

Mathematical Problems in Engineering

Theory, Methods, and Applications

Special Issue

Mathematical Problems for Complex Networks

Guest Editors: Zidong Wang, Jinling Liang, and Yurong Liu



Mathematical Problems for Complex Networks

Mathematical Problems in Engineering

**Mathematical Problems for
Complex Networks**

Guest Editors: Zidong Wang, Jinling Liang, and Yurong Liu



Copyright © 2012 Hindawi Publishing Corporation. All rights reserved.

This is an issue published in "Mathematical Problems in Engineering." All articles are open access articles distributed under the Creative Commons Attribution License, which permits unrestricted use, distribution, and reproduction in any medium, provided the original work is properly cited.

Editorial Board

- E. M. Abdel-Rahman, Canada
Hamdy Nabih Agiza, Egypt
Sebastian Anita, Romania
W. Assawinchaichote, Thailand
K. V. Avramov, Ukraine
Erwei Bai, USA
Ezzat G. Bakhom, USA
J. M. Balthazar, Brazil
Shankar P. Bhattacharyya, USA
Stefano Boccaletti, Spain
Michael J. Brennan, UK
John Burns, USA
Piermarco Cannarsa, Italy
Carlo Cattani, Italy
Miguel Cerrolaza, Venezuela
Michael J. Chappell, UK
Kue-Hong Chen, Taiwan
Kui Fu Chen, China
Michele Chiumenti, Spain
Jyh Horng Chou, Taiwan
Slim Choura, Tunisia
Biswa N. Datta, USA
M. do R. de Pinho, Portugal
Joao B. R. Do Val, Brazil
Horst Ecker, Austria
Alex Elias-Zuniga, Mexico
Anders Eriksson, Sweden
Qi Fan, USA
Moez Feki, Tunisia
Ricardo Femat, Mexico
Rolf Findeisen, Germany
R. A. Fontes Valente, Portugal
Zoran Gajic, USA
Ugo Galvanetto, Italy
Furong Gao, Hong Kong
Oleg V. Gendelman, Israel
Paulo Batista Gonçalves, Brazil
Oded Gottlieb, Israel
Muhammad R. Hajj, USA
Thomas Hanne, Switzerland
Katica R. Hedrih, Serbia
M. I. Herreros, Spain
Wei-Chiang Hong, Taiwan
J. Horacek, Czech Republic
Gordon Huang, Canada
Anuar Ishak, Malaysia
Reza Jazar, Australia
Zhijian Ji, China
J. Jiang, China
J. J. Judice, Portugal
Tadeusz Kaczorek, Poland
Tamas Kalmar-Nagy, USA
Tomasz Kapitaniak, Poland
Hamid R. Karimi, Norway
Nikolaos Kazantzis, USA
Jurgen Kurths, Germany
Claude Lamarque, France
Stefano Lenci, Italy
Ming Li, China
Shanling Li, Canada
Teh-Lu Liao, Taiwan
P. Liatsis, UK
Jui-Sheng Lin, Taiwan
Wanquan Liu, Australia
Bin Liu, Australia
Angelo Luongo, Italy
Alexei Mailybaev, Brazil
R. Martinez-Guerra, Mexico
B. Maslowski, Czech Republic
Yuri V. Mikhlin, Ukraine
G. V. Milovanović, Serbia
Trung Nguyen Thoi, Vietnam
Hung Nguyen-Xuan, Vietnam
Ben T. Nohara, Japan
Anthony Nouy, France
Francesco Pellicano, Italy
F. Lobo Pereira, USA
A. Pogromsky, The Netherlands
Seppo Pohjolainen, Finland
Stanislav Potapenko, Canada
Sergio Preidikman, USA
Serge Prudhomme, USA
Dane Quinn, USA
K. R. Rajagopal, USA
Sivaguru Ravindran, USA
G. Rega, Italy
Pedro Ribeiro, Portugal
J. Rodellar, Spain
Rosana Rodríguez-López, Spain
A. J. Rodriguez-Luis, Spain
Rubén Ruiz García, Spain
Miguel A. F. Sanjuán, Spain
Ilmar Ferreira Santos, Denmark
Nickolas S. Sapidis, Greece
Andrey V. Savkin, Australia
Massimo Scalia, Italy
Alexander P. Seyranian, Russia
Tony Sheu, Taiwan
Zhan Shu, UK
Christos H. Skiadas, Greece
Davide Spinello, Canada
Sri Sridharan, USA
Jitao Sun, China
Xi-Ming Sun, China
Andrzej Swierniak, Poland
Allen Tannenbaum, USA
Cristian Toma, Romania
Irina N. Trendafilova, UK
Kuppapalle Vajravelu, USA
Victoria Vampa, Argentina
Blas M. Vinagre, Spain
Yongqi Wang, Germany
Moran Wang, USA
Gerhard-Wilhelm Weber, Turkey
Peter R. Wolenski, USA
Kwok W. Wong, HongKong
Christine Qiong Wu, Canada
Ligang Wu, China
Zheng-Guang Wu, China
Xuping Xu, USA
Xing-Gang Yan, UK
Jun-Juh Yan, Taiwan
Xing-Gang Yan, UK
Mahmoud T. Yassen, Egypt
Mohammad I. Younis, USA
Ion Zaballa, Spain
Xu Zhang, China

Contents

Mathematical Problems for Complex Networks, Zidong Wang, Jinling Liang, and Yurong Liu
Volume 2012, Article ID 934680, 5 pages

An Immune Cooperative Particle Swarm Optimization Algorithm for Fault-Tolerant Routing Optimization in Heterogeneous Wireless Sensor Networks, Yifan Hu, Yongsheng Ding, and Kuangrong Hao
Volume 2012, Article ID 743728, 19 pages

Mixed H_2/H_∞ Performance Analysis and State-Feedback Control Design for Networked Systems with Fading Communication Channels, Adrian-Mihail Stoica
Volume 2012, Article ID 291714, 16 pages

On the Complexities of the Design of Water Distribution Networks, Joaquín Izquierdo, Idel Montalvo, Rafael Pérez-García, and Agustín Matías
Volume 2012, Article ID 947961, 25 pages

Enhancement of the Quality and Robustness in Synchronization of Nonlinear Lur'e Dynamical Networks, Shiyun Xu, Yong Tang, Huadong Sun, Ziguan Zhou, and Ying Yang
Volume 2012, Article ID 236782, 22 pages

Recent Advances on Filtering and Control for Nonlinear Stochastic Complex Systems with Incomplete Information: A Survey, Bo Shen, Zidong Wang, Jinling Liang, and Yurong Liu
Volume 2012, Article ID 530759, 16 pages

Impulsive Synchronization of Nonlinearly Coupled Complex Networks, Guizhen Feng, Jinde Cao, and Jianquan Lu
Volume 2012, Article ID 969402, 10 pages

Second-Order Consensus for Multiagent Systems under Directed and Switching Topologies, Lixin Gao, Jingjing Zhang, and Wenhai Chen
Volume 2012, Article ID 273140, 21 pages

Structural Models of Cortical Networks with Long-Range Connectivity, Nicole Voges, Ad Aertsen, and Stefan Rotter
Volume 2012, Article ID 484812, 17 pages

A Quasi-ARX Model for Multivariable Decoupling Control of Nonlinear MIMO System, Lan Wang, Yu Cheng, and Jinglu Hu
Volume 2012, Article ID 570498, 13 pages

Practical Stability in the p th Mean for Itô Stochastic Differential Equations, Enguang Miao, Huisheng Shu, and Yan Che
Volume 2012, Article ID 380304, 12 pages

p th Mean Practical Stability for Large-Scale Itô Stochastic Systems with Markovian Switching, Yan Yun, Huisheng Shu, and Yan Che
Volume 2012, Article ID 573439, 11 pages

The Practical Stabilization for a Class of Networked Systems with Actuator Saturation and Input Additive Disturbances, Dongyan Chen, Shanqiang Li, and Yujing Shi
Volume 2012, Article ID 326876, 19 pages

Geometric Buildup Algorithms for Sensor Network Localization, Zhenzhen Zheng, Xinlong Luo, and Zhijun Wu
Volume 2012, Article ID 927031, 18 pages

Global Robust Stability of Switched Interval Neural Networks with Discrete and Distributed Time-Varying Delays of Neural Type, Huaiqin Wu, Ning Li, Kewang Wang, Guohua Xu, and Qiangqiang Guo
Volume 2012, Article ID 361871, 18 pages

H_∞ Neural-Network-Based Discrete-Time Fuzzy Control of Continuous-Time Nonlinear Systems with Dither, Zhi-Ren Tsai and Jiing-Dong Hwang
Volume 2012, Article ID 314964, 18 pages

Further Stability Criterion on Delayed Recurrent Neural Networks Based on Reciprocal Convex Technique, Guobao Zhang, Tao Li, and Shumin Fei
Volume 2012, Article ID 829037, 14 pages

Abstract Description of Internet Traffic of Generalized Cauchy Type, Ming Li and Wei Zhao
Volume 2012, Article ID 821215, 18 pages

Energy-Aware Topology Evolution Model with Link and Node Deletion in Wireless Sensor Networks, Xiaojuan Luo, Huiqun Yu, and Xiang Wang
Volume 2012, Article ID 281465, 14 pages

A Novel Algorithm of Stochastic Chance-Constrained Linear Programming and Its Application, Xiaodong Ding and Chengliang Wang
Volume 2012, Article ID 139271, 17 pages

Adaptive-Impulsive Control of the Projective Synchronization in Drive-Response Complex Dynamical Networks with Time-Varying Coupling, Song Zheng
Volume 2012, Article ID 501843, 12 pages

Two Quarantine Models on the Attack of Malicious Objects in Computer Network, Bimal Kumar Mishra and Aditya Kumar Singh
Volume 2012, Article ID 407064, 13 pages

Editorial

Mathematical Problems for Complex Networks

Zidong Wang,^{1,2} Jinling Liang,³ and Yurong Liu⁴

¹ *School of Information Sciences and Technology, Donghua University, Shanghai 200051, China*

² *Department of Information Systems and Computing, Brunel University, Uxbridge, Middlesex UB8 3PH, UK*

³ *Department of Mathematics, Southeast University, Nanjing 210096, China*

⁴ *Department of Mathematics, Yangzhou University, Yangzhou 225002, China*

Correspondence should be addressed to Zidong Wang, zidong.wang@brunel.ac.uk

Received 16 November 2011; Accepted 16 November 2011

Copyright © 2012 Zidong Wang et al. This is an open access article distributed under the Creative Commons Attribution License, which permits unrestricted use, distribution, and reproduction in any medium, provided the original work is properly cited.

Complex networks do exist in our lives. The brain is a neural network. The global economy is a network of national economies. Computer viruses routinely spread through the Internet. Food-webs, ecosystems, and metabolic pathways can be represented by networks. Energy is distributed through transportation networks in living organisms, man-made infrastructures, and other physical systems. Dynamic behaviors of complex networks, such as stability, periodic oscillation, bifurcation, or even chaos, are ubiquitous in the real world and often reconfigurable. Networks have been studied in the context of dynamical systems in a range of disciplines. However, until recently there has been relatively little work that treats dynamics as a function of network structure, where the states of both the nodes and the edges can change, and the topology of the network itself often evolves in time. Some major problems have not been fully investigated, such as the behavior of stability, synchronization and chaos control for complex networks, as well as their applications in, for example, communication and bioinformatics.

Complex networks have already become an ideal research area for control engineers, mathematicians, computer scientists, and biologists to manage, analyze, and interpret functional information from real-world networks. Sophisticated computer system theories and computing algorithms have been exploited or emerged in the general area of computer mathematics, such as analysis of algorithms, artificial intelligence, automata, computational complexity, computer security, concurrency and parallelism, data structures, knowledge discovery, DNA and quantum computing, randomization, semantics, symbol manipulation, numerical analysis, and mathematical software. This special issue aims to bring together the latest approaches to understanding complex networks from a dynamic system perspective. Topics include, but are not limited to the following aspects of dynamics analysis for complex

networks: (1) synchronization and control; (2) topology structure and dynamics; (3) stability analysis; (4) robustness and fragility.

This special issue aims to bring together the latest approaches to understanding the mathematical issues of complex networks from a dynamic system perspective. We have solicited submissions to this special issue from electrical engineers, control engineers, mathematicians, and computer scientists. After a rigorous peer-review process, 21 papers have been selected that provide overviews, solutions, or early promises, to manage, analyze, and interpret dynamical behaviors of complex networks. These papers have covered both the practical and theoretical aspects of complex networks in the broad areas of dynamical systems, mathematics, statistics, operational research, and engineering.

This special issue starts with a survey paper on the recent advances of filtering and control for complex networked systems with incomplete information. Specifically, in the paper entitled "*Recent advances on filtering and control for nonlinear stochastic complex systems with incomplete information*" by Z. Wang, the focus is mainly on the filtering and control problem for complex systems with incomplete information and the main aim is to give a survey on some recent advances in this area. The incomplete information under consideration includes missing measurements, randomly varying sensor delays, signal quantization, sensor saturations, and signal sampling. The modeling issues are first discussed to reflect the real complexity of the nonlinear stochastic systems. Based on the models established, various filtering and control problems with incomplete information are reviewed in detail. Then, the complex systems, are dealt with from three aspects, that is, nonlinear stochastic systems, complex networks and sensor networks. Both theories and techniques for dealing with complex systems are reviewed and, at the same time, some challenging issues for future research are raised. Subsequently, the filtering problems for the stochastic nonlinear complex networks with incomplete information are paid particular attention by summarizing the latest results. Finally, some conclusions are drawn and several possible related research directions are pointed out.

Complex networks are composed of a large number of highly interconnected dynamical units and therefore exhibit very complicate dynamics. Examples of such complex networks include the Internet, which is a network of routers domains, the World Wide Web, which is a network of web sites, the brain, which is a network of neurons, and an organization, which is a network of people. Synchronization for complex networks is attracting more and more research attention due to its ubiquity in many system models of the natural world. In another paper "*Impulsive synchronization of nonlinearly-coupled complex networks*" by J. Cao, the impulsive synchronization problem is investigated for nonlinearly coupled complex networks. Based on the stability analysis of impulsive functional differential equations, some sufficient synchronization criteria are established in terms of average impulsive interval. The model addressed is a nonlinearly coupled network that covers the linearly coupled network and an array of linearly coupled systems as special cases. In the work "*Enhancement of the quality and robustness in synchronization of nonlinear lur'e dynamical networks*" by Y. Yang, the synchronization is studied for a class of nonlinear dynamical networks with faults and external disturbances. Sufficient conditions are given to guarantee the global robust synchronization for the network by means of solving the linear matrix inequalities. By using adaptive-impulsive control approach, the projective synchronization problem is dealt with in "*Adaptive-impulsive control of the projective synchronization in drive-response complex dynamical networks with time-varying coupling*" by S. Zheng for drive-response time-varying coupling complex dynamical networks with time delay and time-varying weight links. An adaptive feedback controller with impulsive control effects is designed. In

the paper entitled *"Second-order consensus for multi-agent systems under directed and switching topologies"* by L. Gao, based on the graph theory and Lyapunov method, sufficient conditions of the consensus stability are established for systems with neighbor-based feedback laws in leader-following case and leaderless case. As special cases, the consensus criteria for balanced and undirected interconnection topology cases can be readily established.

Sensor networks have recently been undergoing a quiet revolution in all aspects of the hardware implementation, software development, and theoretical research. Sensor networks possess their own characteristics due mainly to the large number of inexpensive wireless devices (nodes) densely distributed and loosely coupled over the region of interest. The past decade has seen successful applications of sensor networks in many practical areas ranging from military sensing, physical security, air traffic control, to industrial and manufacturing automation. In the paper addressed *"Energy-aware topology evolution model with link and node deletion in wireless sensor networks"* by X. Luo, based on the complex network theory, a new topological evolving model is proposed. In the evolution of the topology of sensor networks, the energy-aware mechanism is taken into account, and the phenomenon of change of the link and node in the network is discussed. Theoretical results and numerical simulation are given to analyze the topology characteristics and network performance with different node energy distributions. It is shown that, when nodes energy is more heterogeneous, the network is better clustered and the higher performance is achieved in terms of the network efficiency and the average path length of transmitting data. In order to maintain k disjoint communication paths from source sensors to the macronodes, a hybrid routing scheme is developed in *"An immune cooperative particle swarm optimization algorithm for fault-tolerant routing optimization in heterogeneous wireless sensor networks"* by Y.-S. Ding, where multiple paths are calculated and maintained in advance, and alternative paths are created on demand. Also, an immune cooperative particle swarm optimization algorithm (ICPSOA) is developed to guarantee the fast routing recovery and reconstruct the network topology from path failure in heterogeneous wireless sensor networks (H-WSNs). In another paper *"Geometric buildup algorithms for sensor network localization"* by Z. Wu, a geometric build-up algorithm is given for the sensor network localization problem with either accurate or noisy distance data. Moreover, an algorithm with two buildup phases is presented to handle the noisy and sparse distance data. By comparing with the existing approaches, the advantages of the proposed algorithms are shown.

In the past few decades, neural networks have received considerable research interests and have found successful applications in a variety of areas such as pattern recognition, associative memory, and combinatorial optimization. The dynamical characteristics of neural networks with time delays have become a subject of intense research activities. In the paper entitled *"Global robust stability of switched interval neural networks with discrete and distributed time-varying delays of neural type"* by H. Wu, a switched interval neural network is discussed with discrete and distributed time-varying delays. Together with the Lyapunov approach and linear matrix inequality (LMI) technique, a delay-dependent criterion is given such that the switched interval neural network is globally asymptotically stable. By constructing the Lyapunov-Krasovskii functional and using the reciprocal convex technique, a new sufficient condition is derived in *"Further stability criterion on delayed recurrent neural networks based on reciprocal convex technique,"* by T. Li to guarantee the global stability for recurrent neural networks with both time-varying and continuously distributed delays. Numerical examples are given to show the effectiveness and less conservatism of the proposed method. In another paper *" H_∞ Neural-network-based discrete-time fuzzy control of continuous-time nonlinear systems with dither,"* by J.-D. Hwang, and by constructing a discrete-time (DT) fuzzy controller, the

stabilization problem is investigated for a class of continuous-time (CT) nonlinear systems. After discretizing the CT nonlinear system, a neural-network (NN) system is established to approximate the DT nonlinear system. Then, a Takagi-Sugeno DT fuzzy controller is designed to stabilize this NN system. It is shown that when the discretized frequency or sampling frequency of the CT system is sufficiently high, the DT system can maintain the dynamic of the original CT system. Moreover, the trajectory of the DT system and the CT system can be made as close as desired by designing the sampling frequency.

As being well known, the cyber world brings massive changes to the society. There have been many cyber-related challenging problems that arise inevitably and should be handled. In the paper addressed "*Two quarantine models on the attack of malicious objects in computer network*," by B. K. Mishra, SEIQR (susceptible, exposed, infectious, quarantined, and recovered) models for the transmission of malicious objects are discussed in computer network with simple mass action incidence and standard incidence rate. Sufficient conditions for global stability and asymptotic stability of endemic equilibrium are given for simple mass action incidence. Also, the behaviors are analyzed for the susceptible, exposed, infected, quarantined, and recovered nodes in the computer network. The spatially embedded networks are tackled in "*Structural models of cortical networks with long-range connectivity*," by S. Rotter with specific distance-dependent connectivity profiles. By applying the stochastic graph theory, the structure and the topology of such networks are considered. In another paper "*Abstract description of internet traffic of generalized cauchy type*," by M. Li, the set-valued analyses are investigated for the traffic of the fractional Gaussian noise (fGn) type and the generalized Cauchy (GC) type. Meanwhile, a design procedure of the autocorrelation function (ACF) is presented for the GC process in Hilbert spaces. Multiple complex tasks commonly occur in the water distribution networks, such as design, planning, operation, maintenance, and management. In the paper entitled "*On the complexities of the design of water distribution networks*," by J. Izquierdo, a synergetic association between swarm intelligence and multiagent systems is discussed for water distribution networks, where human interaction is simultaneously enabled. In the paper addressed "*A novel algorithm of stochastic chance-constrained linear programming and its application*," by C. Wang, the stochastic chance-constrained linear programming problem is investigated. A simplex algorithm is developed based on the stochastic simulation and a practical example is presented to illustrate the applicability of the proposed algorithm.

Stability analysis and stabilization problems of stochastic systems have attracted much attention in the past decades, since stochastic modeling has come to play an important role in many real-world systems, including nuclear, thermal, chemical processes, biology, socioeconomics, immunology, and so forth. In another paper "*Mixed H_2/H_∞ performance analysis and state-feedback control design for networked systems with fading communication channels*," by A.-M. Stoica, the aim is to develop a performance analysis approach for networked systems with fading communication channels. A state feedback controller is designed to accomplish a mixed H_2/H_∞ performance requirement. A numerical iterative procedure is presented which can be utilized to compute the stabilizing solution for system with jumps. The practical stabilization problem is investigated in "*The practical stabilization for a class of networked systems with actuator saturation and input additive disturbances*," by D. Chen for a class of linear systems with actuator saturation and input additive disturbances. The time-invariant and time-varying input additive disturbances are considered, respectively. By applying the Riccati equation approach and designing the linear state feedback controllers, sufficient conditions are established to guarantee the semiglobal practical stabilization for the closed-loop systems. In the paper entitled "*A quasi-ARX model for multivariable decoupling*

control of nonlinear MIMO system,” by J. Hu, a multiinput and multioutput (MIMO) quasi-autoregressive exogenous (ARX) model is presented and a multivariable-decoupling proportional integral differential (PID) controller is designed for the MIMO nonlinear systems. An adaptive control algorithm is given by using the MIMO quasi-ARX radial basis function network (RBFN) prediction model. In another paper “*Practical stability in the p th mean for $It\delta$ stochastic differential equations,*” by H. Shu, the p th mean practical stability problem is investigated for a general class of $It\delta$ -type stochastic differential equations over both finite-time and infinite-time horizons. Sufficient conditions are established such that the addressed differential equations are p th moment practically stable. The practical stability problem is studied in “ *p th mean practical stability for large-scale $It\delta$ stochastic systems with markovian switching,*” by H. Shu for Markovian switching systems in the p th mean sense. By using the Lyapunov method, some criteria are presented such that various types of practical stability in the p th mean are guaranteed for the nonlinear stochastic systems.

Acknowledgments

This special issue is a timely reflection of the research progress in the area of mathematical problems for complex networks. We would like to acknowledge all authors for their efforts in submitting high-quality papers. We are also very grateful to the reviewers for their thorough and ontime reviews of the papers.

Zidong Wang
Jinling Liang
Yurong Liu

Research Article

An Immune Cooperative Particle Swarm Optimization Algorithm for Fault-Tolerant Routing Optimization in Heterogeneous Wireless Sensor Networks

Yifan Hu,^{1,2} Yongsheng Ding,^{1,2} and Kuangrong Hao^{1,2}

¹ College of Information Sciences and Technology, Donghua University, Shanghai 201620, China

² Engineering Research Center of Digitized Textile and Fashion Technology, Ministry of Education, Donghua University, Shanghai 201620, China

Correspondence should be addressed to Yongsheng Ding, ysding@dhu.edu.cn

Received 26 May 2011; Accepted 3 August 2011

Academic Editor: Jinling Liang

Copyright © 2012 Yifan Hu et al. This is an open access article distributed under the Creative Commons Attribution License, which permits unrestricted use, distribution, and reproduction in any medium, provided the original work is properly cited.

The fault-tolerant routing problem is important consideration in the design of heterogeneous wireless sensor networks (H-WSNs) applications, and has recently been attracting growing research interests. In order to maintain k disjoint communication paths from source sensors to the macronodes, we present a hybrid routing scheme and model, in which multiple paths are calculated and maintained in advance, and alternate paths are created once the previous routing is broken. Then, we propose an immune cooperative particle swarm optimization algorithm (ICPSOA) in the model to provide the fast routing recovery and reconstruct the network topology for path failure in H-WSNs. In the ICPSOA, mutation direction of the particle is determined by multi-swarm evolution equation, and its diversity is improved by immune mechanism, which can enhance the capacity of global search and improve the converging rate of the algorithm. Then we validate this theoretical model with simulation results. The results indicate that the ICPSOA-based fault-tolerant routing protocol outperforms several other protocols due to its capability of fast routing recovery mechanism, reliable communications, and prolonging the lifetime of WSNs.

1. Introduction

The complex networks have attracted growing research interests in topology structure and dynamic problems. Many kinds of system can be described with the complex network model, and these models are constructed by several nodes connected with each other, such as the Internet and the wireless sensor networks (WSNs). Due to the ability of collecting data from the environment and reporting it back to the sink without human supervision [1, 2], WSNs, especially heterogeneous ones, have come to pervade every aspect of our lives, such as habitat monitoring, industrial sensing, and traffic control [3–5]. The heterogeneous WSNs always

deploy an appropriate number of heterogeneous wireless sensor nodes (called macronodes), which contain devices with more capabilities, storage space, and energy than ordinary nodes. They cannot only improve the success rate of data transmission of WSNs, but also reduce the energy consumption of transmission, thus can effectively prolong the network lifetime. The benefits of using heterogeneous WSNs (H-WSNs) have been presented in the literature [6–9]. It is reported that when properly deployed, heterogeneity can triple the average delivery rate and provide a fivefold increase in the network lifetime [6].

However, in practical applications, unpredictable events such as environmental impairment, communication link broken, and battery depletion may cause the sensor devices to fail, partitioning the network and disrupting network functions. Therefore, fault tolerance becomes a critical issue for the successful communication of H-WSNs. It is expected that the network topology broken by software or hardware failure of sensor nodes could be automatically reconstructed and self-healed by the fault-tolerant routing technology so as to be recovered from path failure and ensured the performance of the communication tasks.

The objective of this paper is to solve the fault-tolerant routing problem for the H-WSNs while maintaining k disjoint communication paths from each source sensor to the macronode it belongs to (called k -disjoint-path routing recovery problem). For this purpose, we propose a swarm intelligence algorithm, immune cooperative particle swarm optimization algorithm (ICPSOA), to provide fast recovery from path failure in the H-WSNs. In this way, the network can tolerate the failure of up to $k - 1$ sensor paths with reconstructed topology, traditional retransmissions can be decreased, and reliability can be provided with lower energy consumption. Our problem is specifically tailored to the situation that data is forwarded from sensors to macronodes.

The main contributions of this paper are as follows: firstly, we formulate the k -disjoint-path routing recovery problem for the H-WSNs. Then, in order to maintain k disjoint communication paths from each source sensor to the set of macronodes, we propose the ICPSOA-based protocol to reconstruct the network topology and provide fast routing recovery from path failure in the H-WSNs. The proposed method can provide simplicity, robustness, and effectiveness for routing recovery problem of the WSNs.

The remainder of this paper is organized as follows: Section 2 overviews the related work on fault-tolerant routing problem, especially routing recovery problem in the H-WSNs. Then, we propose the H-WSNs architecture and fault model and the ICPSOA-based approach for solving the routing recovery problem in Section 3. The simulation results are presented in Section 4. Section 5 provides a conclusion of our paper and discusses a few future directions for further improving the performance of our approach.

2. Related Work

2.1. The Fault-Tolerant Routing Algorithms of WSNs

Fault-tolerant routing protocols proposed for WSNs can be classified into three groups: (1) proactive routing, called disjoint multipath, in which several paths from source node to sink are calculated, maintained in advance, and stored in a routing table, but greater energy consumption and the requirement to predict the global topology information are the disadvantages [10–12], (2) reactive routing, where all paths are created on demand [7], and (3) hybrid routing, which is a mix of the above two groups [8, 9].

One of the common fault-tolerant routing solutions is to establish disjoint multipath with proactive routing mechanism. Disjoint multipath constructs a number of alternative

paths which are node/links disjoint with the primary path and other alternative paths. Thus, a failure in any or all nodes/links on the primary path does not affect the alternative paths. Using this multipath scheme in a network with k disjoint paths from source to destination can tolerate at most $k - 1$ intermediate network component failures. A secure and energy-efficient multipath routing protocol proposed by Nasser and Chen [10] is effectively resistive to some specific attacks, and has the character of pulling all traffic through the malicious nodes by advertising an attractive route to the destination.

A considerable amount of work has also been done on the hybrid routing scheme, which combines multipath scheme and reactive routing scheme. In this scheme, multiple paths are calculated and maintained in advance, and then, alternative paths are created on demand. EARQ (energy-aware routing for real-time and reliable communication) is a hybrid routing scheme proposed by Heo and Hong [9], which selected a path that expended less energy than others, among paths that delivered a packet in time, which enabled even distribution of energy expenditure to sensor nodes. It also provided reliable communication and fast recovery from path failure, because it only sent a redundant packet via an alternative path if the reliability of a path was less than a predefined value. Pandana and Liu [11] sought to propose an algorithm which designed the connectivity weight of each node and established a most reliable path in order to keep the other nodes' connectivity.

Our work differs from the above existing ones [13–16] by considering a different architecture and routing objective. We consider the H-WSNs architecture with a number of macronodes and concern with providing k -connectivity from each source node to the set of macronodes, and as such, we provide a hybrid routing scheme to maintain the multipath routing. The H-WSNs usually consist of two types of wireless devices [12]: a large number of resource-constrained wireless sensor nodes deployed randomly and a much smaller number of resource-rich macronodes placed at known locations. The macronode network, which provides more energy, transmission bandwidth, computing ability, and storage space, is used to quickly forward sensor data packets to the sink. With this setting, data gathering in the H-WSNs has two steps. Firstly, sensor nodes transmit and relay information on multihop paths toward any macronode. Then, it is forwarded to the sink using fast macronode-to-macronode communication once a packet encounters a macronode.

The similar hybrid routing schemes for the H-WSNs are as follows: CPEQ (cluster-based periodic, event-driven, and query-based protocol) [17] groups sensor nodes to efficiently relay data to the sink by uniformly distributing energy dissipation among the nodes. It can provide fast broken path reconfiguration and high reliability in the delivery of event packets and speed up new subscriptions by using the reverse path. Cardei and Yang [18] proposed $GATC_k$ and $DATC_k$ in the H-WSNs, with the objective of minimizing the total energy consumption while providing k independent paths from each node to macronodes. Such a topology provides the infrastructure for fault-tolerant data-gathering applications robust to the failure of up to $k - 1$ sensors. Boukerche et al. [8] used a protocol of ICE (intercluster communication-based energy-aware and fault-tolerant protocol) by alternating the nodes responsible for intercluster communication inside one cluster. If one of multiple paths has faulty nodes, the other ones will be used for the event notification's propagation. But the fast routing recovery mechanism for path failure has rarely been considered. Further, as the fault-tolerant optimization problem to find the optimal routing is NP-hard, these heuristic deterministic methods would always get the likely optimal routing result, and is easy to fall into local optimum. So, we employ a swarm intelligence algorithm, the ICPSOA, to improve the performance of solving these problems.

In this paper, we propose an ICPSOA-based fault-tolerant routing algorithm, which reconstructs the network topology of H-WSNs and provides a fast recovery from path failure with alternative path. We also compare the performance of the protocols of EARQ, CPEQ, and ICE with that of our approach. As we known, EARQ is an effective fault-tolerant routing protocol for homogeneous WSNs, while ICE and CPEQ are for H-WSNs to provide routing recovery from path failure. In this way, we can evaluate the fault-tolerant routing recovery mechanism with different network types.

2.2. SPSOA, CPSOA, and ICPSOA

The EA-based bionic randomized algorithm has become the important tools for solving complex optimization problems because of its intelligence and widely used and global search ability. But the algorithm dealing with fault-routing problem of WSNs should support the characteristic of energy saving. In general, better fault-tolerant performance always needs more energy consumption. Therefore, we choose light-weight algorithm based on the particle swarm optimization algorithm (PSOA), which has a simple structure and is easy to realize.

The PSOA is a new EA based method to search an optimal solution in the high-dimensional problem space [13], where each particle is a potential solution to the problem under analysis. In updating a population of particles with regard to their internal position and velocity, the PSOA is informed by the experiences of all the particles. It provides an idea to find solutions to complex problems using group advantage without global model and centralized control and can be suitable to apply in a dynamical modeling environment. It has been applied to many optimization problems, such as control problems and protocol design [14]. A remarkable difference between the PSOA and other EA-based algorithms is that the PSOA is very simple and has few parameters to be adjusted. Therefore, in general, it requires less computational complexity.

In the standard PSOA (SPSOA), each particle is a potential solution to the problem. Assume N particles fly in the D -dimensional search space, the position of the i th particle is $\mathbf{x}_i^t = (x_{i1}^t, x_{i2}^t, \dots, x_{iD}^t)^T$, and its velocity is $\mathbf{v}_i^t = (v_{i1}^t, v_{i2}^t, \dots, v_{iD}^t)^T$. $\mathbf{p}_i = (p_{i1}^t, p_{i2}^t, \dots, p_{iD}^t)$ is the best previous position of the particle, and \mathbf{p}_g is the global best position of the whole particle swarm. Therefore, the velocity and position of each particle will be updated according to [15]

$$\begin{aligned} v_{id}^{t+1} &= w v_{id}^t + c_1 \text{rand}_1 (p_{id}^t - x_{id}^t) + c_2 \text{rand}_2 (p_{gd}^t - x_{id}^t), \\ x_{id}^{t+1} &= x_{id}^t + v_{id}^{t+1}, \end{aligned} \quad (2.1)$$

where $1 \leq d \leq D$, c_1 and c_2 are learning factors, and usually, we make $c_1 = c_2 = 2$; w is the inertia weight and used to control the tradeoff between the global and local exploration ability of the swarm. Random numbers rand_1 and rand_2 are uniformly distributed in $[0,1]$.

The SPSOA also exhibits several disadvantages: it sometimes poses the problem of converging to undesired local optimum, for the diversity of population decreases in the latter iteration of evolution; optimizing stops when reaching a likely optimal solution, and thus the accuracy of the algorithm is limited. Therefore, a cooperative PSOA (CPSOA), which uses cooperative behavior of multiple swarms to improve the SPSOA, is proposed in [16]. In the CPSOA, limitation of an individual can be compensated by a number of other individuals from other symbiotic groups in the interaction. It can avoid misjudgment caused by single

exchange of information [16]. However, it still uses the formula of the SPSOA to evolve. The trajectory of each particle is unable to yield high diversity of particles to increase search space. Therefore, the CPSOA may get a suboptimal solution.

For this reason, we draw on good diversity characteristic of immune mechanism and develop an immune CPSOA (ICPSOA), in which each particle is considered as an antibody. Particle clone is used to generate a new population with offspring. Mutation is used to diversify the search process. Immune restrain is considered to restrain the inferior ones in order to keep the stable population. Immune memory is used to store the feasible solutions [19]. The affinity between antibody and antigen can measure the optimal path, and the affinity between antibodies and antibodies can evaluate the diversity of population [20]. In the ICPSOA, mutation direction of the particle (called antibody) is determined by evolution equation, and its diversity is increased by immune mechanism [21]. Although the addition of the immune mechanism may add more time complexity to the system, the proposed ICPSOA largely improves the capability of jumping out of local optima. The use of the ICPSOA for the fault-tolerant routing problem in H-WSNs has been presented in the following sections.

3. Fault-Tolerant Routing Problem in H-WSNs Based on the ICPSOA

3.1. Model of the Proposed H-WSNs

3.1.1. The Architecture for the Model of H-WSNs

The architecture for the model of H-WSNs contains two types of wireless sensor devices as shown in Figure 1. The lower layer is formed by sensor nodes with constrained resource, including small amount of source nodes and other relay nodes. The main tasks performed by the source nodes are sensing, data processing, and data transmission. The tasks performed by the relay nodes are data processing and relaying. The dominant energy consumer is the radio transceiver. The upper layer consists of resource-rich macronodes overlaid on the H-WSNs. Wireless communication links between macronodes have considerably longer ranges and higher data rates, allowing the macronode network to bridge remote regions of the interest area. The tasks performed by a macronode are data aggregation and transmission, complex computations, and decision making. The ICPSOA is also executed by macronodes.

Therefore, in-network data transmission can be performed by forming a spanning tree among all the tree nodes. As shown in Figure 1, transmission starts with the leaf nodes (source node) of the tree sending their values to their parent nodes (macronode, nodes $1, 2, \dots, 12$) in the tree, until the final data is obtained at the root node (sink, node 13). Thus, the overall architecture would have a tree of macronodes and then each macronode can serve as the root of a subtree of ordinary nodes. Here, we are only interested in the fault-tolerant routing between sensor-sensor and sensor-macronode communications.

Assume that the network has the following characters: (1) the H-WSNs is a static network, where the nodes will not move after deployment, (2) every node knows its own position and that of the macronodes and the sink. The location can be obtained by GPS or localization protocols for estimating the location of a node, (3) the wireless transmission energy of macronode can be adjusted based on the distance between the receiver and itself, (4) the adjacent nodes would acquire the state information of their 1-hop neighbors and the links between them through periodically broadcast. The meanings of used symbols is provided in Table 1.

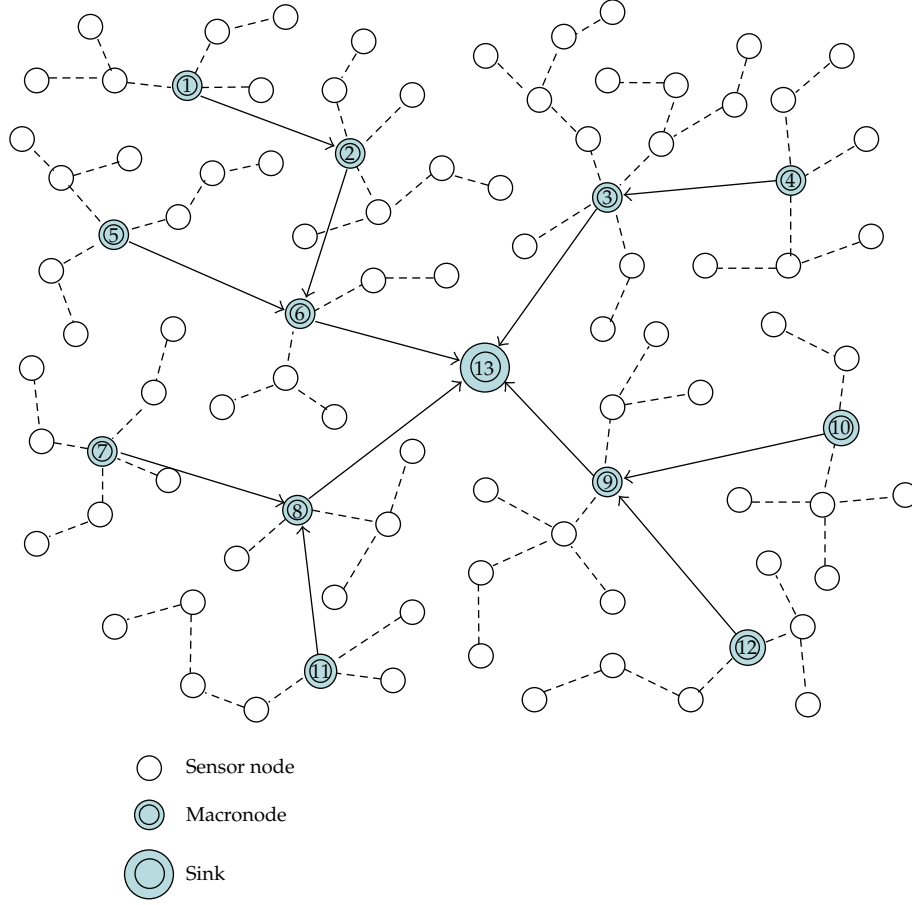


Figure 1: The architecture of H-WSNs.

Table 1: The main symbols.

ST_i	The i th subtree of the tree of the H-WSNs
N_{ST_i}	The number of the sensor nodes in ST_i
P_{ST_i}	The state information of all the nodes in ST_i
n_s	One of the source nodes in ST_i
n_r	The root node (macronode) in ST_i
$P(s, r)$	The set of all the possible paths between n_s and n_r in ST_i
$p_i(s, r)$	The i th path between n_s and n_r in ST_i
n_{fail}	The failed relay node of $p_i(s, r)$ in ST_i
n_{fail-c}	The child node of n_{fail} of $p_i(s, r)$ in ST_i
n_{fail-p}	The parent node of n_{fail} of $p_i(s, r)$ in ST_i
n_i	The i th sensor node of $p_i(s, r)$ in ST_i
p_b	The optimal path of $P(s, r)$ with optimal fitness in ST_i
$n_{p_b, i}$	The i th sensor node of p_b in ST_i

3.1.2. The k -Disjoint-Path Spanning Graph in the Subtree

The subtree ST_i of the network is modeled as a directed, connected graph $G(V, E)$, where V is a finite set of subtree nodes and E is the set of subtree edges representing connection between these nodes, where source node $n_s \in V$ and macronode (root) $n_r \in \{V - \{n_s\}\}$. $p_i(s, r)$ is a valid path between n_s and n_r , and $P(s, r)$ is the set of all the paths $p_i(s, r)$. $n(n \in p_i(s, r))$ represents a node in $p_i(s, r)$, and $e(e \in p_i(s, r))$ represents direct edge between any two adjacent nodes in $p_i(s, r)$. Then, we can get the k -disjoint-path spanning graph in the subtree ST_i . The factors affecting the choice of path $p_i(s, r)$ include (1) the available energy function of each node, $ene(n)$, (2) distance function of the edge between adjacent nodes, $dist(e)$, (3) energy consumption function, $ene(e)$, (4) communication delay function of the node, $delay(n)$. Then, these parameters can determine the fitness function of $p_i(s, r)$, $fitness(p_i)$

$$\begin{aligned} fitness(p_i) &= \frac{\sum_{n \in p_i(s, r)} ene(n)}{f_1 + f_2 + f_3}, \\ f_1 &= \frac{\sum_{e \in p_i(s, r)} ene(n)}{\sum_{e \in E} ene(n)}, \\ f_2 &= \frac{\sum_{n \in p_i(s, r)} delay(n)}{\sum_{n \in N} delay(n)}, \\ f_3 &= \frac{\sum_{e \in p_i(s, r)} dist(e)}{\sum_{e \in E} dist(e)}, \end{aligned} \quad (3.1)$$

where f_1 is the ratio of the energy consumed by the edges of path p_i and the energy consumed by all the edges in the subtree, f_2 is the delay of the edges and nodes of path p_i versus the delay of all the nodes in the subtree, and f_3 is the distance of the edges of path p_i versus the distance of all the edges in the subtree. f_1, f_2, f_3 are the weight of effective energy, delay and distance constraints in the fitness function, and $f_1 + f_2 + f_3 = 1$. We set $f_1 = 0.4, f_2 = 0.2, f_3 = 0.4$. The higher fitness value indicates the more suitable path.

As illustrated in Figure 2, we assume $k = 3$, the three disjoint paths between source node (node 2) and root (node 30) are 2-3-9-15-20-25-28-30, 2-8-13-18-23-30, and 2-7-12-16-21-27-30, respectively. The detailed protocol dealing with routing recovery problem is presented in the following sections.

3.1.3. The Proposed Fault Model and Energy Model

We use the simple fault model proposed in [22] and identify the node failure in it. The fault-model should be simple enough to analyze, but also sophisticated enough to capture the fault behavior effectively. The probability of sensor nodes failure of subtree is given by p_{node} . As we use the more reliable macronodes to sustain the failure during transmission process, the probability of macronode failure is assumed to be $p_{macro} \approx 0$. If any of the sensor nodes fails, our routing recovery approach for node failure in subtree can be implemented.

We introduce the energy model adopted in [18], and the equation of energy model of a sensor node is as follows:

$$ene(m, d) = ene_{tx}(m, d) + ene_{rx}(m) = (a_{11} + a_{21}d^n)m + a_{12}m, \quad (3.2)$$

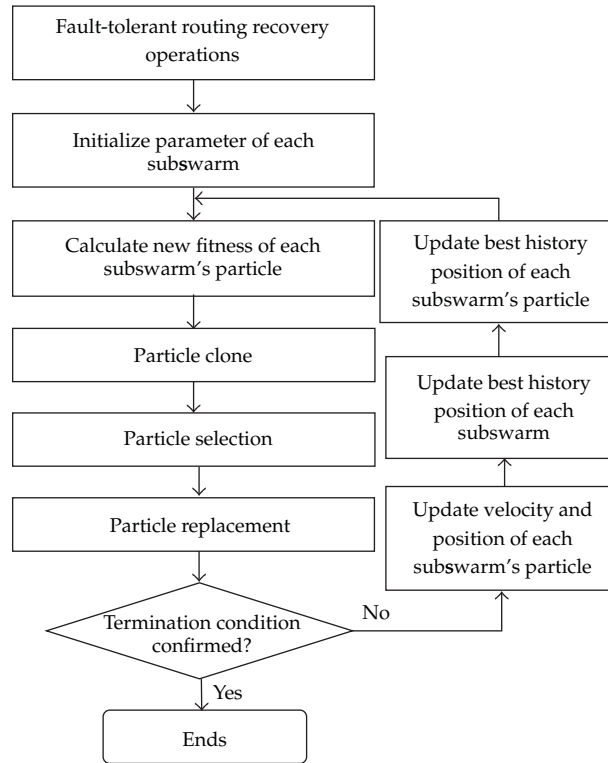


Figure 3: The architecture of the ICPSOA for the H-WSNs.

Input: P_{ST_0} : The information parameters of nodes
 P_{Gen} : The iterated generations for searching process

Output: $fitness(p_i)$: The global optimal fitness

Process:

Step 1: Initialization: Generate initial particle swarm parameter.

Step 2: Immunization: Immune clone, mutation, particle selection and restrain.

Step 3: If termination criterion conditions are satisfied, **go to Step 5**; else **go to Step 4**.

Step 4: Update: Update the velocity and position of each sub-swarm and particle.

Step 5: Output: Output the global optimal fitness of the particle swarm. **Ends**.

Algorithm 1: The ICPSOA for fault-routing problem.

Algorithm 2, $b(g)$ is a complete vector function consisting of all subswarms' optimal position vector, $x_m S_i$ represents position vector of the m th particle in the i th swarm, $p_m S_i$ is the optimal history position vector of the m th particle in the i th swarm, and $p_g S_i$ represents optimal experience position vector of the i th swarm.

(2) Immunization

In this step, each particle can be considered as an antibody, resulting in the clonal mutation set C . The clone number and the fitness of particle are proportional. The clonal number N_c is

Input:	P_{ST_0} : The information parameters of nodes n : The population size of particle k : The population size of swarm
Output:	S_i : The vector of the i th particle swarm $b(g)$: Each sub-swarm's optimal position vector function
Process:	Particle's D -dimensional vector is divided into k particle swarms. $b(L, i) = (p_g S_1, \dots, p_g S_{i-1}, L, p_g S_{i+1}, \dots, p_g S_k)$

Algorithm 2: Initialization mechanism in the ICPSOA.

usually calculated as follows:

$$N_c = N, \quad (3.3)$$

where c_i is the clone factor and is proportional to particle's fitness value. N is the number of particles. Mutation rule can be setup according to experience. The particle mutation rule for the function optimization problem is

$$c_i = x_i + \text{rand}, \quad (3.4)$$

where c_i is the clonal individual, x_i is the original antibody, rand represents the mutation factor, and rand is uniformly distributed in $[0,1]$.

For the particles replacement rule, we need to calculate the antigen stimulus degree of the original particles and select clonal mutation particles. The Euclidean distance between any particle C_t and antigen Y_t is

$$d(i, j) = \sqrt{\sum_{i=1}^n (c_{it} - Y_{jt})^2}. \quad (3.5)$$

Therefore, the stimulus degree of antibody particle is

$$A(i, j) = \frac{1}{d(i, j)}. \quad (3.6)$$

After that, each particle is compared with stimulus threshold; the higher one will maintain in the subswarm, and the lower one will be replaced (called restrain). The process of this step is as shown in Algorithm 3. Then, go to Step 2 in Algorithm 1.

(3) Termination Criterion

If the solution is satisfied with the termination criterion, $\text{fitness}(p_i)$ is the optimal fitness or P_{Gen} decreases to zero, the optimal path p_i will be the desired optimal solution, and this procedure ends; otherwise, returns to Step 4 in Algorithm 1. Then, the k th path is established.

Input: n : The population size of particles
 P_{Gen} : The iterated generations for searching process
 k : The population size of swarm
Output: The allele of the offspring's antibodies (particles)
Process:
For each swarm $i \in [1 \cdots k]$
For each particle $m \in [1 \cdots n/k]$
Clone operation: $N_c = N$
Mutation operation: $c_i = x_i + \text{rand}$
Replacement (restrain) operation:

$$d(i, j) = \sqrt{\sum_{j=1}^n (c_{ij} - y_{ij})^2}, \quad A(i, j) = 1/d(i, j)$$
If $A(i, j) > \text{threshold}$, the particle (antibody) is replaced
End For
End For

Algorithm 3: Immune mechanism in the ICPSOA.

(4) Update

In this step, the velocity and position of the particle is updated as (2.1). The process is as shown in Algorithm 4. The updating equation of particles' optimal position vector in each subswarm is as follows:

$$b(p_m S_i, i) = \begin{cases} b(x_m S_i, i), & \text{fitness}(b(x_m S_i, i)) \geq \text{fitness}(b(p_m S_i, i)), \\ b(p_m S_i, i), & \text{fitness}(b(x_m S_i, i)) < \text{fitness}(b(p_m S_i, i)), \end{cases} \quad (3.7)$$

where $1 \leq i \leq k$. The updating equation of optimal position of each subswarm is

$$b(p_g S_i, i) = \arg \max_{P(p_m S_i, i)} \text{fitness}(b(p_m S_i, i)), \quad 1 \leq m \leq \frac{n}{k}, \quad 1 \leq i \leq k. \quad (3.8)$$

Equation (3.8) indicates that the optimal position of the m th subswarm will select the personal optimal position with the optimal fitness of particle in the swarm.

Inertia weight w plays an important role to the convergence of the result among the adjustable parameters. The larger weight can help the particle escape from the local best solution, and the smaller one is better for the convergence, thus the inertia weight can achieve balance between global search and local search. To overcome the limitations of other general strategies, the linear differential decreasing strategy is used [23]. Here, we select $w_{\text{start}} = 0.85$, $w_{\text{end}} = 0.35$

$$\begin{aligned} \frac{dw(t)}{dt} &= \frac{2(w_{\text{start}} - w_{\text{end}})}{t_{\text{max}}^2} t, \\ w(t) &= w_{\text{start}} - \frac{(w_{\text{start}} - w_{\text{end}})}{t_{\text{max}}^2} t^2. \end{aligned} \quad (3.9)$$

Input:	P_{ST_c} : The information parameters of nodes S_i : The i th particle swarm $b(L, i)$: Each sub-swarm's optimal position vector function P_{Gen} : The iterated generations for searching process
Output:	v_{id}^{t+1} and x_{id}^{t+1} : The velocity and position of each sub-swarm and its particle $fitness(p_i)$: The global optimal fitness
Process:	For each swarm $i \in [1 \cdots k]$ For each particle $m \in [1 \cdots n/k]$ Update velocity and position of each sub swarm's particle If $fitness(b(x_m S_i, i)) \geq fitness(b(p_m S_i, i))$, $b(p_m S_i, i) = b(x_m S_i, i)$ Else If $fitness(b(x_m S_i, i)) < fitness(b(p_m S_i, i))$, $b(p_m S_i, i) = b(x_m S_i, i)$ Calculate $fitness(p_i)$ of the particle (path) End For $b(p_g S_i, i) = \arg \max_{P(p_m S_i, i)} fitness(b(p_m S_i, i))$ End For

Algorithm 4: Update mechanism in the ICPSOA.

The computational complexity is an important issue in designing our optimization algorithms. In the n th iteration of the ICPSOA, the time to calculate fitness function for immune clone is N_c , the time to calculate fitness function for particle mutation and selection is N_c , and the time to calculate fitness function for particle update is tN . So the total calculating time P_n in the n th iteration should be

$$P_n \leq [N_c + N_c] + tN = (1 +)N_c + tN . \quad (3.10)$$

Therefore, the computational complexity of the ICPSOA is $O(N_c)$, which indicates that the size of clone group has a direct impact on the search speed of the ICPSOA with the same size of particle.

3.3. The ICPSOA-Based Fault-Tolerant Routing Protocol Framework for H-WSNs

The ICPSOA is the kernel of fault-tolerant routing protocol. As shown in Figure 2, once n_{fail} (node 18) fails, the macronode n_r (node 30) constructs subgraph $G'(G' \subset G)$ according to the current topology information of nodes and extracts the set of nodes N_p which can be used to construct an alternative path $p_i(s, r)$ from G' . Each node represents a particle, and the population size of particle is n . Some nodes of N_p can form a particle sequence $\{n_{p_1}, n_{p_2}, n_{p_3}, \dots, n_{p_m}\}$ ($m \leq n$) according to their order, which can construct a path $p_i(s, r)$ from source n_s to n_r . The algorithm ICPSOA would optimize the particle sequence to obtain the optimal path $p_b(s, r)$ with optimal fitness $fitness(p_b)$, and $p_b(s, r)$ includes the following nodes $\{n_s, n_{p_b1}, n_{p_b2}, \dots, n_{p_bm}, n_r\}$. Each node owns a routing table recording the paths it belongs to and the nodes' information on these paths. We now demonstrate with an example how the routing recovery process is accomplished in our protocol. In the example (Figure 2), n_{fail} 's child node n_{fail-c} and parent node n_{fail-p} are node 23 and 13.

Step 1. $n_{\text{fail-c}}$ reports the failure of n_{fail} to n_r , and $n_{\text{fail-p}}$ reports the failure to n_s (node 2), then n_s starts up another backup path to transmit data. n_s broadcasts a path request (PR) packet, with routing table including its own available energy and coordinate.

Step 2. If an intermediate node n_i receives PR, it will relay the packet according to its own state of information: if n_i is on one of the other existed $k - 1$ paths between n_s and n_r , it will ignore the packet; else, n_i will calculate $\text{dist}(e)$, $\text{ene}(e)$ and $\text{delay}(e)$ between n_i and n_{i-1} according to the information provided by n_{i-1} . Then, it continues to relay packet RP, with routing table including above information, n_i and n_{i-1} 's ID, and its $\text{ene}(n)$.

Step 3. Each intermediate node in the subtree repeats Step 2 until n_r receives the PR. Then n_r extracts the information, calculates $\text{fitness}(p_i)$ using the ICPSOA and selects the path p_b with optimal fitness. Then, it broadcasts packet RP_ACK, including the IDs of selected nodes $\{n_{p_b1}, n_{p_b2}, n_{p_b3}, \dots, n_{p_bn}\}$ on p_b (path 2-8-14-19-24-30 in Figure 2) in routing table.

Step 4. If $n_{p_b,i}$ has received PR_ACK, it checks whether its ID is in the packet's routing table. Then it establishes a connection between child $n_{p_b,i-1}$ and parent $n_{p_b,i+1}$ and delivers PR_ACK to parent until n_s receives the packet. Go to Step 5.

Step 5. n_s broadcasts packet PR_END, and $n_{p_b,i}$ on p_b delivers it to n_r . Once n_r receives PR_END, the k th path from source node to its root in the subtree is established, the network topology is reconstructed, and protocol ends.

During this process, n_r will broadcast one packet and receive three packets, n_s will broadcast two packets and receive two packets, a part of relay nodes n_i in the subtree will deliver four packets. We assume the number of hops of $p_i(s,r)$ ($i \in (1, k - 1)$) is $N_{p_i(s,r)_i}$, then the number of the packets received by n_r before running the ICPSOA is $N = N_{ST_{ii}} - \sum_{i=1}^{k-1} N_{p_i(s,r)_i}$. In this way the energy consumption of packet receiving and broadcasting of n_r can be calculated.

4. Simulation Results

4.1. Simulation Model

To evaluate the performance of the ICPSOA, we design a corresponding simulation scenario upon Matlab. The simulation experiment is constructed on Windows XP with Intel Pentium 4 processor (2.4 GHz) and 2 GB RAM. The goal of the simulation is to show that the ICPSOA can provide a more stable transport environment in an error-prone network. The results are also compared to the protocols of ICE, CPEQ, and EARQ.

In Table 2, we present the parameters configured for the conducted simulation experiments. The sensor nodes are randomly deployed on area A , and the macronodes are located at known coordinates. 500 rounds are taken and five packets are delivered in each round. The size of the network is the same for different algorithms and the fitness function is then measured. The parameters used for the ICPSOA are function dimension $D = 30$, iterated generations $P_{\text{Gen}} = 1000$, division factor $k = 5$, clone factor $= 4$, mutation factor $= 0.5$. According to the description of the ICPSOA in Section 3.1.3, we set energy consumption $\text{ene}_{\text{PU}} = 80 \text{ pJ}$, $\text{ene}_{\text{IC}} = 5 \text{ pJ}$, $\text{ene}_{\text{IM}} = 10 \text{ pJ}$, $\text{ene}_{\text{PS}} = 15 \text{ pJ}$, $\text{ene}_{\text{PR}} = 10 \text{ pJ}$ per iteration. The metrics that we use in our experiments are average number of alive nodes per round, average energy depletion ratio per round (measured as the energy dissipation versus

Table 2: Simulation parameters.

Simulation parameter	Value
Network area A	10000 m \times 10000 m
Number of sensor node n_{node}	50–500
Number of macronode n_{macro}	10
Available energy on sensors E_{node}	120 J
Sensing radius of sensor node $R_{\text{node-s}}$	300 m
Communication radius of sensor node $R_{\text{node-c}}$	600 m
Communication radius of macronode $R_{\text{macro-c}}$	3500 m
Bandwidth of sensor node B_{node}	250 kb/s
Number of disjoint multipath k	3
Number of simulation rounds	500
Number of packet in each round	1
Size of packet in each round m	400 bits
Probability of node failure P_{node}	0.02
Energy consumption of sending circuit a_{11}	40 nJ/bit
Energy consumption of receiving circuit a_{12}	80 nJ/bit
Energy consumption of sending amplifier a_2	200 pJ/bit/m ²
Channel attenuation index n	2
Energy consumption of data fusion e_{neDF}	4 nJ/bit
Energy consumption of updating routing table e_{neRT}	2 nJ/bit

the initial energy), average delay of packet delivery, and packet delivery ratio (measured as the number of successfully delivered packet versus required packet).

4.2. Evaluation of the Simulation Results

To illustrate the effect of the proposed protocol, we take a snapshot during a simulation. Figure 4 shows a small area (2000 m \times 2000 m), which illustrates a subtree with the existed three paths between source node (node 29) and macronode (node 18). We can see when an intermediate node (node 24) fails, source node immediately establishes an alternative path to connect the macronode in order to replace the previous 3rd path.

The simulation ends after 1000 rounds. We compare the number of alive nodes per round for these four protocols. As shown in Figure 5 for different network sizes, the number of nodes died in the ICPSOA, ICE, and CPEQ is less than EARQ over the same number of rounds. This is because comparing with heterogenous WSNs, all the nodes only need to transmit data to its root (macronode) of the subtree in the H-WSNs, which indirectly shortens the transmission distance between sensor nodes to the sink, and prolongs their lifetime. The fast routing recovery mechanism of the ICPSOA also makes its number of alive nodes 5% ~ 10% more than that of ICE, and CPEQ in the same rounds. Then, we would only compare the ICPSOA, ICE, and CPEQ with the same network style (H-WSNs) in the remaining simulation process.

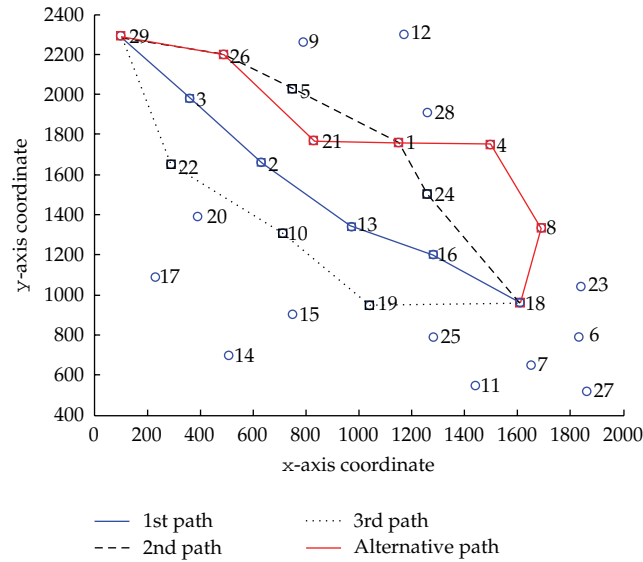


Figure 4: Snapshot of establishing the alternative path using ICPSOA.

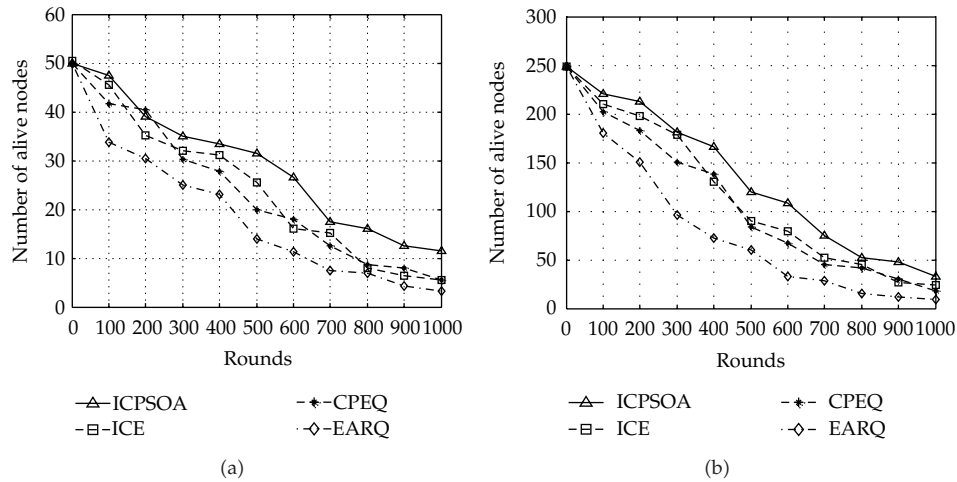


Figure 5: Experimental results for number of alive nodes per round with variant scale of network. (a) Size of 50 nodes. (b) Size of 250 nodes.

As shown in Figure 6 for different network sizes, energy depletion ratio of the ICPSOA based protocol is 5% ~ 15% smaller than that of ICE and CPEQ. And the dispersion between them is more obvious as the size of the cluster increases. That is because firstly, each source node has k paths to the macronode, and the total energy consumed is minimized; secondly, the ICPSOA can select the nodes with better QoS parameters (such as more available energy and less distance of path) to establish alternative path and construct a more reliable transmission environment to reduce the retransmission caused by unstable paths, therefore, prolong the network lifetime as compared to ICE and CPEQ.

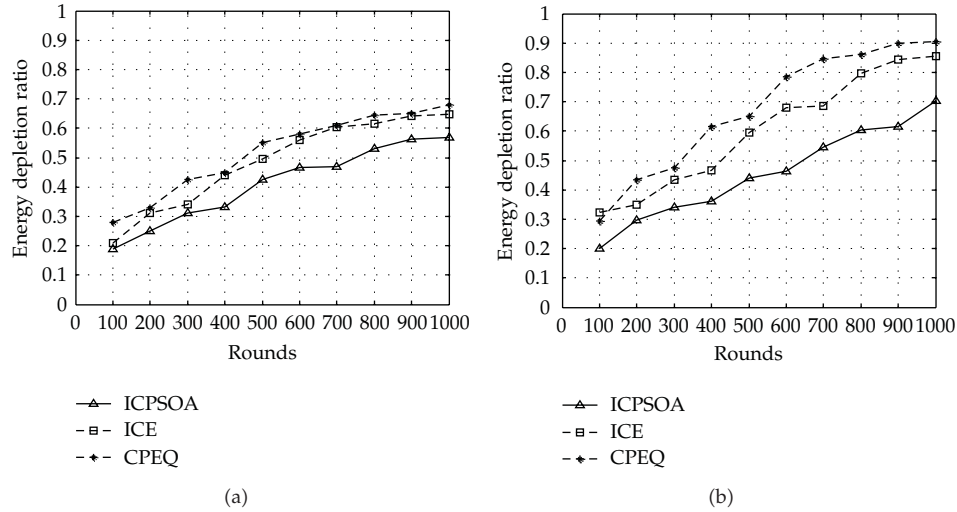


Figure 6: Experimental results for energy depletion ratio per round with variant scale of networks. (a) Size of 50 nodes. (b) Size of 250 nodes.

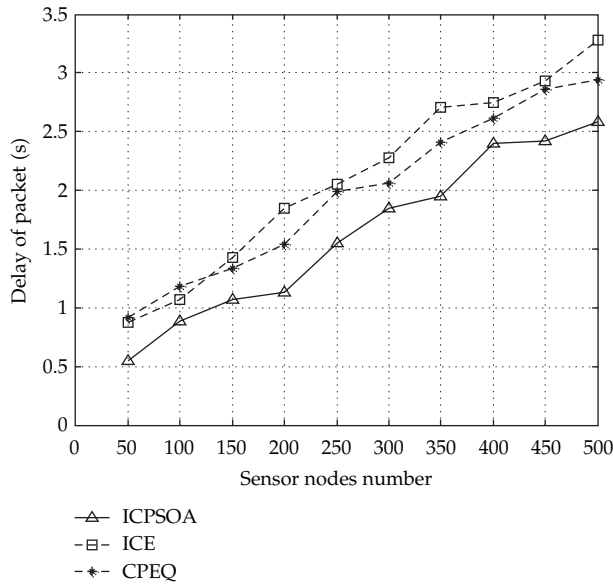


Figure 7: Experimental results for average delay of packet delivery.

Figure 7 shows the average delay of packet delivery (average delay of each packet delivered from source node to the sink). We can observe that the ICPSOA outperforms ICE and CPEQ in terms of average delay for the same networks. The ICPSOA has demonstrated a lower delay when network size grows. A low delay of packets can be explained by the multipath property and shortest alternative path selection of the proposed ICPSOA-based protocol for fault tolerance.

Figure 8(a) shows that the H-WSNs with the ICPSOA can deliver more packets to the sink than the network with EARQ and ICE with the value of 0.02 of p_{node} . In most cases,

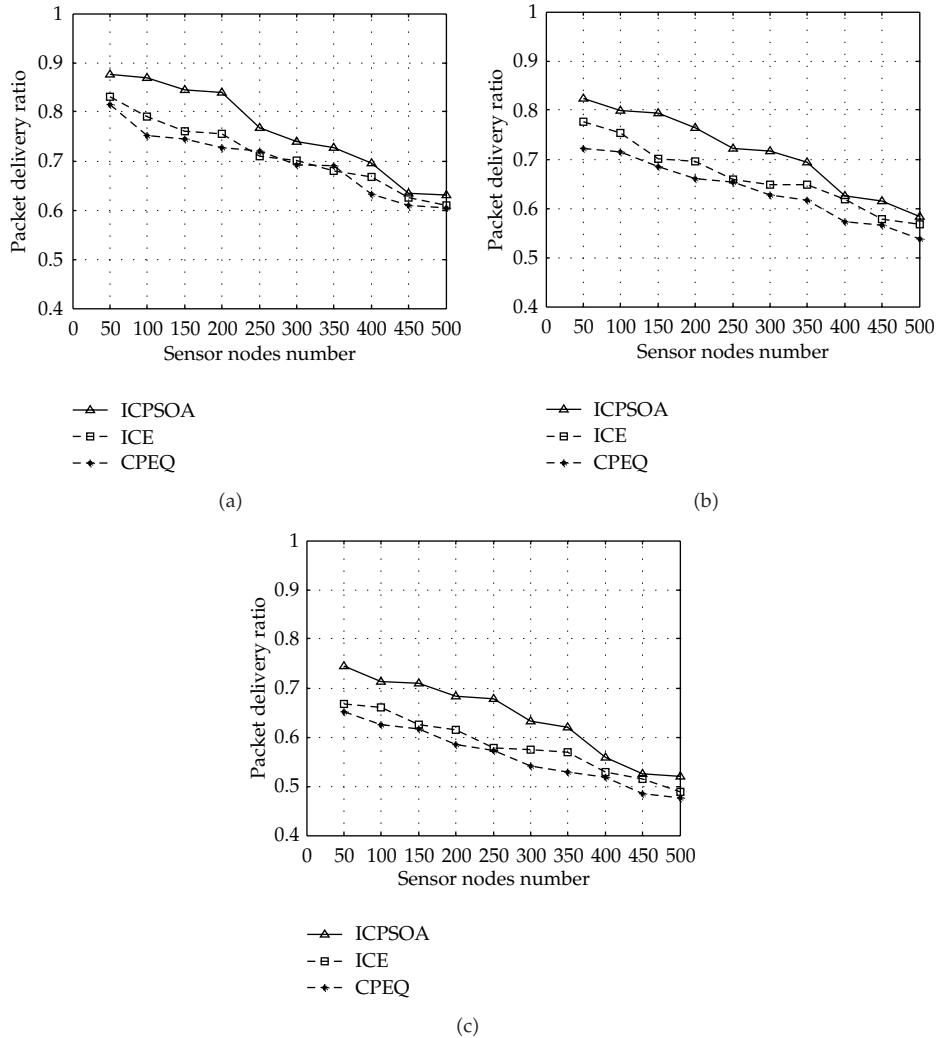


Figure 8: Experimental results for average successful packet delivery ratio with variant failure probability. (a) $P_{node} = 0.02$. (b) $P_{node} = 0.04$. (c) $P_{node} = 0.08$.

the ICPSOA can send 5% ~ 15% more packets to the sink. A bigger value of packet delivery ratio indicates a lower packet dropout probability [24, 25] and a better network capability of delivering useful information. This result can be explained by the fact that the ICPSOA provides a fast recovery from path failure with an optimal alternative path, which improves the success rate of data transmission. Note that the packets in the ICPSOA experience a higher delivery ratio as the size of the network grows, which indicates the ICPSOA-based protocol of the H-WSNs is more feasible for practical deployment of large-scale WSNs than ICE and CPEQ.

We should also compare the performance trend of the three algorithms with different probability of node failure P_{node} . We plot the packet delivery ratio against the number of nodes in Figure 8 for various P_{node} (value of 0.02, 0.05, and 0.08). As shown in Figure 8(a), 8(b), and 8(c), the observed packet delivery ratio of the proposed schemes degrades as P_{node}

ascends, which means the performance of proposed scheme is reduced as the percentage of failed nodes increases. But the ICPSOA can still deliver more packets than ICE and CPEQ for different size of the sensor network.

5. Conclusions

We propose the ICPSOA-based fault-tolerant routing protocol for H-WSNs, which focuses on a solution to the problem of energy depletion and packet delivery of nodes, by trying to reconstruct the topology structure and recover the routing for the path failure and achieve energy conservation by avoiding unnecessary retransmission. The conserved energy can be used to increase the quantity of information received by the sink. The experiment presents the promising ability of the ICPSOA, and better solutions of fault tolerance and prolonging the network lifetime can be obtained by the ICPSOA-based protocol than the protocols of EARQ, ICE and CPEQ. The results have illustrated the advantage of H-WSNs and backup disjoint multipath, which can reduce the risk of data delivery loss and energy consumption on the path exploring. It also aims at shortening delay of packet delivery, evening energy dissipation among the nodes by constructing the optimal alternative paths in the H-WSNs with the swarm intelligence algorithm. The strength of the ICPSOA is its simplicity, robustness and effectiveness for fast routing recovery compared to other approaches and makes the ICPSOA a potential solution to meet the requirements of critical conditions monitoring applications.

As for future studies, the following directions are under the way: firstly, the proposed protocol ignores the fault-tolerant routing between macronode-macronode communications, which could be considered to form a more complete protocol architecture; secondly, we should further reduce the computational complexity of the proposed ICPSOA such that it converges faster to a better solution, providing robustness against failure in the network.

Acknowledgments

This work was supported in part by the Key Project of the National Nature Science Foundation of China (no. 61134009), the National Nature Science Foundation of China (no. 60975059), Specialized Research Fund for the Doctoral Program of Higher Education from Ministry of Education of China (no. 20090075110002), Specialized Research Fund for Shanghai Leading Talents, Project of the Shanghai Committee of Science and Technology (nos. 11XD1400100, 11JC1400200, 10JC1400200, 10DZ0506500).

References

- [1] D. Wang, J. Zheng, Y. Zhou, and J. Li, "A scalable support vector machine for distributed classification in ad hoc sensor networks," *Neurocomputing*, vol. 74, no. 1–3, pp. 394–400, 2010.
- [2] J. Liang, Z. Wang, and X. Liu, "Distributed state estimation for discrete-time sensor networks with randomly varying nonlinearities and missing measurements," *IEEE Transactions on Neural Networks*, vol. 22, no. 3, pp. 486–496, 2011.
- [3] B. Shen, Z. Wang, and X. Liu, "A stochastic sampled-data approach to distributed H-infinity filtering in sensor networks," *IEEE Transactions on Circuits and Systems I: Regular Papers*, vol. 58, no. 9, pp. 2237–2246, 2011.
- [4] B. Shen, Z. Wang, and Y. S. Hung, "Distributed consensus H-infinity filtering in sensor networks with multiple missing measurements: the finite-horizon case," *Automatica*, vol. 46, no. 10, pp. 1682–1688, 2010.

- [5] B. Shen, Z. Wang, Y. S. Hung, and G. Chesi, "Distributed H-infinity filtering for polynomial nonlinear stochastic systems in sensor networks," *IEEE Transactions on Industrial Electronics*, vol. 58, no. 5, pp. 1971–1979, 2011.
- [6] C. Laukik, D. Alin, and S. Ranka, "Fault tolerant aggregation in heterogeneous sensor networks," *Journal of Parallel and Distributed Computing*, vol. 69, no. 2, pp. 210–219, 2009.
- [7] K. Akkaya and M. Younis, "A survey on routing protocols for wireless sensor networks," *Ad Hoc Networks*, vol. 3, no. 3, pp. 325–349, 2005.
- [8] A. Boukerche, A. Martirosyan, and R. Pazzi, "An inter-cluster communication based energy aware and fault tolerant protocol for wireless sensor networks," *Mobile Networks and Applications*, vol. 13, no. 6, pp. 614–626, 2008.
- [9] J. Heo and J. Hong, "EARQ: energy aware routing for real-time and reliable communication in wireless industrial sensor networks," *IEEE Transactions on Industrial Informatics*, vol. 5, no. 1, pp. 3–11, 2009.
- [10] N. Nasser and Y. F. Chen, "SEEM: secure and energy-efficient multipath routing protocol for wireless sensor networks," *Computer Communications*, vol. 30, no. 11-12, pp. 2401–2412, 2007.
- [11] C. Pandana and K. J. R. Liu, "Robust connectivity-aware energy-efficient routing for wireless sensor networks," *IEEE Transaction on Wireless Communications*, vol. 10, no. 7, pp. 3904–3916, 2008.
- [12] X. Han and X. Cao, "Fault-tolerant relay node placement in heterogeneous wireless sensor networks," *IEEE Transactions on Mobile Computing*, vol. 9, no. 5, pp. 643–656, 2010.
- [13] C. H. Lin, J. L. Chen, and Z. L. Gaing, "Combining biometric fractal pattern and particle swarm optimization-based classifier for fingerprint recognition," *Mathematical Problems in Engineering*, vol. 2010, Article ID 328676, pp. 1–30, 2010.
- [14] T. Wimalajeewa and S. K. Jayaweera, "Optimal power scheduling for correlated data fusion in wireless sensor networks via constrained PSO," *IEEE Transactions on Wireless Communications*, vol. 7, no. 9, pp. 3608–3618, 2008.
- [15] T. S. Zhan and C. C. Kao, "Modified PSO method for robust control of 3RPS parallel manipulators," *Mathematical Problems in Engineering*, vol. 2010, Article ID 302430, 25 pages, 2010.
- [16] C. J. Lin, C. H. Chen, and C. T. Lin, "A hybrid of cooperative particle swarm optimization and cultural algorithm for neural fuzzy networks and its prediction applications," *IEEE Transactions on Systems, Man and Cybernetics C*, vol. 39, no. 1, pp. 55–68, 2009.
- [17] A. Boukerche, R. W. N. Pazzi, and R. B. Araujo, "Fault-tolerant wireless sensor network routing protocols for the supervision of context-aware physical environments," *Journal of Parallel and Distributed Computing*, vol. 66, no. 4, pp. 586–599, 2006.
- [18] M. Cardei and S. H. Yang, "Algorithms for fault-tolerant topology in heterogeneous wireless sensor networks," *IEEE Transactions on Parallel and Distributed Systems*, vol. 19, no. 4, pp. 545–558, 2008.
- [19] Y. S. Ding, Z. H. Hu, and W. B. Zhang, "Multi-criteria decision making approach based on immune co-evolutionary algorithm with application to garment matching problem," *Expert Systems with Applications*, vol. 38, no. 8, pp. 10377–10383, 2011.
- [20] Y. S. Ding, X. J. Lu, K. R. Hao, L. F. Li, and Y. F. Hu, "Target coverage optimization of wireless sensor networks using multi-objective immune co-evolutionary algorithms," *International Journal of Systems Science*, vol. 42, no. 9, pp. 1531–1541, 2011.
- [21] Z. Hu and Y. S. Ding, "Immune co-evolutionary algorithm based partition balancing optimization for tobacco distribution system," *Expert Systems with Applications*, vol. 36, no. 3, pp. 5248–5255, 2009.
- [22] L. Chitnis and A. Dobra, "Aggregation methods for large-scale sensor networks," *ACM Transactions on Sensor Networks*, vol. 4, no. 2, pp. 1–36, 2008.
- [23] S. Q. Ren and J. Park, "Fault-tolerance data aggregation for clustering wireless sensor network," *Wireless Personal Communications*, vol. 51, no. 1, pp. 179–192, 2009.
- [24] H. Dong, Z. Wang, D. W. C. Ho, and H. Gao, "Robust H-infinity fuzzy output-feedback control with multiple probabilistic delays and multiple missing measurements," *IEEE Transactions on Fuzzy Systems*, vol. 18, no. 4, pp. 712–725, 2010.
- [25] B. Shen, Z. Wang, H. Shu, and G. Wei, "Robust H-infinity finite-horizon filtering with randomly occurred nonlinearities and quantization effects," *Automatica*, vol. 46, no. 11, pp. 1743–1751, 2010.

Research Article

Mixed H_2/H_∞ Performance Analysis and State-Feedback Control Design for Networked Systems with Fading Communication Channels

Adrian-Mihail Stoica

Faculty of Aerospace Engineering, University Politehnica of Bucharest, 01106 Bucharest, Romania

Correspondence should be addressed to Adrian-Mihail Stoica, adrian.stoica@upb.ro

Received 1 July 2011; Accepted 2 September 2011

Academic Editor: Zidong Wang

Copyright © 2012 Adrian-Mihail Stoica. This is an open access article distributed under the Creative Commons Attribution License, which permits unrestricted use, distribution, and reproduction in any medium, provided the original work is properly cited.

The purpose of the present paper is to provide a performance analysis approach of networked systems with fading communication channels. For a Ricean model of the fading communication channel, it is shown that the resulting system has a hybrid structure including the continuous-time dynamics of the networked systems and a discrete-time dynamics of the communication channels. Moreover, this resulting hybrid system has both multiplicative and additive noise terms. The performance analysis naturally leads to an H_2/H_∞ -type norm evaluation for systems with finite jumps and multiplicative noise. It is proved that this norm depends on the stabilizing solution of a specific system of coupled Riccati's equations with jumps. A state-feedback design problem to accomplish a mixed H_2/H_∞ performance is also considered. A numerical iterative procedure allowing to compute the stabilizing solution of the Riccati-type system with jumps is presented. The theoretical results are illustrated by numerical results concerning the tracking performances of a flight formation with fading communication channel. The paper ends with some concluding remarks.

1. Introduction

The analysis and synthesis of networked control systems have received a major attention over the last decade due to their wide area of applications (see, e.g., [1–3] and their references). These applications include aerial and terrestrial surveillance [3], formation atmospheric flight [4], terrain mapping, and satellites formations for space science missions [5]. In all these applications, the formation members are autonomous vehicles from which the human pilots have been removed in order to avoid their participation at dangerous and repetitive tasks. The specific feature of such networked systems is that the control loop is closed through a communication channel shared by all autonomous vehicles. This communication

network is required since the control law of each formation member usually depends on the measurements from all other vehicles. Even in the distributed control architectures when each vehicle uses only the information about its neighboring vehicles, a communication network is very useful. Indeed, in [6] it is proved that in a *predecessor following* approach, the relative positioning error between vehicles is amplified if the members of the formation have no information about the leader position. This conclusion motivates the use of a *predecessor and leader following* method in which both information about the predecessor and about the leader position are available for each formation member. In [6] it is also proved that in this case the relative spacing errors can be attenuated. These interesting results emphasize the importance of the communication in networked control systems. Most of the communication systems are based on wireless networks which, in contrast with the wired systems, are much more sensitive to information transmission errors.

The main goal of this paper is to analyze the interaction between the control and the communication system with fading. To this end, a model of the fading communication channel is required. There are many such models developed in the recent literature (see, e.g., [7, 8]). Deterministic models of communication networks with time-varying delays are considered in [9–11], in which the maximum admissible delays are determined using the Lyapunov stability theory. In other deterministic models of fading communication channels, the transmission errors are represented as uncertain parameters, and, the control system is designed via specific robust synthesis procedures including linear quadratic Gaussian (LQG) and μ -synthesis. Another class of representations of fading communication channels is based on stochastic models either with Markovian jumps or with white noise [7, 12]. Many useful results concerning the stability, control, and disturbance attenuation of such systems are available in the control literature (see, e.g., [13–15] and their references). In [8], an H_∞ -type design is used to determine a controller for a system with fading communication channel represented as a Markovian system. A Markovian representation of the network status is also used to solve robust fault detection problems by H_∞ techniques for communication systems which may be found in [16]. An extended version for the case of random measurement delays and stochastic data-missing phenomenon is treated in [17]. In the present paper, a discrete-time Ricean model of the communication channel is considered. The stochastic Rice models are often used for models of wireless links [7]. They include both additive and multiplicative white noise terms. The problem analyzed in this paper is the influence of the fading communication channel over the tracking performance of a flight formation. The control system of the flight formation is the one derived in [4]. Since the exogenous inputs in the networked system are both deterministic (the reference signals for the formation control) and stochastic (the white noise terms in the fading communication channel model), a mixed H_2/H_∞ -type approach is appropriate for this analysis. Moreover, the networked system has a hybrid structure due to its continuous-time component represented by the vehicles dynamics and a discrete-time one corresponding to the communication channel. The above mentioned considerations lead to a mixed H_2/H_∞ analysis problem for stochastic systems with finite jumps. The systems with finite jumps are used to represent dynamic systems with continuous-time and discrete-time components. Useful results and developments concerning these systems may be found, for instance, in [18, 19]. The paper provides an analysis and an optimization approach of the mixed H_2/H_∞ performance for a hybrid model of networked systems with fading communication channels. This model is derived in Section 2 of the paper. In Section 3, the expression of the H_2/H_∞ performance is determined in terms of the stabilizing solution of a specific system of coupled Riccati equations with finite jumps. A state-feed-

back design procedure to optimize the mixed performance is presented in Section 4. Numerical aspects concerning the computation of the stabilizing solution are given in Section 5. The theoretical results are illustrated by a numerical example concerning the tracking performance of an aircraft formation. The paper ends with some final remarks and future work.

2. A Model of Networked Systems over Fading Communication Channel

In this section a control problem of a formation of unmanned air vehicles (UAVs) will be briefly presented. Such problems have been intensively analyzed over the last fifteen years (see, e.g., [3]) both for their wide area of applications and for the challenges addressed to the control engineer. In [4], a dynamic inversion-type approach is used to linearize the nonlinear dynamic and kinematic equations of the UAV motion. A simplified linearized model of a flight formation member has the form:

$$\begin{aligned} \dot{\bar{x}} &= Y \bar{x}, \\ \dot{\bar{x}} &= -K_d \bar{x} - K_x \bar{x}, \end{aligned} \quad (2.1)$$

where $\bar{x} \in \mathbb{R}^3$ denotes the deviation of the aircraft with respect to its desired position and $\bar{x} \in \mathbb{R}^3$ stands for the deviation of its state $x = [V \quad \theta \quad \psi]^T$ (V representing the airspeed, the heading angle, and ψ the flight path angle) with respect to some specified value \bar{x} . The input vector \bar{x} includes the desired derivatives of \bar{x} and plays the role of a reference signal in the model (2.1). The constant matrix Y has the diagonal form $Y = \text{diag}(1, V_0, V_0)$, and the state-feedback control gains K_d and K_x are diagonal, too. In the present paper, the case when the reference signal \bar{x} is transmitted from the ground station or from the formation leader using a fading communication channel is considered. The aim is to analyze how the tracking performances of the flight formation are altered due to the communication system. To this end, a model of the fading communication channel is required. In this paper, the L th-order Rice model was adopted. This model is frequently used in wireless mobile links, and it is given by the discrete-time equation:

$$r(i) = \sum_{k=0}^L a_k(i) v(i-k) + n(i), \quad (2.2)$$

where i denotes the moment of time, $v(\cdot)$ denotes the transmitted information, $r(\cdot)$ is the received information, n is a Gaussian white noise with zero mean and unit variance, and $a_k(i)$, $k = 0, \dots, L$ are independent random variables with known mean \bar{a}_k and variance $\frac{2}{k}$. In the case of the application considered in this paper, $v(\cdot)$ is just the transmitted reference signal \bar{x} . A state-space representation of (2.2) is

$$\begin{aligned} p(i+1) &= M p(i) + N v(i), \\ r(i) &= \sum_{k=1}^L a_k(i) P_k p(i) + a_0(i) v(i) + n(i), \quad i = 0, 1, \dots, \end{aligned} \quad (2.3)$$

where, by definition,

$$M = \begin{bmatrix} 0 & 0 & \cdots & 0 \\ I & 0 & \cdots & 0 \\ \vdots & \ddots & & \\ 0 & \cdots & I & 0 \end{bmatrix}, \quad N = \begin{bmatrix} I \\ 0 \\ \vdots \\ 0 \end{bmatrix}, \quad P_k = [0 \cdots 0 \ I \ 0 \cdots 0], \quad (2.4)$$

and $p(i) \in \mathbb{R}^{L \cdot n_v \times 1}$ stands for the state vector of the communication channel, n_v denoting the dimension of the transmitted information vector $v(\cdot)$. In (2.4), the identity and the zero matrices have the size $n_v \times n_v$, and the identity matrix in P_k is on the k th position. The configuration of the communication system (2.3) coupled with the system (2.1) is illustrated in Figure 1. The resulting system from Figure 1 is in fact a hybrid system since the dynamics of (2.1) is a continuous-time one, and (2.3) is a discrete-time system. A state-space realization of such hybrid system can be given using systems with finite jumps of the general form:

$$\begin{aligned} \dot{x}(t) &= A x(t) + B w(t), \quad t \neq ih, \\ x(ih^+) &= A_d x(ih) + B_d w_d(i), \quad i = 0, 1, \dots, \end{aligned} \quad (2.5)$$

in which $h > 0$ denotes the sampling period, the state $x(t)$ is left continuous and right discontinuous at the sampling moments $t = ih$, $i = 0, 1, \dots$, and $w(t)$, $t \neq ih$, and $w_d(i)$, $i = 0, 1, \dots$, are the continuous-time and the discrete-time inputs, respectively, of the system (see, e.g., [19, 20]). Since the received information r is constant between the sampling moments, it can be represented as

$$\begin{aligned} \dot{r}(t) &= 0, \quad t \neq ih, \\ r(ih^+) &= \sum_{k=1}^L a_k(i) P_k p(ih) + a_0(i) v(i) + n(i), \quad i = 0, 1, \dots, \end{aligned} \quad (2.6)$$

where the state p of the communication system is given by

$$\begin{aligned} \dot{p}(t) &= 0, \quad t \neq ih, \\ p(ih^+) &= M p(ih) + N v(i), \quad i = 0, 1, \dots \end{aligned} \quad (2.7)$$

A similar model can be adopted for the continuous-time control system (2.1) which can be represented as

$$\dot{q}(t) = \bar{A} q(t) + \bar{B} r(t), \quad t \geq 0, \quad (2.8)$$

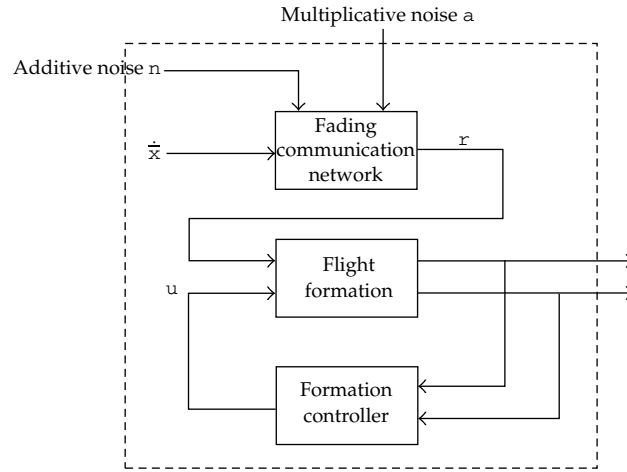


Figure 1: Control configuration of networked systems with fading communication channel.

where

$$\begin{aligned}
 q(t) &:= \begin{bmatrix} r^T(t) & p^T(t) \end{bmatrix}^T, \\
 \bar{A} &:= \begin{bmatrix} 0 & Y \\ -K_d & -K_x \end{bmatrix}, \quad \bar{B} := \begin{bmatrix} 0 \\ -I \end{bmatrix}.
 \end{aligned} \tag{2.9}$$

In (2.8) the state $q(t)$ is continuous-time, and therefore,

$$q(ih^+) = q(ih), \tag{2.10}$$

and $r(t)$ is the received perturbed reference signal described by (2.6). From (2.6)–(2.10), it follows that the hybrid networked system with fading communication channels can be represented using a model with finite jumps of the form (2.5) where $x = [q^T \ r^T \ p^T]^T$. Moreover, since in (2.6) the coefficients $a_k(i)$, $k = 0, \dots, L$ and $i = 0, 1, \dots$, are random variables, one may consider the following stochastic version of (2.5) which includes both multiplicative noise components and additive white noise terms:

$$\begin{aligned}
 dx(t) &= (A_0 x(t) + B_0 w(t))dt + (A_1 x(t) + B_1 w(t))d\beta(t) + G d\alpha(t), \quad t \neq ih, \\
 x(ih^+) &= A_{0d} x(ih) + B_{0d} w_d(i) + (A_{1d} x(ih) + B_{1d} w_d(i)) \alpha_d(i) + G_d \alpha_d(i), \quad i = 0, 1, \dots, \\
 y(t) &= Cx(t), \quad t \neq ih, \\
 Y_d(i) &= C_d x(ih), \quad i = 0, 1, \dots,
 \end{aligned} \tag{2.11}$$

where the random variables $\beta(t) \in \mathbb{R}$, $t \geq 0$, and $\alpha(t) \in \mathbb{R}^r$, $t \geq 0$, are such that the pair $(\beta(t), \alpha(t))$ is an $r + 1$ -dimensional standard Wiener process, and $\alpha_d(i) \in \mathbb{R}$ and

$w_d(i) \in \mathbb{R}^{n_d}$, $i = 0, 1, \dots$ are sequences of independent random variables on a probability space $(\Omega, \mathcal{P}, \mathcal{F})$. It is assumed that $w(t)$, $w_d(i)$, $t \geq 0$, $w_d(i)$, $i = 0, 1, \dots$, are independent stochastic processes with zero mean and unitary second moments. The outputs $y(t)$ and $y_d(i)$ denote the continuous-time and the discrete-time outputs, respectively. By virtue of standard results from the theory of stochastic differential equations (see, e.g., [21]), the system (2.11) has a unique \mathcal{F}_t -adapted solution for any initial condition $x(0)$, \mathcal{F}_t denoting the σ -algebra generated by the random vectors $w(s)$, $w_d(i)$, and $w_d(i)$, $0 \leq s \leq t$, $0 \leq i \leq \lfloor t \rfloor$. This solution is almost surely left continuous.

A mixed H_2/H_∞ problem for this class of stochastic systems with jumps will be treated in the next section.

3. Mixed H_2/H_∞ -Type Norm for Systems with Jumps Corrupted with Multiplicative Noise

Before defining and computing the mixed H_2/H_∞ norm for systems of the form (2.11), some useful definitions and preliminary results will be briefly presented.

3.1. Notations, Definitions, and Some Useful Results

Consider the stochastic system with jumps (2.11) in which w and w_d denote continuous-time and discrete-time energy bounded inputs, respectively. It means that $w \in L^2[0, \infty)$, where $L^2[0, \infty)$ denotes the space of the functions $f(t)$, $t \geq 0$ for which $\|f\|_{L^2}^2 := \int_0^\infty |f(t)|^2 dt < \infty$, and $w_d \in \ell^2$ where ℓ^2 is the space of the discrete-time vectors $g(i)$, $i = 0, 1, \dots$ with the property $\|g\|_{\ell^2}^2 := \sum_{i=0}^\infty |g(i)|^2 < \infty$, where $|\cdot|$ stands for the Euclidian norm.

Definition 3.1. The stochastic system with jumps and with multiplicative noise

$$\begin{aligned} dx(t) &= A_0 x(t) dt + A_1 x(t) d w(t), \quad t \neq i h, \\ x(i h^+) &= A_{0d} x(i h) + A_{1d} x(i h) w_d(i), \quad i = 0, 1, \dots \end{aligned} \quad (3.1)$$

is *exponentially stable in mean square* (ESMS) if there exist $\alpha > 0$ and $\beta \geq 1$ such that $E[|x(t)|^2] \leq e^{-\alpha t} E[|x(0)|^2]$ for any initial condition $x(0)$ and for all $t \geq 0$, $E[\cdot]$ denoting the mean of the random variable and $x(t)$ representing the solution of (3.1) with the initial condition $x(0)$.

The following result gives necessary and sufficient conditions in which the system with finite jumps (3.1) is ESMS, and its proof may be found in [13].

Proposition 3.2. *The system (3.1) is ESMS if and only if the system of coupled Lyapunov equations*

$$\begin{aligned} -\dot{X}(t) &= A_0^T X(t) + X(t) A_0 + A_1^T X(t) A_1, \quad t \neq i h, \\ X(i h^-) &= A_{0d}^T X(i h) A_{0d} + A_{1d}^T X(i h) A_{1d}, \quad i = 0, 1, \dots \end{aligned} \quad (3.2)$$

has a unique symmetric solution $X(t) \geq 0$, $t \geq 0$, right continuous and h -periodic.

Another useful result is the differentiation rule of functions of solutions to stochastic differential equations, well known in the literature as Itô's formula [21].

Proposition 3.3. Let $v(t, x)$ be a continuous function with respect to $(t, x) \in [0, T] \times \mathbb{R}^n$. If $x(t)$ is a solution of the stochastic differential equation

$$dx(t) = a(t)dt + b(t)dW(t), \quad (3.3)$$

then

$$\begin{aligned} dv(t, x(t)) = & \left[\frac{\partial v}{\partial t}(t, x(t)) + \left(\frac{\partial v}{\partial x}(t, x(t)) \right)^T a(t) + \frac{1}{2} \text{Tr} \left(b^T(t) \frac{\partial^2 v}{\partial x^2}(t, x(t)) b(t) \right) \right] dt \\ & + \left(\frac{\partial v}{\partial x}(t, x(t)) \right)^T b(t) dW(t), \end{aligned} \quad (3.4)$$

where $\text{Tr}(\cdot)$ denotes the trace of the matrix (\cdot) .

The next result will be used in the following sections, and its proof may be found in [13, page 162].

Proposition 3.4. Consider the stochastic system with multiplicative noise

$$dx(t) = (A_0 x(t) + B_0 u(t))dt + (A_1 x(t) + B_1 u(t))dW(t) \quad (3.5)$$

and the cost function

$$J(t_0, x_0, u) = E \left[\int_{t_0}^T \begin{bmatrix} x^T(t) & u^T(t) \end{bmatrix} \begin{bmatrix} M & L \\ L^T & R \end{bmatrix} \begin{bmatrix} x(t) \\ u(t) \end{bmatrix} dt \right], \quad (3.6)$$

then

$$\begin{aligned} J(t_0, x_0, u) = & x_0^T X(t_0) x_0 - E \left[x^T(T) X(T) x(T) \right] \\ & + E \left[\int_{t_0}^T \left(u(t) - \tilde{F}(t) x(t) \right)^T \left(R + B_1^T X(t) B_1 \right) \left(u(t) - \tilde{F}(t) x(t) \right) dt \right], \end{aligned} \quad (3.7)$$

where $X(t)$ verifies the equation

$$\begin{aligned} -\dot{X}(t) = & A_0^T X(t) + X(t) A_0 + A_1^T X(t) A_1 - \left(X(t) B_0 + A_1^T X(t) B_1 \right) \\ & \times \left(R + B_1^T X(t) B_1 \right)^{-1} \left(B_0^T X(t) + B_1^T X(t) A_1 \right) + M \end{aligned} \quad (3.8)$$

and where $\tilde{F}(t) = -(R + B_1^T X(t) B_1)^{-1} (B_0^T X(t) + B_1^T X(t) A_1 + L^T)$.

3.2. The Mixed H_2/H_∞ Norm of the System (2.11)

Assume that the system (2.11) which will be denoted below by \mathcal{G} is ESMS and that $x(0) = 0$. As in the deterministic case, H_2 and H_∞ norms can be defined as follows.

(i) For $w(t) \equiv 0$ and $w_d(i) \equiv 0$, the *impulse-to-energy gain* induced from (u, u_d) to (y, y_d) stands for the H_2 -type norm of the system (2.11). The H_2 -type norm of (2.11) denoted by $\|\mathcal{G}\|_2$ can be determined as

$$\|\mathcal{G}\|_2^2 = \text{Tr} \left(G_d^T Q(\bar{h}) G_d \right) + \frac{1}{h} \int_0^h \text{Tr} \left(G^T Q(t) G \right) dt, \quad (3.9)$$

where $Q(t)$, $t \geq 0$ is the solution of the Lyapunov-type system

$$\begin{aligned} -\dot{Q}(t) &= A_0^T Q(t) + Q(t) A_0 + A_1^T Q(t) A_1 + C^T C, \quad t \neq \bar{h}, \\ Q(\bar{h}^-) &= A_{0d}^T Q(\bar{h}) A_{0d} + A_{1d}^T Q(\bar{h}) A_{1d} + C_d^T C_d, \quad i = 0, 1, \dots, \end{aligned} \quad (3.10)$$

(see also [18]).

(ii) For $w(t) \equiv 0$ and $w_d(i) \equiv 0$, the *energy-to-energy gain* induced from (w, w_d) to (y, y_d) stands for the H_∞ -type norm of the system (2.11), denoted by $\|\mathcal{G}\|_\infty$. It represents the smallest $\gamma > 0$ for which the following system of coupled Riccati equations

$$\begin{aligned} -\dot{X}(t) &= A_0^T X(t) + X(t) A_0 + A_1^T X(t) A_1 + C^T C + \left(X(t) B_0 + A_1^T X(t) B_1 \right) \\ &\quad \times \left({}^2I - B_1^T X(t) B_1 \right)^{-1} \left(B_0^T X(t) + B_1^T X(t) A_1 \right), \quad t \neq \bar{h}, \\ X(\bar{h}^-) &= A_{0d}^T X(\bar{h}) A_{0d} + A_{1d}^T X(\bar{h}) A_{1d} + C_d^T C_d + \left(A_{0d}^T X(\bar{h}) B_{0d} + A_{1d}^T X(\bar{h}) B_{1d} \right) \\ &\quad \times \left({}^2I - B_{1d}^T X(\bar{h}) B_{1d} \right)^{-1} \left(B_{0d}^T X(\bar{h}) A_{0d} + B_{1d}^T X(\bar{h}) A_{1d} \right), \quad i = 0, 1, \dots \end{aligned} \quad (3.11)$$

has a *stabilizing solution* $X(t) \geq 0$, $t \geq 0$. Recall that a symmetric right continuous, h -periodic function $X(t)$ verifying (3.11) is called a stabilizing solution of (3.11) if

$$\begin{aligned} {}^2I - B_1^T X(t) B_1 &> 0, \quad t \neq \bar{h}, \\ {}^2I - B_{1d}^T X(\bar{h}) B_{1d} &> 0, \quad i = 0, 1, \dots, \end{aligned} \quad (3.12)$$

and the system with jumps

$$\begin{aligned} dx(t) &= (A_0 + B_0 F(t))x(t)dt + (A_1 + B_1 F(t))x(t)d(t), \quad t \neq \bar{h}, \\ x(\bar{h}^+) &= (A_{0d} x(\bar{h}) + B_{0d} F(\bar{h}))x(\bar{h}) + (A_{1d} + B_{1d} F(\bar{h}))x(\bar{h})_d(i), \quad i = 0, 1, \dots \end{aligned} \quad (3.13)$$

is ESMS, where, by definition,

$$\begin{aligned} F(\vartheta) &= \left({}^2I - B_1^T X(\vartheta) B_1 \right)^{-1} \left(B_0^T X(\vartheta) + B_1^T X(\vartheta) A_1 \right), \quad \vartheta \neq \text{ih}, \\ F(\text{ih}) &= \left({}^2I - B_{1d}^T X(\text{ih}) B_{1d} \right)^{-1} \left(B_{0d}^T X(\text{ih}) A_{0d} + B_{1d}^T X(\text{ih}) A_{1d} \right), \quad \text{ih} = 0, 1, \dots \end{aligned} \quad (3.14)$$

Similarly with the deterministic case (see, e.g., [22, 23]), a mixed H_2/H_∞ -type norm of (2.11) can be defined solving the optimization problem:

$$\mathcal{J}_0 = \sup_{(w, w_d)} \mathbb{E} \left[\|Y\|_{L^2}^2 + \|Y_d\|_{L^2}^2 - {}^2 \left(\|w\|_{L^2}^2 + \|w_d\|_{L^2}^2 \right) \right], \quad (3.15)$$

where $(w, w_d) \in L^2[0, \infty) \times L^2[0, \infty)$, the white-noise-type random inputs w and w_d are as in previous subsection and $\gamma > \|G\|_\infty$ with $\|G\|_\infty$. Notice that, if w and w_d are null in (3.15), then \mathcal{J}_0 gives the square of the H_2 -type norm induced by the random inputs w and w_d . The main result of this subsection is the following theorem.

Theorem 3.5. *The optimum \mathcal{J}_0 defined in (3.15) is given by*

$$\mathcal{J}_0 = \text{Tr} \left(G_d^T X(\text{ih}) G_d \right) + \frac{1}{h} \int_0^h \text{Tr} \left(G^T X(\vartheta) G \right) d\vartheta, \quad (3.16)$$

where $X(\vartheta)$ is the stabilizing solution of the system of coupled Riccati equations (3.11).

Proof. The proof follows applying Itô's formula (Proposition 3.3) for the function $v(\vartheta, x) = x^T(\vartheta) X(\vartheta) x(\vartheta)$ with $x(\vartheta)$ being the solution of (2.11) and with $X(\vartheta)$ the stabilizing solution to the system (3.11). Thus, by direct computations, one obtains

$$\begin{aligned} \dot{v}(x(\vartheta), x(\vartheta)) &= \left[-\mathcal{P}_c(\vartheta) - Y^T(\vartheta) Y(\vartheta) + {}^2 w^T(\vartheta) w(\vartheta) + \text{Tr} \left(G^T X(\vartheta) G \right) \right] d\vartheta \\ &\quad + 2x^T(\vartheta) X(\vartheta) G d(\vartheta) + 2x^T(\vartheta) X(\vartheta) (A_1 x(\vartheta) + B_1 w(\vartheta)) d(\vartheta), \end{aligned} \quad (3.17)$$

where, by definition,

$$\begin{aligned} \mathcal{P}_c(\vartheta) &:= \left[x^T(\vartheta) \left(X(\vartheta) B_0 + A_1^T X(\vartheta) B_1 \right) - w^T(\vartheta) \left({}^2I - B_1^T X(\vartheta) B_1 \right) \right] \\ &\quad \times \left({}^2I - B_1^T X(\vartheta) B_1 \right)^{-1} \left[\left(B_0^T X(\vartheta) + B_1^T X(\vartheta) A_1 \right) x(\vartheta) - \left({}^2I - B_1^T X(\vartheta) B_1 \right) w(\vartheta) \right] \geq 0. \end{aligned} \quad (3.18)$$

On the other hand using the second equations of (2.11) and of (3.11), it follows that

$$\begin{aligned}
\mathbb{E} \left[\int_{\mathfrak{ih}^+}^{(\mathfrak{i}+1)\mathfrak{h}} d \left(x^T X x \right) \right] &= \mathbb{E} \left[x^T((\mathfrak{i}+1)\mathfrak{h}) X((\mathfrak{i}+1)\mathfrak{h}) x((\mathfrak{i}+1)\mathfrak{h}) - x^T(\mathfrak{ih}^+) X(\mathfrak{ih}^+) x(\mathfrak{ih}^+) \right] \\
&= \mathbb{E} \left[x^T((\mathfrak{i}+1)\mathfrak{h}) X((\mathfrak{i}+1)\mathfrak{h}) x((\mathfrak{i}+1)\mathfrak{h}) - x^T(\mathfrak{ih}) X(\mathfrak{ih}^-) x(\mathfrak{ih}) + Y_d^T(\mathfrak{i}) Y_d(\mathfrak{i}) \right. \\
&\quad \left. - {}^2w_d^T(\mathfrak{i}) w_d(\mathfrak{i}) + \rho_d(\mathfrak{i}) \right] - \text{Tr} \left(G_d^T X(\mathfrak{ih}) G_d \right),
\end{aligned} \tag{3.19}$$

where

$$\begin{aligned}
\rho_d(\mathfrak{i}) &: \\
&= \left[x^T(\mathfrak{ih}) \left(A_{0d}^T X(\mathfrak{ih}) B_{0d} + A_{1d}^T X(\mathfrak{ih}) B_{1d} \right) - w^T(\mathfrak{i}) \left({}^2I - B_{1d}^T X(\mathfrak{ih}) B_{1d} \right) \right] \left({}^2I - B_{1d}^T X(\mathfrak{ih}) B_{1d} \right)^{-1} \\
&\quad \times \left[x^T(\mathfrak{ih}) \left(A_{0d}^T X(\mathfrak{ih}) B_{0d} + A_{1d}^T X(\mathfrak{ih}) B_{1d} \right) - w^T(\mathfrak{i}) \left({}^2I - B_{1d}^T X(\mathfrak{ih}) B_{1d} \right) \right]^T \geq 0.
\end{aligned} \tag{3.20}$$

Integrating (3.17) from $t = 0$ to ∞ and equalizing it with (3.19) summed up from $i = 0$ to ∞ , based on the fact that $\rho_c(t) \geq 0$ and $\rho_d(i) \geq 0$ and that $X(t)$ is h -periodic, one obtains (3.16). \square

4. State-Feedback Mixed H_2/H_∞ Control Design

Consider the following linear stochastic system with multiplicative noise and finite jumps:

$$\begin{aligned}
dx(t) &= (A_0 x(t) + B_0 w(t) + B_2 u(t)) dt + (A_1 x(t) + B_1 w(t)) d\mathfrak{t} + G d\mathfrak{t}, \quad t \neq \mathfrak{ih}, \\
x(\mathfrak{ih}^+) &= A_{0d} x(\mathfrak{ih}) + B_{0d} w_d(\mathfrak{i}) + (A_{1d} x(\mathfrak{ih}) + B_{1d} w_d(\mathfrak{i})) d_d(\mathfrak{i}) + G_d d_d(\mathfrak{i}), \quad i = 0, 1, \dots, \\
y_1(t) &= C x(t) + D u(t), \quad t \neq \mathfrak{ih}, \\
y_2(t) &= x(t), \quad t \neq \mathfrak{ih}, \\
y_d(i) &= C_d x(\mathfrak{ih}), \quad i = 0, 1, \dots,
\end{aligned} \tag{4.1}$$

where $w(t) \in L^2[0, \infty)$ is an exogenous input, $u(t)$ denotes the control variable, $y_1(t)$ stands for the regulated output, and $y_2(t)$ is the measured output. For the simplicity of the computations, the following orthogonality assumption is made:

$$D^T [C \ D] = [0 \ I]. \tag{4.2}$$

As seen from the above system, the state vector $x(t)$ is assumed measurable. It is not the purpose of the present paper to analyze the case when the state variables must be estimated.

For some results concerning the discrete-time filtering methods associated to networked systems, see, for instance, [24–26].

The second equation of the system (4.1) does not include a discrete-time control input since, in the application presented in the previous section, the control law has only a continuous-time component.

The problem analyzed in this section consists in finding a state-feedback gain $F(t), t \neq \bar{h}$, such that the resulting system obtained with $u(t) = F(t)x(t), t \neq \bar{h}$, satisfies the following conditions.

- (i) It is ESMS.
- (ii) The H_∞ -type norm of the stochastic system with jumps obtained by ignoring the noises $w(t)$ and $d_a(i)$ is less than a given $\gamma > 0$.
- (iii) The performance index (3.16) is minimized, where $X(t)$ in (3.16) denotes the stabilizing solution of the norm-type Riccati system (3.11) corresponding to the resulting system obtained with $u(t) = F(t)x(t), t \neq \bar{h}$, namely, replacing A_0 by $A_0 + B_2F(t)$.

The solution of this problem is given by the following result.

Theorem 4.1. *The solution of the state-feedback mixed H_2/H_∞ control problem considered above is given by*

$$F(t) = -B_2^T X(t), \quad t \neq \bar{h}, \quad (4.3)$$

where $X(t)$ denotes the h -periodic stabilizing solution of the game-theoretic Riccati type system with jumps

$$\begin{aligned} -\dot{X}(t) &= A_0^T X(t) + X(t)A_0 + A_1^T X(t)A_1 + C^T C + \left(X(t)B_0 + A_1^T X(t)B_1 \right) \\ &\quad \times \left(I - B_1^T X(t)B_1 \right)^{-1} \left(B_0^T X(t) + B_1^T X(t)A_1 \right) - X(t)B_2 B_2^T X(t), \quad t \neq \bar{h}, \\ X(\bar{h}^-) &= A_{0d}^T X(\bar{h})A_{0d} + A_{1d}^T X(\bar{h})A_{1d} + C_d^T C_d + \left(A_{0d}^T X(\bar{h})B_{0d} + A_{1d}^T X(\bar{h})B_{1d} \right) \\ &\quad \times \left(I - B_{1d}^T X(\bar{h})B_{1d} \right)^{-1} \left(B_{0d}^T X(\bar{h})A_{0d} + B_{1d}^T X(\bar{h})A_{1d} \right), \quad i = 0, 1, \dots \end{aligned} \quad (4.4)$$

Proof. Consider the cost function

$$J(x_0, w, u) = E \left[\int_0^\infty \left(|y_1(t)|^2 - \gamma^2 |w(t)|^2 \right) dt \right] \quad (4.5)$$

associated with the system

$$\begin{aligned} dx(t) &= (A_0 x(t) + B_0 w(t) + B_2 u(t))dt + (A_1 x(t) + B_1 w(t))d(t), \quad t \neq \bar{h}, \\ x(\bar{h}^+) &= A_{0d} x(\bar{h}) + B_{0d} w_d(i) + (A_{1d} x(\bar{h}) + B_{1d} w_d(i)), \quad i = 0, 1, \dots, \\ y_1(t) &= C x(t) + D u(t), \quad t \neq \bar{h}, \end{aligned} \quad (4.6)$$

with the initial condition $x(0) = x_0$. Applying Proposition 3.4 for $u_1 = w$ and $u_2 = u$, one obtains that

$$\begin{aligned} J(x_0, w, u) &= x_0^T X(0)x_0 - \mathbb{E} \left[x^T(\cdot) X(\cdot) x(\cdot) \right] \\ &+ \mathbb{E} \int_0^\infty \left[\left(u(t) + B_2^T X(t)x(t) \right)^T \left(u(t) + B_2^T X(t)x(t) \right) - \tilde{\rho}(w(t), x(t), X(t)) \right] dt, \end{aligned} \quad (4.7)$$

where the following notation has been introduced

$$\begin{aligned} \tilde{\rho}(w(t), x(t), X(t)) &:= \left[w(t) - \left(I - B_1^T X(t)B_1 \right)^{-1} \left(B_0^T X(t) + B_1 X(t)A_1 \right) x(t) \right]^T \\ &\times \left(I - B_1^T X(t)B_1 \right) \\ &\times \left[w(t) - \left(I - B_1^T X(t)B_1 \right)^{-1} \left(B_0^T X(t) + B_1 X(t)A_1 \right) x(t) \right], \end{aligned} \quad (4.8)$$

$X(t)$, $t \geq 0$, denoting the stabilizing solution of the Riccati-type system (4.4).

Equation (4.7) shows that the minimum of J with respect to the control input u is obtained for $u(t) = -B_2^T X(t)x(t)$.

Further, consider a stabilizing state-feedback control $\hat{u}(t) = \hat{F}(t)\hat{x}(t)$, $t \geq 0$, for which the H_∞ norm of the resulting system without additive white noise (see the requirement (ii) above)

$$\begin{aligned} d\hat{x}(t) &= \left[\left(A_0 + B_2 \hat{F}(t) \right) \hat{x}(t) + B_0 w(t) \right] dt + \left(A_1 \hat{x}(t) + B_1 w(t) \right) d\beta(t), \\ y(t) &= (C + D F(t))\hat{x}(t) \end{aligned} \quad (4.9)$$

is less than γ .

Using again Proposition 3.4 for the system (4.9), direct computations give

$$J(x_0, w, \hat{u}) = x_0^T \hat{X}(0)x_0 - \mathbb{E} \left[\hat{x}^T(\cdot) \hat{X}(\cdot) \hat{x}(\cdot) \right] - \mathbb{E} \left[\int_0^\infty \tilde{\rho}(w(t), \hat{x}(t), \hat{X}(t)) dt \right], \quad (4.10)$$

where $\tilde{\rho}(\cdot, \cdot, \cdot)$ is defined by (4.8) and $\hat{X}(t)$ is the stabilizing solution of the Riccati system of form (3.11) corresponding to (4.9). Then, defining $\tilde{u}(t) := F(t)x(t)$ and

$$\tilde{w}(t) := \left(I - B_1^T X(t)B_1 \right)^{-1} \left(B_0^T X(t) + B_1^T X(t)A_1 \right) x(t), \quad (4.11)$$

one obtains that $J(x_0, \tilde{w}, \tilde{u}) \leq J(x_0, \tilde{w}, \hat{u})$; namely,

$$\begin{aligned} x_0^T X(0)x_0 - E \left[x^T(\cdot) X(\cdot) x(\cdot) \right] &\leq x_0^T \hat{X}(0)x_0 - E \left[\hat{x}^T(\cdot) \hat{X}(\cdot) \hat{x}(\cdot) \right], \\ -E \left[\int_0^{\infty} \tilde{\rho}(\hat{w}(\cdot), \hat{x}(\cdot), \hat{X}(\cdot)) d\tau \right] &\leq x_0^T \hat{X}(0)x_0 - E \left[\hat{x}^T(\cdot) \hat{X}(\cdot) \hat{x}(\cdot) \right]. \end{aligned} \quad (4.12)$$

Since $x(\cdot)$ and $\hat{x}(\cdot)$ are stabilizing solutions of the Riccati systems, it follows that $\lim_{t \rightarrow \infty} x(\cdot) = \lim_{t \rightarrow \infty} \hat{x}(\cdot) = 0$. Therefore, making $t \rightarrow \infty$ in (4.12), one obtains that $x(0) \leq \hat{X}(0)$.

Further, using a similar reasoning for the cost function

$$J_t(x_0, w, u) = E \left[\int_t^{\infty} \left(|y_1(\tau)|^2 - w(\tau)^2 \right) d\tau \right] \quad (4.13)$$

with $t \in (0, h)$, one obtains that $x(t) \leq \hat{x}(t)$, and; thus, one concludes that the minimum of (3.16) is obtained for the stabilizing solution $x(t)$ of the Riccati-type system (4.4). \square

5. A Numerical Procedure to Compute the Stabilizing Solution of the Riccati System with Jumps

In order to determine J_0 with the expression given in the statement of Theorem 3.5, the stabilizing solution $x(t)$, $t \geq 0$, of the Riccati-type system (3.11) must be determined. Since the two Riccati equations of this system are coupled, an iterative procedure will be used. The proposed iterative method is similar with the iterative numerical methods used to solve Riccati equations of norm in the deterministic continuous-time and discrete-time cases (see, for instance, [27, 28]). These Newton-type iterative procedures are adapted to the particularities of the Riccati systems with jumps derived in the previous sections, and a detailed proof of the convergence towards the stabilizing solution is not the purpose of the present paper. Roughly speaking, the proof based follows showing that the solutions obtained at each iteration determine a monotonic and bounded sequence. An important particular feature of the Riccati systems with jumps, already mentioned above, is that their solution $x(t)$ is h -periodic and right continuous. The proposed iterative procedure is the following:

$$\begin{aligned} \dot{X}_{k+1}(t) + (A_0 + B_0 F_k(t))^T X_{k+1}(t) + X_{k+1}(t)(A_0 + B_0 F_k(t)) + M_k(t) &= 0, \quad t \neq ih, \\ X_{k+1}(ih^-) = (A_{0d} + B_{0d} F_{d,k}(i))^T X_{k+1}(ih)(A_{0d} + B_{0d} F_{d,k}(i)) + N_k(i), \quad &i = 0, 1, \dots, \end{aligned} \quad (5.1)$$

where

$$\begin{aligned} F_k(t) &= \left({}^2I - B_1^T X_k(t) B_1 \right)^{-1} \left(B_0^T X_k(t) + B_1^T X_k(t) A_1 \right), \\ M_k(t) &= A_1^T X_k(t) B_1 \left({}^2I - B_1^T X_k(t) B_1 \right)^{-1} B_1^T X_k(t) A_1 \\ &\quad - X_k(t) B_0 \left({}^2I - B_1^T X_k(t) B_1 \right)^{-1} B_0^T X_k(t) + A_1^T X_k(t) A_1 + C^T C, \end{aligned}$$

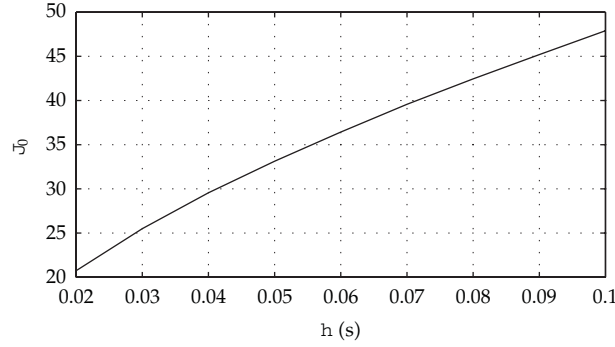


Figure 2: Variation of J_0 with respect to the sampling period h .

$$\begin{aligned}
 F_{d,k}(\dot{i}) &= \left({}^2I - B_{1d}^T X_k(\dot{i}h) B_{1d} \right)^{-1} \left(B_{0d}^T X_k(\dot{i}h) A_{0d} + B_{1d}^T X_k(\dot{i}h) A_{1d} \right), \\
 N_k(\dot{i}) &= -F_{d,k}^T B_{0d}^T X_k(\dot{i}h) (A_{0d} + B_{0d} F_{k,d}(\dot{i})) - A_{0d}^T X_k(\dot{i}h) B_{0d} F_{k,d}(\dot{i}) \\
 &\quad + (A_{1d} + B_{1d} F_{k,d}(\dot{i}))^T X_k(\dot{i}h) (A_{1d} + B_{1d} F_{k,d}(\dot{i})) + C_d^T C_d.
 \end{aligned} \tag{5.2}$$

For the initial step of the above iterative procedure, one takes $x(0) = 0$, $t \in (0, h)$, and $F_0(t)$ and $F_{0,d}(\dot{i})$ stabilizing (5.1). In order to solve (5.1) at each iteration, one solves the first equation (5.1) obtaining

$$X_{k+1}(\dot{i}h) = e^{(A_{0d} + B_{0d} F_k)^T h} X_{k+1}(\dot{i}h^-) e^{(A_{0d} + B_{0d} F_k)h} + \int_0^h e^{(A_{0d} + B_{0d} F_k)^T (h-\tau)} M_k(\tau) e^{(A_{0d} + B_{0d} F_k)(h-\tau)} d\tau, \tag{5.3}$$

which is substituted then in the second equation (5.1) obtaining, thus, a Lyapunov-type equation with the unknown variable $X_{k+1}(\dot{i}h^-)$. Then, by backward integration on the interval $[(i-1)h, \dot{i}h^-)$ with the initial condition $X_{k+1}(\dot{i}h^-)$, one obtains $X_{k+1}(t)$ for $t \in [(i-1)h, \dot{i}h^-)$.

In the final part of this section, some of the above theoretical results will be used to analyze the mixed performance of the UAVs formation networked with fading communication channel considered in Section 2. The values of the gains considered in this example are $K_d = \text{diag}(0.7, 0.05, 0.05)$ and $K_x = \text{diag}(7, 5, 5)$, for $v_0 = 150 \text{ m/s}$ (see Section 2). One determined the performance index H_2/H_∞ performance computing the value of the index J_0 defined by (3.15). The results are illustrated in Figure 2. One can see the the tracking performances of the flight formation are severely deteriorated when the sampling period of the transmission in the communication channel increases. In Figure 3, the variation of σ_{\min} with respect to the sampling period and the variance of the multiplicative noise, in the absence of the additive white noise, are shown in Figure 3. It can be seen that σ_{\min} is not very much influenced by the multiplicative noise at small sampling periods, but it becomes very sensitive with respect to this noise when the sampling period increases.

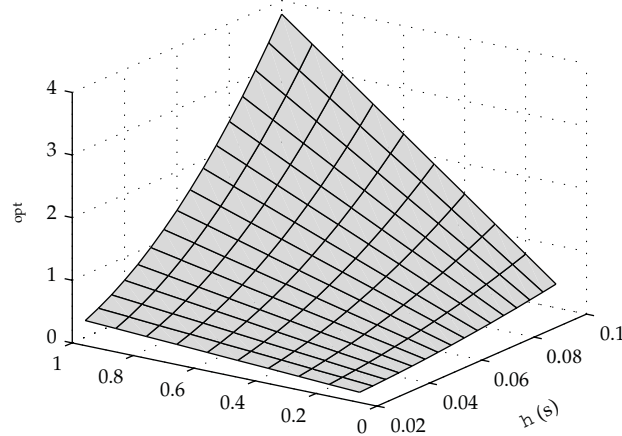


Figure 3: Variation of \min with respect to h and \dots .

6. Conclusions

The purpose of the paper was to provide an appropriate methodology to evaluate the performance of networked systems interconnected via fading communication channels. The main difficulty arises from the hybrid structure of the resulting system which includes a continuous-time component specific to the network individual members and a discrete-time component given by the communication system. It is shown that such a hybrid configuration can be analyzed from the point of view of stability and disturbance attenuation performances using dynamic models with finite jumps. In the actual stage of the research, a method to compute a mixed H_2/H_∞ -type performance has been developed, and a state-feedback control law to optimize it has been designed. Further research will be focused on the state estimation problems arising in the implementation of such control laws.

Acknowledgments

The author thanks the anonymous reviewers for their useful comments and suggestions. This work was sponsored by the National University Research Council (CNCS) under Grant 1721.

References

- [1] R. W. Beard, J. Lawton, and F. Y. Hadaegh, "A coordination architecture for spacecraft formation control," *IEEE Transactions on Control Systems Technology*, vol. 9, no. 6, pp. 777–790, 2001.
- [2] J. Carbaugh, D. N. Godbole, and R. Sengupta, "Safety and capacity analysis of automated and manual highway systems," *Transportation Research Part C*, vol. 6, no. 1-2, pp. 69–99, 1998.
- [3] S. Banda, J. Doyle, R. Murray, J. Paduano, J. Speyer, and G. Stein, "Research needs in dynamics and control of uninhabited aerial vehicles," Panel Report, 1997.
- [4] F. Giulietti and G. Mengali, "Dynamics and control of different aircraft formation structures," *Aeronautical Journal*, vol. 108, no. 1081, pp. 117–124, 2004.
- [5] TechSat 21, "Space missions using satellite clusters," 1998, <http://www.vs.afri.af.mil/>.
- [6] P. J. Seiler, *Coordinated control of unmanned aerial vehicles*, Ph.D. thesis, University of California, Berkeley, Calif, USA, 2001.

- [7] N. Elia, "Remote stabilization over fading channels," *Systems & Control Letters*, vol. 54, no. 3, pp. 237–249, 2005.
- [8] P. Seiler and R. Sengupta, "An H_∞ approach to networked control," *IEEE Transactions on Automatic Control*, vol. 50, no. 3, pp. 356–364, 2005.
- [9] A. Hassibi, S. P. Boyd, and J. P. How, "Control of asynchronous dynamical systems with rate constraints on events," in *Proceedings of the 38th IEEE Conference on Decision and Control (CDC '99)*, pp. 813–814, December 1999.
- [10] G. C. Walsh, O. Beldiman, and L. G. Bushnell, "Asymptotic behavior of nonlinear networked control systems," *IEEE Transactions on Automatic Control*, vol. 46, no. 7, pp. 1093–1097, 2001.
- [11] W. Zhang, M. S. Branicky, and S. M. Phillips, "Stability of networked control systems," *IEEE Control Systems Magazine*, vol. 21, no. 1, pp. 84–99, 2001.
- [12] H. Chan and U. Özgüner, "Optimal control of systems over a communication network with queues via a jump system approach," in *Proceedings of the 4th IEEE Conference on Control Applications*, pp. 1148–1153, September 1995.
- [13] V. Dragan, T. Morozan, and A.-M. Stoica, *Mathematical Methods in Robust Control of Linear Stochastic Systems*, vol. 50 of *Mathematical Concepts and Methods in Science and Engineering*, Springer, New York, NY, USA, 2006.
- [14] P. V. Pakshin, "State estimation and control synthesis for discrete linear systems with additive and multiplicative noise," *Automation and Remote Control*, vol. 39, no. 4, pp. 526–535, 1978.
- [15] J. Zabczyk, "Stochastic control of discrete-time systems," in *Control Theory and Topics in Functional Analysis*, vol. 1, pp. 187–224, International Atomic Energy Agency, Vienna, Austria, 1976.
- [16] X. He, Z. Wang, Y. D. Ji, and D. H. Zhou, "Robust fault detection for networked systems with distributed sensors," *IEEE Transactions on Aerospace and Electronic Systems*, vol. 47, no. 1, pp. 166–177, 2011.
- [17] X. He, Z. Wang, and D. H. Zhou, "Robust fault detection for networked systems with communication delay and data missing," *Automatica*, vol. 45, no. 11, pp. 2634–2639, 2009.
- [18] A. Ichikawa and H. Katayama, " H_∞ control for a general jump system with application to sampled-data systems," in *Proceedings of the 35th IEEE Conference on Decision and Control (CDC '96)*, pp. 446–451, Kobe, Japan, December 1996.
- [19] N. Sivashankar and P. P. Khargonekar, "Characterization and Computation of the H_2 induced norm of sampled-data systems," *SIAM Journal on Control and Optimization*, vol. 32, no. 4, pp. 1128–1150, 1994.
- [20] V. Dragan and A.-M. Stoica, "Riccati type equations for stochastic systems with jumps," in *Proceedings of the 17th International Symposium on Mathematical Theory of Networks and Systems (MTNS '06)*, Kyoto, Japan, July 2006.
- [21] E. Biglieri, J. Proakis, and S. Shamai, "Fading channels: information-theoretic and communications aspects," *IEEE Transactions on Information Theory*, vol. 44, no. 6, pp. 2619–2692, 1998.
- [22] J. Doyle, K. Zhou, K. Glover, and B. Bodenheimer, "Mixed H_2 and H_∞ performance objectives. II. Optimal control," *IEEE Transactions on Automatic Control*, vol. 39, no. 8, pp. 1575–1587, 1994.
- [23] K. Zhou, K. Glover, B. Bodenheimer, and J. Doyle, "Mixed H_2 and H_∞ performance objectives. I. Robust performance analysis," *IEEE Transactions on Automatic Control*, vol. 39, no. 8, pp. 1564–1574, 1994.
- [24] H. Dong, Z. Wang, and H. Gao, "Robust H_∞ filtering for a class of nonlinear networked systems with multiple stochastic communication delays and packet dropouts," *IEEE Transactions on Signal Processing*, vol. 58, no. 4, pp. 1957–1966, 2010.
- [25] H. Dong, Z. Wang, D. W. C. Ho, and H. Gao, "Variance-constrained H_∞ filtering for a class of nonlinear time-varying systems with multiple missing measurements: the finite-horizon case," *IEEE Transactions on Signal Processing*, vol. 58, no. 5, pp. 2534–2543, 2010.
- [26] A. S. Matveev and A. V. Savkin, "Optimal state estimation in networked systems via sensor control," in *Proceedings of the 15th IFAC World Congress*, Barcelona, Spain, 2002.
- [27] R. R. Bitmead, M. R. Gevers, I. R. Petersen, and R. J. Kaye, "Monotonicity and stabilizability properties of solutions of the Riccati difference equation: propositions, lemmas, theorems, fallacious conjectures and counter-examples," *Systems & Control Letters*, vol. 5, no. 5, pp. 309–315, 1985.
- [28] H. K. Wimmer, "Monotonicity of maximal solutions of algebraic Riccati equations," *Systems & Control Letters*, vol. 5, no. 5, pp. 317–319, 1985.

Research Article

On the Complexities of the Design of Water Distribution Networks

Joaquín Izquierdo,¹ Idel Montalvo,² Rafael Pérez-García,¹
and Agustín Matías³

¹ *FluIng-IMM, Universitat Politècnica de València, Camino Vera s/n, 46022 Valencia, Spain*

² *3S Consult Büro Karlsruhe, Albtalstrasse 13D, 76137 Karlsruhe, Germany*

³ *Universidad de Extremadura, Avda. Universidad, s/n, 10071 Cáceres, Spain*

Correspondence should be addressed to Joaquín Izquierdo, jizquier@upv.es

Received 10 July 2011; Accepted 13 September 2011

Academic Editor: Zidong Wang

Copyright © 2012 Joaquín Izquierdo et al. This is an open access article distributed under the Creative Commons Attribution License, which permits unrestricted use, distribution, and reproduction in any medium, provided the original work is properly cited.

Water supply is one of the most recognizable and important public services contributing to quality of life. Water distribution networks (WDNs) are extremely complex assets. A number of complex tasks, such as design, planning, operation, maintenance, and management, are inherently associated with such networks. In this paper, we focus on the design of a WDN, which is a wide and open problem in hydraulic engineering. This problem is a large-scale combinatorial, nonlinear, nonconvex, multiobjective optimization problem, involving various types of decision variables and many complex implicit constraints. To handle this problem, we provide a synergetic association between swarm intelligence and multiagent systems where human interaction is also enabled. This results in a powerful collaborative system for finding solutions to such a complex hydraulic engineering problem. All the ingredients have been integrated into a software tool that has also been shown to efficiently solve problems from other engineering fields.

1. Introduction

Water distribution networks (WDNs) are important and dynamic systems. Most people are unaware of their importance, despite the fact that they routinely open the water tap every day. The existence of WDNs is generally ignored, except when disruption occurs. Politicians tend to neglect them because they are buried assets. Nevertheless, WDNs provide citizens with an essential public service. They supply drinking water, which is a crucial requirement for the normal development of most basic activities of life, such as feeding and hygiene [1].

For most of the people, perhaps with the exception of those directly involved in their management, WDNs are simply static infrastructures. However, WDNs are dynamic

and living beings. They are born, when they are designed and built; they grow, as a consequence of increasing urban development and the appearance of new demands; they age and deteriorate, since they suffer a number of operational and environmental conditions that cause progressive and insidious deterioration; they need care, preventive care but also sometimes surgery; they are expected to work properly, despite the great amount of uncertainty involved and defective information about the state and operation of these systems due to their geographical dispersion and the fact that they are hidden assets; they have to meet basic requirements even under adverse circumstances, hence they must show resilience; and so on.

Our aim is to achieve a quality long-lasting life for WDNs. Nevertheless, it is a fact that with the passing of time these systems become gradually, but substantially, impaired. Some of the reasons include increasing loss of pressure triggered by increasing roughness of the inner pipes; breakage or cracking of pipes provoked by corrosion and mechanical or thermal charges; loss of water (leaks) and pathogen intrusion due to pipe breaks and cracks, with their corresponding economic loss, third party damage, and risk of contamination.

Several complex tasks, such as design, planning, operation, maintenance, and management, are inherently associated with WDNs. These tasks are not simple at all and require considerable investment. Efficiency and reduction of costs have been compelling reasons for practitioners to progressively move away from manual design based on experience and support the development of suitable automatic or semiautomatic tools. Support, of course, is increasingly multidisciplinary and receives contributions from various scientific areas. Mathematics is one of the areas contributing most effectively with suitable and efficient methods and tools.

We focus on the design of a WDN, a wide and open problem in hydraulic engineering that involves the addition of new elements in a system; the rehabilitation or replacement of existing elements; decision making on operation; reliability and protection of the system; among other actions. Designs are necessary to carry out new configurations or enlarge and improve existing configurations to meet new conditions. The design of a WDN involves finding acceptable trade-offs among various conflicting objectives: finding the lowest costs for layout and sizing using new components and rehabilitating, reusing, or substituting existing components; creating a working system configuration that fulfils all water demands, including water quality; adhering to the design constraints; guaranteeing a certain degree of reliability for the system [2–4].

The formulation of the optimal WDN design problem has traditionally been influenced by the available mathematical support for solving the problem; formulations have been adapted (restricted and/or simplified) to the available mathematical techniques [5]. However, in its more general setting, the optimal design of a large WDN is a formidable problem because of the very high computational complexity involved if it has to be solved within a reasonable time framework. There are various explanations for this complexity. One reason is the huge number of expensive hydraulic analyses that must be performed during the process. In addition, WDN optimal design is a nonlinear, nonconvex problem that cannot be formulated in just one way and has various objective functions because of the plurality of situations that can be found and the different aims that each situation may involve. Last but not least, even for the simplest cases and the smallest of WDNs, design can easily become an NP-hard problem.

In this paper, we provide a detailed description of the various objectives involved in the WDN optimal design problem. We argue that classical optimization techniques are unable to satisfactorily solve these problems and describe an evolutionary, multiagent approach

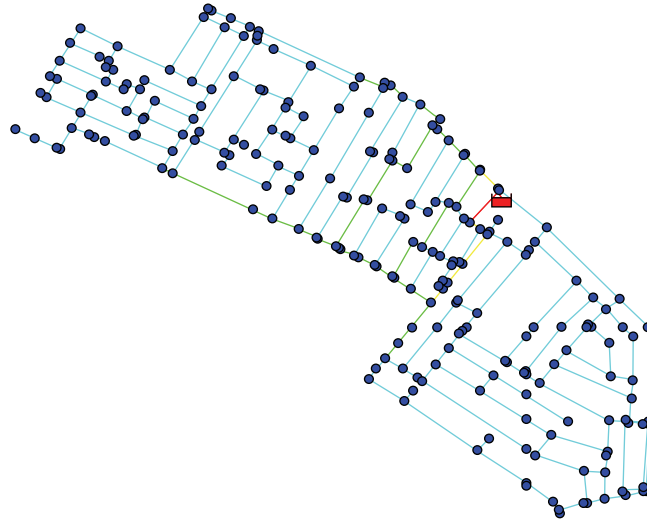


Figure 1: A WDN.

to tackle this task. We then provide the solution for some real-world water distribution networks.

2. The WDN Optimal Design Problem

The layout of a network is usually conditioned by urban plans and/or various other reasons. Street positions, location of sources, main consumption points, and so forth are perfectly known before starting the design. Therefore, design does not generally consider the layout and is usually restricted to sizing the necessary network components. Figure 1 presents a network fed by one tank (small red box), with 294 pipes (lines) amounting to 18.34 km and 240 nodes (blue points). This network has already been designed, and the different colors (light blue, green, yellow, and red) represent different pipe diameters.

Various objectives may be considered in the WDN optimal design problem. In this section, we describe these objectives, namely, cost of components; adherence to hydraulic constraints; satisfaction of water demand quality; resilience of the system during stressed conditions.

2.1. Cost of Components

Apart from the basic variables of the problem, which are the diameters of the new pipes, additional variables that depend on the design characteristics of the system may be required: storage volume, pump head, type of rehabilitation to be carried out for various parts of the network, and so forth. The estimation of individual costs will always depend on these variables. The correct approach to assess the costs for each element is important when defining the objective function, which has to be fully adapted to the problem under consideration in terms of design, enlargement, rehabilitation, operational design, and so forth. For example, in the network shown in Figure 1, some of the areas may be already built,

while others must be newly designed. For the already existing pipes, the objective may consist in one of various actions: rehabilitation (with several available alternatives with associated costs), replacement, or simply duplication.

In addition, it is important that the objective function reflects with utmost reliability the total cost of the system during its lifetime [6].

Many authors have used, in their optimization, an objective function that only considers the cost of pipelines, new and/or additional, duplicated pipelines, while others have taken into account other various costs [7, 8]. For the sake of simplicity, we only describe in detail here the cost related to the L pipes of the network, which includes the cost of new pipes, L_{new} , and the cost of rehabilitated pipes, L_{reh} . This function, besides contributing most of the total cost, exhibits the characteristics we are interested in underlining. Costs corresponding to other elements (tanks, pumps, valves, etc.), which are typically nonlinear, are just new terms to be added within this fitness function (see [7], for example).

The cost of the pipes is expressed as

$$C(D) = \sum_{i=1}^L c(D_i) \cdot l_i, \quad (2.1)$$

and the sum extended to all ($L = L_{\text{new}} + L_{\text{reh}}$) individual pipes. $D = (D_1, \dots, D_L)^T$ is the vector of the pipe diameters. The costs per meter, depending on the diameter of pipe i , D_i , are given by $c(D_i)$; l_i is the i th pipe length. Note that D_i is chosen from a discrete set of commercially available diameters, and $c(\cdot)$ is a nonlinear function of diameter.

Typically, the unitary cost of a new pipe, including purchase, transport, and installation costs, takes the form

$$c(D) = (T_1 + T_2 D), \quad (2.2)$$

where T_1 , T_2 , and α are characteristic constants of the pipes (information provided by pipe manufacturers, market costs of construction works, etc.). Typically, α takes values different from 1. Maintenance costs are usually considered as a fraction of the installation costs.

There are various rehabilitation options: no rehabilitation, relining, duplication, and replacement are the most usual. Relining costs may be evaluated by the nonlinear function

$$c(D) = T_4 D^\alpha, \quad (2.3)$$

with T_4 and α , other characteristic constants. Duplication is equivalent to the installation of a new pipe, and replacement involves, in addition, the cost of removing the old pipe.

2.1.1. Working Conditions or Scenarios

The working conditions of a WDN depend on the values adopted by two types of variables, namely, demand models and roughness coefficient values. Typically, independent random variables are used to model both types of variables. Under the assumption that design is made to work for N_{dm} demand models and N_{rc} sets of roughness coefficient values, the design is performed for $N_{\text{wc}} = N_{\text{dm}} \cdot N_{\text{rc}}$ working conditions. Each of these conditions

has individual probabilities, P_{wc}^k , $k = 1, \dots, N_{wc}$, given by the product of the corresponding probabilities regarding demand models and roughness values. In addition, these probabilities verify

$$\sum_k P_{wc}^k = 1. \quad (2.4)$$

In the case of inclusion of the operational costs of the network along a certain temporal horizon, the necessary amortization rates must be considered. In this case, the objective cost function, omitting for simplicity the independent variables, may be represented by

$$C_{Net} = \sum_k \left[P_{wc}^k (a_{pipe} \cdot C_{pipe} + a_{pump} \cdot C_{pump} + a_{valv} \cdot C_{valv} + a_{tank} \cdot C_{tank} + C_{Oper}) \right]. \quad (2.5)$$

In this case, values a_{xxx} correspond to amortization rates, C_{pipe} is given by expression (2.1), and the costs of pumps, tanks, valves, and operation (which have not been detailed in this paper, as stated) are also considered. Observe that, in general, C_{Net} is a nonlinear, partially stochastic function depending on continuous, discrete, and binary variables.

2.2. Hydraulic Constraints

When modeling physical processes where the underlying functions are known, the deterministic equations can be solved to forecast the model output to a certain degree of accuracy. In hydraulic modeling, different governing laws, [9], can provide a very accurate description of the process provided that the initial and/or boundary conditions and the forcing terms are precisely defined.

Analyzing pressurized water systems is a mathematically complex task that hydraulic engineers must face, especially for the large systems found in even medium-sized cities, since it involves solving many nonlinear simultaneous equations. Several formulations are available (see, for example, [9]). One formulation considers the $N - 1$ continuity equations, which are linear, plus the L energy equations, typically nonlinear

$$\sum_{j \in N_i} Q_{ij} = Q_i, \quad i = 1, \dots, N - 1, \quad (2.6)$$

$$H_{k1} - H_{k2} = R_k Q_k |Q_k|, \quad k = 1, \dots, L.$$

N is the number of demand junctions, and L is the number of lines in the system. N_i is the number of nodes directly connected to node i ; Q_i is the demand associated to node i ; $k1$ and $k2$ represent the end nodes of line k , which carries an unknown flowrate Q_k and is characterized by its resistance R_k , which depends on the diameter D_k and on Q_k through the Reynolds number (the nonlinearity of the energy equations arises not only from the quadratic term, but also from the function R_k). H_{k1} and H_{k2} , piezometric heads at nodes $k1$ and $k2$, are

unknown for consumption nodes and are given for fixed head nodes. The complete set of equations may be written by using block matrix notation as

$$\begin{pmatrix} A_{11}(q) & A_{12} \\ A_{12}^t & 0 \end{pmatrix} \begin{pmatrix} Q \\ H \end{pmatrix} = \begin{pmatrix} -A_{10}H_f \\ Q \end{pmatrix}, \quad (2.7)$$

where A_{12} is the connectivity matrix describing the way demand nodes are connected through the lines. Its size is $L \times N_p$, N_p being the number of demand nodes; q is the vector of the flowrates through the lines; H is the vector of unknown heads at demand nodes; A_{10} describes the way fixed head nodes are connected through the lines and is an $L \times N_f$ matrix, N_f being the number of fixed head nodes with known head H_f ; Q is the N_p -dimensional vector of demands. Finally, $A_{11}(q)$ is an $L \times L$ diagonal matrix, with elements

$$a_{ii} = R_i Q_i + B_i + \frac{A_i}{Q_i}, \quad (2.8)$$

with $R_i = R_i(D_i, Q_i)$ being the line resistance and A_i, B_i coefficients characterizing a potential pump. System (2.7) is a nonlinear problem, whose solution is the state vector $x = (Q^t, H^t)^t$ (flowrates through the lines and heads at the demand nodes) of the system.

Since most water systems involve a huge number of equations and unknowns, the system (2.7) is usually solved using some gradient-like technique. Various tools to analyze water networks using gradient-like techniques have been developed in the past. Among them, EPANET2, [10], is used in a generalized way.

To be integrated in the algorithm later described, we have modified the EPANET Toolkit to support pressure-driven demands as described in [11]; the idea of pressure-driven demands has also been considered in other works [12, 13]. The demand at a certain node is formulated for pressure (piezometric head) values, H_{real} , between the minimum pressure allowed, H_{inf} , and the required pressure, H_{req} , with $0 < H_{inf} < H_{req}$, at the node by

$$\frac{Q_{real}}{D_{req}} = \left(\frac{H_{real} - H_{inf}}{H_{req} - H_{inf}} \right)^{0.5}, \quad \text{if } H_{req} \leq H_{real} \leq H_{inf}, \quad (2.9)$$

a function of Q_{real} and D_{req} representing the real flow delivered and the demand requested at the node, respectively. Along with this equation, two other conditions complete the definition of the demand at the node

$$\begin{aligned} \text{(i) if } H_{real} \geq H_{req}, \quad \text{then } Q_{real} &= D_{req}, \\ \text{(ii) if } H_{real} \leq H_{inf}, \quad \text{then } Q_{real} &= 0. \end{aligned} \quad (2.10)$$

The integration of such software to run different analyses or simulations for potential solutions of the problem is performed during the optimization process that is developed within the evolutionary algorithms [14–16], such as the algorithm presented in this paper.

2.3. Satisfaction of Demand Quality

WDN design is typically performed subject to several performance constraints in order to achieve an adequate service level. The most used constraint requires a certain minimum pressure level at each node of the system. Other constraints may include maximum pipe flow velocities and minimum concentrations of chlorine, for example. For many years, nodal pressure constraints have been considered as strong constraints in the sense that they should be strictly satisfied. Nevertheless, the possibility of violating by a small degree some of these constraints opens the door to various strategies for adopting suboptimal designs or soft solutions that may be more convenient from other (global or political) perspectives. This fact has been openly favored by multiobjective approaches such as the one we present in this paper.

In many studies, these constraints have been included as penalty terms in the cost function. However, in this paper, we consider the satisfaction of demand quality as a new objective that must be fulfilled.

There are various ways of expressing lack of compliance with pressure, velocity, disinfectant, and so forth conditions. For example, an objective function considering nodal and velocity constraints given by minimum values of node pressures and pipe velocities may be given by

$$P = \sum_{j=1}^N H(p_{\min} - p_j) \cdot (p_{\min} - p_j) + \sum_{i=1}^L H(v_{\min} - v_i) \cdot (v_{\min} - v_i), \quad (2.11)$$

where all the functions involved depend on the D , the vector of diameters, through the hydraulic model presented in the previous section.

Here, N is the number of demand nodes in the network, and L is the number of pipes. For nodes with pressures greater than this minimal value, the associated individual terms vanish, and the Heaviside step function H is used in this explicit expression. The same argument applies to pipe velocities (note that absolute values for velocities are considered since flow may occur in any direction). Parameters α and β help normalize the importance of the different scales between pressure and velocity, and this enables a more meaningful aggregation of different types of constraint violation and can also be used to balance the importance of one over the other. Extensions of (2.11) may be provided to consider maximum bounds for both variables. It is also straightforward to extend (2.11) to consider additional objectives, such as limiting the level of chlorine in each pipe in the case of water quality optimization. This expression is also a function of the selected pipe diameters through the hydraulic model presented in the next subsection.

2.4. Reliability and Tolerance

WDNs have almost always been designed with loops so as to provide alternative paths from the source to every network node or junction. This reduces the number of affected consumers when a pipe is withdrawn from service for various reasons. Under normal operating conditions, there is no need for loops, meaning that a looped network is redundant. Redundancy is the capacity of the network to distribute water to users using alternative routes. Redundancy is only needed to maintain service, reduce deficit, and minimize the number of affected consumers when a pipe is withdrawn from service. Redundancy includes

two important concepts: firstly, the connectivity necessary to provide alternative flow paths to each node; secondly, the provision of an adequate flow capacity (diameter) for those paths [17].

The concept of redundancy is closely related to reliability [18–20]. The concept of reliability was introduced to quantitatively measure the possibility of maintaining an adequate service for a given period.

The reliability calculation in looped water supply networks is formulated in the literature as a function of the causes affecting consumer demand. The causes usually considered include real demand exceeding the design demand (e.g., a fire demand); growth of population served by the network; pipe aging; pipe failure.

An explicit formulation of all these causes in probabilistic terms and their further integration implies considerable mathematical and algorithmic complexity. Thus, although numerous WDN reliability quantification schemes exist [17, 21], most are computationally expensive.

This paper considers a simple reliability formulation as in [11, 22, 23] which only considers pipe failures. It is assumed that a pipe temporarily withdrawn from service can be isolated, and so only those consumers connected to that pipe are affected. Only one pipe failure at a time is considered in the formulation of reliability. This is supported by the well-known fact that the probability of simultaneous failure by two or more pipes is extremely small [11, 19, 20, 24–29].

Accordingly, it is accepted that the probability of simultaneous pipe failures is practically zero. In this case, the probability pf_0 of the whole network working without failure is

$$pf_0 = 1 - \sum_{k=1}^L pf_k, \quad (2.12)$$

where k is a pipe counter; L is the total number of pipes in the network; pf_k is the failure probability of pipe k .

The value of pf_k can be obtained from empirical formulae as a function of pipe diameter and length [20, 27, 28, 30, 31].

Considering an average time for the duration of pipe failure, reliability R is defined as

$$R = \frac{1}{q^{\text{req}}} \left(q^{\text{nf}} pf_0 + \sum_{k=1}^L q^k pf_k \right), \quad (2.13)$$

where q^{req} is the total required demand by the network (the sum of all nodal demands); q^{nf} is the total flow delivered to the network when there are no failures; q^k is the total flow delivered to the network when pipe k fails. Again, R is a function of D , the vector of diameters, through the hydraulic model.

After this definition, it can be seen that reliability R represents the expected fraction of q^{req} that can be maintained for a certain time horizon, providing the network properties used for this reliability calculation are maintained.

By calling $r_0 = q^{nf} / q^{req}$ and $r_k = q^k / q^{req}$, as follows(2.13) can be written:

$$R = r_0 p f_0 + \sum_{k=1}^L r_k p f_k. \quad (2.14)$$

As WDNs should behave satisfactorily under normal conditions when there are no failures ($r_0 = 1$), it is worthwhile making a separate and specific analysis of their behavior under only failure states. Accordingly, the concept of *tolerance* to failure T has been introduced [22, 23] using the expression

$$T = \frac{R - r_0 p f_0}{1 - p f_0} = \frac{\sum_{k=1}^L r_k p f_k}{\sum_{k=1}^L p f_k}. \quad (2.15)$$

In this expression, the variables are related to the whole network, and T is a function of D . However, tolerance can also be formulated for each individual node if desired.

This tolerance to failure represents the expected q^{req} fraction that the network supplies as an average when it is in a state of failure. In other words, this index answers the question of how well the network behaves, on average, when a pipe is removed from service.

From (2.15), a very important conclusion can be derived: the value of tolerance is not influenced by the value of r_0 .

Kalungi and Tanyimboh [23] showed that despite the fact that tolerance is not an explicit measure of redundancy, the tolerance index is a good measure of the impact of redundancy. Moreover, tolerance seems to give an adequate inverse measure of network vulnerability, or of the vulnerability of the whole system if other components are included in the calculation. It is an inverse measure, because the greater the tolerance, the lesser the vulnerability.

In short, the reliability concept, as defined above, can be regarded as simply a measure of the behavior of the network under normal conditions: meaning that reliability is not a good measure of behavior under failure situations. This is because the term $r_0 p f_0$ from (2.15) is absolutely predominant. Moreover, tolerance T refers only to the time during which the network is in a failure state. The main aim in looping the network is to reduce the consequences of failures. Therefore, we will use both reliability and tolerance objectives in the optimal design of WDNs.

An additional factor considered by various authors (see, for example, [17]) is that both reliability and tolerance assessment depends on the real demand expected to be required at each node. Demands are considered not as fixed values but as random variables, and a fixed design demand will not be established a priori. However, it is usual to estimate design demands as a fixed value that is the result of multiplying an average demand (usually an estimated value of liters per person per day) by some coefficient reflecting expected peaks of demand.

3. Combining Swarm Optimization and Multiagent Paradigm for Multiobjective WDN Design

Given the complexity of the problem described above, we now develop suitable tools to handle the problem. Our approach is a synergetic combination of swarm intelligence

principles together with multiagent system properties aimed at solving the above multiobjective problems. Let us first briefly introduce the necessary details around multiobjective optimization.

In multiobjective optimization, the goal is to find the vector, X , in the decision or search space $S \subseteq \mathbb{R}^d$, of decision variables, x_1, \dots, x_d , that satisfy a set of constraints, and optimizes a vector function, $F(x) = (f_1(x), \dots, f_m(x))^t$ in the objective space $F(S) \subset \mathbb{R}^m$, with m components representing the various objective functions considered. As a consequence, a multiobjective optimization problem may be formulated as follows

$$\text{optimize } F(x) = (f_1(x), \dots, f_m(x))^t \quad (3.1)$$

subject to

$$\begin{aligned} g_i(x) &> 0, \quad i = 1, 2, \dots, k, \\ h_j(x) &= 0, \quad j = 1, 2, \dots, l, \end{aligned} \quad (3.2)$$

where k and l are inequality and equality constraints, respectively.

Both the decision and the objective spaces are multidimensional, and a change in the decision variables producing a positive increment in one of the components of F often simultaneously causes worse values in other components of F . If the objectives are conflicting in this way, the goal is to find, from all the sets of solutions satisfying the constraints, the set of solutions that yield optimal values with respect to all the objective functions. This set is called the Pareto optimal solution set, $P \subset S$, and its image $F(P)$ in the objective space is called the Pareto front [32]. This set represents a cost-benefit trade-off among the considered objectives and enables informed decision making.

Each solution in the Pareto optimal set is optimal because improvements in one of the components are not possible without impairing at least one of the other components. Two solutions are compared based on the concept of *dominance*. The concept of dominance (for a minimization problem) is concisely defined by stating that solution X dominates another solution Y , and we write $X \leq Y$ if $X \neq Y$ and X is not worse than Y for any of the objectives, that is,

$$X \text{ dominates } Y \text{ if } \{f_i(X) \leq f_i(Y), i = 1, \dots, m\}, \{\exists j, 1 \leq j \leq m : f_j(X) < f_j(Y)\}. \quad (3.3)$$

Two solutions are termed indifferent or incomparable if neither dominates the other. In general, the goal of a multiobjective optimization algorithm is to identify P and its image $F(P)$. However, finding solutions in P may be too difficult, or the Pareto optimal set may consist of a prohibitory large number of decision alternatives. In fact, what is frequently sought is an approximation of the global Pareto-optimal set of design solutions.

The design of a WDN is a large-scale combinatorial, nonlinear, multiobjective optimization problem, involving various types of decision variables and many complex implicit constraints, such as the hydraulic constraints already mentioned. There is no single search algorithm for solving such real-world optimization problems without compromising solution accuracy, computational efficiency, and problem completeness.

Classical methods of optimization involve the use of gradients or higher-order derivatives of the fitness function. But these methods are not well suited for many real-world problems since they are unable to process inaccurate, noisy, discrete, and complex data. Robust methods of optimization are often required to generate suitable results. Several works (e.g., [33–35]) have shown that evolutionary algorithms and, in particular, genetic algorithms are suitable for handling this type of problem.

Many researchers have shifted direction and embarked on the implementation of various evolutionary algorithms: genetic algorithms, ant colony optimization, particle swarm optimization, simulated annealing, shuffled complex evolution, harmony search, and memetic algorithms, among many others. These derivative-free global search algorithms have been shown to obtain better solutions for large network design problems. Recent examples of the use of evolutionary algorithms for multiobjective design of WDN include [36–38].

The advantages of the growing use of evolutionary algorithms in the optimal design of WDN include [5]

- (1) evolutionary algorithms can deal with problems in a discrete manner, which unlike other optimization methods, enables the use of naturally discrete variables and the use of the binary variables in yes/no decisions so frequently in many real-world problems;
- (2) evolutionary algorithms work with only the information of the objective function, and this prevents complications associated with the determination of the derivatives and other auxiliary information;
- (3) evolutionary algorithms are generic optimization procedures and can directly adapt to any objective function, even if it is not described by closed expressions, but by whole, complex procedures;
- (4) because evolutionary algorithms work with a population of solutions, various optimal solutions can be obtained, or many solutions can be obtained with values close to the optimal objective function, and this can be of great value from an engineering point of view;
- (5) an analysis of systems with various loading conditions or forcing terms can be performed within the optimal design process.

A particle swarm optimization-based environment has been developed by the authors that mimics the judgment of an engineer. It was built by using various prior features and improvements regarding swarm intelligence, multiagent systems, and the necessary adaptation to multiobjective performance, including human interaction.

3.1. Swarm Intelligence Approach

The first feature derives from the philosophy behind PSO (particle swarm optimization) [39]. It consists of a variant of the standard PSO that can deal with various types of variables [40], includes a mechanism for increased diversity [15, 41], and enables the self-management of the parameters involved so that engineers are spared the task of parameter selection and fine-tuning [16]. A concise description follows.

A swarm of M particles is initially randomly generated. A particle, X , is represented by its location in a d -dimensional subset, $S \subset \mathbb{R}^d$ (search space). Any set of values

of the d variables, determining the particle location, represents a candidate solution for the optimization problem. The optimal solution is then searched for by iteration. The performance of each particle is measured using one or more fitness functions, according to the problem in hand. During the process, a particle X is associated with three vectors;

- (i) current position, $X = (x_1 \dots x_d)$;
- (ii) best position, $Y = (y_1 \dots y_d)$, reached in previous cycles; and
- (iii) flight velocity $V = (v_1 \dots v_d)$, which makes it evolve.

The particle which is in the best position, Y^* , is identified in every iteration.

In each generation, the velocity of each particle is updated as in (3.4) based on its recent trajectory, its best encountered position, the best position encountered by any particle, and a number of parameters as follows: ω is a factor of inertia suggested in [42] that controls the impact of the velocity history on the new velocity; c_1 and c_2 are two positive acceleration constants, called the cognitive and social parameters, respectively,

$$V \leftarrow V + c_1 R_1(Y - X) + c_2 R_2(Y^* - X), \quad (3.4)$$

where R_1 and R_2 are $d \times d$ diagonal matrices with their in-diagonal elements randomly distributed within the interval $[0,1]$.

For discrete variables, we use

$$V \leftarrow \text{fix}(V + c_1 R_1(Y - X) + c_2 R_2(Y^* - X)), \quad (3.5)$$

where $\text{fix}(\cdot)$ is a function that takes the integer part of its argument.

Expressions (3.4) and (3.5) are used to calculate the particle's new velocity, a determination that takes into consideration three main terms: the particle's previous velocity; the distance of the particle's current position to its own best position; the distance of the particle's current position to the swarm's best experience (position of the best particle).

In each dimension, particle velocities are clamped to minimum and maximum velocities, which are user-defined parameters,

$$V_{\min} \leq V_j \leq V_{\max}, \quad (3.6)$$

in order to control excessive roaming by particles outside the search space. These very important parameters are problem dependent. They determine the resolution with which regions between the present position and the target (best so far) positions are searched. If velocities are too great, particles might fly through good solutions. On the other hand, if they are too slow then, particles may not explore sufficiently beyond locally good regions, becoming easily trapped in local optima and unable to move far enough to reach a better position in the problem space. Usually, V_{\min} is taken as $-V_{\max}$.

There is, however, a singular aspect regarding velocity bounds that must be taken into consideration so that the algorithm can treat both continuous and discrete variables in a balanced way. In [40], it was found that using different velocity limits for discrete and continuous variables produces better results.

Finally, the position of each particle is updated every generation. This is performed by adding the velocity vector to the position vector,

$$X \leftarrow X + V. \quad (3.7)$$

Thus, each particle or potential solution moves to a new position according to expression (3.7).

The main drawback of PSO is the difficulty in maintaining acceptable levels of population diversity while balancing local and global searches [43]; as a result, suboptimal solutions are prematurely obtained [44]. Some evolutionary techniques maintain population diversity by using some more or less sophisticated operators or parameters. Several other mechanisms for forcing diversity in PSO can be found in the literature [45–47]. In general, the random character that is typical of evolutionary algorithms adds a degree of diversity to the manipulated populations. Nevertheless, in PSO, those random components are unable to add sufficient diversity.

Frequent collisions of birds in the search space, especially with the leader, can be detected—as shown in [15]. This causes the effective size of the population to decrease and the algorithm's effectiveness to be consequently impaired. The study in [41] introduces a PSO derivative in which a few of the best birds are selected to check collisions, and colliding birds are randomly regenerated after collision. This random re-generation of the many birds that collide with the best birds has been shown to avoid premature convergence because it prevents clone populations from dominating the search. The inclusion of this procedure into PSO greatly increases diversity, as well as improving convergence characteristics and the quality of the final solutions.

The role of inertia, w , in (3.4) and (3.5) is considered critical for the convergence behavior of the PSO algorithm. Although inertia was constant in the early stages of the algorithm, it is currently allowed to vary from one cycle to the next. As inertia facilitates the balancing of global and local searches, it has been suggested that w could be allowed to adaptively decrease linearly with time, usually in a way that initially emphasizes global search and then, with each cycle of the iteration, increasingly prioritizes local searches [48]. A significant improvement in the performance of PSO, with decreasing inertia weight across the generations, is achieved by using the proposal in [49],

$$w = 0.5 + \frac{1}{2(\ln(k) + 1)}, \quad (3.8)$$

where k is the iteration counter.

In the variant, we propose that, the acceleration coefficients and the clamping velocities are neither set to a constant value, as in standard PSO, nor set as a time-varying function, as in adaptive PSO variants [50]. Instead, they are incorporated into the optimization problem [16]. Each particle is allowed to self-adaptively set its own parameters by using the same process used by PSO—and given by expressions (3.4) or (3.5), and (3.7). These three parameters are considered as three new variables that are incorporated into position vectors X . In general, if d is the dimension of the problem, and p is the number of self-adapting parameters, the new position vector for X will be

$$X = (x_1, \dots, x_d, x_{d+1}, \dots, x_{d+p}). \quad (3.9)$$

Clearly, these new variables do not enter the fitness function, but rather they are manipulated by using the same mixed individual-social learning paradigm used in PSO. Also, V and Y , which give the velocity and thus-far best position for the particle, increase their dimension, correspondingly.

By using expressions (3.4) or (3.5), and (3.7), each particle is additionally endowed with the ability to self-adjust its parameters by taking into account the parameters it had at its best position in the past, as well as the parameters of the leader, which facilitated this best particle's move to its privileged position. As a consequence, particles use their cognition of individual thinking and social cooperation to improve their positions, as well as improving the way they better their position by accommodating themselves to the best-known conditions, namely, their conditions and their leader's conditions when they achieved the thus-far best position.

Although the authors have applied this algorithm mainly to WDN design, it has proven very efficient in solving optimization problems in other fields [51–54].

3.2. Multiagent Paradigm Adoption

The emergent behavior of a PSO swarm is strongly reminiscent of the philosophy behind the multiagent (MA) paradigm [55, 56]. In an MA system each agent has a limited capacity and/or incomplete information to resolve a problem, and, therefore, has a limited view of the solution. There is no overall control of the system; values are decentralized, and the computation is asynchronous [55]. Each agent acting alone cannot solve the problem in all its entirety, but a group of agents, with the coexistence of different views, is better able to find a solution by interacting together. This idea can be clearly extrapolated to the case of multiobjective optimization, since the result of the many interactions occurring within an MA, as explained above, is an improved performance.

For the optimal design of WDNs, an MA system offers considerable added value because of the introduction of several agents with different visions of the evaluation of solutions for the same problem, so enabling a multiobjective optimization that is qualitatively much closer to reality. From a practical standpoint, the development of a multiobjective optimization process enables the combination of economic, engineering, and policy viewpoints when searching for a solution.

Taking into account the desirability of solving the optimal design of WDNs with a multiobjective approach and the benefits offered by MA systems, a departure from the standard behavior of particles in PSO must be performed. In addition to using the concept of dominance, various other aspects must also be restated.

3.3. Adaptation to Multiobjective Performance

Firstly, the concept of leadership in a swarm must be redefined. The most natural option is to select as leader the closest particle to the so-called *utopia point* in the objective space. The utopia point is defined as the point in the objective space whose components give the best values for every objective. The *utopia point* is an unknown point since the best value for every objective is something unknown at the start (and perhaps during the whole process). Accordingly, we use a dynamic approximation of this utopia point, termed *singular point*, which is updated with the best values found so far during the evolution of the algorithm

[38]. Even though this idea resembles the concept of *reference point* [57–59], it is simpler while effective.

Secondly, because each objective may be expressed in different units, it is necessary to make some regularization for evaluating distances in the objective space. Once a regularization mechanism has been enforced, to establish the distance between any two objective vectors, the Euclidean distance between them is calculated. Note that the worst and best objective values are not usually known a priori; they are updated while the solution space is explored.

Thirdly, arguably, the most interesting solutions are located near the singular point and not too far from the peripheral areas of the Pareto front. Therefore, instead of seeking a complete and detailed Pareto front, we may be more interested in precise details around the singular point. Nevertheless, situations can occur when unbalanced Pareto fronts develop with respect to the singular point. Consequently, poorly detailed sections on the Pareto front may appear to be worth exploring. It seems plausible that problem complexity is the cause of this asymmetry in many real-world, multiobjective optimization problems.

It is not easy to find a general heuristic rule for deciding which parts of the Pareto front should be more closely represented and how much detail the representation of the Pareto front should contain. Various ways of favoring the completeness of a Pareto front may be devised. We describe one possible approach based on dynamic population increases to raise the Pareto front density [60, 61] and another approach based on human-computer interaction to complete poorly represented areas of the Pareto front.

3.3.1. Increasing the Density of the Pareto Front

In the first approach, during the search process, swarms can increase their population when needed in order to better define the Pareto front; a particle whose solution already belongs to the Pareto front may, on its evolution, find another solution belonging to the front. In this situation, a new clone of the particle is placed where the new solution is found, thus increasing the density of particles on the Pareto front. Greater densities on the Pareto front must be restricted to the case where the new clone has at least one of its neighbors located further away than some minimal permissible distance in the objective space. It must be noted that two particles are considered to be neighbors when no other particle is located between them for at least one of the objectives considered in the problem.

3.3.2. Human-Computer Interaction

In the second approach, users are allowed to add new swarms for searching in the desired region of the objective space. The concept of a singular point is now extended to any desired point in the objective space for particles to search around.

Decisions are strongly dependent on the people solving the problem and on the problem itself. The user can specify additional points where the algorithm should focus the search and specify how much detail a region should contain. This must be achieved in real time during the execution of the algorithm. Once a new singular point is added, a new swarm is created with the same characteristics as the first created swarm. Swarms will run in parallel, but they share (and can modify) the information related to the Pareto set. Particles from any swarm can be added to the Pareto set. If the user changes the fixed values for a singular point, then the corresponding swarm selects a new leader considering the location of the new singular point.

Human interaction with the algorithm in real time also enables the incorporation of human behavior, so that the human becomes another member of the swarm by proposing new candidate solutions. Eventually, such a solution can be incorporated into the Pareto front or lead the behavior of a group of particles. User solutions will always be evaluated in the first swarm created. If a particle is being evaluated, then the user request waits until the evaluation of the particle is finished. If a solution proposed by the user is being evaluated, then any particle belonging to the first swarm should wait for evaluation. Once any solution is evaluated, the algorithm checks whether it could be incorporated in the Pareto front. Synchronization is effected among all the swarms in order to open access for managing the Pareto front. Proposed solutions could even become leaders of the swarm(s) if they are good enough. At this point, human behavior begins to have a proactive role during the evolution of the algorithm.

The participation of several human agents with different perspectives on a problem is very close to what happens in the practice of engineering decision making, where politicians, economists, engineers, and environmental specialists are involved in final decisions. The idea of incorporating user experience into the search process is a step forward in the development of computer-aided design.

The combination of various swarms within the same algorithm is efficient because it conducts a neighborhood search in which each of the swarms specializes, and the best improvement step in terms of Pareto optimality is followed to yield a new solution. The practice of incorporating different search mechanisms also reduces the probability of the search becoming trapped in local optima.

3.4. The Algorithm

In the approach presented, as explained above, new particles are used that are based on the behavior of particles in PSO. Swarms running in parallel may be distributed in different computers, and it must be ensured that the swarms can communicate amongst themselves—a peer-to-peer scenario would be a good choice for this task. The steps of the algorithm for every swarm may be summarized in Pseudocode 1.

The algorithm and its connection with EPANET2 (modified with the pressure-driven demand feature explained above) were implemented in a software program called WaterIng (<http://www.ingeniousware.net/>) [62], which was developed for water distribution system design and analysis. WaterIng is in constant development and may be downloaded from its website; the installation includes a file with network data as an example. A first step guide is also available to learn the main concepts of how to design a water distribution system using the software.

4. Case Studies

This software has been used to perform the design of the case studies shown below. The multiobjective model implemented by this software has shown robustness and good explanatory outcomes. Decision makers are provided with a set of informed solutions to select the best design with regard, for example, to available resources and/or other criteria.

Some parameters of the algorithm were established a priori for running the case studies; the initial population size was set equal to 20. The inertia weight was calculated using (3.8). Finally, fine-tuning the other parameters is performed by using the self-adaptive

- (1) Set up parameters and initialize the number of iterations to zero.
- (2) Generate a random population of M particles: $\{x_i(k)\}_{i=1}^M$
- (3) Evaluate the fitness of the particles and set the local best location for each particle equal to its current location.
- (4) Form the Pareto front and make a list of particles belonging to the front.
- (5) Build the singular point.
- (6) Find the closest particle to the singular point and establish it as swarm leader.
- (7) While not in termination-condition, do the following:
 - (a) Execute from $i = 1$ to number of particles.
 - Start
 - (i) Change the position of the particle:
 - Determine the inertia parameter $w(k)$, according to (3.8).
 - Calculate the new velocity, $v_i(k+1)$, for particle i according to (3.4) or (3.5).
 - Set a new position, $x_i(k+1)$, for particle i according to (3.7).
 - (ii) Calculate the new fitness function vector for particle i in its new position.
 - (iii) If the new fitness function vector for particle i dominates the fitness function vector that the particle had before moving to the new position; then set the new position as the best position currently found by particle i .
 - (iv) If particle i is in the list of particles belonging to the Pareto front then:
 - if the new fitness function vector may also be a point on the Pareto front and this new position has at least one of its neighbors located further than the minimal permissible distance from any of the objectives, then add a new particle j (a clone of i) with P_k and P_{kbest} located at the current position of i ;
 - else
 - try to add (if possible) the particle i (at its new position) to the Pareto front; if the particle is added, remove from the list any dominated solution; dominated clones are eliminated from the swarm.
 - (v) If particle i is closer to the singular point than any other particle in the swarm, then set particle i as the leader of the swarm with regard to the singular point.
 - (vi) If particle i is not currently the leader of the swarm, but coincides in position with the leader, then re-generate particle i randomly.
 - End
 - (b) Increase the iteration number.
- (8) Show the Pareto front and related results.

PSEUDOCODE 1

techniques described above. As a termination condition, we ran the algorithm until 600 iterations were completed without improvement. However, the figures presented in this work were taken during the first moments and not after reaching the number of iterations without improvements. An improvement is understood as any positive change in the approximated Pareto front that the algorithm obtains. It must be noted that even if the algorithm reaches its own termination condition, it could still be receiving requests from users or other swarms running in parallel; each swarm can, in addition, restart the search by itself when an update in its Pareto front is needed after the interaction with a user or another swarm.

4.1. Hanoi Network

This is a well-known problem, one of the most explored systems in the research literature, and it has been included in this paper for comparison purposes. In this problem, the

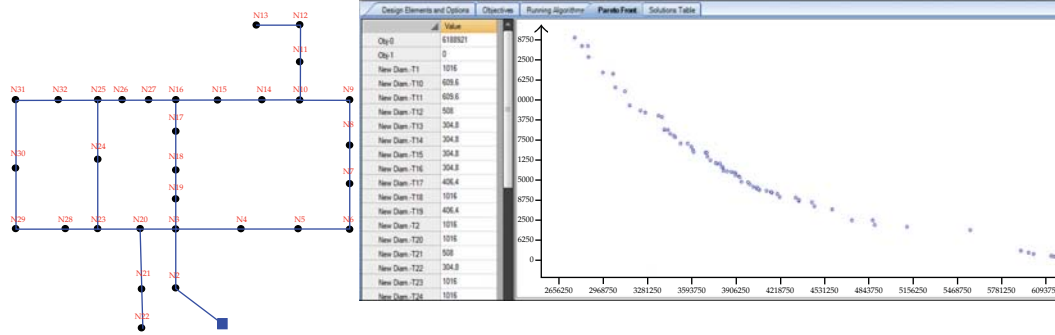


Figure 2: Hanoi network. Approximated Pareto front regarding investment and lack of pressure.

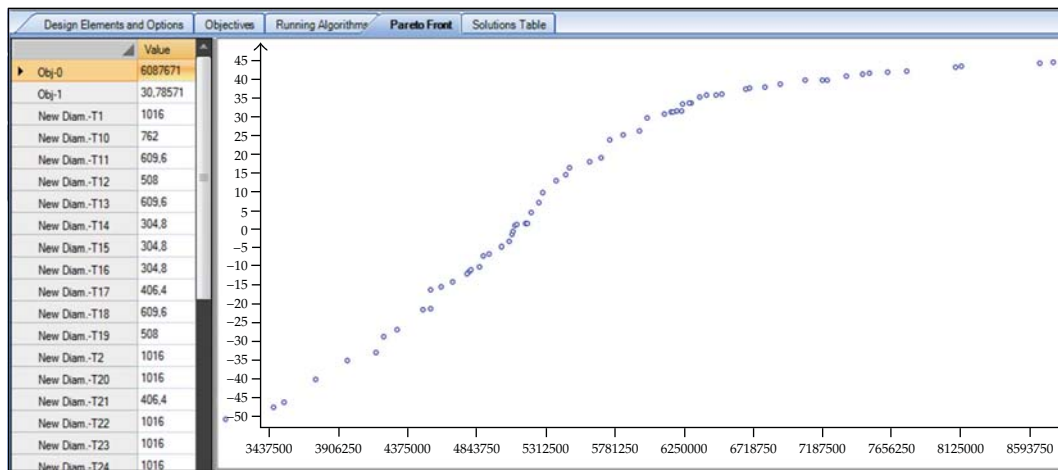


Figure 3: Approximated Pareto front regarding investment and minimum pressure in the network.

engineer seeks the minimum investment cost for a water network, constrained to have at least a minimum pressure value at demand nodes. This constraint was turned into an objective for considering a multiobjective approach: to find solutions minimizing the investment and minimizing the lack of pressure at demand nodes. More information about the original problem can be found in [63]. Figure 2 represents the network layout and an approximated Pareto front considering as objectives the minimization of investment costs and the minimization of the lack of pressure. The estimation of the lack of pressure was made without considering any failure condition in the network.

This problem was also run considering as objectives the minimization of the investment costs and the maximization of the minimum expected pressure in the network (see Figure 3).

All approximated Pareto fronts were obtained in less than 25 seconds (in a Pentium core2duo, 2 GB RAM). Although images were taken when the algorithm was still running (without reaching the termination condition), some similarities with results obtained in other works may be identified (see [7, 14–16, 64, 65] among others). From Figure 2, it can be seen that a solution without lack of pressure is found around 6.2×10^6 \$. After a zoom in the Pareto front it can be seen that the algorithm found a solution without lack of pressure and with a

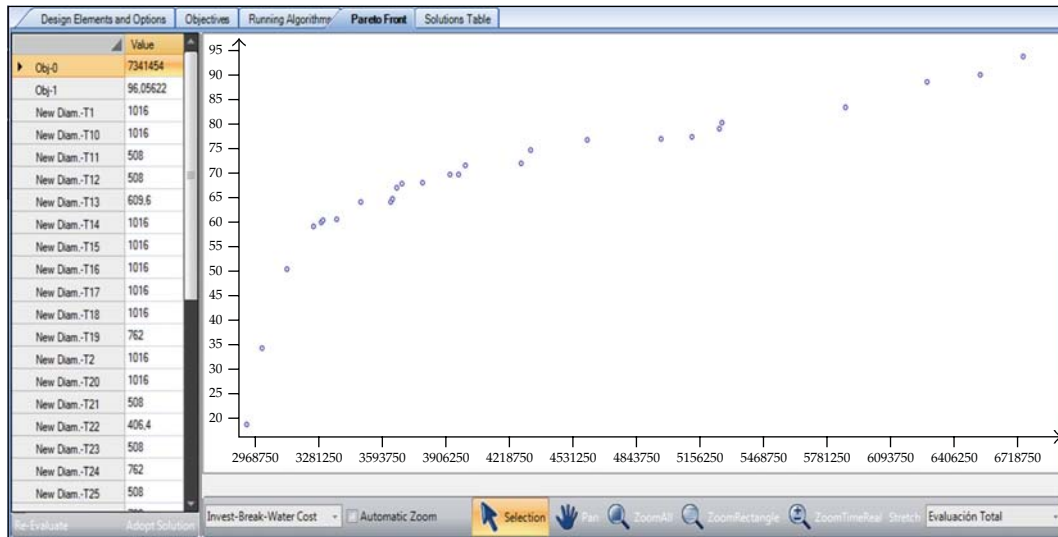


Figure 4: Approximated Pareto front regarding investment and reliability.

cost of 6.12×10^6 \$. This result is very close to the best results obtained by other authors for this problem under the same conditions.

Finally, in Figure 4, an approximated Pareto front considering as objectives the investment costs and the reliability of the network is represented.

4.2. Real Case I: Modified Sector of Lima, Peru

The second case study is a real-world design with three objectives: minimizing the investment cost, minimizing the lack of pressure at demand nodes, and minimizing additional costs caused by reliability problems. This case is a modification of a network designed in collaboration with Wasser SL, a company located at Madrid, Spain.

Results obtained in this design showed a good tolerance to failure conditions. Consideration of tolerance made it possible to find a solution (Figure 5, left) that could distribute all the required water with a pressure satisfying the requirement, even if failure conditions occur in any pipe. In contrast, in Figure 5 (centre and right) problems for the network designed without considering any tolerance to failure condition are presented. Red points indicate a pressure lower than the minimum requirement if the pipe marked with an arrows fails.

Figure 6 represents the solutions initiating the Pareto front. The best solution found for this project when considering a good performance under failure was just 3% more expensive than any solution obtained without consideration of tolerance.

4.3. Real Case II: Modified San José Town

This case was taken from studies developed in San José de las Lajas, Havana, Cuba. A modified variant of the network of this town (see Figure 7) was used for testing the algorithm.

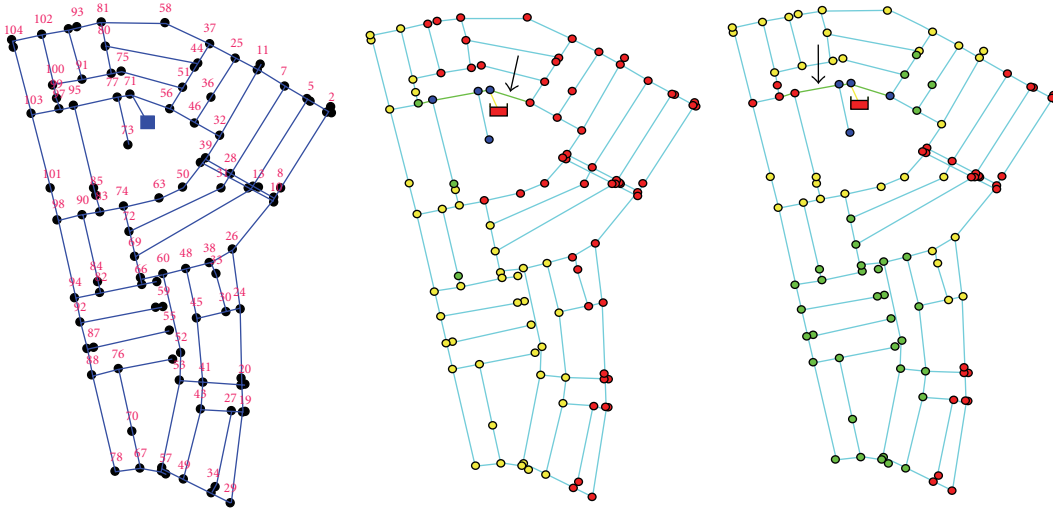


Figure 5: Lima sector, a modified real case example.

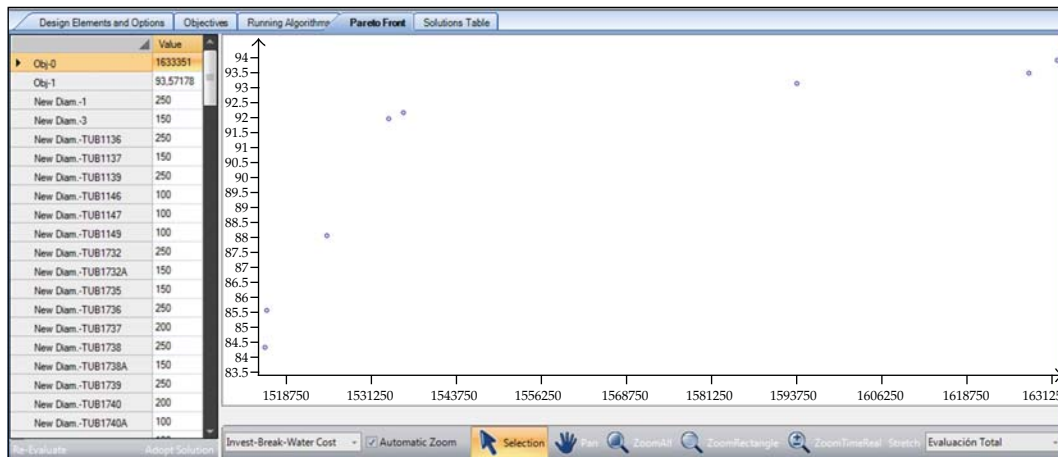


Figure 6: Approximated Pareto front regarding cost and tolerance to failure condition.

In this network, a significant investment is necessary for increasing the minimum pressure at demand nodes. The layout and configuration of the network do not contribute to good pressure distribution throughout the network. This system is currently working without distributing water 24 hours a day; various zones have been determined that receive water at specific moments of the day. Even if this system was designed anew, with the presented configuration and the proposed commercial pipes, the network would have pressure problems at various points. The addition of another tank and different layouts were proposed for analysis in future works. Figure 8 provides relevant information for sound decision making as it shows an approximated relation between investment cost and minimum pressure in the network.

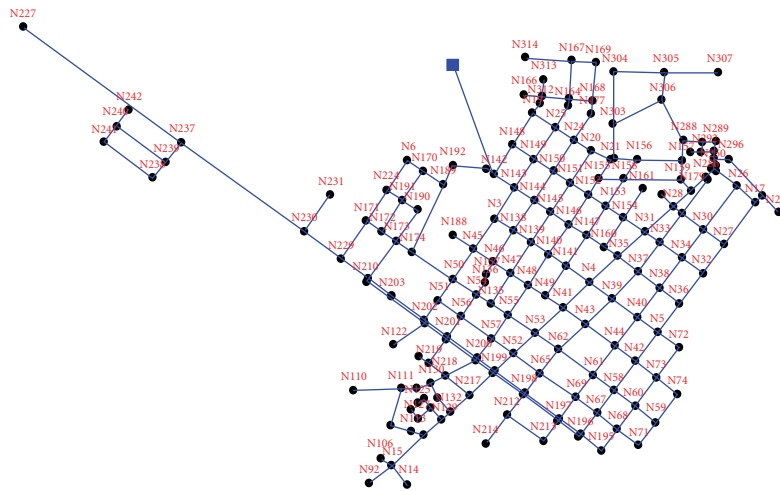


Figure 7: San José town, a modified real case example.

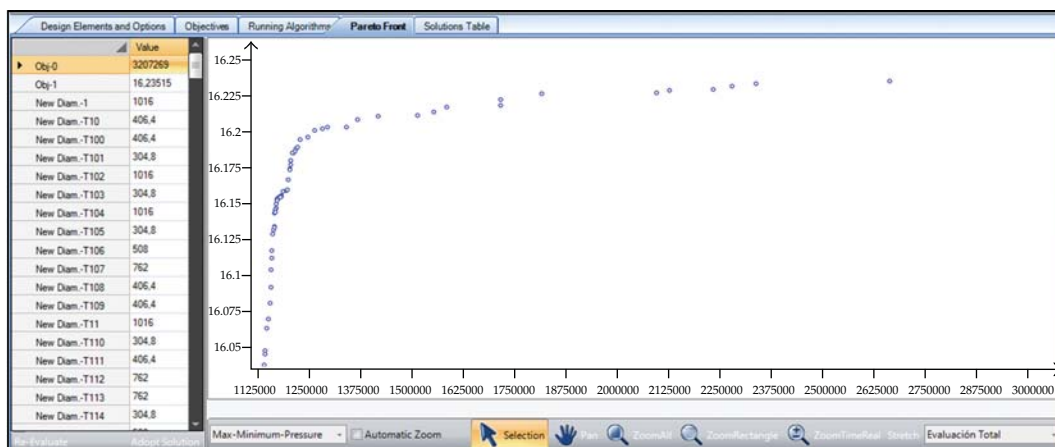


Figure 8: San José town. Approximated Pareto front regarding investment and minimum pressure in the network.

5. Conclusions

In this paper, one of the aspects that reflects the huge complexity of WDNs, namely, the design of these infrastructures, is addressed. We have described the various design elements that render the problem into a large-scale combinatorial, nonlinear, nonconvex, multiobjective optimization problem, involving various types of decision variables and many complex implicit constraints. We then argued that this type of problem is not accessible for classical optimization techniques and discussed the great interest and impact produced by the many evolutionary algorithms.

Based on PSO, we have developed the necessary tools to build an MA algorithm that has proven to be efficient for solving the stated problem. We described some features that substantially improve the searching ability of PSO, paying special attention to two aspects: increase in diversity and self-management of parameters. We then provided the necessary

adaptations to deal with multiobjective problems. We proposed the possibility that various swarms could explore different areas of the Pareto front. And finally, we have integrated human interaction into the process. This offers a special platform for finding solutions in a human-computer cooperative framework. Integrating the search capacity of algorithms with the ability of specialists to redirect the search towards specific points of interest—based on their experience in solving problems—results in a powerful collaborative system for finding solutions to complex engineering problems. Agents can profit from the creativity and ideas of human experts to improve their own solutions; and in turn, human experts can profit from the speed and search capabilities of artificial agents to explore broader solution spaces.

WaterIng is just a first step for engineers working in WDN decision making. The development of the software has not stopped with the contents of this paper; it continues to meet new challenges. Extensions to this work are possible for solving more complex problems, especially in the field of hydraulic engineering. The ideas presented in this paper can also be applied to other engineering fields or, in general, to problems where the search for optimal solutions needs the use of a computer.

One of the aspects we have not explicitly addressed in this paper is the partial stochastic character of the considered problem due to demand variations and the probability, or even the possibility from a fuzzy theory point of view, of the evolution (due to aging) of the roughness within the pipes. Future research topics could explore this aspect, perhaps using recently developed ideas regarding stochastic complex networks, as in [66–69].

Acknowledgments

This work has been developed with the support of the project IDAWAS, DPI2009-11591, of the Dirección General de Investigación of the Ministerio de Educación y Ciencia, and ACOMP/2010/146 of the Conselleria d'Educació of the Generalitat Valenciana. The first author is also indebted to the Universitat Politècnica de València for the sabbatical leave granted during the first semester of 2011. The use of English in this paper was revised by John Rawlins.

References

- [1] J. Izquierdo and R. Pérez-García, Eds., *Applications of Intelligent Data Analysis in Urban Supply Systems*, Universitat Politècnica de València, Valencia, Spain, 2011.
- [2] I. C. Goulter and A. V. Colas, "Quantitative approaches to reliability assessment in pipe networks," *Journal of Transportation Engineering*, vol. 112, no. 3, pp. 287–301, 1986.
- [3] I. C. Goulter and F. Bouchart, "Reliability-constrained pipe network model," *Journal of Hydraulic Engineering—ASCE*, vol. 116, no. 2, pp. 211–229, 1990.
- [4] T. M. Walski, Ed., *Advanced Water Distribution Modeling and Management*, Haestad Press, Waterbury, Conn, USA, 2003.
- [5] I. Montalvo, *Diseño óptimo de sistemas de distribución de agua mediante agent swarm optimization*, Ph.D. thesis, Universitat Politècnica de València, Valencia, Spain, 2011.
- [6] Y. Kleiner, B. J. Adams, and J. S. Rogers, "Water distribution network renewal planning," *Journal of Computing in Civil Engineering*, vol. 15, no. 1, pp. 15–26, 2001.
- [7] A. S. Matías, *Diseño de redes de distribución de agua contemplando la fiabilidad, mediante algoritmos genéticos*, Ph.D. thesis, Universidad Politécnica de Valencia, Valencia, Spain, 2003.
- [8] G. C. Dandy and M. O. Engelhardt, "Multi-objective trade-offs between cost and reliability in the replacement of water mains," *Journal of Water Resources Planning and Management*, vol. 132, no. 2, pp. 79–88, 2006.

- [9] J. Izquierdo, R. Pérez, and P. L. Iglesias, "Mathematical models and methods in the water industry," *Mathematical and Computer Modelling*, vol. 39, no. 11-12, pp. 1353–1374, 2004.
- [10] L. A. Rossman, *EPANET 2 User's Manual*, Environmental Protection Agency, Cincinnati, Ind, USA, 2000.
- [11] C. Xu and I. C. Goulter, "Simulation-based optimal design of reliable water distribution networks," in *Proceedings of the 3rd International Conference on Modeling and Simulation*, Victoria University of Technology, Melbourne, Australia, 1997.
- [12] Z. Y. Wu, R. H. Wang, T. Walski, S. Y. Yang, D. Bowdler, and C. C. Baggett, "Efficient pressure dependent demand model for large water distribution system analysis," in *Proceedings of the 8th Annual Water Distribution System Analysis Symposium*, Cincinnati, Ohio, USA, 2006.
- [13] O. Giustolisi, D. Savic, and Z. Kapelan, "Pressure-driven demand and leakage simulation for water distribution networks," *Journal of Hydraulic Engineering—ASCE*, vol. 134, no. 5, pp. 626–635, 2008.
- [14] I. Montalvo, J. Izquierdo, R. Pérez, and M. M. Tung, "Particle swarm optimization applied to the design of water supply systems," *Computers & Mathematics with Applications*, vol. 56, no. 3, pp. 769–776, 2008.
- [15] I. Montalvo, J. Izquierdo, R. Pérez, and P. L. Iglesias, "A diversity-enriched variant of discrete PSO applied to the design of water distribution networks," *Engineering Optimization*, vol. 40, no. 7, pp. 655–668, 2008.
- [16] I. Montalvo, J. Izquierdo, R. Pérez, and M. Herrera, "Improved performance of PSO with self-adaptive parameters for computing the optimal design of water supply systems," *Engineering Applications of Artificial Intelligence*, vol. 23, no. 5, pp. 727–735, 2010.
- [17] J. B. Martínez, "Cost and reliability comparison between branched and looped water supply networks," *Journal of Hydroinformatics—IWA*, vol. 12, no. 2, pp. 150–160, 2010.
- [18] I. C. Goulter, "Systems analysis in water-distribution network design: from theory to practice," *Journal of Water Resources Planning and Management—ASCE*, vol. 118, no. 3, pp. 238–248, 1992.
- [19] H. Park and J. Liebman, "Redundancy-constrained minimum-cost design of water-distribution nets," *Journal of Water Resources Planning and Management—ASCE*, vol. 119, no. 1, pp. 83–98, 1993.
- [20] D. Khomsi, G. A. Walters, A. R. D. Thorley, and D. Ouazar, "Reliability tester for water-distribution networks," *Journal of Computing in Civil Engineering—ASCE*, vol. 10, no. 1, pp. 10–19, 1996.
- [21] I. C. Goulter, T. M. Walski, L. W. Mays, A. B. A. Sekarya, R. Bouchart, and Y. K. Tung, "Reliability analysis for design," in *Water Distribution Systems Handbook*, L. W. Mays, Ed., McGraw-Hill, New York, NY, USA, 2000.
- [22] T. T. Tanyimboh, M. Tabesh, and R. Burrows, "Appraisal of source head methods for calculating reliability of water distribution networks," *Journal of Water Resources Planning and Management—ASCE*, vol. 127, no. 4, pp. 206–213, 2001.
- [23] P. Kalungi and T. T. Tanyimboh, "Redundancy model for water distribution systems," *Reliability Engineering and System Safety*, vol. 82, no. 3, pp. 275–286, 2003.
- [24] D. R. Morgan and I. C. Goulter, "Optimal urban water distribution design," *Water Resources Research*, vol. 21, no. 5, pp. 642–652, 1985.
- [25] G. A. Walters and J. Knezevic, "Discussion of "Reliability based optimization model for water distribution systems" by Su, Y., Mays, L. W., Duan, N., and Lansey, K.," *Journal of Hydraulic Engineering—ASCE*, vol. 115, no. 8, pp. 1157–1158, 1989.
- [26] G. V. Loganathan, M. P. Shah, and H. P. Sherali, "A two-phase network design heuristic for minimum cost water distribution systems under a reliability constraint," *Engineering Optimization*, vol. 15, no. 4, pp. 311–336, 1990.
- [27] F. Bouchart and I. Goulter, "Reliability improvements in design of water distribution networks recognizing valve location," *Water Resources Research*, vol. 27, no. 12, pp. 3029–3040, 1991.
- [28] R. Gupta and R. Bhave, "Reliability analysis of water-distribution systems," *Journal of Environmental Engineering*, vol. 120, no. 2, pp. 447–460, 1994.
- [29] C. Xu and I. C. Goulter, "Reliability-based optimal design of water distribution networks," *Journal of Water Resources Planning and Management—ASCE*, vol. 125, no. 6, pp. 352–362, 1999.
- [30] Y. Su, L. W. Mays, N. Duan, and K. E. Lansey, "Reliability based optimization model for water distribution systems," *Journal of Hydraulic Engineering—ASCE*, vol. 113, no. 12, pp. 1539–1556, 1987.
- [31] M. J. Cullinane, K. E. Lansey, and L. W. Mays, "Optimization-availability-based design of water-distribution networks," *Journal of Hydraulic Engineering—ASCE*, vol. 118, no. 3, pp. 420–441, 1992.
- [32] V. Pareto, *Cours d'Economie Politique*, Université de Lausanne, Lausanne, Switzerland, 1896.
- [33] D. E. Goldberg, *Genetic Algorithms in Search, Optimization and Machine Learning*, Addison-Wesley, Boston, Mass, USA, 1989.

- [34] K. Deb, *Multi-Objective Optimization Using Evolutionary Algorithms*, John Wiley & Sons, New York, NY, USA, 2001.
- [35] D. A. Savic, "Single-objective vs. multiobjective optimisation for integrated decision support integrated assessment and decision support," in *Proceedings of the 1st Biennial Meeting of the International Environmental Modeling and Software Society*, A. E. Rizzoli and A. J. Jakeman, Eds., vol. 1, pp. 7–12, University of Lugano, Lugano, Switzerland, 2002.
- [36] L. S. Vamvakieridou-Lyroudia, G. A. Walters, and D. A. Savic, "Fuzzy multiobjective optimization of water distribution networks," *Journal of Water Resources Planning and Management—ASCE*, vol. 131, no. 6, pp. 467–476, 2005.
- [37] G. C. Dandy and M. O. Engelhardt, "Multi-objective trade-offs between cost and reliability in the replacement of water mains," *Journal of Water Resources Planning and Management—ASCE*, vol. 132, no. 2, pp. 79–88, 2006.
- [38] I. Montalvo, J. Izquierdo, S. Schwarze, and R. Pérez-García, "Multi-objective particle swarm optimization applied to water distribution systems design: an approach with human interaction," *Mathematical and Computer Modelling*, vol. 52, no. 7-8, pp. 1219–1227, 2010.
- [39] J. Kennedy and R. C. Eberhart, "Particle swarm optimization," in *Proceedings of the IEEE International Conference on Neural Networks*, pp. 1942–1948, Piscataway, NJ, USA, 1995.
- [40] J. Izquierdo, I. Montalvo, R. Pérez, and V. S. Fuertes, "Design optimization of wastewater collection networks by PSO," *Computers & Mathematics with Applications*, vol. 56, no. 3, pp. 777–784, 2008.
- [41] M. Herrera, J. Izquierdo, I. Montalvo, and R. Pérez-García, "Injecting diversity into particle swarm optimization. Application to water distribution system design," *Advances in Computer Science and Engineering*, vol. 6, no. 2, pp. 159–179, 2011.
- [42] Y. F. Shi and R. C. Eberhart, "A modified particle swarm optimizer," in *Proceedings of the IEEE International Conference on Evolutionary Computation*, pp. 69–73, Anchorage, Alaska, USA, 1998.
- [43] C. A. C. Coello, G. B. Lamont, and D. A. van Veldhuizen, *Evolutionary Algorithms for Solving Multi-Objective Problems*, Springer, New York, NY, USA, 2007.
- [44] Y. Dong, J. Tang, B. Xu, and D. Wang, "An application of swarm optimization to nonlinear programming," *Computers & Mathematics with Applications*, vol. 49, no. 11-12, pp. 1655–1668, 2005.
- [45] P. J. Angeline, "Using selection to improve particle swarm optimization," in *Proceedings of the IEEE Congress on Evolutionary Computation*, pp. 84–89, Anchorage, Alaska, USA, 1998.
- [46] M. Løvbjerg, T. K. Rasmussen, and T. Krink, "Hybrid particle swarm optimiser with breeding and subpopulations," in *Proceedings of the Genetic and Evolutionary Computation Conference*, San Francisco, Calif, USA, 2001.
- [47] K. E. Parsopoulos, V. P. Plagianakos, G. D. Magoulas, and M. N. Vrahatis, "Stretching technique for obtaining global minimizers through particle swarm optimization," in *Proceedings of the Workshop on Particle Swarm Optimization*, Indianapolis, Ind, USA, 2001.
- [48] Y. Shi and R. C. Eberhart, "Empirical study of particle swarm optimization," in *Proceedings of the IEEE Congress on Evolutionary Computation*, Washington, DC, USA, 1999.
- [49] Y. X. Jin, H. Z. Cheng, J. I. Yan, and L. Zhang, "New discrete method for particle swarm optimization and its application in transmission network expansion planning," *Electric Power Systems Research*, vol. 77, no. 3-4, pp. 227–233, 2007.
- [50] M. S. Arumugam and M. V. C. Rao, "On the improved performances of the particle swarm optimization algorithms with adaptive parameters, cross-over operators and root mean square (RMS) variants for computing optimal control of a class of hybrid systems," *Applied Soft Computing*, vol. 8, no. 8, pp. 324–336, 2008.
- [51] J. Izquierdo, R. Minciardi, I. Montalvo, M. Robba, and M. Tavera, "Particle Swarm Optimization for the biomass supply chain strategic planning," in *Proceedings of the 4th Biennial Meeting, iEMSs 2008: International Congress on Environmental Modelling and Software*, pp. 1272–1280, Barcelona, Spain, 2008.
- [52] J. L. Díaz, M. Herrera, J. Izquierdo, I. Montalvo, and R. Pérez-García, "A particle swarm optimization derivative applied to cluster analysis," in *Proceedings of the 4th Biennial Meeting, iEMSs 2008: International Congress on Environmental Modelling and Software*, Barcelona, Spain, 2008.
- [53] J. Izquierdo, I. Montalvo, R. Pérez, and V. S. Fuertes, "Forecasting pedestrian evacuation times by using swarm intelligence," *Physica A*, vol. 388, no. 7, pp. 1213–1220, 2009.
- [54] M. Herrera, J. Izquierdo, I. Montalvo, J. García-Armengol, and J. V. Roig, "Identification of surgical practice patterns using evolutionary cluster analysis," *Mathematical and Computer Modelling*, vol. 50, no. 5-6, pp. 705–712, 2009.
- [55] K. P. Sycara, "Multiagent systems," *American Association for Artificial Intelligence—AI Magazine*, vol. 19, no. 2, pp. 79–92, 1998.

- [56] M. Wooldridge, *An Introduction to Multiagent Systems*, John Wiley & Sons, New York, NY, USA, 2002.
- [57] A. P. Wierzbicki, "The use of reference objectives in multiobjective optimization," in *Multiple Criteria Decision Making Theory and Application*, T. Gal and G. Fandel, Eds., Springer-Verlag, Berlin, Germany, 1980.
- [58] K. Deb, J. Sundar, N. U. B. Rao, and S. Chaudhuri, "Reference point based multiobjective optimization using evolutionary algorithms," *International Journal of Computational Intelligence Research*, vol. 2, no. 3, 2006.
- [59] J. Molina, L. V. Santana, A. G. Hernández-Díaz, C. A. Coello Coello, and R. Caballero, "G-dominance: reference point based dominance for multiobjective metaheuristics," *European Journal of Operational Research*, vol. 197, no. 2, pp. 685–692, 2009.
- [60] M. Reyes-Sierra and C. A. Coello Coello, "Multi-objective particle swarm optimizers: a survey of the state-of-the-art," *International Journal of Computational Intelligence Research*, vol. 2, no. 3, pp. 287–308, 2006.
- [61] G. Dupont, S. Adam, Y. Lecourtier, and B. Grilheres, "Multi objective particle swarm optimization using enhanced dominance and guide selection," *International Journal of Computational Intelligence Research*, vol. 4, no. 2, pp. 145–158, 2008.
- [62] I. Montalvo, J. B. Martínez-Rodríguez, J. Izquierdo, and R. Pérez-García, "Water distribution system design using agent swarm optimization," in *Proceedings of the 12th Annual Water Distribution Systems Analysis conference (WDSA '10)*, Tucson, Ariz, USA, 2010.
- [63] O. Fujiwara and B. Khang, "A two-phase decomposition method for optimal design of looped water distribution networks," *Water Resources Research*, vol. 26, no. 4, pp. 539–549, 1990.
- [64] D. A. Savic and G. A. Walters, "Genetic algorithms for least-cost design of water distribution networks," *Journal of Water Resources Planning and Management—ASCE*, vol. 123, no. 2, pp. 67–77, 1997.
- [65] A. C. Zecchin, A. R. Simpson, H. R. Maier, and J. B. Nixon, "Parametric study for an ant algorithm applied to water distribution system optimization," *IEEE Transactions on Evolutionary Computation*, vol. 9, no. 2, pp. 175–191, 2005.
- [66] Y. Liu, Z. Wang, J. Liang, and X. Liu, "Stability and synchronization of discrete-time Markovian jumping neural networks with mixed mode-dependent time delays," *IEEE Transactions on Neural Networks*, vol. 20, no. 7, pp. 1102–1116, 2009.
- [67] J. Liang, Z. Wang, and X. Liu, "State estimation for coupled uncertain stochastic networks with missing measurements and time-varying delays: The discrete-time case," *IEEE Transactions on Neural Networks*, vol. 20, no. 5, pp. 781–793, 2009.
- [68] Z. Wang, Y. Wang, and Y. Liu, "Global synchronization for discrete-time stochastic complex networks with randomly occurred nonlinearities and mixed time delays," *IEEE Transactions on Neural Networks*, vol. 21, no. 1, pp. 11–25, 2010.
- [69] B. Shen, Z. Wang, and X. Liu, "Bounded H-infinity synchronization and state estimation for discrete time-varying stochastic complex networks over a finite-horizon," *IEEE Transactions on Neural Networks*, vol. 22, no. 1, pp. 145–157, 2011.

Research Article

Enhancement of the Quality and Robustness in Synchronization of Nonlinear Lur'e Dynamical Networks

**Shiyun Xu,¹ Yong Tang,¹ Huadong Sun,¹
Ziguan Zhou,¹ and Ying Yang²**

¹ China Electric Power Research Institute, Beijing 100192, China

² The State Key Laboratory for Turbulence and Complex Systems, Department of Mechanics and Aerospace Technology, College of Engineering, Peking University, Beijing 100871, China

Correspondence should be addressed to Ying Yang, yy@water.pku.edu.cn

Received 28 June 2011; Accepted 9 September 2011

Academic Editor: Zidong Wang

Copyright © 2012 Shiyun Xu et al. This is an open access article distributed under the Creative Commons Attribution License, which permits unrestricted use, distribution, and reproduction in any medium, provided the original work is properly cited.

In order to improve the synchronous reliability and dependability of complex dynamical networks, methods need to be proposed to enhance the quality and robustness of the synchronization scheme. The present study focuses on the robust fault detection issue within the synchronization for a class of nonlinear dynamical networks composed by identical Lur'e systems. Sufficient conditions in terms of linear matrix inequalities (LMIs) are established to guarantee global robust $\mathcal{H}_2/\mathcal{H}_\infty$ synchronization of the network. Under such a synchronization scheme, the error dynamical system is globally asymptotically stable, the effect of external disturbances is suppressed, and at the same time, the network is sensitive to possible faults based on a mixed $\mathcal{H}_2/\mathcal{H}_\infty$ performance. The fault sensitivity \mathcal{H}_2 index, moreover, can be optimized via a convex optimization algorithm. The effectiveness and applicability of the analytical results are demonstrated through a network example composed by the Chua's circuit, and it shows that the quality and robustness of synchronization has been greatly enhanced.

1. Introduction

In daily life, many physical systems can be characterized by various complex network models whose nodes are the elements of the network and the edges represent the interactions among them [1]. Treated as typical versions of large-scale systems, the notion of complex dynamical networks has drawn more and more attentions in recent years [2, 3]. One of the interesting and significant phenomena in complex dynamical networks is the synchronization of all dynamical nodes, which is a kind of typical collective behaviors and basic motions

in nature [4–9]. Aiming at deriving global synchronization conditions, attempts have been made to consider the synchronization for a special class of networks composed of nonlinear Lur'e systems [10–12]. The main reason is that, in various fields of theory and engineering applications, vast amounts of nonlinear systems can be represented as the Lur'e type, including the Chua's circuit [13], the Goodwin model [14], and the swarm model [15]. Primary methods of dealing with such problems, among others, are developed under the framework of absolute stability theory [16].

In order to improve the synchronous reliability and dependability, methods have been proposed to enhance the quality and robustness of the synchronization scheme. Due to the instability and poor performance that caused by noise or disturbances, it is reasonable to take the noise phenomenon into account during the synchronization process of complex dynamical networks [17, 18]. On the other hand, research in fault diagnosis has been gaining increasing consideration worldwide in the past decades [19–23]. One of the key issues related to fault detection is concerned with its robustness. Large amounts of the relevant jobs have been done for the linear systems in order to examine the robust fault detection (RFD) problem (see [22, 23] and the references therein). In a recent work, we have investigated the robust fault sensitive synchronization of nonlinear Lur'e systems coupled in a master-slave fashion [24]. Similarly, in complex dynamical networks, since it is inevitable for faults to happen within each of the single node, a fault-free synchronization process cannot always be guaranteed. Even though, there is a few work concentrating upon the RFD problem of large-scale nonlinear systems, and hardly there is any previous work that brought the notion "fault" into physical aspects such as synchronization of nonlinear dynamical networks.

Based on these considerations, this present study considers the fault detection and disturbance rejection problem within robust synchronization for a class of dynamical networks. The network model is composed by identical nodes with each node being a perturbed nonlinear Lur'e system, while at the same time, subject to possible faults. The main challenge in evaluating the synchronization scheme is to distinguish failures from other disturbances, and accordingly, the $\mathcal{H}_- / \mathcal{H}_\infty$ paradigm is introduced [25]. For the purpose of description, the robustness objectives during synchronization are considered in virtue of the \mathcal{H}_∞ norm, while the fault sensitivity specifications are expressed by utilizing the formulation of \mathcal{H}_- index. In this manner, the closed-loop error system is asymptotically stable with the \mathcal{H}_∞ -norm from the disturbance input to controlled output reduced to a prescribed level, and at the same time, with the \mathcal{H}_- performance index maximized. By transforming the synchronization problem of dynamical networks into absolute stability problem of corresponding error systems as well as applying Lur'e system method in control theory [16], sufficient conditions to the global robust $\mathcal{H}_- / \mathcal{H}_\infty$ synchronization within nonlinear Lur'e networks are developed in terms of sets of linear matrix inequalities (LMI) [26]. Furthermore, the derived high-dimensional LMI condition is simplified into three groups of lower-dimensional LMIs, which are easier to handle. It should be pointed out that no linearization technique is involved through derivation of all the synchronization criteria.

The rest of the paper is organized as follows. Section 2 proposes the model to be examined in this study, and gives the mathematical formulations of the global robust $\mathcal{H}_- / \mathcal{H}_\infty$ synchronization problem to be solved. In Section 3, the global robust \mathcal{H}_∞ synchronization scheme of the networks is firstly studied, based on which the criteria on $\mathcal{H}_- / \mathcal{H}_\infty$ synchronization are then proposed in virtue of the LMI technique. Moreover, performance analysis of the network is also discussed in this part. The dynamical network composed by ten identical Chua's circuits is adopted as a numerical example in Section 4, and Section 5 closes the paper.

2. Notations and Preliminaries

The notations used in this study are fairly standard. $\mathbb{R}^{n \times n}$ is the set of $n \times n$ real matrices. For a matrix A , A^T denotes its transpose. He is the Hermit operator with $\text{He } A = A + A^T$. If A is a real symmetric negative definite matrix, it is shown by $A < 0$. $\text{diag}(\cdot)$ implies a diagonal or block-diagonal matrix. $A \otimes B$ indicates the Kronecker product of an $n \times m$ matrix A and a $p \times q$ matrix B , that is,

$$A \otimes B = \begin{pmatrix} a_{11}B & \cdots & a_{1m}B \\ \vdots & \ddots & \vdots \\ a_{n1}B & \cdots & a_{nm}B \end{pmatrix}. \quad (2.1)$$

If not explicitly stated, matrices are assumed to have compatible dimensions, and the terms replaced by $*$ of a matrix refer to the terms in a symmetric position that do not need to be written out.

2.1. Basic Knowledge on Lur'e Systems

The basic model of nonlinear Lur'e systems subject to input noise and possible faults considered in this paper is described by

$$\begin{aligned} \dot{x} &= A x + B(y) + B_d d_0 + B_f f_0, \quad y = C x, \\ z &= H x + D f, \end{aligned} \quad (2.2)$$

where $x \in \mathbb{R}^n$ is the state vector and $z \in \mathbb{R}^m$ represents the measurement output vector. $d_0 \in \mathbb{R}^p$ is an unknown input vector (including disturbance, uninterested fault as well as some norm-bounded unstructured model uncertainty) belonging to $L_2[0, +\infty)$, while $f_0 \in \mathbb{R}^q$ denotes the process, sensor, or actuator fault vector to be detected and isolated. Depending on specific situations under consideration, f_0 and d_0 can be modeled as different types of signals. The matrices A, B, C, D, B_d, B_f and H , are known constant matrices with appropriate dimensions. Nonlinearity $\gamma: \mathbb{R}^m \times \mathbb{R}_+ \rightarrow \mathbb{R}^m$ is continuous and locally Lipschitz in the first argument with $\gamma(0) = 0, \gamma = (\gamma_1^T, \dots, \gamma_m^T)^T$ and $\gamma(y) = (\gamma_1^T(y_1), \dots, \gamma_m^T(y_m))^T$, where the functions $\gamma_l(y_l), l = 1, 2, \dots, m$ are assumed to satisfy the following inequalities:

$$0 \leq \gamma_l(y_l) y_l \leq \gamma_{l1}^2 y_l^2, \quad l = 1, 2, \dots, m, \quad (2.3)$$

where $\gamma_{l1} \in \mathbb{R}, l = 1, 2, \dots, m$. Denoting $\Theta_0 = \text{diag}(\gamma_{11}, \gamma_{21}, \dots, \gamma_{m1})$, it is obvious to get

$$\gamma^T(y) (\gamma(y) - \Theta_0 y) \leq 0, \quad (2.4)$$

and the nonlinearity $\gamma(y)$ is said to be in the sector $[0, \Theta_0]$ if it satisfies (2.4).

Definition 2.1. Nonlinear system (2.2) is said to be absolutely stable with respect to the sector $[0, \Theta_0]$, if the equilibrium point $x = 0$ is globally asymptotically stable for the nonlinearity (y) satisfying (2.4).

In order to characterize the influence of the disturbance and fault input, several definitions are introduced.

Definition 2.2. Consider the following transfer function $d_0 \mapsto z$ of system (2.2):

$$K_{zd0}(s) \triangleq H (sI - A)^{-1} B_d. \quad (2.5)$$

Then its \mathcal{H}_∞ norm is defined as $\|K_{zd0}\|_\infty = \sup_{d_0 \in \mathbb{L}_2} \bar{\sigma}[K_{zd0}(j\omega)] = \sup_{d_0 \in \mathbb{L}_2} (\|K_{zd0}d_0\|_2 / \|d_0\|_2)$, where $\bar{\sigma}$ represents the maximal singular value.

Definition 2.3. For system (2.2), the transfer function from the input f_0 to output z is given as:

$$K_{zf0}(s) \triangleq H (sI - A)^{-1} B_f + D, \quad (2.6)$$

whose \mathcal{H}_- index is defined by $\|K_{zf0}(s)\|_-^{[0, \bar{\omega}]} \triangleq \inf_{\omega \in [0, \bar{\omega}]} \underline{\sigma}[K_{zf0}(j\omega)] = \inf_{f_0 \in \mathbb{L}_2} (\|K_{zf0}f_0\|_2 / \|f_0\|_2)$, where $\underline{\sigma}$ stands for the minimum singular value and $\bar{\omega}$ denotes the frequency band $[0, \bar{\omega}]$.

Remark 2.4. The \mathcal{H}_- index defined has been widely adopted to measure the sensitivity of residual to fault in the frequency domain. A system is said to possess a better level of RFD, if the \mathcal{H}_∞ norm of its transfer function from the disturbances to the performance variable is small; meanwhile, the \mathcal{H}_- index of the transfer function from fault to the output variable is large [19]. Various kinds of $\mathcal{H}_- / \mathcal{H}_\infty$ performance criteria have been proposed to determine the RFD issue [21], and the performance is mostly adopted as a trade-off between robustness and sensitivity. In this study, for the sake of simplicity, we will consider the case of maximizing the fault sensitivity $\|K_{rf}(s)\|_-$ with disturbance attenuation $\|K_{rd}(s)\|_\infty$ being a prescribed constant.

2.2. Dynamical Networks Composed of Lur'e Nodes

Consider a class of complex dynamical network model with each node being a general Lur'e system (2.2) shown as follows:

$$\dot{x}_i = A x_i + B (y_i) + \sum_{j=1}^N g_{ij} \Gamma z_j + B_d d_0 + B_f f_0, \quad y_i = C x_i, \quad (2.7)$$

$$z_i = H x_i + D f_0, \quad i = 1, 2, \dots, N,$$

where $x_i \in \mathbb{R}^n$ and $z_i \in \mathbb{R}^m$ are the state and measurement output of the i th node, respectively. d_0 and f_0 are defined as in system (2.2), which are supposed to be the same with respect to each node. The inner coupling matrix $\Gamma = (\gamma_{ij})_{n \times n}$ denotes the coupling pattern between two nodes. $G = (g_{ij})_{N \times N}$ is the outer coupling matrix, standing for the coupling configuration

of the network. If there is a connection between node i and node j ($i \neq j$), then $g_{ij} = g_{ji} = 1$; otherwise, $g_{ij} = g_{ji} = 0$ ($i \neq j$). The row sums of G are zero, that is, $\sum_{j=1, j \neq i}^N g_{ij} = -g_{ii}$, $i = 1, 2, \dots, N$. Let $\mathbf{y}_i = (y_{i1}, \dots, y_{im})^T \in \mathbb{R}^m$ and $(Y_i) = (y_{i1}, \dots, y_{im})^T \in \mathbb{R}^m$ with the following properties:

$$0 \leq y_{i1} y_{i1} \leq y_{i1}^2, \quad 0 \leq y_{i1} \leq 1, \quad i = 1, 2, \dots, N, \quad l = 1, 2, \dots, m. \quad (2.8)$$

Denote $\Theta_1 = \text{diag}(1, \dots, 1)$ then the nonlinear function (Y) belongs to the sector $[0, \Theta_1]$.

Lemma 2.5 (Wu [27]). *The eigenvalues of an irreducible matrix $G_0 = (G_{0ij}) \in \mathbb{R}^{N \times N}$ with $\sum_{j=1, j \neq i}^N G_{0ij} = -G_{0ii}$, $i = 1, 2, \dots, N$ satisfy the following.*

- (i) 0 is an eigenvalue of G_0 associated with the eigenvector $(1, 1, \dots, 1)^T$.
- (ii) If $G_{0ij} \geq 0$ for all $1 \leq i, j \leq N$, $i \neq j$, then the real parts of all eigenvalues of G_0 are less than or equal to 0 and all possible eigenvalues with zero part are 0 . In fact, 0 is its eigenvalue of multiplicity 1 .

Assume that the network (2.7) has no isolate clusters; namely, the network is connected. Under this circumstance, the coupling matrix G is symmetric and irreducible; hence it satisfies all the properties given in Lemma 2.5. Besides, suppose that the coupling matrix G has q distinct different eigenvalues $\lambda_1, \dots, \lambda_q$; then there exists a nonsingular matrix U with $U^T U = I_N$ such that $U^T G U = \Lambda$, where Λ is in the following form:

$$\Lambda = \text{diag} \left(\underbrace{1, 2, \dots, 2}_{m_2}, \underbrace{3, \dots, 3}_{m_3}, \dots, \underbrace{q, \dots, q}_{m_q} \right). \quad (2.9)$$

Here, $\lambda_1 = 0$ is the maximum eigenvalue of multiply 1 and λ_i is the eigenvalue of multiply m_i , $i = 2, 3, \dots, q$ satisfying $m_2 + \dots + m_q = N - 1$ and $\lambda_2 > \lambda_3 > \dots > \lambda_q$.

Definition 2.6. When $d_0 = f_0 = 0$, the dynamical network (2.7) is said to achieve global (asymptotical) synchronization if

$$\lim_{t \rightarrow \infty} \|x_i - x_s\|_2 = 0, \quad i = 1, 2, \dots, N, \quad (2.10)$$

where $\|\cdot\|_2$ means the Euclidean norm. $x_s \in \mathbb{R}^n$ is a solution of an isolate node given by

$$\begin{aligned} \dot{x}_s &= A x_s + B(Y_s), \quad Y_s = C x_s, \\ z_s &= H x_s, \end{aligned} \quad (2.11)$$

which can be an equilibrium point, a periodic orbit, or even a nonperiodic orbit.

From the properties of the internal coupling matrix G , the following condition holds:

$$\dot{x}_s = A x_s + B (C x_s) + \sum_{j=1}^N g_{ij} \Gamma H x_s. \quad (2.12)$$

Define error signals $e_i = x_i - x_s$ and residual signals $r_i = z_i - z_s$ for $i = 1, 2, \dots, N$. By subtracting (2.12) from (2.7), one arrives at the dynamics of synchronization residual error:

$$\dot{e}_i = A e_i + B (C e_i; x_s) + \sum_{j=1}^N g_{ij} \Gamma H e_j + B_d d_0 + B_f f_0 + \sum_{j=1}^N g_{ij} \Gamma D f_0, \quad (2.13)$$

$$r_i = H e_i + D f_0, \quad i = 1, 2, \dots, N,$$

where $(C e_i; x_s) = (C e_i + C x_s) - (C x_s)$. Let $(\cdot) = ({}^T_1(\cdot), \dots, {}^T_m(\cdot))^T$; it is not difficult to derive from (2.8) that for $c_1^T e \neq 0$, the nonlinear functions ${}_1(c_1^T e; x_s)$, $l = 1, 2, \dots, m$, satisfy the following sector restrictions:

$$0 \leq \frac{{}_1(c_1^T e; x_s)}{c_1^T e} = \frac{(c_1^T e_i + c_1^T x_s) - (c_1^T x_s)}{c_1^T e_i} \leq \theta_1, \quad i = 1, 2, \dots, N, \quad l = 1, 2, \dots, m, \quad (2.14)$$

which leads to

$${}_1(c_1^T e; x_s) ({}_1(c_1^T e; x_s) - \theta_1 c_1^T e_i) \leq 0, \quad i = 1, 2, \dots, N, \quad l = 1, 2, \dots, m, \quad (2.15)$$

and thus $(C e; x_s)$ also belongs to the sector $[0, \Theta_1]$.

Remark 2.7. Based on the basic knowledge of synchronization, the residual error dynamics must be asymptotically stable in order for the whole process to work. Note that the dynamics of the residual error signal r depends not only on f_0, d_0 , and (y) but also on the states of each isolated node x_j . In consequence, this study aims at ensuring the residual error dynamical system to be sensitive to possible faults in the regard of \mathcal{H}_∞ index, but the error dynamics also remain robustly asymptotically stable to external disturbance in the \mathcal{H}_∞ sense. Under such circumstances, the dynamical network composed of Lur'e nodes is said to achieve global synchronization with a guaranteed $\mathcal{H}_\infty / \mathcal{H}_\infty$ performance.

Reformulating system (2.13) in virtue of the Kronecker product [28] as

$$\begin{aligned} \dot{e} &= (\mathbb{I}_N \otimes A + G \otimes \Gamma H) e + (\mathbb{I}_N \otimes B) \Phi((\mathbb{I}_N \otimes C) e; X_s) + (\mathbb{I}_N \otimes B_d) d + (\mathbb{I}_N \otimes B_f + G \otimes \Gamma D) f \\ &\triangleq \bar{A} e + \bar{B} \Phi(\bar{C} e; X_s) + \bar{B}_d d + \bar{B}_f f, \\ r &= (\mathbb{I}_N \otimes H) e + (\mathbb{I}_N \otimes D) f \triangleq \bar{H} e + \bar{D} f, \end{aligned} \quad (2.16)$$

where

$$\begin{aligned}
 e &= \begin{pmatrix} e_1 \\ e_2 \\ \vdots \\ e_N \end{pmatrix} \in \mathbb{R}^{N \times n}, & d &= \begin{pmatrix} d_0 \\ d_0 \\ \vdots \\ d_0 \end{pmatrix} \in \mathbb{R}^{N \times p}, & f &= \begin{pmatrix} f_0 \\ f_0 \\ \vdots \\ f_0 \end{pmatrix} \in \mathbb{R}^{N \times q}, \\
 \Phi(\bar{C}; X_s) &= \begin{pmatrix} (C e_1; x_s) \\ (C e_2; x_s) \\ \vdots \\ (C e_N; x_s) \end{pmatrix} \in \mathbb{R}^{N \times m}, & X_s &= \begin{pmatrix} x_s \\ x_s \\ \vdots \\ x_s \end{pmatrix} \in \mathbb{R}^{N \times n},
 \end{aligned} \tag{2.17}$$

with $\Theta = \mathbb{I}_N \otimes \Theta_1 \in \mathbb{R}^{N \times m} > 0$ and $\Phi(\bar{C}; X_s)$ belonging to the sector $[0, \Theta]$. accordingly, the residual error dynamical system (2.16) can be treated as an N n -dimensional nonlinear Lur'e system, and the \mathcal{L}_- / \mathcal{L}_∞ synchronization of the nonlinear dynamical networks (2.7) can be transformed into the performance analysis and stabilization problem of the corresponding residual error dynamics (2.16).

For system (2.16), the transfer function $d \mapsto r$ is given by $K_{rd}(s) \triangleq \bar{H}(sI - \bar{A})^{-1} \bar{B}_d$, while $K_{rf}(s) \triangleq \bar{H}(sI - \bar{A})^{-1} \bar{B}_f + \bar{D}$ denotes the transfer function $f \mapsto r$. Specifically speaking, the main objective of this present study is to determine under what condition the residual error dynamics (2.16) could be asymptotically stable and, at the same time, satisfy the following conditions:

$$\|K_{rf}(s)\|_- > \gamma, \quad \|K_{rd}(s)\|_\infty < \gamma, \tag{2.18}$$

where γ is a prescribed positive constant, and γ is a constant to be optimized. By applying the well-known Parseval theorem to the frequency-domain expressions (2.18), where the ratios \mathcal{L}_∞ norm and \mathcal{L}_- index are presented in Definitions 2.2 and 2.3, respectively, we arrive at the equivalent statements as follows:

$$\mathcal{J}_1 = \int_0^\infty \left[r(t)^T r(t) - \gamma^2 d^T(t) d(t) \right] dt < 0, \tag{2.19}$$

$$\mathcal{J}_2 = \int_0^\infty \left[r(t)^T r(t) - \gamma^2 f^T(t) f(t) \right] dt > 0. \tag{2.20}$$

Accordingly, the definition of robust \mathcal{L}_- / \mathcal{L}_∞ synchronization is derived as follows.

Definition 2.8. The dynamical networks composed of nonlinear Lur'e nodes in (2.7) are said to achieve global robust \mathcal{L}_- / \mathcal{L}_∞ synchronization with disturbance attenuation γ and fault sensitivity γ over the frequency range $[0, \bar{\omega}]$ (where $\bar{\omega}$ could be both finite and infinite), if with zero disturbance and zero fault, the synchronization residual error signal (2.16) is asymptotically stable, while with zero initial condition and given constants $\gamma > 0$, $\gamma > 0$, conditions (2.19)-(2.20) hold.

3. Main Results

The intention of this part is to investigate the fault sensitivity as well as disturbance rejection ability of the complex dynamical network (2.7). In order to quantify these two performance indices, one borrows the concept of \mathcal{H}_∞ -index and \mathcal{H}_∞ -norm defined in the previous section.

3.1. Global \mathcal{H}_∞ Synchronization of Nonlinear Lur'e Networks

In this subsection, we first consider the case that there is no fault existed in the network by extending previous results on \mathcal{H}_∞ synchronization between two identical Lur'e systems to that of nonlinear Lur'e dynamical networks. Accordingly, the network model is described by

$$\begin{aligned} \dot{x}_i &= A x_i + B \left(Y_i \right) + \sum_{j=1}^N G_{ij} \Gamma z_j + B_d d_0, \quad Y_i = C x_i, \\ z_i &= H x_i, \quad i=1,2,\dots,N, \end{aligned} \quad (3.1)$$

and the corresponding error dynamics in form of Kronecker product is expressed as

$$\begin{aligned} \dot{e} &= \bar{A} e + \bar{B} \Phi(\bar{C} e; X_s) + \bar{B}_d d, \\ r &= \bar{H} e. \end{aligned} \quad (3.2)$$

The disturbance rejection problem within the synchronization of nonlinear dynamical network (3.1) is summarized in the following definition.

Definition 3.1. Given constant scalar $\gamma > 0$, the dynamical network (3.1) is said to achieve global robust \mathcal{H}_∞ synchronization, if system (3.2) is globally asymptotically stable with zero disturbance, and meanwhile, the performance index (2.19) is satisfied with zero initial conditions.

The robust \mathcal{H}_∞ synchronization can be determined in virtue of the following criterion.

Theorem 3.2. Suppose that $\gamma > 0$ is a prescribed constant. For a given scalar μ , if there exist positive-definite matrices $P = P^T > 0$, diagonal matrices $\Delta_1 = \text{diag}(\mu_1, \dots, \mu_m) > 0$, $\Pi_1 = \text{diag}(\mu_1, \dots, \mu_m) > 0$, and $\Omega_1 = \text{diag}(\mu_1, \dots, \mu_m) > 0$, and matrices \bar{Q}_1 and \bar{Q}_2 such that the following LMI

$$\Xi_1 = \begin{pmatrix} -\text{He}(\bar{Q}_1 \bar{A}) + \bar{H}^T \bar{H} \bar{C}^T \Theta \Delta - \bar{Q}_1 \bar{B} \bar{P} + \bar{Q}_1 - \bar{A}^T \bar{Q}_2^{-T} \bar{C}^T \Theta \Omega & -\bar{Q}_1 \bar{B}_d \\ * & -\text{He} \Delta & -\bar{B}^T \bar{Q}_2^{-T} & 0 & 0 \\ * & * & \text{He} \bar{Q}_2 & \bar{C}^T \Pi & -\bar{Q}_2 \bar{B}_d \\ * & * & * & -\text{He} \Omega & 0 \\ * & * & * & * & -\gamma^2 \mathbf{I} \end{pmatrix} < 0 \quad (3.3)$$

holds, where $\Delta = \mathbb{I}_N \otimes \Delta_1, \Pi = \mathbb{I}_N \otimes \Pi_1$, and $\Omega = \mathbb{I}_N \otimes \Omega_1$, then the dynamical network (3.1) achieves global robust \mathcal{H}_∞ synchronization with disturbance attenuation γ .

Proof. See Appendix A. \square

Remark 3.3. Theorem 3.2 has provided a sufficient condition for the global robust \mathcal{H}_∞ synchronization of nonlinear Lur'e networks by introducing slack matrices \bar{Q}_1 and \bar{Q}_2 into LMI (3.3). It is thus expected that Theorem 3.2 will be less conservative than some existing results due to the increasing freedom of these slack variables [29]. With the derived \mathcal{H}_∞ synchronization conditions on Lur'e networks, the fault detection issue will then be examined in the next subsection. However, if the number of nodes is large, condition (3.3) would become a high-dimensional LMI, which is rather tedious to verify. To this end, both of these criteria will be further simplified to the test of three groups of lower-dimensional LMIs.

3.2. Fault Detection within Global \mathcal{H}_∞ Synchronization

The RFD within a synchronization configuration can be treated as a multiple objective design task; that is, the design objective is not only being as sensitive as possible to faults such that early detection of faults is possible, but on the other hand, the sensitivity of possible faults is maximized, also suppressing the effect of disturbances and modeling errors on the synchronization error and subsequently on the residual, in order to prevent the synchronization process from being destroyed. Next theorem gives an LMI formulation for global robust $\mathcal{H}_- / \mathcal{H}_\infty$ synchronization.

Theorem 3.4. Suppose that $\gamma > 0$, $\beta > 0$ are prescribed constant scalars. For a given constant α , if there exist a positive-definite matrix $P = P^T > 0$, diagonal matrices $\Delta_1 = \text{diag}(\delta_{11}, \dots, \delta_{1m}) > 0$, $\Pi_1 = \text{diag}(\pi_{11}, \dots, \pi_{1m}) > 0$, and $\Omega_1 = \text{diag}(\omega_{11}, \dots, \omega_{1m}) > 0$, and matrices \bar{Q}_1 and \bar{Q}_2 such that LMIs (3.3) as well as

$$\Xi_2 = \begin{pmatrix} -\text{He}(\bar{Q}_1 \bar{A}) - \bar{H}^{-T} \bar{H}^{-T} \bar{C}^T \Theta \Delta - \bar{Q}_1 \bar{B} \bar{P} + \bar{Q}_1 - \bar{A}^{-T} \bar{Q}_2^{-T} \bar{C}^T \Theta \Omega & -\bar{H} \bar{D} - \bar{Q}_1 \bar{B}_f \\ * & -\text{He} \Delta & -\bar{B}^{-T} \bar{Q}_2^{-T} & 0 & 0 \\ * & * & \text{He} \bar{Q}_2 & \bar{C}^T \Pi & -\bar{Q}_2 \bar{B}_f \\ * & * & * & -\text{He} \Omega & 0 \\ * & * & * & * & 2\mathbb{I} - \bar{D}^{-T} \bar{D} \end{pmatrix} < 0 \quad (3.4)$$

hold, then the dynamical network in (2.7) achieves global robust $\mathcal{H}_- / \mathcal{H}_\infty$ synchronization with disturbance attenuation γ and fault sensitivity β .

Proof. See Appendix B. \square

Theorem 3.5. Suppose that $\alpha_i > 0$ and $\beta_i > 0$ are given scalars. If there exist matrices $W_i > 0, V_i$, and diagonal matrices $\Delta_1 > 0, \Pi_1 > 0$, and $\Omega_1 > 0$ such that the following conditions for $i = 1, 2$ and α_i hold:

$$\begin{pmatrix} Y_{11} + H^T H & C^T \Theta_1 \Delta_1 - V_i B & Y_{31} & C^T \Theta_1 \Omega_1 & -V_i B_d \\ * & -\text{He} \Delta_1 & -B^T V_i^T & 0 & 0 \\ * & * & \text{He} V_i & C^T \Pi_1 & -V_i B_d \\ * & * & * & -\text{He} \Omega_1 & 0 \\ * & * & * & * & -2I \end{pmatrix} < 0, \quad (3.5)$$

$$\begin{pmatrix} Y_{11} - H^T H & C^T \Theta_1 \Delta_1 - V_i B & Y_{31} & C^T \Theta_1 \Omega_1 & -H D - V_i B_f - \alpha_i V_i \Gamma D \\ * & -\text{He} \Delta_1 & -B^T V_i^T & 0 & 0 \\ * & * & \text{He} V_i & C^T \Pi_1 & -V_i B_f - \alpha_i V_i \Gamma D \\ * & * & * & -\text{He} \Omega_1 & 0 \\ * & * & * & * & 2I - D^T D \end{pmatrix} < 0, \quad (3.6)$$

where $Y_{11} = -\text{He}(V_i A + \alpha_i V_i \Gamma H)$ and $Y_{31} = W_i + V_i - A^T V_i^T - \alpha_i H^T \Gamma^T V_i^T$, then the conditions given in Theorem 3.4 are ensured.

Proof. See Appendix C. □

Corollary 3.6. For a constant α_i , let $\beta_i > 0$ and $\gamma_i > 0$ be prescribed constant scalars. The dynamical network (2.7) is said to achieve global robust $\mathcal{L}_2 / \mathcal{L}_\infty$ synchronization with disturbance attenuation β_i and fault sensitivity γ_i , if there exist matrices $W_i > 0, V_i \Gamma_i$, and diagonal matrices $\Delta_1 > 0, \Omega_1 > 0, \Pi_1 > 0$ such that the LMI conditions (3.5)-(3.6) hold for $i = 1, 2$ and α_i (corresponding to the largest, second largest, and smallest eigenvalues, resp.).

Remark 3.7. If the number of nodes N is large, the $\mathcal{L}_2 / \mathcal{L}_\infty$ synchronization criterion of the dynamical network would become a group of LMIs with rather high dimensions. In order to tackle this problem, the synchronization of the $nN \times nN$ -dimensional network has been disposed in a lower n -dimensional space through verifying three groups of n -dimensional LMIs in Corollary 3.6, and the derived conditions are quite convenient to use.

As an immediate consequence, we arrive at the simplified criterion for global robust \mathcal{L}_∞ synchronization of nonlinear dynamical network (3.1) summarized as in the following corollary.

Corollary 3.8. For a constant α_i , let $\beta_i > 0$ and $\gamma_i > 0$ be prescribed constant scalars. If there exist matrices $W_i > 0, V_i \Gamma_i$, and diagonal matrices $\Delta_1 > 0, \Omega_1 > 0, \Pi_1 > 0$ such that the LMIs (3.5) for $i = 1, 2$ and α_i are feasible, then the dynamical network (2.7) is said to achieve global robust \mathcal{L}_∞ synchronization.

3.3. \mathcal{L}_- / \mathcal{L}_∞ Performance Analysis

It comes from Corollary 3.6 that the \mathcal{L}_- / \mathcal{L}_∞ synchronization within a dynamical network can be cast into that of three sets of independent systems whose dimensions are the same as that of each isolate node. Namely, if the following systems

$$\begin{aligned} \dot{e}_i &= (A + \Gamma H) e_i + B (C e_i) + (B_f + \Gamma D) f_0 + B_d d_0, \\ r_i &= H e_i + D f_0, \end{aligned} \quad (3.7)$$

satisfy (3.5)-(3.6) for $i = 1, 2$ and \mathcal{G} , then the conditions given in Definition 2.8 will be guaranteed. Suppose the transfer function of system (3.7) from $d_0 \mapsto r_i$ and $f_0 \mapsto r_i$ for $i = 1, 2, \dots, N$ as K_{rdi} and K_{rfi} , respectively. Then denote

$$\begin{aligned} K_{rd} &= \text{diag}(K_{rd1}, \dots, K_{rdN}), \\ K_{rf} &= \text{diag}(K_{rf1}, \dots, K_{rfN}), \end{aligned} \quad (3.8)$$

where K_{rd} and K_{rf} are in the following form:

$$\begin{aligned} K_{rd} &= (\mathbb{I}_N \otimes H) (s\mathbb{I} - \mathbb{I}_N \otimes A - \Lambda \otimes \Gamma H)^{-1} (\mathbb{I}_N \otimes B_d), \\ K_{rf} &= (\mathbb{I}_N \otimes H) (s\mathbb{I} - \mathbb{I}_N \otimes A - \Lambda \otimes \Gamma H)^{-1} (\mathbb{I}_N \otimes B_f - \Lambda \otimes \Gamma D) + (\mathbb{I}_N \otimes D). \end{aligned} \quad (3.9)$$

On the other hand, consider the following system:

$$\begin{aligned} \dot{e} &= (\mathbb{I}_N \otimes A + \Lambda \otimes \Gamma H) e + (\mathbb{I}_N \otimes B) \Phi((\mathbb{I}_N \otimes C) e; X_s) + (\mathbb{I}_N \otimes B_d) d + (\mathbb{I}_N \otimes B_f + \Lambda \otimes \Gamma D) f \\ r &= (\mathbb{I}_N \otimes H) e + (\mathbb{I}_N \otimes D) f, \end{aligned} \quad (3.10)$$

where $e = (e_1^T, \dots, e_N^T)^T$ and $r = (r_1^T, \dots, r_N^T)^T$. It can be found that the transfer functions from $d \mapsto r$ and $f \mapsto r$ of system (3.10) are just those defined in (3.8). Moreover, by carrying out unitary transformation, K_{rd} is similar to K_{rd} , and so do K_{rf} and K_{rf} . Recall the definition of the \mathcal{L}_∞ norm and \mathcal{L}_- index previously stated in Definitions 2.2 and 2.3; then we arrive at the following relationships between the \mathcal{L}_∞ norms of K_{rd} and K_{rdi} as well as the \mathcal{L}_- indexes of K_{rf} and K_{rfi} for $i = 1, 2, \dots, N$:

$$\begin{aligned} \|K_{rd}\|_\infty &= \|K_{rd}\|_\infty = \max_{i=1, \dots, N} \|K_{rdi}\|_\infty, \\ \|K_{rf}\|_- &= \|K_{rf}\|_- = \min_{i=1, \dots, N} \|K_{rfi}\|_-. \end{aligned} \quad (3.11)$$

Conditions (3.11) show that the \mathcal{L}_∞ norm of the transfer function from $d \mapsto r$ in (2.16) equals to the maximum of those of the N systems (3.7), whilst the corresponding \mathcal{L}_- index is the minimum value within those of (3.7). Accordingly, the RFD of the network (2.7) can be cast into those of (3.7); thus we have the following corollary.

Corollary 3.9. For a given scalar $\epsilon > 0$, the performance indexes of the dynamical network (2.7) satisfy $\|K_{rd}\|_\infty < \epsilon$, and $\|K_{rf}\|_\infty > \epsilon$, if $\max_{i=1,\dots,N} \|K_{rdi}\|_\infty < \epsilon$ and $\min_{i=1,\dots,N} \|K_{rfi}\|_\infty > \epsilon$ hold in the decoupled systems (3.7) for $i=1,2,\dots,N$.

The following corollary presents a method of deriving the maximum value of fault sensitivity and, at the same time, suppresses the external disturbance to a prescribed level for the global robust \mathcal{H}_∞ synchronization of network (2.7).

Corollary 3.10. The nonlinear dynamical networks (2.7) are said to achieve global synchronization with guaranteed \mathcal{H}_∞ performance γ and the maximum fault detection sensitivity $\beta_0 = \sqrt{\gamma}$, where γ is the global minimum of the following generalized eigenvalue minimization problem with respect to matrices $W_i > 0, V_i$ for $i = \{1, 2, \dots, N\}$ as well as diagonal matrices $\Delta_1 > 0, \Pi_1 > 0$, and $\Omega_1 > 0$:

$$\min - \left(\begin{array}{cccc} Y_{11} - H^T H & C^T \Theta_1 \Delta_1 - V_i B & Y_{13} & -H D - V_i B_f \\ * & -H \epsilon \Delta_1 & \Pi_1 C - B^T V_i^T & 0 \\ * & * & H \epsilon V_i & -V_i B_f \\ * & * & * & I - D^T D \end{array} \right) < 0, \quad (3.12)$$

as well as the LMI condition (3.5) holds. Here, Y_{11} and Y_{13} are described in Theorem 3.5 with constant scalars ϵ and $\gamma > 0$ prescribed.

4. Numerical Examples

A lower-dimensional dynamical network model is concerned in this part so as to demonstrate the applicability and effectiveness of the approaches proposed in the previous sections. Throughout our numerical simulations, each node of the network is supposed to be a concrete Chua's circuit, which is frequently observed in various fields of theory and engineering applications [30].

In the first stage, it will be shown that how the results derived in Section 3.1 can be used to guarantee the global robust \mathcal{H}_∞ synchronization of the dynamical network (2.7). Let us take a group of ten dimensionless state equations of Chua's oscillators, for example, where one of the node system is shown as system S_a in Figure 1, $a = 1, 2, \dots, 10$:

$$\begin{pmatrix} \dot{v}_{a1} \\ \dot{v}_{a2} \\ \dot{i}_{a3} \end{pmatrix} = \begin{pmatrix} \frac{1}{C_1} \left(\frac{v_{a2} - v_{a1}}{R} - g(v_{a1}) \right) + \sum_{j=1}^{10} \frac{G_{aj}}{R_1 C_1} H v_{j1} \\ \frac{1}{C_2} \left(\frac{v_{a1} - v_{a2}}{R} + i_{a3} + i_{ad} \right) \\ -\frac{1}{L} (v_{a2} + R_0 i_{a3}) \end{pmatrix}. \quad (4.1)$$

Here, R_0 and R are linear resistors. The voltages across the capacitors C_1 and C_2 are denoted by v_{a1} and v_{a2} , i_{a3} is the current through the inductances L , and i_{ad} is an external disturbance

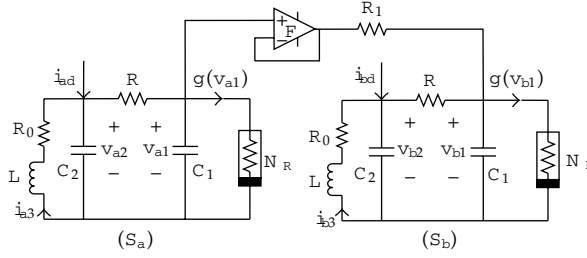


Figure 1: Coupling of any of the two identical Chua's circuits with disturbance signal, $a = 1, 2, \dots, N$, and $b = 1, 2, \dots, N$.

current that system S_a subjects to. The nonlinear characteristic $g(v_1)$ represents the current through the nonlinear resistor N_R , which is a piecewise-linear function expressed as

$$g(v_{a1}) = M_{-1}v_{a1} + \frac{1}{2}(M_0 - M_{-1})[|v_{a1} + 1| - |v_{a1} - 1|], \quad (4.2)$$

and it satisfies $\min\{M_0, M_{-1}\} \leq g'(v_1) \leq \max\{M_0, M_{-1}\}$.

Suppose that each node of the dynamical network developed by (2.7) is a circuit in the form of (4.1). The possible coupling between two arbitrary Chua's circuits, as shown in Figure 1, indicates that there is a connection from S_b to S_a but none from S_a to S_b , where the element F plays the role of unidirectional communication. Depending on different values of the controller gain, the resistor R_1 can be adjusted. It is straightforward to reformulate system (4.1) into the Lur'e form as

$$\dot{x}_i = A x_i + B (C x_i) + \sum_{j=1}^{10} g_{ij} \Gamma H x_j + B_d d_i, \quad (4.3)$$

where

$$x = \begin{pmatrix} v_1 \\ v_2 \\ \dot{b} \end{pmatrix}, \quad A = \begin{pmatrix} -p(M_0 + 1) & p & 0 \\ 1 & -1 & 1 \\ 0 & -q & -s \end{pmatrix}, \quad B = \begin{pmatrix} -p(M_{-1} - M_0) \\ 0 \\ 0 \end{pmatrix}, \quad (4.4)$$

$$C = (1 \ 0 \ 0), \quad B_d = \begin{pmatrix} 0 \\ \frac{1}{C_2} \\ 0 \end{pmatrix}, \quad d_i = \dot{i}_{ad},$$

and the nonlinear function $(C x) = (1/2)(|x_1 + 1| - |x_1 - 1|)$ satisfies the sector condition on $[0, 1]$. Furthermore, suppose the output equation to be as

$$z_i = H x_i, \quad (4.5)$$

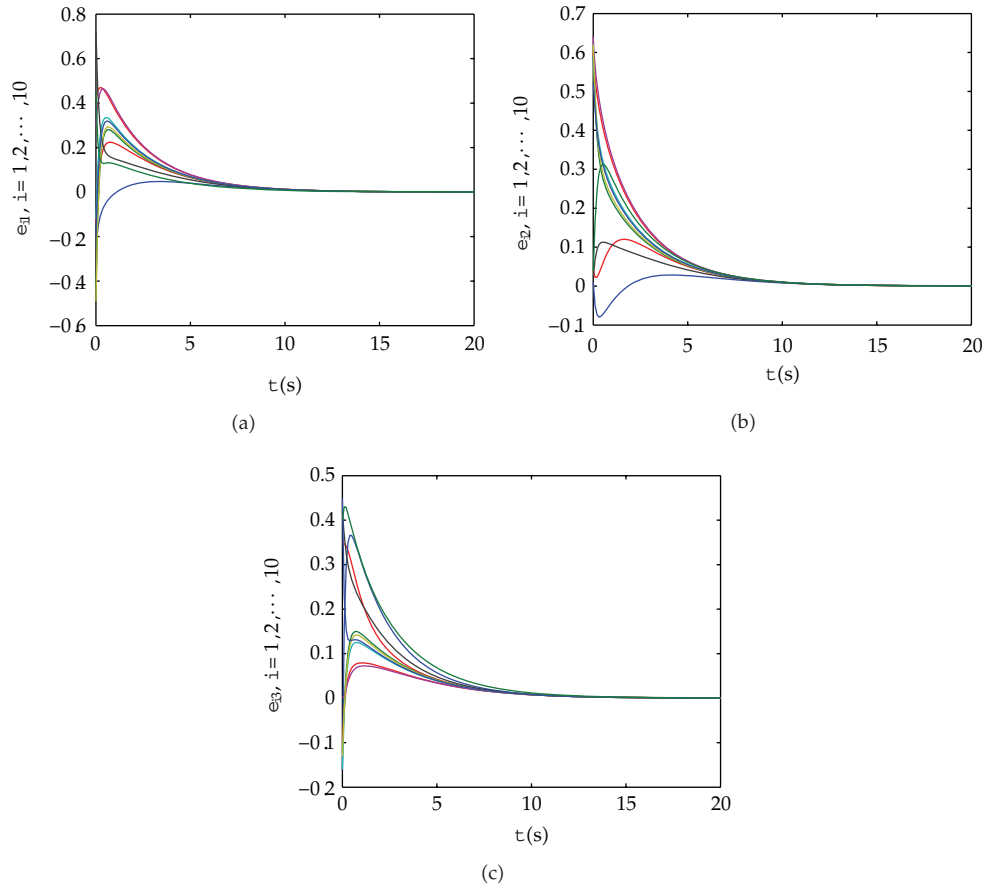


Figure 2: The time responses of synchronization errors of the nominal dynamical network.

with parameter matrix $H = (1 \ 0 \ 0)$. Choose system parameters as $R = C_2 = 1$, $p = 1/RC_1 = 5.5$, $q = 1/L = 7.3$, $s = R_0/L = 4$, $M_0 = -1/7$, $M_1 = 2/7$. In the following, $R_1 = 0.3 \Omega$ is taken. The network topology is assumed as star-like with ten nodes; thus G has the eigenvalues as follows:

$$\lambda_1 = 0, \quad \lambda_2 = \dots = \lambda_9 = -1, \quad \lambda_{10} = -10. \quad (4.6)$$

Picking $\gamma = 3$, and prescribing disturbance attenuation $\gamma = 0.9$, we arrive at the feasible solutions given in Appendix B by solving the LMIs (3.5), which, according to Corollary 3.8, implies that the dynamical network composed of Chua's circuits has achieved the global robust \mathcal{H}_∞ synchronization.

Simulation results also confirm the effectiveness of the design. Figure 2 depicts the time response of synchronization error of the nominal dynamical network without disturbance signal $d(t)$, and it shows that the synchronization error converges to zero exponentially. Herein, initial values are taken arbitrarily.

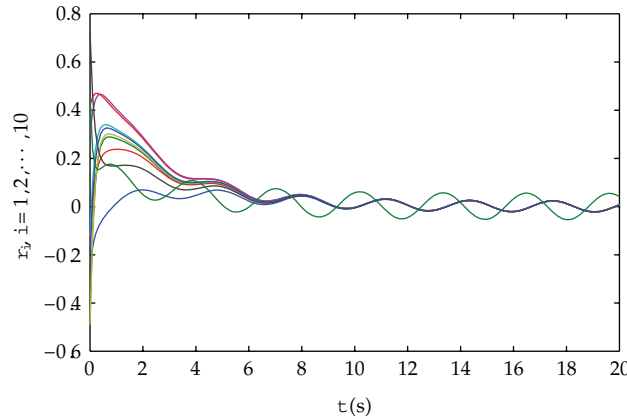


Figure 3: The fault-free residual responses r_i with $d_i(t) = 0.5 \sin(2t)$, $i = 1, 2, \dots, 10$.

To observe the \mathcal{H}_∞ performance with disturbance attenuation, assume the unknown input noise disturbance d_i to be as

$$d_i(t) = 0.5 \sin(2t), \quad t \geq 0, \quad i = 1, 2, \dots, 10. \tag{4.7}$$

Accordingly, the time response of the output residual error of Lur'e dynamical network with the above disturbance signals and zero initial conditions are shown in Figure 3.

In what follows, let us consider the global robust $\mathcal{H}_- / \mathcal{H}_\infty$ synchronization of the dynamical network (4.4) in the presence of fault signal f . For the purpose of illustration, the process fault is supposed to be a faulty current flowing in the same direction as i_{m3} along with the leftmost branch of each of the circuits, which will be simulated as two different types. Accordingly, it leads to

$$\begin{aligned} \dot{x}_i &= A x_i + B (C x_i) + \sum_{j=1}^{10} g_{ij} \Gamma H x_j + B_d d_i + B_f f, \\ z_i &= H x_i + D f, \quad i = 1, 2, \dots, 10 \end{aligned} \tag{4.8}$$

with $B_f = (0 \ 1/C_2 \ -R_0/L)^T$ and $D = 1$.

Remaining $\gamma = 0.9$ and picking the fault sensitivity $\beta = 0.6$, we arrive at solution of the LMI (3.5)-(3.6) with $\beta = 3$ presented in Appendix C, which on its turn ensures that the network (4.4) has achieved global robust $\mathcal{H}_- / \mathcal{H}_\infty$ synchronization in the presence of possible faults and external disturbances.

As for the corresponding simulation results, first let the process fault be a pulse of unit amplitude occurred from 5s to 10s (and is zero otherwise). The generated residual signals $r_i(t)$, $i = 1, 2, \dots, 10$ are depicted in Figure 4(a), from which one observes that the effect of the disturbance input $d_i(t)$ on the residual error signal $r_i(t)$, $i = 1, 2, \dots, 10$ has been greatly reduced, and the residuals have rather large amplitudes so that the synchronization process

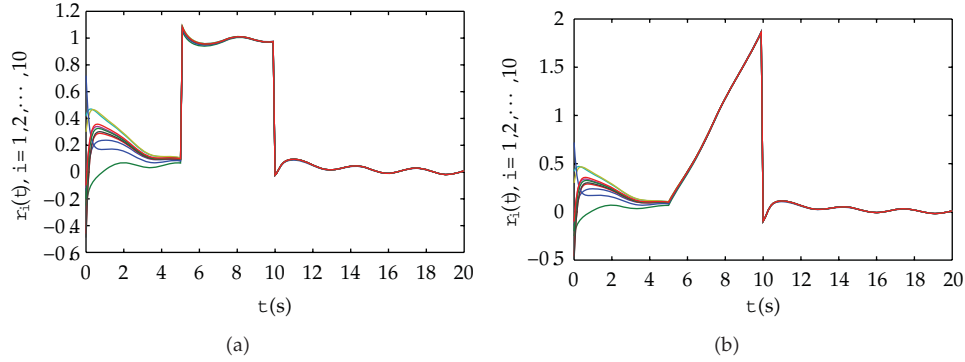


Figure 4: The residual responses $r_i(t)$ with $d_i(t) = 0.5 \sin(2t)$ and (a) $f(t) = f_1(t)$; (b) $f(t) = f_2(t)$, $i = 1, 2, \dots, 10$.

remains sensitive to fault. With the same disturbance $d_i(t)$, then redo the simulation with a different:

$$f_2(t) = \begin{cases} 0.4(t-5), & 10 \leq t < 20, \\ 0, & \text{elsewhere,} \end{cases} \quad (4.9)$$

and the results are plotted in Figure 4(b).

By solving the generalized eigenvalue problem corresponding to the minimization problem given in Corollary 3.6, we get estimates of the maximum values of fault sensitivity as $\alpha_{1m} = 0.7961$, $\alpha_{2m} = \dots = \alpha_{9m} = 0.8548$, and $\alpha_{10m} = 0.9524$, which also guarantees in terms of Corollary 3.6 that Lur'e dynamical networks achieve $\mathcal{H}_-/\mathcal{H}_\infty$ synchronization with $\gamma < \alpha_{0m}$, where $\alpha_{0m} = \min_{i=1,\dots,10} \{ \alpha_{im} \} = 0.7961$.

5. Conclusion and Future Work

Aiming at enhancing the reliability and robustness of synchronization, the global robust $\mathcal{H}_-/\mathcal{H}_\infty$ synchronization scheme has been introduced into a class of nonlinear dynamical networks in the existence of possible faults and external disturbances. The criterion on synchronization was developed in virtue of the LMI technique such that each of the node systems of the network is robustly synchronized as well as sensitive to faults according to a mixed $\mathcal{H}_-/\mathcal{H}_\infty$ performance. Since both of the external disturbance and system fault are, respectively, considered, such synchronization scheme proposed here may be more practical than the synchronization in the previous literature. Moreover, the fault sensitivity \mathcal{H}_- index could be optimized via a convex optimization algorithm. In order to demonstrate the effectiveness and applicability of the derived results, a low-dimensional dynamical network with each node being a Chua's circuit has been adopted as an example.

As for future work, it will be interesting to study the synchronization of complex networks with different disturbance from various sources. Also, it is possible to extend the present results to stochastic complex networks [31–34].

Appendices

A. Proof of Theorem 3.2

Proof. First, we will show the global asymptotical stability of the residual error dynamics (3.2) with $\bar{d} = 0$ (no fault is taken into account here), and accordingly (3.2) is represented as

$$\dot{e} = \bar{A}e + \bar{B}\Phi(\bar{C}e; X_s). \quad (\text{A.1})$$

Under the given conditions, the performance indexes J_1 in condition (2.19) are then proven to be satisfied.

Choose a Lyapunov functional candidate in the form of

$$V = e^T P e + 2 \sum_{i=1}^N \sum_{j=1}^m c_{ij}^T \int_0^{c_{ij}^T e_i} \varphi_j(\cdot) d\cdot, \quad (\text{A.2})$$

where $P > 0$ and $\Pi = I_N \otimes \Pi_1$ with $\Pi_1 = \text{diag}(\pi_1, \dots, \pi_m) > 0$ need to be determined. By calculating the time derivative of V along with the trajectory of the residual error dynamics (3.2), it yields

$$\dot{V} = 2e^T P \dot{e} + 2 \sum_{i=1}^N \sum_{j=1}^m c_{ij}^T \varphi_j(c_{ij}^T e_i) c_{ij}^T \dot{e}_i = 2e^T P \dot{e} + 2\Psi^T(\bar{C}e) \Pi \bar{C} \dot{e}, \quad (\text{A.3})$$

where $\Psi(\bar{C}e) = (\varphi_1^T(c_{11}e_1), \dots, \varphi_m^T(c_{mN}e_N))$. Then consider the sector restrictions that nonlinearities $\Phi(\bar{C}e; X_s)$ and $\Psi(\bar{C}e)$ satisfy, namely, for any diagonal matrices $\Delta_1 = \text{diag}(\delta_1, \dots, \delta_m) > 0$ and $\Omega_1 = \text{diag}(\omega_1, \dots, \omega_m) > 0$:

$$\begin{aligned} & 2 \sum_{i=1}^N \sum_{j=1}^m c_{ij}^T \varphi_j(c_{ij}^T e_i; X_s) \left(c_{ij}^T \dot{e}_i - c_{ij}^T \dot{e}_i \right) \\ & = 2\Phi^T(\bar{C}e; X_s) \Delta \Phi(\bar{C}e; X_s) - 2\Phi^T(\bar{C}e; X_s) \Delta \Theta \bar{C} e \leq 0, \\ & 2 \sum_{i=1}^N \sum_{j=1}^m c_{ij}^T \varphi_j(c_{ij}^T e_i) \left(c_{ij}^T \dot{e}_i - c_{ij}^T \dot{e}_i \right) \\ & = 2\Psi^T(\bar{C}e) \Omega \Psi(\bar{C}e) - 2\Psi^T(\bar{C}e) \Omega \Theta \bar{C} e \leq 0 \end{aligned} \quad (\text{A.4})$$

with $\Omega = I_N \otimes \Omega_1$ and $\Delta = I_N \otimes \Delta_1$. The results are obtained with the assumption that each subsystem has the same diagonal matrices Π_1 , Ω_1 , and Δ_1 which does not affect the feasibility of inequality (2.18). For the sake of simplicity, denote $\Phi \triangleq \Phi(\bar{C}e; X_s)$ and $\Psi \triangleq \Psi(\bar{C}e)$ in the following contexts. Moreover, it is known from (A.1) that there exist free-weighting matrices \bar{Q}_1 and \bar{Q}_2 with appropriate dimensions such that

$$e^T \bar{Q}_1 (\dot{e} - \bar{A}e - \bar{B}\Phi) = \dot{e}^T \bar{Q}_2 (\dot{e} - \bar{A}e - \bar{B}\Phi) = 0. \quad (\text{A.5})$$

Incorporating formulations (A.4)-(A.5) into equality (A.3) derives

$$\begin{aligned} \dot{V} &\leq 2e^T P \dot{e} + 2\Psi^T \Pi \bar{C} \dot{e} - 2\Phi^T \Delta \Phi + 2\Phi^T \Delta \Theta \bar{C} e - 2\Psi^T \Omega \Psi + 2\Psi^T \Omega \Theta \bar{C} e \\ &\quad + 2e^T \bar{Q}_1 (\dot{e} - \bar{A} e - \bar{B} \Phi) + 2\dot{e}^T \bar{Q}_2 (\dot{e} - \bar{A} e - \bar{B} \Phi) \\ &= \Xi^T \Xi, \end{aligned} \quad (\text{A.6})$$

where

$$\Xi = \begin{pmatrix} e \\ \Phi \\ \dot{e} \\ \Psi \end{pmatrix}, \quad \Xi = \begin{pmatrix} \text{He} \bar{Q}_1 \bar{A} - \bar{C}^T \Theta \Delta - \bar{Q}_1 \bar{B} P + \bar{Q}_1 - \bar{A}^T \bar{Q}_2^{-T} & \bar{C}^T \Theta \Omega \\ * & -\text{He} \Delta - \bar{B}^T \bar{Q}_2^{-T} & 0 \\ * & * & \text{He} \bar{Q}_2 & \bar{C}^T \Pi \\ * & * & * & -\text{He} \Omega \end{pmatrix}, \quad (\text{A.7})$$

and it follows that $\Xi < 0$ is guaranteed by the upper left block of LMI (3.3); hence the synchronization residual error dynamics (3.2) is globally asymptotically stable.

In the following, we will show that the restriction on performance index J_1 given in (2.19) is satisfied under zero initial conditions for all nonzero $d \in L_2[0, \infty)$. In this case, the error dynamics (3.2) is expressed by

$$\dot{e} = \bar{A} e + \bar{B} \Phi(\bar{C} e; X_s) + \bar{B}_d d, \quad r = \bar{H} e. \quad (\text{A.8})$$

Based on (A.6) and (A.8), it is not difficult to derive

$$r^T r - d^T d + \dot{V} \leq \Xi_1^T \Xi_1, \quad (\text{A.9})$$

where $\Xi_1 = [e^T \Phi^T \dot{e}^T \Psi^T d^T]^T$, and Ξ_1 is described in condition (3.3) with $\Xi_1 < 0$. It further implies that for any $d \neq 0$, $r(t)^T r(t) - d^T d(t) + \dot{V}(t) < 0$. Under zero initial condition, the Lyapunov function V defined in (A.2) satisfies $V(0) = 0$ and $V(t) \geq 0$ for $t > 0$, hence

$$\begin{aligned} J_1 &\leq \int_0^\infty [r(t)^T r(t) - d^T d(t)] dt + V(t)|_{t \rightarrow \infty} - V(0) \\ &= \int_0^\infty [r(t)^T r(t) - d^T d(t) + \dot{V}(t)] dt < 0, \end{aligned} \quad (\text{A.10})$$

and (2.19) is satisfied, which completes the proof. \square

B. Proof of Theorem 3.4

Proof. On the basis of Theorem 3.2, it is known that if there exist solutions to LMI (3.3), the network achieves global synchronization and robust to input disturbances. As for the

condition of fault detection within the \mathcal{L}_∞ synchronization, namely, the synchronization process should be sensitive to possible input faults, it then comes to an extra verification of condition (2.20) under zero initial conditions for all nonzero $f \in \mathbb{L}_2[0, \infty]$. In this situation, the error dynamics is given by

$$\dot{e} = \bar{A}e + \bar{B}\Phi(\bar{C}e; X_s) + \bar{B}_f f, \quad r = \bar{H}e + \bar{D}f. \quad (\text{B.1})$$

Following the same line of the proof of $\mathcal{J}_1 < 0$ in Theorem 3.2, we know that if

$$\begin{aligned} -\mathcal{J}_2 &\leq \int_0^\infty \left[{}^2 f^T(\vartheta) f(\vartheta) - r(\vartheta)^T r(\vartheta) \right] dt + v(\vartheta)|_{\vartheta \rightarrow \infty} - v(0) \\ &= \int_0^\infty \left[{}^2 f^T(\vartheta) f(\vartheta) - r(\vartheta)^T r(\vartheta) + \dot{v}(\vartheta) \right] dt < 0 \end{aligned} \quad (\text{B.2})$$

holds, then the constraint (2.20) will be satisfied where v is defined in (A.2), and further, the inequality condition (B.2) is guaranteed by

$${}^2 f^T f - r^T r + \dot{v} \leq \frac{\tau}{2} \Xi_2 \frac{\tau}{2} < 0, \quad (\text{B.3})$$

where $\Xi_2 = [e^T \Phi^T \dot{e}^T \Psi^T f^T]^T$ with $\Xi_2 < 0$ given in (3.4). Thus the performance index $\mathcal{J}_2 > 0$ is satisfied, and the proof is completed. \square

C. Proof of Theorem 3.5

Proof. To facilitate the design of the coupling matrix Γ , we designate $\bar{Q}_1 = \bar{S}$ and $\bar{Q}_2 = \bar{S}$, respectively, where \bar{S} is a constant scalar; also it can be seen from (3.3) that $(\bar{S} + \bar{S}^T) < 0$, and thus \bar{S} is nonsingular.

Recall that there exists a unitary matrix U such that $U^T G U = \Lambda$ with Λ defined in (2.9). Pre- and postmultiplying to both sides of LMIs (3.3) by $\bar{U} = \text{diag}(U^T \otimes I_N, U^T \otimes I_m, U^T \otimes I_m, U^T \otimes I_m)$ and \bar{U}^T yields

$$\begin{pmatrix} -\text{He}(\bar{V} \bar{A}_\Lambda) + \bar{H}^T \bar{H} & \bar{C}^T \Theta \Delta - \bar{V} \bar{B} & \bar{W} + \bar{V} & -\bar{A}^T \bar{V}^T & \bar{C}^T \Theta \Omega & -\bar{V} \bar{B}_d \\ * & -\text{He} \Delta & & -\bar{B}^T \bar{V}^T & 0 & 0 \\ * & * & \text{He} \bar{V} & \bar{C}^T \Pi & -\bar{V} \bar{B}_d & \\ * & * & * & -\text{He} \Omega & 0 & \\ * & * & * & * & * & -{}^2 I \end{pmatrix} < 0, \quad (\text{C.1})$$

where $\bar{V} = (U^T \otimes I_N) \bar{S} (U \otimes I_N)$, $\bar{W} = (U^T \otimes I_N) \bar{P} (U \otimes I_N)$, and $\bar{A}_\Lambda = I \otimes A + \Lambda \otimes \Gamma H$. It implies from (C.1) that all the matrices appearing in this LMI are diagonal except for matrices \bar{V}, \bar{W} . To this end, suppose that there exist matrices V_i and W_i such that for $i = 1, 2, \dots, N$, the N LMIs (3.5) hold; then there must exist diagonal matrices $\bar{V} = \text{diag}(V_1, V_2, \dots, V_N)$

and $\bar{W} = \text{diag}(W_1, W_2, \dots, W_N)$ as solutions to condition (C.1), and accordingly (3.3) holds. In a similar pattern, the feasibility of LMI (3.6) means that condition (3.4) holds.

Moreover, since the coupling matrix G has q distinct different eigenvalues as (2.9), it is evident to find that the number of LMI groups to be examined in (3.5)-(3.6) can be reduced from N to q . On the other hand, it is noted that due to the convex property of LMI [26], each of the rest $q-3$ groups of LMIs for $i=3, \dots, q-1$ can be written as a linear combination of the two groups of LMIs corresponding to the second-maximum λ_2 and the minimum eigenvalue λ_q . In this situation, the synchronization condition only requires the feasibility of three groups LMIs (3.5)-(3.6) with $i=1, 2$ and q ; thus it completes the proof. \square

D. Solution of LMIs (3.5) for $i=1, 2$ and q

One has

$$\begin{aligned} W_1 &= \begin{pmatrix} 14.4037 & -10.8380 & 0.4396 \\ -10.8380 & 30.5854 & 3.0167 \\ 0.4396 & 3.0167 & 7.0477 \end{pmatrix}, & V_1 &= \begin{pmatrix} -1.6269 & -2.0020 & -0.2305 \\ -1.0598 & -6.5768 & -0.7952 \\ 0.0584 & 0.3076 & -0.2281 \end{pmatrix}, \\ \Pi_1 &= 1.9512, & \Delta_1 &= 7.6035, & \Lambda_1 &= 2.5538, \\ W_2 = \dots = W_9 &= \begin{pmatrix} 11.0778 & -5.0711 & 1.8522 \\ -5.0711 & 17.0729 & 3.4321 \\ 1.8522 & 3.4321 & 9.6299 \end{pmatrix}, \\ V_2 = \dots = V_9 &= \begin{pmatrix} -0.9218 & -1.0373 & -0.1830 \\ -0.3643 & -3.0024 & -0.4393 \\ -0.0293 & 0.3875 & -0.3124 \end{pmatrix}, \\ \Pi_2 = \dots = \Pi_9 &= 1.8828, & \Delta_2 = \dots = \Delta_9 &= 5.0301, & \Lambda_2 = \dots = \Lambda_9 &= 2.9445, \\ W_{10} &= \begin{pmatrix} 7.1144 & -1.1548 & 0.5316 \\ -1.1548 & 5.1002 & 1.5201 \\ 0.5316 & 1.5201 & 4.5129 \end{pmatrix}, & V_{10} &= \begin{pmatrix} -0.1892 & -0.1842 & -0.0411 \\ -0.0345 & -0.7973 & -0.1416 \\ 0.0078 & 0.2423 & -0.1422 \end{pmatrix}, \\ \Pi_{10} &= 1.0396, & \Delta_{10} &= 1.9588, & \Lambda_{10} &= 2.0045. \end{aligned} \tag{D.1}$$

E. Solution of LMIs (3.5)-(3.6) for $i=1, 2$ and q

One has

$$W_1 = \begin{pmatrix} 19.4357 & -10.2421 & -0.2580 \\ -10.2421 & 50.9203 & 4.7464 \\ -0.2580 & 4.7464 & 0.5780 \end{pmatrix}, \quad V_1 = \begin{pmatrix} -2.5375 & -4.4290 & -0.4708 \\ -2.4266 & -15.4850 & -1.8584 \\ -0.3124 & -1.6514 & -0.2009 \end{pmatrix},$$

$$\begin{aligned}
\Pi_1 &= 2.1700 \times 10^{-6}, & \Delta_1 &= 12.8948, & \Lambda_1 &= 1.0216 \times 10^{-12}, \\
W_2 = \cdots = W_9 &= \begin{pmatrix} 31.7702 & -9.3411 & 0.1724 \\ -9.3411 & 56.7357 & 5.3885 \\ 0.1724 & 5.3885 & 0.6592 \end{pmatrix}, \\
V_2 = \cdots = V_9 &= \begin{pmatrix} -3.0576 & -6.0476 & -0.6670 \\ -1.8406 & -15.4908 & -1.8934 \\ -0.2677 & -1.7028 & -0.2106 \end{pmatrix}, \\
\Pi_2 = \cdots = \Pi_9 &= 1.5037 \times 10^{-6}, & \Delta_2 = \cdots = \Delta_9 &= 20.8139, \\
\Lambda_2 = \cdots = \Lambda_9 &= 2.0313 \times 10^{-12}, \\
W_{10} &= \begin{pmatrix} 275.7624 & -44.0445 & 1.2220 \\ -44.0445 & 59.4247 & 5.0031 \\ 1.2220 & 5.0031 & 0.6368 \end{pmatrix}, & V_{10} &= \begin{pmatrix} -7.0320 & -9.6985 & -1.1098 \\ 0.4957 & -10.1060 & -1.2957 \\ -0.0845 & -1.1706 & -0.1522 \end{pmatrix}, \\
\Pi_{10} &= 3.6238 \times 10^{-6}, & \Delta_{10} &= 114.4167, & \Lambda_{10} &= 3.0198 \times 10^{-12}.
\end{aligned} \tag{E.1}$$

Acknowledgments

This work is supported by the National Science and Technology Infrastructure Program (Grant no. 2008BAA13B07), the China Postdoctoral Science Foundation-funded project (Grant no. 20100480242), the Science Technology Project of State Grid Corporation of China (Research on Safety and Stability of large-scale power system based on complex system theory), and the National Science Foundation of China (Grant no. 60874011).

References

- [1] R. Albert and A. Barabási, "Statistical mechanics of complex networks," *Reviews of Modern Physics*, vol. 74, no. 1, pp. 47–97, 2002.
- [2] X. F. Wang and G. Chen, "Complex networks: small-world, scale-free and beyond," *IEEE Circuits and Systems Magazine*, vol. 3, no. 1, pp. 6–20, 2003.
- [3] S. Boccaletti, V. Latora, Y. Moreno, M. Chavez, and D.-U. Hwang, "Complex networks: structure and dynamics," *Physics Reports*, vol. 424, no. 4-5, pp. 175–308, 2006.
- [4] X. F. Wang and G. Chen, "Synchronization in small-world dynamical networks," *International Journal of Bifurcation and Chaos*, vol. 12, no. 1, pp. 187–192, 2002.
- [5] M. Barahona and L. M. Pecora, "Synchronization in small-world systems," *Physical Review Letters*, vol. 89, no. 5, Article ID 054101, pp. 1–4, 2002.
- [6] S. Strogatz, *Sync: The Emerging Science of Spontaneous Order*, Hyperion Books, New York, NY, USA, 2003.
- [7] J. Lü and G. Chen, "A time-varying complex dynamical network model and its controlled synchronization criteria," *IEEE Transactions on Automatic Control*, vol. 50, no. 6, pp. 841–846, 2005.
- [8] S. Xu and Y. Yang, "Global asymptotical stability and generalized synchronization of phase synchronous dynamical networks," *Nonlinear Dynamics*, vol. 59, no. 3, pp. 485–496, 2010.
- [9] C. W. Wu, *Synchronization in Complex Networks of Nonlinear Dynamical Systems*, World Scientific, 2006.

- [10] X. Liu, J. Wang, and L. Huang, "Global synchronization for a class of dynamical complex networks," *Physica A*, vol. 386, no. 1, pp. 543–556, 2007.
- [11] X. Liu, J. Wang, and L. Huang, "Stabilization of a class of dynamical complex networks based on decentralized control," *Physica A*, vol. 383, no. 2, pp. 733–744, 2007.
- [12] S. Xu and Y. Yang, "Synchronization for a class of complex dynamical networks with time-delay," *Communications in Nonlinear Science and Numerical Simulation*, vol. 14, no. 8, pp. 3230–3238, 2009.
- [13] L. O. Chua, "Chua's circuit: an overview ten years later," *Journal of Circuits, Systems, and Computers*, vol. 4, pp. 117–159, 1994.
- [14] P. Ruoff, M. Vinsjevik, C. Monnerjahn, and L. Rensing, "The goodwin model: simulating the effect of light pulses on the circadian sporulation rhythm of *Neurospora crassa*," *Journal of Theoretical Biology*, vol. 209, no. 1, pp. 29–42, 2001.
- [15] V. Gazi and K. M. Passino, "Stability analysis of swarms," *IEEE Transactions on Automatic Control*, vol. 48, no. 4, pp. 692–697, 2003.
- [16] M. Vidyasagar, *Nonlinear Systems Analysis*, Prentice-Hall, Upper Saddle River, NJ, USA, 1993.
- [17] B. Shen, Z. Wang, and X. Liu, "Bounded H_∞ synchronization and state estimation for discrete time-varying stochastic complex networks over a finite horizon," *IEEE Transactions on Neural Networks*, vol. 22, no. 1, pp. 145–157, 2011.
- [18] Y. Tang, Z. Wang, W. K. Wong, J. Kurths, and J. Fang, "Multiobjective synchronization of coupled systems," *Chaos*, vol. 21, no. 2, Article ID 025114, 2011.
- [19] J. Chen and R. J. Patton, *Robust Model-Based Fault Diagnosis for Dynamic Systems*, Kluwer Academic Publishers, Boston, Mass, USA, 1999.
- [20] P. M. Frank, "Enhancement of robustness in observer-based fault detection," *International Journal of Control*, vol. 59, no. 4, pp. 955–981, 1994.
- [21] S. X. Ding, *Model-Based Fault Diagnosis Techniques, Design Schemes, Algorithms, and Tools*, Springer, Berlin, Germany, 2008.
- [22] J. L. Wang, G.-H. Yang, and J. Liu, "An LMI approach to H_∞ index and mixed H_-/H_∞ fault detection observer design," *Automatica*, vol. 43, no. 9, pp. 1656–1665, 2007.
- [23] X. Li and K. Zhou, "A time domain approach to robust fault detection of linear time-varying systems," *Automatica*, vol. 45, no. 1, pp. 94–102, 2009.
- [24] S. -Y. Xu, Y. Yang, X. Liu, Y. Tang, and H. -D. Sun, "Robust fault-sensitive synchronization of a class of nonlinear systems," *Chinese Physics B*, vol. 20, no. 2, Article ID 020509, 2011.
- [25] M. Hou and R. J. Patton, "An LMI approach to H_-/H_∞ fault detection observers," in *Proceedings of the UKACC International Conference on Control*, pp. 305–310, 1996.
- [26] S. Boyd, L. ELGhaoui, E. Feron, and V. Balakrishnam, *Linear Matrix Inequalities in Systems and Control*, SIMA, Philadelphia, Pa, USA, 1994.
- [27] C. W. Wu, *Synchronization in Coupled Chaotic Circuits and Systems*, World Scientific, Singapore, 2002.
- [28] C. W. Wu and L. O. Chua, "Application of Kronecker products to the analysis of systems with uniform linear coupling," *IEEE Transactions on Circuits and Systems I*, vol. 42, no. 10, pp. 775–778, 1995.
- [29] M. Wu, Y. He, J. H. She, and G. P. Liu, "Delay-dependent criteria for robust stability of time-varying delay systems," *Automatica*, vol. 40, no. 8, pp. 1435–1439, 2004.
- [30] *Chua's Circuit: A Paradigm for Chaos*, vol. 1, World Scientific, Singapore, 1993.
- [31] Z. Wang, Y. Wang, and Y. Liu, "Global synchronization for discrete-time stochastic complex networks with randomly occurred nonlinearities and mixed time delays," *IEEE Transactions on Neural Networks*, vol. 21, no. 1, Article ID 5342442, pp. 11–25, 2010.
- [32] J. Liang, Z. Wang, and X. Liu, "State estimation for coupled uncertain stochastic networks with missing measurements and time-varying delays: the discrete-time case," *IEEE Transactions on Neural Networks*, vol. 20, no. 5, pp. 781–793, 2009.
- [33] Y. Liu, Z. Wang, J. Liang, and X. Liu, "Synchronization and state estimation for discrete-time complex networks with distributed delays," *IEEE Transactions on Systems, Man, and Cybernetics, Part B: Cybernetics*, vol. 38, no. 5, pp. 1314–1325, 2008.
- [34] J. Liang, Z. Wang, Y. Liu, and X. Liu, "Global synchronization control of general delayed discrete-time networks with stochastic coupling and disturbances," *IEEE Transactions on Systems, Man, and Cybernetics, Part B: Cybernetics*, vol. 38, no. 4, pp. 1073–1083, 2008.

Review Article

Recent Advances on Filtering and Control for Nonlinear Stochastic Complex Systems with Incomplete Information: A Survey

Bo Shen,¹ Zidong Wang,^{1,2} Jinling Liang,³ and Yurong Liu⁴

¹ School of Information Science and Technology, Donghua University, Shanghai 200051, China

² Department of Information Systems and Computing, Brunel University, Uxbridge, Middlesex UB8 3PH, UK

³ Department of Mathematics, Southeast University, Nanjing 210096, China

⁴ Department of Mathematics, Yangzhou University, Yangzhou 225002, China

Correspondence should be addressed to Zidong Wang, zidong.wang@brunel.ac.uk

Received 16 August 2011; Accepted 28 September 2011

Academic Editor: Zhan Shu

Copyright © 2012 Bo Shen et al. This is an open access article distributed under the Creative Commons Attribution License, which permits unrestricted use, distribution, and reproduction in any medium, provided the original work is properly cited.

Some recent advances on the filtering and control problems for nonlinear stochastic complex systems with incomplete information are surveyed. The incomplete information under consideration mainly includes missing measurements, randomly varying sensor delays, signal quantization, sensor saturations, and signal sampling. With such incomplete information, the developments on various filtering and control issues are reviewed in great detail. In particular, the addressed nonlinear stochastic complex systems are so comprehensive that they include conventional nonlinear stochastic systems, different kinds of complex networks, and a large class of sensor networks. The corresponding filtering and control technologies for such nonlinear stochastic complex systems are then discussed. Subsequently, some latest results on the filtering and control problems for the complex systems with incomplete information are given. Finally, conclusions are drawn and several possible future research directions are pointed out.

1. Introduction

Filtering and control problems have long been a fascinating focus of research attracting constant attention from a variety of engineering areas. In recent years, with the rapid development of the network technology, the study of networked control systems (NCSs) has gradually become an active research area due to the advantages of using networked media in many aspects such as low cost, reduced weight and power requirements, simple installation and maintenance, as well as high reliability. It is well known that the devices in networks are mutually connected via communication cables which are of limited capacity. Therefore, some

new network-induced phenomena have inevitably emerged in the areas of signal processing and control engineering. These phenomena include, but are not limited to, network-induced time delay, data missing (also called packet dropout or missing measurement), quantization, saturation, and channel fading. Note that these phenomena could drastically deteriorate the performance of the networked filtering or control systems and, as such, the aim of this paper is to deal with the filtering and control problems for nonlinear stochastic complex systems with aforementioned network-induced phenomena. In this paper, the information with respect to the network-induced phenomena is customarily referred to as the incomplete information.

Nowadays, practical engineering systems typically exhibit a great deal of complexity which poses significant challenges for the analysis and synthesis of such systems. Among others, the nonlinearity and stochasticity serve as two of the main sources in reality that have resulted in considerable system complexity and have received recurring research attention. Moreover, due to the unavoidable modeling errors and coupled dynamics, some new interesting phenomena (such as parameter uncertainties and coupling between control nodes) should be taken into account to achieve the desired performance. The complexity sources mentioned above give rise to the urgent necessity for developing new filtering and control technologies for various kinds of complex systems in order to meet the needs of practical engineering. It is not surprising that, in the past few years, the control and filtering problems for complex systems with incomplete information have been extensively investigated by many researchers.

In this paper, we focus mainly on the filtering and control problem for complex systems with incomplete information and aim to give a survey on some recent advances in this area. The incomplete information under consideration includes missing measurements, randomly varying sensor delays, signal quantization, sensor saturations, and signal sampling. The modeling issues are first discussed to reflect the real complexity of the nonlinear stochastic systems. Based on the models established, various filtering and control problems with incomplete information are reviewed in detail. Then, we deal with the complex systems from three aspects, that is, nonlinear stochastic systems, complex networks, and sensor networks. Both theories and techniques for dealing with complex systems are reviewed and, at the same time, some challenging issues for future research are raised. Subsequently, the filtering problems for the stochastic nonlinear complex networks with incomplete information are paid particular attention by summarizing the latest results. Finally, some conclusions are drawn and several possible related research directions are pointed out.

The remainder of this paper is organized as follows. In Section 2, the motivation for addressing the incomplete information is discussed. Section 3 reviews the developments of filtering and control issues for three kinds of complex systems. Section 4 gives latest results on filtering problems for the stochastic nonlinear complex networks with incomplete information. The conclusions and future work are given in Section 5.

2. Incomplete Information

Recently, the signal transmission via networked systems has become prevalent and, accordingly, network-induced issues have drawn considerable research interests. These issues mainly include missing measurements (also called packet dropouts), randomly varying sensor delays, signal quantization, sensor saturations, and signal sampling whose mathematical models are listed in Table 1, where v_k is the external disturbance while w_k represents both the exogenous random inputs and parameter uncertainty of the system. Let

Table 1: Mathematical models of incomplete information.

Types	Mathematical models
Missing measurements	$x_{k+1} = f(x_k) + E_1 v_k + g(x_k) w_k, Y_k = \gamma_k h(x_k) + E_2 v_k$, where γ_k is a stochastic variable taking value on 1 or 0.
Randomly varying sensor delays	$x_{k+1} = f(x_k) + E_1 v_k + g(x_k) w_k$, $Y_k = \gamma_k h(x_k) + (1 - \gamma_k) h(x_{k-1}) + E_2 v_k$, where γ_k is a stochastic variable taking value on 1 or 0.
Signal quantization	$x_{k+1} = f(x_k) + E_1 v_k + g(x_k) w_k, Y_k = q(h(x_k)) + E_2 v_k$, where $q(\cdot)$ is a quantization function.
Sensor saturations	$x_{k+1} = f(x_k) + E_1 v_k + g(x_k) w_k, Y_k = \text{Sat}(h(x_k)) + E_2 v_k$, where $\text{Sat}(\cdot)$ is a saturation function.
Signal sampling	$\dot{x}_t = f(x_t) + E_1 v_t + g(x_t) w_t, Y_t = h(x_{t_k}) + E_2 v_{t_k}, t_k \leq t < t_{k+1}$.

we now discuss the network-induced issues one by one as follows in order to motivate the research problem to be investigated.

2.1. Missing Measurements

It is quite common in practice that the measurement output of a discrete-time stochastic system is not consecutive but contains missing observations due to a variety of causes such as sensor temporal failure and network-induced packet loss, see, for example, [1–3]. Therefore, it is not surprising that the filtering problem for systems with missing measurements has recently attracted much attention. For example, a binary switching sequence has been used in [4–6], which can be viewed as a Bernoulli distributed white sequence taking values of 0 and 1, to model the measurement missing phenomena. A Markovian jumping process has been employed in [7] to reflect the measurement missing problem. In [8, 9], the data missing (dropout) rate has been converted into the signal transmission delay that has both the upper and lower bounds. In [10], a model of multiple missing measurements has been presented by using a diagonal matrix to account for the different missing probability for individual sensors. By introducing a certain set of indicator functions, the packet dropouts and random sensor delays have been modeled in a unified way in [11]. The optimal H_2 filtering problem for linear systems with multiple packet dropouts has been studied in [12], whereas the optimal H_∞ filtering problem has been dealt with in [13] for the same systems. Moreover, the optimal filter design problem has been tackled in [14] for systems with multiple packet dropouts by solving a recursive difference equation (RDE).

2.2. Randomly Varying Sensor Delays

In practical applications such as engineering, biological, and economic systems, the measured output may be delayed. Therefore, the problem of filtering with delayed measurements has been attracting considerable research interests, see [7, 15, 16], for some recent publications, where the time-delay in the measurement is customarily assumed to be deterministic. However, it is quite common in practice that the time-delays occur in a random way, rather than a deterministic way, for a number of engineering applications such as real-time distributed decision-making and multiplexed data communication networks. Hence, there is a great need to develop new filtering approaches for the systems with randomly varying

delayed measurements, and some efforts have been made in this regard so far. For example, in [17], a linear unbiased state estimation problem has been examined for discrete-time systems with random sensor delays over both finite- and infinite-horizons where the full and reduced-order filters have been designed to achieve specific estimation error covariances. These results have been extended in [18] to the case where parameter uncertainties are taken into account. A robust suboptimal filter design problem has been considered for uncertain discrete time-varying systems with randomly varying sensor delay in [19], where some sufficient conditions have been developed for the filter design such that the upper-bound of the state estimation error variance is minimized. Very recently, in [20], a linear matrix inequality (LMI) approach [21] has been developed to discuss the infinite-horizon H_∞ filtering problem for linear discrete-time systems with randomly varying sensor delays.

2.3. Signal Quantization

The signal quantization is considered as another source that has significant impact on the achievable performance of the networked systems and, therefore, it is necessary to conduct analysis on the quantizers and understand how much effect the quantization makes on the overall networked systems. In fact, the problem of quantized control for nonnetworked systems has been reported as early as in 1990 [22]. So far, a great number of results have been available in the literature, see for example, [22–27]. In [23], the feedback stabilization problems have been considered for linear time-invariant control systems with saturating quantized measurements. In [27], some general types of quantizers have been developed to solve the problem of feedback stabilization for general nonlinear systems. Recently, a new type of quantizer (called logarithmic quantizer) has attracted considerable research interest. Such a quantizer has proven to be the coarsest one in the problem of quadratic stabilization for discrete-time single-input-single-output linear time-invariant systems using quantized feedback under the assumption that the quantizer is static and time-invariant [25]. Based on that, a number of quantized feedback design problems have been studied in [26] for linear systems, where the major contribution of [26] lies in that many quantized feedback design problems have been found to be equivalent to the well-known robust control problems with sector-bounded uncertainties. Later, the elegant results obtained in [25] have been generalized to the multiple-input-multiple-output systems and to control design with performance constraints. Inspiringly, in recent years, there have appeared some new results on NCSs with the consideration of signal quantization effects. In [28], the network-based guaranteed cost problem has been dealt with for linear systems with state and input quantization by using the method of sector bound uncertainties. Moreover, in [29], the problem of quantized state feedback H_∞ stabilization has been addressed for linear time-invariant systems over data networks with limited network quality-of-service. Following that, the problem of output feedback control for NCSs with limited communication capacity has been investigated in [30], where the packet losses and quantization effects are taken into account simultaneously.

2.4. Sensor Saturations

In reality, the obstacles in delivering the high performance promises of traditional filter theories are often due to the physical limitations of system components, of which the most commonly encountered one stems from the saturation that occurs in any actuators, sensors,

or certain system components. Saturation brings in nonlinear characteristics that can severely restrict the amount of deployable filter scheme. Such a characteristic not only limits the filtering performance that can otherwise be achieved without saturation, it may also lead to undesirable oscillatory behavior or, even worse, instability. Therefore, the control problems for systems under actuator/sensor saturations have attracted considerable research interests (see e.g., [31–37]), and the related filtering problem has also gained some scattered research attention [38, 39].

It should be pointed out that, in almost all the relevant literature, the saturation is implicitly assumed to occur already. However, in networked environments such as wireless sensor networks, the sensor saturation itself may be subject to random abrupt changes, for example, random sensor failures leading to intermittent saturation, sensor aging resulting in changeable saturation level, repairs of partial components, changes in the interconnections of subsystems, sudden environment changes, modification of the operating point of a linearized model of a nonlinear systems, and so forth. In other words, the sensor saturations may occur in a probabilistic way and are randomly changeable in terms of their types and/or intensity. Such a phenomenon of sensor saturation, namely, randomly occurring sensor saturation (ROSS), has been largely overlooked in the area.

2.5. Signal Sampling

With the rapid development of high-speed computers, modern control systems tend to be controlled by digital controllers, that is, only the samples of the control input signals at discrete time instants will be employed. The traditional approach is to use periodic sampling technique to obtain a discrete-time system for modeling the real plant. However, such a discrete-time model might not capture the intersample behavior of the real system, especially for the case when the sampling period is time-varying. On this account, considerable research efforts have been made on various aspects of sampled-data systems. For example, the H_2 optimal and H_∞ suboptimal control problems for sampled-data systems have been studied in [40, 41] and [42, 43], respectively. As for the sampled-data filtering problem, let us mention some representative work here. In [44], the robust H_∞ filtering problem has been investigated for a class of systems with parametric uncertainties and unknown time delays under sampled measurements. The nonlinear H_∞ filtering problem for sampled-data systems has been considered in [45], where a set of certain continuous and discrete Hamilton-Jacobi equations has been established for the existence of the desired filter. In [46], the performance criterion in terms of the estimation error covariance has been proposed and the corresponding sampled-data filtering problem has been solved. It is worth pointing out that, in [47, 48], a new approach to dealing with the sampled-data control problems has been proposed by converting the sampling period into a time-varying but bounded delay, and then the sampled-data H_∞ control problem has been investigated by recurring to the H_∞ control theory for the time-delay systems. Based on this method, the sampled-data H_∞ control and filtering problems have been thoroughly investigated in [49] and [50], respectively, where the stochastic sampling has been taken into account.

3. Complex Systems

In this section, we take a look at the theories and technologies for handling the filtering and control problems for the complex systems including nonlinear stochastic systems, complex

networks, and sensor networks. Afterwards, we point out some challenging issues to be studied.

3.1. Nonlinear Stochastic Systems

The nonlinearity and stochasticity are arguably two of the main resources in reality that have resulted in considerable system complexity [40]. In the past few years, nonlinear H_∞ filtering and H_∞ control have been an active branch within the general research area of nonlinear control problems, and a great deal of results have been available in the literature. For the H_∞ control problems, we refer the readers to [51–54] and the references therein. With respect to the H_∞ filtering problems, we mention some representative work as follows. In [16], the H_∞ filtering problem has been investigated for a class of uncertain stochastic time-delay systems with sector-bounded nonlinearities. The H_∞ reduced-order approximation of two-dimensional digital filters has been considered in [55], while [56] has designed a full-order H_∞ filter for 2D Markovian jump systems. In [45], a nonlinear H_∞ filtering problem has been studied for sampled-data systems. In [57, 58], the H_∞ filtering problem has been considered for systems with constant and time-varying delay, respectively. It should be pointed out that, in all the papers mentioned above, the nonlinearities have been assumed to be bounded by a linearity-like form (e.g., Lipschitz and sector conditions), and the filters have been designed by solving a set of LMIs. With respect to general stochastic systems, the nonlinear H_∞ filtering problem has been considered for discrete-time systems in [59], and a great effort has been paid in [60] to investigate the H_∞ filtering problem for continuous stochastic systems with a very general form.

3.2. Complex Networks

Complex networks are made up of interconnected nodes and are used to describe various systems of real world. Many real world systems can be described by complex networks, such as the World Wide Web, telephone call graphs, neural networks, scientific citation web, and so forth. Since the discoveries of the “small-world” and “scale-free” properties of complex networks [61, 62], complex networks become a focus point of research which has attracted increasing attention from various fields of science and engineering. In particular, special attention has been paid to the synchronization problem for dynamical complex networks, in which each node is regarded as a dynamical element [63–65]. It has been shown that the synchronization is ubiquitous in many system models of the natural world, for example, the large-scale and complex networks of chaotic oscillators [66–73], the coupled systems exhibiting spatiotemporal chaos and autowaves [74], and the array of coupled neural networks [75–84].

Recently, the synchronization problem for discrete-time stochastic complex networks has drawn much research attention since it is rather challenging to understand the interaction topology of complex networks because of the discrete and random nature of network topology [85]. On one hand, discrete-time networks could be more suitable to model digitally transmitted signals in many application areas such as image processing, time series analysis, quadratic optimization problems, and system identification. On the other hand, the stochastic disturbances over a real complex network may result from the release of probabilistic causes such as neurotransmitters [86], random phase-coupled oscillators [87], and packet dropouts [88]. A great number of results have been available in the recent literature on the general topic of stochastic synchronization problem for discrete-time complex networks. For example,

in [89], the synchronization stability problem has been studied for a class of complex dynamical networks with Markovian jumping parameters and mixed time delays.

Although the synchronization problem for discrete-time stochastic complex networks is now attracting an increasing research attention, there are still several open problems deserving further investigation. In a real world, virtually all complex networks are time-varying, that is, all the network parameters are explicitly dependent on time. For example, a major challenge in biological networks is to understand and model, quantitatively, the dynamic topological and functional properties of biological networks. Such time, or condition specific biological circuitries are referred to as time-varying networks or structural nonstationary networks, which are common in biological systems. The synchronization problem for time-varying complex networks has received some scattered research interest, where most literature has focused on time-varying coupling or time-varying delay terms. For example, in [90], a time-varying complex dynamical network model has been introduced and it has been revealed that the synchronization of such a model is completely determined by the innercoupling matrix, the eigenvalues, and the corresponding eigenvectors of the coupling configuration matrix of the network. Very recently, in [91], a class of controlled time-varying complex dynamical networks with similarity has been investigated and a decentralized holographic-structure controller has been designed to stabilize the network asymptotically at its equilibrium states. It should be pointed out that, up to now, the general synchronization results for complex networks with time-varying network parameters have been very few, especially when the networks exhibit both discrete-time and stochastic natures.

Closely associated with the synchronization problem is the so-called state estimation problem for complex networks. For large-scale complex networks, it is quite common that only partial information about the network nodes (states) is accessible from the network outputs. Therefore, in order to make use of key network nodes in practice, it becomes necessary to estimate the network nodes through available measurements. Note that the state estimation problem for neural networks (a special class of complex networks) was first addressed in [92] and has then drawn particular research interests, see, for example, [93, 94], where the networks are deterministic and continuous-time. Recently, the state estimation problem for complex networks has also gained much attention, see [95].

3.3. Sensor Networks

Sensor networks have recently received increasing interests due to their extensive application in areas such as information collection, environmental monitoring, industrial automation, and intelligent buildings [96, 97]. In particular, the distributed filtering or estimation for sensor networks has been an ongoing research issue that attracts increasing attention from researchers in the area. Compared to the single sensor, filter i in a sensor network estimates the system state based not only on the sensor i 's measurement but also on its neighboring sensors' measurements according to the topology of the given sensor network. Such a problem is usually referred to as the distributed filtering or estimation problem. The main difficulty in designing distributed filters lies in how to deal with the complicated coupling between one sensor and its neighboring sensors.

Recently, considerable research efforts have been made with respect to distributed filtering, and some novel distributed filters have been proposed. For example, a distributed estimation algorithm for sensor networks has been proposed in [98], where each node computes its estimate as a weighted sum of its own and its neighbors' measurements and estimates, and the weights are adaptively updated to minimize the variance of the estimation

error. In [99], diffusion strategies have been suggested and then successfully applied to the distributed Kalman filtering, where nodes communicate with their direct neighbors only and the information is diffused across the network. By using the same diffusion strategies, the distributed Kalman smoother has been designed in [100]. In [101], the notion of distributed bounded consensus filters has been proposed and the convergence analysis has been conducted for the corresponding distributed filters. It has been shown in [101] that, in view of the pinning control approach, only a small fraction of sensors are needed to measure the target information while the whole network can be controlled.

In the past few years, the consensus problems of multiagent networks have stirred a great deal of research interests, and a rich body of research results has been reported in the literature, see, for example, [102–110]. Representatively, in [102], a systematical framework of consensus problem has been proposed, and three kinds of networks including directed networks with fixed topology, directed networks with switching topology, and undirected networks with communication delay and fixed topology have been discussed by using the Lyapunov approach and the frequency domain theory. In [105], the H_∞ performance constraint has been introduced to the consensus context, and a distributed robust H_∞ consensus controller has been designed for the directed networks of agents with time-delay. The consensus protocol has been extended in [107], where the measurement noises have also been taken into account in constructing the consensus protocol. Comparing to the work mentioned above, in [110], the average consensus problems have been studied for agents with integrator dynamics in presence of communication delays. Recently, the consensus problem has also been studied for designing distributed Kalman filters (DKFs). For example, a distributed filter has been introduced in [111] that allows the nodes of a sensor network to track the average of n sensor measurements using an average consensus-based distributed filter called consensus filter. The DKF algorithm presented in [111] has been modified in [112], where another two novel DKF algorithms have been proposed and the communication complexity as well as packet-loss issues have been discussed. The DKF problem considered in [113] is also based on the average consensus, where the node hierarchy has been used with nodes performing different types of processing and communications. Very recently, the consensus-based overlapping decentralized estimation problem has been dealt with in [114] for systems with missing observations and communication faults.

It is worth mentioning that, in almost all the literature concerning the distributed filtering problems, the filter design algorithm has been mainly based on the traditional Kalman filtering theory. Unfortunately, it is now well known that the robust performance of Kalman filters cannot always be guaranteed since Kalman filters tend to be sensitive to model structure drift [7, 45, 57, 60, 115–118]. As such, a variety of robust and/or H_∞ filtering approaches have been proposed in the literature to improve the robustness of the filters against parameter uncertainties and exogenous disturbances. In this sense, it seems natural to include the robust and/or H_∞ performance requirements for the distributed consensus filtering problems, and this deserves deep investigation.

4. Latest Progress

Very recently, the filtering problem for the stochastic nonlinear complex systems with incomplete information has been intensively studied and some elegant results have been reported. In this section, we highlight some of the newest work with respect to this topic.

(i) In [119], the H_∞ filtering problem has been studied for a general class of nonlinear discrete-time stochastic systems with missing measurements and a filter of very general form

has been designed such that the filtering process is stochastically stable and the filtering error satisfies H_∞ performance constraint for all admissible missing observations and nonzero exogenous disturbances under the zero-initial condition. The existence conditions of the desired filter have been derived in terms of the Hamilton-Jacobi-Isaacs inequalities (HJIs). Then, by using similar analysis techniques, the H_∞ filtering problem with randomly varying sensor delays has been considered in [120], and a set of parallel results has been derived.

(ii) In order to describe the phenomena of a nonlinear disturbance appearing in a random way, a notion of the randomly occurring nonlinearity has been introduced in [121, 122]. In [121], a new robust H_∞ filtering technique has been developed for the Itô-type discrete time-varying stochastic systems with polytopic uncertainties, quantization effects, and randomly occurring nonlinearities. Then, the robust H_∞ finite-horizon filtering problem has been studied in [122] for a class of discrete time-varying stochastic systems with norm-bounded uncertainties, multiple randomly occurred nonlinearities, and successive packet dropouts.

(iii) The H_∞ filtering problem has been studied in [123] for a class of nonlinear systems with randomly occurring incomplete information, where the considered incomplete information includes both the sensor saturations and the missing measurements. A new phenomenon of sensor saturation, namely, randomly occurring sensor saturation, has first been put forward in order to better reflect the reality in a networked environment. Then, a novel sensor model has been established to account for both the randomly occurring sensor saturation and missing measurement in a unified representation. Based on this sensor model, a regional H_∞ filter with a certain ellipsoid constraint has been designed such that the filtering error dynamics is locally mean-square asymptotically stable and the H_∞ -norm requirement is satisfied.

(iv) In [124], a new distributed H_∞ -consensus filtering problem over a finite-horizon has been addressed for sensor networks with multiple missing measurements. The so-called H_∞ -consensus performance requirement is defined to quantify bounded consensus regarding the filtering errors (agreements) over a finite-horizon. A sufficient condition has first been established in terms of a set of difference linear matrix inequalities (DLMI) under which the expected H_∞ -consensus performance constraint is guaranteed. Then, the filter parameters have been explicitly parameterized by means of the solutions to a certain set of DLMI that can be computed recursively. Subsequently, two kinds of robust distributed H_∞ -consensus filters have been designed for the systems with norm-bounded uncertainties and polytopic uncertainties.

(v) In [125], the distributed H_∞ filtering problem is dealt with for a class of polynomial nonlinear stochastic systems in sensor networks. A Lyapunov function candidate whose entries are polynomials has been adopted and then, a sufficient condition for the existence of a feasible solution to the addressed distributed H_∞ filtering problem has been derived in terms of parameter-dependent linear matrix inequalities (PDLMI). For computational convenience, these PDLMI have further been converted into a set of sums of squares (SOS) that can be solved effectively by using the semidefinite programming technique.

(vi) In [126], the problem of distributed H_∞ filtering in sensor networks using a stochastic sampled-data approach has been investigated. The signal received by each sensor is sampled by a sampler separately with stochastic sampling periods before it is employed by the corresponding filter. By using the method of converting the sampling periods into bounded time-delays, the design problem of the stochastic sampled-data-based distributed H_∞ filters amounts to solving the H_∞ filtering problem for a class of stochastic nonlinear systems with multiple bounded time-delays. Then, by constructing a new Lyapunov functional and employing both the Gronwall's inequality and the Jensen

integral inequality, a sufficient condition has been derived to guarantee the H_∞ performance as well as the exponential mean-square stability of the resulting filtering error dynamics.

Subsequently, the desired sampled-data-based distributed H_∞ filters have been designed in terms of the solution to certain matrix inequalities.

(vii) In [127], new synchronization and state estimation problems have been considered for an array of coupled discrete time-varying stochastic complex networks over a finite-horizon. A novel concept of bounded H_∞ synchronization has been proposed to handle the time-varying nature of the complex networks. By utilizing a time-varying real-valued function and the Kronecker product, criteria have been established that ensure the bounded H_∞ synchronization in terms of a set of recursive linear matrix inequalities (RLMIs). The bounded H_∞ state estimation problem has then been studied for the same complex network, where the purpose is to design a state estimator to estimate the network states through available output measurements such that, over a finite-horizon, the dynamics of the estimation error is guaranteed to be bounded with a given disturbance attenuation level. Again, an RLMI approach has been developed for the state estimation problem.

5. Conclusions and Future Work

In this paper, we have surveyed some recent advances on the filtering and control for complex systems with incomplete information. The developments of the incomplete information models have been reviewed and various filtering and control problems based on these incomplete information have been discussed. Then, we have introduced basic theories and methods for dealing with filtering and control problems of complex systems and raised a few challenging issues. Subsequently, we have paid particular attention to the filtering problems of the stochastic nonlinear complex systems with incomplete information and given the latest results. Related topics for the future research work are listed below.

- (i) In practical engineering, there still exist many more complex yet important network-induced issues which, however, have not been studied. Therefore, these new phenomena of incomplete information should be paid great attention to, and a unified measurement model accounting for these issues simultaneously also remains to be established.
- (ii) The polynomial nonlinear system is one of the most important classes of nonlinear systems. The control and filtering problems for polynomial nonlinear systems with kinds of incomplete information are interesting and deserve further investigation. The analysis and synthesis of polynomial nonlinear controllers and filters for the polynomial nonlinear systems would be a challenging research topic.
- (iii) The problems of fault detection and fault tolerant control in the presence of incomplete information are of engineering significance, especially when the system is time varying. Hence, the problems of fault detection and fault tolerant control for time-varying systems with incomplete information over a finite time-horizon would be another interesting topic.
- (iv) Note that the incomplete information usually occurs in a random way which makes the considered system stochastic. In this case, the performance objection is only required to be achieved in the desired probability. Therefore, the control and filtering problems for nonlinear stochastic systems with probabilistic performance are of significant engineering importance.

- (v) Applications of the existing theories and methodologies to some practical engineering problems such as the mobile robot navigation would be another one of the future work.

Acknowledgments

This work was supported in part by the National Natural Science Foundation of China under Grant nos. 61134009, 61104125, 61028008, 61174136, 60974030, and 61074129, the Qing Lan Project of Jiangsu Province of China, the Project sponsored by SRF for ROCS of SEM of China, the Engineering and Physical Sciences Research Council (EPSRC) of the UK under Grant GR/S27658/01, the Royal Society of the UK, and the Alexander von Humboldt Foundation of Germany.

References

- [1] M. Basin, E. Sanchez, and R. Martinez-Zuniga, "Optimal linear filtering for systems with multiple state and observation delays," *International Journal of Innovative Computing, Information and Control*, vol. 3, no. 5, pp. 1309–1320, 2007.
- [2] M. Basin, J. Perez, and D. Calderon-Alvarez, "Optimal filtering for linear systems over polynomial observations," *International Journal of Innovative Computing, Information and Control*, vol. 4, no. 2, pp. 313–320, 2008.
- [3] M. S. Mahmoud, Y. Shi, and H. N. Nounou, "Resilient observer-based control of uncertain time-delay systems," *International Journal of Innovative Computing, Information and Control*, vol. 3, no. 2, pp. 407–418, 2007.
- [4] Z. Wang, D. W. C. Ho, and X. Liu, "Variance-constrained filtering for uncertain stochastic systems with missing measurements," *IEEE Transactions on Automatic Control*, vol. 48, no. 7, pp. 1254–1258, 2003.
- [5] Z. Wang, F. Yang, D. W. C. Ho, and X. Liu, "Robust H_∞ filtering for stochastic time-delay systems with missing measurements," *IEEE Transactions on Signal Processing*, vol. 54, no. 7, pp. 2579–2587, 2006.
- [6] B. Sinopoli, L. Schenato, M. Franceschetti, K. Poolla, M. I. Jordan, and S. S. Sastry, "Kalman filtering with intermittent observations," *IEEE Transactions on Automatic Control*, vol. 49, no. 9, pp. 1453–1464, 2004.
- [7] P. Shi, M. Mahmoud, S. K. Nguang, and A. Ismail, "Robust filtering for jumping systems with mode-dependent delays," *Signal Processing*, vol. 86, no. 1, pp. 140–152, 2006.
- [8] H. Gao and T. Chen, " H_∞ estimation for uncertain systems with limited communication capacity," *IEEE Transactions on Automatic Control*, vol. 52, no. 11, pp. 2070–2084, 2007.
- [9] H. Gao, T. Chen, and T. Chai, "Passivity and passification for networked control systems," *SIAM Journal on Control and Optimization*, vol. 46, no. 4, pp. 1299–1322, 2007.
- [10] G. Wei, Z. Wang, and H. Shu, "Robust filtering with stochastic nonlinearities and multiple missing measurements," *Automatica*, vol. 45, no. 3, pp. 836–841, 2009.
- [11] X. He, Z. Wang, and D. Zhou, "Robust H_∞ filtering for networked systems with multiple state delays," *International Journal of Control*, vol. 80, no. 8, pp. 1217–1232, 2007.
- [12] M. Sahebsara, T. Chen, and S. L. Shah, "Optimal H_2 filtering in networked control systems with multiple packet dropout," *IEEE Transactions on Automatic Control*, vol. 52, no. 8, pp. 1508–1513, 2007.
- [13] M. Sahebsara, T. Chen, and S. L. Shah, "Optimal H_∞ filtering in networked control systems with multiple packet dropouts," *Systems & Control Letters*, vol. 57, no. 9, pp. 696–702, 2008.
- [14] S. Sun, L. Xie, and W. Xiao, "Optimal full-order and reduced-order estimators for discrete-time systems with multiple packet dropouts," *IEEE Transactions on Signal Processing*, vol. 56, no. 8, pp. 4031–4038, 2008.
- [15] X. Lu, L. Xie, H. Zhang, and W. Wang, "Robust Kalman filtering for discrete-time systems with measurement delay," *IEEE Transactions on Circuits and Systems II*, vol. 54, no. 6, pp. 522–526, 2007.
- [16] Z. Wang, Y. Liu, and X. Liu, " H_∞ filtering for uncertain stochastic time-delay systems with sector-bounded nonlinearities," *Automatica*, vol. 44, no. 5, pp. 1268–1277, 2008.

- [17] E. Yaz and A. Ray, "Linear unbiased state estimation for random models with sensor delay," in *Proceedings of the 35th IEEE Conference on Decision and Control*, pp. 47–52, Kobe, Japan, December 1996.
- [18] Z. Wang, D. W. C. Ho, and X. Liu, "Robust filtering under randomly varying sensor delay with variance constraints," *IEEE Transactions on Circuits and Systems II*, vol. 51, no. 6, pp. 320–326, 2004.
- [19] F. Yang, Z. Wang, G. Feng, and X. Liu, "Robust filtering with randomly varying sensor delay: the finite-horizon case," *IEEE Transactions on Circuits and Systems I*, vol. 56, no. 3, pp. 1310–1314, 2009.
- [20] S. Zhou and G. Feng, " H_∞ filtering for discrete-time systems with randomly varying sensor delays," *Automatica*, vol. 44, no. 7, pp. 1918–1922, 2008.
- [21] S. Xu and J. Lam, "A survey of linear matrix inequality techniques in stability analysis of delay systems," *International Journal of Systems Science*, vol. 39, no. 12, pp. 1095–1113, 2008.
- [22] D. F. Delchamps, "Stabilizing a linear system with quantized state feedback," *IEEE Transactions on Automatic Control*, vol. 35, no. 8, pp. 916–924, 1990.
- [23] R. W. Brockett and D. Liberzon, "Quantized feedback stabilization of linear systems," *IEEE Transactions on Automatic Control*, vol. 45, no. 7, pp. 1279–1289, 2000.
- [24] J.-C. Delvenne, "An optimal quantized feedback strategy for scalar linear systems," *IEEE Transactions on Automatic Control*, vol. 51, no. 2, pp. 298–303, 2006.
- [25] N. Elia and S. K. Mitter, "Stabilization of linear systems with limited information," *IEEE Transactions on Automatic Control*, vol. 46, no. 9, pp. 1384–1400, 2001.
- [26] M. Fu and L. Xie, "The sector bound approach to quantized feedback control," *IEEE Transactions on Automatic Control*, vol. 50, no. 11, pp. 1698–1711, 2005.
- [27] D. Liberzon, "Hybrid feedback stabilization of systems with quantized signals," *Automatica*, vol. 39, no. 9, pp. 1543–1554, 2003.
- [28] D. Yue, C. Peng, and G. Y. Tang, "Guaranteed cost control of linear systems over networks with state and input quantisations," *IEE Proceedings Control Theory and Applications*, vol. 153, no. 6, pp. 658–664, 2006.
- [29] C. Peng and Y.-C. Tian, "Networked H_∞ control of linear systems with state quantization," *Information Sciences*, vol. 177, no. 24, pp. 5763–5774, 2007.
- [30] E. Tian, D. Yue, and C. Peng, "Quantized output feedback control for networked control systems," *Information Sciences*, vol. 178, no. 12, pp. 2734–2749, 2008.
- [31] Y. Cao, Z. Lin, and B. M. Chen, "An output feedback H_∞ controller design for linear systems subject to sensor nonlinearities," *IEEE Transactions on Circuits and Systems I*, vol. 50, no. 7, pp. 914–921, 2003.
- [32] Y. Cao, Z. Lin, and D. G. Ward, "An antiwindup approach to enlarging domain of attraction for linear systems subject to actuator saturation," *IEEE Transactions on Automatic Control*, vol. 47, no. 1, pp. 140–145, 2002.
- [33] Y. Y. Cao, Z. Lin, and D. G. Ward, " H_∞ antiwindup design for linear systems subject to input saturation," *Journal of Guidance, Control, and Dynamics*, vol. 25, no. 3, pp. 455–463, 2002.
- [34] T. Hu, Z. Lin, and B. M. Chen, "Analysis and design for discrete-time linear systems subject to actuator saturation," *Systems & Control Letters*, vol. 45, no. 2, pp. 97–112, 2002.
- [35] Z. Zuo, D. W. C. Ho, and Y. Wang, "Fault tolerant control for singular systems with actuator saturation and nonlinear perturbation," *Automatica*, vol. 46, no. 3, pp. 569–576, 2010.
- [36] Z. Zuo, J. Wang, and L. Huang, "Output feedback H_∞ controller design for linear discrete-time systems with sensor nonlinearities," *IEE Proceedings Control Theory and Applications*, vol. 152, no. 1, pp. 19–26, 2005.
- [37] E. Fridman and M. Dambrine, "Control under quantization, saturation and delay: an LMI approach," *Automatica*, vol. 45, no. 10, pp. 2258–2264, 2009.
- [38] Y. Xiao, Y.-Y. Cao, and Z. Lin, "Robust filtering for discrete-time systems with saturation and its application to transmultiplexers," *IEEE Transactions on Signal Processing*, vol. 52, no. 5, pp. 1266–1277, 2004.
- [39] F. Yang and Y. Li, "Set-membership filtering for systems with sensor saturation," *Automatica*, vol. 45, no. 8, pp. 1896–1902, 2009.
- [40] T. Chen and B. A. Francis, "Linear time-varying H_2 -optimal control of sampled-data systems," *Automatica*, vol. 27, no. 6, pp. 963–974, 1991.
- [41] L. Qiu and T. Chen, " H_2 -optimal design of multirate sampled-data systems," *IEEE Transactions on Automatic Control*, vol. 39, no. 12, pp. 2506–2511, 1994.
- [42] T. Chen and L. Qiu, " H_∞ design of general multirate sampled-data control systems," *Automatica*, vol. 30, no. 7, pp. 1139–1152, 1994.

- [43] L. Qiu and T. Chen, "Multirate sampled-data systems: all H_∞ suboptimal controllers and the minimum entropy controller," *IEEE Transactions on Automatic Control*, vol. 44, no. 3, pp. 537–550, 1999.
- [44] P. Shi, "Filtering on sampled-data systems with parametric uncertainty," *IEEE Transactions on Automatic Control*, vol. 43, no. 7, pp. 1022–1027, 1998.
- [45] S. K. Nguang and P. Shi, "Nonlinear H_∞ filtering of sampled-data systems," *Automatica*, vol. 36, no. 2, pp. 303–310, 2000.
- [46] Z. Wang, B. Huang, and P. Huo, "Sampled-data filtering with error covariance assignment," *IEEE Transactions on Signal Processing*, vol. 49, no. 3, pp. 666–670, 2001.
- [47] E. Fridman, A. Seuret, and J.-P. Richard, "Robust sampled-data stabilization of linear systems: an input delay approach," *Automatica*, vol. 40, no. 8, pp. 1441–1446, 2004.
- [48] E. Fridman, U. Shaked, and V. Suplin, "Input/output delay approach to robust sampled-data H_∞ control," *Systems & Control Letters*, vol. 54, no. 3, pp. 271–282, 2005.
- [49] H. Gao, J. Wu, and P. Shi, "Robust sampled-data H_∞ control with stochastic sampling," *Automatica*, vol. 45, no. 7, pp. 1729–1736, 2009.
- [50] J. Wu, X. Chen, and H. Gao, " H_∞ filtering with stochastic sampling," *Signal Processing*, vol. 90, no. 4, pp. 1131–1145, 2010.
- [51] J. A. Ball, J. W. Helton, and M. L. Walker, " H_∞ control for nonlinear systems with output feedback," *IEEE Transactions on Automatic Control*, vol. 38, no. 4, pp. 546–559, 1993.
- [52] N. Berman and U. Shaked, " H_∞ control for discrete-time nonlinear stochastic systems," *IEEE Transactions on Automatic Control*, vol. 51, no. 6, pp. 1041–1046, 2006.
- [53] N. Berman and U. Shaked, " H_∞ -like control for nonlinear stochastic systems," *Systems & Control Letters*, vol. 55, no. 3, pp. 247–257, 2006.
- [54] A. J. van der Schaft, " L_2 -gain analysis of nonlinear systems and nonlinear state feedback H_∞ control," *IEEE Transactions on Automatic Control*, vol. 37, no. 6, pp. 770–784, 1992.
- [55] C. Du, L. Xie, and Y. C. Soh, " H_∞ reduced-order approximation of 2-D digital filters," *IEEE Transactions on Circuits and Systems I*, vol. 48, no. 6, pp. 688–698, 2001.
- [56] L. Wu, P. Shi, H. Gao, and C. Wang, " H_∞ filtering for 2D Markovian jump systems," *Automatica*, vol. 44, no. 7, pp. 1849–1858, 2008.
- [57] G. Wei and H. Shu, " H_∞ filtering on nonlinear stochastic systems with delay," *Chaos, Solitons and Fractals*, vol. 33, no. 2, pp. 663–670, 2007.
- [58] S. Xu, J. Lam, and X. Mao, "Delay-dependent H_∞ control and filtering for uncertain Markovian jump systems with time-varying delays," *IEEE Transactions on Circuits and Systems I*, vol. 54, no. 9, pp. 2070–2077, 2007.
- [59] U. Shaked and N. Berman, " H_∞ nonlinear filtering of discrete-time processes," *IEEE Transactions on Signal Processing*, vol. 43, no. 9, pp. 2205–2209, 1995.
- [60] W. Zhang, B.-S. Chen, and C.-S. Tseng, "Robust H_∞ filtering for nonlinear stochastic systems," *IEEE Transactions on Signal Processing*, vol. 53, no. 2, pp. 589–598, 2005.
- [61] D. J. Watts and S. H. Strogatz, "Collective dynamics of "small-world" networks," *Nature*, vol. 393, no. 6684, pp. 440–442, 1998.
- [62] A.-L. Barabasi and R. Albert, "Emergence of scaling in random networks," *Science*, vol. 286, no. 5439, pp. 509–512, 1999.
- [63] Z. Duan, G. Chen, and L. Huang, "Disconnected synchronized regions of complex dynamical networks," *IEEE Transactions on Automatic Control*, vol. 54, no. 4, pp. 845–849, 2009.
- [64] Z. Li, Z. Duan, G. Chen, and L. Huang, "Consensus of multiagent systems and synchronization of complex networks: a unified viewpoint," *IEEE Transactions on Circuits and Systems I*, vol. 57, no. 1, pp. 213–224, 2010.
- [65] Z. Zuo, C. Yang, and Y. Wang, "A unified framework of exponential synchronization for complex networks with time-varying delays," *Physics Letters A*, vol. 374, no. 19–20, pp. 1989–1999, 2010.
- [66] X. F. Wang and G. Chen, "Synchronization in small-world dynamical networks," *International Journal of Bifurcation and Chaos in Applied Sciences and Engineering*, vol. 12, no. 1, pp. 187–192, 2002.
- [67] J. Jost and M. P. Joy, "Spectral properties and synchronization in coupled map lattices," *Physical Review E*, vol. 65, no. 1, p. 016201, 2002.
- [68] J. Liang, Z. Wang, Y. Liu, and X. Liu, "Robust synchronization of an array of coupled stochastic discrete-time delayed neural networks," *IEEE Transactions on Neural Networks*, vol. 19, no. 11, pp. 1910–1921, 2008.
- [69] R. Palm, "Synchronization of decentralized multiple-model systems by market-based optimization," *IEEE Transactions on Systems, Man, and Cybernetics, Part B*, vol. 34, no. 1, pp. 665–672, 2004.

- [70] W. He and J. Cao, "Exponential synchronization of hybrid coupled networks with delayed coupling," *IEEE Transactions on Neural Networks*, vol. 21, no. 4, pp. 571–583, 2010.
- [71] F. O. Souza and R. M. Palhares, "Synchronisation of chaotic delayed artificial neural networks: an H_∞ control approach," *International Journal of Systems Science*, vol. 40, no. 9, pp. 937–944, 2009.
- [72] W. Lu and T. Chen, "Synchronization of coupled connected neural networks with delays," *IEEE Transactions on Circuits and Systems I*, vol. 51, no. 12, pp. 2491–2503, 2004.
- [73] W. Lu and T. Chen, "Global synchronization of discrete-time dynamical network with a directed graph," *IEEE Transactions on Circuits and Systems II*, vol. 54, no. 2, pp. 136–140, 2007.
- [74] V. Perez-Munuzuri, V. Perez-Villar, and L. O. Chua, "Autowaves for image processing on a two-dimensional CNN array of excitable nonlinear circuits: flat and wrinkled labyrinths," *IEEE Transactions on Circuits and Systems I*, vol. 40, no. 3, pp. 174–181, 1993.
- [75] L. M. Pecora and T. L. Carroll, "Synchronization in chaotic systems," *Physical Review Letters*, vol. 64, no. 8, pp. 821–824, 1990.
- [76] Z. Li and G. Chen, "Global synchronization and asymptotic stability of complex dynamical networks," *IEEE Transactions on Circuits and Systems II*, vol. 53, no. 1, pp. 28–33, 2006.
- [77] J. Cao and J. Lu, "Adaptive synchronization of neural networks with or without time-varying delay," *Chaos. An Interdisciplinary Journal of Nonlinear Science*, vol. 16, no. 1, p. article 013133, 2006.
- [78] X. Hu and J. Wang, "Design of general projection neural networks for solving monotone linear variational inequalities and linear and quadratic optimization problems," *IEEE Transactions on Systems, Man, and Cybernetics, Part B*, vol. 37, no. 5, pp. 1414–1421, 2007.
- [79] H. R. Karimi and H. Gao, "New delay-dependent exponential H_∞ synchronization for uncertain neural networks with mixed time delays," *IEEE Transactions on Systems, Man, and Cybernetics, Part B*, vol. 40, no. 1, pp. 173–185, 2010.
- [80] Z. Fei, H. Gao, and W. X. Zheng, "New synchronization stability of complex networks with an interval time-varying coupling delay," *IEEE Transactions on Circuits and Systems II*, vol. 56, no. 6, pp. 499–503, 2009.
- [81] H. Gao, J. Lam, and G. Chen, "New criteria for synchronization stability of general complex dynamical networks with coupling delays," *Physics Letters A*, vol. 360, no. 2, pp. 263–273, 2006.
- [82] S. Mou, H. Gao, J. Lam, and W. Qiang, "A new criterion of delay-dependent asymptotic stability for Hopfield neural networks with time delay," *IEEE Transactions on Neural Networks*, vol. 19, no. 3, pp. 532–535, 2008.
- [83] P. Li, J. Lam, and Z. Shu, "On the transient and steady-state estimates of interval genetic regulatory networks," *IEEE Transactions on Systems, Man, and Cybernetics, Part B*, vol. 40, no. 2, pp. 336–349, 2010.
- [84] Z. Shu and J. Lam, "Global exponential estimates of stochastic interval neural networks with discrete and distributed delays," *Neurocomputing*, vol. 71, no. 13–15, pp. 2950–2963, 2008.
- [85] Z. Toroczkai, "Complex networks: the challenge of interaction topology," *Los Alamos Science*, no. 29, pp. 94–109, 2005.
- [86] J. Buhmann and K. Schulten, "Influence of noise on the function of a "physiological" neural network," *Biological Cybernetics*, vol. 56, no. 5-6, pp. 313–327, 1987.
- [87] K. Wood, C. Van den Broeck, R. Kawai, and K. Lindenberg, "Continuous and discontinuous phase transitions and partial synchronization in stochastic three-state oscillators," *Physical Review E*, vol. 76, no. 4, p. 041132, 2007.
- [88] Z. Wang, D. W. C. Ho, Y. Liu, and X. Liu, "Robust H_∞ control for a class of nonlinear discrete time-delay stochastic systems with missing measurements," *Automatica*, vol. 45, no. 3, pp. 684–691, 2009.
- [89] H. Li and D. Yue, "Synchronization of Markovian jumping stochastic complex networks with distributed time delays and probabilistic interval discrete time-varying delays," *Journal of Physics A*, vol. 43, no. 10, p. article 105101, 2010.
- [90] J. Lü and G. Chen, "A time-varying complex dynamical network model and its controlled synchronization criteria," *IEEE Transactions on Automatic Control*, vol. 50, no. 6, pp. 841–846, 2005.
- [91] W. Zhong, J. D. Stefanovski, G. M. Dimirovski, and J. Zhao, "Decentralized control and synchronization of time-varying complex dynamical network," *Kybernetika*, vol. 45, no. 1, pp. 151–167, 2009.
- [92] Z. Wang, D. W. C. Ho, and X. Liu, "State estimation for delayed neural networks," *IEEE Transactions on Neural Networks*, vol. 16, no. 1, pp. 279–284, 2005.
- [93] Y. Liu, Z. Wang, and X. Liu, "Design of exponential state estimators for neural networks with mixed time delays," *Physics Letters A*, vol. 364, no. 5, pp. 401–412, 2007.
- [94] Y. He, Q. G. Wang, M. Wu, and C. Lin, "Delay-dependent state estimation for delayed neural networks," *IEEE Transactions on Neural Networks*, vol. 17, no. 4, pp. 1077–1081, 2006.

- [95] Y. Liu, Z. Wang, J. Liang, and X. Liu, "Synchronization and state estimation for discrete-time complex networks with distributed delays," *IEEE Transactions on Systems, Man, and Cybernetics, Part B*, vol. 38, no. 5, pp. 1314–1325, 2008.
- [96] B. Lu and V. C. Gungor, "Online and remote motor energy monitoring and fault diagnostics using wireless sensor networks," *IEEE Transactions on Industrial Electronics*, vol. 56, no. 11, pp. 4651–4659, 2009.
- [97] G. Cimatti, R. Rovatti, and G. Setti, "Chaos-based spreading in DS-UWB sensor networks increases available bit rate," *IEEE Transactions on Circuits and Systems I*, vol. 54, no. 6, pp. 1327–1339, 2007.
- [98] A. Speranzon, C. Fischione, K. Johansson, and A. Sangiovanni-Vincentelli, "A distributed minimum variance estimator for sensor networks," *IEEE Journal on Selected Areas in Communications*, vol. 26, no. 4, pp. 609–621, 2008.
- [99] F. S. Cattivelli, C. G. Lopes, and A. H. Sayed, "Diffusion strategies for distributed Kalman filtering: formulation and performance analysis," in *Proceedings of the IAPR Workshop on Cognitive Information*, Santorini, Greece, June 2008.
- [100] F. S. Cattivelli and A. H. Sayed, "Diffusion mechanisms for fixed-point distributed Kalman smoothing," in *Proceedings of the European Signal Processing Conference*, pp. 1–4, Lausanne, Switzerland, August 2008.
- [101] W. Yu, G. Chen, Z. Wang, and W. Yang, "Distributed consensus filtering in sensor networks," *IEEE Transactions on Systems, Man, and Cybernetics, Part B*, vol. 39, no. 6, pp. 1568–1577, 2009.
- [102] R. Olfati-Saber and R. M. Murray, "Consensus problems in networks of agents with switching topology and time-delays," *IEEE Transactions on Automatic Control*, vol. 49, no. 9, pp. 1520–1533, 2004.
- [103] G. Shi and Y. Hong, "Global target aggregation and state agreement of nonlinear multi-agent systems with switching topologies," *Automatica*, vol. 45, no. 5, pp. 1165–1175, 2009.
- [104] L. Xiao and S. Boyd, "Fast linear iterations for distributed averaging," *Systems & Control Letters*, vol. 53, no. 1, pp. 65–78, 2004.
- [105] P. Lin, Y. Jia, and L. Li, "Distributed robust H_∞ consensus control in directed networks of agents with time-delay," *Systems & Control Letters*, vol. 57, no. 8, pp. 643–653, 2008.
- [106] Z. G. Hou, L. Cheng, and M. Tan, "Decentralized robust adaptive control for the multiagent system consensus problem using neural networks," *IEEE Transactions on Systems, Man, and Cybernetics, Part B*, vol. 39, no. 3, pp. 636–647, 2009.
- [107] T. Li and J. F. Zhang, "Mean square average-consensus under measurement noises and fixed topologies: necessary and sufficient conditions," *Automatica*, vol. 45, no. 8, pp. 1929–1936, 2009.
- [108] F. Xiao and L. Wang, "Consensus protocols for discrete-time multi-agent systems with time-varying delays," *Automatica*, vol. 44, no. 10, pp. 2577–2582, 2008.
- [109] Y. G. Sun, L. Wang, and G. Xie, "Average consensus in networks of dynamic agents with switching topologies and multiple time-varying delays," *Systems & Control Letters*, vol. 57, no. 2, pp. 175–183, 2008.
- [110] P. A. Bliman and G. Ferrari-Trecate, "Average consensus problems in networks of agents with delayed communications," *Automatica*, vol. 44, no. 8, pp. 1985–1995, 2008.
- [111] R. Olfati-Saber and J. S. Shamma, "Consensus filters for sensor networks and distributed sensor fusion," in *Proceedings of the 44th IEEE Conference Decision and Control and European Control Conference*, pp. 6698–6703, Seville, Spain, December 2005.
- [112] R. Olfati-Saber, "Distributed Kalman filtering for sensor networks," in *Proceedings of the 46th IEEE Conference on Decision and Control, (CDC '07)*, pp. 5492–5498, New Orleans, LA, USA, December 2007.
- [113] I. D. Schizas, S. I. Roumeliotis, G. B. Giannakis, and A. Ribeiro, "Anytime optimal distributed Kalman filtering and smoothing," in *Proceedings of the IEEE 14th Workshop on Statistical Signal Processing, (SSP '07)*, pp. 368–372, Madison, Wis, USA, August 2007.
- [114] S. S. Stanković, M. S. Stanković, and D. M. Stipanović, "Consensus based overlapping decentralized estimation with missing observations and communication faults," *Automatica*, vol. 45, no. 6, pp. 1397–1406, 2009.
- [115] B. D. O. Anderson and J. B. Moore, *Optimal Filtering*, Prentice-Hall, Englewood Cliffs, NJ, USA, 1979.
- [116] H. Gao, X. Meng, and T. Chen, " H_∞ filter design for discrete delay systems: a new parameter-dependent approach," *International Journal of Control*, vol. 82, no. 6, pp. 993–1005, 2009.
- [117] H. Gao, Y. Zhao, J. Lam, and K. Chen, " H_∞ fuzzy filtering of nonlinear systems with intermittent measurements," *IEEE Transactions on Fuzzy Systems*, vol. 17, no. 2, pp. 291–300, 2009.
- [118] S. K. Nguang and P. Shi, " H_∞ filtering design for uncertain nonlinear systems under sampled measurements," *International Journal of Systems Science*, vol. 32, no. 7, pp. 889–898, 2001.

- [119] B. Shen, Z. Wang, H. Shu, and G. Wei, "On nonlinear H_∞ filtering for discrete-time stochastic systems with missing measurements," *IEEE Transactions on Automatic Control*, vol. 53, no. 9, pp. 2170–2180, 2008.
- [120] B. Shen, Z. Wang, H. Shu, and G. Wei, " H_∞ filtering for nonlinear discrete-time stochastic systems with randomly varying sensor delays," *Automatica*, vol. 45, no. 4, pp. 1032–1037, 2009.
- [121] B. Shen, Z. Wang, H. Shu, and G. Wei, "Robust H_∞ finite-horizon filtering with randomly occurred nonlinearities and quantization effects," *Automatica*, vol. 46, no. 11, pp. 1743–1751, 2010.
- [122] B. Shen, Z. Wang, H. Shu, and G. Wei, " H_∞ filtering for uncertain time-varying systems with multiple randomly occurred nonlinearities and successive packet dropouts," *International Journal of Robust and Nonlinear Control*, vol. 21, no. 14, pp. 1693–1709, 2011.
- [123] Z. Wang, B. Shen, and X. Liu, " H_∞ filtering with randomly occurring sensor saturations and missing measurements," *Automatica*. In press.
- [124] B. Shen, Z. Wang, and Y. S. Hung, "Distributed H_∞ -consensus filtering in sensor networks with multiple missing measurements: the finite-horizon case," *Automatica*, vol. 46, no. 10, pp. 1682–1688, 2010.
- [125] B. Shen, Z. Wang, Y. S. Hung, and G. Chesi, "Distributed H_∞ filtering for polynomial nonlinear stochastic systems in sensor networks," *IEEE Transactions on Industrial Electronics*, vol. 58, no. 5, pp. 1971–1979, 2011.
- [126] B. Shen, Z. Wang, and X. Liu, "A stochastic sampled-data approach to distributed H_∞ filtering in sensor networks," *IEEE Transactions on Circuits and Systems I*, vol. 58, no. 9, pp. 2237–2246, 2011.
- [127] B. Shen, Z. Wang, and X. Liu, "Bounded H_∞ synchronization and state estimation for discrete time-varying stochastic complex networks over a finite horizon," *IEEE Transactions on Neural Networks*, vol. 22, no. 1, pp. 145–157, 2010.

Research Article

Impulsive Synchronization of Nonlinearly Coupled Complex Networks

Guizhen Feng,^{1,2} Jinde Cao,^{1,3} and Jianquan Lu³

¹ School of Automation, Southeast University, Nanjing 210096, China

² Department of Mathematics and Physics, Nanjing Institute of Industry Technology, Nanjing 210046, China

³ Department of Mathematics, Southeast University, Nanjing 210096, China

Correspondence should be addressed to Jinde Cao, jdcao@seu.edu.cn

Received 25 June 2011; Revised 5 September 2011; Accepted 5 September 2011

Academic Editor: Jinling Liang

Copyright © 2012 Guizhen Feng et al. This is an open access article distributed under the Creative Commons Attribution License, which permits unrestricted use, distribution, and reproduction in any medium, provided the original work is properly cited.

This paper investigates synchronization problem of nonlinearly coupled dynamical networks, and an effectively impulsive control scheme is proposed to synchronize the network onto the objective state. Based on the stability analysis of impulsive differential equations, a low-dimensional sufficient condition is derived to guarantee the exponential synchronization in virtual of average impulsive interval. A numerical example is given to illustrate the effectiveness and feasibility of the proposed methods and results.

1. Introduction

Synchronization of complex networks is an important topic that has drawn a great deal of attention from diverse fields including physics, biology, neuroscience, and mathematics [1–3]. It is also a fundamental phenomenon that enables coherent behavior in networks as a result of interactions. In our real life, there are many interesting and useful network synchronization phenomena, such as, fireflies in the forest, applause, description of heart, and routing messages in the internet.

Due to its potential applications in many different areas, the synchronization of complex dynamical networks has been widely discussed in the last decade. For example, in [4, 5], the authors studied the synchronization in two specific kinds of networks including scale-free networks and small-world networks. In [6–8], the authors introduced a time-varying dynamical network with the same prototype of [4, 5] and further investigated its synchronization. In order to simulate more realistic complex networks, the researchers

studied the influences of time delays on synchronization in [9–12]. In [9], the authors extended the model of [4, 5] to a uniform model with coupling delays, and some synchronization criteria for complex networks are derived for both delay-independent and delay-dependent exponential stability of the synchronous state. In [10], the authors are concerned with global synchronization of coupled delayed neural network. In [11], the authors studied the globally exponential synchronization in arrays of coupled identical delayed neural networks by using Lyapunov functional method and Kronecker product techniques. Some interesting results about synchronization and consensus of sensor networks with communication constraints have been obtained in [12–14]. However, previous studies on synchronization mainly concerned with linearly coupled dynamical networks, with the coupling matrix constant or time varying, and so forth. Only some papers investigated nonlinearly-coupled networks, such as [15–17].

Most recently, another synchronization technique, based on impulsive control, has been reported and developed in [18–22]. This technique is very effective and robust and with a low cost since the control input is implemented by the “sudden jumps” of some state variables at some instants. Therefore it is of great importance to study the coupled dynamical networks under impulsive control. Based on the theory of impulsive differential equations, in [18], the authors proposed an impulsive synchronization criterion for an uncertain dynamical network. In [19], the authors studied the synchronization of complex dynamical networks with time-varying delays and impulsive effects by introducing the concept of control topology. In [20], the authors investigated the exponential synchronization of the complex dynamical networks with a coupled delay and impulsive control. By referring to the concept of average dwell time, a unified synchronization criterion was derived by proposing a concept named “average impulsive interval” in [21]. In [22], the authors investigate the globally exponential synchronization for linearly coupled neural networks with time varying delay and impulsive disturbances under the concept of average impulsive interval.

Motivated by the above discussions, the aim of this paper is to discuss the impulsive synchronization of nonlinearly-coupled complex networks. Based on the stability analysis of impulsive functional differential equations, some sufficient synchronization criteria are derived in virtual of average impulsive interval.

The main contributions of this paper are as follows. First, this paper uses the concept of “average impulsive interval” to obtain the synchronization criterion. It makes the result much less conservative than previous results since the strict requirement on the upper bound and lower bound of the impulsive interval, which always appear in the previous results, is not necessary any more. Second, the model considered in this paper is nonlinearly coupled network, which includes linearly coupled network and array of linearly coupled systems as special cases.

The outline of this paper is given as follows. In Section 2, a model of nonlinearly-coupled complex networks with impulsive control and some necessary definitions are proposed. In Section 3, a sufficient criterion is derived based on the stability analysis of impulsive functional differential equations. In Section 4, a numerical example is given to illustrate the effectiveness and feasibility of the synchronization criterion.

Notation 1. Throughout this paper, some mathematical notations are used. \mathbb{I} represents the identity matrix and $\mathbb{R} = \{-\infty, +\infty\}$. Denote the transpose of the vector x as x^T . Without explicitly state, the dimension of the vectors and matrices are assumed to be compatible in the context.

2. Model Description and Preliminaries

Consider a complex dynamical network consisting of N nonlinearly-coupled identical nodes, which is described by

$$\dot{x}_i(t) = f(x_i(t)) + c \sum_{j=1}^N a_{ij} \Gamma h(x_j(t)), \quad i = 1, 2, \dots, N, \quad (2.1)$$

where the nonlinear coupling function $h(x_j(t)) = (h(x_{j1}(t)), h(x_{j2}(t)), \dots, h(x_{jn}(t)))^T$ satisfies the following condition: $[(h(u) - h(v)) / (u - v)] \geq \gamma > 0$ for any $u, v \in \mathbb{R}$. The configuration coupling matrix $L = (a_{ij})_{N \times N}$ is defined as follows: if there is a connection between node i and node j ($j \neq i$), then $a_{ij} = a_{ji} > 0$; otherwise, $a_{ij} = a_{ji} = 0$; the diagonal elements are defined as $a_{ii} = -\sum_{j=1, j \neq i}^N a_{ij}$. $\Gamma = \text{diag}\{\gamma_1, \gamma_2, \dots, \gamma_n\}$ > 0 is the inner coupling positive definite matrix between two connected nodes i and j .

In order to achieve the synchronization of the complex dynamical network (2.1) at the original point, we design an impulsive control law:

$$u_i(t) = \sum_{k=1}^{\infty} \mu x_i(t) \delta(t - t_k), \quad i = 1, 2, \dots, N, \quad (2.2)$$

where the impulsive instant sequence $\{t_k\}_{k=1}^{\infty}$ satisfies $0 \leq t_1 < t_2 < \dots < t_k < \dots$ and $\lim_{k \rightarrow \infty} t_k = \infty$, μ is the impulsive control gain, and $\delta(\cdot)$ is the Dirac delta function. Then, we obtain the following impulsive dynamical network with nonlinear coupling as follows:

$$\dot{x}_i(t) = f(x_i(t)) + c \sum_{j=1}^N a_{ij} \Gamma h(x_j(t)), \quad t \neq t_k, k \in \mathbb{N}, t \geq t_0, \quad (2.3)$$

$$\Delta x_i(t_k) = \mu x_i(t_k), \quad t = t_k,$$

where $i = 1, 2, \dots, N$, and $\Delta x_i(t_k) = x_i(t_k^+) - x_i(t_k^-)$ is the "jump" in the state variable at the time instant t_k , with $x_i(t_k^+) = \lim_{t \rightarrow t_k^+} x_i(t)$, and $x_i(t_k^-) = \lim_{t \rightarrow t_k^-} x_i(t)$. For simplicity, we assume that $x(t)$ is left continuous at $t = t_k$, that is, $x_i(t_k^-) = x_i(t_k)$.

There are some definitions and denotations that are necessary for presenting the main results as follows.

Definition 2.1. The nonlinear-coupled dynamical network is said to be exponentially synchronized to the original point if there exist some constants $\alpha > 0$ and $M > 0$ such that for any initial conditions

$$\|x_i(t)\| \leq M e^{-\alpha t}, \quad \forall t \geq 0. \quad (2.4)$$

Now, we give the following definition on quadratic (QUAD) inequality, which plays an important role in the discussion of synchronization.

Definition 2.2. The function $f(\cdot)$ is said to satisfy $f(\cdot) \in \text{QUAD}(P, \Delta, \mu)$, if there exists a positive definite diagonal matrix $P = \text{diag}(p_1, \dots, p_n)$, a diagonal matrix $\Delta = \text{diag}(\delta_1, \dots, \delta_n)$, and a scalar $\mu > 0$, such that

$$(x - y)^T P [f(x) - f(y) - \Delta(x - y)] \leq -\mu (x - y)^T (x - y) \quad (2.5)$$

holds for any $x, y \in \mathbb{R}^n$.

Definition 2.3 (see [20] average impulsive interval). The average impulsive interval of the impulsive sequence $\tau = \{\tau_1, \tau_2, \dots\}$ is less than T_a , if there exist positive integer N_0 and positive number T_a , such that

$$N(\tau, t) \geq \frac{t - \tau}{T_a} - N_0, \quad \forall t \geq \tau \geq 0, \quad (2.6)$$

where $N(\tau, t)$ denotes the number of impulsive times of the impulsive sequence τ in the time interval (τ, t) .

3. Main Result

Suppose that we are mainly interested in achieving synchronization of the network (2.3) by defining the controlled synchronization state as original point $x^* = 0$, which satisfies $f(x^*) = 0$. Now the main result will be presented in this section.

Theorem 3.1. Consider the nonlinearly-coupled complex network (2.1) with impulsive controller. Suppose that $f(\cdot) \in \text{QUAD}(I, \Delta, \mu)$, and the average impulsive interval of impulsive sequence $\tau = \{\tau_1, \tau_2, \dots\}$ is less than T_a . Then the impulsive dynamical system (2.3) is exponentially synchronized with convergence rate λ if

$$\lambda = \frac{2 \ln(|1 + \mu|)}{T_a} + \mu < 0, \quad (3.1)$$

where $\mu = -2\alpha + 2 \max_k \{ \beta_k \}$.

Proof. Construct a Lyapunov function in the form of

$$V(\tau) = \sum_{i=1}^N x_i^T(\tau) x_i(\tau). \quad (3.2)$$

When $t \in (t_{k-1}, t_k]$, the derivative of $V(t)$ with respect to (2.3) can be calculated as follows:

$$\begin{aligned} \dot{V}(t) &= 2 \sum_{i=1}^N x_i^T(t) \dot{x}_i(t) \\ &= 2 \sum_{i=1}^N x_i^T(t) \left[f(x_i(t)) + c \sum_{j=1}^N \Gamma_{ij} h(x_j(t)) \right] \\ &= 2 \sum_{i=1}^N x_i^T(t) f(x_i(t)) + 2c \sum_{i=1}^N \sum_{j=1}^N \Gamma_{ij} x_i^T(t) h(x_j(t)). \end{aligned} \quad (3.3)$$

Since $f(\cdot) \in \text{QUAD}(\mathcal{I}, \Delta, \cdot)$, the following inequality can be obtained:

$$\begin{aligned} 2 \sum_{i=1}^N x_i^T(t) f(x_i(t)) &= 2 \sum_{i=1}^N \left[x_i^T(t) (f(x_i(t)) - \Delta x_i(t)) + x_i^T(t) \Delta x_i(t) \right] \\ &\leq 2 \sum_{i=1}^N \left[-x_i^T(t) x_i(t) + \max_k \{ \lambda_k \} x_i^T(t) x_i(t) \right] \\ &= (-2 + 2 \max_k \{ \lambda_k \}) \sum_{i=1}^N x_i^T(t) x_i(t) \\ &= V(t), \end{aligned} \quad (3.4)$$

where $\lambda_k = -2 + 2 \max_k \{ \lambda_k \}$.

Let $x(t) = (x_1(t), x_2(t), \dots, x_N(t))^T$ and $h(x(t)) = (h(x_1(t)), h(x_2(t)), \dots, h(x_N(t)))^T$. Since $[(h(u) - h(v))/(u - v)] \geq \lambda_k > 0$, it follows from the diffusive property of matrix L that

$$\begin{aligned} 2c \sum_{i=1}^N \sum_{j=1}^N \Gamma_{ij} x_i^T(t) h(x_j(t)) &= 2c \sum_{i=1}^N \sum_{j=1}^N \Gamma_{ij} \left[\sum_{i=1}^n x_i(t) h(x_j(t)) \right] \\ &= 2c \sum_{i=1}^n \left[\sum_{i=1}^N \sum_{j=1}^N \Gamma_{ij} x_i(t) h(x_j(t)) \right] \\ &= 2c \sum_{i=1}^n (x(t))^T L h(x(t)) \\ &= -c \sum_{i=1}^n \sum_{j=1}^N \sum_{j \neq i}^N \Gamma_{ij} (x_i(t) - x_j(t)) (h(x_i(t)) - h(x_j(t))) \\ &\leq -c \sum_{i=1}^n \sum_{j=1}^N \sum_{j \neq i}^N \Gamma_{ij} (x_i(t) - x_j(t))^2 \\ &\leq 0. \end{aligned} \quad (3.5)$$

From the inequalities (3.4) and (3.5), we can obtain that

$$\dot{V}(\vartheta) \leq -\mu V(\vartheta), \quad \vartheta \in (t_{k-1}, t_k], \quad k = 1, 2, \dots \quad (3.6)$$

Therefore,

$$V(\vartheta) \leq V(t_{k-1}^+) \exp[-\mu(\vartheta - t_{k-1})], \quad \vartheta \in (t_{k-1}, t_k), \quad k = 1, 2, \dots \quad (3.7)$$

On the other hand, when $\vartheta = t_k^+$, $k = 1, 2, \dots$,

$$V(t_k^+) = \sum_{i=1}^N x_i^T(t_k^+) x_i(t_k^+) = \sum_{i=1}^N (1 + \mu)^2 x_i^T(t_k) x_i(t_k) = (1 + \mu)^2 V(t_k). \quad (3.8)$$

From (3.7) and (3.8), we know that for any $\vartheta \in (t_0, t_1]$, $V(\vartheta) \leq V(t_0) e^{-\mu(\vartheta - t_0)}$, which leads to $V(t_1) \leq V(t_0) e^{-\mu(t_1 - t_0)}$. When $\vartheta = t_1^+$, one has $V(t_1^+) \leq (1 + \mu)^2 V(t_1) \leq (1 + \mu)^2 V(t_0) e^{-\mu(t_1 - t_0)}$. By induction, for $\vartheta \in (t_k, t_{k+1}]$, $k = 1, 2, \dots$,

$$V(\vartheta) \leq V(t_0) (1 + \mu)^{2k} e^{-\mu(\vartheta - t_0)}. \quad (3.9) \quad \square$$

Let $N(\vartheta, t_0)$ be the number of impulsive times of the impulsive sequence on the interval (t_0, ϑ) . Hence for any $\vartheta \in \mathbb{R}$ we can obtain

$$V(\vartheta) \leq (1 + \mu)^{2N(\vartheta, t_0)} e^{-\mu(\vartheta - t_0)} V(t_0). \quad (3.10)$$

Since $\mu \in (-2, 0)$, it follows from Definition 2.3 that

$$\begin{aligned} V(\vartheta) &\leq (1 + \mu)^{2((\vartheta - t_0)/T_a - N_0)} e^{-\mu(\vartheta - t_0)} V(t_0) \\ &\leq (1 + \mu)^{-2N_0} e^{(2 \ln(|1 + \mu|)/T_a)(\vartheta - t_0)} e^{-\mu(\vartheta - t_0)} V(t_0) \\ &= (1 + \mu)^{-2N_0} e^{(2 \ln(|1 + \mu|)/T_a + \mu)(\vartheta - t_0)} V(t_0) \\ &= (1 + \mu)^{-2N_0} e^{(\vartheta - t_0)} V(t_0). \end{aligned} \quad (3.11)$$

Since $(2 \ln(|1 + \mu|)/T_a) + \mu < 0$, the system (2.1) can be exponentially stabilized to the original point, which implies exponential synchronization of the impulsive dynamical network (2.3). The proof is completed.

Remark 3.2. Due to the introduction of the concept ‘‘average impulsive interval’’, the requirement on the lower bound and upper bound of impulsive interval is removed in Theorem 3.1. It makes our result less conservative.

4. Numerical Example

In this section, based on the results obtained in the previous section, we consider the impulsive control of four nonlinearly-coupled canonical Lorenz systems to show the effectiveness of our results. The network is described as follows:

$$\begin{aligned}\dot{x}_i &= f(x_i(t)) + c \sum_{j=1}^4 a_{ij} \Gamma h(x_j(t)), \quad t \neq t_k, \\ \Delta x_i(t_k) &= \mu x_i(t_k), \quad t = t_k,\end{aligned}\tag{4.1}$$

where $x_i = (x_{i1}, x_{i2}, x_{i3})^T \in \mathbb{R}^3$ is the state vector of i th node, $h(x_i(t)) = (h(x_{i1}(t)), h(x_{i2}(t)), h(x_{i3}(t)))^T = (3x_{i1}(t) + \sin(x_{i1}(t)), 3x_{i2}(t) + \sin(x_{i2}(t)), 3x_{i3}(t) + \sin(x_{i3}(t)))^T$ satisfying the condition: $[(h(u) - h(v))/(u - v)] \geq \alpha > 0$ for any $u, v \in \mathbb{R}$ with $\alpha = 2$. The Laplacian coupling matrix is

$$L = \begin{bmatrix} -5 & 4 & 1 & 0 \\ 4 & -6 & 0 & 2 \\ 1 & 0 & -1 & 0 \\ 0 & 2 & 0 & -2 \end{bmatrix}.\tag{4.2}$$

The uncoupled canonical Lorenz system $\dot{y}(t) = f(y(t))$ is described as

$$\begin{aligned}\dot{y}_1 &= 10(y_2 - y_1), \\ \dot{y}_2 &= 28y_1 - y_2 - y_1y_3, \\ \dot{y}_3 &= y_1y_2 - \frac{8}{3}y_3,\end{aligned}\tag{4.3}$$

and the respective double-scroll attractor is shown in Figure 1.

In this case, we can prove that the coupled Lorenz system satisfies the QUAD condition with $P = I$, $\Delta = \text{diag}\{10, 19, -5/3\}$ and $\alpha = 1$, which can be verified in the following:

$$\begin{aligned}& x_i^T(t) (f(x_i(t)) - \Delta x_i(t)) \\ &= x_i^T(t) \left(10x_{i2} - 10x_{i1}, 28x_{i1} - x_{i2} - x_{i1}x_{i3}, x_{i1}x_{i2} - \frac{8}{3}x_{i3} \right) - x_i^T(t) \Delta x_i(t) \\ &= x_{i1}(10x_{i2} - 10x_{i1}) + x_{i2}(28x_{i1} - x_{i2} - x_{i1}x_{i3}) + x_{i3} \left(x_{i1}x_{i2} - \frac{8}{3}x_{i3} \right) \\ &\quad - 10x_{i1}^2 - 19x_{i1}^2 + \frac{5}{3}x_{i3}^2 = -20x_{i1}^2 - 20x_{i1}^2 - x_{i3}^2 + 38x_{i1}x_{i2} \\ &\leq -x_{i1}^2 - x_{i1}^2 - x_{i3}^2 = -x_i^T(t)x_i(t).\end{aligned}\tag{4.4}$$

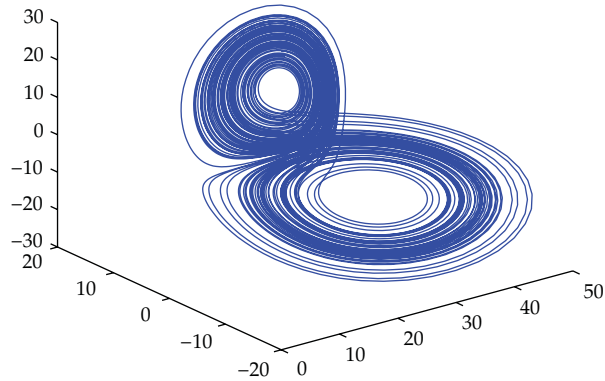


Figure 1: The double-scroll attractor of the Lorenz system.

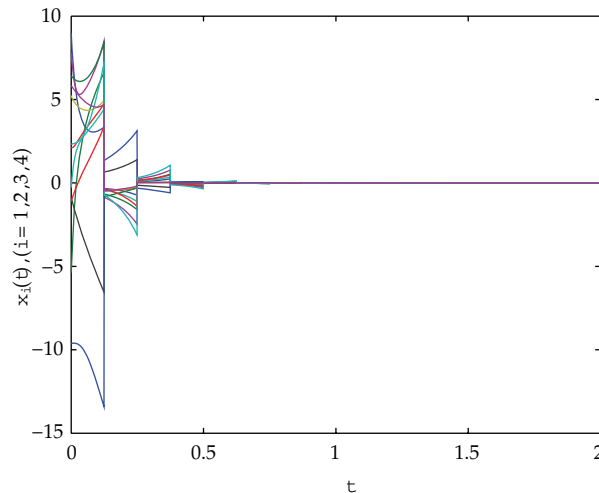


Figure 2: Evolution of the state variable $x_i(t)$, $i = 1, 2, 3, 4$.

Then $\lambda = -2 + 2 \max_k \{ \lambda_k \} = 36$. If we choose average impulsive interval $T_a = 0.125$ and $\mu = -1.1$, the sufficient condition in the Theorem 3.1 will be satisfied with $2 \ln(|1 + \mu|) / T_a + \lambda < 0$. The simulation results of $x_i(t)$, $i = 1, 2, 3, 4$ are shown in Figure 2 with the coupling strength $c = 1$.

5. Conclusion

In this paper, the synchronization of nonlinearly-coupled networks has been investigated. By using the impulsive controllers, the nonlinearly-coupled dynamical networks can be synchronized to the original point. A criterion for the synchronization is derived by using the stability analysis of impulsive differential equations and the concept of average impulsive interval. A numerical example is finally given to illustrate the effectiveness and feasibility of the proposed method and result. One of the future research topics would be extending

the present results to the synchronization of nonlinearly coupled networks by impulsively controlling a small fraction of nodes.

Acknowledgments

The work of J. D. Cao was supported by the National Natural Science Foundation of China under Grant 11072059, the Specialized Research Fund for the Doctoral Program of Higher Education under Grant 20070286003, and the Natural Science Foundation of Jiangsu Province of China under Grant BK2009271. The work of J. Q. Lu was supported by the National Natural Science Foundation of China (NSFC) under Grants 11026182 and 61175119, the Natural Science Foundation of Jiangsu Province of China under Grant BK2010408, Program for New Century Excellent Talents in University (NCET-10-0329), and the Alexander von Humboldt Foundation of Germany.

References

- [1] S. H. Strogatz, "Exploring complex networks," *Nature*, vol. 410, no. 6825, pp. 268–276, 2001.
- [2] A. L. Barabási and R. Albert, "Emergence of scaling in random networks," *Science*, vol. 286, no. 5439, pp. 509–512, 1999.
- [3] D. J. Watts and S. H. Strogatz, "Collective dynamics of 'small-world' networks," *Nature*, vol. 393, no. 6684, pp. 440–442, 1998.
- [4] X. Wang and G. Chen, "Synchronization in small-world dynamical networks," *International Journal of Bifurcation and Chaos in Applied Sciences and Engineering*, vol. 12, no. 1, pp. 187–192, 2002.
- [5] X. Wang and G. Chen, "Synchronization in scale-free dynamical networks: robustness and fragility," *IEEE Transactions on Circuits and Systems. I*, vol. 49, no. 1, pp. 54–62, 2002.
- [6] J. Lü, X. Yu, and G. Chen, "Chaos synchronization of general complex dynamical networks," *Physica A*, vol. 334, no. 1-2, pp. 281–302, 2004.
- [7] J. Lü, X. Yu, G. Chen, and D. Cheng, "Characterizing the synchronizability of small-world dynamical networks," *IEEE Transactions on Circuits and Systems. I. Regular Papers*, vol. 51, no. 4, pp. 787–796, 2004.
- [8] J. Lü and G. Chen, "A time-varying complex dynamical network model and its controlled synchronization criteria," *IEEE Transactions on Automatic Control*, vol. 50, no. 6, pp. 841–846, 2005.
- [9] C. Li and G. Chen, "Synchronization in general complex dynamical networks with coupling delays," *Physica A*, vol. 343, no. 1-4, pp. 263–278, 2004.
- [10] G. Chen, J. Zhou, and Z. Liu, "Global synchronization of coupled delayed neural networks and applications to chaotic CNN models," *International Journal of Bifurcation and Chaos in Applied Sciences and Engineering*, vol. 14, no. 7, pp. 2229–2240, 2004.
- [11] J. Cao, P. Li, and W. Wang, "Global synchronization in arrays of delayed neural networks with constant and delayed coupling," *Physics Letters, Section A*, vol. 353, no. 4, pp. 318–325, 2006.
- [12] B. Shen, Z. Wang, H. Shu, and G. Wei, "Robust H^∞ finite-horizon filtering with randomly occurred nonlinearities and quantization effects," *Automatica*, vol. 46, no. 11, pp. 1743–1751, 2010.
- [13] B. Shen, Z. Wang, Y. S. Hung, and G. Chesi, "Distributed H^∞ filtering for polynomial nonlinear stochastic systems in sensor networks," *IEEE Transactions on Industrial Electronics*, vol. 58, no. 5, pp. 1971–1979, 2011.
- [14] B. Shen, Z. Wang, and Y. S. Hung, "Distributed H^∞ -consensus filtering in sensor networks with multiple missing measurements: the finite-horizon case," *Automatica*, vol. 46, no. 10, pp. 1682–1688, 2010.
- [15] H. Jiang and Q. Bi, "Impulsive synchronization of networked nonlinear dynamical systems," *Physics Letters. A*, vol. 374, no. 27, pp. 2723–2729, 2010.
- [16] A. Das and F. L. Lewis, "Distributed adaptive control for synchronization of unknown nonlinear networked systems," *Automatica*, vol. 46, no. 12, pp. 2014–2021, 2010.
- [17] X. Liu and T. Chen, "Robust μ -stability for uncertain stochastic neural networks with unbounded time-varying delays," *Physica A*, vol. 387, no. 12, pp. 2952–2962, 2008.

- [18] B. Liu, X. Liu, G. Chen, and H. Wang, "Robust impulsive synchronization of uncertain dynamical networks," *IEEE Transactions on Circuits and Systems. I. Regular Papers*, vol. 52, no. 7, pp. 1431–1441, 2005.
- [19] Z. Guan, Z. Liu, G. Feng, and Y. Wang, "Synchronization of complex dynamical networks with time-varying delays via impulsive distributed control," *IEEE Transactions on Circuits and Systems. I. Regular Papers*, vol. 57, no. 8, pp. 2182–2195, 2010.
- [20] Y. Yang and J. Cao, "Exponential synchronization of the complex dynamical networks with a coupling delay and impulsive effects," *Nonlinear Analysis. Real World Applications*, vol. 11, no. 3, pp. 1650–1659, 2010.
- [21] J. Lu, D. W. C. Ho, and J. Cao, "A unified synchronization criterion for impulsive dynamical networks," *Automatica*, vol. 46, no. 7, pp. 1215–1221, 2010.
- [22] J. Lu, D. W. C. Ho, J. Cao, and J. Kurths, "Exponential synchronization of linearly coupled neural networks with impulsive disturbances," *IEEE Transactions on Neural Networks*, vol. 22, no. 2, pp. 329–336, 2011.

Research Article

Second-Order Consensus for Multiagent Systems under Directed and Switching Topologies

Lixin Gao, Jingjing Zhang, and Wenhai Chen

Institute of Intelligent Systems and Decision, Wenzhou University, Zhejiang 325027, China

Correspondence should be addressed to Lixin Gao, gao-lixin@163.com

Received 24 June 2011; Accepted 25 August 2011

Academic Editor: Zidong Wang

Copyright © 2012 Lixin Gao et al. This is an open access article distributed under the Creative Commons Attribution License, which permits unrestricted use, distribution, and reproduction in any medium, provided the original work is properly cited.

We consider multiagent consensus problems in a decentralized fashion. The interconnection topology among the agents is switching and directed. The agent dynamics is expressed in the form of a double-integrator model. Two different cases are considered: one is the leader-following case and the other is the leaderless case. Based on graph theory and the common Lyapunov function method, some sufficient conditions are established for the consensus stability of the considered systems with the neighbor-based feedback laws in both leader-following case and leaderless case, respectively. As special cases, the consensus conditions for balanced and undirected interconnection topology cases can be established directly. Finally, two numerical examples are given to illustrate the obtained results.

1. Introduction

In recent years, the coordination problem of multiple autonomous agents has drawn an increasing attention. It is because there are many applications of multiagent systems in many areas including cooperative control of unmanned air vehicles, flocking of birds, schooling for underwater vehicles, distributed sensor networks, attitude alignment for cluster of satellites, collective motion of particles, and distributed computations [1–5].

Although these practical backgrounds are different, the fundamental principles in the coordination of multiple spacecraft, robots, and even animals are very similar, that is, coordinating multiple agents to achieve a goal of the whole system by local information. As a result, a critical problem for coordinated control is to design appropriate protocols and algorithms such that the group of agents can reach consensus on the shared information in the presence of limited and unreliable information exchange and dynamically changing interaction topologies [6]. In [5], the author also pointed out that a key technology in cooperative control is the problem of consensus. The investigated feedback scheme associated

with those problems is inspired by the aggregates of individuals in nature. Reynolds first proposed a computer animation model to simulate collective behaviors of multiple agents in [2]. In the fields of system and control, the development of consensus theory is primarily impelled by Vicsek's particle swarm model mentioned in [3]. In [1], Jadbabaie et al. gave a theoretical explanation of the consensus behavior of Vicsek's model and proved that the states of all the jointly connected agents converged to the same value or the value of a given leader. Ren and Beard [6] extended the work of Jadbabaie et al. [1] to the case of directed graphs and explored the minimum requirements to reach global consensus. Olfati-Saber and Murray studied the average-consensus problem with strongly connected and balanced directed topologies in [7], which is essentially the same problem as in [1, 6] for continuous-time consensus scheme. Similar or generalized consensus problems have also been studied in [8–12]. There are also many interesting results about the similar topic for stochastic complex networks [13–15].

In real applications, the interacting topology between agents may change dynamically since the communication links between agents may be unreliable due to disturbances and/or subject to communication time delay. It is well known that switching of the communication topology and communication time delays may lower the system performance and even cause the network system to diverge or oscillate. Theoretically, the consensus in undirected switching topology is much easier than that of directed switching topology. Recently, some preliminary results have been reported to deal with the directed switching topology [16, 17].

Furthermore, with many practical applications, especially involving mechanical systems, the dynamics of agents is usually modeled as a double integrator $\ddot{x} = u$. There are many interesting agent-related works, such as in [18–20], involving double-integrator dynamics under switching and undirected interconnection topology among the agents. Most existing results are obtained under undirected interconnection topology. In directed topology case, [21] discussed this topic under the simple fixed topology. In [9], the authors pointed out that the system matrix related to this multiagent system with double-integrator dynamics does not satisfy the properties related to stochastic matrix and the norm-based method proposed by [1] may fail for the double-integrator form agent dynamic. Therefore, the Lyapunov-based approach is often chosen to solve consensus problem of multi-agent systems with double integrator model.

Motivated by the above works, we study a group of agents with the double-integrator dynamics. The main purpose of this paper is to develop a decentralized control strategy to reach the global consensus of the multi-agent systems under directed switching interconnection topology among the agents. Two different cases are considered: one is the leader-following case and the other is the leaderless case. First, we establish a sufficient consensus condition by constructing a parameter-dependent common Lyapunov function in leader-following formulation. The established consensus condition is expressed as a reduced-order Lyapunov matrix inequalities. As commonly known, it is not an easy task to construct a common Lyapunov function for a switching system, let alone the parameter-dependent common Lyapunov function. As for the leaderless case, the common Lyapunov method cannot be used directly. By using the Schur orthogonal transformation, we decomposes the group tracking dynamics into two subsystems: one represses the leader and the other represses a leader-following subsystem. Then, a sufficient condition is established by applying the obtained leader-following consensus condition to leader-following subsystem. As special cases, we can obtain consensus conditions directly for the multi-agent system with undirected and balanced switching interconnection topology. The jointly connected convergence condition can guarantee that the multi-agent with linear dynamical model

achieves consensus. But for double-integrator model, we construct a counterexample to show that the jointly connected condition may not guarantee that the multi-agent system achieves consensus, which implies that the proposed globally reachable convergence condition may be moderatable and acceptable. By using similar analysis method, we also can probe consensus problems of [9, 18, 19] with switching and directed interconnection topology. Finally, the numerical examples also show that the established consensus condition is solvable.

The rest of the paper is organized as follows. In Section 2, we give a formulation of the coordination problem with help of graph theory. Then in Section 3, some results on the consensus stability are obtained for the multi-agent system with fixed and varying interconnection topologies in the leader-following case, while in Section 4, the leaderless case is studied. In Section 5, two simulation examples are presented to illustrate our theoretical results. Finally, concluding remarks with discussions of the future work are given in Section 6.

The notation of this paper is standard. \mathbb{R} is the real number set. \mathbf{I} is an identity matrix with compatible dimension. \mathbf{A}^T denotes as transpose of a matrix \mathbf{A} . For symmetric matrices \mathbf{A} and \mathbf{B} , $\mathbf{A} > (\geq) \mathbf{B}$ means $\mathbf{A} - \mathbf{B}$ is positive (semi-)definite. $\lambda(\mathbf{A})$ represents an eigenvalue of \mathbf{A} . For symmetric matrices \mathbf{A} , $\lambda_{\min}(\mathbf{A})$ and $\lambda_{\max}(\mathbf{A})$ represent the minimum and maximum eigenvalue of \mathbf{A} , respectively. $\|\bullet\|$ denotes the Euclidean norm. \otimes denotes the Kronecker product, which satisfies (1) $(\mathbf{A} \otimes \mathbf{B})(\mathbf{C} \otimes \mathbf{D}) = (\mathbf{A}\mathbf{C}) \otimes (\mathbf{B}\mathbf{D})$; (2) if $\mathbf{A} \geq 0$ and $\mathbf{B} \geq 0$, then $\mathbf{A} \otimes \mathbf{B} \geq 0$.

2. Problem Formulation

Stability analysis of the group of agents is based on several results of algebraic graph theory. In this section, we first introduce some basic concepts and notations in graph theory that will be used throughout this paper. More details are available in [22].

We denote by $\mathcal{G} = (\mathcal{V}, \mathcal{E}, \mathbf{A})$ with an index set $\mathcal{J} = \{1, 2, \dots, n\}$, where $\mathcal{V} = \{v_1, v_2, \dots, v_n\}$ is the set of vertices, $\mathcal{E} \subset \mathcal{V} \times \mathcal{V}$ is the set of edges of the digraph, and each edge is denoted by $(v_i, v_j) \in \mathcal{E}$, $i, j \in \mathcal{J}$, and a weighted adjacency matrix $\mathbf{A} = [a_{ij}]$ has nonnegative adjacency elements a_{ij} . Throughout this paper, we assume that all the graphs have no edges from a node to itself. A weighted graph is called undirected if for all $(v_i, v_j) \in \mathcal{E} \Rightarrow (v_j, v_i) \in \mathcal{E}$ and $a_{ij} = a_{ji}$. Otherwise, the graph is called a directed graph or digraph. The adjacency elements associated with the edges of the graph are positive, that is $a_{ij} > 0 \Leftrightarrow (v_i, v_j) \in \mathcal{E}$. Obviously, we also have $a_{ij} = 0 \Leftrightarrow (v_i, v_j) \notin \mathcal{E}$. A path from vertex v_i to vertex v_j is a sequence of distinct vertices starting with v_i and ending with v_j such that consecutive pair of vertices make an edge of digraph. If there is a path from one node v_i to another node v_j , then v_j is said to be reachable from v_i . If a node v_i is reachable from every other node of the digraph, then it is said to be globally reachable. Obviously, every node of an undirected connected graph is globally reachable.

The relationships between n agents can be conveniently described by a simple digraph \mathcal{G} . We denote the set of all neighbor vertices of vertex v_i by $\mathcal{N}_i = \{j \mid (v_i, v_j) \in \mathcal{E}\}$. Neighboring relations reflect physical proximity between two agents, or the existence of a communication channel [6]. Its degree matrix $\mathbf{D} = \text{diag}\{d_1, \dots, d_n\} \in \mathbb{R}^{n \times n}$ is a diagonal matrix, where diagonal elements $d_i = \sum_{j \in \mathcal{N}_i} a_{ij}$ for $i = 1, \dots, n$. Then the Laplacian matrix of \mathcal{G} is defined as

$$\mathbf{L} = \mathbf{D} - \mathbf{A}. \quad (2.1)$$

The following lemma relates the Laplacian matrix with its directed graph, as well as supplying an algebraic characterization. It is well known that the Laplacian matrix captures many interesting properties of the graphs. The result of Lemma 2.1 can be found in [6].

Lemma 2.1. *The weighted graph Laplacian matrix L associated with graph G has at least one zero eigenvalue, and all of the nonzero eigenvalues are located on the open right half plane. Furthermore, L has exactly one zero eigenvalue if and only if the directed graph G has a globally reachable node.*

Moreover, for a digraph with a globally reachable node, the n -dimensional eigenvector associated with the single zero eigenvalue is the vector of ones, $\mathbf{1} := (1, 1, \dots, 1)^T$. For undirected weight graph G , L is symmetric, positive and semidefinite, and all eigenvalues of L are real and nonnegative.

A weighted graph $G = (\mathcal{U}, \mathcal{A})$ is said to be balanced if

$$\sum_{j=1}^n a_{ij} = \sum_{j=1}^n a_{ji}, \quad i = 1, 2, \dots, n, \quad (2.2)$$

Any undirected weighted graph is balanced. Furthermore, a weighted graph is balanced if and only if $\mathbf{1}^T L = 0$ (see [7]).

Let $\tilde{\mathcal{G}}$ be the set of reverse edges of G obtained by reversing the order of all the pairs in \mathcal{A} . The mirror of G is denoted by an undirected graph in the form $\hat{G} = (\mathcal{U}, \hat{\mathcal{A}})$ with the same set of nodes of G , the set of edges $\hat{\mathcal{A}} = \mathcal{A} \cup \tilde{\mathcal{A}}$, and the symmetric adjacency matrix $\hat{A} = [\hat{a}_{ij}]$ with elements $\hat{a}_{ij} = (a_{ij} + a_{ji})/2$. The Laplacian matrix for mirror graph \hat{G} is $L(\hat{G}) = (1/2)(L(G) + L^T(G))$ if and only if G is balanced graph [7].

In what follows, we mainly consider a graph \bar{G} associated with the system with n agents (labeled by $v_i, i = 1, 2, \dots, n$) and one leader (labeled by v_0). A simple and directed graph G describing the topology relation of these n followers, and \bar{G} contains graph G and v_0 with the directed edges from some agents to the leader describes the topology relation among all agents. In other words, we denote a weighted digraph of order $n + 1$ by $\bar{G} = \{\bar{\mathcal{U}}, \bar{\mathcal{A}}\}$, where $\bar{\mathcal{U}} = \{v_0, v_1, \dots, v_n\}$, and the weighted matrix has the following form:

$$\bar{A} = \begin{pmatrix} 0 & 0 \\ \mathbf{b} & A \end{pmatrix}, \quad \mathbf{b} = (b_1, b_2, \dots, b_n)^T \in \mathbb{R}^n, \quad A = (a_{ij}) \in \mathbb{R}^{n \times n}. \quad (2.3)$$

The element $a_{ij} > 0$ represents that agent i is connected to agent j , and $b_i > 0$ represents that agent i is connected to leader. Meanwhile, $a_{ij} = 0$ and $b_i = 0$ represents that agent i is not connected to agent j and leader, respectively. The induced subgraph $G = \{\mathcal{U}, \mathcal{A}\}$ of \bar{G} represses the interconnection topology among n following agents.

For the multi-agent system under consideration, the relationships between neighbors can change over time and the interconnection topology may be dynamically changing. Let $t_1 = 0, t_2, t_3, \dots$ be an infinite time sequence at which the interconnection graph of the considered multi-agent system switches. Usually, it is assumed that chattering does not occur; that is, there is a constant $\tau_0 > 0$, often called dwell time, with $t_{i+1} - t_i \geq \tau_0$, for all i . Moreover, we assume that only finite possible interconnection topologies can be switched. In the leaderless case, denote $\mathcal{S} = \{G_1, G_2, \dots, G_M\}$ as a set of the graphs of all possible topologies, while in the leader-following case, denote $\bar{\mathcal{S}} = \{\bar{G}_1, \bar{G}_2, \dots, \bar{G}_{N_0}\}$ as a set of the

graphs of all possible topologies. Denote $\mathcal{D} = \{1, 2, \dots, N\}$ and $\mathcal{D}_0 = \{1, 2, \dots, N_0\}$ as index sets, respectively.

In this paper, we intend to coordinate n mobile agents with each agent expressed in the form of a double integrator:

$$\begin{aligned} \dot{r}_i &= p_i, \\ \dot{p}_i &= u_i, \end{aligned} \quad i = 1, \dots, n, \quad (2.4)$$

where $r_i \in \mathbb{R}^m$ is the position of agent i , $p_i \in \mathbb{R}^m$ its velocity and $u_i \in \mathbb{R}^m$ its control inputs. In the leader-following case, the dynamics of the leader is taken as

$$\begin{aligned} \dot{r}_0 &= p_0 \\ \dot{p}_0 &= a_0(t), \end{aligned} \quad (2.5)$$

where $r_0 \in \mathbb{R}^m$ and $p_0 \in \mathbb{R}^m$ are the position and velocity vectors of the leader, respectively, and $a_0(t) \in \mathbb{R}^m$ is a known input, which may be regarded as some given policy known to all the agents. Particularly, $a_0(t) \equiv 0$ expresses that the leader moves in constant velocity.

The n mobile agents are said to achieve global consensus if for any given initial values $r_i(0)$ and $p_i(0)$ ($i = 1, 2, \dots, n$), $\lim_{t \rightarrow +\infty} (r_i(t) - r_j(t)) = 0$ and $\lim_{t \rightarrow +\infty} (p_i(t) - p_j(t)) = 0$ for any $i, j = 1, 2, \dots, n$. Thus, in the leader-following case, the multi-agent system achieves global consensus if and only if $\lim_{t \rightarrow +\infty} (r_i(t) - r_0(t)) = 0$ and $\lim_{t \rightarrow +\infty} (p_i(t) - p_0(t)) = 0$ for any initial values.

The control law is said to be neighbor control law or local control law if all the control inputs u_i only depend on the states of agent i and its neighbors. We are interested in using neighbor control law to solve the consensus problem. To this end, the controller u_i of agent i , regarded as node i in a graph, requires state information from a subset of the agent's flockmates, called the neighbor set \mathcal{N}_i and defined as above. There are two cases considered for multi-agent system as follows.

Leader-Following Case

For any $i \in \mathcal{D}$, take the local control law, which is neighbor-based feedback law as follows:

$$\begin{aligned} u_i &= a_0(t) - \left(\sum_{j \in \mathcal{N}_i(t)} a_{ij}(t) (r_i - r_j) + b_i(t) (r_i - r_0) \right) \\ &\quad - \left(\sum_{j \in \mathcal{N}_i(t)} a_{ij}(t) (p_i - p_j) + b_i(t) (p_i - p_0) \right), \end{aligned} \quad (2.6)$$

where \bar{a}_{ij} is considered as a "control" parameter, which is positive constant and will be determined later, and \bar{b}_i is a positive weighted parameter. The set of switching interconnection topology graph is assumed to be $\bar{\mathcal{G}}_1 = \{\bar{\mathcal{U}}, \bar{A}_1\}$, $1 \in \mathcal{D}_0$, where the \bar{A}_1 has the following form:

$$\bar{A}_1 = \begin{pmatrix} 0 & 0 \\ b_1 & A_1 \end{pmatrix}, \quad b_1 = (b_1^{(1)}, b_2^{(1)}, \dots, b_n^{(1)})^T \in \mathbb{R}^n, \quad A_1 = (a_{ij}^{(1)}) \in \mathbb{R}^{n \times n}. \quad (2.7)$$

In time t the interconnection topology graph is assumed to be switched to $\bar{\mathcal{G}}_{1, l \in \mathcal{D}_0}$, so $a_{ij}(t)$ and $b_i(t)$ are chosen by $a_{ij}(t) = a_{ij}^{(l)}$ and $b_i(t) = b_i^{(l)}$.

Denote $s_j = r_j - r_0$ and $q_j = p_j - p_0$. Take $s := (s_1^T, \dots, s_n^T)^T \in \mathbb{R}^{mn}$, $q := (q_1^T, \dots, q_n^T)^T \in \mathbb{R}^{mn}$, and $u := (u_1^T - a_0^T, u_2^T - a_0^T, \dots, u_n^T - a_0^T)^T \in \mathbb{R}^{mn}$. Then error dynamics of closed system (2.4)–(2.6) can be rewritten as

$$\begin{aligned} \dot{s} &= q, \\ \dot{q} &= u - (H \otimes I_m)s - (H \otimes I_m)q, \end{aligned} \quad (2.8)$$

where $H = L + B$, $\sigma : [0, +\infty) \rightarrow \mathcal{D}_0 = \{1, 2, \dots, N_0\}$ is a piecewise constant switching signal with successive times when the topology of graph $\bar{\mathcal{G}}$ switches. L is the Laplacian matrix of the switching graph \mathcal{G} consisting of n vertices (presenting agents $1, \dots, n$), and B is a diagonal matrix whose i diagonal entry is $b_i(t)$ at time t .

Leaderless Case

Because there is no leader dynamics (2.5), take the local control law for any $i \in \mathcal{I}$ as follows:

$$u_i = - \sum_{j \in \mathcal{N}_i(t)} a_{ij}(t)(r_i - r_j) - \sum_{j \in \mathcal{N}_i(t)} a_{ij}(t)(p_i - p_j). \quad (2.9)$$

Let $r := (r_1^T, \dots, r_n^T)^T$ and $p := (p_1^T, \dots, p_n^T)^T$. Then we can rewrite the closed-loop system (2.4) and (2.9) as

$$\begin{aligned} \dot{r} &= p, \\ \dot{p} &= u - (L \otimes I_m)r - (L \otimes I_m)p, \end{aligned} \quad (2.10)$$

where $\sigma : [0, +\infty) \rightarrow \mathcal{D} = \{1, 2, \dots, N\}$ is a piecewise constant switching signal to describe the switch of the interconnection graph \mathcal{G} . The $a_{ij}(t)$ is chosen by $a_{ij}(t) = a_{ij}^{(l)}$, $l \in \mathcal{D}$.

The next lemma shows well-known results and will be used later, which is given in [23].

Lemma 2.2. *Suppose that a symmetric matrix is partitioned as*

$$\begin{pmatrix} C_1 & C_2 \\ C_2^T & C_3 \end{pmatrix}, \quad (2.11)$$

where C_1 and C_3 are square. This matrix is positive definite if and only if C_1 is positive definite and $C_3 - C_2^T C_1^{-1} C_2$ is positive definite.

In what follows, we first focus on the analysis of the leader-following case and then study the leaderless case in a similar trace.

3. Leader-Following Case

In this section, we concentrate on the analysis of the multi-agent systems with a leader. If the information of the input $a_0(t)$ can be used in local control design, then we can prove that although the leader keeps changing, the agents can follow the leader that is, consensus is achieved.

Using neighbor-based feedback law (2.6), the error dynamics system (2.8) will be expressed in a compact form as follows:

$$\dot{x} = (F \otimes I_m)x, \quad (3.1)$$

where

$$x = \begin{pmatrix} s \\ q \end{pmatrix}, \quad F = \begin{pmatrix} 0 & I \\ -H & -H \end{pmatrix}. \quad (3.2)$$

The interconnection topology graph is $\bar{\mathcal{G}}(t)$, and the interconnection graphs associated with all followers are $\mathcal{G}(t)$.

Note that F is not directly related to a stochastic matrix, and therefore, the method reported in [1] cannot be applied directly. In what follows, we will propose an approach based on common Lyapunov function for the system (3.1) to demonstrate the convergence of the dynamics system (3.1).

Now we give the main result in the leader-following case as follows.

Theorem 3.1. *Suppose that the interconnection graph is connected for any interval $[t_j, t_{j+1})$. If there exist a positive definite matrix \bar{P}_1 and a positive constant μ such that*

$$H^T \bar{P}_1 + \bar{P}_1 H \geq \mu I, \quad \forall t \in \mathcal{D}_0, \quad (3.3)$$

and taking a constant

$$\gamma > \frac{2}{\mu} \max(\bar{P}_1), \quad (3.4)$$

then the local control law (2.6) can guarantee that multi-agent system (2.4), (2.5) achieves consensus for any given initial condition $x(0)$ and $p(0)$.

Proof. To prove the theorem, we consider the dynamics in each interval at first. Note that, in any interval (say $[t_j, t_{j+1})$), the interconnection topology does not change. Therefore, $F(t)$ is a constant matrix for $t \in [t_j, t_{j+1})$ for any $j \geq 0$, and then the solution to (3.1) is well defined. Thus, we can assume that $F(t) = F, \forall t \in \mathcal{D}_0, t \in [t_j, t_{j+1})$. Choose matrix \tilde{P}_1 as

$$\tilde{P}_1 = \begin{pmatrix} 2\bar{P}_1 & \bar{P}_1 \\ \bar{P}_1 & 2\bar{P}_1 \end{pmatrix}. \quad (3.5)$$

We can verify that \tilde{P}_1 is positive definite by applying Lemma 2.2. Consider a common Lyapunov function $V(x) = x^T(\tilde{P}_1 \otimes I_m)x$, where \tilde{P}_1 is defined in (3.5). Then, for any $l \in \mathcal{D}_0$ which corresponds to interval $[t_j, t_{j+1})$, we have

$$\begin{aligned} \dot{V}(x)|_{(3.1)} &= x^T \left[\left(F_1^T \otimes I_m \right) \left(\tilde{P}_1 \otimes I_m \right) + \left(\tilde{P}_1 \otimes I_m \right) \left(F_1 \otimes I_m \right) \right] x \\ &= x^T \left[\left(F_1^T \tilde{P}_1 + \tilde{P}_1 F_1 \right) \otimes I_m \right] x := -x^T (Q_1 \otimes I_m) x, \end{aligned} \quad (3.6)$$

where

$$Q_1 = \begin{pmatrix} \left(H_1^T \bar{P}_1 + \bar{P}_1 H_1 \right) & {}^2 \left(H_1^T \bar{P}_1 + \bar{P}_1 H_1 \right) - 2 \bar{P}_1 \\ {}^2 \left(H_1^T \bar{P}_1 + \bar{P}_1 H_1 \right) - 2 \bar{P}_1 & {}^3 \left(H_1^T \bar{P}_1 + \bar{P}_1 H_1 \right) - 2 \bar{P}_1 \end{pmatrix}. \quad (3.7)$$

Note that

$$\begin{pmatrix} & {}^2 \\ {}^2 & {}^3 \end{pmatrix} \otimes \left(H_1^T \bar{P}_1 + \bar{P}_1 H_1 - \mu I \right) \geq 0. \quad (3.8)$$

Then we have

$$Q_1 \geq Q := \begin{pmatrix} \mu I & {}^2 \mu I - 2 \bar{P}_1 \\ {}^2 \mu I - 2 \bar{P}_1 & {}^3 \mu I - 2 \bar{P}_1 \end{pmatrix}. \quad (3.9)$$

By using Lemma 2.2, (3.4) guarantees that matrix Q is positive definite.

In addition, the maximum eigenvalue of \tilde{P}_1 is

$$\begin{aligned} \max(\tilde{P}_1) &= \frac{2 + {}^2 + 2\sqrt{1 + {}^4}}{2} \max(\bar{P}_1), \\ \min \frac{x^T (Q_1 \otimes I) x}{x^T (\tilde{P}_1 \otimes I) x} &\geq \frac{\min(Q)}{\max(\tilde{P}_1)}. \end{aligned} \quad (3.10)$$

Let $\gamma := \min(Q) / 2 \max(\tilde{P}_1)$. Then, we have $\dot{V}(x) \leq -2\gamma V(x)$, which implies $V(x) \leq V(x(0))e^{-2\gamma t}$. Moreover, we have

$$\|x(t)\| \leq \frac{\sqrt{V(x)}}{\sqrt{\min(\tilde{P}_1)}} \leq \frac{\sqrt{V(0)}}{\sqrt{\min(\tilde{P}_1)}} e^{-\gamma t} \leq \frac{\sqrt{\max(\tilde{P}_1)}}{\sqrt{\min(\tilde{P}_1)}} \|x(0)\| e^{-\gamma t}. \quad (3.11)$$

Thus we have $\lim_{t \rightarrow +\infty} x(t) = 0$ with at least an exponent rate γ . The proof is now completed. \square

Remark 3.2. Obviously, the consensus problem of closed-loop multi-agent system (2.4), (2.5) and (2.6) is equivalent to stability problem of error system (3.1). The closed-loop multi-agent system and the error system are both $2n$ -order systems, and the consensus condition (3.3) given in Theorem 3.1 is n -order Lyapunov matrix inequalities. Thus, the established consensus condition is a reduced order condition. In many applications, the system normally switches in finite model. The assumption that the system switches only in finite model is often used. Because the interconnection topology is modeled by weighted digraph, different weight will lead different interconnection topology. Although the set of nodes and the set of possible edges are finite, the set of possible interconnection topology may be infinite, but from the point of mathematics, the assumption that the index set \mathcal{P} is finite in Theorem 3.1 may be not necessary. From the proof of Theorem 3.1, we can also obtain the result of Theorem 3.1 by the assumption that condition (3.3) is satisfied for any element of an infinite index set \mathcal{P} .

Note that the matrix $H = L + B$ plays a key role in the convergence analysis of system (3.1). A matrix is said to be a positive stable matrix if all its eigenvalues have positive real parts. The matrix $H = L + B$ is positive stable if and only if node v_0 is globally reachable in $\bar{\mathcal{G}}$ (see [18]).

Of course, the result of Theorem 3.1 can be applied to fixed topology case directly. Because H is positive stable, there exists a positive definite matrix $\bar{P}_2 \in \mathbb{R}^{n \times n}$ such that

$$H^T \bar{P}_2 + \bar{P}_2 H = I. \quad (3.12)$$

Therefore, we can obtain the following corollary for fixed topology case.

Corollary 3.3. *Suppose the interconnection topology $\bar{\mathcal{G}}$ is fixed. If node v_0 is globally reachable in $\bar{\mathcal{G}}$ and the constant $\bar{\alpha}$ satisfies*

$$\bar{\alpha} > \frac{2}{\lambda_{\min}(\bar{P}_2)}, \quad (3.13)$$

then the local control law (2.6) can guarantee that system (2.4), (2.5) achieves consensus for any given initial condition $x(0)$ and $p(0)$.

Moreover, let $\lambda_i(H) = \alpha_i + j\beta_i$ ($i = 1, 2, \dots, n$) be i th eigenvalue of H . A necessary and sufficient condition for fixed topology case obtained by [21] is given as follows. The local control law (2.6) can guarantee that the multi-agent system in leader-following case achieves consensus for any given initial condition $x(0)$ and $p(0)$ if and only if node v_0 is globally reachable in $\bar{\mathcal{G}}$ and the constants $\bar{\alpha}$ and $\bar{\beta}$ satisfy

$$\bar{\alpha} > \frac{1}{2} \max_i \frac{\beta_i^2}{\alpha_i \left[\frac{2}{\alpha_i} + \frac{2}{\beta_i} \right]}. \quad (3.14)$$

The assumption that node v_0 is globally reachable in $\bar{\mathcal{G}}$ can guarantee that $\alpha_i > 0$. For any given $\bar{\alpha} > 0$, $\beta_i > 0$, and $\bar{\beta}$, it is not difficult to see (3.14) can be satisfied for larger enough $\bar{\alpha}$. Obviously, (3.14) always holds for any $\bar{\alpha} > 0$, $\bar{\beta} > 0$ if all $\beta_i = 0$. When the interconnection graphs \mathcal{G} associated with all followers are undirected and node v_0 is globally reachable in $\bar{\mathcal{G}}$,

all eigenvalues of H are real and positive (see [9]). Thus, in this fixed undirected case, multi-agent system (2.4)–(2.6) achieves consensus for any given initial condition $r(0)$ and $p(0)$ if and only if node v_0 is globally reachable in \bar{G} .

Consider the special case that the graph G associated with all followers is balanced. The matrix $L + L^T$ is positive semidefinite. Moreover, we have (see [18]).

Lemma 3.4. *Suppose G_1 is balanced. Then $H_1^T + H_1$ is positive definite if and only if node v_0 is globally reachable in \bar{G}_1 .*

Based on Lemma 3.4 and the fact that the set \mathcal{P}_0 is finite, define

$$\bar{\alpha}_1 := \frac{1}{2} \min_{\mathbb{K} \in \mathcal{P}_0} \left\{ \min(H_1^T + H_1) \mid \text{node } 0 \text{ is globally reachable of } \bar{G}_1 \text{ and } G_1 \text{ is balanced} \right\} > 0 \quad (3.15)$$

which is fixed and depends directly on the constants $a_{ij}^{(l)}$ and $b_i^{(l)}$ for $i, j = 1, \dots, n$ and $l = 1, 2, \dots, N$. Obviously, if all the interconnection graphs G_l associated with followers are undirected and node v_0 is globally reachable in \bar{G} , $\bar{\alpha}_1$ can be expressed as $\bar{\alpha}_1 = \min_{\mathbb{K} \in \mathcal{P}_0} \{ \min(H_1) \}$. Now we propose following the corollary for the balanced graph case.

Corollary 3.5. *In any interval $[t_j, t_{j+1})$, suppose that node v_0 is globally reachable in the interconnection graph \bar{G}_1 and G_1 associated with all followers is balanced. Taking a constant*

$$\alpha_1 > \frac{1}{2\bar{\alpha}_1}, \quad (3.16)$$

then multi-agent system (2.4)–(2.6) achieves consensus for any given initial condition $r(0)$ and $p(0)$.

Proof. According to Lemma 3.4 and the definition of $\bar{\alpha}_1$, we have

$$H_1^T I + H_1 \geq 2\bar{\alpha}_1 I. \quad (3.17)$$

Then we can obtain the corollary directly by using the result of Theorem 3.1. \square

Because the interconnection graph considered in this paper is weighted graph, two graphs with same edge set and different weighted adjacency matrices are different interconnection graphs. Although the node set and edge are finite, the set of possible interconnection graph may be infinite. For the case that all the graphs G_l , $l \in \mathcal{P}_0$ are associated with all followers are balanced and the switching index set \mathcal{P}_0 is infinite, we also can prove that multi-agent system achieves consensus by only assumption that there exists a positive constant a_{\min} such that all nonzero weighted factors $a_{ij}^{(l)}, b_i^{(l)}$ are equal or greater than a_{\min} .

To probe the consensus stability condition in this case, let $\Gamma_0 = \{\bar{G}_p, p \in \mathcal{P}_0\}$ denote the class of all possible interconnection graphs with the following properties: (1) v_0 is globally reachable node; (2) the interconnection graph G_p related to all followers is balanced; (3) all constant weighted factors a_{ij}, b_i are equal or greater than a positive constant a_{\min} . \mathcal{P}_0 is index set of Γ_0 , which is infinite set. Let $\tilde{\Gamma}_0$ denote the class of all possible

nonweighted interconnection graphs with the properties: (1) v_0 is globally reachable node; (2) the interconnection graph \mathcal{G} related to all followers is undirected; (3) all nonzero weights are 1.

For any graph $\bar{\mathcal{G}} \in \Gamma_0$, we construct a related graph $\tilde{\mathcal{G}}$ by replacing all directed edges between all follower agents with undirected edges and all nonzero weights with 1. Because v_0 is globally reachable node in the interconnection graph $\bar{\mathcal{G}}$, v_0 is also globally reachable node in $\tilde{\mathcal{G}}$. Thus, we have $\tilde{\mathcal{G}} \in \tilde{\Gamma}_0$. Moreover, $H(\tilde{\mathcal{G}}) = B(\tilde{\mathcal{G}}) + L(\tilde{\mathcal{G}})$ is symmetric and positive definite by Lemma 3.4. Because of the finiteness of node set and edge set, $\tilde{\Gamma}_0$ is a finite set. Define

$$\tilde{\alpha}_1 := \min_{\tilde{\mathcal{G}} \in \tilde{\Gamma}_0} \left\{ \min \left(\tilde{H}(\tilde{\mathcal{G}}) \right) \right\}, \quad (3.18)$$

which is fixed, and $\tilde{\alpha}_1 > 0$.

On the other hand, consider a weighted graph $\hat{\mathcal{G}}$ with same node set and edge set as $\tilde{\mathcal{G}}$. In addition, its weight of edge (i, j) is taken as $(a_{ij} + a_{ji})/2 - a_{\min} \geq 0$ and weight of edge $(0, i)$ is taken as $2b_i - a_{\min} \geq 0$. It is not difficult to see that

$$\begin{aligned} H(\hat{\mathcal{G}}) &= B(\hat{\mathcal{G}}) + L(\hat{\mathcal{G}}) \\ &= 2B(\bar{\mathcal{G}}) + L(\bar{\mathcal{G}}) + L^T(\bar{\mathcal{G}}) - a_{\min} [B(\tilde{\mathcal{G}}) + L(\tilde{\mathcal{G}})] \\ &= H(\bar{\mathcal{G}}) + H^T(\bar{\mathcal{G}}) - a_{\min} H(\tilde{\mathcal{G}}). \end{aligned} \quad (3.19)$$

Noticing that $H(\hat{\mathcal{G}})$ is symmetric and positive semidefinite matrix, we have

$$H(\bar{\mathcal{G}}) + H^T(\bar{\mathcal{G}}) \geq a_{\min} H(\tilde{\mathcal{G}}) \geq a_{\min} \tilde{\alpha}_1 \mathbb{I}. \quad (3.20)$$

Similarly, we can get the following result.

Corollary 3.6. *Suppose that the interconnection graph $\bar{\mathcal{G}}(t)$ of any interval $[t_j, t_{j+1})$ belongs in Γ_0 . Take a constant*

$$\gamma > \frac{2}{a_{\min} \tilde{\alpha}_1}. \quad (3.21)$$

Then the local control law (2.6) can guarantee that the multi-agent system in leader-following case achieves consensus for any given initial condition $x(0)$ and $p(0)$.

4. Leaderless Case

In this section, similar to the analysis given in the last section, we probe the consensus problem for leaderless case. The involved interconnection graph is \mathcal{G} instead of $\bar{\mathcal{G}}$. The closed-loop system (2.10) will be expressed in a compact form as follows:

$$\dot{x} = (F \otimes I_m)x \quad (4.1)$$

with

$$x = \begin{pmatrix} r \\ p \end{pmatrix}, \quad F = \begin{pmatrix} 0 & I \\ -L & -L \end{pmatrix}. \quad (4.2)$$

Noticing that vector $\mathbf{1}$ is the eigenvector of the Laplacian matrix L corresponding to its zero eigenvalue by Lemma 2.1, we choose an orthogonal matrix with form

$$U = \begin{pmatrix} \frac{1}{\sqrt{n}} & * & \cdots & * \\ \frac{1}{\sqrt{n}} & * & \cdots & * \\ \vdots & \vdots & \vdots & \vdots \\ \frac{1}{\sqrt{n}} & * & \cdots & * \end{pmatrix}, \quad (4.3)$$

where $*$ denotes the other entries in this matrix. We have

$$U^T L U = \begin{pmatrix} 0 & \bar{B} \\ 0 & \bar{L} \end{pmatrix}, \quad (4.4)$$

where $\bar{B} \in \mathbb{R}^{1 \times (n-1)}$, $\bar{L} \in \mathbb{R}^{(n-1) \times (n-1)}$. Taking $\bar{s} = U^T r$ and $\bar{q} = U^T p$, system (4.1) is equivalent to be described by

$$\begin{aligned} \dot{\bar{s}} &= \bar{q} \\ \dot{\bar{q}} &= \left[\begin{pmatrix} 0 & -\bar{B} \\ 0 & -\bar{L} \end{pmatrix} \otimes I_m \right] \bar{s} + \left[\begin{pmatrix} 0 & -\bar{B} \\ 0 & -\bar{L} \end{pmatrix} \otimes I_m \right] \bar{q}. \end{aligned} \quad (4.5)$$

For convenience, set

$$\begin{aligned} 0 &= \bar{s}_1, \\ 1 &= \left(\bar{s}_2^T, \bar{s}_3^T, \dots, \bar{s}_n^T \right)^T, \end{aligned}$$

$$\begin{aligned} \dot{0} &= \bar{q}_1, \\ \dot{1} &= \left(\bar{q}_2^T, \bar{q}_3^T, \dots, \bar{q}_n^T \right)^T. \end{aligned} \quad (4.6)$$

Then the whole system decomposes into two subsystems as follows: one is

$$\begin{aligned} \dot{1} &= -1, \\ \dot{1} &= - \left(\bar{L} \otimes I_m \right) 1 - \left(\bar{L} \otimes I_m \right) 1, \end{aligned} \quad (4.7)$$

and the other one is

$$\begin{aligned} \dot{0} &= 0, \\ \dot{0} &= - \left(\bar{B} \otimes I_m \right) 0 - \left(\bar{B} \otimes I_m \right) 0. \end{aligned} \quad (4.8)$$

Notice that all eigenvalues of the matrix \bar{L} are eigenvalues of L from (4.4), which means all of the nonzero eigenvalues of \bar{L} are located on the open right half plane by Lemma 2.1. If the graph has a globally reachable node, the rank of \bar{L} is $n - 1$, and therefore all the eigenvalues of matrix \bar{L} are located on the open right half plane, which implies matrix \bar{L} is positive stable matrix. Now we give the main result in leaderless case as follows.

Theorem 4.1. *Suppose that the interconnection graph has a globally reachable node for any interval $[t_j, t_{j+1})$. If there exist a matrix $U_1 \in \mathbb{R}^{n \times (n-1)}$, a positive definite $\bar{P}_3 \in \mathbb{R}^{(n-1) \times (n-1)}$, and a positive constant μ such that*

$$\begin{aligned} U_1^T \mathbf{1} &= 0, \\ U_1^T U_1 &= I_{n-1}, \\ \left(U_1^T L U_1 \right)^T \bar{P}_3 + \bar{P}_3 \left(U_1^T L U_1 \right) &\geq \mu I, \quad \forall l \in \mathcal{D}, \end{aligned} \quad (4.9)$$

and taking a constant

$$> \frac{2}{\mu} \max \left(\bar{P}_3 \right), \quad (4.10)$$

then the local control law (2.9) can guarantee that the multi-agent system in leaderless case achieves consensus for any given initial condition $x(0)$ and $p(0)$.

Proof. Take $U = ((1/\sqrt{n})\mathbf{1}, U_1)$. Due to $U_1^T \mathbf{1} = 0$ and $U_1^T U_1 = I_{n-1}$, it is easy to know that U is an orthogonal matrix and satisfies (4.4). Because the interconnection graph \mathcal{G}_1 has a globally

reachable node, $\bar{L}_1 = U_1^T L_1 U_1$ is positive stable matrix. Applying the result of Theorem 3.1 to system (4.7), we have

$$\lim_{t \rightarrow \infty} \begin{pmatrix} 1 \\ 1 \end{pmatrix} = 0. \quad (4.11)$$

Noticing that $U^T \mathbf{1} = (\sqrt{n}, 0, \dots, 0)^T$, we have

$$\begin{aligned} r(t) - \frac{1}{\sqrt{n}} \mathbf{0}(t) \mathbf{1} &= U \left(\bar{s} - \frac{1}{\sqrt{n}} \mathbf{0}(t) U^T \mathbf{1} \right) = U \begin{pmatrix} 0 \\ 1(t) \end{pmatrix} \rightarrow 0 \quad (t \rightarrow +\infty), \\ p(t) - \frac{1}{\sqrt{n}} \mathbf{0}(t) \mathbf{1} &= U \left(\bar{q} - \frac{1}{\sqrt{n}} \mathbf{0}(t) U^T \mathbf{1} \right) = U \begin{pmatrix} 0 \\ 1(t) \end{pmatrix} \rightarrow 0 \quad (t \rightarrow +\infty), \end{aligned} \quad (4.12)$$

which imply $\lim_{t \rightarrow +\infty} (r_i(t) - r_j(t)) = 0$ and $\lim_{t \rightarrow +\infty} (p_i(t) - p_j(t)) = 0$ for any $i, j = 1, 2, \dots, n$. This completes the proof. \square

Similarly, consider the special case that all the interconnection graphs \mathcal{G}_i are balanced. Due to $\mathbf{1}^T L_i = L_i \mathbf{1} = 0$ for balanced graph \mathcal{G}_i , we have

$$U^T L_i U = \begin{pmatrix} 0 & 0 \\ 0 & \bar{L}_i \end{pmatrix}, \quad \bar{L}_i \in \mathbb{R}^{(n-1) \times (n-1)}, \quad (4.13)$$

where U is orthogonal matrix having form (4.3). The next lemma is given for $\bar{L}_i^T + \bar{L}_i$.

Lemma 4.2. *If \mathcal{G}_i is balanced and has a globally reachable node, then $\bar{L}_i^T + \bar{L}_i$ is positive definite.*

Proof. $1/2(L_i^T + L_i)$ is the Laplacian matrix of the mirror graph of \mathcal{G}_i . Because \mathcal{G}_i is balanced and has a globally reachable node, the mirror graph is undirected and connected. Therefore, $1/2(L_i^T + L_i)$ is positive semidefinite and its rank is $n - 1$. From (4.13), we have $\bar{L}_i^T + \bar{L}_i$ is positive definite. \square

Based on Lemma 4.2 and the fact that the set \mathcal{D} is finite, define

$$\bar{\lambda}_2 := \min_{i \in \mathcal{D}} \left\{ \frac{1}{2} \min \left(\bar{L}_i^T + \bar{L}_i \right) \mid \mathcal{G}_i \text{ is balanced and has a globally reachable node} \right\} > 0. \quad (4.14)$$

$\bar{\lambda}_2$ is also well defined. From (4.13), $\bar{\lambda}_2$ is equivalent to be expressed as

$$\bar{\lambda}_2 = \min_{i \in \mathcal{D}} \left\{ \frac{1}{2} \lambda_2(L_i^T + L_i) \mid \mathcal{G}_i \text{ is balanced and has a globally reachable node} \right\} > 0, \quad (4.15)$$

where $\lambda_2(L_1^T + L_1)$ is the second small eigenvalue of $L_1^T + L_1$. Moreover, if all the interconnection graphs \mathcal{G} associated with any time interval are undirected and connected, then we have $\lambda_2 = \min_{\mathcal{P}} \{ \lambda_2(L_1) \}$. For balanced graph case, the following corollary is similarly obtained as in Corollary 3.5.

Corollary 4.3. *In any interval $[t_j, t_{j+1})$, suppose that the interconnection graph $\mathcal{G}(t)$ is balanced and has a globally reachable node. Taking a constant*

$$\lambda_2 > \frac{1}{2 - \alpha_{\min}}, \quad (4.16)$$

then the local control law (2.9) can guarantee the multi-agent system in leaderless case achieves consensus for any given initial condition $x(0)$ and $p(0)$.

Similarly, denote by $\Gamma = \{\mathcal{G}_p, p \in \mathcal{D}\}$ the class of all possible interconnection graphs with the following properties: (1) the interconnection graph \mathcal{G}_p is balanced and has a globally reachable node; (2) all constant weighted factors α_j are equal or greater than a positive constant α_{\min} . \mathcal{D} is index set of Γ , which is infinite set. Let $\tilde{\Gamma}$ denote the class of all possible nonweighted interconnection graphs with the properties that the graph is balanced and connected. Thus $\tilde{\Gamma}$ is a finite set. Define

$$\tilde{\lambda}_2 := \min_{\tilde{\mathcal{G}} \in \tilde{\Gamma}} \left\{ \lambda_2 \left[L^T(\tilde{\mathcal{G}}) + L(\tilde{\mathcal{G}}) \right] \right\}, \quad (4.17)$$

which is fixed, and $\tilde{\lambda}_2 > 0$. By applying similar analysis of leader-following case, we propose the following result directly.

Corollary 4.4. *Suppose that any interconnection graph $\mathcal{G}(t)$ associated with interval $[t_j, t_{j+1})$ belongs in Γ . Take a constant*

$$\lambda_2 > \frac{2}{\alpha_{\min} \tilde{\lambda}_2}. \quad (4.18)$$

Then the local control law (2.6) can guarantee that the multi-agent system in leader-following case achieves consensus for any given initial condition $x(0)$ and $p(0)$.

Remark 4.5. We define the center of the multi-agent system as $\bar{r} = (1/n) \sum_{i=1}^n r_i$. The velocity of the center is expressed as $\bar{p} = (1/n) \sum_{i=1}^n p_i$. If all the interconnection graphs \mathcal{G} associated with any time interval are balanced, the dynamics of center is given by

$$\begin{aligned}
\dot{\bar{r}} &= \frac{1}{n} \sum_{i=1}^n \dot{x}_i = \frac{1}{n} \sum_{i=1}^n v_i = \bar{v}, \\
\dot{\bar{p}} &= \frac{1}{n} \sum_{i=1}^n \dot{p}_i = \frac{1}{n} \sum_{i=1}^n u_i, \\
&= \frac{1}{n} \sum_{i=1}^n \left[- \sum_{j \in \mathcal{N}_i} a_{ij} (r_i - r_j) - \sum_{j \in \mathcal{N}_i} a_{ij} (p_i - p_j) \right] = 0.
\end{aligned} \tag{4.19}$$

Then, we can get that

$$\begin{aligned}
\bar{p}(t) &= \bar{p}(0) = \frac{1}{n} \sum_{i=1}^n p_i(0) = \frac{1}{\sqrt{n}} v_0(t), \\
\bar{r}(t) &= \bar{r}_0(0) + \bar{p}(0)t = \frac{1}{\sqrt{n}} v_0(t).
\end{aligned} \tag{4.20}$$

The center \bar{r} of the closed-loop system (2.10) will move at a constant speed $(1/n) \sum_{i=1}^n p_i(0)$, which is the average initial velocity of all agents. The position and velocity of every agent will tend to the position and velocity of center, respectively, which means that the multi-agent network achieves consensus.

Remark 4.6. If the dynamics of the agent is linear, that is, $\dot{x} = u_i$, and the interconnection graph is jointly connected, as pointed out in the local control law can guarantee the multi-agent system achieves consensus [1, 8]. But for double-integrator model, the jointly connected condition may not guarantee that the multi-agent system achieves consensus. We propose a counterexample as follows. Thus the assumption that the interconnection graph has a globally reachable node in many references and also in this paper may be moderatable and acceptable.

Counterexample 1

The multi-agent system contains two agents, labeled by agent 1 and agent 2. Without loss of generality, we assume $m = 1$. For any positive constant ϵ , let $t_0 = 0, t_1, t_2, \dots$ be an infinite time sequence, which satisfies $t_{k+1} = t_k + 1$ and $t_{k+2} = t_{k+1} + (1/2^{-2k}) + (1/4^{-2k}) (e^2 + e^{-2})$, $k = 0, 1, 2, \dots$. Suppose that the two agents are connected in time interval $[t_{2k}, t_{2k+1})$ and not connected in time interval $[t_{2k+1}, t_{2k+2})$. The dynamics of the two agents can be expressed as

$$\begin{aligned}
\dot{r}_i &= p_i, \\
\dot{p}_i &= u_i,
\end{aligned} \quad i = 1, 2. \tag{4.21}$$

Take $\tau = 2$, $\sigma = 1$. All nonzero weighted elements of graph are taken as 1. Applying the local law (2.9) to the multi-agent system, the control input u_i has the following form:

$$\begin{aligned} u_1(t) &= \begin{cases} -2(r_1 - r_2) - 2^{-2}(p_1 - p_2), & t \in [\tau_k, \tau_{k+1}), \\ 0, & t \in [\tau_{k+1}, \tau_{k+2}), \end{cases} \\ u_2(t) &= \begin{cases} -2(r_2 - r_1) - 2^{-2}(p_2 - p_1), & t \in [\tau_k, \tau_{k+1}), \\ 0, & t \in [\tau_{k+1}, \tau_{k+2}). \end{cases} \end{aligned} \quad (4.22)$$

The initial position and velocity of agents are taken as $r_1(0) = -r_2(0) = (e^2 - 2 + 1)/4^{-2}$ and $p_1(0) = -p_2(0) = 1$. From the symmetry of the input and initial values, we can know that $r_1 = -r_2$ and $p_1 = -p_2$. Then, we can obtain

$$\begin{aligned} r_1(t) = -r_2(t) &= \begin{cases} \left[\frac{e^2 - 2 + 1}{4^{-2}} + \frac{e^2 + 1}{2}(t - \tau_k) \right] e^{-2(t - \tau_k)}, & t \in [\tau_k, \tau_{k+1}), \\ \frac{1 + 2}{4^{-2}} + \frac{1}{4^{-2}} e^{-2^{-2}} - (t - \tau_{k+1}), & t \in [\tau_{k+1}, \tau_{k+2}), \\ - \left[\frac{e^2 - 2 + 1}{4^{-2}} + \frac{e^2 + 1}{2}(t - \tau_k) \right] e^{-2(t - \tau_k)}, & t \in [\tau_{k+2}, \tau_{k+3}), \\ - \frac{1 + 2}{4^{-2}} - \frac{1}{4^{-2}} e^{-2^{-2}} + (t - \tau_{k+3}), & t \in [\tau_{k+3}, \tau_{k+4}), \end{cases} \\ p_1(t) = -p_2(t) &= \begin{cases} e^{-2(t - \tau_k)} - (e^2 + 1)(t - \tau_k) e^{-2(t - \tau_k)}, & t \in [\tau_k, \tau_{k+1}), \\ -1, & t \in [\tau_{k+1}, \tau_{k+2}), \\ -e^{-2(t - \tau_k)} + (e^2 + 1)(t - \tau_{k+2}) e^{-2(t - \tau_{k+2})}, & t \in [\tau_{k+2}, \tau_{k+3}), \\ 1, & t \in [\tau_{k+3}, \tau_{k+4}), \end{cases} \end{aligned} \quad (4.23)$$

for $k = 0, 1, 2, \dots$. Although the interconnection graph related with any time interval $[\tau_{k+1}, \tau_{k+2})$ is not connected, the jointed graph related to the multi-agent system is jointly connected in any interval $[\tau_k, \tau_{(k+1)})$. Thus, the interconnection topology of the multi-agent system satisfies jointly connected condition proposed by [1]. On the other hand, it is easy to see that the multi-agent system cannot achieve consensus for any positive constant ϵ in this case.

5. Simulation Examples

In this section, to illustrate our theoretical results derived in the above sections, we will provide two numerical simulations. Without loss of generality, we take $m = 1$ in numerical simulation. In leader-follower case, consider a multi-agent system with one leader and six followers. The interconnection topology is arbitrarily switched with switching period 1

among four graphs $\bar{G}_i(i = 1, 2, 3, 4)$. The Laplacian matrices $L_i(i = 1, 2, 3, 4)$ for the four subgraphs $G_i(i = 1, 2, 3, 4)$ are

$$\begin{aligned}
 L_1 &= \begin{pmatrix} 3 & 5 & -15 & 0 & 0 & 0 & -2 \\ -1 & 5 & 5 & -25 & 0 & -2 & 0 \\ 0 & -1 & 2 & -1 & 0 & 0 & 0 \\ 0 & 0 & -2 & 5 & -1 & -2 & 0 \\ 0 & -2 & 0 & -1 & 5 & -2 & 0 \\ -1 & 0 & 0 & -1 & -2 & 4 & 0 \end{pmatrix}, & L_2 &= \begin{pmatrix} 5 & -1 & -2 & 0 & -2 & 0 \\ -15 & 4 & 5 & -1 & 0 & 0 & -2 \\ -2 & -1 & 4 & 0 & -1 & 0 & 0 \\ 0 & 0 & 0 & 2 & 0 & -2 & 0 \\ -1 & 0 & -1 & 0 & 2 & 0 & 0 \\ 0 & -2 & 0 & -2 & 0 & 4 & 0 \end{pmatrix}, \\
 L_3 &= \begin{pmatrix} 3 & 0 & 0 & -2 & 0 & -1 \\ 0 & 2 & 0 & -1 & -1 & 0 \\ 0 & 0 & 2 & 0 & 0 & -2 \\ -2 & -1 & 0 & 5 & -2 & 0 \\ 0 & -1 & 0 & -2 & 3 & 0 \\ -2 & 0 & -2 & 0 & 0 & 4 \end{pmatrix}, & L_4 &= \begin{pmatrix} 2 & 0 & 0 & -1 & -1 & 0 \\ 0 & 4 & -2 & 0 & -2 & 0 \\ 0 & -2 & 5 & -2 & 0 & -1 \\ -2 & 0 & -2 & 4 & 0 & 0 \\ -1 & -2 & 0 & 0 & 5 & -2 \\ 0 & 0 & -1 & 0 & -2 & 3 \end{pmatrix},
 \end{aligned} \tag{5.1}$$

and the diagonal matrices for the interconnection relationship between the leader and the followers are

$$\begin{aligned}
 B_1 &= \text{diag}(1, 0, 0, 1, 0, 0), & B_2 &= \text{diag}(0, 1, 0, 1, 0, 0), \\
 B_3 &= \text{diag}(1, 0, 0, 0, 1, 1), & B_4 &= \text{diag}(0, 0, 1, 1, 0, 0).
 \end{aligned} \tag{5.2}$$

The positive definite

$$\bar{P}_2 = \begin{pmatrix} 4.60 & 0.58 & 0.18 & 0.65 & 0.78 & 0.67 \\ 0.58 & 4.01 & 0.95 & 0.41 & 0.92 & 0.85 \\ 0.18 & 0.95 & 6.12 & 0.74 & 0.80 & 1.38 \\ 0.65 & 0.41 & 0.74 & 3.51 & 0.59 & 0.61 \\ 0.78 & 0.92 & 0.80 & 0.59 & 5.08 & 1.05 \\ 0.67 & 0.85 & 1.38 & 0.61 & 1.05 & 4.92 \end{pmatrix} \tag{5.3}$$

and $\mu = 1$ satisfy condition (3.3). Take $\alpha = 2.5$ and $\beta = 3 > (2/\mu^2) \max(\bar{P}_2)$, where $\max(\bar{P}_2) = 8.81$.

The initial positions and velocities of the all agents are randomly produced. The position and velocity errors in Figure 1 are defined as $r_i - r_0$ and $p_i - p_0$, respectively. Figure 1 shows that the follower agents can track the leader.

In leaderless case, consider a multi-agent system with six agents. The interconnection topology is also arbitrarily switched with switching period 1 among four graphs $G_i(i =$

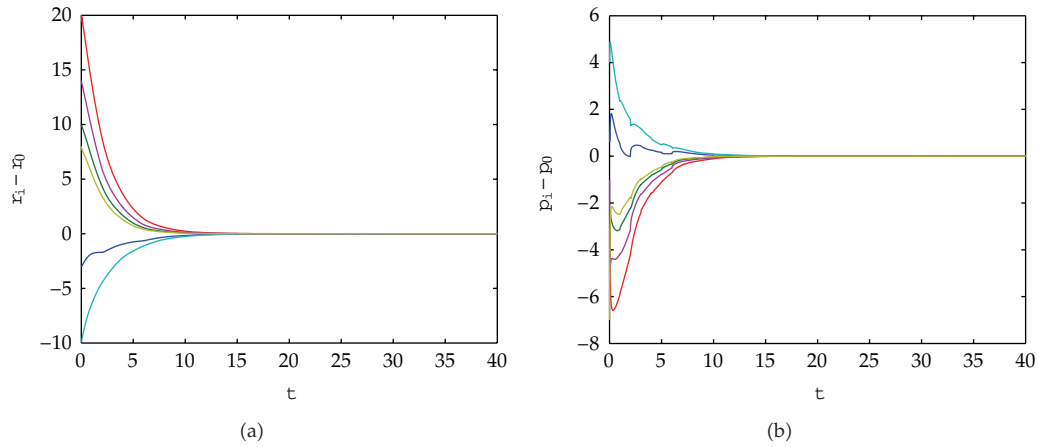


Figure 1: Position and velocity tracking errors of six followers.

1, 2, 3, 4). The Laplacian matrices \$L_i(i = 1, 2, 3, 4)\$ of graphs \$G_i\$ are also defined as above. The matrix

$$U_1 = \begin{pmatrix} -0.4695 & 0.4926 & 0.3434 & 0.3596 & -0.3507 \\ -0.5804 & -0.5372 & -0.0859 & -0.4456 & -0.0433 \\ 0.3598 & 0.3469 & -0.5239 & -0.3718 & -0.4133 \\ 0.5426 & -0.2934 & 0.6559 & -0.0941 & -0.1174 \\ 0.0109 & 0.3577 & 0.0222 & -0.1558 & 0.8249 \\ 0.1366 & -0.3666 & -0.4118 & 0.7077 & 0.0998 \end{pmatrix}, \tag{5.4}$$

the positive definite

$$\bar{P}_3 = \begin{pmatrix} 0.7577 & -0.0131 & -0.0377 & 0.0021 & -0.0559 \\ -0.0131 & 0.6863 & 0.0262 & 0.0109 & -0.0595 \\ -0.0377 & 0.0262 & 0.8184 & 0.0813 & 0.0027 \\ 0.0021 & 0.0109 & 0.0813 & 0.8299 & 0.0194 \\ -0.0559 & -0.0595 & 0.0027 & 0.0194 & 0.8698 \end{pmatrix} \tag{5.5}$$

and \$\mu = 1\$ such that they satisfy condition (4.9). Take \$\gamma = 2.5\$ and \$\beta = 1 > (2/\mu^2) \max(\bar{P}_3)\$, where \$\max(\bar{P}_3) = 0.93\$. The position and velocity errors in Figure 2 are defined as \$x_i - \bar{x}\$ and \$p_i - \bar{p}\$, respectively. Figure 2 shows the multi-agent system in leaderless case can achieve consensus.

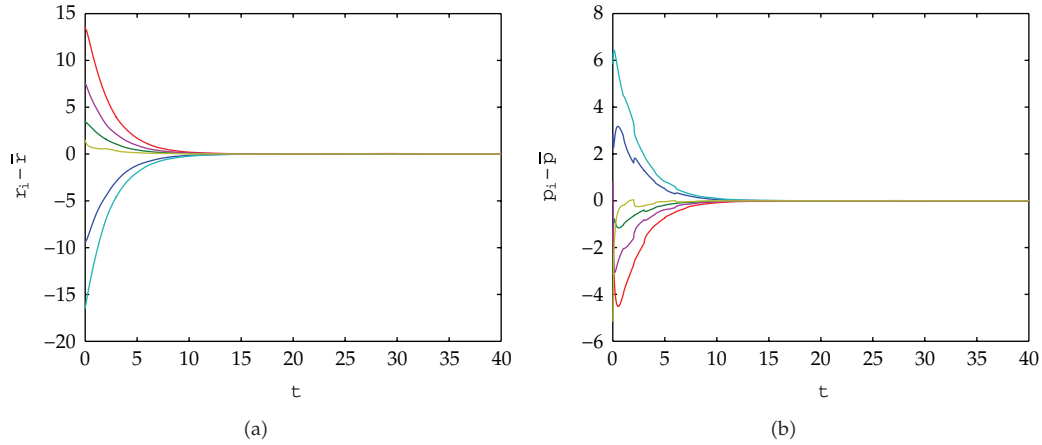


Figure 2: Position and velocity tracking errors of six followers.

6. Conclusion

In this paper, we have investigated the control of multi-agent systems with varying directed interconnection topologies using graph theory and stability theory. The proposed consensus strategy is neighbor-based law that is, each agent regulated its position and velocity based on its neighbor agents. There are two different cases considered in this study. One is the leader-following case and the other the leaderless case. To make this less conservative, a parameter-dependent common Lyapunov function (CLF) was constructed to analyze the stability of the closed system. Some sufficient conditions are given to achieve consensus of these mobile agents with the proposed local control strategies in both leader-following and leaderless cases, respectively. Of course, we can obtain consensus condition directly for the multi-agent system with the switching and undirected interconnection topology or directed balanced interconnection topology. Due to conservativeness of the common Lyapunov function method, we will probe less conservative method in our future work. We also will probe multi-agent H_∞ consensus control problems with external disturbance under time delay directed switching topologies in our future work. Moreover, several numerical simulations were shown to verify the theoretical analysis.

Acknowledgment

This work was supported by the National Nature Science Function of China under Grants nos. 61074123, 60674071, and 61174063.

References

- [1] A. Jadbabaie, J. Lin, and A. S. Morse, "Coordination of groups of mobile autonomous agents using nearest neighbor rules," *IEEE Transactions on Automatic Control*, vol. 48, no. 6, pp. 988–1001, 2003.
- [2] C. W. Reynolds, "Flocks, herds, and schools: a distributed behavioral model," *Computer Graphics*, vol. 21, no. 4, pp. 25–34, 1987.
- [3] T. Vicsek, A. Czirak, E. Ben-Jacob, I. Cohen, and O. Shochet, "Novel type of phase transition in a system of self-driven particles," *Physical Review Letters*, vol. 75, no. 6, pp. 1226–1229, 1995.

- [4] S. Mu, T. Chu, and L. Wang, "Coordinated collective motion in a motile particle group with a leader," *Physica A*, vol. 351, no. 2–4, pp. 211–226, 2005.
- [5] R. M. Murray, "Recent research in cooperative control of multivehicle systems," *Journal of Dynamic Systems, Measurement and Control, Transactions of the ASME*, vol. 129, no. 5, pp. 571–583, 2007.
- [6] W. Ren and R. W. Beard, "Consensus seeking in multiagent systems under dynamically changing interaction topologies," *IEEE Transactions on Automatic Control*, vol. 50, no. 5, pp. 655–661, 2005.
- [7] R. Olfati-Saber and R. M. Murray, "Consensus problems in networks of agents with switching topology and time-delays," *IEEE Transactions on Automatic Control*, vol. 49, no. 9, pp. 1520–1533, 2004.
- [8] L. Gao and D. Cheng, "Comment on coordination of groups of mobile autonomous agents using nearest neighbor rules," *IEEE Transactions on Automatic Control*, vol. 50, no. 11, pp. 1913–1916, 2005.
- [9] Y. Hong, J. Hu, and L. Gao, "Tracking control for multi-agent consensus with an active leader and variable topology," *Automatica*, vol. 42, no. 7, pp. 1177–1182, 2006.
- [10] F. Xiao and L. Wang, "Asynchronous consensus in continuous-time multi-agent systems with switching topology and time-varying delays," *IEEE Transactions on Automatic Control*, vol. 53, no. 8, pp. 1804–1816, 2008.
- [11] B. Shen, Z. Wang, and Y. S. Hung, "Distributed H_∞ -consensus filtering in sensor networks with multiple missing measurements: the finite-horizon case," *Automatica*, vol. 46, no. 10, pp. 1682–1688, 2010.
- [12] W. Ni and D. Cheng, "Leader-following consensus of multi-agent systems under fixed and switching topologies," *Systems and Control Letters*, vol. 59, no. 3–4, pp. 209–217, 2010.
- [13] J. Liang, Z. Wang, and X. Liu, "State estimation for coupled uncertain stochastic networks with missing measurements and time-varying delays: the discrete-time case," *IEEE Transactions on Neural Networks*, vol. 20, no. 5, pp. 781–793, 2009.
- [14] Z. Wang, Y. Wang, and Y. Liu, "Global synchronization for discrete-time stochastic complex networks with randomly occurred nonlinearities and mixed time delays," *IEEE Transactions on Neural Networks*, vol. 21, no. 1, Article ID 5342442, pp. 11–25, 2010.
- [15] B. Shen, Z. Wang, and X. Liu, "Bounded H_∞ synchronization and state estimation for discrete time-varying stochastic complex networks over a finite horizon," *IEEE Transactions on Neural Networks*, vol. 22, no. 1, pp. 145–157, 2011.
- [16] P. Lin, Y. Jia, and L. Li, "Distributed robust H_∞ consensus control in directed networks of agents with time-delay," *Systems and Control Letters*, vol. 57, no. 8, pp. 643–653, 2008.
- [17] Y. Sun, L. Wang, and G. Xie, "Average consensus in networks of dynamic agents with switching topologies and multiple time-varying delays," *Systems and Control Letters*, vol. 57, no. 2, pp. 175–183, 2008.
- [18] J. Hu and Y. Hong, "Leader-following coordination of multi-agent systems with coupling time delays," *Physica A*, vol. 374, no. 2, pp. 853–863, 2007.
- [19] Y. Hong, G. Chen, and L. Bushnell, "Distributed observers design for leader-following control of multi-agent networks," *Automatica*, vol. 44, no. 3, pp. 846–850, 2008.
- [20] L. X. Gao, H. J. Yan, and D. Jin, "Consensus problems in multi-agent systems with double integrator model," *Chinese Physics B*, vol. 19, no. 5, Article ID 050520, 8 pages, 2010.
- [21] W. Yu, G. Chen, and M. Cao, "Some necessary and sufficient conditions for second-order consensus in multi-agent dynamical systems," *Automatica*, vol. 46, no. 6, pp. 1089–1095, 2010.
- [22] C. Godsil and G. Royle, *Algebraic Graph Theory*, Springer, New York, NY, USA, 2001.
- [23] R. Horn and C. Johnson, *Matrix Analysis*, Cambridge University Press, New York, NY, USA, 1985.

Research Article

Structural Models of Cortical Networks with Long-Range Connectivity

Nicole Voges,^{1,2} Ad Aertsen,^{1,3} and Stefan Rotter^{1,3}

¹ Faculty of Biology, University of Freiburg, 79104 Freiburg, Germany

² Eye Clinic, University Medical Center Freiburg, 79106 Freiburg, Germany

³ Bernstein Center Freiburg, University of Freiburg, Hansastr. e9a, 79104 Freiburg, Germany

Correspondence should be addressed to Stefan Rotter, stefan.rotter@biologie.uni-freiburg.de

Received 4 July 2011; Accepted 17 August 2011

Academic Editor: Zidong Wang

Copyright © 2012 Nicole Voges et al. This is an open access article distributed under the Creative Commons Attribution License, which permits unrestricted use, distribution, and reproduction in any medium, provided the original work is properly cited.

Most current studies of neuronal activity dynamics in cortex are based on network models with completely random wiring. Such models are chosen for mathematical convenience, rather than biological grounds, and additionally reflect the notorious lack of knowledge about the neuroanatomical microstructure. Here, we describe some families of new, more realistic network models and explore some of their properties. Specifically, we consider spatially embedded networks and impose specific distance-dependent connectivity profiles. Each of these network models can cover the range from purely local to completely random connectivity, controlled by a single parameter. Stochastic graph theory is then used to describe and analyze the structure and the topology of these networks.

1. Introduction

The architecture of any network can be an essential determinant of its respective function. Signal processing in the brain, for example, relies on a large number of mutually connected neurons that establish a complex network [1]. Since the seminal work of Ramón y Cajal more than a hundred years ago, enormous efforts have been put into uncovering the microcircuitry of the various parts of the brain, including the neocortex [2–6]. On the level of networks, however, our knowledge is still quite fragmentary, rendering computational network models for cortical function notoriously underdetermined.

Networks with a probabilistically defined structure represent, from a modeler's perspective, a viable method to deal with this lack of detailed knowledge concerning cell-to-cell connections [7]. In such models, data from statistical neuroanatomy (e.g., coupling probabilities) are directly used to define ensembles of networks where only few parameters

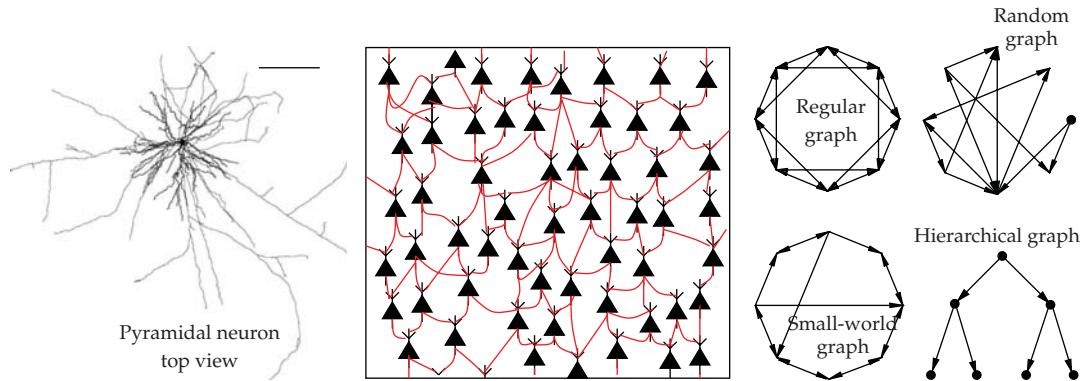


Figure 1: Left: reconstruction of a pyramidal cell stained in a tangential slice of the rat neocortex (top view). Middle: schematic 2D section representing a spatially embedded network composed of locally (red lines) connected pyramidal cells (black triangles). Right: different types of abstract networks.

are needed to define relatively complex network structures. Properties that all members of such a statistical ensemble have in common are then regarded as “generic” for this type of network.

Random graphs [8, 9] and more general stochastic graph models have been mathematically analyzed in great detail. The main motivation was that striking threshold behavior and phase transitions could be observed when certain parameters of such systems were varied. Recently the theory of “complex networks” began to raise even more interest as it was discovered that real-world networks of very different nature (e.g., social networks, the Internet, and metabolic networks) share a number of universal properties [10–12]. Applications to large-scale brain organization were among the earliest applications of the new concepts [13–15]. Here, we suggest to import some of the ideas and methods that came up in the abstract theory of complex networks and apply them to neuronal networks at a cellular level (Figure 1). Specifically, we provide several parametric models for spatially embedded networks. These models allow us to synthesize biologically realistic networks with controlled statistical properties, which serve as candidate models for cortical networks. Providing such models supports the joint structural analysis of synthetic and biological networks.

The graph-theoretic analysis of cortical networks raises the following problem: graphs usually do not deal with space (right part Figure 1), even though a spatial embedding of the physical network implicitly determines some of its properties. Horizontal wiring between cortical neurons, for example, exhibits a clear dependence on the distance of the involved cells, indicated by the left part of Figure 1. Many synaptic contacts are formed between close neighbors, in accordance with, and constrained by, the geometry of neuronal dendrites and local axons [16–18]. However, there is also an appreciable number of axons that travel for longer distances within the gray matter before making synaptic contacts with cells further away [6, 7, 19, 20]. Absolute numbers of local and nonlocal synaptic connections are still a matter of debate among neuroanatomists, and the same is true for the details of the spatial organisation of synaptic projections [1, 6, 7]. Here, we consider three different candidate network models, each representing one possible concept for the geometric layout of distance-dependent connectivity. The uncertainty concerning the ratio of local versus nonlocal synapses is reflected by the systematic variation of a suitable parameter in each model. Moreover, if spatial aspects are included in simulating and analyzing cortical network

dynamics, neurons are commonly placed on the grid points of a regular lattice [21, 22]. Cortical neurons, however, are unlikely to be arranged in a crystal-like fashion [1], neither in three dimensions nor in a two-dimensional projection.

Altogether, we face a spatially embedded and very sparsely connected network, where only a very small fraction of neuron pairs are synaptically coupled to each other directly. What is the impact of these general structural features of synaptic wiring in the cortex? Do these features matter in determining the global topology of the network? Sparse couplings save cable material, but they also constrain communication in the network. Can the sparsity, in principle, be overcome by smart circuit design? Likewise, admitting only neighborhood couplings saves cable length but increases the topological distance between nodes in the network, that is, the number of synapses engaged in transmitting a signal between remote neurons becomes quite large [23, 24]. On the other hand, allowing for distant projections reduces the topological distance, but it induces a higher consumption of wiring material. These wires occupy space that is clearly limited within the skull. Has cortex optimized its design by making use of such tricks? Here, we approach these and related biological questions by establishing suitable parametric families of stochastic network models and by exploring their properties numerically.

Preliminary results of this study have been presented previously in abstract form [25, 26].

2. Methods

We considered network models that comprised neurons with directed synaptic connections. Therefore, our cortical networks were represented by directed graphs G (see Figure 2, left), specified by nonsymmetric adjacency matrices $A(G) = (a_{ij})$. We had $a_{ij} = 1$ if a link $i \rightarrow j$ existed, otherwise $a_{ij} = 0$ (see Figure 2, middle). We did neither allow for autapses (self-coupling) nor for multiple synapses for any pair of neurons. Also, our choice of the adjacency matrix approach did not allow, at this point, to differentiate between excitatory and inhibitory synaptic contacts. Our networks were composed of $N = 1024$ sparsely connected nodes. On average, only a fraction $c \approx 0.012$ of all $N(N - 1)$ possible links was realized in each particular network. These synaptic connections were established according to probabilistic rules common to all neurons. In general, the expected number of both incoming and outgoing synapses was fixed to $\bar{k} \approx 12$; see Table 1. The same distribution for incoming ($P(k_{in})$) and outgoing ($P(k_{out})$) links, respectively, held for all nodes. However, in any specific network realization, each node had random in- and out-degrees. Along the same lines, all other network properties assumed random values if computed from individual networks. To obtain characteristic mean values, we generated 20 independent realizations for each type of network and calculated the corresponding averages and the standard errors of the means (SEM).

2.1. Spatially Embedded Graphs

Each neuron was situated in a quadratic domain of extent $R = 1$, wrapped to a torus to avoid boundary effects (see Figure 2, right). We considered the following two types of 2D spatially embedded networks, random position networks (RPNs), and lattice position networks (LPNs). In RPNs, the positions of all nodes were drawn independently from the

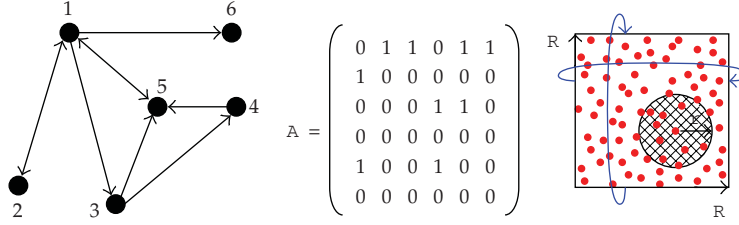


Figure 2: Left: simple ring graph composed of 6 nodes. Middle: the corresponding adjacency matrix. Right: scheme describing the construction of spatially embedded networks with distance-dependent connectivity. Each node (red dots) has a connectivity disk (filled circle); blue arrows indicate periodic boundary conditions (torus topology).

Table 1: List of randomness parameters used to construct the spatially embedded RPNs. ρ is the rewiring probability for the SW model, (r, p) describe range and probability of connectivity in the FN model, and (ρ, p_0) are the parameters for the adjusted GN networks.

SW:	0	0.01	0.02	0.05	0.1	0.2	0.5	0.8	1
FN: p	1	0.99	0.98	0.95	0.9	0.8	0.5	0.2	0.01
FN: r	0.0611	0.0614	0.0617	0.0627	0.0644	0.0683	0.0864	0.1366	0.5
\bar{k} (FN, LPN)	12	—	11.76	11.4	10.8	10.2	12.00	12.00	11.9
GN: p_0	1	—	—	0.95	0.9	0.8	0.5	0.2	0.05
GN:	0.0432	—	—	0.0443	0.0455	0.0483	0.061	0.0965	0.197

same uniform probability distribution. In LPNs, the nodes were placed on the grid points of a rectangular lattice. For a comparison, we also analyzed the corresponding 1D ring graphs.

In a network with no long-range connections, nodes placed within a circular neighborhood of radius r were linked to the center node with connection probability p , according to

$$c_{R^2} = pr^2 \quad \text{with } r \leq R. \quad (2.1)$$

For the LPNs, the smallest possible neighborhood compatible with this rule was obtained for full connectivity ($p = 1$), implying a radius $r_{\min} = R\sqrt{c/\rho} \approx 0.061$. This neighborhood consisted of 8 nearest neighbors and 4 additional next-to-nearest neighbors, compatible with $\bar{k} = 12$ for all networks considered in this study.

We considered the following three families of networks, each spanning the full range from regular to random connectivity.

- (i) Fuzzy neighborhood (FN) network: this model assumed uniform connectivity of probability p within a circular neighborhood of radius r . No connections were established with nodes further away. Starting from a symmetric adjacency matrix $A(G)$ with $(r, p) = (r_{\min}, 1)$, the transition to a completely random graph was induced by simultaneously increasing r and decreasing p accordingly to $(r, p) = (0.5, 0.015)$.
- (ii) Small-world- (SW-) like network: again starting from $(r, p) = (r_{\min}, 1)$, we applied a rewiring procedure in order to introduce long-range links, that is, connections spanning larger distances than r_{\min} . Each individual link of the graph was, with

probability p , replaced by a randomly selected one. For $p = 1$ we again ended up with a completely random graph.

- (iii) Gaussian neighborhood (GN) network: Gaussian profiles were used to define a smooth distance-dependent connection probability, adjusted to the connectivity parameters of the FN networks. The corresponding parameter pairs were (σ, p_0) , where σ was the width of the Gaussian profile used. For technical reasons, we confined our investigation here to RPN models. In contrast to the FN and SW models, the initial adjacency matrix $A(G)$ for $(\sigma, p_0) = (0.043, 1)$ was nonsymmetrical. Motivated by neuroanatomical data [16], GN models represent a biologically more realistic connectivity model.

2.2. Characteristic Network Properties

The following descriptors were used to characterize and compare the network models described above. Most quantities are well established in the context of graph theory (see, eg., [10, 11]).

(a) Degree distributions and correlations: counting incoming and outgoing links for each node of a graph yield an estimate of the distribution of in-degrees $P_{in}(k)$ and out-degrees $P_{out}(k)$, respectively. Here, we only used the out-degree for analysis. The two-node degree correlation $K_c = \langle \sum_{i \rightarrow j} k_i k_j \rangle$ describes out-degree correlations between connected nodes $i \rightarrow j$. In addition, to account for the spatial embedding aspect of our graphs, we considered histograms of the number of links between any two nodes depending on their spatial distance.

(b) Small-world characteristics: the cluster coefficient describes the probability that two nodes, both connected to a common third node, are also directly linked to each other. Let C_i be the fraction of links actually established between any two nodes receiving a link from node i . We considered the mean cluster coefficient $C = (1/N) \sum_i C_i$. Additionally, we calculated the degree-dependent cluster coefficient $C(k)$, where the average was formed over all nodes with a given out-degree [27]. The shortest path L_{ij} is the minimal number of hops necessary to get from node i to node j respecting link directions. We considered the average shortest path length $L = (1/N(N-1)) \sum_{i \neq j} L_{ij}$ for all pairs of distinct nodes, referred to as “characteristic” path length. If delays in a neuronal network are mainly generated by *synaptic* and *dendritic* integration times, L is a natural measure for the total delay to transmit a signal from neuron i to neuron j . The two measures C and L together constitute the so-called small-world characteristics [10–12].

(c) Wiring length: since we deal with spatially embedded networks, any pair of nodes i and j can be assigned a spatial distance D_{ij} . Of interest here was the total pairwise distance of connected nodes $D = \sum_{i \rightarrow j} D_{ij}$. It provides a measure of the total wiring length of the network, assuming straight cables [28, 29]. If delays in a neuronal network are mainly generated by *axonal* conduction times, D is a natural measure for the total delay to transmit a signal from neuron i to neuron j .

(d) Eigenvalues and eigenvectors: for any graph G with N nodes, we numerically determined the N (complex) eigenvalues of its adjacency matrix $A(G)$ and estimated the eigenvalue density $P(\lambda)$ based on 20 samples of graphs of the same type [10, 30, 31]. The corresponding eigenvectors v of $A(G)$ were also numerically determined [10]. To quantify

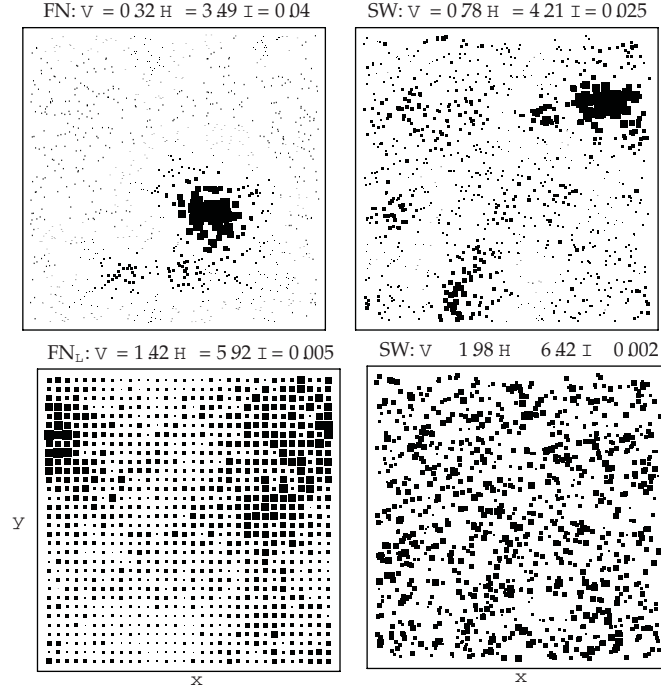


Figure 3: Localization of four sample eigenvectors of spatially embedded graphs. The squared value of each component of an eigenvector is represented by a rectangle of proportional area, centered at the position of the corresponding node. Top left: FN random position network with $p = 0.9$. Bottom right: FN lattice position network with $p = 0.5$. Right top and bottom: Two different eigenvectors of a SW RPN for $p = 0.1$.

the spatial spread of a normalized eigenvector v , we used three different measures: firstly, the weighted 2D circular variance

$$V = 4 - 2 \left| \sum_k |v_k|^2 e^{2i x_k/R} \right| - 2 \left| \sum_k |v_k|^2 e^{2i y_k/R} \right|, \quad (2.2)$$

where v_k are the components of v satisfying $\sum_k v_k^2 = 1$ and (x_k, y_k) denotes the spatial coordinates of node k . Complex numbers were used here to conveniently account for the fact that the neurons in our model are arranged on a torus. The circular mean [32, 33] of x -coordinates across all neurons $\mu_c = \sum_k e^{(2i x_k)/R}$ was used to obtain the average x -coordinate in a consistent manner. The circular variance $\frac{V}{2} = 2(1 - |\mu_c|)$ provides a measure for the dispersion of x -coordinates and small values of $\frac{V}{2}$ indicate a high concentration on the circle. For any eigenvector v , we considered the sum of the circular variances for x - and y -coordinates, respectively, each weighed according to the participation of individual nodes k described by the coefficient $|v_k|^2$. This definition gives values for $0 \leq V \leq 4$. Small values of V indicate that the “mass” encoded by the squared components of v is concentrated in a compact spatial region (see Figure 3 (top-left)), while larger values of V imply that it is more

uniformly spread over the whole domain (see Figure 3 (bottom-right)). For comparison, we also considered two other measures, the entropy H and the inverse participation ratio \mathcal{I}

$$H = -\sum_{k=1}^N |v_k|^2 \log(|v_k|^2), \quad \mathcal{I} = \sum_{k=1}^N |v_k|^4. \quad (2.3)$$

The entropy H assumes its maximal value $H_{\max} = \log N$ if the mass encoded by the squared coefficients of v is uniformly distributed over its N components. Its minimal value $H_{\min} = 0$ is assumed if the mass is concentrated in one point in space. The inverse participation ratio was suggested for the analysis of 1D ring graphs [31]. In contrast to H , it assumes its minimal value $\mathcal{I}_{\min} = 1/N$ if the mass encoded by the squared coefficients of v is uniformly distributed over its N components. Its maximal value $\mathcal{I}_{\max} = 1$ is assumed if the mass is concentrated in one point in space. As the circular variance, both measures were used to assess the spatial concentration of eigenfunctions. Figure 3 shows four sample eigenvectors arising from different networks, with the corresponding values for the three locality measures indicated above each plot.

3. Results

We employed several characteristic network properties to compare different types of spatially embedded networks (FN, SW, and GN). Comparing FN and SW connectivity, we aimed to analyze the effect of unconstrained long-range connections, as opposed to the compact FN connectivity. We also asked if GN connectivity provides an appropriate compromise, involving long-range links combined with a compact local connectivity range. We focused on networks with random node positions (RPN), while the results for lattice position networks (LPNs) and the corresponding 1D ring graphs are only discussed in case of a significant deviation.

3.1. Degree Distributions and Degree Correlations

In the FN, SW, and GN scenarios, networks with random node positions exhibited binomial distributions for both the in- and out-degree (Figure 4 (top-left)), irrespective of the relative abundance of nonlocal connections. For networks with nodes positioned on a regular lattice, however, these distributions were binomial only in the case of random connectivity. Here, a more regular wiring ($p < 0.5$, $p > 0.5$), that is, fewer nonlocal connections, implied less spread in the distribution [28]. For RPNs, the variability of the degree of each node depended both on the randomness parameter characterizing its connectivity and on the fluctuations of the number of nodes located within its neighborhood (connectivity disk). In case of LPNs, however, this variability was only determined by the randomness parameter.

Figure 4 (top-right) shows the two node degree correlations of RPNs for the three types of connectivity considered in this study (FN, GN, and SW). Additionally shown are the results of calculating κ_c for 1D ring graphs with SW and FN connectivity. These were comparable to those of the LPN models but much less influenced by the strong sensitivity to fluctuations in \bar{k} as they occurred for LPNs with FN connectivity. For regularly connected 1D ring graphs ($p = 1$ or $p = 0$) the degree correlations exhibited smaller values ($\kappa_c = \bar{k}\bar{k}$) than for random connections ($p \approx 0$, $p \approx 1$), resulting in an increasing κ_c curve. In contrast,

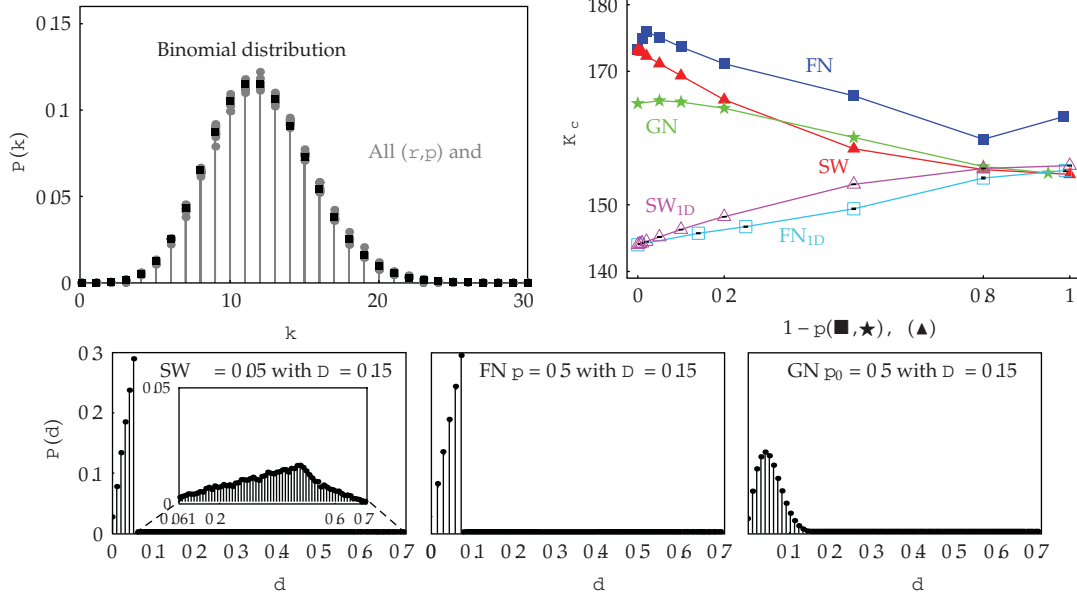


Figure 4: Top left: binomial out-degree distributions (gray) for RPNs based on FN and SW connectivity for different parameter settings. The fitted binomial distribution is superimposed (black). Top right: degree correlations depending on the randomness parameters p and r , respectively, for FN (blue), SW (red), and GN (green) RPNs. The results for the corresponding 1D ring graphs are also indicated, for both SW (magenta) and FN (light blue). Each data point represents the mean outcome of 20 simulations, the largest occurring SEM is 0.54. Bottom: three histograms $P(d)$ of the number of links in dependence of their spatial distance d . Each histogram represents one connectivity type (SW, FN, or GN). The specific parametric realizations are chosen according to an approximately equal mean distance of connected nodes $D = 0.15$, corresponding to a horizontal line in Figure 5, bottom left.

for RPNs, K_c started with rather high values and decreased with increasing randomness parameter, terminating at the same value of approximately $K_c = 156$ as observed for randomly connected 1D ring graphs. RPNs with GN connectivity exhibited rather small K_c values for $r < 0.2$ compared to the other two models. Thus, $P(k)$ and K_c clearly depended on the type of spatial embedding (RPN versus LPN), whereas there were only small deviations with respect to the type of connectivity (FN versus SW versus GN).

The three histograms in Figure 4 (bottom) indicate the frequency of connections $P(d)$ at a given distance d for SW, FN, and GN RPNs, respectively. Each of these networks was established with the same total wiring length $D = 0.15$ (cf. Figure 5). In contrast to the out-degree distribution $P(k)$, the distributions $P(d)$ reflect the specific distance-dependent connectivity profiles. For uniform connection probability, as given in the local neighborhood $d < r_{\min} = 0.0611$ in SW networks, $P(d)$ exhibited a linear slope; see Figure 4, bottom-left. We also observed a linear increase of $P(d)$ within the connectivity range r of FN networks, as well as for the number of long-range links ($r_{\min} < r < R$) in SW models. This feature is due to the linear increase of the circumference of a circle with increasing radius. Therefore, in case of a 2D spacial embedding with uniformly distributed node positions and a constant connection probability, the number of nodes connected at a given distance grows linearly with increasing distance. For GN networks, however, the connection probability is not constant but decreases with increasing distance, leading to the nonlinear rise, and decline, as displayed in Figure 4, bottom-right.

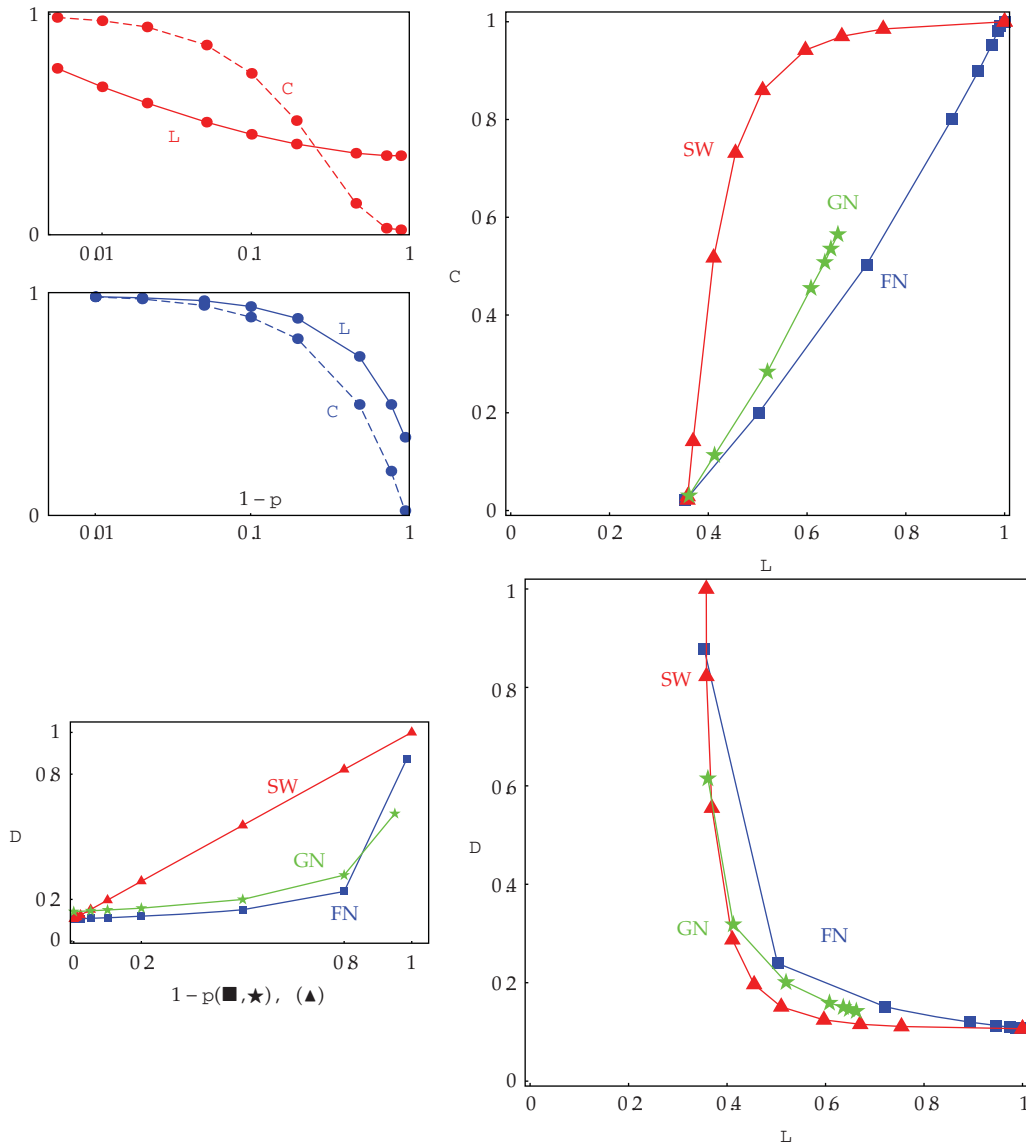


Figure 5: Top left: cluster coefficient C and average shortest path length L for RPN with SW (upper) and FN (lower) connectivity, for different parameters p and $1-p$, respectively. All curves are normalized to the common maximum ($C_{\max} = 0.586$, $L_{\max} = 8.53$). Shown are mean values obtained from 20 simulations for each parameter, the SEM is always below 0.003. Top right: scatter plot of the normalized values of C versus L for RPNs with FN, SW, and GN connectivity. The leftward bending of the SW curve reflects the small-world effect: Strong clustering (high values of C) coexists with short paths linking pairs of nodes (low values of L). Bottom left: mean distance of connected nodes D for FN, GN, and SW RPNs, depending on p or $1-p$, respectively. All values are normalized as described above ($D_{\max} = 0.38$). The SEM is below 0.00009. Bottom right: scattering of D versus L for the same FN, GN, and SW RPNs.

3.2. Small-World Characteristics and Wiring Length

In this section, most results are shown for RPNs. Concerning the average shortest path length and the mean distance of connected nodes, any differences between RPNs and LPNs were

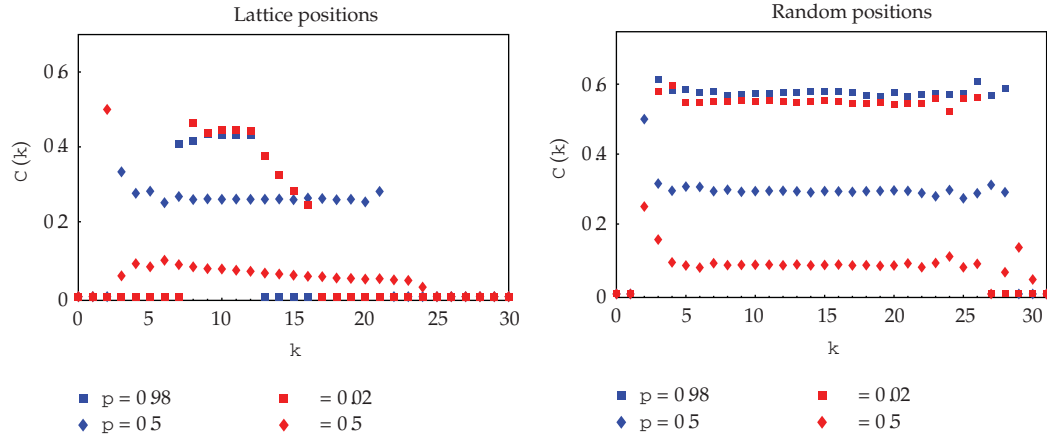


Figure 6: Degree-dependent cluster coefficient for RPNs (left) and LPNs (right) with SW (red symbols) and FN (blue symbols) connectivity. Each figure shows the results for several different values of the parameters p and β , respectively.

negligible. Only the cluster coefficient was significantly higher in case of RPNs; for a detailed analysis of this issue, see [28].

The well-known characteristic feature of small-world networks is the L - C ratio depending on the rewiring probability p . Starting from a regular graph with increasing p , the average shortest path length, L , initially decreases much more than the cluster coefficient C . This is exactly what we observed for our spatially embedded SW networks; see Figure 5, top left (red curves). In contrast, we found $C \leq L$ for all p in case of FN connectivity (blue curves). These findings are summarized in Figure 5, top-right, plotting C versus L for the three types of connectivity. Randomness now progresses from top-right to bottom-left. Spatially embedded SW networks showed a strong small-world effect, according to which very few long-range connections sufficed to dramatically decrease the characteristic path length L , while the cluster coefficient C remained relatively high. Neither FN nor GN networks shared this behavior. Any given clustering C was associated with much shorter paths L in SW networks than in FN or GN networks.

Figure 5, bottom, shows the mean Euclidean distance D between pairs of connected nodes, again depending on the randomness parameters p , and β . For SW connectivity, D increased linearly, while again both FN and GN curves exhibited a different behavior: initially, there was a comparably weak increase, which became steeper at $p_0 = 0.8$ and $p = 0.8$. Wiring length D and graph distance L are jointly displayed for all networks considered here in Figure 5, bottom-right. For all network models, D increased as L decreased from regular (bottom-right) to random (top) connectivity. Non-local connections decreased the graph-theoretic path length L , but they increased the total wiring length D . To realize a given graph-theoretic path length, SW networks had the smallest wiring expenses, followed by GN and FN networks, which make the least effective use of cables.

We also computed the degree-dependent cluster coefficient $C(k)$, another well-established measure for 1D networks [27]. For random graphs, $C(k)$ is known to be independent of the degree k . This is what we observed for RPNs, independently of the type of connectivity, as well as for LPNs with FN and GN connectivity, as indicated by the horizontal lines in Figure 6. Only for LPNs with a less random SW connectivity ($\beta < 0.5$) we found a decreasing $C(k)$ for degrees k larger than a certain threshold (depending on the specific value of

). This effect cannot be traced back to the degree distribution since $P(k)$ is identical for the corresponding SW and FN LPNs (see above). In LPNs, thus, the nonconstant $C(k)$ carries information about deviations from a uniform connectivity. In turn, for more regular connectivity, $C(k)$ behaved differently for RPNs and LPNs, respectively.

To summarize, FN and GN models did not exhibit any small-world characteristics. There was no reduction of L compared to C with increasing randomness because unconstrained long-range connections were only present in the SW model. Long-range links also induced the strong increase of D in the SW model, as well as the decrease in $C(k)$ in case of LPNs.

3.3. Eigenvalues and Eigenvectors

Concerning the eigenvalue distribution of the adjacency matrix, we again found characteristic differences due to the spatial embedding, especially in the case of near-regular connectivity. We observed, however, again only small deviations between different types of connectivity.

Figure 7, bottom rows, shows the density of eigenvalues (real part on the x -axis, imaginary part on the y -axis) for the FN (left) and SW (right) RPNs. From top to bottom randomness progresses, indicated by p ranging from 0.95 to 0.015 and c ranging from 0.05 to 1.0. For regular networks ($p = 1$ or $c = 0$), these networks had a symmetric adjacency matrix and, therefore, only real eigenvalues. The corresponding eigenvalue spectrum $P(\lambda)$ is shown in Figure 7, top. Note the prominent peak at $\lambda = -1$ in an otherwise smooth and asymmetric distribution. The GN network, however, even at $p_0 = 1$ exhibited an asymmetric disk-like structure, due to the initially asymmetrical adjacency matrix (data not shown). In contrast to the smooth distributions of RPNs, the eigenvalue density of LPNs was rugged, with many peaks; see Figure 8.

For both the FN and SW scenarios, the distribution of eigenvalues smoothly changed its shape from circular (most eigenvalues complex) with radius $\sqrt{N c(1-c)}$ in the case of a completely randomly connected network to degenerate (all eigenvalues real) with a heavy tail of large positive eigenvalues for networks with only local couplings; see Figure 7. Additionally, both distributions exhibited a prominent peak at $\text{Re}(\lambda) = -1$, clearly visible only for $p > 0.9$ and $c < 0.1$, respectively. In the FN model, there were more large real eigenvalues, corresponding to the prominent horizontal line. For the SW model, particularly in the range of $c = 0.5$, we observed a higher frequency of eigenvalues with $2.5 < \text{Re}(\lambda) < 7.5$ and $-1.5 < \text{Im}(\lambda) < 1.5$.

Although the spectra of FN and SW networks were quite similar, the average spatial concentration of eigenvectors turned out to be a quite sensitive indicator for both the type of spatial embedding (RPN versus LPN) and the type of wiring (FN versus SW) assumed for the construction of the graph. Figure 9 shows the results of calculating the locality of all eigenvectors. As explained in Section 2 we considered three measures, two of them are displayed in Figure 9. In the top row, we present the entropy H for RPNs, the middle row shows the square-root of the circular variance $v^{1/2}$ for RPNs, and the bottom row shows the same quantity for LPNs. In each figure, dots correspond to the eigenvectors and eigenvalues of one particular network realization. The different colors represent different randomness parameters p and c , respectively.

In general, the eigenvectors corresponding to the largest absolute values of λ were the most local ones. Additionally, we found that the more regular the connectivity is, the more spatial concentration occurs: there were more localized eigenvectors in the regular

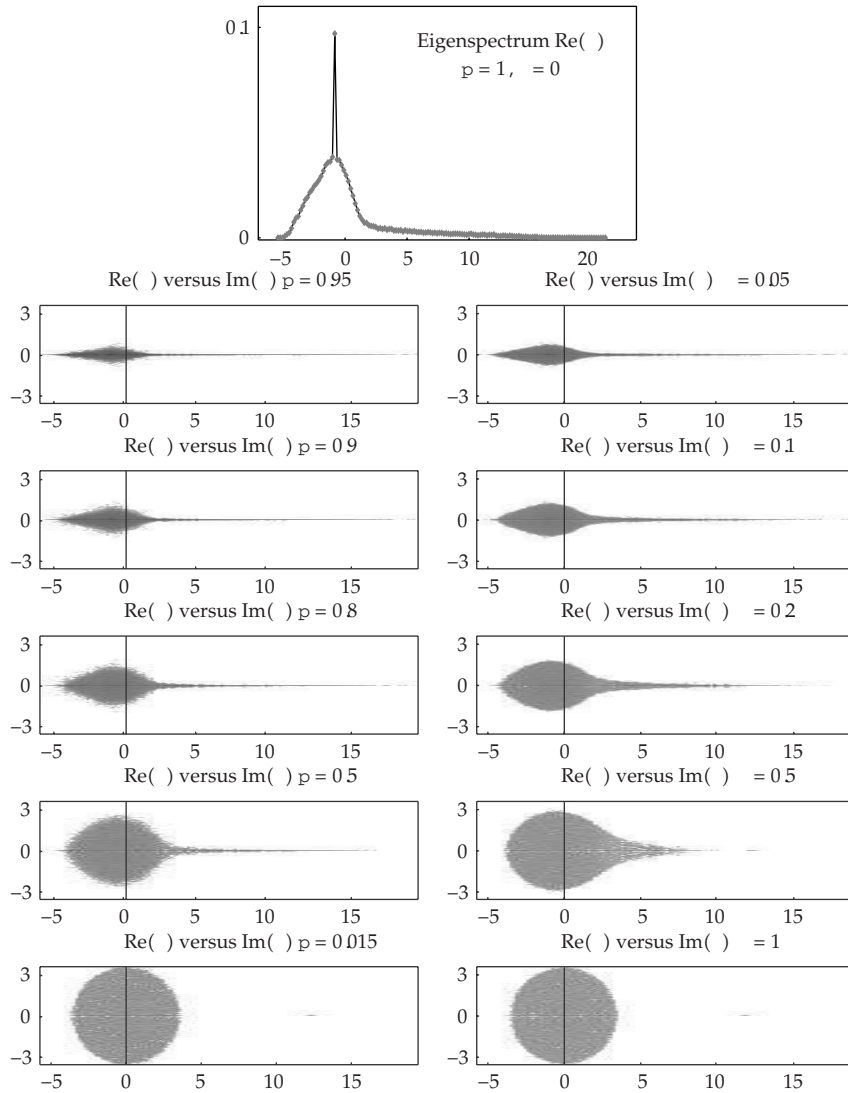


Figure 7: Eigenvalue density of FN (left) and SW (right) RPNs ranging from local (top) to random (bottom) networks. Top: real eigenvalue spectrum of a (symmetric) locally connected network ($r = 0.061$, $p = 1$, $r = 0$). Note the exceptional peak of the density at small negative values around -1 . Bottom: complex eigenvalue density for (nonsymmetric) RPNs with FN and SW connectivity. The corresponding parameters p and r are indicated within the plot. The logarithmic gray scale indicates densities up to about 16 per unit square (black).

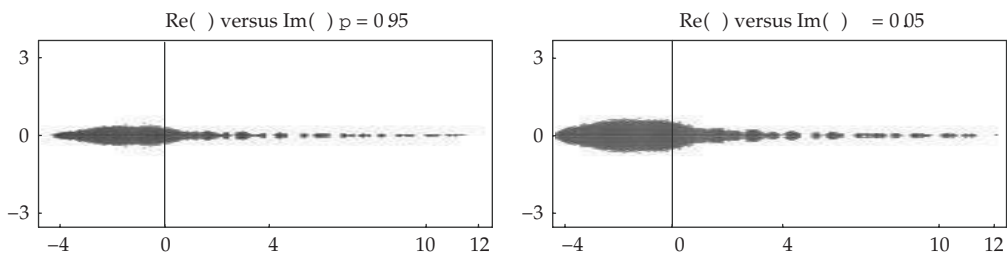


Figure 8: Complex eigenvalue density for LPNs with FN ($p = 0.95$) and SW ($r = 0.05$) connectivity. The logarithmic gray scale indicates densities up to about 16 per unit square (black).

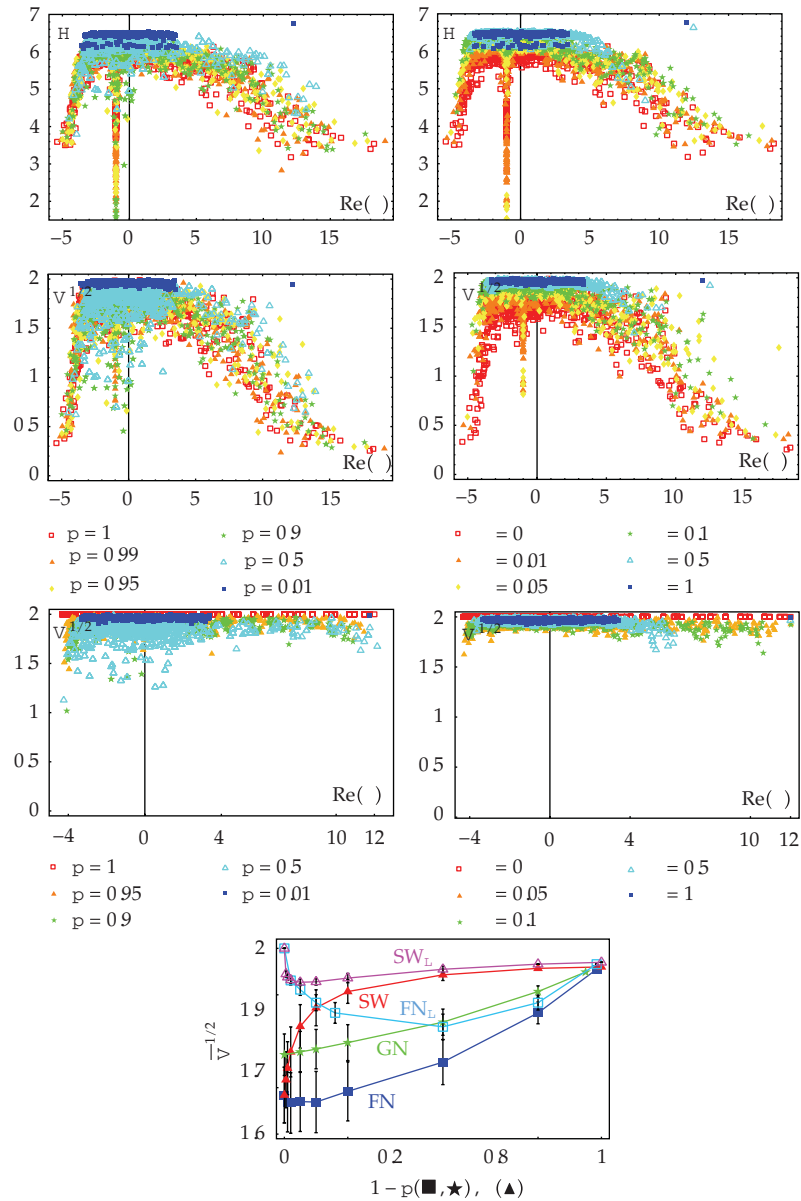


Figure 9: Locality of eigenvectors for RPNs and LPNs, either with FN (left) or SW (right) connectivity. Top: entropy H and square-root of circular variance $V^{1/2}$ for RPNs. Middle: circular variance for LPNs. In each plot the randomness parameters p or γ range from purely local (red) to random (blue) connectivity. Bottom: mean $V^{1/2}$ of all analyzed networks in dependence of p or γ , respectively. Shown are FN and SW connectivity for RPN and LPN and GN connectivity for RPNs only. Each data point represents the mean of 20 simulations; error bars indicate the SEM.

connectivity range (red), and these exhibited smaller values of both $V^{1/2}$ and H . (the \mathcal{I} measure behaved similar to H ; data not shown). In addition to the features discussed above, we again found a prominent aggregation for $\gamma = -1$ which can be traced back to the peak at $\text{Re}(\lambda = -1)$ in the eigenvalue spectrum. Comparing our two connectivity models, we found

that the eigenvectors of the FN networks were clearly more local than those for SW networks: There were more points with small $v^{1/2}$ values on the left than on the right side of Figure 9.

Figure 9, bottom, indicates a prominent difference between RPNs and LPNs. Lattice positions produced significantly less spatial concentration. We found only very few eigenvectors for $v^{1/2} < 1.5$. The most local eigenvectors were not to be found in the regular connectivity range but for values of p and β at approximately 0.5. Hence, a certain amount of randomness was important for the emergence of locality. There was less locality in the LPNs and less locality in the SW model. However, for more random connectivity these differences were less expressed. With respect to the circular variance, the GN model showed indeed intermediate behavior: the eigenvectors were not as local as in the SW network, but there was more spatial concentration than in the FN model.

4. Discussion and Conclusions

We introduced two families of network models, each describing a sheet, or layer, of cortical tissue with different types of horizontal connections. We assumed no particular structure in the vertical dimension. Neurons were situated in space, and the probability for a synaptic coupling between any two cells depended only on their distance. Both models could be made compatible with basic neuroanatomy by adjusting the parameters of the coupling appropriately. Both families of networks spanned the full range from purely local, or regular, to completely random connectivity by variation of a single parameter. The paths they took through the high-dimensional manifold of possible networks, however, were very different.

The first model (fuzzy neighborhood) assumed a homogeneous coupling probability for neurons within a disk of a given diameter centered at the source neuron. The probability was matched to the size of the disk such that the total connectivity assumed a prescribed value. The related Gaussian neighborhood model was based on similar assumptions but its smoothly decreasing connection probabilities were defined by Gaussian profiles, adapted to those of the fuzzy neighborhood model. For very small disks, only close neighbors formed synapses with each other, and, for very large disks spanning the whole network, couplings were effectively random. The second model (small world) started with the same narrow neighborhoods but departed in a different direction by replacing more and more local connections with nonlocal ones, randomly selecting targets that were located anywhere in the network.

For most models considered in this study, the initial random positioning of neurons in space guaranteed that both in-degrees and out-degrees had always the same binomial distribution, irrespective of the size of the disk defining the neighborhood and irrespective of the number of non-local connections. This means that none of the statistical differences between the various candidate models described in the paper can be due to specific degree distributions. This is in marked contrast to the original demonstration of the small-world effect in ring graphs [34], where the locally coupled networks were at the same time completely regular, that is, all degrees were identical. Finally, we also relaxed the random positioning of neurons before linking them and put them on a (jittered) grid instead [28]. It is striking to see (and a warning to the modeler) that this had indeed a strong impact on several parameters considered (Figures 6 and 9).

The first main result of this study is that networks residing in two dimensions—very much like one-dimensional ring graphs [34]—can also exhibit the small-world effect (Figure 5). As a prerequisite, though, the non-local shortcut links must be allowed to invade

also remote parts of the network without any constraints on the distance they might need to travel. In our small-world model, strong clustering (provided by intense neighborhood coupling) and short graph-theoretical paths (provided by the long-distance bridges) coexisted for certain parameter constellations. Such a smart circuit design is the prevailing assumption for cortical connectivity [14, 15, 29]. In the fuzzy neighborhood models, in contrast, the global limit imposed on the physical length of connections was strictly prohibitive for this combination of properties. The Gaussian neighborhood model, finally, shows comparably weak clustering but shorter graph-theoretical paths than the corresponding fuzzy neighborhood model.

It seems reasonable to assume that, in neocortex, the length of a cable realizing a connection is roughly proportional to the physical distance it has to bridge. The second main result of this study is that the length of the average shortest graph-theoretical path was always inversely related to the total length of cable that is necessary to realize it (Figure 5 (bottom part)), considering networks with fixed global connectivity. Completely random networks had very short graph-theoretical paths, but they needed a lot of cable to be wired up. In contrast, networks with local couplings were only very economical in terms of cable, for the price of quite long graph-theoretical paths. Networks from the small-world regime with short graph-theoretical paths were relatively inefficient in terms of necessary cable length, compared to the fuzzy and Gaussian neighborhood models (Figure 5). Only networks with patchy long-range connectivity [7, 20, 29] provide a near-to-optimal solution since they are very efficient in terms of both cable and graph-theoretical path lengths, in addition to high clustering. Networks with patchy connectivity are, however, beyond the scope of this paper. In view of the results presented here, an optimized model would employ a Gaussian connectivity profile for local connections, combined with some long-distance bridges to overcome the sparsity in cortical connectivity.

What conclusions can be drawn from graph spectral analyses? First of all, the complex eigenvalue spectrum of the adjacency matrix of a graph is a true graph invariant in the sense that any equivalent graph (obtained by renaming the nodes) has exactly the same spectrum. To some degree, the opposite is also the case: significantly different graphs give rise to differently shaped eigenvalue spectra. Empirically, it seems that similar graphs also yield similar spectra, but a rigorous mathematical foundation of such a result would be very difficult to establish. So we informally state the result that the shape of eigenvalue spectra reflects characteristic properties of graph ensembles, very much like a fingerprint. With an appropriate catalog at hand, major characteristics of a network might be recognized from its eigenvalue spectrum.

More can be said once the eigenvalue spectrum is interpreted in an appropriate dynamical context. Linearizing the firing rate dynamics about a stationary state allows the direct interpretation of eigenvalues in terms of the transient dynamic properties of an eigenstate. Real parts give the damping time constant, and imaginary parts yield the oscillation frequency. Although some care must be taken to correctly account for inhibition in the network [35], it is safe to predict that networks with more local connections tend to have a greater diversity with respect to the life times of their states and a reduced tendency to produce fast oscillations (Figure 7). The spatial properties of the eigenstates (Figures 3 and 9) are potentially relevant for describing network-wide features of activity, which can be observed in the brain using modern methods like real-time optical imaging. More specific predictions about the network dynamics based on a network model, however, would certainly depend on the precise neuron model, further parameters describing the circuit, in particular

synaptic transmission delays [36], but also on the type of signal the dynamic properties of which are considered [37].

Finally, we would like to stress once more the importance of identifying characteristic parameters in stochastic graphs and their potential yield for the analysis of neuroanatomical data. Measurable quantities, or combinations of such characteristic numbers, could be of invaluable help to find signatures and to eventually identify the type of neuronal network represented by neocortex.

Acknowledgments

The authors thank A. Schüz and V. Braitenberg for stimulating discussions. This work was funded by a grant to N. Voges from the IGPP Freiburg. Further support was received from the German Federal Ministry for Education and Research (BMBF; Grant no. 01GQ0420 to BCCN Freiburg) and the 6th RFP of the EU (Grant no. 15879-FACETS).

References

- [1] V. Braitenberg and A. Schüz, *Cortex: Statistics and Geometry of Neuronal Connectivity*, Springer, Berlin, Germany, 2nd edition, 1998.
- [2] R. J. Douglas and K. A. C. Martin, "Neuronal circuits of the neocortex," *Annual Review of Neuroscience*, vol. 27, pp. 419–451, 2004.
- [3] J. S. Lund, A. Angelucci, and C. P. Bressloff, "Anatomical substrates for functional columns in macaque monkey primary visual cortex," *Cerebral Cortex*, vol. 13, no. 1, pp. 15–24, 2003.
- [4] A. M. Thomson, "Selectivity in the inter-laminar connections made by neocortical neurones," *Journal of Neurocytology*, vol. 31, no. 3–5, pp. 239–246, 2002.
- [5] K. S. Rockland, "Non-uniformity of extrinsic connections and columnar organization," *Journal of Neurocytology*, vol. 31, no. 3–5, pp. 247–253, 2002.
- [6] C. Boucsein, M. P. Nawrot, and P. Schnepel, "Beyond the cortical column: abundance and physiology of horizontal connections imply a strong role for inputs from the surround," *Frontiers in Neuroscience*, vol. 5, article 32, 2011.
- [7] N. Voges, A. Schüz, A. Aertsen, and S. Rotter, "A modeler's view on the spatial structure of intrinsic horizontal connectivity in the neocortex," *Progress in Neurobiology*, vol. 92, no. 3, pp. 277–292, 2010.
- [8] P. Erdős and A. Rényi, "On random graphs. I," *Publicationes Mathematicae Debrecen*, vol. 6, pp. 290–297, 1959.
- [9] B. Bollobás, *Random Graphs*, vol. 73 of *Cambridge Studies in Advanced Mathematics*, Cambridge University Press, Cambridge, UK, 2nd edition, 2001.
- [10] R. Albert and A. L. Barabási, "Statistical mechanics of complex networks," *Reviews of Modern Physics*, vol. 74, no. 1, pp. 47–97, 2002.
- [11] M. E. J. Newman, "The structure and function of complex networks," *SIAM Review*, vol. 45, no. 2, pp. 167–256, 2003.
- [12] S. H. Strogatz, "Exploring complex networks," *Nature*, vol. 410, no. 6825, pp. 268–276, 2001.
- [13] O. Sporns, G. Tononi, and G. M. Edelman, "Theoretical neuroanatomy: relating anatomical and functional connectivity in graphs and cortical connection matrices," *Cerebral Cortex*, vol. 10, no. 2, pp. 127–141, 2000.
- [14] D. S. Bassett and E. Bullmore, "Small-world brain networks," *Neuroscientist*, vol. 12, no. 6, pp. 512–523, 2006.
- [15] F. Gerhard, G. Pipa, B. Lima, S. Neuenschwander, and W. Gerstner, "Extraction of network topology from multi-electrode recordings: is there a small-world effect?" *Frontiers in Computational Neuroscience*, vol. 5, article 4, 2011.
- [16] B. Hellwig, "A quantitative analysis of the local connectivity between pyramidal neurons in layers 2/3 of the rat visual cortex," *Biological Cybernetics*, vol. 82, no. 2, pp. 111–121, 2000.
- [17] N. Kalisman, G. Silberberg, and H. Markram, "Deriving physical connectivity from neuronal morphology," *Biological Cybernetics*, vol. 88, no. 3, pp. 210–218, 2003.

- [18] A. Stepanyants, J. A. Hirsch, L. M. Martinez, Z. F. Kisvárdy, A. S. Ferecskó, and D. B. Chklovskii, "Local potential connectivity in cat primary visual cortex," *Cerebral Cortex*, vol. 18, no. 1, pp. 13–28, 2008.
- [19] H. Ojima, C. N. Honda, and E. G. Jones, "Patterns of axon collateralization of identified supragranular pyramidal neurons in the cat auditory cortex," *Cerebral Cortex*, vol. 1, no. 1, pp. 80–94, 1991.
- [20] Z. F. Kisvárdy and U. T. Eysel, "Cellular organization of reciprocal patchy networks in layer III of cat visual cortex (area 17)," *Neuroscience*, vol. 46, no. 2, pp. 275–286, 1992.
- [21] C. Mehring, U. Hehl, M. Kubo, M. Diesmann, and A. Aertsen, "Activity dynamics and propagation of synchronous spiking in locally connected random networks," *Biological Cybernetics*, vol. 88, no. 5, pp. 395–408, 2003.
- [22] A. Kumar, S. Rotter, and A. Aertsen, "Propagation of synfire activity in locally connected networks with conductance-based synapses," in *Proceedings of the Computational and Systems Neuroscience (Cosyne '06)*, 2006.
- [23] D. B. Chklovskii, "Optimal sizes of dendritic and axonal arbors in a topographic projection," *Journal of Neurophysiology*, vol. 83, no. 4, pp. 2113–2119, 2000.
- [24] D. B. Chklovskii, "Synaptic connectivity and neuronal morphology: two sides of the same coin," *Neuron*, vol. 43, no. 5, pp. 609–617, 2004.
- [25] N. Voges, A. Aertsen, and S. Rotter, "Statistical analysis and modeling of cortical network architecture based on neuroanatomical data," Göttingen Neurobiology Report, Thieme, 2005.
- [26] N. Voges, A. Aertsen, and S. Rotter, "Anatomy-based network models of cortex and their statistical analysis," in *Proceedings of the 15th Annual Computational Neuroscience Meeting (CNS '06)*, Edinburgh, UK.
- [27] A. L. Barabási and Z. N. Oltvai, "Network biology: understanding the cell's functional organization," *Nature Reviews Genetics*, vol. 5, no. 2, pp. 101–113, 2004.
- [28] N. Voges, A. Aertsen, and S. Rotter, "Statistical analysis of spatially embedded networks: from grid to random node positions," *Neurocomputing*, vol. 70, no. 10–12, pp. 1833–1837, 2007.
- [29] N. Voges, C. Guijarro, A. Aertsen, and S. Rotter, "Models of cortical networks with long-range patchy projections," *Journal of Computational Neuroscience*, vol. 28, no. 1, pp. 137–154, 2010.
- [30] I. J. Farkas, I. Derényi, A. L. Barabási, and T. Vicsek, "Spectra of "real-world" graphs: beyond the semicircle law," *Physical Review E*, vol. 64, no. 2, Article ID 26704, pp. 267041–2670412, 2001.
- [31] I. Farkas, I. Derényi, H. Jeong et al., "Networks in life: scaling properties and eigenvalue spectra," *Physica A*, vol. 314, no. 1–4, pp. 25–34, 2002.
- [32] E. Batschelet, *Circular Statistics in Biology*, Mathematics in Biology, Academic Press, London, UK, 1981.
- [33] N. I. Fisher, *Statistical Analysis of Circular Data*, Cambridge University Press, Cambridge, UK, 1993.
- [34] D. J. Watts and S. H. Strogatz, "Collective dynamics of 'small-world networks,'" *Nature*, vol. 393, no. 6684, pp. 440–442, 1998.
- [35] B. Kriener, T. Tetzlaff, A. Aertsen, M. Diesmann, and S. Rotter, "Correlations and population dynamics in cortical networks," *Neural Computation*, vol. 20, no. 9, pp. 2185–2226, 2008.
- [36] N. Voges and L. Perrinet, "Phase space analysis of networks based on biologically realistic parameters," *Journal of Physiology Paris*, vol. 104, no. 1–2, pp. 51–60, 2010.
- [37] M. Timme, F. Wolf, and T. Geisel, "Topological speed limits to network synchronization," *Physical Review Letters*, vol. 92, no. 7, Article ID 74101, pp. 741011–741014, 2004.

Research Article

A Quasi-ARX Model for Multivariable Decoupling Control of Nonlinear MIMO System

Lan Wang, Yu Cheng, and Jinglu Hu

Graduate School of Information, Production and Systems, Waseda University, Hibikino 2-7, Wakamatsu-ku, Kitakyushu-shi, Fukuoka 808-0135, Japan

Correspondence should be addressed to Jinglu Hu, jinglu@waseda.jp

Received 27 June 2011; Accepted 17 August 2011

Academic Editor: Jinling Liang

Copyright © 2012 Lan Wang et al. This is an open access article distributed under the Creative Commons Attribution License, which permits unrestricted use, distribution, and reproduction in any medium, provided the original work is properly cited.

This paper proposes a multiinput and multioutput (MIMO) quasi-autoregressive exogenous (ARX) model and a multivariable-decoupling proportional integral differential (PID) controller for MIMO nonlinear systems based on the proposed model. The proposed MIMO quasi-ARX model improves the performance of ordinary quasi-ARX model. The proposed controller consists of a traditional PID controller with a decoupling compensator and a feed-forward compensator for the nonlinear dynamics based on the MIMO quasi-ARX model. Then an adaptive control algorithm is presented using the MIMO quasi-ARX radial basis function network (RBFN) prediction model and some stability analysis of control system is shown. Simulation results show the effectiveness of the proposed control method.

1. Introduction

Nonlinear system control has become a considerable topic in the field of control engineering [1, 2]. Many control results have been obtained for nonlinear single-input and single-output (SISO) systems based on the black box models, such as neural networks (NNs), wavelet networks (WNs), neurofuzzy networks (NFNs), and radial basis function networks (RBFNs), because of their abilities to approximate arbitrary mapping to any desired accuracy [3–9]. These black box models have been directly used to identify and control nonlinear dynamical systems.

Due to the complexity of nonlinear Multi-Input and Multi-Output (MIMO) systems, most of the control techniques developed for SISO systems cannot be extended directly for MIMO systems. One of the main difficulties in MIMO nonlinear system control is coupling problem. As such, it is important to investigate the realization of decoupling control. Many adaptive decoupling control algorithms have been proposed to deal with coupling in nonlinear system based on linear methods and nonlinear networks [10–14]. Some decoupling control methods of them are difficult not only to achieve accurate requirement and stability but also to be implemented in industrial applications. On the other hand, PID controller has been widely applied in controlling the SISO system because of its simple structure and relatively easy industrial application [15, 16]. However, PID controller cannot be directly used for MIMO model. Lang et al. [17] proposed a multivariable decoupling PID controller for MIMO linear systems based on the linear PID control and generalized minimum variance control law. What's more, Zhai & Chai [18] presented a multivariable PID control method using neural network to deal with nonlinear multivariable processes. In this control system, the nonlinear unmodeled part estimated by neural network is considered as a black box. The initial weights of neural network, local minima, and overfitting are the problems which need to be resolved.

In our previous work, a quasi-autoregressive exogenous (ARX) model with an ARX-like macromodel part and a kernel part was proposed, and a controller was designed for SISO systems [4, 19–21]. The kernel part is an ordinary network model, but it is used to parameterize the nonlinear coefficients of macromodel. As we know, RBFNs have played an important role in control engineering, especially in nonlinear system control because of their simple topological structure and precision in nonlinear approximation [22, 23]. Especially, RBFNs can be regarded as nonlinear models which are linear in parameters when fixing the nonlinear parameters by *a priori* knowledge [24, 25]. Incorporating the network models with this property, the quasi-ARX models become linear in parameters. Therefore, the RBFNs are chosen to replace the NNs as in [4].

The SISO model and control methods based on quasi-ARX model cannot directly be applied to MIMO nonlinear systems. Motivated by the above discussions, an MIMO quasi-ARX model is first proposed for MIMO nonlinear systems and then a nonlinear multivariable decoupling PID controller is proposed based on the MIMO quasi-ARX model, which consists of a traditional PID controller with a decoupling compensator and a feed-forward compensator for the nonlinear dynamics based on the MIMO quasi-ARX model. Then an adaptive controller is presented using the MIMO quasi-ARX RBFN prediction model. The parameters of such controller are selected based on the generalized minimum control variance. In this paper, quasi-ARX RBFN model is divided into two parts: the linear part is used to guarantee the stability and decoupling, and the nonlinear part is used to improve the accuracy.

The paper is organized as follows: in Section 2 the nonlinear MIMO system considered is first described, and then a hybrid system expression is obtained and an MIMO quasi-ARX RBFN model is proposed. In Section 3, a multivariable decoupling PID controller is developed based on the proposed model and generalized minimum variance control law. Then an adaptive control algorithm is presented using the MIMO quasi-ARX RBFN prediction model, and the corresponding parameter estimation methods are proposed in Section 4. Section 5 carries out numerical simulations to show the effectiveness of the proposed control method. Finally, Section 6 presents the conclusions.

2. An MIMO Quasi-ARX Model

2.1. Systems

Consider an MIMO nonlinear dynamical system with input-output relation as

$$\begin{aligned} \mathbf{y}(t+d) &= \mathbf{f}(\boldsymbol{\vartheta}), \\ \boldsymbol{\vartheta} &= \left[\mathbf{y}(t+d-1)^T, \dots, \mathbf{y}(t+d-n_y)^T, \mathbf{u}(t)^T, \dots, \mathbf{u}(t-n_u+1)^T \right]^T, \end{aligned} \quad (2.1)$$

where $\mathbf{y} = [y_1, \dots, y_n]^T \in \mathbb{R}^n$ and $\mathbf{u} = [u_1, \dots, u_n]^T \in \mathbb{R}^n$ are system input and output vectors, respectively, d the known integer time delay, $\boldsymbol{\vartheta}$ the regression vector, and n_y, n_u the system orders. $\mathbf{f}(\cdot) = [f_1(\cdot), \dots, f_n(\cdot)]^T$ is a vector-valued nonlinear function, and, at a small region around $\boldsymbol{\vartheta} = \mathbf{0}$ ($\mathbf{0} = [0, \dots, 0]^T$), they are C^∞ continuous. The origin is an equilibrium point, then $\mathbf{f}(\mathbf{0}) = \mathbf{0}$. The system is controllable, in which a reasonable unknown controller may be expressed by $\mathbf{u}(t) = \mathbf{u}(\boldsymbol{\vartheta})$, where $\boldsymbol{\vartheta}$ is defined in Section 2.4.

2.2. ARX-Like Expression

Under the continuous condition, the unknown nonlinear function $f_k(\boldsymbol{\vartheta})$, ($i = 1, \dots, n$) can be performed Taylor expansion on a small region around $\boldsymbol{\vartheta} = \mathbf{0}$:

$$y_k(t+d) = f'_k(0) \boldsymbol{\vartheta} + \frac{1}{2} \boldsymbol{\vartheta}^T f''_k(0) \boldsymbol{\vartheta} + \dots, \quad (2.2)$$

where the prime denotes differentiation with respect to $\boldsymbol{\vartheta}$. Then the following notations are introduced:

$$\left(f'_k(0) + \frac{1}{2} \boldsymbol{\vartheta}^T f''_k(0) \boldsymbol{\vartheta} + \dots \right)^T = \left[a_{1,t}^{1k} \dots a_{n_y,t}^{1k} \dots a_{n_y,t}^{nk} b_{1,t}^{1k} \dots b_{n_u,t}^{1k} \dots b_{n_u,t}^{nk} \right]^T, \quad (2.3)$$

where $a_{i,t}^{1k} = a_i^{1k}(\boldsymbol{\vartheta})$ ($i = 1, \dots, n_y$) and $b_{j,t}^{1k} = b_j^{1k}(\boldsymbol{\vartheta})$ ($j = 0, \dots, n_u - 1$) are nonlinear functions of $\boldsymbol{\vartheta}$.

However, we need to get $\mathbf{y}(t+d)$ by using the input-output data up to time t in a model. The coefficients $a_{i,t}^{1k}$ and $b_{j,t}^{1k}$ need to be calculable using the input-output data up to time t . To do so, let us iteratively replace $y(t+1)$ in the expressions of $a_{i,t}^{1k}$ and $b_{j,t}^{1k}$ with functions:

$$\mathbf{y}(t+s) \Rightarrow \mathbf{g}(\tilde{\boldsymbol{\vartheta}}(t+s)), \quad s = 1, \dots, d-1, \quad (2.4)$$

where $\tilde{\boldsymbol{\vartheta}}(t+s)$ is $\boldsymbol{\vartheta}(t+s)$ whose elements $y(t+m)$, $s+1 < m \leq d-s$ are replaced by (2.4), and define the new expressions of the coefficients by

$$a_{i,t}^{1k} = \tilde{a}_{i,t}^{1k} = \tilde{a}_i^{1k}(\boldsymbol{\vartheta}), \quad b_{j,t}^{1k} = \tilde{b}_{j,t}^{1k} = \tilde{b}_j^{1k}(\boldsymbol{\vartheta}), \quad (2.5)$$

where $\mathbf{v}(t)$ is a vector:

$$\mathbf{v}(t) = \left[\mathbf{y}(t)^T \cdots \mathbf{y}(t-n_y+1)^T \mathbf{u}(t)^T \cdots \mathbf{u}(t-n_u-d+2)^T \right]^T. \quad (2.6)$$

Now, introduce two polynomial matrices $\mathbf{A}(q^{-1}, t)$ and $\mathbf{B}(q^{-1}, t)$ based on the coefficients, defined by

$$\begin{aligned} \mathbf{A}(q^{-1}, t) &= \mathbf{I} - \mathbf{a}_{1,t}q^{-1} - \cdots - \mathbf{a}_{n_y,t}q^{-n_y}, \\ \mathbf{B}(q^{-1}, t) &= \mathbf{b}_{0,t} + \cdots + \mathbf{b}_{n_u-1,t}q^{-n_u+1}, \end{aligned} \quad (2.7)$$

where $\mathbf{a}_{i,t} = (a_{i,t}^{1k})_{N \times N}$, $i = 1, \dots, n_y$ and $\mathbf{b}_{j,t} = (b_{j,t}^{1k})_{N \times N}$, $j = 1, \dots, n_u$. Then, the nonlinear system (2.1) can be equivalently represented as the following ARX-like expression:

$$\mathbf{A}(q^{-1}, t)\mathbf{y}(t+d) = \mathbf{B}(q^{-1}, t)\mathbf{u}(t). \quad (2.8)$$

By (2.8), let $\mathbf{y}(t+d)$ satisfies the following equation:

$$\mathbf{y}(t+d) = \mathcal{A}(q^{-1}, t)\mathbf{y}(t) + \mathcal{B}(q^{-1}, t)\mathbf{u}(t), \quad (2.9)$$

where

$$\begin{aligned} \mathcal{A}(q^{-1}, t) &= \mathbf{A}_{0,t} + \mathbf{A}_{1,t}q^{-1} + \cdots + \mathbf{A}_{n_y-1,t}q^{-n_y+1}, \\ \mathcal{B}(q^{-1}, t) &= \mathbf{F}(q^{-1}, t)\mathbf{B}(q^{-1}, t), \\ &= \mathbf{B}_{0,t} + \mathbf{B}_{1,t}q^{-1} + \cdots + \mathbf{B}_{n_u+d-2,t}q^{-n_u-d+2}, \end{aligned} \quad (2.10)$$

$\mathbf{A}_{i,t}$ ($i = 0, \dots, n_y - 1$) and $\mathbf{B}_{j,t}$ ($j = 0, \dots, n_u + d - 2$) are coefficient matrices. And $\mathbf{G}(q^{-1}, t)$, $\mathbf{F}(q^{-1}, t)$ are unique polynomials satisfying

$$\mathbf{F}(q^{-1}, t)\mathbf{A}(q^{-1}, t) = \mathbf{I} - \mathbf{A}(q^{-1}, t)q^{-d}. \quad (2.11)$$

2.3. Hybrid Expression

The coefficients matrices $\mathbf{A}_{i,t}$ ($i = 0, \dots, n_y - 1$) and $\mathbf{B}_{j,t}$ ($j = 0, \dots, n_u + d - 2$) can be considered as a summation of two parts: the constant part $\mathbf{A}_{i,t}^1$ and $\mathbf{B}_{j,t}^1$ and the nonlinear function part on $\mathbf{v}(t)$ which are denoted $\mathbf{A}_{i,t}^n$ and $\mathbf{B}_{j,t}^n$. Then, the expression of system in the predictor form (2.9) can be described by

$$\mathbf{y}(t+d) = \mathcal{A}^1(q^{-1})\mathbf{y}(t) + \mathcal{B}^1(q^{-1})\mathbf{u}(t) + \mathcal{A}^n(q^{-1}, t)\mathbf{y}(t) + \mathcal{B}^n(q^{-1}, t)\mathbf{u}(t), \quad (2.12)$$

where

$$\begin{aligned}
\mathcal{A}^1(\bar{q}^{-1}) &= A_0^1 + A_1^1 \bar{q}^{-1} + \cdots + A_{n_y-1}^1 \bar{q}^{-n_y+1}, \\
\mathcal{A}^n(\bar{q}^{-1}, (\bar{t})) &= A_{0,t}^1 + A_{1,t}^1 \bar{q}^{-1} + \cdots + A_{n_y-1,t}^1 \bar{q}^{-n_y+1}, \\
\mathcal{B}^1(\bar{q}^{-1}) &= B_0^1 + B_1^1 \bar{q}^{-1} + \cdots + B_{n_y-d+2}^1 \bar{q}^{-n_u+d-2}, \\
\mathcal{B}^n(\bar{q}^{-1}, (\bar{t})) &= B_{0,t}^1 + B_{1,t}^1 \bar{q}^{-1} + \cdots + B_{n_y-d+2,t}^1 \bar{q}^{-n_u+d-2}.
\end{aligned} \tag{2.13}$$

Similar with [18], the linear polynomial matrix $\mathcal{B}^1(\bar{q}^{-1})$ can be expressed as $\mathcal{B}^1(\bar{q}^{-1}) = \overline{\mathcal{B}}^1(\bar{q}^{-1}) + \overline{\overline{\mathcal{B}}}^1(\bar{q}^{-1})$ with $\overline{\mathcal{B}}^1(\bar{q}^{-1})$ being diagonal and $\overline{\overline{\mathcal{B}}}^1(\bar{q}^{-1})$ being a polynomial matrix with zero diagonal elements.

Then, the linear and nonlinear expression of system (2.12) can be obtained as

$$\begin{aligned}
\mathbf{y}(t+d) &= \mathcal{A}^1(\bar{q}^{-1})\mathbf{y}(\bar{t}) + \overline{\mathcal{B}}^1(\bar{q}^{-1})\mathbf{u}(\bar{t}) + \overline{\overline{\mathcal{B}}}^1(\bar{q}^{-1})\mathbf{u}(\bar{t}) \\
&\quad + \mathcal{A}^n(\bar{q}^{-1}, (\bar{t}))\mathbf{y}(\bar{t}) + \mathcal{B}^n(\bar{q}^{-1}, (\bar{t}))\mathbf{u}(\bar{t}).
\end{aligned} \tag{2.14}$$

2.4. Quasi-ARX RBFN Model

Now, we will propose an MIMO quasi-ARX RBFN model. However, the $\mathbf{v}(\bar{t})$ are based on $\Psi(\bar{t})$ whose elements contain $\mathbf{u}(\bar{t})$. To solve this problem, an *extravariabile* $\mathbf{x}(\bar{t})$ Obviously, in a control system, the reference signal $\mathbf{y}^*(t+d)$ can be used as the extra variable $\mathbf{x}(t+d)$, is introduced, and an unknown nonlinear function $\mathcal{N}(\bar{t})$ is used to replace the variable $\mathbf{u}(\bar{t})$ in $\mathcal{B}^n(\bar{q}^{-1}, (\bar{t}))\mathbf{u}(\bar{t})$. Under the assumption of the system is controllable in Section 2.1, the function $\mathcal{N}(\bar{t})$ exists. Define

$$\mathcal{N}(\bar{t}) = \left[\mathbf{y}(\bar{t})^T \cdots \mathbf{y}(t-n_1)^T \mathbf{x}(t+d)^T \cdots \mathbf{x}(t-n_3+d)^T \mathbf{u}(t-1)^T \cdots \mathbf{u}(t-n_2)^T \right]^T, \tag{2.15}$$

including the extra variable $\mathbf{x}(t+d)$ as an element. A typical choice for n_1, n_2 , and n_3 in $\mathcal{N}(\bar{t})$ is $n_1 = n_y - 1$, $n_2 = n_u + d - 2$, and $n_3 = 0$. We can express (2.14) by

$$\mathbf{y}(t+d) = \mathcal{T}(\bar{t})\Omega_0 + \mathcal{N}(\bar{t}), \tag{2.16}$$

where $\mathcal{T}(\bar{t}) = \mathcal{B}^1(\bar{q}^{-1})$. The elements of $\mathcal{N}(\bar{t})$ are unknown nonlinear function of $\mathcal{N}(\bar{t})$, which can be parameterized by NN or RBFN. In this paper, the RBFN is used which has local property:

$$\mathcal{N}(\bar{t}) = \sum_{j=1}^M \Omega_j \mathcal{R}_j(\mathbf{p}_j, \mathcal{N}(\bar{t})), \tag{2.17}$$

where M is the number of RBFs. $\Omega_j = [\Omega_{j1}, \dots, \Omega_{jn}]$ is the coefficient matrix with $\Omega_{j,i} = [\frac{1}{j,i}, \dots, \frac{N}{j,i}]^T$, $j = 1, \dots, M$. And $\mathcal{R}_j(\mathbf{p}_j, (\vartheta))$ the RBFs defined by

$$\mathcal{R}_j(\mathbf{p}_j, (\vartheta)) = e^{-\beta_j \|\vartheta - \mathbf{Z}_j\|^2}, \quad j = 1, 2, \dots, M, \quad (2.18)$$

where $\mathbf{p}_j = \{\beta_j, \mathbf{Z}_j\}$ is the parameters set of the RBF; \mathbf{Z}_j is the center vector of RBF and β_j are the scaling parameters; $\|\bullet\|_2$ denotes the vector two norm. Then we can express the quasi-ARX RBFN prediction model for (2.16) in a form of

$$\mathbf{y}(t+d) = \mathbf{A}^T(t)\Omega_0 + \mathbf{A}^T(t) \sum_{j=1}^M \Omega_j \mathcal{R}_j(\mathbf{p}_j, (\vartheta)). \quad (2.19)$$

3. Controller Design

3.1. Nonlinear Multivariable Decoupling PID Controller

Introduce the following performance index:

$$J_M(t+d) = \left\| \mathbf{y}(t+d) - \mathbf{R}(q^{-1})\mathbf{y}^*(t+d) + \mathbf{S}(q^{-1})\mathbf{u}(t) + \mathbf{Q}(q^{-1})\mathbf{u}(t) \right\|, \quad (3.1)$$

where \mathbf{R} and \mathbf{S} are the diagonal weighting polynomial matrices, and \mathbf{Q} is a weighting polynomial matrix with diagonal elements.

The optimal control law minimizing (3.1) is

$$\mathbf{y}(t+d) - \mathbf{R}(q^{-1})\mathbf{y}^*(t+d) + \mathbf{S}(q^{-1})\mathbf{u}(t) + \mathbf{Q}(q^{-1})\mathbf{u}(t) = 0. \quad (3.2)$$

Substituting (2.14) into (3.2), the following equation is obtained:

$$\begin{aligned} \left(\overline{\mathbf{B}}^{-1}(q^{-1}) + \mathbf{Q}(q^{-1}) \right) \mathbf{u}(t) &= \mathbf{R}(q^{-1})\mathbf{y}^*(t+d) - \mathcal{A}^1(q^{-1})\mathbf{y}(t) - \left(\overline{\mathbf{B}}^{-1}(q^{-1}) + \mathbf{S}(q^{-1}) \right) \mathbf{u}(t) \\ &\quad - \left(\mathcal{B}^n(q^{-1}, (\vartheta))\mathbf{u}(t) + \mathcal{A}^n(q^{-1}, (\vartheta))\mathbf{y}(t) \right), \end{aligned} \quad (3.3)$$

where $\overline{\mathbf{B}}^{-1}(q^{-1}) + \mathbf{Q}(q^{-1}) = q^{-1}\overline{\mathbf{H}}(q^{-1})$, with $\overline{\mathbf{H}} = \text{diag}\{\beta_1, \dots, \beta_n\}$ and $\overline{\mathbf{H}}(q^{-1}) = (1 - q^{-1}) \cdot \mathbf{I}$. By introducing $\mathbf{R}(q^{-1}) = \mathcal{A}^1(q^{-1})$ and $\overline{\mathbf{B}}^{-1}(q^{-1})\mathbf{S}(q^{-1}) = \mathbf{Q}(q^{-1})\overline{\mathbf{B}}^{-1}(q^{-1})$, when $n_y - 1 \leq 2$, a nonlinear decoupling PID controller is obtained, similar to a traditional PID controller:

$$\overline{\mathbf{H}}(q^{-1})\mathbf{u}(t) = \mathcal{A}^1(q^{-1})\mathbf{e}(t) - \overline{\mathbf{H}}(q^{-1})\mathbf{u}(t) - \mathbf{v}(t), \quad (3.4)$$

where $\overline{\mathbf{H}}(q^{-1}) = \overline{\mathbf{B}}^{-1}(q^{-1}) + \mathbf{S}(q^{-1})$ and $\mathbf{v}(t) = \left(\mathcal{B}^n(q^{-1}, (\vartheta))\mathbf{u}(t) + \mathcal{A}^n(q^{-1}, (\vartheta))\mathbf{y}(t) \right)$. $\mathbf{e}(t) = \mathbf{y}^*(t+d) - \mathbf{y}(t)$.

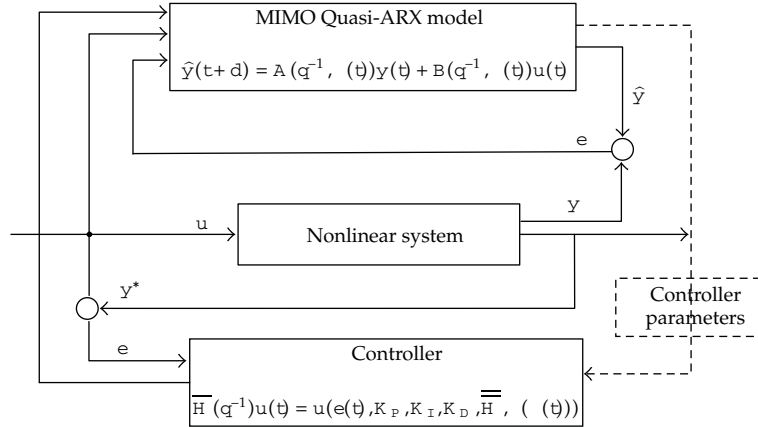


Figure 1: The multivariable decoupling PID control system based on MIMO quasi-ARX model.

The controller (3.4) is substituted into the system (3.2), the obtained closed-loop system which is shown in Figure 1 will be stable, and the decoupling control effect and tracking errors can be eliminated.

A velocity-type form of the PID controller is given:

$$\begin{aligned} \bar{H}(q^{-1})u(t) &= K_p(e(t) - e(t-1)) + K_I e(t) + K_D(e(t) - 2e(t-1) + e(t-2)) \\ &\quad - \bar{H}(q^{-1})u(t) - v(t). \end{aligned} \tag{3.5}$$

The gain can be selected as

$$\begin{aligned} K_p &= -(2A_2 + A_1), \\ K_I &= (A_0 + A_1 + A_2), \\ K_D &= A_2, \end{aligned} \tag{3.6}$$

where when $n_y = 1, A_1 = A_2 = 0$ and when $n_y = 2, A_2 = 0$.

3.2. Parameter Estimation

3.2.1. A Simple Strategy for Determining p_j

Now let us initialize p_j , denoted as follows:

$$p_j = [\bar{z}_1^j \bar{z}_2^j \cdots \bar{z}_N^j, j]^T \quad (j = 1, \dots, M), \tag{3.7}$$

where $N = \dim(\hat{y}(t))$. Since p_j is associated with partition of $\hat{y}(t)$, the bounds of $\hat{y}(t)$ can be used to determine a fairly good initial value. It will not be discussed here, and the interested readers are referred to [26].

3.2.2. Estimation of Parameter Vector Ω_0

If the process is known, Ω_0 is obtained by using Taylor expansion at its equilibrium; otherwise, it will be replaced by its estimation $\hat{\Omega}_0$.

3.2.3. Estimation of Parameter Vector Ω_j

Parameter vector $\Omega_j (j = 1, \dots, M)$ can be estimated by a simplified multivariable least-squares algorithm as in [27]. By introducing the notations:

$$\Omega = \left[\Omega_1^T, \dots, \Omega_M^T \right]^T, \quad \Phi(t) = \left[(t)^T \otimes \Psi_{\mathcal{R}}^T(t) \right]^T, \quad (3.8)$$

where the symbol \otimes denotes Kronecker production, then $\Psi_{\mathcal{R}}^T(t) = [\mathcal{R}_j(\mathbf{p}_j, (t)), j = 1, \dots, M]$, the MIMO quasi-ARX model (2.12) can be expressed in a regression form:

$$\mathbf{y}(t+d) = (t)^T \Omega_0 + \Phi^T(t) \Omega. \quad (3.9)$$

The parameter Ω is updated by an LS algorithm while fixing \mathbf{p}_j and Ω_0 :

$$\hat{\Omega}(t) = \hat{\Omega}(t-d) + \frac{\mathbf{p}(t)\Phi(t-d)\mathbf{e}(t)}{1 + \Phi(t-d)^T \mathbf{p}(t)\Phi(t-d)}, \quad (3.10)$$

where $\hat{\Omega}(t)$ is the estimate of Ω at time instant t , $\mathbf{e}(t)$ is the error vector of MIMO quasi-ARX model, defined by

$$\begin{aligned} \mathbf{e}(t) &= \mathbf{y}(t) - (t)^T \Omega_0 - \Phi(t-d)^T \hat{\Omega}(t-d), \\ \mathbf{p}(t) &= \frac{\mathbf{P}(t-d) - \mathbf{P}^T(t-d)\Phi(t-d)^T \Phi(t-d)\mathbf{P}(t-d)}{1 + \Phi(t-d)^T \mathbf{P}(t)\Phi(t-d)}. \end{aligned} \quad (3.11)$$

Remark 3.1. Comparing with [18], there are three improvements: the unmodeled part is modeled in this paper by quasi-ARX model, RBFN is used to replace NN, and some priori knowledge can be used to determine the parameters.

4. Stability Analysis

There are some assumption made.

Assumption 1. (i) $\mathbf{y}^*(t)$ is a bounded deterministic sequence; (ii) $\forall (t)$ is globally bounded, $|\forall (t)| \leq \Delta$, where the boundary Δ is known; (iii) the choices of \mathbf{p} and $\mathbf{S}(\alpha^{-1})$ are such that $\det\{\tilde{\mathbf{H}}(\alpha^{-1})\mathbf{A}(\alpha^{-1}) + \alpha^{-d}\tilde{\mathbf{B}}(\alpha^{-1}) \mathcal{A}^{-1}(\alpha^{-1})\} \neq 0$.

Theorem 4.1. For the MIMO nonlinear (2.1) with the controller (3.5), together with the parameters of the controller selected by Section 3.2, all the signals in the closed-loop system described above can be

bounded, and the tracking error can be made less than any specified constant over a compact set by properly choosing the structures and parameters of quasi-ARX RBFN model, that is, $\lim_{t \rightarrow \infty} \|\mathbf{y}(t+d) - \mathbf{y}^*(t+d)\| \leq \epsilon$.

Proof. The nonlinear part estimation error vector can be described by

$$\mathbf{e}(t) = \mathbf{v}(t+d) - \mathbf{v}^T(t+d) \sum_{j=1}^M \hat{\Omega}(t+d)_j \mathcal{R}_j(\mathbf{p}_j, \mathbf{v}(t+d)). \quad (4.1)$$

We can see that, if the nonlinear decoupling PID controller (3.5) is used to the system (2.14), the following input-output dynamics are obtained as in [18]:

$$\begin{aligned} & (\tilde{\mathbf{H}}(\mathbf{q}^{-1})\mathbf{A}(\mathbf{q}^{-1}) + \mathbf{q}^{-d}\tilde{\mathbf{B}}(\mathbf{q}^{-1}) \mathcal{A}^1(\mathbf{q}^{-1}))\mathbf{y}(t+d) \\ &= \tilde{\mathbf{B}}(\mathbf{q}^{-1}) \mathcal{A}^1(\mathbf{q}^{-1})\mathbf{y}^*(t+d) + \tilde{\mathbf{H}}(\mathbf{q}^{-1})\mathbf{v}(t+d) - \tilde{\mathbf{B}}(\mathbf{q}^{-1})\hat{\mathbf{v}}(t+d), \\ & (\mathbf{A}(\mathbf{q}^{-1})\mathbf{H}(\mathbf{q}^{-1}) + \mathbf{q}^{-d} \mathbf{A}(\mathbf{q}^{-1})\mathcal{A}^1(\mathbf{q}^{-1}))\mathbf{u}(t+d) \\ &= \tilde{\mathbf{A}}(\mathbf{q}^{-1}) \mathcal{A}^1(\mathbf{q}^{-1})\mathbf{y}^*(t+d) - \mathbf{q}^{-d} \mathcal{A}^1(\mathbf{q}^{-1})\mathbf{v}(t+d) - \mathbf{A}(\mathbf{q}^{-1})\hat{\mathbf{v}}(t+d). \end{aligned} \quad (4.2)$$

Substitute (4.1) into (4.2), the equations are given as follows:

$$\begin{aligned} & (\tilde{\mathbf{H}}(\mathbf{q}^{-1})\mathbf{A}(\mathbf{q}^{-1}) + \mathbf{q}^{-d}\tilde{\mathbf{B}}(\mathbf{q}^{-1}) \mathcal{G}(\mathbf{q}^{-1}))\mathbf{y}(t+d) \\ &= \tilde{\mathbf{B}}(\mathbf{q}^{-1}) \mathcal{G}(\mathbf{q}^{-1})\mathbf{y}^*(t+d) + (\tilde{\mathbf{H}}(\mathbf{q}^{-1}) - \tilde{\mathbf{B}}(\mathbf{q}^{-1}))\mathbf{v}(t+d) + \tilde{\mathbf{B}}(\mathbf{q}^{-1}) \mathbf{e}(t), \\ & (\mathbf{A}(\mathbf{q}^{-1})\mathbf{H}(\mathbf{q}^{-1}) + \mathbf{q}^{-d} \mathbf{A}(\mathbf{q}^{-1})\mathcal{A}^1(\mathbf{q}^{-1}))\mathbf{u}(t+d) \\ &= \tilde{\mathbf{A}}(\mathbf{q}^{-1}) \mathcal{A}^1(\mathbf{q}^{-1})\mathbf{y}^*(t+d) - (\mathbf{q}^{-d} \mathcal{A}^1(\mathbf{q}^{-1}) + \mathbf{A}(\mathbf{q}^{-1}))\mathbf{v}(t+d) - \mathbf{A}(\mathbf{q}^{-1}) \mathbf{e}(t). \end{aligned} \quad (4.3)$$

From (4.3) and Assumption 1, there exist constants C_1, C_2, C_3, C_4 satisfying

$$\begin{aligned} \|\mathbf{y}(t+d)\| &\leq C_1 + C_2 \max_{0 \leq \tau \leq t} \|\mathbf{e}(\tau)\|, \\ \|\mathbf{u}(t)\| &\leq C_3 + C_4 \max_{0 \leq \tau \leq t} \|\mathbf{e}(\tau)\|. \end{aligned} \quad (4.4)$$

Because of the universal approximations of the RBFNs, the estimation error $\mathbf{e}(t)$ can be achieved less than any constant over a compact set by properly choosing their structures and parameters. It can be got that

$$\|\mathbf{e}(t+d)\| \leq C_5 + C_6 \max_{0 \leq \tau \leq t} \|\mathbf{e}(\tau)\| \leq C_7 + C_8 \leq C_9. \quad (4.5)$$

where C_5, C_6, C_7, C_8, C_9 are constants.

Then, the boundness of all the signals in the closed-loop system is got. \square

The tracking error of the system is obtained as

$$e = \lim_{t \rightarrow \infty} \|y(t+d) - y^*(t+d)\| \leq C, \quad (4.6)$$

where $C > 0$ is a constant.

5. Numerical Simulations

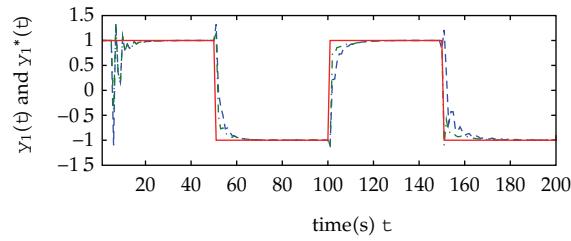
In order to study the behavior of the proposed control method, a numerical simulation is described in this section. The MIMO nonlinear system to be controlled is described by

$$\begin{aligned} y_1(t+1) &= 0.9y_1(t) - \frac{0.3y_1(t-1)}{1+y_2^2(t-1)} + 0.4\sin(u_1(t)) + 0.7u_1(t-1) + 0.3u_2(t) - 0.5u_2(t-1), \\ y_2(t+1) &= -0.4\sin(y_2^2(t)) - 0.1y_2(t-1) + u_2(t-1) - 0.3\sin(u_1(t)) \\ &\quad + 0.2u_1(t-1 + 0.8\sin(u_2(t))) + 0.5u_2^2(t-1), \quad \text{for } t \in [0, 150), \\ y_1(t+1) &= 0.6y_1(t) - \frac{0.4y_1(t-1)}{1+y_2^2(t-1)} + 0.4\sin(u_1(t)) + 0.6u_1(t-1) + 0.4u_2(t) - 0.5u_2(t-1), \\ y_2(t+1) &= -0.5\sin(y_2^2(t)) - 0.1y_2(t-1) + u_2(t-1) - 0.3\sin(u_1(t)) + 0.3u_1(t-1) \\ &\quad + 0.9\sin(u_2(t)) + 0.5u_2^2(t-1), \quad \text{for } t \in [150, \infty). \end{aligned} \quad (5.1)$$

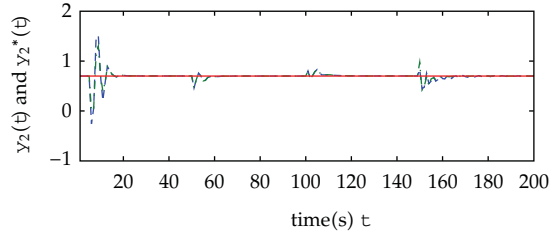
In this example, a system disturbance appears when $t = 150$. The desired output of system is given $y_1^*(t) = \text{sign}(\sin(t/50))$ and $y_2^*(t) = 0.7$.

In this example, the proposed control method in Sections 3 and 4 is illustrated effective in the control stability and robustness. The order is chosen as $n_y = n_u = 2$, and time delay $d = 1$. The regression $\varphi(t) = [y_1(t-1)y_2(t-1)y_1(t-2)y_2(t-2)u_1(t-1)u_2(t-1)u_1(t-2)u_2(t-2)]^T$ and $\psi(t) = [y_1(t-1)y_2(t-1)y_1(t-2)y_2(t-2)y_1^*(t)y_1^*(t)y_2^*(t)y_2^*(t)u_1(t-2)u_2(t-2)]^T$. Based on the priori knowledge, we choose $Z_{\max} = [22224141]$ and $Z_{\min} = [-2-2-2-2-4-1-4-1]$. The parameters p_j can be determined by the proposed method in Section 3.2.

Under the same simulation conditions and with the same parameters value, the control output results by a typical PID controller are given for comparison, where the PID controller has neither the decoupling compensator nor the nonlinear part. The control outputs are shown in Figure 2, the solid red line is the desired outputs, the dashed blue line is the typical PID control outputs, and the dotted green line is the proposed method control outputs. The corresponding control inputs $u_1(t)$ and $u_2(t)$ are given in Figures 3 and 4. We can see that our proposed method is nearly consistent with the desired output at most of the time which is better than typical PID control method when $t \in [0, 150)$. Obviously, the control performance of our proposed method is much better than typical PID control method when the system has disturbance when $t = 150$. The input signals have small fluctuation as shown in Figure 4.

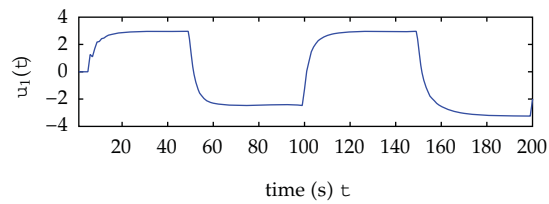


(a)

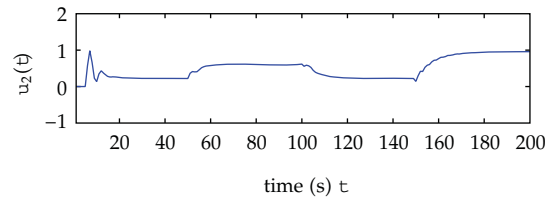


(b)

Figure 2: Control outputs.



(a)



(b)

Figure 3: Corresponding control inputs of the PID control method.

Table 1 gives the comparison results of the errors. Obviously, the mean and variance of errors of the proposed method are smaller than the typical PID control method.

6. Conclusions

In this paper, an MIMO quasi-ARX model is first introduced, and a nonlinear multivariable decoupling PID controller is proposed based on the proposed model for MIMO nonlinear systems. The proposed controller consists of a traditional PID controller with a decoupling compensator and a feed-forward compensator for the nonlinear dynamics based on the

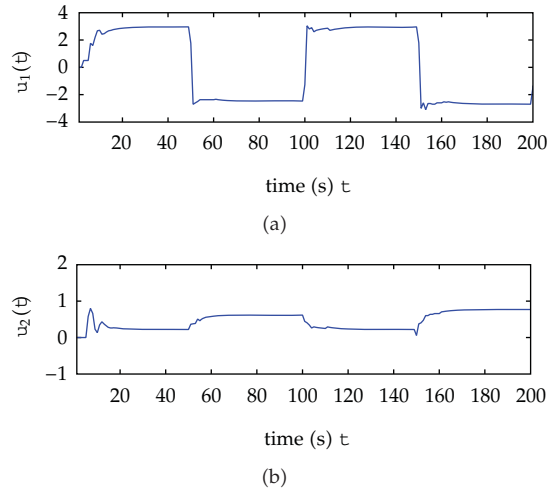


Figure 4: Corresponding control inputs of the proposed control method.

Table 1: Comparison results of errors based on two control method.

	Mean of errors	Variance of errors
$y_1(t)$ typical method	0.0132	0.1350
: proposed method	-0.0090	0.0668
$y_2(t)$ typical method	-0.0067	0.0157
: proposed method	-0.0039	0.0098

MIMO quasi-ARX model. And an adaptive control system is presented using the MIMO quasi-ARX RBFN prediction model. The parameters of such controller are selected based on the generalized minimum control variance. The proposed control method has more simplicity structures and better control performance. The nonlinear part is not a black box whose parameters can be determined by *a priori* acknowledge. Simulation results show the effectiveness of the proposed method on control accuracy and robustness when a disturbance appears in the system. Because the PID controller can be realized on standard DCS/PLC modules, the algorithm is more useful for industrial process control. Otherwise, because the parameters of controller are chosen from the generalized minimum variance control law, it is easier for engineers and process operators to relate the parameter settings.

References

- [1] G. Wei, Z. Wang, and H. Shu, "Robust filtering with stochastic nonlinearities and multiple missing measurements," *Automatica*, vol. 45, no. 3, pp. 836–841, 2009.
- [2] B. Shen, Z. Wang, Y. S. Hung, and G. Chesi, "Distributed H_∞ filtering for polynomial nonlinear stochastic systems in sensor networks," *Automatica*, vol. 58, no. 5, pp. 1971–1979, 2011.
- [3] K. Narendra and K. Parthasarathy, "Identification and control of dynamical systems using neural networks," *IEEE Transactions on Neural Networks*, vol. 1, no. 1, pp. 4–27, 1990.
- [4] L. Wang, Y. Cheng, and J. Hu, "A quasi-ARX neural network with switching mechanism to adaptive control of nonlinear systems," *SICE Journal of Control, Measurement, and System Integration*, vol. 3, no. 4, pp. 246–252, 2010.
- [5] Q. Zhang and A. Benveniste, "Wavelet networks," *IEEE Transactions on Neural Networks*, vol. 3, no. 6, pp. 889–898, 1992.

- [6] S. A. Billings and H. Wei, "A new class of wavelet networks for nonlinear system identification," *IEEE Transactions on Neural Networks*, vol. 16, no. 4, pp. 862–874, 2005.
- [7] J. Jang and C.-T. Sun, "Neuro-fuzzy modeling and control," *Proceedings of the IEEE*, vol. 83, no. 3, pp. 378–406, 1995.
- [8] J. Hu, K. Hirasawa, and K. Kumamaru, "A neurofuzzy-based adaptive predictor for control of nonlinear systems," *Transactions of the Society of Instrument and Control Engineers*, vol. 35, no. 8, pp. 1060–1068, 1999.
- [9] S. Chen, S. A. Billings, and P. M. Grant, "Recursive hybrid algorithm for nonlinear system identification using radial basis function networks," *International Journal of Control*, vol. 55, no. 5, pp. 1051–1070, 1992.
- [10] P. E. McDermott and D. A. Mellichamp, "A decoupling pole placement self-tuning controller for a class of multivariable processes," *Optimal Control Applications and Methods*, vol. 7, no. 1, pp. 55–79, 1986.
- [11] R. Yusof, S. Omatu, and M. Khalid, "Self-tuning PID control: a multivariable derivation and application," *Automatica*, vol. 30, no. 12, pp. 1975–1981, 1994.
- [12] S. S. S. Ge and C. Wang, "Adaptive neural control of uncertain MIMO nonlinear systems," *IEEE Transactions on Neural Networks*, vol. 15, no. 3, pp. 674–692, 2004.
- [13] L. C. Hung and H. Y. Chung, "Decoupled control using neural network-based sliding-mode controller for nonlinear systems," *Expert Systems with Applications*, vol. 32, no. 4, pp. 1168–1182, 2007.
- [14] Y. Fu and T. Chai, "Nonlinear multivariable adaptive control using multiple models and neural networks," *Automatica*, vol. 43, no. 6, pp. 1101–1110, 2007.
- [15] P. J. Gawthrop, "Self-tuning PID controllers: algorithms and implementation," *IEEE Transactions on Automatic Control*, vol. 31, no. 3, pp. 201–209, 1986.
- [16] W. D. Chang, R. C. Hwang, and J. G. Hsieh, "A self-tuning PID control for a class of nonlinear systems based on the Lyapunov approach," *Journal of Process Control*, vol. 12, no. 2, pp. 233–242, 2002.
- [17] S. Lang, X. Gu, and T. Chai, "A multivariable generalized self-tuning controller with decoupling design," *IEEE Transactions on Automatic Control*, vol. 31, no. 5, pp. 474–477, 1986.
- [18] L. Zhai and T. Chai, "Nonlinear decoupling PID control using neural networks and multiple models," *Journal of Control Theory and Applications*, vol. 4, no. 1, pp. 62–69, 2006.
- [19] J. Hu and K. Hirasawa, "Neural network based prediction model for control of nonlinear systems," *Transactions of the Society of Instrument and Control Engineers*, vol. 39, no. 2, pp. 166–175, 2003 (Japanese).
- [20] J. Hu and K. Hirasawa, "A method for applying neural networks to control of nonlinear systems," in *Neural Information Processing: Research and Development*, J. Rajapakse and L. Wang, Eds., vol. 5, pp. 351–369, Springer, 2004.
- [21] L. Wang, Y. Cheng, and J. Hu, "Nonlinear adaptive control using a fuzzy switching mechanism based on improved quasi-ARX neural network," in *Proceedings of the International Joint Conference on Neural Networks, (IJCNN '10)*, vol. 7, pp. 1–7, 2010.
- [22] Q. Zhu, S. Fei, T. Zhang, and T. Li, "Adaptive RBF neural-networks control for a class of time-delay nonlinear systems," *Neurocomputing*, vol. 71, no. 16–18, pp. 3617–3624, 2008.
- [23] H. Peng, J. Wu, G. Inoussa, Q. Deng, and K. Nakano, "Nonlinear system modeling and predictive control using the RBF nets-based quasi-linear ARX model," *Control Engineering Practice*, vol. 17, no. 1, pp. 59–66, 2009.
- [24] Y. Lu, N. Sundararajan, and P. Saratchandran, "A sequential learning scheme for function approximation using minimal radial basis function neural networks," *Neural Computation*, vol. 9, no. 2, pp. 461–478, 1997.
- [25] C. Panchapakesan, M. Palaniswami, D. Ralph, and C. Manzie, "Effects of moving the centers in an RBF network," *IEEE Transactions on Neural Networks*, vol. 13, no. 6, pp. 1299–1307, 2002.
- [26] J. Hu, K. Hirasawa, C. Jin, and T. Matsuoka, "Control of nonlinear systems based on a probabilistic learning network," in *Proceedings of the 14th International Federation of Automatic Control World Congress, (IFAC '99)*, pp. 447–452, Beijing, China, 1999.
- [27] G. C. Goodwin and K. S. Sin, *Adaptive Filtering Prediction and Control*, Prentice-Hall, 1984.

Research Article

Practical Stability in the p th Mean for Itô Stochastic Differential Equations

Enguang Miao,¹ Huisheng Shu,¹ and Yan Che^{2,3}

¹ Department of Applied Mathematics, Donghua University, Shanghai 201620, China

² Department of Electronics and Information Engineering, Putian University, Fujian, Putian 351100, China

³ College of Information Sciences and Technology, Donghua University, Shanghai 201620, China

Correspondence should be addressed to Huisheng Shu, huisheng.shu@gmail.com

Received 29 June 2011; Accepted 6 September 2011

Academic Editor: Zidong Wang

Copyright © 2012 Enguang Miao et al. This is an open access article distributed under the Creative Commons Attribution License, which permits unrestricted use, distribution, and reproduction in any medium, provided the original work is properly cited.

The p th mean practical stability problem is studied for a general class of Itô-type stochastic differential equations over both finite and infinite time horizons. Instead of the comparison principle, a function $\psi(t)$ which is nonnegative, nondecreasing, and differentiable is cooperated with the Lyapunov-like functions to analyze the practical stability. By using this technique, the difficulty in finding an auxiliary deterministic stable system is avoided. Then, some sufficient conditions are established that guarantee the p th moment practical stability of the considered equations. Moreover, the practical stability is compared with traditional Lyapunov stability; some differences between them are given. Finally, the results derived in this paper are demonstrated by an illustrative example.

1. Introduction

Lyapunov stability is one of the most important conceptions of stability and has been widely applied to many fields involving nearly all aspects of reality. As we all know, however, the Lyapunov stability is usually employed to study the steady-state property over an infinite horizon and cannot cope with the transient behavior of the trajectory. Therefore, even a stable system in the sense of Lyapunov cannot be applied in the practice since the trajectory exhibits undesirable transient behaviors such as exceeding certain boundary imposed on the trajectory. Moreover, for a Lyapunov stable system, the domain of the desired attractor may be too small to control the initial perturbation in it, which also limits the uses of the Lyapunov stability. On the other hand, for an unstable system in the sense of Lyapunov, it is often the case that its trajectory oscillates sufficiently near by the desired state, which is absolutely acceptable in the practical engineering. As such, we are more interested in the transient behavior over a finite or infinite horizon rather than the steady-state property over

an infinite horizon. For this purpose, a new notion of stability, that is, the practical stability has first been proposed in [1], where it has been shown that the Lyapunov stability may not assure the practical stability and vice versa. Subsequently, the theory on the practical stability has been developed in [2–4].

Up to now, the practical stability problem has been well investigated for deterministic differential equations and many desirable results have been achieved. For example, in [5], a concept of finite time stability, as one special case of practical stability proposed in [6], has been introduced to examine the behavior of systems contained within prespecified bounds during a fixed time interval. The practical stability with respect to a set rather than the particular state $x = 0$ has been extended. In [7, 8], some results on the practical stability have been obtained for discontinuous systems and some differences between the practical stability and the Lyapunov stability have been given. In [9], by using the method of Lyapunov function and Dini derivative, some sufficient conditions have been derived for various types of practical stability. In [10], a new definition of generalized practical stability is introduced. By making use of Lyapunov-like functions, some sufficient conditions are established.

With respect to the stochastic differential systems, we just mention the following representative works. The practical stability in the p th mean has been proposed for discontinuous systems in [11]. In [12], by using the Lyapunov-like functions and the comparison principle, a unified approach is developed to deal with the problems of both the p th mean Lyapunov stability and the p th mean practical stability for the delayed stochastic systems. In [13], some criteria of practical stability in probability have been established in terms of deterministic auxiliary systems with initial conditions. The results obtained in [11, 13] have been further extended to a class of large-scale Itô-type stochastic systems in [14], where the initial conditions of the resulting auxiliary systems are random. In all papers mentioned above, the practical stability of the stochastic systems is determined through testing one corresponding auxiliary deterministic system, whereas, in [15], the sufficient conditions for practical stability in the mean square for a class of stochastic dynamical systems are established by using an integrable function and Lyapunov-like functions instead of the comparison principle.

In this paper, we are concerned with the problem of the practical stability in the p th mean for a general class of Itô-type stochastic differential equations over both finite and infinite time intervals. By using Lyapunov-like functions and a nonnegative, nondecreasing, and differentiable function $v(t)$, some criteria are established to ensure the p th mean practical stability for the considered stochastic system. This technique avoids the difficulty in finding an auxiliary deterministic stable system. Moreover, the practical stability is compared with traditional Lyapunov stability and some differences between them are presented. Finally, an illustrative example is provided to demonstrate the results derived in this paper.

Notation. \mathbb{R}^n denotes the n -dimensional Euclidean space. T_0 denotes the interval $[t_0, T)$, where $t_0, T \in \mathbb{R}_+$ (in this paper, T can be finite or infinite). $M[t_0, T)$ represents the family of nonnegative, nondecreasing, and differentiable functions on $[t_0, T)$. $C^{1,2}(T_0 \times \mathbb{R}^n, \mathbb{R}_+)$ represents the family of all real-valued functions $v(t, x(t))$ defined on $T_0 \times \mathbb{R}^n$ which are continuously twice differentiable in $x(t) \in \mathbb{R}^n$ and once differentiable in $t \in \mathbb{R}_+$. Let (Ω, \mathcal{F}, P) be a complete probability space. For a random variable ξ , $E\|\xi\|^p$ means the p th mean of ξ . The followings are the other notions in this paper:

$$S_0(t) = \{x(t) \in \mathbb{R}^n : E\|x(t)\|^p < \infty\},$$

$$S(A)(t) = \{x(t) \in \mathbb{R}^n : E\|x(t)\|^p \leq A\},$$

$$\begin{aligned} V_M^{\hat{S}_0}(\vartheta) &= \sup\{EV(\vartheta, x(\vartheta)) : x(\vartheta) \in S_0(\vartheta)\}, \\ V_m^{\hat{S}}(\vartheta) &= \inf\{EV(\vartheta, x(\vartheta)) : x(\vartheta) \in S(\vartheta)\}, \end{aligned} \quad (1.1)$$

where ϑ, A ($\vartheta < A$) are given.

2. Preliminaries and Definitions

Consider the stochastic system described by the following n -dimensional stochastic differential equation:

$$\begin{aligned} dx(\vartheta) &= f(\vartheta, x(\vartheta))d\vartheta + g(\vartheta, x(\vartheta))dB(\vartheta) \quad \text{on } \vartheta \in T_0, \\ x(\vartheta_0) &= x_0, \end{aligned} \quad (2.1)$$

where $dx(\vartheta)$ is the stochastic increment in the sense of Itô and $B(\vartheta)$ is an m -dimensional Brownian motion. $f(\vartheta, x(\vartheta))$ and $g(\vartheta, x(\vartheta))$ are $n \times 1$ and $n \times m$ matrix functions, respectively. And $x(\vartheta_0) = x_0$ is the initial value. Then, we let $x(\vartheta) = x(\vartheta; \vartheta_0, x_0)$ be any solution process of (2.1) with the initial value $x(\vartheta_0) = x_0$. Furthermore, we assume that (2.1) satisfies the theorem of the existence and uniqueness of solutions [16] as follows.

(i) (Lipschitz condition) for all $x(\vartheta), y(\vartheta) \in \mathbb{R}^n$, and $\vartheta \in T_0$,

$$\|f(\vartheta, x(\vartheta)) - f(\vartheta, y(\vartheta))\|^2 \vee \|g(\vartheta, x(\vartheta)) - g(\vartheta, y(\vartheta))\|^2 \leq K \|x(\vartheta) - y(\vartheta)\|^2. \quad (2.2)$$

(ii) (Linear growth condition) for all $x(\vartheta), y(\vartheta) \in \mathbb{R}^n$, and $\vartheta \in T_0$,

$$\|f(\vartheta, x(\vartheta))\|^2 \vee \|g(\vartheta, x(\vartheta))\|^2 \leq K^* (1 + \|x(\vartheta)\|^2), \quad (2.3)$$

where K and K^* are two positive constants.

Note that $S_0(\vartheta)$ and $S(\vartheta)$ satisfy the conditions

$$S_0(\vartheta) \subset S(\vartheta), \quad S_0(\vartheta) \cap S(\vartheta) = \emptyset. \quad (2.4)$$

By using Itô formula, The derivative of the Lyapunov-like function $V(\vartheta, x(\vartheta)) \in C^{1,2}(T_0 \times \mathbb{R}^n, \mathbb{R}_+)$ with respect to ϑ along the solution $x(\vartheta)$ of (2.1) is given by

$$dV(\vartheta, x(\vartheta)) = LV(\vartheta, x(\vartheta))d\vartheta + V_x(\vartheta, x(\vartheta))g(\vartheta, x(\vartheta))dB(\vartheta), \quad (2.5)$$

where

$$LV(\vartheta, x(\vartheta)) = V_\vartheta(\vartheta, x(\vartheta)) + V_x(\vartheta, x(\vartheta))f(\vartheta, x(\vartheta)) + \frac{1}{2} \text{trace}[g^T(\vartheta, x(\vartheta))V_{xx}(\vartheta, x(\vartheta))g(\vartheta, x(\vartheta))]. \quad (2.6)$$

Now, we give the definitions on the practical stability in the p th mean for (2.1).

Definition 2.1. System (2.1) is said to be practically stable in the p th mean (PSM) with respect to (ϵ, A) , $0 < \epsilon < A$; if there exist (δ, A) , then one has $E\|x_0\|^p < \delta$; one implies that

$$E\|x(\tau, t_0, x_0)\|^p < A \quad \forall \tau \in T_0. \quad (2.7)$$

Remark 2.2. In Definition 2.1, for $T_0 = [t_0, T)$, if the T is finite time, then the system (2.1) is called finite time practically stable, which is one special case of practical stability.

Noticing the notations of $S_0(t)$ and $S(t)$ above, we can see that $S_0(t_0)$ is a subset of the initial-state set when the initial time is t_0 , and $S(t)$ is a subset of the state space at time τ . Therefore, it is easy to see that $E\|x_0\|^p < \delta$; one implies that $x(t_0) \in S_0(t_0)$, $E\|x(\tau, t_0, x_0)\|^p < A$, and $x(\tau, t_0, x_0) \in \text{int } S(\tau)$. Thus, we give the following definition which is equal to Definition 2.1.

Definition 2.3. System (2.1) is said to be PSM with respect to (ϵ, A) , $0 < \epsilon < A$, if, for given $S_0(t), S(t)$ with $S_0(t) \subset S(t)$ and $S_0(t) \cap S(t) = \emptyset$, one has $x(t_0) \in S_0(t_0)$ then it is implied that

$$x(\tau, t_0, x_0) \in \text{int } S(\tau) \quad \forall \tau \in T_0. \quad (2.8)$$

Remark 2.4. If the conditions of Definition 2.3 are satisfied, then the system (2.1) is also said to be practically stable in the p th mean with respect to $(S_0(t_0), S(t))$.

In Section 3, the criteria for practical stability in the p th mean will be established for (2.1).

3. Practical Stability Criteria

In this section, the practical stability in the p th mean will be investigated in detail, and some stability criteria will be derived for (2.1) by using a Lyapunov-like function and a nonnegative, nondecreasing, and differentiable function $V(t)$.

Theorem 3.1. *If the following conditions are met:*

- (1) $S_0(t) \subset S(t)$ and $S_0(t) \cap S(t) = \emptyset$ for all $t \in T_0$,
- (2) there exists a function $V(t, x(t)) \in C^{1,2}(T_0 \times \mathbb{R}^n, \mathbb{R}_+)$, which is satisfying the following conditions:

(a)

$$ELV(t, x(t)) \leq 0 \quad t \in T_0, x(t) \in S(t), \quad (3.1)$$

(b)

$$V_M^{S_0}(t_0) < V_m^{\hat{S}}(t) \quad \forall t \in T_0, \quad (3.2)$$

then (2.1) is PSM with respect to (ϵ, A) .

Proof. For all $x_0 \in S_0(t_0)$, let $x(t) = x(t, t_0, x_0)$ be a solution of (2.1) with the initial value x_0 . For contradiction, we assume that there exists a first time $t_1 \in T_0$ such that $E\|x(t)\|^p < A$ for $t_0 \leq t < t_1$ and $E\|x(t_1)\|^p = A$.

By the notations of $V_M^{S_0}(t)$, $V_m^{\hat{S}}(t)$, and (2)-(b), we have

$$V_M^{S_0}(t_0) < V_m^{\hat{S}}(t_1) \leq EV(t_1, x(t_1)). \quad (3.3)$$

Noticing the $V(t, x(t))$ and (2.5), (2.6), it can be obtained that

$$V(t_1, x(t_1)) - V(t_0, x(t_0)) = \int_{t_0}^{t_1} LV(s, x(s))ds + \int_{t_0}^{t_1} V_x(s, x(s))g(s, x(s))dB(s). \quad (3.4)$$

By the assumption (2)-(a) and taking the expected value on the both sides of (3.4), we have

$$\begin{aligned} E[V(t_1, x(t_1)) - V(t_0, x(t_0))] &= E\left[\int_{t_0}^{t_1} LV(s, x(s))ds\right] \\ &= \int_{t_0}^{t_1} ELV(s, x(s))ds \\ &\leq 0 \end{aligned} \quad (3.5)$$

because

$$E\left[\int_{t_0}^{t_1} V_x(s, x(s))g(s, x(s))dB(s)\right] = 0, \quad (3.6)$$

then we have

$$V_M^{S_0}(t_0) < V_m^{\hat{S}}(t_1) \leq EV(t_1, x(t_1)) \leq EV(t_0, x(t_0)) \leq V_M^{S_0}(t_0). \quad (3.7)$$

This is a contradiction, so the proof is complete. \square

Remark 3.2. In Theorem 3.1, if the T_0 is a finite time interval, then (2.1) is practically stable on finite time. Furthermore, it should be pointed out that the condition $ELV(t, x(t)) \leq 0$ is necessary to guarantee the p th moment stability for (2.1) in the sense of Lyapunov. However, it would be too strict for the p th mean practical stability of (2.1). In the following theorem, this condition is replaced by

$$ELV(t, x(t)) \leq \frac{d(t)}{dt}, \quad (3.8)$$

where $(t) \in M[t_0, T]$.

Theorem 3.3. *If the following conditions are met:*

- (1) $S_0(t) \subset S(t)$ and $S_0(t) \cap S(t) = \emptyset$ for all $t \in T_0$,
 (2) there exists a function $(t) \in M [t_0, T)$, which satisfies the following conditions:

(a)

$$ELV(t, x(t)) \leq \frac{d}{dt} (t) \quad t \in T_0, x(t) \in S(t), \quad (3.9)$$

(b)

$$(t_0) = V_M^{S_0}(t_0), \quad (3.10)$$

(c)

$$(t) < V_m^{\hat{S}}(t) \quad \forall t \in T_0, \quad (3.11)$$

then (2.1) is PSM with respect to $(, A)$.

Proof. Let $x(t)$ be a solution of (2.1) with the initial value $x_0 \in S_0(t_0)$. For contradiction, we assume that the result is not true, which means that there exists a first time $t_1 \in T_0$ such that $E \|x(t)\|^p < A$ for $t_0 \leq t < t_1$ and $E \|x(t_1)\|^p = A$.

Noticing the notation of $V_m^{\hat{S}}(t)$, we have

$$V_m^{\hat{S}}(t_1) \leq EV(t_1, x(t_1)). \quad (3.12)$$

By using (2.5), (2.6), it follows that

$$V(t_1, x(t_1)) - V(t_0, x(t_0)) = \int_{t_0}^{t_1} LV(s, x(s)) ds + \int_{t_0}^{t_1} V_x(s, x(s)) g(s, x(s)) dB(s). \quad (3.13)$$

Taking the expectation on the both sides of (3.13), considering

$$E \left[\int_{t_0}^{t_1} V_x(s, x(s)) g(s, x(s)) dB(s) \right] = 0 \quad (3.14)$$

and the assumption (2)-(a), we obtain

$$\begin{aligned} EV(t_1, x(t_1)) &= EV(t_0, x(t_0)) + \int_{t_0}^{t_1} ELV(s, x(s)) ds \\ &\leq EV(t_0, x(t_0)) + \int_{t_0}^{t_1} d(s) \end{aligned}$$

$$\begin{aligned}
 &= EV(t_0, x(t_0)) + \psi(t_1) - \psi(t_0) \\
 &= \psi(t_1) - \left[V_M^{S_0}(t_0) - EV(t_0, x(t_0)) \right] \\
 &\leq \psi(t_1).
 \end{aligned} \tag{3.15}$$

Then, it follows from (3.12) and (3.15) that

$$V_m^{\hat{S}}(t_1) \leq EV(t_1, x(t_1)) \leq \psi(t_1) \tag{3.16}$$

which contradicts with the condition (2)-(c) of Theorem 3.3, and, hence, the proof is complete. \square

Remark 3.4. In Theorem 3.3, we mainly use the function $\psi(t)$ and the Lyapunov-like functions but not the comparison principle in [11–14] to achieve the result, which avoids the difficulty in finding an auxiliary deterministic stable system. Here, we assume that

$$ELV(t, x(t)) \leq \frac{d}{dt} \psi(t) \tag{3.17}$$

holds on $x(t) \in S(t)$. Next, the condition $x(t) \in S(t)$ will be replaced by a weaker one, that is, $x(t) \in S(t)/S_0(t)$.

Theorem 3.5. *If the following conditions are met:*

- (1) $S_0(t) \subset S(t)$ and $S_0(t) \cap S(t) = \emptyset$ for all $t \in T_0$,
- (2) there exists a function $\psi(t) \in M[t_0, T]$, which satisfies the following conditions:

(a)

$$ELV(t, x(t)) \leq \frac{d}{dt} \psi(t) \quad t \in T_0, x(t) \in \frac{S(t)}{S_0(t)}, \tag{3.18}$$

(b)

$$\psi(t) = V_M^{S_0}(t), \quad x(t) \in S_0(t), \tag{3.19}$$

(c)

$$\psi(t) < V_m^{\hat{S}}(t) \quad \forall t \in T_0, \tag{3.20}$$

then (2.1) is PSM with respect to (ψ, A) .

Proof. Let $x(t)$ be a solution of (2.1) with the initial value $x_0 \in S_0(t_0)$. For contradiction, we assume that there exists a first time $t_2 \in T_0$ such that $E\|x(t)\|^p < A$ for $t_0 \leq t < t_2$ and

$E\|x(t_2)\|^p = A$. Due to the continuity of $E\|x(t)\|^p$ and the connectivity of $S(t), S_0(t)$, there exists such a time t_1 and $E\|x(t_1)\|^p = A$ holds for the last time before the time t_2 . So, we get that $x(t) \in S(t)/S_0(t)$ when $t \in [t_1, t_2]$.

Noticing the (2.5), (2.6), it can be obtained that, when $t \in [t_1, t_2]$,

$$V(t_2, x(t_2)) - V(t_1, x(t_1)) = \int_{t_1}^{t_2} LV(s, x(s)) ds + \int_{t_1}^{t_2} V_x(s, x(s)) g(s, x(s)) dB(s). \quad (3.21)$$

By virtue of

$$E \left[\int_{t_1}^{t_2} V_x(s, x(s)) g(s, x(s)) dB(s) \right] = 0, \quad (3.22)$$

we take the conditional expectation of (3.21) conditioning on the initial value $x(t_0) = x_0$; it can be seen from condition (2)-(a) that

$$\begin{aligned} E[V(t_2, x(t_2)) - V(t_1, x(t_1)) \mid x(t_0) = x_0] &= E \left[\int_{t_1}^{t_2} LV(s, x(s)) ds \mid x(t_0) = x_0 \right] \\ &= \int_{t_1}^{t_2} E LV(s, x(s)) ds \\ &\leq \int_{t_1}^{t_2} d(s) \\ &= (t_2) - (t_1). \end{aligned} \quad (3.23)$$

Taking the expectation on the both sides of (3.23) and using the assumption (2)-(b), we obtain

$$\begin{aligned} EV(t_2, x(t_2)) &= EV(t_1, x(t_1)) + (t_2) - (t_1) \\ &= (t_2) - [(t_1) - EV(t_1, x(t_1))] \\ &\leq (t_2) - [(t_1) - V_M^{S_0}(t_1)] \\ &= (t_2). \end{aligned} \quad (3.24)$$

Then,

$$V_m^{\hat{S}}(t_2) \leq EV(t_2, x(t_2)) \leq (t_2). \quad (3.25)$$

Noticing the assumption (2)-(c), this is a contradiction, Then, the proof is complete. \square

In the theorems above, some sufficient conditions that guarantee the p th mean practical stability are derived for (2.1). It is worth mentioning that the establishment of the practical stability criteria here avoids introducing other auxiliary stable systems, which make

it convenient to determine whether an Itô-type stochastic differential system is the p th mean practically stable. In Section 4, an example will be employed to demonstrate the obtained results.

4. Example

In this section, one numerical example is given to demonstrate the result in Theorem 3.3. The results obtained in Theorems 3.1 and 3.5 can be verified in the same way.

Example 4.1. Consider the one-dimensional stochastic differential equation as follow:

$$\begin{aligned} dx(t) &= x(t) \sin(t) dt + dB(t) \quad \text{on } t \in [t_0, T), \\ x(t_0) &= x_0, \end{aligned} \quad (4.1)$$

where $B(t)$ is a one-dimensional Brownian motion.

Let $\kappa = \kappa^* = 1$; it is obvious that (4.1) satisfies both the Lipschitz condition and the Linear growth condition, so the existence and uniqueness of the solution $x(t)$ of (4.1) is guaranteed.

Now, we investigate the practical stability in the 1st mean for (4.1) with respect to $\alpha = 1$ and $A = 2$. One assumes that the initial value $x(t_0)$ satisfies the conditions $E|x(t_0)| < 1$ and $E|x(t_0, x_0)| < 2$ for $t \in T_0$. Then, we approximate the value of t_0 and T .

We define a Lyapunov-like function as

$$V(t, x(t)) = |x(t)|. \quad (4.2)$$

Due to the fact that $V(t, x(t))$ is a positive-definite function, one can easily get $V(t, x(t)) > 0$ when $x(t) \neq 0$.

So, when $x(t) \neq 0$, it is obvious that

$$V_t(t, x(t)) = 0, \quad V_x(t, x(t)) = \begin{cases} 1, & x > 0, \\ -1, & x < 0, \end{cases} \quad V_{xx}(t, x(t)) = 0. \quad (4.3)$$

By using the Itô formula, we calculate the derivative of the Lyapunov-like function $V(t, x(t))$ along the solution $x(t)$ of (4.1), and noticing the (2.6), we have

$$\begin{aligned} LV(t, x(t)) &= V_t(t, x(t)) + V_x(t, x(t))f(t, x(t)) + \frac{1}{2} \text{trace} \left[g^T(t, x(t)) V_{xx}(t, x(t)) g(t, x(t)) \right] \\ &= 0 \pm x(t) \sin(t) + 0 \\ &\leq |x(t)|. \end{aligned} \quad (4.4)$$

Taking the expectation on both sides of (4.4), one obtains

$$E[LV(t, x(t))] \leq E|x(t)| < A = 2, \quad (4.5)$$

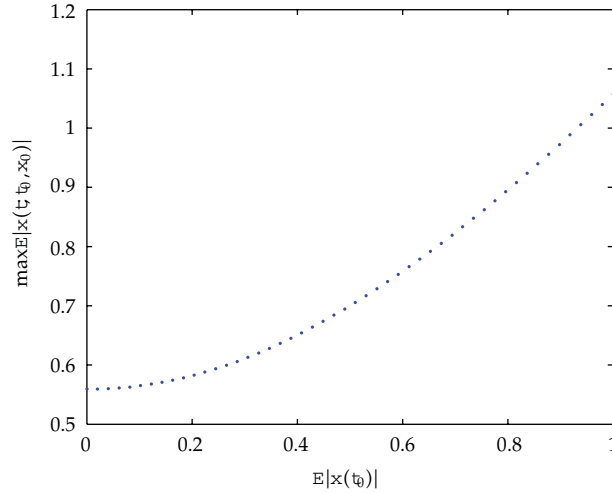


Figure 1: Illustration of the practical stability in the 1st mean.

so we define

$$\tau = 2t. \quad (4.6)$$

From (4.4)–(4.6), it can be easily verified that the condition (2)-(a) of Theorem 3.3 is satisfied. Then, by the condition (2)-(b) of Theorem 3.3, we have

$$\tau_0 = V_M^{S_0}(\tau_0) = \sup\{E|x(\tau_0)|; x(\tau_0) \in S_0(\tau_0)\} = 1 \quad (4.7)$$

and hence, it can be obtained from (4.6) that

$$\tau_0 = \frac{1}{2}. \quad (4.8)$$

On the other hand, from the condition (2)-(c) of Theorem 3.3, we have

$$\tau < V_m^{\hat{S}}(\tau) = \inf\{E|x(\tau)| : x(\tau) \in \hat{S}(\tau)\} = A = 2. \quad (4.9)$$

So, we have

$$\tau < 1. \quad (4.10)$$

Now, we have the fact that $\tau_0 = 1/2$ and $T = 1$. According to Theorem 3.3, (4.1) is practically stable in the 1st mean with respect to $\tau_0 = 1$ and $A = 2$ on $\tau \in [1/2, 1)$. In the simulation, we take 50 initial values satisfying $E|x(1/2)| < 1$. For every initial value, the 1st mean orbit and the maximum of $E|x(\tau)|$ for $\tau \in [1/2, 1)$ are computed numerically. The simulation result is depicted in Figure 1.

5. Conclusion

This paper mainly establishes the sufficient conditions of practical stability in the p th mean for the Itô-type stochastic differential equation over finite or infinite time interval. By using Lyapunov-like functions and a nonnegative, nondecreasing, and differentiable function (ψ) instead of the comparison principle, the difficulty in finding an auxiliary deterministic stable system is avoided. Moreover, this paper indicates that the practical stability can be examined over finite or infinite time interval and it can be used to depict the transient behavior of the trajectory.

For further studies, we can extend practical stability in the p th mean to uniformly practical stability and strict practical stability in the p th mean by the same methods in this paper. And, we can also consider other techniques to establish the sufficient conditions for the practical stability in probability and the almost sure practical stability instead of the comparison principle. Other future research topics include the investigation on the filtering and control problems for uncertain nonlinear stochastic systems; see, for example, [17–26].

Acknowledgment

This paper is supported by the National Natural Science Foundation of China (No. 60974030) and the Science and Technology Project of Education Department in Fujian Province, China (No. JA11211).

References

- [1] J. P. LaSalle and S. Lefschetz, *Stability Theory by Liapunov's Direct Method with Applications*, Academic Press, New York, NY, USA, 1961.
- [2] S. R. Bernfeld and V. Lakshmikantham, "Practical stability and Lyapunov functions," *The Tôhoku Mathematical Journal*, vol. 32, no. 4, pp. 607–613, 1980.
- [3] A. A. Martynyuk, "Methods and problems of practical stability of motion theory," *Nonlinear Vibration Problems*, vol. 22, pp. 19–46, 1984.
- [4] A. A. Martynyuk and Z. Q. Sun, *Practical Stability and its Application*, Science Press, Beijing, China, 2003.
- [5] L. Weiss and E. F. Infante, "On the stability of systems defined over a finite time interval," *Proceedings of the National Academy of Sciences of the United States of America*, vol. 54, pp. 44–48, 1965.
- [6] L. Weiss and E. F. Infante, "Finite time stability under perturbing forces and on product spaces," *IEEE Transactions on Automatic Control*, vol. 12, pp. 54–59, 1967.
- [7] J. X. He, "Practical stability of discontinuous systems with external perturbations," *Journal of Mathematics*, vol. 3, no. 4, pp. 385–398, 1983.
- [8] J. X. He, "Practical stability of discontinuous systems," *Journal of Mathematical Research and Exposition*, vol. 5, pp. 55–60, 1985.
- [9] X. X. Liao, *Stability Theory and Applications*, Huazhong Normal University Press, 1988.
- [10] G. Zhai and A. N. Michel, "Generalized practical stability analysis of discontinuous dynamical systems," in *Proceedings of the 42nd IEEE Conference on Decision and Control*, pp. 1663–1668, December 2003.
- [11] Z. S. Feng, Y. Q. Liu, and F. W. Guo, "Criteria for practical stability in the p th mean of nonlinear stochastic systems," *Applied Mathematics and Computation*, vol. 49, no. 2-3, pp. 251–260, 1992.
- [12] Z. S. Feng, "Lyapunov stability and practical stability of nonlinear delay stochastic systems: a unified approach," in *Proceedings of the 32nd Conference on Decision and Control*, pp. 865–870, December 1993.
- [13] A. H. Tsoi and B. Zhang, "Practical stabilities of Itô type nonlinear stochastic differential systems and related control problems," *Dynamic Systems and Applications*, vol. 6, no. 1, pp. 107–124, 1997.

- [14] S. Sathananthan and S. Suthaharan, "Practical stability criteria for large-scale nonlinear stochastic systems by decomposition and aggregation," *Dynamics of Continuous, Discrete & Impulsive Systems Series A*, vol. 8, no. 2, pp. 227–248, 2001.
- [15] A. N. Michel and L. Hou, "Finite-time and practical stability of a class of stochastic dynamical systems," in *Proceedings of the 47th IEEE Conference on Decision and Control*, pp. 3452–3456, December 2008.
- [16] X. Mao, *Stochastic Differential Equations and Applications*, International Publishers in Science and Technology, England, UK, 2nd edition, 2008.
- [17] H. Dong, Z. Wang, D. W. C. Ho, and H. Gao, "Robust H_∞ filtering for Markovian jump systems with randomly occurring nonlinearities and sensor saturation: the finite-horizon case," *IEEE Transactions on Signal Processing*, vol. 59, no. 7, pp. 3048–3057, 2011.
- [18] Y. Tang, Z. Wang, W. K. Wong, J. Kurths, and J. Fang, "Multiobjective synchronization of coupled chaotic systems," *Chaos*, vol. 21, no. 2, Article ID 025114, 2011.
- [19] Z. Wang, J. Lam, L. Ma, Y. Bo, and Z. Guo, "Variance-constrained dissipative observer-based control for a class of nonlinear stochastic systems with degraded measurements," *Journal of Mathematical Analysis and Applications*, vol. 377, no. 2, pp. 645–658, 2011.
- [20] B. Shen, Z. Wang, Y. S. Hung, and G. Chesi, "Distributed H_∞ filtering for polynomial nonlinear stochastic systems in sensor networks," *IEEE Transactions on Industrial Electronics*, vol. 58, no. 5, pp. 1971–1979, 2011.
- [21] J. Liang, Z. Wang, and X. Liu, "Distributed state estimation for discrete-time sensor networks with randomly varying nonlinearities and missing measurements," *IEEE Transactions on Neural Networks*, vol. 22, no. 3, pp. 486–496, 2011.
- [22] X. He, Z. Wang, Y. Ji, and D. Zhou, "Robust fault detection for networked systems with distributed sensors," *IEEE Transactions on Aerospace and Electronic Systems*, vol. 47, no. 1, pp. 166–177, 2011.
- [23] B. Shen, Z. Wang, and X. Liu, "Bounded H_∞ synchronization and state estimation for discrete time-varying stochastic complex networks over a finite-horizon," *IEEE Transactions on Neural Networks*, vol. 22, no. 1, pp. 145–157, 2011.
- [24] B. Shen, Z. Wang, H. Shu, and G. Wei, " H_∞ filtering for uncertain time-varying systems with multiple randomly occurred nonlinearities and successive packet dropouts," *International Journal of Robust and Nonlinear Control*, vol. 21, no. 14, pp. 1693–1709, 2011.
- [25] Z. Wang, D. W. C. Ho, H. Dong, and H. Gao, "Robust H_∞ finite-horizon control for a class of stochastic nonlinear time-varying systems subject to sensor and actuator saturations," *IEEE Transactions on Automatic Control*, vol. 55, no. 7, pp. 1716–1722, 2010.
- [26] Z. Wang, Y. Liu, and X. Liu, "Exponential stabilization of a class of stochastic system with Markovian jump parameters and mode-dependent mixed time-delays," *IEEE Transactions on Automatic Control*, vol. 55, no. 7, pp. 1656–1662, 2010.

Research Article

p th Mean Practical Stability for Large-Scale Itô Stochastic Systems with Markovian Switching

Yan Yun,¹ Huisheng Shu,¹ and Yan Che^{2,3}

¹ *Department of Applied Mathematics, Donghua University, Shanghai 201620, China*

² *Department of Electronics and Information Engineering, Putian University, Fujian Putian 351100, China*

³ *College of Information Sciences and Technology, Donghua University, Shanghai 201620, China*

Correspondence should be addressed to Huisheng Shu, huisheng.shu@gmail.com

Received 29 June 2011; Accepted 6 September 2011

Academic Editor: Zidong Wang

Copyright © 2012 Yan Yun et al. This is an open access article distributed under the Creative Commons Attribution License, which permits unrestricted use, distribution, and reproduction in any medium, provided the original work is properly cited.

Motivated by the study of a class of large-scale stochastic systems with Markovian switching, this correspondence paper is concerned with the practical stability in the p th mean. By investigating Lyapunov-like functions and the basic comparison principle, some criteria are derived for various types of practical stability in the p th mean of nonlinear stochastic systems. The main contribution of these results is to convert the problem of practical stability in the p th mean of stochastic systems into the one of practical stability of the comparative deterministic systems.

1. Introduction

The practical dynamical systems in real-world applications, such as engineering, physics, and economics, usually exhibit the stochastic nature due to the uncertain resulting from the external environment. Examples include traffic systems, flexible manufacturing systems, and economic systems. All of these dynamical systems can be modeled by Itô stochastic differential equations. Therefore, it is not surprising that various problems of Itô stochastic differential equations have received considerable attention. As the development of the stochastic theory including stochastic processes, stochastic integral, and stochastic partial differential equations, the theory on the stochastic differential equations in infinite dimensional spaces has advanced greatly, and, so far, a rich body of literature has been reported.

Stability is one of the most important issues in the analysis and synthesis of stochastic systems and often regarded as the first characteristic of the dynamical systems (or models) to be studied. Currently, there have already been many kinds of stability concepts such as asymptotic stability, stability in probability, almost sure exponential stability, and mean-square

exponential stability. These stabilities are analyzed in terms of the theory of functional analysis which, however, makes it difficult for a newcomer to enter this interesting and important field. The concepts of stability mentioned above are defined in the sense of Lyapunov. In many real-world applications, however, the systems might not be asymptotically stable in the sense of Lyapunov and stay nearby a state with an acceptable fluctuation. For example, an aircraft or a missile may oscillate around a mathematically unstable course, and its performance may be acceptable yet. To treat with such situations, a new stability concept, that is, the practical stability, has been proposed by LaSalle and Lefschetz [1] and, subsequently, has been developed in [2–4].

With respect to stochastic systems, the practical stability in the p th mean and the stability in probability have been introduced in [5] and [6], respectively. In these papers, both the stochastic system and its corresponding auxiliary equation have deterministic initial conditions. By using the powerful comparison theorem, which is developed in [7, 8], these concepts have been extended to a more general class of stochastic systems in [9], where the resulting auxiliary system has random initial conditions. Recently, stochastic differential equations with Markovian switching have also stirred a great deal of research interests due primarily to their insight into applications. The fundamental theory of existence and uniqueness of the solution of stochastic differential equations with Markovian switching has been studied well in [10, 11], while the stability issues have been investigated in [12–15].

To be more specific, during the research of practical stability, one of the foremost challenges to system theory in the present-day advanced technological world is to overcome the increasing size and complexity of the corresponding mathematical models [9, 16]. This is the so-called large-scale systems, which is more closed to the actual circumstances, and, therefore, it has a wider significance. However, since the computational efforts are enormous, the practical stability of large-scale systems has received relatively little attention. Recently, several important results have been obtained in the area of practical stability for large-scale Itô stochastic systems, see [17], for example, in which the large amount of computational efforts of a large-scale complex system become simpler and more economical by decomposition into a number of interconnected subsystems; these subsystems, to some extent, can be considered to be independent so that some of the qualitative behaviors of the corresponding subsystems can be combined with interconnection constraints to come up with the qualitative behavior of the overall large-scale systems. Like all other systems, the stability issue should be examined first in the large-scale systems. However, the problem of p th mean practical stability for large-scale Itô stochastic systems with Markovian switching has not been addressed properly, which motivates the current research.

In this paper, the problem of the p th mean practical stability for large-scale Itô stochastic systems with Markovian switching is studied. First, the notion of practical stability in the p th mean is introduced and extended for the large-scale stochastic systems with Markovian switching. Then, the concepts of Lyapunov-like vector-valued functions coupled with the decomposition-aggregation techniques are utilized to develop a comparison principle. In addition, some general criteria of practical stability for the large-scale Itô stochastic systems with Markovian switching are obtained. Finally, an example is given to show the usefulness of the developed criteria.

2. Preliminaries

Let $\{\Omega, \mathcal{F}, \mathcal{F}_{\geq 0}, \mathbb{P}\}$ be a complete probability space with a filtration satisfying the usual conditions, that is, the filtration is continuous on the right and \mathcal{F}_0 contains all \mathbb{P} -zero sets.

$W(t) = (W_1(t), W_2(t), \dots, W_m(t))^T$ is an m -dimensional Wiener process defined on the probability space. $\{r(t), t \in \mathbb{R}_+\}$ denotes a right-continuous Markov chain on the probability space $\{\Omega, \mathcal{F}, \mathcal{F}_{\geq 0}, P\}$, taking values in a finite state space $S = \{1, 2, \dots, N\}$ with generator $\Gamma = (\gamma_{ij})_{N \times N}$ given by

$$P\{r(t+\Delta) = j \mid r(t) = i\} = \begin{cases} \gamma_{ij}\Delta + o(\Delta), & \text{if } i \neq j, \\ 1 + \gamma_{ii}\Delta + o(\Delta), & \text{if } i = j, \end{cases} \quad (2.1)$$

where $\Delta > 0$ and $\gamma_{ij} \geq 0$ is the transition rate from i to j if $i \neq j$ while $\gamma_{ii} = -\sum_{j \neq i} \gamma_{ij}$. We assume that the Markov chain $r(\cdot)$ is independent of Wiener process $W(\cdot)$. It is known that almost every sample path of $r(t)$ is a right-continuous step function with a finite number of simple jumps in any finite subinterval of \mathbb{R} .

Consider the following Itô stochastic differential equations with Markovian switching:

$$dx(t) = f(t, r(t), x(t))dt + \sigma(t, r(t), x(t))dW(t) \quad (2.2)$$

with the initial condition $x_0 = x$. Here x is assumed to be independent of $W(\cdot)$. The nonlinear functions $f: \mathbb{R}_+ \times S \times \mathbb{R}^n \rightarrow \mathbb{R}^n$ and $\sigma: \mathbb{R}_+ \times S \times \mathbb{R}^n \rightarrow \mathbb{R}^{n \times m}$ satisfy Lipschitz condition and Linear growth condition.

In this paper, we always assume that (2.2) has a unique continuous solution $x(t, x)$ such that $\mathbb{E}(\sup_{0 \leq t \leq p} \|x(t, x)\|^p) < \infty$ for each $t \geq 0$ and $p \geq 0$. Further, it is also assumed that $f(t, j, 0) = 0$ and $\sigma(t, j, 0) = 0$ for all $j \in S$ and, accordingly, (2.2) has a trivial solution $x(t, 0) \equiv 0$.

Now, we decompose (2.2) into n interconnected subsystems described by

$$\begin{aligned} dx_i &= [p_i(t, r(t), x_i) + h_i(t, r(t), x)]dt + \sum_{r=1}^m \left[\Gamma_r^i(t, r(t), x_i) + k_r^i(t, r(t), x) \right] dW_r(t), \\ x_i(t_0) &= x_0, \quad i = 1, 2, \dots, n, \end{aligned} \quad (2.3)$$

where nonlinear functions $p_i(t, r(t), x_i)$, and $\Gamma_r^i(t, r(t), x_i) \in \mathbb{R}_+ \times S \times \mathbb{R} \rightarrow \mathbb{R}$, $h_i(t, r(t), x)$ and $k_r^i(t, r(t), x) \in \mathbb{R}_+ \times S \times \mathbb{R}^n \rightarrow \mathbb{R}$, respectively.

3. Comparison Principle

The comparison principle has proved to be a useful tool in the study of the qualitative and quantitative properties of solution processes of Itô-type stochastic system with Markovian switching. In this section, by employing the concept of Lyapunov vector-valued function coupled with decomposition-aggregation techniques, and together with the theory of differential inequalities, the comparison theorems for the large-scale system (2.3) are developed.

The \mathcal{L} -operator for the n -interconnected subprocedures (2.3) is defined as

$$\begin{aligned} \mathcal{L}^c V_i(t, j, x(t)) &= \frac{V_i(x(t), t, j)}{t} + \sum_{j=1}^n \left(\frac{V_i(x(t), t, j)}{x_j} \right) [p_j(t, j, x_i) + h_j(t, j, x)] \\ &+ \frac{1}{2} \sum_{j,r=1}^n \frac{V_i^2(t, j, x)}{x_j x_r} a_{jr} + \sum_{j=1}^N \gamma_{ij} V_i(t, j, x), \end{aligned} \quad (3.1)$$

where

$$(a_{jr}) = \dot{f}_j^i(t, i, x_i)^T \dot{f}_r^i(t, i, x_i) + \dot{f}_j^i(t, i, x_i)^T k_r^i(t, i, x) + k_j^i(t, i, x)^T \dot{f}_r^i(t, i, x_i) + k_j^i(t, i, x)^T k_r^i(t, i, x),$$

$$j, r = 1, 2, \dots, n, \quad s = 1, 2, \dots, N. \quad (3.2)$$

Now, consider now the following auxiliary random differential system:

$$du = g(t, u)dt, \quad u(t_0) = u_0, \quad (3.3)$$

where $g(t, u) \in C[\mathcal{J} \times \mathcal{R}_+^n, \mathcal{R}^n]$ is concave and quasi-monotone nondecreasing in u for each fixed $t \in \mathcal{J}$ and u_0 is an n -dimensional random vector. Let $u(t, t_0, u_0)$ be any solution of the system (3.3) and $r(t, t_0, u_0)$ the maximal solution process of the system (3.3) through (t_0, u_0) .

We need the following corresponding definitions of practical stability for the auxiliary system (3.3).

Definition 3.1. System (3.3) is said to be practically stable, if for all given $(\mathcal{A}, \mathcal{B})$ with $0 < \mathcal{A} < \mathcal{B}$, $E \sum_{i=1}^n u_{i_0} < \mathcal{A}$ implies $\sum_{i=1}^n u_i(t, t_0, u_0) < \mathcal{B}$, for all $t \geq t_0$ for some $t_0 \in \mathcal{R}_+$.

Definition 3.2. Set $\mathcal{I} = (i_1, i_2, \dots, i_s)$ and $\mathcal{J} = (j_1, j_2, \dots, j_s)$. If $i_i \leq j_i, \forall i = 1, 2, \dots, s$, one denotes $\mathcal{I} < \mathcal{J}$.

In this section, by employing the Lyapunov-like functions and the basic comparison principle of stochastic systems, some results on various types of practical stability in the p th mean are obtained for the interconnected system (2.3).

Theorem 3.3. Assume that there exist functions $V_i(t, x)$ and $g(t, u)$ satisfying the following conditions:

- (i) for every $V_i(t, x) \in C[\mathcal{J} \times \mathcal{R}^n, \mathcal{R}_+]$, $V_i(t, x)/t, V_i(t, x)/x^2$, and ${}^2V_i(t, x)/x^2$ exist and are continuous for $(t, x) \in (\mathcal{J} \times \mathcal{R}^n)$, and $\mathcal{L}V_i(t, j, x) \leq g_i(t, V_i(t, j, x))$ holds for all $(t, x) \in \mathcal{J} \times \mathcal{R}^n, i = 1, 2, \dots, n, j = 1, 2, \dots, N$;
- (ii) $g(t, u) \in C[\mathcal{J} \times \mathcal{R}^n, \mathcal{R}_+^n]$ is a quasi-monotone nondecreasing concave function in u for each $t \in \mathcal{J}$, and satisfies $g(t, 0) \equiv 0$;
- (iii) the maximal solution of the auxiliary differential system (3.3), that is, $r(t, t_0, u_0)$ exists for all $t \geq t_0$, where u_0 is an n -dimensional random vector;
- (iv) for the solution process $x_i(t) = x_i(t, t_0, x_0)$ of system (2.3), if $E[V_i(t, x(t), j)]$ exists for all $t \geq t_0$, then

$$E[V(t, x(t), j)] \leq r(t, t_0, u_0) \quad (3.4)$$

whenever $t \geq t_0$ and $V(t_0, x_0, j) \leq u_0$, where

$$V(t, x, j) = [V_1(t, x, j), V_2(t, x, j), \dots, V_n(t, x, j)]^T. \quad (3.5)$$

Proof. By applying generalized Itô formula, we have

$$EV_i(x, t, j) - EV_i(x(t_0), t_0, j) = \int_{t_0}^t E \mathcal{L}V_i(x, s, j) d_s. \quad (3.6)$$

Setting $m_i(t) = EV_i(x, t, j)$, we obtain

$$m_i(t) - m_i(t_0) = \int_{t_0}^t E \mathcal{L}V_i(x, s, j) d_s, \quad (3.7)$$

based on which, letting $\Delta t \rightarrow 0^+$, it can be obtained that

$$\begin{aligned} m_i(t + \Delta t) - m_i(t) &= \int_t^{t+\Delta t} E \mathcal{L}V_i(x, s, j) d_s \\ &\leq \int_t^{t+\Delta t} E g_i(t, V_i(x, s, j)) d_s \\ &\leq \int_t^{t+\Delta t} g_i(t, EV_i(x, s, j)) d_s. \end{aligned} \quad (3.8)$$

That is, for each $i = 1, 2, \dots, n$, we have

$$D^+ m_i(t) \leq g_i(t, m_i(t)), \quad (3.9)$$

where D^+ denotes the upper right Dini-derivative operator and $m_i(t) = EV_i(x, t, j)$.

Denoting $D^+ m(t) = (D^+ m_1(t), D^+ m_2(t), \dots, D^+ m_n(t))$, we have

$$D^+ m(t) \leq g(t, m(t)). \quad (3.10)$$

According to comparison theorem in [17], it immediately follows that

$$E[V(t, x(t), j)] \leq r(t, t_0, u_0) \quad (3.11)$$

whenever $t \geq t_0$ and $V(t_0, x_0, j) \leq u_0$, and hence the proof is complete. \square

4. Practical Stability Criteria

In this section, by employing Lyapunov-like functions and basic comparison principles for interconnected systems developed in the previous section, we give various types of practical stability in the p th mean of the interconnected system (2.3).

Definition 4.1. System (2.3) is said to be practically stable in the p th mean, if for all given $(\mathcal{A}, \mathcal{B})$ with $0 < \mathcal{A} < \mathcal{B}$, $E\|x_0\|^p < \mathcal{B}$ implies $E\|x(t, t_0, x_0)\|^p < \mathcal{A}$ for all $t \geq t_0$.

Definition 4.2. A function $v(t, u)$ is said to belong to the class \mathcal{K} , if $v \in \mathcal{K}(\mathcal{R}_+, \mathcal{R}_+)$ satisfies $v(0) = 0$; $v(t, u)$ is said to belong to the class \mathcal{CK} , if $v \in \mathcal{CK}(\mathcal{R}_+ \times \mathcal{R}_+, \mathcal{R}_+)$ is continuous, concave, and strictly increasing in u for each $t \in \mathcal{R}_+$ and satisfies $v(t, 0) = 0$; $v(t, u)$ is said to belong to the class \mathcal{UK} , if $v \in \mathcal{UK}[\mathcal{R}_+, \mathcal{R}_+]$ is continuous, convex, and strictly increasing for each $u \in \mathcal{R}_+$ and satisfies $v(0) = 0$.

The following theorem gives the criteria of practical stability.

Theorem 4.3. *Assume that*

- (i) *all the hypotheses of Theorem 3.3 hold;*
- (ii) *for $(t, x) \in \mathcal{J} \times \mathcal{R}^n$, the following inequality holds:*

$$b(\|x\|^p) \leq \sum_{i=1}^n V_i(t, x, j) \leq a(t, \|x\|^p), \quad (4.1)$$

where $b \in \mathcal{UK}[\mathcal{R}_+, \mathcal{R}_+]$ and $a \in \mathcal{CK}[\mathcal{R}_+, \mathcal{R}_+]$ satisfy $b(0) = 0$ and $a(t, 0) = 0$, respectively;

- (iii) *the maximal solutions of the auxiliary differential system (3.3) on $t \geq t_0$, that is, $r(t) = r(t, t_0, u_0)$ and $E[r(t, t_0, u_0)]$ both exist;*
- (iv) *for the given α and \mathcal{A} ($0 < \alpha < \mathcal{A}$), system (3.3) is practically stable with $a(t_0, \alpha) < b(\mathcal{A})$.*

Then, the interconnected system (2.3) is practically stable in the p th mean.

Proof. Let $x_i(t) = x_i(t, t_0, x_0)$ ($i = 1, 2, \dots, n$) be any solution process of system (2.3). It can be obtained from Theorem 3.3 that

$$E[V(t, x(t), j)] \leq r(t, t_0, u_0) \quad (4.2)$$

whenever $t \geq t_0$ and $V(t_0, x_0, j) \leq u_0$, where $r(t, t_0, u_0)$ is the maximal solution of system (3.3) on $[t_0, \infty)$, and thus,

$$\sum_{i=1}^n E[V_i(t, j, x(t))] \leq \sum_{i=1}^n r_i(t, t_0, u_0). \quad (4.3)$$

Considering that $r(t, t_0, u_0)$ is practically stable, we have

$$\sum_{i=1}^n u_{i_0} < a(t_0, \alpha), \quad (4.4)$$

which implies that

$$\sum_{i=1}^n r_i(t, t_0, u_0) < b(\mathcal{A}) \quad \forall t \geq t_0. \quad (4.5)$$

We claim that $E\|x_0\|^p < \mathcal{A}$ implies $E\|x(t, t_0, x_0)\|^p < \mathcal{A}$, for all $t \geq t_0$ for some $t_0 \in \mathcal{R}_+$, where $x(t) = (x_1(t), x_2(t), \dots, x_n(t))$ is any solution of system (2.3) with $E\|x_0\|^p < \mathcal{A}$. Suppose that this claim is not true, then there exists a $t_1 > t_0$ and a solution $x(t) = x(t, t_0, x_0)$ of system (2.3) with $E\|x_0\|^p < \mathcal{A}$ satisfying

$$E\|x(t_1)\|^p = \mathcal{A}, \quad E\|x(t)\|^p < \mathcal{A} \quad \text{for } t_0 \leq t < t_1. \quad (4.6)$$

Then, it follows from assumption (ii) that

$$\sum_{i=1}^n E[V_i(t, j, x(t_1))] \geq b(E\|x(t_1)\|^p) = b(\mathcal{A}). \quad (4.7)$$

Choosing u_0 such that $V(t_0, x_0) = u_0$ and $\sum_{i=1}^n u_{i_0} = a(t_0, E\|x_0\|^p)$, we have

$$\sum_{i=1}^n E[V_i(t_1, j, x(t_1))] \leq \sum_{i=1}^n r_i(t_1, t_0, u_0) < b(\mathcal{A}). \quad (4.8)$$

Therefore, we arrive at the following contradiction:

$$b(\mathcal{A}) \leq \sum_{i=1}^n E[V_i(t_1, j, x(t_1))] < b(\mathcal{A}). \quad (4.9)$$

This completes the proof. \square

Theorem 4.4. Assume the following:

- (i) all hypotheses of Theorem 3.3 hold;
- (ii) for $(t, x) \in \mathcal{T} \times \mathcal{R}^n$, $V(t, x)$ satisfies the following inequality:

$$\Phi(\|x\|^p) \leq \sum_{i=1}^n V_i(t, x, j), \quad (4.10)$$

where $\Phi \in \mathcal{U}\mathcal{K}[\mathcal{R}_+, \mathcal{R}_+]$ and $\mathcal{U}\mathcal{K}[\mathcal{R}_+, \mathcal{R}_+]$ is the collection of all continuous, convex, and increasing functions defined on \mathcal{R}_+ into itself with $\Phi(0) = 0$;

- (iii) the maximal solution $r(t)$ of system (3.3) through (t_0, u_0) converges to the zero vector as $t \rightarrow \infty$. Then, the interconnected system (2.3) is practically stable in the p th mean.

Proof. An application of Theorem 3.3 gives the following inequality:

$$EV(t, j, x(t)) \leq r(t, t_0, u_0), \quad (4.11)$$

where $r(t, t_0, u_0)$ is the maximal solution of system (3.3).

From assumption (ii), it can be seen that $\Phi(\cdot) > 0$ for every $\mathcal{A} > 0$. Let ϵ be a positive real number satisfying $\|x_0\|^p < \mathcal{A}$. By choosing u_0 such that $V(t_0, x_0) = u_0$ and noting as-

sumption (ii) and the continuity of V , there exists ϵ^* such that $\|x_0\|^p < \epsilon^*$ implies $\sum_{i=1}^n E[V_i(t, j, x_0)] \leq \epsilon^*$.

From assumption (iii) and the practical stability of $r(t)$ of system (3.3), we have $\sum_{i=1}^n V_i(t, j, x_0) = \sum_{i=1}^n u_{i_0} < \epsilon^*$ which implies that

$$\sum_{i=1}^n r_i(t, t_0, u_0) < \Phi(\mathcal{A}). \quad (4.12)$$

It follows from (4.11) that

$$\sum_{i=1}^n E[V_i(t, j, x(t))] \leq \sum_{i=1}^n r_i(t, t_0, u_0), \quad t \geq t_0, \quad (4.13)$$

and from (4.10), we arrive at the following inequality:

$$E[\Phi(\|x\|^p)] \leq \sum_{i=1}^n E[V_i(t, j, x(t))]. \quad (4.14)$$

By noting that Φ is a convex function and using the Jensen's inequality [18], we have

$$\Phi[E(\|x\|^p)] \leq E[\Phi(\|x\|^p)]. \quad (4.15)$$

Then, from (4.12)–(4.15), we obtain

$$\Phi[E(\|x\|^p)] < \Phi(\mathcal{A}) \quad (4.16)$$

whenever $\|x_0\|^p < \epsilon^*$, which implies

$$E[(\|x(t)\|^p)] < \mathcal{A}, \quad \forall t \geq t_0. \quad (4.17)$$

Thus the proof is complete. \square

5. Example

Consider the following stochastic differential equation with Markovian switching:

$$dx(t) = f(t, r(t), x(t))dt + \sigma(t, r(t), x(t))dw(t), \quad (5.1)$$

where $x = [x_1 \ x_2]^T \in \mathcal{R}^2$ is the state vector, $w(t)$ is a normalized scalar Wiener process.

The nonlinear vector function $\sigma = [\sigma_1 \ \sigma_2]^T \in \mathcal{C}[\mathcal{R}_+ \times \mathcal{S} \times \mathcal{R}^2, \mathcal{R}^2]$ satisfies $\sigma(t, r(t), 0) \equiv 0$,

$$\begin{aligned} [\sigma_1(t, r(t), x(t)) + \sigma_2(t, r(t), x(t))]^2 &\leq (x_1 + x_2)^2(t), \\ [\sigma_1(t, r(t), x(t)) - \sigma_2(t, r(t), x(t))]^2 &\leq (x_1 - x_2)^2(t), \end{aligned} \quad (5.2)$$

where $\sigma \in \mathcal{C}[\mathcal{R}_+, \mathcal{R}_+] \cap L_1[0, \infty)$.

The nonlinear function $f(t, r(t), x(t))$ is taken as

$$f(t, r(t), x(t)) = \begin{pmatrix} e^{-t} + \sin(t)x_1 \\ e^{-t} + \sin(t)x_2 \end{pmatrix}. \quad (5.3)$$

We choose

$$V(t, r(t), x) = \begin{pmatrix} V_1(t, x) \\ V_2(t, x) \end{pmatrix} = \begin{pmatrix} (x_1 + x_2)^2 \\ (x_1 - x_2)^2 \end{pmatrix} \quad (5.4)$$

as the Lyapunov function for (5.1). It is not difficult to obtain

$$|x|^2 \leq \sum_{i=1}^2 V_i(t, r(t), x(t)) \leq 2|x|^2. \quad (5.5)$$

Now, consider the following auxiliary random differential system:

$$du = g(t, u)dt \quad u(t_0) = u_0, \quad (5.6)$$

where $u \in \mathcal{R}^2$, $g(t, u)$ is given by

$$g(t, u) = \begin{pmatrix} (2e^{-t} + 2\sin(t) + \cos(t))u_1 \\ (2e^{-t} + 2\sin(t) + \cos(t))u_2 \end{pmatrix}. \quad (5.7)$$

We obtain

$$\mathcal{L}V_i(t, r(t), x(t)) \leq g_i(t, V_i(t, r(t), x(t))) \quad \text{for } (t, x) \in \mathcal{R}_+ \times \mathcal{R}^2; \quad (5.8)$$

let $a(r) = b(r) = r$. Obviously, the functions $a(r)$ and $b(r)$ are both convex and concave. Moreover, it is easy to see that $g(t, u)$ is concave and quasi-monotone nondecreasing in u for the fixed t and hence the system (5.1) is uniformly practically stable.

6. Conclusions

In this paper, the notion of practical stability in the p th mean is introduced and extended for the large-scale stochastic systems with Markovian switching. By employing Lyapunov-like functions and the basic comparison principle, sufficient conditions are established for various types of practical stability in the p th mean of nonlinear stochastic systems. The advantage of these results is to convert the problem of practical stability in the p th mean of stochastic systems into the problem of practical stability of the comparative deterministic systems. Future research topics include the investigation on the filtering and control problems for uncertain nonlinear stochastic systems, see for example, [19–28].

Acknowledgment

This work is supported by the National Natural Science Foundation of China (No. 60974030) and the Science and Technology Project of Education Department in Fujian Province, China (No. JA11211).

References

- [1] J. P. LaSalle and S. Lefschetz, *Stability Theory by Liapunov's Direct Method with Applications*, Academic Press, New York, NY, USA, 1961.
- [2] A. A. Martynyuk, *Practical Stability of Motion*, Naukav a Dumka, Kiev, Ukraine, 1983.
- [3] A. A. Martynyuk, "Averaging method in the theory of motion stability," *Nonlinear Vibration Problems*, vol. 14, pp. 71–79, 1973.
- [4] V. Lakshmikantham, S. Leela, and A. A. Martynyuk, *Practical Stability of Nonlinear Systems*, World Scientific, Singapore, 1990.
- [5] Z. S. Feng, Y. Q. Liu, and F. W. Guo, "Criteria for practical stability in the p -th mean of nonlinear stochastic systems," *Applied Mathematics and Computation*, vol. 49, no. 2-3, pp. 251–260, 1992.
- [6] A. H. Tsoi and B. Zhang, "Practical stabilities of Itô type nonlinear stochastic differential systems and related control problems," *Dynamic Systems and Applications*, vol. 6, no. 1, pp. 107–124, 1997.
- [7] G. S. Ladde and B. A. Lawrence, "Stability and convergence of large scale stochastic approximation procedures," *International Journal of Systems Science*, vol. 26, no. 3, pp. 595–618, 1995.
- [8] L. Shaikhet, "Stability of stochastic differential systems with Markovian Switching," *Stochastic Processes*, vol. 2, no. 18, pp. 180–184, 1996.
- [9] S. Sathananthan, *Practical Stability Criteria for Nonlinear Ito-Type Stochastic Control Systems*, Academic Press, New York, NY, USA, 2000.
- [10] M. A. O. Xuerong, A. Matasov, and A. B. Piunovskiy, "Stochastic differential delay equations with Markovian switching," *Bernoulli*, vol. 6, no. 1, pp. 73–90, 2000.
- [11] P. Zhao, "Practical stability, controllability and optimal control of stochastic Markovian jump systems with time-delays," *Automatica*, vol. 44, no. 12, pp. 3120–3125, 2008.
- [12] X. Mao, "Robustness of stability of stochastic differential delay equations with Markovian Switching," *Stability and Control: Theory and Applications*, vol. 3, no. 1, pp. 48–61, 2000.
- [13] H. Gilsing, "On the stability of the Euler scheme for an affine stochastic delay differential equation with the delay," Tech. Rep. 20,SFB 373, Humboldt University, Berlin, Germany, 2001.
- [14] A. V. Swishchuk and Y. I. Kazmerchuk, "Stability of stochastic of differential delay Ito's equations with Poisson Jumps and with Markovian Switching. Application to Financial Models," *Teoriya Veroyatnostei i Matematicheskaya Statistika*, vol. 63 (63), 2001.
- [15] J. Luo, J. Zou, and Z. Hou, "Comparison principle and stability criteria for stochastic differential delay equations with Markovian switching," *Science in China. Series A*, vol. 46, no. 1, pp. 129–138, 2003.
- [16] D. D. Šiljak, *Large-Scale Dynamic Systems: Stability and Structure*, vol. 3 of *North-Holland Series in System Science and Engineering*, North-Holland, New York, NY, USA, 1979.
- [17] S. Sathananthan and S. Suthaharan, "Practical stability criteria for large-scale nonlinear stochastic systems by decomposition and aggregation," *Dynamics of Continuous, Discrete & Impulsive Systems. Series A*, vol. 8, no. 2, pp. 227–248, 2001.
- [18] G. S. Ladde and V. Lakshmikantham, *Random Differential Inequalities*, vol. 150 of *Mathematics in Science and Engineering*, Academic Press, New York, NY, USA, 1980.
- [19] H. Dong, Z. Wang, D. W.C. Ho, and H. Gao, "Robust H_∞ filtering for Markovian jump systems with randomly occurring nonlinearities and sensor saturation: the finite-horizon case," *IEEE Transactions on Signal Processing*, vol. 59, no. 7, pp. 3048–3057, 2011.
- [20] Y. Tang, Z. Wang, W. K. Wong, J. Kurths, and J. Fang, "Multiobjective synchronization of coupled systems," *Chaos*, vol. 21, no. 2, Article ID 025114, 2011.
- [21] Z. Wang, J. Lam, L. Ma, Y. Bo, and Z. Guo, "Variance-constrained dissipative observer-based control for a class of nonlinear stochastic systems with degraded measurements," *Journal of Mathematical Analysis and Applications*, vol. 377, no. 2, pp. 645–658, 2011.
- [22] B. Shen, Z. Wang, Y. S. Hung, and G. Chesi, "Distributed H_∞ filtering for polynomial nonlinear stochastic systems in sensor networks," *IEEE Transactions on Industrial Electronics*, vol. 58, no. 5, pp. 1971–1979, 2011.

- [23] J. Liang, Z. Wang, and X. Liu, "Distributed state estimation for discrete-time sensor networks with randomly varying nonlinearities and missing measurements," *IEEE Transactions on Neural Networks*, vol. 22, no. 3, pp. 486–496, 2011.
- [24] X. He, Z. Wang, Y. D. Ji, and D. H. Zhou, "Robust fault detection for networked systems with distributed sensors," *IEEE Transactions on Aerospace and Electronic Systems*, vol. 47, no. 1, pp. 166–177, 2011.
- [25] B. Shen, Z. Wang, and X. Liu, "Bounded H_∞ synchronization and state estimation for discrete time-varying stochastic complex networks over a finite horizon," *IEEE Transactions on Neural Networks*, vol. 22, no. 1, pp. 145–157, 2011.
- [26] B. Shen, Z. Wang, H. Shu, and G. Wei, " H_∞ filtering for uncertain time-varying systems with multiple randomly occurred nonlinearities and successive packet dropouts," *International Journal of Robust and Nonlinear Control*, vol. 21, no. 14, pp. 1693–1709, 2011.
- [27] Z. Wang, D. W. C. Ho, H. Dong, and H. Gao, "Robust H_∞ finite-horizon control for a class of stochastic nonlinear time-varying systems subject to sensor and actuator saturations," *IEEE Transactions on Automatic Control*, vol. 55, no. 7, pp. 1716–1722, 2010.
- [28] Z. Wang, Y. Liu, and X. Liu, "Exponential stabilization of a class of stochastic system with Markovian jump parameters and mode-dependent mixed time-delays," *IEEE Transactions on Automatic Control*, vol. 55, no. 7, pp. 1656–1662, 2010.

Research Article

The Practical Stabilization for a Class of Networked Systems with Actuator Saturation and Input Additive Disturbances

Dongyan Chen, Shanqiang Li, and Yujing Shi

Department of Applied Mathematics, Harbin University of Science and Technology, Harbin 150080, China

Correspondence should be addressed to Dongyan Chen, dychen_2004@yahoo.com.cn

Received 28 May 2011; Revised 9 August 2011; Accepted 17 August 2011

Academic Editor: Yurong Liu

Copyright © 2012 Dongyan Chen et al. This is an open access article distributed under the Creative Commons Attribution License, which permits unrestricted use, distribution, and reproduction in any medium, provided the original work is properly cited.

The practical stabilization problem is investigated for a class of linear systems with actuator saturation and input additive disturbances. Firstly, the case of the input additive disturbance being a bounded constant and a variety of different situations of system matrices are studied for the three-dimensional linear system with actuator saturation, respectively. By applying the Riccati equation approach and designing the linear state feedback control law, sufficient conditions are established to guarantee the semiglobal practical stabilization or oscillation for the addressed system. Secondly, for the case of the input additive disturbances being time-varying functions, a more general class of systems with actuator saturation is investigated. By employing the Riccati equation approach, a low-and-high-gain linear state feedback control law is designed to guarantee the global or semiglobal practical stabilization for the closed-loop systems.

1. Introduction

Actuator saturation (control saturation), as a common and typical nonlinear constraint for control systems, is often encountered in various industrial systems, especially in many physical-controlled systems with magnitude limitation in the input. In general, linear systems can be completely controlled by using the linear state feedback, and the semiglobal (or local) stabilization can be achieved [1–3]. Linear systems with actuator saturation are also a special class of nonlinear systems [4]. The occurrence of actuator saturation inevitably affects the control systems performance and may even result in the instability of the controlled systems. Consequently, the actuator saturation has attracted significant attention, and a variety of approaches have been developed in the literature with respect to various types of systems [5–13]. Specifically, the problems of the global (or semiglobal) asymptotic stabilization, the attraction domain estimation, and the practical stabilization have been extensively investigated.

When the dimension of the integrator is greater than or equal to 3, the linear systems with input saturation cannot be stabilized by using the linear state feedback control law, so the global asymptotic stabilization of the system cannot be attained. However, if all eigenvalues of the open-loop system have negative real parts, the global asymptotic stabilization for the addressed system can be guaranteed by designing a globally stable boundary control law. Accordingly, the exponentially semiglobal stabilization problems have been widely studied in [1–3] by designing a linear state feedback control law. By employing the linear matrix inequality (LMI) technique, much work has been done in finding the condition of invariant set and the estimation of attraction domain, see for example, [14–18]. Very recently, networked control systems (NCSs) have attracted considerable attention due to their successful applications in a wide range of areas with the advantage of decreasing the installation cost and implementation difficulties [19–27]. It should be pointed out that, in most related literature concerning the actuator saturation problems, the networked systems with actuator saturation and input additive disturbances have not been thoroughly studied yet.

On the other hand, the study of the linear systems with actuator saturation also covers the practical stabilization problem, that is, a controller is designed such that the trajectories of closed-loop system can enter into an arbitrarily small prescribed neighborhood of the origin in finite time and remain thereafter. The practical stabilization problems have been gaining an increasing research interest, and many important results have been reported, see, for example, [28–30]. To mention a few, the problems of global practical stabilization for planar linear systems have been studied [28, 29] in the presence of actuator saturation and input additive disturbances. By tuning the value of the parameter and designing a parameterized linear state feedback law, sufficient conditions have been established such that all trajectories of the closed-loop systems approach to an arbitrarily small neighborhood of the origin in a finite time and remain thereafter. Moreover, the global stabilization problem has also been studied in [30] for a class of second-order switched systems with input saturation. It is worth mentioning that, because of the mathematical complexity and computational difficulty, the corresponding results for general multidimensional systems with actuator saturation and input additive perturbations have been not reported. By designing the low-and-high-gain and the scheduled low-and-high-gain control laws, the semiglobal asymptotic stabilization problems have been investigated in [31, 32] for general multidimensional linear systems. The feedback control law has been designed to deal with the matched uncertainties and input additive disturbances. However, strict assumptions on the input additive uncertainties and disturbances have been imposed on the systems. It is, therefore, our aim to address the multidimensional systems with general constraints on the input additive disturbances.

Motivated by the above discussion, we aim to investigate the practical stabilization problem for three-dimensional (multidimensional) system with actuator saturation and input additive disturbances. By employing the Riccati equation approach, the linear state feedback control law is designed to guarantee the practical stabilization for the system with actuator saturation and time-invariant input additive disturbances. Moreover, the practical stabilization of a general multidimensional system with actuator saturation and time-varying input additive disturbances is studied, and the low-and-high-gain linear state feedback control law is synthesized by using the Riccati equation approach. The main contributions of this paper can be highlighted as follows: (1) the practical stabilization problem of three-dimensional linear systems is investigated for the first time, which covers actuator saturation as well as input additive disturbances; (2) the low-and-high-gain linear state feedback control

law is designed for multidimensional system with actuator saturation and time-varying input additive disturbances.

Notations. The notations in this paper are quite standard except where otherwise stated. The superscript “ T ” stands for matrix transposition; \mathbb{R}^n ($\mathbb{R}^{n \times m}$) denote, respectively, the n -dimensional Euclidean space, the set of all $n \times m$ matrices; the notation $P > 0$ ($P \geq 0$) means that matrix P is real symmetric and positive definite (positive semi-definite); 0 represents a zero matrix with appropriate dimension, respectively; $\|\cdot\|$ denotes the Euclidean norm of a vector and its induced norm of a matrix. In symmetric block matrices or long matrix expressions, we use a star “ $*$ ” to represent a term that is induced by symmetry. Matrices, if their dimensions are not explicitly stated, are assumed to be compatible for algebraic operations.

2. The Case of Bounded Constant Input Disturbance

Consider the following three-dimensional system with actuator saturation and input additive disturbance:

$$\dot{x} = Ax + B(u + d), \quad (2.1)$$

where $x \in \mathbb{R}^3$ is the state, A and B are real matrices of appropriate dimensions, $u \in \mathbb{R}$ is the control input, and $d \in \mathbb{R}$ is the disturbance.

The saturation function $\text{sat}(\cdot)$ is defined as

$$\text{sat}(u) = \text{sign}(u) \min\{1, |u|\}, \quad (2.2)$$

where the notation of “ sign ” denotes the signum function.

Before proceeding further, we make the following assumptions.

Assumption 2.1. The matrix pair (A, B) is controllable, and the eigenvalues of A have nonpositive real parts.

Assumption 2.2. The input disturbance is bounded, that is, $|d| \leq D$, where D is an arbitrarily large positive scalar.

Based on Assumption 2.1, let $B = [0 \ 0 \ 1]^T$, matrix A is in one of the following forms:

$$(a) \ A = \begin{bmatrix} 0 & 1 & 0 \\ 0 & 0 & 1 \\ 0 & 0 & 0 \end{bmatrix}, \quad (b) \ A = \begin{bmatrix} 0 & 1 & 0 \\ 0 & 0 & 1 \\ 0 & 0 & -a \end{bmatrix}, \quad (c) \ A = \begin{bmatrix} 0 & 1 & 0 \\ 0 & 0 & 1 \\ 0 & -a & 0 \end{bmatrix},$$

$$\begin{aligned}
\text{(d) } A &= \begin{bmatrix} 0 & 1 & 0 \\ 0 & 0 & 1 \\ -a & 0 & 0 \end{bmatrix}, & \text{(e) } A &= \begin{bmatrix} 0 & 1 & 0 \\ 0 & 0 & 1 \\ -a & -b & 0 \end{bmatrix}, & \text{(f) } A &= \begin{bmatrix} 0 & 1 & 0 \\ 0 & 0 & 1 \\ -a & 0 & -b \end{bmatrix}, \\
\text{(g) } A &= \begin{bmatrix} 0 & 1 & 0 \\ 0 & 0 & 1 \\ 0 & -a & -b \end{bmatrix}, & \text{(h) } A &= \begin{bmatrix} 0 & 1 & 0 \\ 0 & 0 & 1 \\ -a & -b & -c \end{bmatrix},
\end{aligned} \tag{2.3}$$

where $a, b,$ and c are positive scalars.

These forms of the matrix pair (A, B) correspond to eight different cases for system (2.1). In the following, the problem of practical stabilization for system (2.1) will be investigated by designing the linear state feedback control law. To facilitate our development, we introduce the following definition.

Definition 2.3. Define an ellipsoid $\Omega(P, \gamma)$ as follows:

$$\Omega(P, \gamma) := \left\{ x \in \mathbb{R}^3, x^T P x \leq \gamma \right\}, \tag{2.4}$$

where $P \in \mathbb{R}^{3 \times 3}$ is a symmetric positive definite matrix and γ is a positive scalar.

For system (2.1), the control law under consideration is of the following structure:

$$u = -\frac{1}{\gamma} B^T P x, \tag{2.5}$$

where $\gamma \in (0, 1]$, and P is a symmetric positive definite matrix to be determined according to the form of (A, B) defined in (2.3).

Lemma 2.4 (see [10]). *Letting $u, v \in \mathbb{R}$ with $|v| \leq 1$, $E_1 = 0$ and $E_2 = 1$, one has*

$$(u) \in \text{co}\{u, v\} = \text{co}\{E_i u + E_i^- v, i = 1, 2\}, \tag{2.6}$$

where “co” denotes the convex hull and $E_i^- = 1 - E_i$.

Theorem 2.5. *Consider the system (2.1) with (A, B) defined in (2.3) and the control law (2.5).*

- (i) *If A satisfies case (g) with $b^2 > 2a$ or case (h) with $bc > a$ in (2.3), then for any given arbitrarily small set $\mathcal{D}_0 \subset \mathbb{R}^3$ containing origin in its interior and for any positive scalar D , there always exists $\gamma^* \in (0, 1]$ such that, for any $\gamma \in (0, \gamma^*]$, all trajectories of the closed-loop system will enter into the set \mathcal{D}_0 in finite time and remain thereafter.*
- (ii) *If A satisfies cases (a) or (b) or (c) in (2.3), when the initial state is in some bounded set, then for any given arbitrarily small set $\mathcal{D}_0 \subset \mathbb{R}^3$ containing origin in its interior and any positive number D , there always exists $\gamma^* \in (0, 1]$, such that, for any $\gamma \in (0, \gamma^*]$, all*

trajectories of the closed-loop system will enter into the set Ω^0 in finite time and remain thereafter.

(iii) If A satisfies cases (d) or (e) or (f) in (2.3), then all trajectories of the closed-loop system are oscillatory.

Proof. Firstly, let us prove (i).

(i₁) Consider the following system

$$\dot{x} = \begin{bmatrix} 0 & 1 & 0 \\ 0 & 0 & 1 \\ 0 & -a & -b \end{bmatrix} x + \begin{bmatrix} 0 \\ 0 \\ 1 \end{bmatrix} \text{sat}(u + d), \quad (2.7)$$

that is, A satisfies the case (g) with $b^2 > 2a$ in (2.3).

Let P be the solution to the following algebra Riccati equation (ARE):

$$A^T P + P A - P B B^T P = - \begin{bmatrix} a^2 & 0 & 0 \\ 0 & b^2 - 2a & 0 \\ 0 & 0 & 1 \end{bmatrix}, \quad (2.8)$$

we have

$$P = \begin{bmatrix} a^2 + ab & ab + a & a \\ * & b^2 + b & b \\ * & * & 1 \end{bmatrix}. \quad (2.9)$$

Define

$$\begin{aligned} \Omega^+ &:= \left\{ x \in \mathbb{R}^3, \frac{1}{-B^T P x} \geq 1 + D \right\}, \\ \Omega^- &:= \left\{ x \in \mathbb{R}^3, \frac{1}{-B^T P x} \leq -1 - D \right\}, \\ \Omega^0 &:= \left\{ x \in \mathbb{R}^3, \left| \frac{1}{-B^T P x} \right| < 1 + D \right\}. \end{aligned} \quad (2.10)$$

For any $x \in \Omega^+$, we have $B^T P x \geq -(1 + D)$, that is, $ax_1 + bx_2 + x_3 \geq -(1 + D)$. From (2.7), we obtain

$$\begin{aligned} \dot{x}_1 &= x_2, \\ \dot{x}_2 &= x_3, \\ \dot{x}_3 &= -ax_2 - bx_3 - 1. \end{aligned} \quad (2.11)$$

Furthermore, there is $a\dot{x}_1 + b\dot{x}_2 + \dot{x}_3 = -1$. It means that $ax_1 + bx_2 + x_3$ will decrease in a constant speed and will be less than $-(1 + D)$ in finite time. Hence, any trajectory departing

from $x \in \Omega^+$ will enter into the interior of Ω^0 in finite time. Similarly, any trajectory departing from $x \in \Omega^-$ will enter into Ω^0 in finite time.

We choose the Lyapunov function $V(x) = x^T P x$ with $P > 0$ being the solution to ARE (2.8). For any $x \in \Omega^0$, we have $|(1/(1+D))B^T P x| < 1$. It follows from Lemma 2.4 that

$$\text{sat}\left\{\frac{1}{-B^T P x - d}\right\} \in \text{co}\left\{E_i\left(\frac{1}{-B^T P x - d}\right) + E_i^- \frac{1}{(1+D)} B^T P x, i=1,2\right\}. \quad (2.12)$$

Noticing that $\epsilon > 0$ is a sufficiently small scalar, we have

$$\begin{aligned} \dot{V}(x) &= x^T P \left[A x - B \text{sat}\left(\frac{1}{-x^T P x - d}\right) \right] + \left[A x - B \text{sat}\left(\frac{1}{-x^T P x - d}\right) \right]^T P x \\ &\leq \max_{i \in \{1,2\}} \left\{ x^T P \left[A x - B E_i \left(\frac{1}{-B^T P x - d} \right) + B E_i^- \frac{1}{(1+D)} B^T P x \right] \right. \\ &\quad \left. + \left[A x - B E_i \left(\frac{1}{-B^T P x - d} \right) + B E_i^- \frac{1}{(1+D)} B^T P x \right]^T P x \right\} \\ &\leq x^T \left[A^T P + P A - \frac{2D}{(1+D)} P B B^T P \right] x + 2x^T P B d \\ &\leq x^T \left[A^T P + P A - P B B^T P \right] x + 2D/(1+D) \\ &= -x^T \begin{bmatrix} a^2 & 0 & 0 \\ 0 & b^2 - 2a & 0 \\ 0 & 0 & 1 \end{bmatrix} x + 2D/(1+D). \end{aligned} \quad (2.13)$$

Define

$$\Omega_d^7 := \left\{ x \in \mathbb{R}^3, x^T \begin{bmatrix} a^2 & 0 & 0 \\ 0 & b^2 - 2a & 0 \\ 0 & 0 & 1 \end{bmatrix} x \leq 2D/(1+D), b^2 > 2a \right\}, \quad (2.14)$$

then there exists a scalar $\epsilon > 0$ such that $\Omega(P, \epsilon)$ is the smallest ellipsoid satisfying $\Omega(P, \epsilon) \cap \Omega^0 \supset \Omega_d^7 \cap \Omega^0$. Hence, we have $\dot{V}(x) < 0$ for all $x \in \Omega(P, \epsilon) \cap \Omega^0$, and $\Omega(P, \epsilon) \cap \Omega^0$ is an invariant set. Hence, any trajectory of the closed-loop system departing from $\Omega(P, \epsilon) \cap \Omega^0$ will enter into $\Omega(P, \epsilon) \cap \Omega^0$ in finite time and remain thereafter. If $\epsilon \rightarrow 0$, then Ω_d^7 tends to origin. Therefore, $\Omega(P, \epsilon) \cap \Omega^0$ approaches to the origin.

(i₂) Assuming that matrix A satisfies the case (h) and $bc > a$, then the system (2.1) can be written as follows:

$$\dot{x} = \begin{bmatrix} 0 & 1 & 0 \\ 0 & 0 & 1 \\ -a & -b & -c \end{bmatrix} x + \begin{bmatrix} 0 \\ 0 \\ 1 \end{bmatrix} \text{sat}(u + d). \quad (2.15)$$

It follows from $bc > a$ that A is stable. Then there exists $P > 0$ satisfying

$$A^T P + P A = -I_3. \quad (2.16)$$

When $x \in \Omega^+$, noting that $B^T P x \geq (1 + D)$, we have $\text{sat}(u + d) = -1$ and

$$\dot{V}(x) = x^T (P A + A^T P) x - 2x^T P B \leq -x^T x - 2(1 + D) < 0. \quad (2.17)$$

Similarly, for any $x \in \Omega^-$, it is easy to obtain $\dot{V}(x) < 0$.

When $x \in \Omega^0$, considering $|(1/(1 + D))B^T P x| < 1$ and noticing that $\epsilon > 0$ is a sufficiently small scalar, we have

$$\begin{aligned} \dot{V}(x) &= x^T (P A + A^T P) x - \frac{2}{1 + D} x^T P B B^T P x + 2 \epsilon D (1 + D) \\ &< -x^T x + 2 \epsilon D (1 + D). \end{aligned} \quad (2.18)$$

Set

$$\Omega_\epsilon^8 := \left\{ x \in \mathbb{R}^3, \|x\|^2 \leq 2 \epsilon D (1 + D) \right\}. \quad (2.19)$$

Then there exists a scalar $\epsilon > 0$ such that $\Omega(P, \epsilon)$ is the smallest ellipsoid which satisfies $\Omega(P, \epsilon) \cap \Omega^0 \supset \Omega_\epsilon^8 \cap \Omega^0$. Now, we can conclude that $\dot{V}(x) < 0$ holds for all $x \notin \Omega(P, \epsilon) \cap \Omega^0$. Therefore, all trajectories will enter into $\Omega(P, \epsilon) \cap \Omega^0$ in finite time. When $\epsilon \rightarrow 0$, $\Omega(P, \epsilon) \cap \Omega^0$ approaches to the origin.

Secondly, let us prove (ii).

(ii₁) Consider the following system:

$$\dot{x} = \begin{bmatrix} 0 & 1 & 0 \\ 0 & 0 & 1 \\ 0 & 0 & 0 \end{bmatrix} x + \begin{bmatrix} 0 \\ 0 \\ 1 \end{bmatrix} \text{sat}(u + d), \quad (2.20)$$

that is, A satisfies the case (a).

In this case, we choose the matrix P to be the solution to the following ARE:

$$A^T P + P A - \frac{2}{(1 + D)} P B B^T P = -\frac{1}{(1 + D)} \begin{bmatrix} 1 & 0 & 0 \\ 0 & 2 & 0 \\ 0 & 0 & \frac{1 - 8(1 + D)}{4} \end{bmatrix}, \quad (2.21)$$

where $0 < \alpha < 1/(8(1+D))$. Then, we obtain

$$P = \begin{bmatrix} \frac{\sqrt{2}}{(1+D)} & \frac{1}{2(1+D)} & \frac{\sqrt{2}}{2} \\ * & \frac{\sqrt{2}}{2} \left(\frac{\sqrt{1-(1+D)}}{(1+D)} \right) & 1 \\ * & * & \frac{\sqrt{2}}{4} \end{bmatrix}. \quad (2.22)$$

For any $x \in \Omega^+$, $B^T P x \geq (1+D)$ and $\text{sat}(u+d) = -1$. The system (2.20) reduces to

$$\dot{x} = \begin{bmatrix} 0 & 1 & 0 \\ 0 & 0 & 1 \\ 0 & 0 & 0 \end{bmatrix} x - \begin{bmatrix} 0 \\ 0 \\ 1 \end{bmatrix}. \quad (2.23)$$

Hence, the solution to (2.23) can be described as:

$$\begin{aligned} x_1 &= -\frac{1}{6}t^3 + \frac{1}{2}x_{03}t^2 + x_{02}t + x_{01}, \\ x_2 &= -\frac{1}{2}t^2 + x_{03}t + x_{02}, \\ x_3 &= -t + x_{03}, \end{aligned} \quad (2.24)$$

where $x(0) = [x_{01} \ x_{02} \ x_{03}]^T$ is the initial state.

By noting $B^T P x \geq (1+D)$, we have $(\sqrt{2}/2)x_1 + x_2 + (\sqrt{2}/4)x_3 \geq (1+D)$. Furthermore, we obtain

$$\begin{aligned} B^T P \dot{x} &= \frac{\sqrt{2}}{2}\dot{x}_1 + \dot{x}_2 + \frac{\sqrt{2}}{4}\dot{x}_3 \\ &= -\frac{\sqrt{2}}{4}t^2 - \left(1 - \frac{\sqrt{2}}{2}x_{03}\right)t - \frac{\sqrt{2}}{4} + x_{03} + \frac{\sqrt{2}}{2}x_{02}. \end{aligned} \quad (2.25)$$

If $B^T P \dot{x} < 0$, then any trajectory departing from Ω^+ will enter into Ω^0 in finite time. Let

$$\frac{\sqrt{2}}{4}t^2 + \left(1 - \frac{\sqrt{2}}{2}x_{03}\right)t + \frac{\sqrt{2}}{4} - x_{03} - \frac{\sqrt{2}}{2}x_{02} > 0. \quad (2.26)$$

For $t > 0$, the discriminant of quadratic inequality is less than zero, then it is accessible to the conditions of the initial point set.

Define

$$X_1^+ := \left\{ x = [x_1 \ x_2 \ x_3]^T \in \Omega^+ : x_1 \in \mathbb{R}, \frac{1}{2}x_3^2 + x_2 + \frac{1}{2} < 0 \right\}, \quad (2.27)$$

then any trajectory departed from X_1^+ will enter into Ω^0 in finite time and remain thereafter.

Similarly, when $x \in \Omega^-$, a set of initial points can also be found such that any trajectory departing from the set will enter into Ω^0 in finite time and remain thereafter. After some algebraic manipulations, the initial set of points can be expressed as follows:

$$X_1^- := \left\{ x = [x_1 \ x_2 \ x_3]^T \in \Omega^- : x_1 \in \mathbb{R}, \frac{1}{2}x_3^2 - x_2 + \frac{1}{2} < 0 \right\}. \quad (2.28)$$

For any $x \in \Omega^0$, $|(1/(1+D))B^T P x| < 1$, we have

$$\begin{aligned} \dot{V}(x) \leq x^T \left[PA + A^T P - \frac{2}{(1+D)} P B B^T P \right] x + 2 D (1+D) \\ - \frac{1}{(1+D)} x^T \begin{bmatrix} 1 & 0 & 0 \\ 0 & 1 & 0 \\ 0 & 0 & \frac{1-8(1+D)}{4} \end{bmatrix} x + 2 D (1+D). \end{aligned} \quad (2.29)$$

Let

$$\Omega_d^1 := \left\{ x \in \mathbb{R}^3, x^T \begin{bmatrix} 1 & 0 & 0 \\ 0 & 1 & 0 \\ 0 & 0 & \frac{1-8(1+D)}{4} \end{bmatrix} x \leq 2^2 D (1+D)^2, \quad < \frac{1}{8(1+D)} \right\}. \quad (2.30)$$

Then there exists a scalar $\epsilon > 0$ such that $\Omega(P, \epsilon)$ is the smallest ellipsoid which satisfies $\Omega(P, \epsilon) \cap \Omega^0 \supset \Omega_d^1 \cap \Omega^0$. Now, we can conclude that $\dot{V}(x) < 0$ holds for all $x \in \Omega(P, \epsilon) \cap \Omega^0$. So $\Omega(P, \epsilon) \cap \Omega^0$ is an invariant set. For the initial state $x \notin \Omega(P, \epsilon) \cap \Omega^0$, any trajectory of the system departing from $x \in X_1^+ \cup X_1^- \cup (\Omega^0 \setminus \Omega(P, \epsilon))$ will enter into $\Omega(P, \epsilon) \cap \Omega^0$ in finite time and remain thereafter. When $\epsilon \rightarrow 0$, $\Omega(P, \epsilon) \cap \Omega^0$ approaches to the origin.

(ii₂) Consider the following system:

$$\dot{x} = \begin{bmatrix} 0 & 1 & 0 \\ 0 & 0 & 1 \\ 0 & 0 & -a \end{bmatrix} x + \begin{bmatrix} 0 \\ 0 \\ 1 \end{bmatrix} \text{sat}(u + d), \quad (2.31)$$

that is, A satisfies the case (b).

In this case, we choose the matrix P to be the solution to the following ARE:

$$A^T P + P A - \frac{2}{\gamma} P B B^T P = -\frac{2}{\gamma} \begin{bmatrix} \frac{1}{16}a^4 & 0 & 0 \\ 0 & \frac{1}{2}a^2 & 0 \\ 0 & 0 & 1 \end{bmatrix}. \quad (2.32)$$

Then, we obtain

$$P = \begin{bmatrix} \frac{a^3}{2} & \frac{a^2}{2} & \frac{1}{4}a^2 \\ * & -a - \frac{1}{4}a^2 & a \\ * & * & 1 \end{bmatrix}, \quad (2.33)$$

where, if $a > 6$, then $\frac{6}{a} < 6/a$, and, if $0 < a \leq 6$, then $\frac{6}{a} \in (0,1]$.

Define

$$\begin{aligned} X_2^+ &:= \left\{ x = [x_1 \ x_2 \ x_3]^T \in \Omega^+ : x_1 \in \mathbb{R}, x_2 \leq \frac{4}{a^2}, x_3 \geq -\frac{1}{a} \right\}, \\ X_2^- &:= \left\{ x = [x_1 \ x_2 \ x_3]^T \in \Omega^- : x_1 \in \mathbb{R}, x_2 \geq \frac{4}{a^2}, x_3 \leq -\frac{1}{a} \right\}, \\ \Omega_d^2 &:= \left\{ x \in \mathbb{R}^3, x^T \begin{bmatrix} \frac{1}{16}a^4 & 0 & 0 \\ 0 & \frac{1}{2}a^2 & 0 \\ 0 & 0 & 1 \end{bmatrix} x \leq \frac{2}{\gamma} D(1+D), \frac{6}{a} < \frac{6}{a}, a > 6, \frac{6}{a} \in (0,1], 0 < a \leq 6 \right\}. \end{aligned} \quad (2.34)$$

Then there exists a scalar $\gamma > 0$ such that $\Omega(P, \gamma)$ is the smallest ellipsoid which satisfies $\Omega(P, \gamma) \cap \Omega^0 \supset \Omega_d^2 \cap \Omega^0$. Therefore, $\dot{V}(x) < 0$ holds for all $x \in \Omega(P, \gamma) \cap \Omega^0$. Hence $\Omega(P, \gamma) \cap \Omega^0$ is an invariant set. For the initial state x outside $\Omega(P, \gamma) \cap \Omega^0$, any trajectory departing from $x \in X_2^+ \cup X_2^- \cup (\Omega^0 \setminus \Omega(P, \gamma))$ will enter into $\Omega(P, \gamma) \cap \Omega^0$ in finite time and remain thereafter. Moreover, when $\gamma \rightarrow 0$, $\Omega(P, \gamma) \cap \Omega^0$ approaches to the origin.

(ii₃) Consider the following system:

$$\dot{x} = \begin{bmatrix} 0 & 1 & 0 \\ 0 & 0 & 1 \\ 0 & -a & 0 \end{bmatrix} x + \begin{bmatrix} 0 \\ 0 \\ 1 \end{bmatrix} \text{sat}(u + d), \quad (2.35)$$

that is, A satisfies the case (c).

In this case, we choose the matrix P to be the solution to the following ARE:

$$A^T P + P A - \frac{2}{\delta} P B B^T P = -\frac{1}{\delta} \begin{bmatrix} 2a^2 & 0 & 0 \\ 0 & \frac{1-6\delta^2 a}{2\delta^3} & 0 \\ 0 & 0 & 1 \end{bmatrix}. \quad (2.36)$$

Then, we obtain

$$P = \begin{bmatrix} a^2 + \frac{a}{2} & \frac{2a}{\delta} & a \\ * & \frac{1}{2} & \frac{1}{2} \\ * & * & 1 \end{bmatrix}, \quad (2.37)$$

where, if $a > 1/6$, then $\delta < \sqrt{(1/6)a}$, and, if $0 < a \leq 1/6$, then $\delta \in (0, 1]$.
Set

$$\begin{aligned} X_3^+ &:= \left\{ x = [x_1 \ x_2 \ x_3]^T \in \Omega^+ : x_1 \in \mathbb{R}, \sqrt{a}x_2 + x_3 < 2 - \frac{1}{\sqrt{a}} \right\}, \\ X_3^- &:= \left\{ x = [x_1 \ x_2 \ x_3]^T \in \Omega^- : x_1 \in \mathbb{R}, \sqrt{a}x_2 + x_3 < 2 + \frac{1}{\sqrt{a}} \right\}, \\ \Omega_d^3 &:= \left\{ x \in \mathbb{R}^3, x^T \begin{bmatrix} 2a^2 & 0 & 0 \\ 0 & \frac{1-6\delta^2 a}{2\delta^3} & 0 \\ 0 & 0 & 1 \end{bmatrix} x \leq 2\delta^2 D(1+D), \right. \\ &\quad \left. \delta < \sqrt{\frac{1}{6}a}, a > \frac{1}{6}, \delta \in (0, 1], 0 < a \leq \frac{1}{6} \right\}. \end{aligned} \quad (2.38)$$

Then, there exists a scalar $\delta > 0$ such that $\Omega(P, \delta)$ is the smallest ellipsoid which satisfies $\Omega(P, \delta) \cap \Omega^0 \supset \Omega_d^2 \cap \Omega^0$. Therefore, $\dot{V}(x) < 0$ is true for all $x \in \Omega(P, \delta) \cap \Omega^0$. Hence, $\Omega(P, \delta) \cap \Omega^0$ is an invariant set. For the initial state $x \notin \Omega(P, \delta) \cap \Omega^0$, any trajectory of the system departing from $x \in X_3^+ \cup X_3^- \cup (\Omega^0 \setminus \Omega(P, \delta))$ will enter into $\Omega(P, \delta) \cap \Omega^0$ in finite time and remain thereafter. Moreover, when $\delta \rightarrow 0$, $\Omega(P, \delta) \cap \Omega^0$ approaches to the origin.

Finally, let us prove (iii).

Assuming that matrix A satisfies any case among (d)–(f), when the actuator is saturated, all the system trajectories departed from Ω^+ and Ω^- are oscillatory, that is, all the trajectories cannot back into any arbitrarily small set containing the origin in finite time. When the actuator is unsaturated, that is, $x \in \Omega^0$. The positive definite symmetric matrix P satisfying certain ARE can be obtained. When $\delta \rightarrow 0$, there exists a small ellipsoid Ω_d^i which contains origin as its interior and approaches to the origin such that $\dot{V}(x) < 0$ for all $x \in \Omega^0 \setminus \Omega_d^i$. Furthermore, there exists $\delta > 0$ such that $\Omega(P, \delta)$ is the smallest ellipsoid which

satisfies $\Omega(\mathcal{P}, \cdot) \cap \Omega^0 \supset \Omega_a^i \cap \Omega^0$, that is, $x \notin \Omega(\mathcal{P}, \cdot) \cap \Omega^0$, the trajectory only starting from $\Omega^0 \setminus \Omega(\mathcal{P}, \cdot)$ can enter into $\Omega(\mathcal{P}, \cdot) \cap \Omega^0$ in finite time.

Based on (i)–(iii), the proof of this theorem is now complete. \square

Remark 2.6. It should be pointed out that, because of the mathematical complexity and computational difficulty, almost all papers concerning the actuator saturation and input additive disturbances have considered the two-dimensional systems. In this paper, we make the first attempt to investigate the practical stabilization problem for three-dimensional system with actuator saturation and input additive disturbances. To the best of our knowledge, the research topic addressed in this paper is new and meaningful. The above attempts distinguish our research results from the existing ones.

Remark 2.7. The sufficient conditions are established in Theorem 2.5 for three-dimensional system with actuator saturation and input additive disturbance. By applying the Riccati equation approach, the linear state feedback control law is designed such that the semiglobal practical stabilization can be guaranteed. It should be pointed out that the simultaneous consideration of actuator saturation and input additive disturbance leads to essential difficulties in the technical development, and the corresponding derivations are nontrivial. More specifically, some constructive strategies are introduced to facilitate the derivation of the main results.

3. The Case of Time-Varying Uncertain Input Disturbance

In this section, we investigate a more general class of systems with actuator saturation and time-varying disturbance input. A low-and-high-gain is designed to guarantee the global or semiglobal practical stabilization for the closed-loop systems.

Consider the following linear system with actuator saturation and time-varying disturbance input

$$\dot{x} = A x + B (u + g(x, t)), \quad (3.1)$$

where $x \in \mathbb{R}^n$ is the state vector, $u \in \mathbb{R}^m$ is the control input, $g(x, t) : \mathbb{R}^n \times \mathbb{R} \rightarrow \mathbb{R}^m$ represents the time-varying uncertainty, and A and B are known real matrices with appropriate dimensions. $(\cdot) : \mathbb{R}^m \rightarrow \mathbb{R}^m$ is the standard saturated function, that is,

$$(s) = [s_1(s_1) \quad s_2(s_2) \quad \cdots \quad s_m(s_m)]^T, \quad s_i(s_i) = \text{sign}(s_i) \min\{1, |s_i|\}, \quad s \in \mathbb{R}^m. \quad (3.2)$$

Before proceeding further, we make the following assumptions.

Assumption 3.1. The matrix pair (A, B) is asymptotically null controllable with bounded control, that is, all the eigenvalues of A are in the left half plane (LHP) and (A, B) is stabilizable.

Assumption 3.2. The uncertain element $g(x, t)$ is piecewise continuous in t and locally Lipschitz in x satisfying

$$\|g(x, t)\| \leq g_0(\|x\|) + D_0, \quad \forall (x, t) \in \mathbb{R}^n \times \mathbb{R}^+, \quad (3.3)$$

where D_0 is a known positive scalar, and the known function $g_0(\cdot) : \mathbb{R}^+ \rightarrow \mathbb{R}^+$ is local Lipschitz and satisfies $g_0(\|x\|) \leq L\|x\|$ with $L > 0$ being a constant.

Problem 1. For the system (3.1), the purpose of this section is to design a state feedback control law $u = Fx$ such that the following requirements are satisfied.

- (1) If $D_0 = 0$, the closed-loop system is globally asymptotically stable at the point of $x = 0$.
- (2) If $D_0 > 0$, the trajectories of the system enter into a given set which contains the origin as an interior point and remain thereafter.

Remark 3.3. As discussed in [31], corresponding to the specific values for D_0 and g_0 , Problem 1 refers to different names. Specifically, when $g_0 = 0, D_0 = 0$, it is called the globally asymptotical stabilization by state feedback problem. When $g_0 = 0, D_0 > 0$, it is called the global disturbance rejection by state feedback problem. When $g_0 \neq 0, D_0 = 0$, it is called the robust globally asymptotical stabilization by state feedback problem. When $g_0 \neq 0, D_0 > 0$, it is called the robust global disturbance rejection by state feedback problem.

For Problem 1, the design of low-and-high gain state feedback control law is composed of three steps. In Steps 1 and 2, the low-gain and high-gain state feedback control law is designed, respectively. Accordingly, the low-and-high-gain control law is designed in Step 3.

Step 1 (low-gain state feedback design). Let $Q : (0,1] \rightarrow \mathbb{R}^{n \times n}$ be a continuously differentiable and strictly increasing function such that $Q(\cdot)$ is symmetric positive definite for each $\epsilon \in (0,1]$ and $\lim_{\epsilon \rightarrow 0} Q(\epsilon) = 0$. Consider the following ARE:

$$A^T P(\epsilon) + P(\epsilon)A - P(\epsilon)BB^T P(\epsilon) = -Q(\epsilon). \tag{3.4}$$

Then, the following lemma is obtained.

Lemma 3.4 (see [32]). *Let Assumption 2.1 be satisfied, then, for all $\epsilon \in (0,1]$, there exists a unique symmetric positive definite matrix $P(\epsilon) > 0$ which solves the ARE (3.4) and $\lim_{\epsilon \rightarrow 0} P(\epsilon) = 0$.*

Now, we construct the low-gain state feedback law as follows:

$$u_L = -B^T P(\epsilon)x, \tag{3.5}$$

where $P(\epsilon)$ is a symmetric positive definite solution to ARE (3.4).

Based on Lemma 3.4, we can conclude that the above low-gain state feedback control law can be arbitrarily small when ϵ is arbitrarily small.

Step 2 (high-gain state feedback design). We design the high-gain state feedback control law as follows:

$$u_H = -\frac{1}{\epsilon} B^T P(\epsilon)x, \tag{3.6}$$

where $\epsilon \geq 0$ is called high-gain parameter, $\epsilon = \frac{\epsilon_0(1 + L + D_0)^2}{\min(Q(\epsilon))}$ with $\epsilon_0 \geq 0$ being an adjustable constant, L and D_0 are defined in Assumption 3.2.

Step 3 (low-and-high-gain state feedback design). Taking the low-gain and high-gain state feedback control law into account, the low-and-high-gain state feedback control law is constructed as follows:

$$u_{LH} = -(1 + \epsilon)B^T P(x). \quad (3.7)$$

Concluded from [32], the state feedback control law (3.7) is one of the optimal control for the linear system (3.1) without any saturation constraint. The following theorem presents a criterion about the solution to Problem 1.

Theorem 3.5. *Let Assumption 3.1 be true. There exist positive scalars ϵ_0 and δ_0^* such that, for all $\epsilon \in (0, \delta_0^*]$ and $\delta_0 \geq \delta_0^*$, the low-and-high-gain state feedback control law (3.7) is a solution to Problem 1.*

Proof. To begin with, the cases of saturation and unsaturation are discussed respectively. For convenience, set $P(\epsilon) = P$ and $Q(\epsilon) = Q$.

Firstly, we choose the Lyapunov function $V(x) = x^T P x$. By calculating the derivative of $V(x)$ along the trajectory of closed-loop system, we have

$$\begin{aligned} \dot{V}(x) &= x^T (A^T P + P A) x + 2x^T P B \left(-(1 + \epsilon)B^T P x + g(x, t) \right) \\ &= -x^T Q x + x^T P B B^T P x + 2x^T P B \left(-(1 + \epsilon)B^T P x + g(x, t) \right) \\ &\leq -x^T Q x + 2x^T P B B^T P x + 2x^T P B \left(-(1 + \epsilon)B^T P x + g(x, t) \right). \end{aligned} \quad (3.8)$$

(1) The actuator is with saturation. Here, it is proved only when $(B^T P x)_i < 0$, where $(\cdot)_i$ denotes the i th element of vector (\cdot) .

When $1 + \epsilon \geq -(1 + \epsilon)B^T P x)_i \geq 1 + L\|x\| + D_0$, we arrive at

$$\begin{aligned} \left(-(1 + \epsilon)B^T P x + g(x, t) \right)_i &\geq 1, \quad \forall (x, t) \in \mathbb{R}^n \times \mathbb{R}^+, \\ \left(-(1 + \epsilon)B^T P x + g(x, t) \right)_i &= 1, \quad i = 1, 2, \dots, m, \quad \forall (x, t) \in \mathbb{R}^n \times \mathbb{R}^+, \end{aligned} \quad (3.9)$$

$$-1 \leq (B^T P x)_i \leq -\frac{1 + L\|x\| + D_0}{1 + \epsilon} \leq -\frac{1}{1 + \epsilon} < 0. \quad (3.10)$$

Thus, we get

$$\left(x^T P B \right)_i \left((B^T P x)_i + 1 \right) \leq 0. \quad (3.11)$$

Hence,

$$x^T P B B^T P x + 2x^T P B H \leq 2 \sum_{i=1}^m \left(x^T P B \right)_i \left((B^T P x)_i + 1 \right) < 0, \quad (3.12)$$

where $H = [1 \ \dots \ 1]^T$.

It follows from (3.8) that

$$\begin{aligned}\dot{V}(\mathbf{x}) &= -\mathbf{x}^T \mathbf{Q} \mathbf{x} + \mathbf{x}^T \mathbf{P} \mathbf{B} \mathbf{B}^T \mathbf{P} \mathbf{x} + 2 \sum_{i=1}^m \left(\mathbf{x}^T \mathbf{P} \mathbf{B} \right)_i \\ &\leq -\mathbf{x}^T \mathbf{Q} \mathbf{x} + 2 \sum_{i=1}^m \left(\mathbf{x}^T \mathbf{P} \mathbf{B} \right)_i \left(\left(\mathbf{B}^T \mathbf{P} \mathbf{x} \right)_i + 1 \right) \\ &< -\mathbf{x}^T \mathbf{Q} \mathbf{x} < 0.\end{aligned}\quad (3.13)$$

If $(\mathbf{B}^T \mathbf{P} \mathbf{x})_i < -1$, for each $(\mathbf{x}, t) \in \mathbb{R}^n \times \mathbb{R}^+$, it can be easily seen that $(-(1 + \epsilon) \mathbf{B}^T \mathbf{P} \mathbf{x} + \mathbf{g}(\mathbf{x}, t))_i \geq 1$, that is, $(-(1 + \epsilon) \mathbf{B}^T \mathbf{P} \mathbf{x} + \mathbf{g}(\mathbf{x}, t))_i = 1 (i = 1, 2, \dots, m)$. Then, we have

$$\dot{V}(\mathbf{x}) = \mathbf{x}^T (\mathbf{A}^T \mathbf{P} + \mathbf{P} \mathbf{A}) \mathbf{x} + 2 \sum_{i=1}^m \left(\mathbf{x}^T \mathbf{P} \mathbf{B} \right)_i \leq \mathbf{x}^T (\mathbf{A}^T \mathbf{P} + \mathbf{P} \mathbf{A}) \mathbf{x} - 2n < 0. \quad (3.14)$$

According to Assumption 3.1, we have $\mathbf{A}^T \mathbf{P} + \mathbf{P} \mathbf{A} < 0$ for any $\mathbf{P} > 0$.

When $-(1 + \epsilon) \leq (-1 + \epsilon) \mathbf{B}^T \mathbf{P} \mathbf{x}_i \leq -1 - L \|\mathbf{x}\| - D_0$, we obtain

$$\begin{aligned}\left(-(1 + \epsilon) \mathbf{B}^T \mathbf{P} \mathbf{x} + \mathbf{g}(\mathbf{x}, t) \right)_i &\leq -1, \quad \forall (\mathbf{x}, t) \in \mathbb{R}^n \times \mathbb{R}^+, \\ \left(-(1 + \epsilon) \mathbf{B}^T \mathbf{P} \mathbf{x} + \mathbf{g}(\mathbf{x}, t) \right)_i &= 1, \quad i = 1, 2, \dots, m, \quad \forall (\mathbf{x}, t) \in \mathbb{R}^n \times \mathbb{R}^+, \\ 1 &\geq \left(\mathbf{B}^T \mathbf{P} \mathbf{x} \right)_i \geq \frac{1 + L \|\mathbf{x}\| + D_0}{1 + \epsilon} \geq \frac{1}{1 + \epsilon} > 0.\end{aligned}\quad (3.15)$$

That is $(\mathbf{B}^T \mathbf{P} \mathbf{x})_i > 0$. Along the same line of the above proof, we can discuss the cases $0 < (\mathbf{B}^T \mathbf{P} \mathbf{x})_i \leq 1$ and $(\mathbf{B}^T \mathbf{P} \mathbf{x})_i > 1$, respectively. Hence, we can conclude that $\dot{V}(\mathbf{x}) < 0$ for $(\mathbf{B}^T \mathbf{P} \mathbf{x})_i > 0$.

(2) The actuator is not saturated. When $|(-1 + \epsilon) \mathbf{B}^T \mathbf{P} \mathbf{x}_i + (\mathbf{g}(\mathbf{x}, t))_i| < 1$, according to (3.8), we have

$$\begin{aligned}\dot{V}(\mathbf{x}) &= -\mathbf{x}^T \mathbf{Q} \mathbf{x} - 2 \mathbf{x}^T \mathbf{P} \mathbf{B} \mathbf{B}^T \mathbf{P} \mathbf{x} + 2 \mathbf{x}^T \mathbf{P} \mathbf{B} \mathbf{g}(\mathbf{x}, t) \\ &\leq -\mathbf{x}^T \mathbf{Q} \mathbf{x} + 2 \sum_{i=1}^m (\mathbf{g}(\mathbf{x}, t))_i - \left(\mathbf{B}^T \mathbf{P} \mathbf{x} \right)_i \left(\mathbf{B}^T \mathbf{P} \mathbf{x} \right)_i.\end{aligned}\quad (3.16)$$

Next, we discuss the following two cases.

If $|(B^T P x)_i| \geq |g_i|$, by noting $(B^T P x)_i(- (B^T P x)_i + (g(x, t))_i) < 0$, we obtain

$$\begin{aligned} \dot{V}(x) &= -x^T Q x - 2x^T P B \left(-(1 + \epsilon) B^T P x + g(x, t) + B^T P x \right) \\ &\leq -x^T Q x + 2 \sum_{i=1}^m \left(- (B^T P x)_i + (g(x, t))_i \right) \\ &\leq -x^T Q x \\ &< 0. \end{aligned} \quad (3.17)$$

If $|(B^T P x)_i| \leq |g_i|$, then

$$\begin{aligned} \dot{V}(x) &= -x^T Q x + 2x^T P B g(x, t) \\ &\leq -x^T Q x + 2 \sum_{i=1}^m \frac{|g_i|^2}{L} \\ &\leq -x^T Q x + 2 \frac{(L \|x\| + D_0)}{L} \\ &\leq - \left(\min(Q) - \frac{4L^2}{D_0} \right) \|x\|^2 + \frac{4D_0^2}{D_0}. \end{aligned} \quad (3.18)$$

Suppose

$$W_0 := \left\{ x \in \mathbb{R}^n : \|x\|^2 \leq \frac{4D_0^2}{D_0(1 + L + D_0)^2 - 4L^2} \right\}. \quad (3.19)$$

Taking $\epsilon = 4$, then all trajectories will enter into W_0 in finite time and remain thereafter for all $t \geq t^*$. Here, W_0 is an arbitrarily small set including the origin point, and t^* is a sufficiently large scalar.

Specifically, it follows from $D_0 = 0$ that $\dot{V}(x) < 0$, that is, $x = 0$ is globally asymptotically stable. To this end, the proof of this theorem is complete. \square

Remark 3.6. In this section, the practical stabilization problem is investigated for a general multidimensional system. From a practical point of view, it is more significant to consider the high-dimensional systems. It is worth mentioning that the system under consideration is comprehensive that includes the actuator saturation and the time-varying input disturbances. By using the Riccati equation approach, the low-and-high-gain state feedback control law is designed such that the global or semiglobal practical stabilization for the multidimensional system can be guaranteed. On the other hand, we are now researching into a method for the system with uncertainties, time-delay, and/or input disturbance in more general cases. The corresponding results will appear in the near future.

4. Conclusions

In this paper, we have made an attempt to investigate the practical stabilization problem for a class of system with actuator saturation and input additive disturbances. For the case of the input additive disturbance being bounded constant, the three-dimensional system has been studied where the system matrices satisfy a class of the controllability canonical form. Eight different forms of the system matrices have been discussed. Subsequently, by applying the Riccati equation approach and designing the linear state feedback control law, the sufficient conditions of the semiglobal practical stabilization or oscillation for the addressed systems have been established. For the case when the input additive disturbances are time-varying functions, by using of the Riccati equation approach as well as combining the low-gain linear state feedback and high-gain linear state feedback, a low-high-gain linear state feedback control law has been designed such that the global or semiglobal practical stabilization for a general multidimensional system with actuator saturation can be guaranteed. One of the future research topics would be the extension of the main results obtained in this paper to networked control systems [27, 33–36].

Acknowledgment

This work was supported by the National Natural Science Foundation of China under Grant 10771047.

References

- [1] A. T. Fuller, "In-the-large stability of relay and saturating control systems with linear controllers," *International Journal of Control*, vol. 10, pp. 457–480, 1969.
- [2] E. D. Sontag and H. J. Sussmann, "Nonlinear output feedback design for linear systems with saturating controls," in *Proceedings of the 29th IEEE Conference on Decision and Control*, pp. 3414–3416, Honolulu, Hawaii, USA, December 1990.
- [3] Z. Lin and A. Saberi, "Semi-global exponential stabilization of linear systems subject to input saturation via linear feedbacks," *Systems & Control Letters*, vol. 21, no. 3, pp. 225–239, 1993.
- [4] H. K. Khali, *Nonlinear Systems*, Prentice Hall, 3rd edition, 2002.
- [5] T. Hu and Z. Lin, *Control Systems with Actuator Saturation: Analysis and Design*, Birkhauser, Boston, Mass, USA, 2001.
- [6] Z. Lin and A. Saberi, "Semi-global exponential stabilization of linear discrete-time systems subject to input saturation via linear feedbacks," *Systems & Control Letters*, vol. 24, no. 2, pp. 125–132, 1995.
- [7] V. Kapila and K. Grigoriadis, *Actuator Saturation Control*, Marcel Dekker, New York, NY, USA, 2002.
- [8] S. Tarbouriech, G. Garcia, and A. H. Glattfelder, *Advanced Strategies in Control Systems with Input and Output Constraints*, vol. 346 of *Lecture Notes in Control and Information Sciences*, Springer, Berlin, Germany, 2007.
- [9] T. Hu and Z. Lin, "Robust stabilization of exponentially unstable linear systems with saturating actuators," in *Proceedings of the American Control Conference (ACC '99)*, pp. 3196–3200, San Diego, Calif, USA, June 1999.
- [10] H. Fang and Z. Lin, "Stability analysis for linear systems under state constraints," *Institute of Electrical and Electronics Engineers. Transactions on Automatic Control*, vol. 49, no. 6, pp. 950–955, 2004.
- [11] D. Fu, H. Liu, and B. Zhou, "Semi-global stabilization of a type of input systems with pole assurance," *Engineering Journal of Wuhan University*, vol. 41, no. 2, pp. 111–115, 2008.
- [12] X. Wu and Z. Lin, "Anti-windup in anticipation of actuator saturation," in *Proceedings of the 49th IEEE Conference on Decision and Control*, pp. 5245–5250, Atlanta, Ga, USA, December 2010.
- [13] S. Tarbouriech and F. Gouaisbaut, "Stabilization of quantized linear systems with saturations," in *Proceedings of the 49th IEEE Conference on Decision and Control*, pp. 3361–3366, Atlanta, Ga, USA, month year.

- [14] T. Hu, A. N. Pitsillides, and Z. Lin, "Null controllability and stabilization of linear systems subject to asymmetric actuator saturation," in *Proceedings of the 39th IEEE Conference on Decision and Control*, pp. 3254–3259, Sydney, Australia, December 2000.
- [15] Y. Cao, Z. Lin, and D. G. Ward, "An antiwindup approach to enlarging domain of attraction for linear systems subject to actuator saturation," *Institute of Electrical and Electronics Engineers. Transactions on Automatic Control*, vol. 47, no. 1, pp. 140–145, 2002.
- [16] T. Hu and Z. Lin, "Exact characterization of invariant ellipsoids for single input linear systems subject to actuator saturation," *Institute of Electrical and Electronics Engineers. Transactions on Automatic Control*, vol. 47, no. 1, pp. 164–169, 2002.
- [17] T. Hu and Z. Lin, "On the necessity of a recent set invariance condition under actuator saturation," in *Proceedings of the American Control Conference*, pp. 1210–1215, May 2002.
- [18] T. Hu and Z. Lin, "The equivalence of several set invariance conditions under saturation," in *Proceedings of the 41st IEEE Conference on Decision and Control*, pp. 4146–4147, December 2002.
- [19] Z. Wang, D. W. C. Ho, Y. Liu, and X. Liu, "Robust H_∞ control for a class of nonlinear discrete time-delay stochastic systems with missing measurements," *Automatica*, vol. 45, no. 3, pp. 684–691, 2009.
- [20] B. Shen, Z. Wang, H. Shu, and G. Wei, "On nonlinear H_∞ filtering for discrete-time stochastic systems with missing measurements," *Institute of Electrical and Electronics Engineers. Transactions on Automatic Control*, vol. 53, no. 9, pp. 2170–2180, 2008.
- [21] B. Shen, Z. Wang, H. Shu, and G. Wei, "Robust H_∞ finite-horizon filtering with randomly occurred nonlinearities and quantization effects," *Automatica*, vol. 46, no. 11, pp. 1743–1751, 2010.
- [22] Z. Wang, Y. Liu, and X. Liu, " H_∞ filtering for uncertain stochastic time-delay systems with sector-bounded nonlinearities," *Automatica*, vol. 44, no. 5, pp. 1268–1277, 2008.
- [23] Z. Wang, G. Wei, and G. Feng, "Reliable H_∞ control for discrete-time piecewise linear systems with infinite distributed delays," *Automatica*, vol. 45, no. 12, pp. 2991–2994, 2009.
- [24] Z. Wang, F. Yang, D. W. C. Ho, and X. Liu, "Robust H_∞ control for networked systems with random packet losses," *IEEE Transactions on Systems, Man, and Cybernetics*, vol. 37, no. 4, pp. 916–924, 2007.
- [25] Z. Wang, F. Yang, D. W. C. Ho, and X. Liu, "Robust H_∞ filtering for stochastic time-delay systems with missing measurements," *IEEE Transactions on Signal Processing*, vol. 54, no. 7, pp. 2579–2587, 2006.
- [26] L. Wu, X. Su, P. Shi, and J. Qiu, "A new approach to stability analysis and stabilization of discrete-time T-S fuzzy time-varying delay systems," *IEEE Transactions on Systems, Man, and Cybernetics*, vol. 41, no. 1, pp. 273–286, 2011.
- [27] H. Dong, Z. Wang, and H. Gao, "Robust H_∞ filtering for a class of nonlinear networked systems with multiple stochastic communication delays and packet dropouts," *IEEE Transactions on Signal Processing*, vol. 58, no. 4, pp. 1957–1966, 2010.
- [28] H. Fang and Z. Lin, "Global practical stabilization of planar linear systems in the presence of actuator saturation and input additive disturbance," *Institute of Electrical and Electronics Engineers. Transactions on Automatic Control*, vol. 51, no. 7, pp. 1177–1184, 2006.
- [29] H. Fang and Z. Lin, "A further result on global stabilization of oscillators with bounded delayed input," *Institute of Electrical and Electronics Engineers. Transactions on Automatic Control*, vol. 51, no. 1, pp. 121–128, 2006.
- [30] Y. Song, Y. Q. Gu, and M. Fei, "Stabilization for a class of second-order switched systems with saturation constrains," *Journal of Shanghai University*, vol. 13, no. 4, pp. 274–275, 2009.
- [31] A. Saberi, Z. Lin, and A. R. Teel, "Control of linear systems with saturating actuators," *Institute of Electrical and Electronics Engineers. Transactions on Automatic Control*, vol. 41, no. 3, pp. 368–378, 1996.
- [32] Z. Lin, "Global control of linear systems with saturating actuators," in *Proceedings of the 35th IEEE Conference on Decision and Control*, pp. 4357–4362, Kobe, Japan, December 1996.
- [33] B. Shen, Z. Wang, Y. S. Hung, and G. Chesi, "Distributed H_∞ filtering for polynomial nonlinear stochastic systems in sensor networks," *IEEE Transactions on Industrial Electronics*, vol. 58, no. 5, pp. 1971–1979, 2011.
- [34] B. Shen, Z. Wang, and X. Liu, "Bounded H_∞ synchronization and state estimation for discrete time-varying stochastic complex networks over a finite horizon," *IEEE Transactions on Neural Networks*, vol. 22, no. 1, pp. 145–157, 2011.
- [35] B. Shen, Z. Wang, and Y. S. Hung, "Distributed H_∞ -consensus filtering in sensor networks with multiple missing measurements: the finite-horizon case," *Automatica*, vol. 46, no. 10, pp. 1682–1688, 2010.

- [36] H. Dong, Z. Wang, D. W. C. Ho, and H. Gao, "Variance-constrained H_∞ filtering for a class of nonlinear time-varying systems with multiple missing measurements: the finite-horizon case," *IEEE Transactions on Signal Processing*, vol. 58, no. 5, pp. 2534–2543, 2010.

Research Article

Geometric Buildup Algorithms for Sensor Network Localization

Zhenzhen Zheng,¹ Xinlong Luo,² and Zhijun Wu³

¹ Department of Mathematics, University of California, Irvine, CA 92697, USA

² School of Information and Communication Engineering, Beijing University of Posts and Telecommunications, Beijing 100876, China

³ Department of Mathematics, Iowa State University, Ames, IA 50011, USA

Correspondence should be addressed to Zhijun Wu, zhijun@iastate.edu

Received 6 June 2011; Revised 22 August 2011; Accepted 22 August 2011

Academic Editor: Jinling Liang

Copyright © 2012 Zhenzhen Zheng et al. This is an open access article distributed under the Creative Commons Attribution License, which permits unrestricted use, distribution, and reproduction in any medium, provided the original work is properly cited.

We present a geometric buildup algorithm for solving the sensor network localization problem with either accurate or noisy distance data. The algorithm determines the locations of the sensors, one at a time, by using the distances between the determined sensors and the undetermined ones. Each time, only a small system of distance equations needs to be solved and therefore, in an ideal case when the required distances are available for every sensor to be determined, the computation can be completed in n steps if n sensors are to be determined. An algorithm with two buildup phases is also implemented to handle not only noisy but also sparse distance data with for example only a few distant anchors. We show our test results and compare them with other approaches.

1. Introduction

Ad hoc wireless sensor networks consist of a large number of spatially distributed sensor nodes that communicate with their nearby sensors within a radio range [1, 2]. The sensor data are relevant only if the sensors' locations are known. The expensive GPS (Global Positioning System) may locate only some of the sensors (called anchors). Most sensors can be located by means of some distance information obtained from the radio signals that the sensors receive [1]. The problem of finding the locations of the sensors given a few anchors and some local distance information among the sensors is called the sensor network localization problem.

Sensor network localization has been applied to many application fields, including environmental studies such as monitoring environmental conditions [3, 4], health cares such as patient tracking [5], and military applications such, as battlefield surveillance [6]. For example, [2, 7] mention that Southern California Edison's Nuclear Generating Station in San Onofre, Calif, USA has deployed wireless mesh-networked sensors from Dust Networks Inc.

to obtain real-time trend data. These data are used to predict which motors are about to fail, so they could be preemptively rebuilt or replaced during scheduled maintenance periods. Implementation of a sensor localization algorithm could provide a service that eliminates the need to record every sensor's location and its associated ID number in the network [2].

Mathematically, the sensor network localization problem can be described as follows. Assume that there are m anchors whose locations denoted by $a_k \in \mathcal{R}^2$, $k = 1, \dots, m$, are known and $n - m$ sensors whose locations denoted by $x_j \in \mathcal{R}^2$, $j = m + 1, \dots, n$ need to be decided. For a pair of sensors x_i and x_j , let their Euclidean distance be denoted by $d_{i,j}$. Similarly, let $d_{i,k}$ denote the Euclidean distance between an anchor a_k and a sensor x_i . Let N_x and N_a be two sets of node pairs,

$$\begin{aligned} N_x &= \{ (i, j) : \|x_i - x_j\| = d_{i,j} < rd \}, \\ N_a &= \{ (i, k) : \|x_i - a_k\| = d_{i,k} < rd \}, \end{aligned} \quad (1.1)$$

where $\|\cdot\|$ represents the Euclidean norm and rd is a fixed parameter called radio range. The sensor network localization problem can be formulated as a 2D distance geometry problem, to find the vectors $x_i \in \mathcal{R}^2$ for all $i = m + 1, \dots, n$ such that

$$\begin{aligned} \|x_i - x_j\|^2 &= d_{i,j}^2 \quad \forall (i, j) \in N_x, \\ \|x_i - a_k\|^2 &= d_{i,k}^2 \quad \forall (i, k) \in N_a. \end{aligned} \quad (1.2)$$

In practice, the distance information is available only if the distance of two nodes is within a certain radio range. Therefore, the available distances are usually sparse, that is, only a small subset of all distances among the nodes is available. The distance data contains errors as well due to the accuracy of the measurements, the power of the sensors, and some other environmental factors. A distance geometry problem with sparse and inexact distances has been proved to be difficult to solve in general [8–10].

More specifically, if exact distances for all pairs of nodes are available, a distance geometry problem can be solved in polynomial time by using for example a singular value decomposition algorithm in $\mathcal{O}(n^2)$ [9] or a geometric buildup algorithm in $\mathcal{O}(n)$ [11], where n is the number of nodes to be determined and $\mathcal{O}(\cdot)$ is the conventional expression for time complexity. If only a sparse set of distances is given, the problem is NP-hard in general [8], even if small distance errors are allowed [10].

Much work has been done on the sensor network localization problem. Biswas et al. [1, 12] proposed an SDP (semidefinite programming) approach to the problem. Wang et al. [13] made further SDP relaxations and developed NSDP (node-based SDP) and ESDP (edge-based SDP) algorithms for large-scale applications. Nie [14] presented an SOS (sum of squares) approach by formulating the problem as a minimization problem for a sum of squares. Tseng [15] developed an SOCP (second-order cone programming) relaxation method. Recent works also include Carter et al. [2], the SFS DP (sparse variant of FSDP [1]) approach by Kim et al. [16], Zhu et al. [17], the LPCGD (log-barrier penalty coordinate gradient descent) approach by Pong and Tseng [18], and the SNLSDPclique approach by Krislock and Wolkowicz [19, 20].

We investigate the solution of the sensor network localization problem within a geometric buildup framework. A basic geometric buildup algorithm [11] was proposed for the

solution of a 3D distance geometry problem with exact distances. The work was later extended to problems with sparse distances [21–23], inexact distances [24], and distance bounds [25]. All these works were applied to protein structure determination problems, which are to determine a set of points given a set of distances between the points. The idea of geometric buildup is to determine the points, one at a time, using the distances between the determined points and the undetermined ones. The algorithm can be applied to distance geometry problems in any finite dimensional Euclidean space including the sensor network localization in 2D.

In every buildup step, for determining a point, a small system of distance equations needs to be solved. However, the point may be overdetermined for there may be more equations than the coordinates for the point. On the other hand, the distances may have errors and the equations are most likely to be inconsistent. To overcome this difficulty, a least-squares approximation method has been developed for solving the distance equations [24]. The method employs a low-rank matrix approximation scheme [26], which requires the singular value decomposition for a small distance matrix. Here, our algorithm is different from [24] in the approximation scheme. We implement a low-rank positive semidefinite approximation scheme [27], which requires a spectral decomposition and guarantees a best-possible approximation to the solution of the distance equations in a least-squares sense.

The availability of an initial set of determined points can be important for a geometric buildup algorithm to start and succeed. Fortunately, for sensor network localization, there is usually a set of anchor nodes that can be used as an initial set of nodes. However, if there are only a few anchors scattered widely in space, the chance is that there may not be many sensors with (at least three) distances to these anchors and the algorithm may be able to determine only a small set of sensors. For this reason, we have also implemented a two-phase buildup algorithm. In the first phase, we determine as many sensors as possible starting with the initial anchors. In the second phase, from the undetermined sensors, if there are any, we find a clique of sensors, that is, a subset of sensors with all distances among them available. We position the sensors in the clique in space (which is possible using their distances) and start from them to determine the remaining sensors. In this way, we can have more sensors determined than a single phase algorithm.

This paper is organized as follows. In Section 2, we present several possible versions of geometric buildup algorithms for sensor network localization. In Section 3, we present the numerical results for a set of simulated sensor network localization problems with exact and inexact sparse distances. We conclude the paper and make some remarks in Section 4.

2. The Geometric Buildup Algorithms

In this section, we present three versions of geometric buildup algorithms for sensor network localization. Three cases of problems are concerned (1) when exact distances are available, (2) when distances have errors, and (3) when there are only a few distant anchors. A geometric buildup algorithm, named as basic, extended, and two-phase geometric buildup algorithms, respectively, is described for each of the three cases.

2.1. The Basic Geometric Buildup Algorithm

When a set of exact distances is given, that is, the distances in (1.1) is accurate, a basic geometric buildup algorithm can be applied. The algorithm works as follows. It first takes the anchors as the initial set of determined sensors. Then, for any undetermined sensor j , it

Input: The positions of the anchors, the distances $d_{i,j}$, $(i,j) \in N_x \cup N_a$.
Output: The positions of a set of determined sensors.
Step 1: Let the anchors be the initial set of determined sensors.
Step 2: **Repeat:**
 For each undetermined sensor j :
 If a basis set of determined sensors is found for sensor j ,
 determine sensor j by solving the linear system (2.2).
 End
 End
If no sensor can be determined in the loop, stop.
If all sensors are determined, stop.

Algorithm 1: The basic geometric buildup algorithm.

tries to find three determined sensors that are not collinear but have distances to sensor j . We call these three determined sensors a basis set of sensors for sensor j . Let $x_i = (x_{i,1}, x_{i,2})^T$ ($i = 1, 2, 3$) be the coordinate vectors of the three determined sensors. Given the distances $d_{i,j}$ ($i = 1, 2, 3$), the coordinate vector $x_j = (x_{j,1}, x_{j,2})^T$ of sensor j can be determined by using the following system of equations:

$$\|x_i\|^2 - 2x_i^T x_j + \|x_j\|^2 = d_{i,j}^2, \quad i = 1, 2, 3. \quad (2.1)$$

Subtracting equation i from equation $i+1$ ($i = 1, 2$) results in a linear system of equations

$$A x_j = b, \quad (2.2)$$

where

$$A = -2 \begin{bmatrix} (x_2 - x_1)^T \\ (x_3 - x_2)^T \end{bmatrix}, \quad b = \begin{bmatrix} (d_{2,j}^2 - d_{1,j}^2) - (\|x_2\|^2 - \|x_1\|^2) \\ (d_{3,j}^2 - d_{2,j}^2) - (\|x_3\|^2 - \|x_2\|^2) \end{bmatrix}. \quad (2.3)$$

The points x_1, x_2, x_3 are not collinear, so the coefficient matrix A is nonsingular and the linear system (2.2) has a unique solution. An outline of the basic geometric buildup algorithm is given in Algorithm 1. Note that if there are at least three anchors in the network and the distances are exact, and if in every step, an undetermined sensor and a basis set of determined sensors associated with it can be found, then the basic geometric buildup algorithm can solve the problem in $O(n)$ computation time, where n is the total number of sensors to be determined.

2.2. The Extended Geometric Buildup Algorithm

Note that for every undetermined sensor, there may be more than three determined sensors that have distances to it. Therefore, there may be more than three distance equations in (2.1) for the sensor to satisfy. Of course, if the distances are accurate, or in other words, are exact, only three equations need to be solved as done in the basic algorithm, while all other

equations are satisfied automatically. However, in practice, the distances may have errors and therefore, the distance equations may not be consistent, and satisfying three of them does not necessarily satisfy all the equations. Besides, (2.1) cannot be reduced to (2.2) any more because there may not be a solution to the equations in (2.1) or, in other words, the equations may never hold and hence cannot add or subtract. The extended geometric buildup algorithm is developed to overcome these difficulties.

An extended geometric buildup algorithm works as follows. It again takes the anchors as the initial set of determined sensor. Then, for each undetermined sensor, it finds all the determined sensors that have distances to the undetermined sensor. If there are at least three such determined sensors and if they are not collinear, then the algorithm tries to find the coordinates for the undetermined sensor by solving a system of distance equations corresponding to all these determined sensors. In particular, since the equations may not be consistent, they are solved approximately in a least-squares sense as described in the following.

Let $x_{+1} = (x_{+1,1}, x_{+1,2})^T$ be the coordinate vector of the sensor to be determined. Let $x_i = (x_{i,1}, x_{i,2})^T$ ($i = 1, \dots, n$) be the coordinate vectors of the determined sensors to be used for the determination of x_{+1} . Let $d_{i,+1}$ be the distances from x_i to x_{+1} , $i = 1, \dots, n$. Then the distance equations to be solved are

$$\|x_i\|^2 - 2x_i^T x_{+1} + \|x_{+1}\|^2 = d_{i,+1}^2, \quad i = 1, \dots, n. \quad (2.4)$$

The equations can be solved by using for example a standard nonlinear least-squares method, but we implement a method similar to that proposed in [24] and obtain a more direct solution to the equations. Instead of working on the system in (2.4), we expand it to the following system:

$$\|x_i\|^2 - 2x_i^T x_j + \|x_j\|^2 = d_{i,j}^2, \quad i, j = 1, \dots, n+1. \quad (2.5)$$

Note that $d_{i,j}$, $i, j = 1, \dots, n+1$ in the added equations may or may not be available in the given distance data, but they can be computed if some of them are not because x_i , $i = 1, \dots, n$ are already known. We then consider all x_i , $i = 1, \dots, n+1$ as unknowns and determine them all by solving the system of equations in (2.5). Since the relative positions of these sensors are invariant under any translation and orthogonal transformation, we can set a reference system so that the sensor to be determined is located at the origin or, in other words, $x_{+1} = (0, 0)^T$. It follows that $\|x_i\| = d_{i,+1}$, $\|x_j\| = d_{j,+1}$ and

$$d_{i,+1}^2 - 2x_i^T x_j + d_{j,+1}^2 = d_{i,j}^2, \quad i, j = 1, \dots, n. \quad (2.6)$$

Define a coordinate matrix X and an induced distance matrix D as follows:

$$X = \{x_{i,k} : i = 1, \dots, n+1, k = 1, 2\},$$

$$D = \left\{ \left(\frac{d_{i,+1}^2 - d_{i,j}^2 + d_{j,+1}^2}{2} : i, j = 1, \dots, n \right) \right\}. \quad (2.7)$$

It is easy to verify that $X X^T = D$, which has been widely studied in the classical multidimensional scaling or "MDS" [27–29]. If the distances have errors, the system $X X^T = D$ may not be consistent. It is natural to consider a least-squares problem

$$\min_{X \in \mathcal{R}^{n \times 2}} \left\| D - X X^T \right\|_F, \quad (2.8)$$

where $\|\cdot\|_F$ is the matrix Frobenius norm. [24] applied the best rank r matrix approximation coming from the classical Eckart-Young Theorem [26], which involves the singular value decomposition. Here, we apply a best positive semidefinite approximation which involves the spectral decomposition. The solution to the problem in (2.8) can be obtained from the following theorem.

Theorem 2.1 (see [19, 27]). *Let $M = \sum_{i=1}^n u_i u_i^T$ be the spectral decomposition of the symmetric matrix M , where $\lambda_1 \geq \dots \geq \lambda_n$. Then $\widetilde{M} = \sum_{i=1}^r \lambda_i^+ u_i u_i^T$, where $\lambda_i^+ = \max\{0, \lambda_i\}$, is the best positive semidefinite approximation to the following problem,*

$$\begin{aligned} \min_{\widetilde{M}} \quad & \left\| M - \widetilde{M} \right\|_F, \\ \text{subj. to} \quad & \text{rank}(\widetilde{M}) \leq r, \quad \widetilde{M} \geq 0. \end{aligned} \quad (2.9)$$

Now suppose that the spectral decomposition of D is $U \Lambda U^T$, where the diagonal entries of Λ are in a decreasing order. Let $V = U(:, 1 : 2)$ and Σ be the diagonal matrix with $\Sigma_{ii} = \max\{0, \Lambda_{ii}\}$, where $i = 1, 2$. Then $X = V \Sigma^{1/2}$ solves the problem in (2.8), and the coordinates of all the sensors are obtained, with the sensor to be determined located at $(0, 0)^T$. To obtain the coordinates of this sensor in the original reference system, it can be transformed along with other sensors so that the recalculated coordinates of those sensors agree with their old ones as much as possible. The latter can be done by minimizing the so-called RMSD (root-mean-square deviation) of the coordinates (details at the end of this subsection).

It seems that the system of equations in (2.4) is simpler and easier to solve than that in (2.5), and the coordinates of x_i , $i = 1, \dots$, are also recalculated in (2.5). It turns out that solving (2.5) instead of (2.4) is critical for the stability of the buildup algorithm. The solution to the system in (2.4) depends on previously calculated coordinates x_i , $i = 1, \dots$, and, therefore, may inherit errors from previous calculations. If such errors are continuously passed down to later calculations, the buildup algorithm is most likely to end up with an incorrect set of coordinates for the sensors. In contrast, the solution to the system in (2.5) depends only on the distances among the sensors, most of which are given in the original distance data. The recalculation of the coordinates x_i , $i = 1, \dots$, also "cutoffs" possible propagations of calculation errors, making the algorithm much more stable [24].

As we have mentioned above, the coordinates of x_i , $i = 1, \dots, + 1$ are determined in an independent reference system. In order to move the coordinates back to their original reference system, we need to make a proper translation and orthogonal transformation for the coordinates. Let $X \in \mathcal{R}^{n \times 2}$ and $Y \in \mathcal{R}^{n \times 2}$ be the previously calculated and recalculated

coordinate matrices of the determined sensors, respectively. We first calculate the geometric centers of X and Y ,

$$X_c = \frac{1}{n} \sum_{i=1}^n X(i,:), \quad Y_c = \frac{1}{n} \sum_{i=1}^n Y(i,:), \quad (2.10)$$

and then update X and Y :

$$\begin{aligned} X &:= X - \mathbf{1}_n X_c, \\ Y &:= Y - \mathbf{1}_n Y_c, \end{aligned} \quad (2.11)$$

where $\mathbf{1}_n$ is an $n \times 1$ vector with all elements 1s. After such a translation, the geometric centers of X and Y coincide at the origin. We then implement an orthogonal transformation on Y so that Y is aligned with X as much as possible. This can be done by choosing an appropriate orthogonal transform Q so that the root-mean-square deviation of X and YQ are minimized, that is,

$$\min_{Q: Q Q^T = I} \text{RMSD}(X, Y) = \frac{\|X - YQ\|_F}{\sqrt{n}}, \quad (2.12)$$

where $Q \in \mathcal{R}^{2 \times 2}$ is an orthogonal matrix. Let $C = Y^T X$, and let $U \Sigma V^T$ be the singular value decomposition of C . It follows that $Q_{\text{opt}} = U V^T$ is the optimal matrix of the above problem [30]. The coordinates of the determined sensors can then be obtained by setting

$$X := Y Q_{\text{opt}} + \mathbf{1}_n X_c, \quad (2.13)$$

and the coordinates of the sensor $i+1$ by

$$x_{i+1}^T := ((0,0) - Y_c) \times Q_{\text{opt}} + X_c. \quad (2.14)$$

An outline of the extended geometric buildup algorithm is given in Algorithm 2.

2.3. The Two-Phase Geometric Buildup Algorithm

The basic and extended geometric buildup algorithms both start building up from the anchors. If only a few anchors are available and if the distance data is also very sparse, the algorithms may not be able to determine any sensors since they may not be able to find an undetermined sensor that has at least three given distances to the anchors. Even if the algorithms can proceed, they may not be able to determine all the sensors if some undetermined sensors do not have enough required distances to the determined sensors. Here, we present a two-phase geometric buildup algorithm to deal with these situations.

In Phase 1, we proceed with the extended geometric buildup algorithm until no sensors can be determined. In Phase 2, we find, in the undetermined sensors, a subset of at least three sensors where the distances between every pair of sensors are given (details are in

Input: The positions of the anchors, the distances $d_{i,j}$, $(i,j) \in N_x \cup N_a$.
Output: The positions of a set of determined sensors.
Step 1: Set the anchors to be the initial set of determined sensors.
Step 2: **Repeat:**
 For each undetermined sensor:
 If the sensor has distances to (≥ 3) required determined sensors,
 determine the positions of all $+ 1$ sensors by solving (2.8),
 and update the coordinates of all $+ 1$ sensors by proper
 translation and orthogonal transformation.
 End
 End
If no sensor can be determined in the loop, stop.
If all the sensors are determined, stop.

Algorithm 2: The extended geometric buildup algorithm.

Input: The set of undetermined sensors (\mathcal{I}_2) in Phase 1.
Output: An initial set of sensors (\mathcal{I}_1) with distances between each other known.
Step 1: Choose the first element in \mathcal{I}_2 to be the first element in \mathcal{I}_1 .
Step 2: **Repeat:**
 For each element in \mathcal{I}_2 :
 If it has given distances to all the elements in \mathcal{I}_1 ,
 add it into \mathcal{I}_1 .
 End
End

Algorithm 3: Choose an initial set in Phase 2.

Algorithm 3 “choose an initial set in Phase 2”). More discussions on finding a clique can be found in [31, 32], and so forth. If such a set of sensors, say $+ 1$ sensors, are found, a system of distance equations as in (2.5) can be formed, and the positions of the sensors can be determined by solving these equations in the same way as we described in the previous subsection: we first set $x_{+1} = (0,0)^T$. We then define X and D as in (2.7). Let the spectral decomposition of D be $U \Lambda U^T$, where the diagonal entries of Λ are in a decreasing order. Let $V = U(:, 1 : 2)$ and Σ be the diagonal matrix with $\Sigma_{ii} = \max\{0, \Lambda_{ii}\}$, where $i = 1, 2$. Then $X = V \Sigma^{1/2}$ gives the positions of the rest of the sensors. Once the positions of these sensors are determined, we can use them as an initial set of sensors to start the extended geometric buildup algorithm again. Upon finishing, another set of determined sensors is obtained.

Hopefully, the two sets of sensors determined in Phases 1 and 2 have an overlapping subset of at least three sensors, say k sensors. Let $X \in \mathcal{R}^{k \times 2}$ and $Y \in \mathcal{R}^{k \times 2}$ be the coordinate matrices of these sensors obtained in Phases 1 and 2, respectively. We can then make a proper translation and orthogonal transformation so that the root-mean-square deviation of X and Y are minimized. An outline of the two-phase buildup algorithm is given in Algorithm 4. Note that the parameter TH is a threshold used in the algorithm. If the percentage of the undetermined sensors in Phase 1 is greater than TH, the algorithm enters Phase 2, otherwise it stops, leaving a few sensors undecided. In principle, if there are a few sensors without

Input: The positions of the anchors, the distances $\bar{d}_{i,j}$, $(i,j) \in N_x \cup N_a$.

Output: The positions of a set of determined sensors.

Step 1: **Phase 1:**

Set the anchors to be the initial set of sensors.

Apply the extended geometric buildup algorithm.

Step 2: **If** the percentage of the undetermined sensors is greater than TH.

Phase 2:

Find and determine an initial set of sensors.

Apply the extended geometric buildup algorithm.

Step 3: Align the sensors determined in the two phases.

Algorithm 4: The two-phase geometric buildup algorithm.

enough distance constraints (e.g., each with fewer than three distances), they are considered to be undecidable.

3. Numerical Results

In this section, we present some numerical results from applying the two-phase geometric buildup algorithm (abbreviated as BU) to a set of test problems for sensor network localization. The test problems were generated in a similar way as used in [1]. We randomly generate n points with a uniform distribution in a square of size 1×1 centered at the origin. Without loss of generality we choose the first m points to be the anchors. We compute the distances $\bar{d}_{i,j}$ between every pair of sensors, but select only those less than the given radio range rd . We also add a multiplicative random noise to every selected distance,

$$\bar{d}_{i,j} = \bar{d}_{i,j}(1 + nf \cdot \text{randn}(1)), \quad (3.1)$$

where nf is a specified noisy factor, and $\text{randn}(1)$ is a standard Gaussian random variable. We set the threshold $TH = 0.1$. The 10% threshold for starting Phase II is indeed arbitrary. It was used for our testing purposes. In real applications, it may be set to a practically acceptable value. That is, if the percentage is lower than that value, the algorithm can terminate.

The output includes three parameters and all of our outputs are the average results from five independent test problems. One parameter is \mathbb{T} , the average CPU time in seconds over five cases except the time to generate the test problems. The buildup algorithm tries to determine all the points, but may terminate with only a subset of points as determined. In the latter case, we use another parameter NumUndet to report the average number of undetermined sensors. This is reasonable because there could be cases that some points are not determinable uniquely, for example, when a point has only one or two distances. If the undetermined points do have more than two distances, we would suggest using a general optimization algorithm to followup. However, in this paper, we have not included followup optimization, for we want to evaluate the performance of the buildup algorithm only. The last parameter is the RMSD value, measuring the average root-mean-square deviation of

Table 1: Input and output of the two-phase geometric buildup algorithm.

Input:
m : number of anchors.
n : number of all the sensors, including anchors.
$\mathbb{P} \mathbb{P}_{n \times 2}$: original coordinates matrix of all sensors.
rd: radio range.
nf :noise factor: $\bar{d}_{i,j} = \bar{d}_{i,j}(1 + \text{nf} \cdot \text{randn}(1))$.
Output:
T: average CPU time in seconds over five cases except the time to generate the test problems.
NumUndet: average number of undetermined sensors.
RMSD: average root-mean-square deviation defined in (3.2).

Table 2: Example 3.1: problems with exact distances.

Approach	n	m	rd	NumUndet	RMSD	T (sec.)
BU	500	50	0.1	1	37e-16	0.25
SFSDP	500	50	0.1	0	47e-3	13.1
SFSDP	500	50	0.3	0	29e-7	7.6
SNLSDPclique	500	50	0.1	0.4	1e-14	0.4
BU	1000	100	0.1	0	46e-16	0.6
SFSDP	1000	100	0.1	0	34e-4	22.7
SFSDP	1000	100	0.3	0	22e-7	16.0
SNLSDPclique	1000	100	0.1	0	4e-15	0.7
BU	2000	100	0.1	0	13e-15	7.0
SFSDP	2000	100	0.1	0	77e-5	42.3
SFSDP	2000	100	0.3	0	52e-7	34.9
SNLSDPclique	2000	100	0.1	0	1e-14	1.8
BU	4000	100	0.06	0	75e-16	9.4
SFSDP	4000	100	0.06	0	21e-3	317.8
SFSDP	4000	100	0.1	0	19e-4	109.2
SNLSDPclique	4000	100	0.06	0	3e-14	3.1

the calculated and actual locations of the determined sensors:

$$\text{RMSD} = \left(\frac{1}{p} \sum_{i=1}^p \|x_i - \bar{x}_i\|^2 \right)^{1/2}, \quad (3.2)$$

where p is the number of the determined sensors, x_i and \bar{x}_i are the true and calculated locations of the determined sensors, respectively. For convenience, we list all the input and output parameters in Table 1. Note that as an input the original coordinates matrix of all sensors (i.e., " $\mathbb{P} \mathbb{P}_{n \times 2}$ ") is used only to generate distances we need and evaluate the accuracy of the algorithms in numerical simulations.

All our calculations are done in MATLAB 7.9.0 (R2009b) on a Dell xps M1330 laptop with 2.00 GHz CPU and 3.00 GB memory.

Table 3: Large-scale problems with exact distances.

Approach	n	m	rd	NumUndet	RMSD	T (sec.)
BU	5000	100	0.06	0	$1.1e-15$	18.0
	6000	200	0.05	0	$7.3e-16$	17.9
	7000	200	0.05	0	$9.9e-16$	28.4
	8000	300	0.04	0	$7.2e-16$	32.1
	9000	300	0.04	0	$7.2e-16$	43.7
	10000	300	0.04	0	$8.1e-16$	51.9
SNLSDPclique	10000	300	0.04	0	$5e-14$	16.3

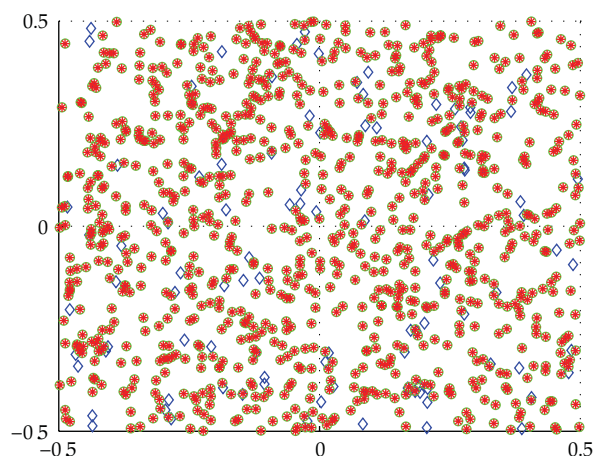


Figure 1: A network determined by the geometric buildup algorithm. $n = 1000$, $m = 100$, $rd = 0.1$, $nf = 0$. The (blue) diamonds refer to the positions of the anchors; the (green) circles to the original locations of the unknown sensors; the (red) asterisks to their estimated positions from the geometric buildup algorithm.

3.1. Problems with Exact Distances

Example 3.1. We have generated a set of sensor networks with 500, 1000, 2000, and 4000 nodes, respectively. We downloaded the code “SFSDP V111” of the SFSDP approach [16] from <http://www.is.titech.ac.jp/~kojima/SFSDP/SFSDP.html>. In Table 2, the “RMSD” of SFSDP are the average results over five cases without post-refinement of locations of sensors by the MATLAB function “lsqnonlin”. The “T” of SFSDP is the average CPU time consumed by SeDuMi with the same accuracy parameter $\text{pars.eps} = 1.0e-5$ as [16]. The numerical results in Table 2 show that for these problems with exact distances, the SFSDP approach performs well when rd is relatively larger, while the BU algorithm can find solutions to the problems with smaller RMSD values in shorter running time with fewer distance data (i.e., smaller rd). Figure 1 shows a graph of 1000 node network determined by the geometric buildup algorithm and all the sensors are accurately positioned.

We have also tested some larger-scale problems with exact distances. The results for each problem size are obtained and shown in Table 2. Note that in particular, a sensor network of 10000 nodes was solved by the geometric buildup algorithm in less than 1 minute.

Table 4: Example 3.2.

n	m	rd	nf	NumUndet	RMSD	T (sec.)
50	3	0.3	0	7.4	$6.0e-16$	0.04
50	3	0.35	0	3.8	$4.5e-16$	0.05

Table 5: Example 3.3.

Approach	n	m	rd	nf	NumUndet	RMSD	Time ^a
BU ^b					12.2	$8.0e-16$	1 sec
SOS ^c	500	4	0.3	0	0	$2.9e-6$	85 min
ESDP ^d					0	$1e-6$	30 sec

^aThis time indicates all the running time including that to generate problems.

^bBU was implemented on a laptop with 3.00 GB memory and 2.00 GHz CPU.

^cSOS [14] was implemented on a Linux machine with 0.98 GB RAM and 1.46 GHz CPU. The “RMSD” and “Time” of SOS come from [14].

^dESDP [13] was implemented on a laptop with 1.99 GB RAM and 1.06 GHz CPU. The “RMSD” and “Time” of ESDP come from [13].

Recently Krislock and Wolkowicz [19, 20] proposed an SNLSDPclique approach which is very efficient for noiseless problems. We also ran “SNLSDPclique-0.2” downloaded from <http://orion.math.uwaterloo.ca/~hwolkowicz/henry/software/EDM.shtml> and present the results in Tables 2 and 3. We find that in these cases when the sensor network is relatively small (e.g., $n = 500, 1000$), the two algorithms perform very closely and the BU algorithm is a little more accurate than the SNLSDPclique algorithm (note that these results of SNLSDPclique have been very accurate); when the sensor network is relatively big (e.g., $n \geq 2000$), the SNLSDPclique algorithm runs faster than the BU algorithm and the BU algorithm is still a little more accurate. We will further demonstrate the performance behaviors of these two algorithms on the noisy problems in Table 7.

3.2. Problems with a Few Anchors

Example 3.2. We have also tested a special network generated by [1, 12]. This network consists of 50 sensors, including 3 anchors. Exact distances are assumed and therefore $nf = 0$. The radio range rd takes values from 0.2 to 0.35. The average performance results for $rd = 0.3, 0.35$ are listed in Table 4. We can see that the problems were solved in less than 1 second. Note that for each rd in these tests, in two runs only Phase 1 was executed, while in the other three runs Phase 2 was also invoked. It showed that sometimes Phase 2 was necessary for sparse distance data. However, when we reduced rd to 0.25 or 0.2, the distances became very sparse, and even in Phase 2, only a few sensors could be determined.

Example 3.3. Another problem we have tested comes from [14]. We have randomly generated 500 sensors $x_1^*, x_2^*, \dots, x_{500}^*$ and the anchors were chosen to be the four points at $(\pm 0.45, \pm 0.45)$. The distance set A was generated as follows. Initially, set $A = \emptyset$. Then for each i from 1 to 500, compute the set $I_i = \{j : \|x_i^* - x_j^*\|_2 \leq 0.3, j \geq i\}$; if $|I_i| \geq 10$, let A_i be the subset of I_i consisting of the 10 smallest integers; otherwise, let $A_i = I_i$; then let $A = A \cup \{(i, j) : j \in A_i\}$. The distance set B is chosen such that $B = \{(i, k) : \|x_i^* - a_k^*\|_2 \leq 0.3\}$, that is, every anchor is connected to all the sensors that are within distance 0.3. The whole distance set is $A \cup B$. Since there are no noises, $nf = 0$.

Table 6: Example 3.4.

n	m	rd	nf	NumUndet	RMSD of BU ^a	T (sec.)	RMSD of ESDP ^a
1000	100	0.06	0	38.6	$3.2e-16$	2.2	$2e-3$
1000	100	0.06	0.001	26.2	$4.7e-3$	2.1	$3e-3$
1000	100	0.06	0.01	36.8	$3.3e-2$	2.5	$2e-2$
4000	400	0.035	0	5.6	$3.2e-16$	41.3	$1e-3$
4000	400	0.035	0.001	4	$3.9e-3$	40.7	$8e-4$
4000	400	0.035	0.01	3.2	$1.2e-2$	40.8	$3e-2$

^aRMSD of ESDP is obtained by implementing the steepest descent local search refinement for noisy sensor network problems. RMSD of BU is obtained without postrefinement. The RMSD values of ESDP come from [13].

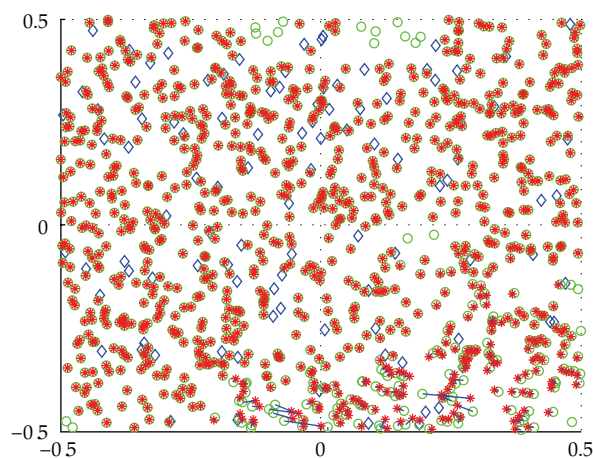


Figure 2: Graphical display of a sensor network with $n = 1000$, $m = 100$, $rd = 0.06$, $nf = 0.001$. The (blue) diamonds refer to the positions of the anchors; the (green) circles to the original locations of the unknown sensors; the (red) asterisks to their estimated positions by BU. The discrepancies between the original and the estimated points are indicated by the solid lines. $RMSD = 5.9e-3$.

In this problem, the four anchors are far away from each other. If one unknown sensor has distances to at least three of them, the radio range has to be at least the distance from one of them to the origin (≈ 0.6364), which is not possible. Therefore, the geometric buildup algorithm has to go to Phase 2 to solve the problem. The average performance results are listed in Table 5. We also list the results of the SOS approach [14] and the ESDP approach [13] in Table 5. Since the SOS code is not published online and the published ESDP code implements the steepest descent local search refinement, while the BU algorithm does not implement any postrefinement, we decided to directly cite their original results. From Table 5 we see that on this test problem the BU algorithm outperforms the SOS approach in the accuracy and running time and it outperforms the ESDP approach in the accuracy at least.

3.3. Problems with Noisy Distances

Example 3.4. We have also tested a set of problems with a large fraction of anchors but low distance noises (e.g., $m = 0.1n$ and $nf \leq 0.01$). These problems are mid- to large-scale, tested by SOCP [15], ESDP [13], and LPCGD [18]. The parameters are set as follows:

$nf = 0, 0.001, 0.01$, $rd = 0.06$ for $n = 1000$, $rd = 0.035$ for $n = 4000$. For each set of parameters, the average results are in Table 6. We see that the numbers of undetermined sensors are relatively small (less than 5% of the total number of sensors). In particular, for the problem with 4000 sensors, there are only a few sensors undetermined. The average RMSD values of the BU algorithm without postrefinement are close to those of ESDP with postrefinement on noisy problems. Figure 2 shows one example of 1000 sensors with $nf = 0.001$ in which the locations of sensors are fairly accurate. Note that in the five cases of 4000 nodes with $nf = 0.001$, although the average RMSD is $3.9e-3$, the best RMSD value is $9.1e-5$ actually without any postrefinement.

We also compared the running time of the BU algorithm with the ESDP [13], SOCP1(SeDuMi) [15], SOCP2(SCGD) [15], and LPCGD [18] approaches. Based on their published results and our running results, we think on these problems the BU algorithm is most likely to run faster than ESDP, SOCP1(Se DuMi), SOCP2(SCGD), and LPCGD may run faster than BU. Since the running environments are quite different and only the ESDP code with a post-refinement is published online, it is hard to compare these approaches exactly in terms of running time, which makes us not list their running time here. Interested readers can refer to the above papers.

We have also tested some problems with larger noises, for example, $nf = 0.1$. The average results are shown in Table 7. As in Example 3.1, the running time of SFSDP is the average CPU time in seconds over five cases consumed by SeDuMi with the accuracy parameter $\text{pars.eps} = 1.0e-5$. Kim et al. [16] used three different values of rd for each problem and we chose the rd with the best result. We also ran “SNLSDPclique-0.2” [19, 20] and show the average results over five cases in Table 7. We can see that although the SFSDP approach is a little more accurate than the BU algorithm, BU obtains similar accuracy with SFSDP (i.e., their RMSD values have the same orders) in shorter running time with fewer distance data. The SNLSDPclique approach runs faster than the BU algorithm, but BU needs fewer distance data with large noises than SNLSDPclique to obtain same orders of RMSD values. We also see that the RMSD values of the BU algorithm become larger than those of problems with low noises. This may be due to the fact that the buildup algorithm is an iterative algorithm and large noises affect the accuracy of calculations. However, we see from Table 7 that the errors of the BU algorithm may be improved by increasing the number of anchors.

Note that for SFSDP, larger rd values result in smaller RMSDs, but for BU, larger rd values may result in larger RMSD, as shown in Table 8. We can see that for the network of 2000 nodes with $nf = 0.1$, when rd varies from 0.05 to 0.11, RMSD increases from $6.9e-2$ to $3.7e+1$. For the network of 1000 nodes with $nf = 0.001$, as rd varies from 0.06 to 0.22, RMSD decreases first, then increases. The reason is that for an undetermined sensor, larger rd may result in more neighboring determined sensors and thus a larger-size noisy least-squares problem, the solution to which may involve larger errors.

3.4. Impact of Noise, the Number of Anchors, and the Radio Range

We now summarize in the following on how the distance noise, the number of anchors, and the radio range affect the performance of the geometric buildup algorithm.

First, as shown in Table 6, the RMSD value of a network determined by the geometric buildup algorithm increases as nf increases. For example, for a network of 4000 nodes, when the noise factor nf increases from 0.001 to 0.01, the RMSD value increases from around $1e-3$ to $1e-2$.

Table 7: Examples with $nf = 0.1$.

Approach	n	m	rd	NumUndet	RMSD	T (sec.)
BU	1000	100	0.08	0	$4.1e-2$	0.53
SFSDP	1000	100	0.2	0	$2.6e-2$	44.0
SNLSDPclique	1000	100	0.2	0	$2e-2$	1
SNLSDPclique	1000	100	0.08	0.2	$5e-1$	0.7
BU	2000	100	0.05	3.4	$7.9e-2$	8.9
SFSDP	2000	100	0.2	0	$2.6e-2$	134.6
SNLSDPclique	2000	100	0.2	0	$4e-2$	2.7
SNLSDPclique	2000	100	0.05	1.8	$2e+1$	1.4
BU	2000	200	0.05	3	$3.6e-2$	6.0
BU	4000	100	0.035	6	$9.99e-2$	75.7
SFSDP	4000	100	0.1	0	$1.6e-2$	269.4
SNLSDPclique	4000	100	0.1	0	$2e-1$	5.6
SNLSDPclique	4000	100	0.035	11.4	$9e+2$	3.9
BU	4000	200	0.035	8.8	$4.7e-2$	65.6
BU	4000	300	0.035	5.8	$3.2e-2$	52.4
BU	4000	400	0.035	5.8	$2.6e-2$	43.0

Table 8: Effect of varying radio ranges.

n	m	rd	nf	NumUndet	RMSD
1000	100	0.06	0.001	20.8	$4.2e-3$
1000	100	0.08	0.001	0.6	$1.3e-3$
1000	100	0.12	0.001	0	$2.5e-4$
1000	100	0.15	0.001	0	$8.9e-4$
1000	100	0.18	0.001	0	$6.7e-2$
1000	100	0.2	0.001	0	$1.3e-1$
1000	100	0.22	0.001	0	$1.3e+1$
2000	100	0.05	0.1	5.4	$6.9e-2$
2000	100	0.07	0.1	0	$7.0e-2$
2000	100	0.08	0.1	0	$1.2e-1$
2000	100	0.1	0.1	0	$7.3e-1$
2000	100	0.11	0.1	0	$3.7e+1$

Second, as shown in Table 7, increasing the number of anchors increases the accuracy of localization. It may reduce the time to find the required determined sensors for an undetermined sensor as well. For example, for a network of 4000 nodes, when m increases from 100 to 400, the RMSD value decreases from $9.99e-2$ to $2.6e-2$ and the running time decreases from 75.7 s to 43.0 s.

Third, as further demonstrated in Table 8, the impact of the radio range depends on the noise. As mentioned in Example 3.4, for an undetermined sensor, larger rd values may result in more neighboring determined sensors and thus a larger-size noisy least-squares problem whose optimal solution may involve larger errors. For example, if nf is small, increasing rd in an appropriate range can improve the accuracy of localization, while if nf is large, increasing rd may increase the RMSD value.

4. Conclusion

In this paper, we have investigated a geometric buildup approach to the sensor network localization problem. We follow the buildup scheme [24] which was applied to protein structure determination problems. The main difference between our algorithm and [24] is that we employ a low-rank positive semidefinite approximation scheme, which requires a spectral decomposition for a small distance matrix and guarantees a best-possible approximation to the solution of the distance equations in a least-squares sense. We have also implemented a two-phase buildup algorithm to handle problems with a few anchors and sparse distances. In principle, the initial clique in Phase II may find only several points while there are still larger cliques in the graph. We would like to consider some efficient clique searching algorithms in our future efforts.

We have tested the geometric buildup algorithm on a set of simulated sensor network localization problems with sparse and exact or inexact distances. The results showed that the algorithm runs fast on the test problems with acceptable accuracy. The algorithm is easy to follow and implement, and if further developed, may particularly be suitable for large-scale applications. The algorithm still needs to be improved to handle problems with large distance noises and problems with extremely sparse distances, which we will work on in our future efforts.

Acknowledgments

Zheng's work was done during her visit to Iowa State University. Her work was supported by the postdoctoral fellowship provided by the Laurence H. Baker Center for Bioinformatics and Biological Statistics and the Department of Mathematics, Iowa State University. Luo's work was done during his visit to Iowa State University. His work was supported by the Grant 2007CB310604 from National Basic Research Program of China and Chinese Scholar Council no. [2007]3091. Wu's work was supported partially by the NIH/NIGMS Grant R01GM081680 from the National Institutes of Health, and the NSF/DMS Grant DMS0914354 from the National Science Foundation, United States. The first author appreciates Professor Yinyu Ye for the SDP code of the sensor network localization given in a workshop (Beijing, 2006) and her advisor Professor Yaxiang Yuan for his encouragement and help all the time. The authors would like to thank Atilla Sit for sharing his initial SVD build-up code and Vladimir Sukhoy and the referees for many helpful discussions and suggestions.

References

- [1] P. Biswas and Y. Ye, "Semidefinite programming for ad hoc wireless sensor network localization," in *Proceedings of the Third International Symposium on Information Processing in Sensor Networks, (IPSN '04)*, pp. 46–54, New York, NY, USA, April 2004.
- [2] M. W. Carter, H. H. Jin, M. A. Saunders, and Y. Ye, "SpaseLoc: an adaptive subproblem algorithm for scalable wireless sensor network localization," *SIAM Journal on Optimization*, vol. 17, no. 4, pp. 1102–1128, 2006.
- [3] D. Culler and W. Hong, "Wireless sensor networks," *Communications of the ACM*, vol. 47, pp. 30–33, 2004.
- [4] T.-H. Yi, H.-N. Li, and M. Gu, "Optimal sensor placement for health monitoring of high-rise structure based on genetic algorithm," *Mathematical Problems in Engineering*, vol. 2011, Article ID 395101, 12 pages, 2011.
- [5] T. Gao, D. Greenspan, M. Welsh, R. R. Juang, and A. Alm, "Vital signs monitoring and patient tracking over a wireless network," in *Proceedings of the 27th Annual International Conference of the*

- IEEE Engineering in Medicine and Biology Society, (EMBS '05)*, pp. 102–105, Shanghai, China, September 2005.
- [6] M. Lawlor, "Small systems, big business," *Signal Magazine*, 2005.
- [7] A. Dragoon, "Small wonders," *CIO Magazine*, 2005.
- [8] J. B. Saxe, "Embeddability of weighted graphs in k-space is strongly NP-hard," in *Proceedings of the 17th Allerton Conference in Communication, Control and Computing*, pp. 480–489, Monticello, Ill, USA, 1979.
- [9] G. M. Crippen and T. F. Havel, *Distance Geometry and Molecular Conformation*, Research Studies Press, Chichester, UK, 1988.
- [10] J. J. More and Z. Wu, "ε-optimal solutions to distance geometry problems via global continuation," in *Global Minimization of Non-Convex Energy Functions*, P. M. Pardalos, D. Shalloway, and G. Xue, Eds., pp. 151–168, American Mathematical Society, Providence, RI, USA, 1996.
- [11] Q. Dong and Z. Wu, "A linear-time algorithm for solving the molecular distance geometry problem with exact inter-atomic distances," *Journal of Global Optimization*, vol. 22, no. 1-4, pp. 365–375, 2002.
- [12] P. Biswas, T.-C. Lian, T.-C. Wang, and Y. Ye, "Semidefinite programming based algorithms for sensor network localization," *ACM Transactions on Sensor Networks*, vol. 2, no. 2, pp. 188–220, 2006.
- [13] Z. Wang, S. Zheng, Y. Ye, and S. Boyd, "Further relaxations of the semidefinite programming approach to sensor network localization," *SIAM Journal on Optimization*, vol. 19, no. 2, pp. 655–673, 2008.
- [14] J. Nie, "Sum of squares method for sensor network localization," *Computational Optimization and Applications*, vol. 43, no. 2, pp. 151–179, 2009.
- [15] P. Tseng, "Second-order cone programming relaxation of sensor network localization," *SIAM Journal on Optimization*, vol. 18, no. 1, pp. 156–185, 2007.
- [16] S. Kim, M. Kojima, and H. Waki, "Exploiting sparsity in SDP relaxation for sensor network localization," *SIAM Journal on Optimization*, vol. 20, no. 1, pp. 192–215, 2009.
- [17] Z. Zhu, A. M.-C. So, and Y. Ye, "Universal rigidity and edge sparsification for sensor network localization," *SIAM Journal on Optimization*, vol. 20, no. 6, pp. 3059–3081, 2010.
- [18] T. K. Pong and P. Tseng, "(Robust) edge-based semidefinite programming relaxation of sensor network localization," *Mathematical Programming*. In press.
- [19] N. Krislock and H. Wolkowicz, "Explicit sensor network localization using semidefinite representations and facial reductions," *SIAM Journal on Optimization*, vol. 20, no. 5, pp. 2679–2708, 2010.
- [20] N. Krislock, *Semidefinite facial reduction for low-rank euclidean distance matrix completion*, Ph.D. thesis, University of Waterloo, Waterloo, Canada, 2010.
- [21] Q. Dong and Z. Wu, "A geometric build-up algorithm for solving the molecular distance geometry problem with sparse distance data," *Journal of Global Optimization*, vol. 26, no. 3, pp. 321–333, 2003.
- [22] D. Wu and Z. Wu, "An updated geometric build-up algorithm for solving the molecular distance geometry problems with sparse distance data," *Journal of Global Optimization*, vol. 37, no. 4, pp. 661–673, 2007.
- [23] D. Wu, Z. Wu, and Y. Yuan, "Rigid versus unique determination of protein structures with geometric buildup," *Optimization Letters*, vol. 2, no. 3, pp. 319–331, 2008.
- [24] A. Sit, Z. Wu, and Y. Yuan, "A geometric buildup algorithm for the solution of the distance geometry problem using least-squares approximation," *Bulletin of Mathematical Biology*, vol. 71, no. 8, pp. 1914–1933, 2009.
- [25] A. Sit and Z. Wu, "Solving a generalized distance geometry problem for protein structure determination," *Bulletin of Mathematical Biology*. In press.
- [26] C. Eckart and G. Young, "The approximation of one matrix by another of lower rank," *Psychometrika*, vol. 1, no. 3, pp. 211–218, 1936.
- [27] R. Mathar and R. Meyer, "Preorderings, monotone functions, and best rank r approximations with applications to classical MDS," *Journal of Statistical Planning and Inference*, vol. 37, no. 3, pp. 291–305, 1993.
- [28] T. F. Cox and M. A. A. Cox, *Multidimensional Scaling*, Chapman and Hall, London, UK, 2en edition, 1994.
- [29] W. S. Torgerson, "Multidimensional scaling. I. Theory and method," *Psychometrika*, vol. 17, pp. 401–419, 1952.

- [30] G. H. Golub and C. F. V. Loan, *Matrix Computations*, Johns Hopkins University Press, Baltimore, Md, USA, 1989.
- [31] R. M. Karp, "Reducibility among combinatorial problems," in *Complexity of Computer Computations*, R. E. Miller and J. W. Thatcher, Eds., pp. 85–103, Plenum Press, New York, NY, USA, 1972.
- [32] J. M. Robson, "Finding a maximum independent set in time $O(2^{n/4})$," Technical Report 1251-01, Université Bordeaux I, Bordeaux, France, 2001.

Research Article

Global Robust Stability of Switched Interval Neural Networks with Discrete and Distributed Time-Varying Delays of Neural Type

**Huaiqin Wu, Ning Li, Kewang Wang, Guohua Xu,
and Qiangqiang Guo**

Department of Applied Mathematics, Yanshan University, Qinhuangdao 066001, China

Correspondence should be addressed to Huaiqin Wu, huaiqinwu@ysu.edu.cn

Received 24 May 2011; Accepted 6 July 2011

Academic Editor: Zidong Wang

Copyright © 2012 Huaiqin Wu et al. This is an open access article distributed under the Creative Commons Attribution License, which permits unrestricted use, distribution, and reproduction in any medium, provided the original work is properly cited.

By combing the theories of the switched systems and the interval neural networks, the mathematics model of the switched interval neural networks with discrete and distributed time-varying delays of neural type is presented. A set of the interval parameter uncertainty neural networks with discrete and distributed time-varying delays of neural type are used as the individual subsystem, and an arbitrary switching rule is assumed to coordinate the switching between these networks. By applying the augmented Lyapunov-Krasovskii functional approach and linear matrix inequality (LMI) techniques, a delay-dependent criterion is achieved to ensure to such switched interval neural networks to be globally asymptotically robustly stable in terms of LMIs. The unknown gain matrix is determined by solving this delay-dependent LMIs. Finally, an illustrative example is given to demonstrate the validity of the theoretical results.

1. Introduction

In the past few decades, neural networks have been a subject of intense research activities due to their wide applications in different areas such as image processing, pattern recognition, associative memory, and combinational optimization. A fundamental problem is the stability which is the prerequisite to ensure that the developed neural network can work [1–40]. In hardware implementation of the neural networks, time delay is inevitably encountered and is usually time varying due to the finite switching speed of amplifiers. It is known that time delay is often the main cause for instability and poor performance of neural networks. Moreover, due to unavoidable factors, such as modeling error, external perturbation, and parameter fluctuation, the neural networks model certainly involves uncertainties such as perturbations and component variations, which will change the stability of neural networks.

To analyze uncertainty of neural networks, one reasonable method is to assume parameters in certain intervals. Therefore, it is of great importance to study the global robust stability of interval neural networks with time-varying delay. Recently, some sufficient conditions for the global robust stability of interval neural networks with time-varying delays and parametric uncertainties have been obtained in terms of LMIs [1–9].

Since neural networks usually have a spatial extent, there is a distribution of propagation delays over a period of time. In these circumstances, the signal propagation is not instantaneous and cannot be modeled with discrete delays, and a more appropriate way is to incorporate continuously distributed delays in neural network model. On the other hand, in certain physical systems, mathematical models have been described by some functional differential equations of neutral type, which depend on the delays of state and state derivative. In practice, neutral type phenomenon always appear in studies of automatic control, chemical reactors, population ecology, heat exchanges, microwave oscillators, and so on. Hence, the stability for neutral type neural networks with time-varying delay has been also considered in the recent years [10–18].

A class of hybrid systems has attracted significant attention because it can model several practical control problems that involve the integration of supervisory logic-based control schemes and feedback control algorithms. As a special class of hybrid systems, switched systems are regarded as nonlinear systems, which are composed of a family of continuous-time or discrete-time subsystems and a rule that orchestrates the switching between the subsystems. Recently, switched neural networks, whose individual subsystems are a set of neural networks, have found applications in fields of high-speed signal processing, artificial intelligence, and gene selection in a DNA microarray analysis [19–21]. Therefore, some researchers have studied the stability issues for switched neural networks [22–27]. In [22], based on the Lyapunov-Krasovskii method and LMI approach, some sufficient conditions were derived for global robust exponential stability of a class of switched Hopfield neural networks with time-varying delay under uncertainty. In [23], by combining Cohen-Grossberg neural networks with an arbitrary switching rule, the mathematical model of a class of switched Cohen-Grossberg neural networks with mixed time-varying delays were established, and the robust stability for such switched Cohen-Grossberg neural networks was analyzed. In [24], by employing nonlinear measure and LMI techniques, some new sufficient conditions were obtained to ensure global robust asymptotical stability and global robust stability of the unique equilibrium for a class of switched recurrent neural networks with time-varying delay. In [25], authors investigated a large class of switched recurrent neural networks with time-varying structured uncertainties and time-varying delay; some delay-dependent robust periodicity criteria guaranteeing the existence, uniqueness, and global asymptotic stability of periodic solution for all admissible parametric uncertainties were devised by taking free weighting matrices and LMIs. In [26], based on multiple Lyapunov functions method and LMI techniques, the authors presented some sufficient conditions in terms of LMIs which guarantee the robust exponential stability for uncertain switched Cohen-Grossberg neural networks with interval time-varying delay and distributed time-varying delay under the switching rule with the average dwell time property.

It should be noted that, in the above literature, almost all results treated of the robust stability for switched neural networks with norm-bounded uncertainty. However, as it well known that there are two forms of parametric uncertainties, namely the interval uncertainty and the norm-bounded uncertainty. To the best of our knowledge, up to now, there are few researchers to deal with the global robust stability for switched neural networks with the interval uncertainty, despite its potential and practical importance.

Motivated by the preceding discussion, the aim of this paper is to present a new class of the switched interval neural networks with discrete and distributed time-varying delays of neural type under interval parameter uncertainties by integrating the theory of switched systems with neural networks. By constructing a suitable Lyapunov-Krasovskii functional and employing Jensen's inequality, a delay-dependent criterion will be derived such that the proposed switched interval neural networks are globally robustly asymptotically stable. The proposed criterion is represented in terms of LMIs, which can be solved efficiently by using recently developed convex optimization algorithms [28].

The rest of this paper is organized as follows. In Section 2, the model formulation and some preliminaries are given. The main results are stated in Section 3. In Section 4, a numerical example is presented to demonstrate the validity of the proposed results. Some conclusions are made in Section 5.

Notations. Throughout this paper, \mathbb{R} denotes the set of real numbers, \mathbb{R}^n denotes the n -dimensional Euclidean space, $\mathbb{R}^{m \times n}$ denotes the set of all $m \times n$ real matrices. For any matrix A , A^T denotes the transpose of A . $A > 0$ ($A < 0$) means that A is a positive definite (negative definite). Given the column vectors $x = (x_1, \dots, x_n)^T$, $y = (y_1, \dots, y_n)^T \in \mathbb{R}^n$, and $x^T y = \sum_{i=1}^n x_i y_i$. $\dot{x}(t)$ denotes the derivative of $x(t)$, and $*$ represents the symmetric form of matrix.

2. Neural Network Model and Preliminaries

Consider the interval neural network model with discrete and distributed time-varying delays of neural type described by the system of differential equations in the form

$$\begin{aligned} \dot{x}(t) = & -Ax(t) + W_1 g(x(t)) + W_2 g(x(t - \tau(t))) + W_3 \int_{t-\tau(t)}^t g(x(s)) ds + W_4 \dot{x}(t - \mu(t)) + u, \\ & A \in A_1, \quad W_k \in W_1^{(k)}, \quad k = 1, 2, 3, 4, \end{aligned} \quad (2.1)$$

where $x(t) = (x_1(t), \dots, x_n(t))^T \in \mathbb{R}^n$ denotes the state vector associated with n neurons; $g(x) = (g_1(x_1), \dots, g_n(x_n))^T : \mathbb{R}^n \rightarrow \mathbb{R}^n$ is a vector-valued neuron activation function; $u = (u_1, \dots, u_n)^T$ is a constant external input vector; $\tau(t)$ denotes the discrete and distributed time-varying delays; $\mu(t)$ represents neutral time-varying delays; $A = \text{diag}(a_1, \dots, a_n)$ is $n \times n$ constant diagonal matrices; $a_i > 0$, $i = 1, \dots, n$, are the neural self-inhibitions; $W_k = [w_{ij}^{(k)}] \in \mathbb{R}^{n \times n}$, $k = 1, 2, 3, 4$, are the connection weight matrices; $A_1 = [\underline{A}, \bar{A}] = \{A = \text{diag}(a_i) : 0 < \underline{a}_i \leq a_i \leq \bar{a}_i, i = 1, 2, \dots, n\}$, $W_1^{(k)} = [\underline{W}_k, \bar{W}_k] = \{W_k = [w_{ij}^{(k)}] : \underline{w}_{ij}^{(k)} \leq w_{ij}^{(k)} \leq \bar{w}_{ij}^{(k)}, i, j = 1, 2, \dots, n\}$ with $\underline{A} = \text{diag}(\underline{a}_1, \underline{a}_2, \dots, \underline{a}_n)$, $\bar{A} = \text{diag}(\bar{a}_1, \bar{a}_2, \dots, \bar{a}_n)$, $\underline{W}_k = [\underline{w}_{ij}^{(k)}]_{n \times n}$, $\bar{W}_k = [\bar{w}_{ij}^{(k)}]_{n \times n}$.

Throughout this paper, the following assumptions are made on the activation functions g_j , $j = 1, 2, \dots, n$, the discrete and distributed time-varying delay $\tau(t)$, and the neutral time-varying delay $\mu(t)$,

$$(\mathcal{H}_1): |g_j(x_1) - g_j(x_2)| \leq k_j |x_1 - x_2|, \quad x_1, x_2 \in \mathbb{R}, \quad j = 1, 2, \dots, n,$$

$$(\mathcal{H}_2): 0 \leq \tau(t) \leq \tau_N, \quad \dot{\tau}(t) < 1, \quad 0 \leq \mu(t) \leq \mu_N, \quad \dot{\mu}(t) \leq \mu < 1,$$

where μ_N, μ_N are constants. The initial value associated with (2.1) is assumed to be $x(s) = \phi(s)$, and $\phi(s)$ is a continuous function on $[-h, 0]$, $h = \max\{\mu_N, \mu_N\}$.

With loss of generality, it is assumed that the above neural networks have only one equilibrium point and are denoted by $x^* = (x_1^*, x_2^*, \dots, x_n^*)^T$. For the purpose of simplicity, the equilibrium x^* will be always shifted to the origin by letting $y(t) = x(t) - x^*$, and the neural network system (2.1) can be represented as follows:

$$\dot{y}(t) = -A y(t) + W_1 f(y(t)) + W_2 f(y(t-\mu(t))) + W_3 \int_{t-\mu(t)}^t f(y(s)) ds + W_4 \dot{y}(t-\mu(t)), \quad (2.2)$$

where $f_j(y_j(t)) = g_j(y_j(t) + x_j^*) - g_j(x_j^*)$, and $f_j(0) = 0$, $j = 1, 2, \dots, n$.

The initial condition associated with (2.2) is given in the form $y(s) = x(s) - x^* = \phi(s) - x^*$, $s \in [-h, 0]$. From the assumption (\mathcal{L}_1) , it follows that $f(y(t)) \leq K y(t)$, $K = \text{diag}(k_1, k_2, \dots, k_n)$. Based on some transformations, the system (2.2) can be written as an equivalent form

$$\begin{aligned} \dot{y}(t) = & -[A_0 + E_A \Sigma_A F_A] y(t) + [W_{10} + E_1 \Sigma_1 F_1] f(y(t)) + [W_{20} + E_2 \Sigma_2 F_2] f(y(t-\mu(t))) \\ & + [W_{30} + E_3 \Sigma_3 F_3] \int_{t-\mu(t)}^t f(y(s)) ds + [W_{40} + E_4 \Sigma_4 F_4] \dot{y}(t-\mu(t)), \end{aligned} \quad (2.3)$$

where $\Sigma_A \in \Sigma$, $\Sigma_k \in \Sigma$, $k = 1, 2, 3, 4$

$$\begin{aligned} \Sigma = & \left\{ \text{diag}[\bar{a}_{11}, \dots, \bar{a}_{1n}, \dots, \bar{a}_{n1}, \dots, \bar{a}_{nn}] \in \mathbb{R}^{n^2 \times n^2} : | \bar{a}_{ij} | \leq 1, i, j = 1, 2, \dots, n \right\}, \\ A_0 = & \frac{\bar{A} + A}{2}, \quad H_A = [\bar{a}_{ij}]_{n \times n} = \frac{\bar{A} - A}{2}, \\ W_{k0} = & \frac{\bar{W}_k + W_k}{2}, \quad H_W^{(k)} = [\bar{w}_{ij}^{(k)}]_{n \times n} = \frac{\bar{W}_k - W_k}{2}, \\ E_A = & [\sqrt{\bar{a}_{11}} e_1, \dots, \sqrt{\bar{a}_{1n}} e_1, \dots, \sqrt{\bar{a}_{n1}} e_n, \dots, \sqrt{\bar{a}_{nn}} e_n]_{n \times n^2}, \\ F_A = & [\sqrt{\bar{a}_{11}} e_1, \dots, \sqrt{\bar{a}_{1n}} e_n, \dots, \sqrt{\bar{a}_{n1}} e_1, \dots, \sqrt{\bar{a}_{nn}} e_n]_{n^2 \times n}^T, \\ E_k = & [\sqrt{\bar{a}_{11}^{(k)}} e_1, \dots, \sqrt{\bar{a}_{1n}^{(k)}} e_1, \dots, \sqrt{\bar{a}_{n1}^{(k)}} e_n, \dots, \sqrt{\bar{a}_{nn}^{(k)}} e_n]_{n \times n^2}, \\ F_k = & [\sqrt{\bar{a}_{11}^{(k)}} e_1, \dots, \sqrt{\bar{a}_{1n}^{(k)}} e_n, \dots, \sqrt{\bar{a}_{n1}^{(k)}} e_1, \dots, \sqrt{\bar{a}_{nn}^{(k)}} e_n]_{n^2 \times n}^T, \end{aligned} \quad (2.4)$$

where $e_i \in \mathbb{R}^n$ denotes the column vector with i th element to be 1 and others to be 0.

The switched interval neural networks with discrete and distributed time-varying delays of neural type consists of a set of interval neural network with discrete and distributed time-varying delays of neural type and a switching rule. Each of the interval neural networks is regarded as an individual subsystem. The operation mode of the switched neural networks

is determined by the switching rule. According to (2.2), the switched interval neural network with discrete and distributed delays of neural type can be described as follows:

$$\begin{aligned} \dot{Y}(t) = & -A_{(\vartheta)}Y(t) + W_{1(\vartheta)}f(Y(t)) + W_{2(\vartheta)}f(Y(t-\mu(t))) + W_{3(\vartheta)}\int_{t-\mu(t)}^t f(Y(s))ds \\ & + W_{4(\vartheta)}\dot{Y}(t-\mu(t)), \quad A_{(\vartheta)} \in A_{1(\vartheta)}, \quad W_{k(\vartheta)} \in W_{1(\vartheta)}^{(k)}, \quad k = 1, 2, 3, 4, \end{aligned} \quad (2.5)$$

where $A_{1(\vartheta)} = [\underline{A}_{(\vartheta)}, \overline{A}_{(\vartheta)}] = \{A_{(\vartheta)} = \text{diag}(a_{i(\vartheta)}) : 0 < \underline{a}_{i(\vartheta)} \leq a_{i(\vartheta)} \leq \overline{a}_{i(\vartheta)}, i = 1, 2, \dots, n\}$,
 $W_{1(\vartheta)}^{(k)} = [\underline{W}_{k(\vartheta)}, \overline{W}_{k(\vartheta)}] = \{W_{k(\vartheta)} = [w_{ij}^{(k)}] : 0 < \underline{w}_{ij}^{(k)} \leq w_{ij}^{(k)} \leq \overline{w}_{ij}^{(k)}, i, j = 1, 2, \dots, n\}$
 with $\underline{A}_{(\vartheta)} = \text{diag}(\underline{a}_{1(\vartheta)}, \underline{a}_{2(\vartheta)}, \dots, \underline{a}_{n(\vartheta)})$, $\overline{A}_{(\vartheta)} = \text{diag}(\overline{a}_{1(\vartheta)}, \overline{a}_{2(\vartheta)}, \dots, \overline{a}_{n(\vartheta)})$, $\underline{W}_{k(\vartheta)} = [\underline{w}_{ij}^{(k)}]_{n \times n}$,
 $\overline{W}_{k(\vartheta)} = [\overline{w}_{ij}^{(k)}]_{n \times n}$

$$\begin{aligned} A_{0(\vartheta)} &= \frac{\overline{A}_{(\vartheta)} + \underline{A}_{(\vartheta)}}{2}, \quad H_{A(\vartheta)} = [h_{ij(\vartheta)}]_{n \times n} = \frac{\overline{A}_{(\vartheta)} - \underline{A}_{(\vartheta)}}{2}, \\ W_{k0(\vartheta)} &= \frac{\overline{W}_{k(\vartheta)} + \underline{W}_{k(\vartheta)}}{2}, \quad H_{W(\vartheta)}^{(k)} = [h_{ij(\vartheta)}^{(k)}]_{n \times n} = \frac{\overline{W}_{k(\vartheta)} - \underline{W}_{k(\vartheta)}}{2}, \\ E_{A(\vartheta)} &= [\sqrt{11(\vartheta)}e_1, \dots, \sqrt{1n(\vartheta)}e_1, \dots, \sqrt{n1(\vartheta)}e_n, \dots, \sqrt{nn(\vartheta)}e_n]_{n \times n^2}, \\ F_{A(\vartheta)} &= [\sqrt{11(\vartheta)}e_1, \dots, \sqrt{1n(\vartheta)}e_n, \dots, \sqrt{n1(\vartheta)}e_1, \dots, \sqrt{nn(\vartheta)}e_n]_{n^2 \times n}^T, \\ E_{k(\vartheta)} &= [\sqrt{11(\vartheta)}^{(k)}e_1, \dots, \sqrt{1n(\vartheta)}^{(k)}e_1, \dots, \sqrt{n1(\vartheta)}^{(k)}e_n, \dots, \sqrt{nn(\vartheta)}^{(k)}e_n]_{n \times n^2}, \\ F_{k(\vartheta)} &= [\sqrt{11(\vartheta)}^{(k)}e_1, \dots, \sqrt{1n(\vartheta)}^{(k)}e_n, \dots, \sqrt{n1(\vartheta)}^{(k)}e_1, \dots, \sqrt{nn(\vartheta)}^{(k)}e_n]_{n^2 \times n}^T, \end{aligned} \quad (2.6)$$

$(\vartheta) : [0, +\infty) \rightarrow \Gamma = \{1, 2, \dots, N\}$ is the switching signal, which is a piecewise constant function of time. For any $i \in \{1, 2, \dots, l\}$, $A_i = A_{0i} + E_{A_i} \Sigma_{A_i} F_{A_i}$, $W_{k_i} = W_{k0i} + E_{k_i} \Sigma_{k_i} F_{k_i}$, and $\Sigma_{A_i} \in \Sigma$, $\Sigma_{k_i} \in \Sigma$, $k = 1, 2, 3, 4$. This means that the matrices $(A_{(\vartheta)}, W_{1(\vartheta)}, W_{2(\vartheta)}, W_{3(\vartheta)}, W_{4(\vartheta)})$ are allowed to take values, at an arbitrary time, in the finite set $\{(A_1, W_{11}, W_{21}, W_{31}, W_{41}), (A_2, W_{12}, W_{22}, W_{32}, W_{42}), \dots, (A_N, W_{1N}, W_{2N}, W_{3N}, W_{4N})\}$. Throughout this paper, it is assumed that the switching rule is not known a priori, and its instantaneous value is available in real time. The initial condition associated with the switching system (2.5) is $Y(s) = \phi(s)$, $s \in [-h, 0]$.

By (2.3), the system (2.5) can be written as

$$\begin{aligned} \dot{Y}(t) = & -A_{0(\vartheta)}Y(t) + W_{10(\vartheta)}f(Y(t)) + W_{20(\vartheta)}f(Y(t-\mu(t))) + W_{30(\vartheta)}\int_{t-\mu(t)}^t f(Y(s))ds \\ & + W_{40(\vartheta)}\dot{Y}(t-\mu(t)) + E_{(\vartheta)}\Delta_{(\vartheta)}(t), \quad A_{(\vartheta)} \in A_{1(\vartheta)}, \quad W_{k(\vartheta)} \in W_{1(\vartheta)}^{(k)}, \quad k = 1, 2, 3, 4, \end{aligned} \quad (2.7)$$

where $E_{(\vartheta)} = [E_{A_{(\vartheta)}}, E_{1_{(\vartheta)}}, E_{2_{(\vartheta)}}, E_{3_{(\vartheta)}}, E_{4_{(\vartheta)}}]$

$$\Delta_{(\vartheta)}(\vartheta) = \begin{bmatrix} -\Sigma_{A_{(\vartheta)}} F_{A_{(\vartheta)}} Y(\vartheta) \\ \Sigma_{1_{(\vartheta)}} F_{1_{(\vartheta)}} f(Y(\vartheta)) \\ \Sigma_{2_{(\vartheta)}} F_{2_{(\vartheta)}} f(Y(\vartheta-\tau)) \\ \Sigma_{3_{(\vartheta)}} F_{3_{(\vartheta)}} \int_{\vartheta-\tau}^{\vartheta} f(Y(s)) ds \\ \Sigma_{4_{(\vartheta)}} F_{4_{(\vartheta)}} \dot{Y}(\vartheta-\mu(\vartheta)) \end{bmatrix} \quad (2.8)$$

$$= \text{diag}\{\Sigma_{A_{(\vartheta)}}, \Sigma_{1_{(\vartheta)}}, \Sigma_{2_{(\vartheta)}}, \Sigma_{3_{(\vartheta)}}, \Sigma_{4_{(\vartheta)}}\} \begin{bmatrix} -F_{A_{(\vartheta)}} Y(\vartheta) \\ F_{1_{(\vartheta)}} f(Y(\vartheta)) \\ F_{2_{(\vartheta)}} f(Y(\vartheta-\tau)) \\ F_{3_{(\vartheta)}} \int_{\vartheta-\tau}^{\vartheta} f(Y(s)) ds \\ F_{4_{(\vartheta)}} \dot{Y}(\vartheta-\mu(\vartheta)) \end{bmatrix},$$

and $\Delta_{(\vartheta)}(\vartheta)$ satisfies the following quadratic inequality:

$$\Delta_{(\vartheta)}^T(\vartheta) \Delta_{(\vartheta)}(\vartheta) \leq \begin{bmatrix} Y(\vartheta) \\ f(Y(\vartheta)) \\ f(Y(\vartheta-\tau)) \\ \int_{\vartheta-\tau}^{\vartheta} f(Y(s)) ds \\ \dot{Y}(\vartheta-\mu(\vartheta)) \end{bmatrix}^T \begin{bmatrix} F_{A_{(\vartheta)}}^T \\ F_{1_{(\vartheta)}}^T \\ F_{2_{(\vartheta)}}^T \\ F_{3_{(\vartheta)}}^T \\ F_{4_{(\vartheta)}}^T \end{bmatrix} \begin{bmatrix} F_{A_{(\vartheta)}}^T \\ F_{1_{(\vartheta)}}^T \\ F_{2_{(\vartheta)}}^T \\ F_{3_{(\vartheta)}}^T \\ F_{4_{(\vartheta)}}^T \end{bmatrix}^T \begin{bmatrix} Y(\vartheta) \\ f(Y(\vartheta)) \\ f(Y(\vartheta-\tau)) \\ \int_{\vartheta-\tau}^{\vartheta} f(Y(s)) ds \\ \dot{Y}(\vartheta-\mu(\vartheta)) \end{bmatrix}. \quad (2.9)$$

Define the indicator function $i(\vartheta) = [i_1(\vartheta), i_2(\vartheta), \dots, i_N(\vartheta)]^T$, where

$$i_i(\vartheta) = \begin{cases} 1, & \text{when the switched system is described by the } i\text{th mode,} \\ A_{0_i}, W_{k0_i}, k = 1, 2, 3, 4, E_i, \\ 0, & \text{otherwise} \end{cases} \quad (2.10)$$

where $i = 1, 2, \dots, N$. Therefore, the system model (2.7) can also be written as

$$\dot{Y}(\vartheta) = \sum_{i=1}^N i_i(\vartheta) \left\{ -A_{0_i} Y(\vartheta) + W_{10_i} f(Y(\vartheta)) + W_{20_i} f(Y(\vartheta-\tau)) \right. \\ \left. + W_{30_i} \int_{\vartheta-\tau}^{\vartheta} f(Y(s)) ds + W_{40_i} \dot{Y}(\vartheta-\mu(\vartheta)) + E_i \Delta_i(\vartheta) \right\}, \quad (2.11)$$

where $\sum_{i=1}^N i_i(\vartheta) = 1$ is satisfied under any switching rules.

To derive the main result in the next section, the following definitions and lemmas will be need.

Definition 2.1. The switched interval neural network model (2.5) is said to be globally robustly asymptotically stable if the neural network model (2.5) is globally asymptotically stable for any $A_{(k)} \in A_{1(k)}, W_{k(k)} \in W_{1(k)}, k = 1, 2, 3, 4$.

Lemma 2.2 (see [6]). Let $\Gamma_0(x)$ and $\Gamma_1(x)$ be two arbitrary quadratic forms over \mathbb{R}^n , then $\Gamma_0(x) < 0$ for all $x \in \mathbb{R}^n - \{0\}$ satisfying $\Gamma_1(x) \leq 0$ if and only if there exists $\alpha \geq 0$ such that

$$\Gamma_0(x) - \alpha \Gamma_1(x) < 0, \quad \forall x \in \mathbb{R}^n - \{0\}. \quad (2.12)$$

Lemma 2.3 (Jensen's inequality, see [23]). For any constant matrix $\Omega \in \mathbb{R}^{n \times n}$, $\Omega = \Omega^T > 0$, scalar $0 < \alpha < \beta$, vector function $\varphi : [t_0, t] \rightarrow \mathbb{R}^n, t \geq 0$ such that the integrations concerned are well defined, then

$$\left(\int_0^{\alpha} \varphi(s) ds \right)^T \Omega \left(\int_0^{\beta} \varphi(s) ds \right) \leq \alpha \left(\int_0^{\beta} \varphi(s)^T \Omega \varphi(s) ds \right). \quad (2.13)$$

3. Main Results

In this section, the global robust asymptotic stability of the proposed model (2.5) will be discussed. By constructing a suitable Lyapunov functional, a robust delay-dependent criterion for the global asymptotic stability of the neural network system (2.5) is derived in terms of LMIs.

Theorem 3.1. Under the assumptions (\mathcal{H}_1) and (\mathcal{H}_2) , if there exist matrices $P > 0, Q_1 > 0, Q_2 > 0, Q_3 > 0, Q_4 > 0, N_i (i = 1, 2, \dots, 7)$ such that the following LMIs hold:

$$\Pi_i = \begin{bmatrix} \prod_{i1} & \prod_{i2} & \prod_{i3} & \prod_{i4} & \prod_{i5} & \prod_{i6} & \prod_{i7} \\ * & -Q_1 & N_3 W_{20_i} & N_3 W_{30_i} & N_3 W_{40_i} & N_3 E_i & -N_3 \\ * & * & \prod_{i3} & \prod_{i4} & \prod_{i5} & \prod_{i6} & N_2 W_{20_i} - N_4 \\ * & * & * & \prod_{i4} & \prod_{i5} & N_5 E_i + N_7 W_{30_i} & N_2 W_{30_i} - N_5 \\ * & * & * & * & \prod_{i5} & N_6 E_i + N_7 W_{40_i} & N_2 W_{40_i} - N_6 \\ * & * & * & * & * & N_7 E_i - I & N_2 E_i - N_7 \\ * & * & * & * & * & * & Q_4 - N_2 - N_2^T \end{bmatrix} < 0, \quad (3.1)$$

where

$$\begin{aligned} \prod_{i11} &= -PA_{0_i} - A_{0_i}^T P + PW_{10_i} W_{10_i}^T P + K^T K + K Q_2 K + N K Q_3 K - N_1 A_{0_i} - A_{0_i}^T N_1^T + N_1 W_{10_i} \\ &\quad + W_{10_i}^T N_1^T + F_{A_i}^T F_{A_i} + F_{A_i}^T F_{1_i} + F_{1_i}^T K F_{1_i}, \end{aligned}$$

$$\prod_{i12} = -N_3 A_{0_i} + N_3 W_{10_i} K,$$

$$\prod_{i13} = -PW_{20_i} + N_1 W_{20_i} - N_4 A_{0_i} + N_4 W_{10_i} K + F_{A_i}^T F_{2_i} + F_{1_i}^T K F_{2_i},$$

$$\prod_{i14} = -PW_{30_i} + N_1 W_{30_i} - N_5 A_{0_i} + N_5 W_{10_i} K + F_{A_i}^T F_{3_i} + F_{1_i}^T K F_{3_i},$$

$$\prod_{i15} = -PW_{40_i} + N_1 W_{40_i} - N_6 A_{0_i} + N_6 W_{10_i} K + F_{A_i}^T F_{4_i} + F_{1_i}^T K F_{4_i},$$

$$\prod_{i16} = -PE_i + N_1 E_i - N_7 A_{0_i} + N_7 W_{10_i} K,$$

$$\prod_{i17} = -N_2 A_{0_i} + N_2 W_{10_i} K - N_1,$$

$$\prod_{i33} = -(1 - \mu) Q_2 + N_4 W_{20_i} + F_{2_i}^T F_{2_i},$$

$$\prod_{i34} = N_4 W_{30_i} + N_5 W_{20_i} + F_{2_i}^T F_{3_i},$$

$$\prod_{i35} = N_4 W_{40_i} + N_6 W_{20_i} + F_{2_i}^T F_{4_i},$$

$$\prod_{i36} = N_4 E_i + N_7 W_{20_i},$$

$$\prod_{i44} = -(1 - \mu) 1/N Q_2 + N_5 W_{30_i} + F_{3_i}^T F_{3_i},$$

$$\prod_{i45} = N_5 W_{40_i} + N_6 W_{30_i} + F_{3_i}^T F_{4_i},$$

$$\prod_{i55} = -(1 - \mu) Q_4 + N_6 W_{40_i} + F_{4_i}^T F_{4_i},$$

(3.2)

then the switched interval neural network model (2.5) is globally robustly asymptotically stable under any switching rules.

Proof. Consider the following Lyapunov-Krasovskii functional:

$$\begin{aligned} V(\vartheta) = & \mathbf{y}^T(\vartheta)P\mathbf{y}(\vartheta) + \int_{t^-(\vartheta)}^{\vartheta} \mathbf{y}(s)^T Q_1 \mathbf{y}(s) ds + \int_{t^-(\vartheta)}^{\vartheta} \mathbf{f}(\mathbf{y}(s))^T Q_2 \mathbf{f}(\mathbf{y}(s)) ds \\ & + \int_{t^-(\vartheta)}^{\vartheta} (s - t^-(\vartheta)) \mathbf{f}(\mathbf{y}(s))^T Q_3 \mathbf{f}(\mathbf{y}(s)) ds + \int_{t-\mu(\vartheta)}^{\vartheta} \dot{\mathbf{y}}(s)^T Q_4 \dot{\mathbf{y}}(s) ds. \end{aligned} \quad (3.3)$$

Calculating the time derivative of $V(\vartheta)$ along the trajectory of (2.11), it can follow that

$$\begin{aligned} \dot{V}(\vartheta) = & 2\mathbf{y}^T(\vartheta)P\dot{\mathbf{y}}(\vartheta) + \mathbf{y}^T(\vartheta)Q_1\mathbf{y}(\vartheta) - \mathbf{y}(t^-(\vartheta))^T Q_1 \mathbf{y}(t^-(\vartheta)) + \mathbf{f}(\mathbf{y}(\vartheta))^T Q_2 \mathbf{f}(\mathbf{y}(\vartheta)) \\ & - (1 - \dot{\cdot}(\vartheta)) \mathbf{f}^T(\mathbf{y}(t^-(\vartheta))) Q_2 \mathbf{f}(\mathbf{y}(t^-(\vartheta))) + (\vartheta) \mathbf{f}^T(\mathbf{y}(\vartheta)) Q_3 \mathbf{f}(\mathbf{y}(\vartheta)) \\ & + \int_{t^-(\vartheta)}^{\vartheta} (-1 + \dot{\cdot}(\vartheta)) \mathbf{f}(\mathbf{y}(s))^T Q_3 \mathbf{f}(\mathbf{y}(s)) ds + \dot{\mathbf{y}}^T(\vartheta) Q_4 \dot{\mathbf{y}}(\vartheta) \\ & - \dot{\mathbf{y}}^T(t - \mu(\vartheta)) Q_4 \dot{\mathbf{y}}(t - \mu(\vartheta)) (1 - \dot{\mu}(\vartheta)) \\ = & 2\mathbf{y}^T(\vartheta)P \left\{ \sum_{i=1}^N \mathbf{i}(\vartheta) \left[-A_{0i} \mathbf{y}(\vartheta) + W_{10i} \mathbf{f}(\mathbf{y}(\vartheta)) + W_{20i} \mathbf{f}(\mathbf{y}(t^-(\vartheta))) \right. \right. \\ & \left. \left. + W_{30i} \int_{t^-(\vartheta)}^{\vartheta} \mathbf{f}(\mathbf{y}(s)) ds + W_{40i} \dot{\mathbf{y}}(t - \mu(\vartheta)) + E_i \Delta_i(\vartheta) \right] \right\} \\ & + \mathbf{y}^T(\vartheta) Q_1 \mathbf{y}(\vartheta) - \mathbf{y}(t^-(\vartheta))^T Q_1 \mathbf{y}(t^-(\vartheta)) + \mathbf{f}(\mathbf{y}(\vartheta))^T Q_2 \mathbf{f}(\mathbf{y}(\vartheta)) \\ & - (1 - \dot{\cdot}(\vartheta)) \mathbf{f}^T(\mathbf{y}(t^-(\vartheta))) Q_2 \mathbf{f}(\mathbf{y}(t^-(\vartheta))) + (\vartheta) \mathbf{f}^T(\mathbf{y}(\vartheta)) Q_3 \mathbf{f}(\mathbf{y}(\vartheta)) \\ & + \int_{t^-(\vartheta)}^{\vartheta} (-1 + \dot{\cdot}(\vartheta)) \mathbf{f}(\mathbf{y}(s))^T Q_3 \mathbf{f}(\mathbf{y}(s)) ds + \dot{\mathbf{y}}^T(\vartheta) Q_4 \dot{\mathbf{y}}(\vartheta) \\ & - \dot{\mathbf{y}}^T(t - \mu(\vartheta)) Q_4 \dot{\mathbf{y}}(t - \mu(\vartheta)) (1 - \dot{\mu}(\vartheta)) \\ = & \sum_{i=1}^N \mathbf{i}(\vartheta) \left\{ \mathbf{y}^T(\vartheta) \left(-PA_{0i} - A_{0i}^T P \right) \mathbf{y}(\vartheta) + 2\mathbf{y}^T(\vartheta) P W_{10i} \mathbf{f}(\mathbf{y}(\vartheta)) \right. \\ & + 2\mathbf{y}^T(\vartheta) P W_{20i} \mathbf{f}(\mathbf{y}(t^-(\vartheta))) \\ & + 2\mathbf{y}^T(\vartheta) P W_{30i} \int_{t^-(\vartheta)}^{\vartheta} \mathbf{f}(\mathbf{y}(s)) ds + 2\mathbf{y}^T(\vartheta) P W_{40i} \dot{\mathbf{y}}(t - \mu(\vartheta)) + 2\mathbf{y}^T(\vartheta) P E_i \Delta_i(\vartheta) \\ & \left. + \mathbf{y}^T(\vartheta) Q_1 \mathbf{y}(\vartheta) - \mathbf{y}(t^-(\vartheta))^T Q_1 \mathbf{y}(t^-(\vartheta)) + \mathbf{f}(\mathbf{y}(\vartheta))^T Q_2 \mathbf{f}(\mathbf{y}(\vartheta)) \right\} \end{aligned}$$

$$\begin{aligned}
& - (1 - \dot{\mu}(\vartheta)) f^T(Y(t - \mu(\vartheta))) Q_2 f(Y(t - \mu(\vartheta))) + \dot{\mu}(\vartheta) f^T(Y(\vartheta)) Q_3 f(Y(\vartheta)) \\
& + \int_{t - \mu(\vartheta)}^t (-1 + \dot{\mu}(s)) f(Y(s))^T Q_3 f(Y(s)) ds + \dot{Y}^T(\vartheta) Q_4 \dot{Y}(\vartheta) \\
& - \dot{Y}^T(t - \mu(\vartheta)) Q_4 \dot{Y}(t - \mu(\vartheta)) (1 - \dot{\mu}(\vartheta)) \}.
\end{aligned} \tag{3.4}$$

By the assumption (\mathcal{L}_1) and Lemma 2.3,

$$2Y^T(\vartheta) P W_{10} f(Y(\vartheta)) \leq Y^T(\vartheta) (P W_{10} W_{10}^T P + K^T K) Y(\vartheta), \tag{3.5}$$

$$f(Y(\vartheta))^T Q_2 f(Y(\vartheta)) \leq Y^T(\vartheta) K Q_2 K Y(\vartheta), \tag{3.6}$$

$$\begin{aligned}
& \int_{t - \mu(\vartheta)}^t (-1 + \dot{\mu}(s)) f(Y(s))^T Q_3 f(Y(s)) ds \\
& \leq -(1 - \dot{\mu}(\vartheta)) \frac{1}{N} \left(\int_{t - \mu(\vartheta)}^t f(Y(s)) ds \right)^T Q_3 \left(\int_{t - \mu(\vartheta)}^t f(Y(s)) ds \right).
\end{aligned} \tag{3.7}$$

Noting the following zero equation with free weighting matrices N_i ($i = 1, 2, \dots, 7$), which indicate the relationship between the terms in the state equation (2.11) and can easily be determined by solving the corresponding LMIs, it follows that

$$\begin{aligned}
& 2 \dot{Y}^T(\vartheta) N \times \left\{ \sum_{i=1}^7 N_i(\vartheta) \left[-\dot{Y}(\vartheta) - A_{0i} Y(\vartheta) + W_{10i} f(Y(\vartheta)) + W_{20i} f(Y(t - \mu(\vartheta))) \right. \right. \\
& \left. \left. + W_{30i} \int_{t - \mu(\vartheta)}^t f(Y(s)) ds + W_{40i} \dot{Y}(t - \mu(\vartheta)) + E_i \Delta_i(\vartheta) \right] \right\} = 0,
\end{aligned} \tag{3.8}$$

$\dot{Y}(\vartheta) = [Y^T(\vartheta) \dot{Y}^T(\vartheta) Y^T(t - \mu(\vartheta)) f^T(Y(t - \mu(\vartheta))) (\int_{t - \mu(\vartheta)}^t f(Y(s)) ds)^T \dot{Y}^T(t - \mu(\vartheta)) \Delta_i^T(\vartheta)]^T \cdot N = [N_1^T N_2^T N_3^T N_4^T N_5^T N_6^T N_7^T]^T$. By substituting (2.9) and (3.5)–(3.8) into (3.4), it follows that

$$\begin{aligned}
& \dot{Y}(\vartheta) - \sum_{i=1}^N N_i(\vartheta) \left(\Delta_i^T(\vartheta) \Delta_i(\vartheta) - \begin{bmatrix} Y(\vartheta) \\ f(Y(\vartheta)) \\ f(Y(t - \mu(\vartheta))) \\ \int_{t - \mu(\vartheta)}^t f(Y(s)) ds \\ \dot{Y}(t - \mu(\vartheta)) \end{bmatrix}^T \begin{bmatrix} F_{A_i}^T \\ F_{1_i}^T \\ F_{2_i}^T \\ F_{3_i}^T \\ F_{4_i}^T \end{bmatrix} \begin{bmatrix} F_{A_i}^T \\ F_{1_i}^T \\ F_{2_i}^T \\ F_{3_i}^T \\ F_{4_i}^T \end{bmatrix}^T \begin{bmatrix} Y(\vartheta) \\ f(Y(\vartheta)) \\ f(Y(t - \mu(\vartheta))) \\ \int_{t - \mu(\vartheta)}^t f(Y(s)) ds \\ \dot{Y}(t - \mu(\vartheta)) \end{bmatrix} \right) \\
& \leq \sum_{i=1}^N N_i(\vartheta) \Pi_i(\vartheta),
\end{aligned} \tag{3.9}$$

where $\dot{y}(t) = [y^T(t) \ y^T(t-\tau(t)) \ f^T(y(t-\tau(t))) \ (\int_{t-\tau(t)}^t f(y(s))ds)^T \ \dot{y}^T(t-\mu(t)) \ \Delta_i^T(t) \ \dot{y}^T(t)]^T$ and $\tau > 0$. From Lemma 2.2 with the conditions (3.1) and (3.9), this implies that $\dot{V}(t) < 0$ for all $\tau(t) \neq 0$. Hence, the neural network system (2.7) is globally asymptotically stable for $A_i(t) \in A_{1(t)}$, $W_k(t) \in W_{1(t)}^{(k)}$, $k = 1, 2, 3, 4$, that is, the switched neural network model (2.5) is globally robustly asymptotically stable. The proof is completed. \square

When the time-varying delay $\tau(t)$ and $\mu(t)$ in (2.5) becomes into $\tau(t) = \tau = \text{const}$, $\mu(t) = \mu = \text{const}$, according to Theorem 3.1, it is easy to obtain the following corollary.

Corollary 3.2. *Under the assumption (\mathcal{H}_1) and (\mathcal{H}_2) , if there exist matrices $P > 0$, $Q_1 > 0$, $Q_2 > 0$, $Q_3 > 0$, $Q_4 > 0$, N_i ($i = 1, 2, \dots, 7$) such that the following LMIs hold:*

$$\begin{bmatrix} \prod_{i1} & \prod_{i2} & \prod_{i3} & \prod_{i4} & \prod_{i5} & \prod_{i6} & \prod_{i7} \\ * & -Q_1 & N_3 W_{20_i} & N_3 W_{30_i} & N_3 W_{40_i} & N_3 E_i & -N_3 \\ * & * & \prod_{i33} & \prod_{i34} & \prod_{i35} & \prod_{i36} & N_2 W_{20_i} - N_4 \\ * & * & * & \prod_{i44} & \prod_{i45} & N_5 E_i + N_7 W_{30_i} & N_2 W_{30_i} - N_5 \\ * & * & * & * & \prod_{i55} & N_6 E_i + N_7 W_{40_i} & N_2 W_{40_i} - N_6 \\ * & * & * & * & * & N_7 E_i - I & N_2 E_i - N_7 \\ * & * & * & * & * & * & Q_4 - N_2 - N_2^T \end{bmatrix} < 0, \quad (3.10)$$

where

$$\begin{aligned} \prod_{i1} &= -PA_{0_i} - A_{0_i}^T P + PW_{10_i} W_{10_i}^T P + K^T K + KQ_2 K + N_1 KQ_3 K - N_1 A_{0_i} - A_{0_i}^T N_1^T \\ &\quad + N_1 W_{10_i} + W_{10_i}^T N_1^T + F_{A_i}^T F_{A_i} + F_{A_i}^T F_{1_i} + F_{1_i}^T K F_{1_i}, \end{aligned}$$

$$\prod_{i2} = -N_3 A_{0_i} + N_3 W_{10_i} K,$$

$$\prod_{i3} = -PW_{20_i} + N_1 W_{20_i} - N_4 A_{0_i} + N_4 W_{10_i} K + F_{A_i}^T F_{2_i} + F_{1_i}^T K F_{2_i},$$

$$\prod_{i4} = -PW_{30_i} + N_1 W_{30_i} - N_5 A_{0_i} + N_5 W_{10_i} K + F_{A_i}^T F_{3_i} + F_{1_i}^T K F_{3_i},$$

$$\prod_{i5} = -PW_{40_i} + N_1 W_{40_i} - N_6 A_{0_i} + N_6 W_{10_i} K + F_{A_i}^T F_{4_i} + F_{1_i}^T K F_{4_i},$$

$$\prod_{i6} = -PE_i + N_1 E_i - N_7 A_{0_i} + N_7 W_{10_i} K,$$

$$\prod_{i7} = -N_2 A_{0_i} + N_2 W_{10_i} K - N_1,$$

$$\begin{aligned}
\Pi_{33} &= -Q_2 + N_4 W_{20_i} + F_{2_i}^T F_{2_i}, \\
\Pi_{34} &= N_4 W_{30_i} + N_5 W_{20_i} + F_{2_i}^T F_{3_i}, \\
\Pi_{35} &= N_4 W_{40_i} + N_6 W_{20_i} + F_{2_i}^T F_{4_i}, \\
\Pi_{36} &= N_4 E_i + N_7 W_{20_i}, \\
\Pi_{44} &= -1/Q_2 + N_5 W_{30_i} + F_{3_i}^T F_{3_i}, \\
\Pi_{45} &= N_5 W_{40_i} + N_6 W_{30_i} + F_{3_i}^T F_{4_i}, \\
\Pi_{55} &= -Q_4 + N_6 W_{40_i} + F_{4_i}^T F_{4_i},
\end{aligned} \tag{3.11}$$

then the switched interval neural network model (2.5) is global robust asymptotically stable.

Remark 3.3. When $N = 1$, the switched system model (2.7) degenerated into the interval neural network model (2.1) with discrete and distributed time-varying delays of neutral type which contain neural network models studied in [1–3, 5, 7]. Moreover, note that when $N = 1$, $W_1 = 0$, and $\mu(t) = \mu(t) = \text{const}$, Theorem 3.1 in this paper coincides with Theorem 1 in [12]. Without considering interval parameter uncertainty, the neural network models presented in [11, 13–15] are the special case. Hence, the results obtained in this paper extend and improve the stability results available in the existing literature [1–3, 5, 7, 11, 13–15].

Remark 3.4. In this paper, augmented Lyapunov functional is used to analyze the stability of the interval neural network model (2.1) with discrete and distributed time-varying delays of neutral type. In the Lyapunov functional, both state and activation function are considered in the same term. Hence, the novel Lyapunov function contains structures more general than the traditional ones, and the negative matrices Π_i in Theorem 3.1 contain more elements. This shows that it is easy to find more appropriate elements in Π_i to ensure that the LMIs (3.1) hold. Thus, sufficient conditions given in this paper are less conservative than the existing results.

Remark 3.5. In this paper, the activation function is Lipschitz continuous, which is first introduced in [29] and used also in [30, 31] is more general than the usual sigmoid functions. Therefore, the stability results obtained in this paper are less conservative than those in [10–13, 27].

Remark 3.6. In [32, 33], the mixed time-delay problems have been considered for the stochastic system with Markovian jump parameters and discrete-time stochastic complex networks with randomly occurred nonlinearities. By applying the Lyapunov-Krasovskii functional approach and linear matrix inequality techniques, the conditions of exponential

stabilization and global synchronization were presented for the stochastic system and discrete-time stochastic complex networks. In [34], Bounded H-infinity synchronization and state estimation were considered for discrete time-varying stochastic complex networks over a finite- horizon via linear matrix inequality. [35] The authors studied the robust H-infinity fuzzy output-feedback control; a controller design is given for the system with multiple probabilistic delays and multiple missing measurements. In the future, based on [32, 33], the model of the switched interval stochastic system and the switched interval discrete-time stochastic complex networks will be expected to be established, and the stability strategy proposed in this paper will be utilized to investigate the stability problems.

4. An Illustrative Example

In this section, an example will be given to illustrate the validity and effectiveness of the proposed stability criterion for the switched interval neural network with discrete and distributed delays of neural type when $N = 2$.

Example 4.1. Consider the following second-order switched interval neural networks with discrete and distributed delays of neural type:

$$\begin{aligned} \dot{Y}_i(t) = & -a_{i(\vartheta)} Y_i(t) + \sum_{j=1}^2 w_{ij}^{(1)}(\vartheta) f_j(Y_j(t)) + \sum_{j=1}^2 w_{ij}^{(2)}(\vartheta) f_j(Y_j(t-\tau(\vartheta))) + \sum_{j=1}^2 w_{ij}^{(3)}(\vartheta) \int_{t-\mu(\vartheta)}^t f_j(Y_j(s)) ds \\ & + \sum_{j=1}^2 w_{ij}^{(4)}(\vartheta) \dot{Y}_j(t-\mu(\vartheta)), \quad a_{i(\vartheta)} \in [\underline{a}_{i(\vartheta)}, \bar{a}_{i(\vartheta)}], \quad w_{ij}^{(k)}(\vartheta) \in [\underline{w}_{ij}^{(k)}(\vartheta), \bar{w}_{ij}^{(k)}(\vartheta)], \\ & k = 1, 2, 3, 4, \quad Y_i(t) = \varphi_i(t), \quad t \in [-h, 0], \quad i, j = 1, 2, \end{aligned} \tag{4.1}$$

where the switching signal $\vartheta : [0, +\infty) \rightarrow \Gamma = \{1, 2\}$, the activation functions $f_i(x) = (2/3) \sin x + (1/3)x$, $i = 1, 2$, the discrete and distributed delays $\tau(\vartheta) = (1/2) \cos t + (1/2)$, and the neural type delay $\mu(\vartheta) = (1/2) \sin t + (1/2)$. Obviously, the assumptions \mathcal{H}_1 and \mathcal{H}_2 are satisfied with $K = \text{diag}(1, 1)$ and $h = 1$, $\tau = \mu = 1/2$. The neural network system parameters are defined as

$$\begin{aligned} \underline{A}_1 &= \begin{pmatrix} 3.99 & 0 \\ 0 & 2.99 \end{pmatrix}, & \bar{A}_1 &= \begin{pmatrix} 4.01 & 0 \\ 0 & 3.01 \end{pmatrix}, \\ \underline{W}_{-11} &= \begin{pmatrix} 1.188 & 0.09 \\ 0.09 & 1.188 \end{pmatrix}, & \bar{W}_{-11} &= \begin{pmatrix} 1.208 & 0.11 \\ 0.11 & 1.208 \end{pmatrix}, \\ \underline{W}_{-21} &= \begin{pmatrix} 0.09 & 0.14 \\ 0.05 & 0.09 \end{pmatrix}, & \bar{W}_{-21} &= \begin{pmatrix} 0.11 & 0.16 \\ 0.07 & 0.11 \end{pmatrix}, \\ \underline{W}_{-31} &= \begin{pmatrix} 0.44 & -0.21 \\ 0.29 & 0.41 \end{pmatrix}, & \bar{W}_{-31} &= \begin{pmatrix} 0.46 & -0.19 \\ 0.31 & 0.43 \end{pmatrix}, \end{aligned} \tag{4.2}$$

$$\begin{aligned}
\underline{W}_{41} &= \begin{pmatrix} 0.09 & -0.01 \\ -0.01 & 0.09 \end{pmatrix}, & \overline{W}_{41} &= \begin{pmatrix} 0.11 & 0.11 \\ 0.11 & 0.11 \end{pmatrix}, \\
\underline{A}_2 &= \begin{pmatrix} 1.99 & 0 \\ 0 & 2.99 \end{pmatrix}, & \overline{A}_2 &= \begin{pmatrix} 2.01 & 0 \\ 0 & 3.01 \end{pmatrix}, \\
\underline{W}_{12} &= \begin{pmatrix} -0.07 & 0.03 \\ -0.01 & 0.02 \end{pmatrix}, & \overline{W}_{12} &= \begin{pmatrix} -0.05 & 0.05 \\ -0.04 & 0.04 \end{pmatrix}, \\
\underline{W}_{22} &= \begin{pmatrix} -0.47 & -0.15 \\ 0.11 & -0.54 \end{pmatrix}, & \overline{W}_{22} &= \begin{pmatrix} -0.45 & -0.13 \\ 0.13 & -0.54 \end{pmatrix}, \\
\underline{W}_{32} &= \begin{pmatrix} -0.31 & 0.09 \\ -0.51 & -0.61 \end{pmatrix}, & \overline{W}_{32} &= \begin{pmatrix} -0.29 & 0.11 \\ -0.49 & -0.59 \end{pmatrix}, \\
\underline{W}_{42} &= \begin{pmatrix} 0.03 & -0.22 \\ -0.21 & -0.44 \end{pmatrix}, & \overline{W}_{42} &= \begin{pmatrix} 0.05 & -0.2 \\ -0.19 & -0.42 \end{pmatrix}.
\end{aligned}
\tag{4.3}$$

Solving the LMI in (3.4) by using appropriate LMI solver in the Matlab, the feasible positive definite matrices P , Q_i , $i = 1, 2, 3, 4$ and the matrices N_i , $i = 1, 2, \dots, 7$ could be as

$$\begin{aligned}
P &= \begin{pmatrix} 6.0192 & -0.5039 \\ -0.5039 & 4.8686 \end{pmatrix}, & Q_1 &= \begin{pmatrix} 3.2386 & 0 \\ 0 & 3.2386 \end{pmatrix}, & Q_2 &= \begin{pmatrix} 4.7009 & 0.3313 \\ 0.3313 & 4.9146 \end{pmatrix}, \\
Q_3 &= \begin{pmatrix} 3.0347 & -0.0788 \\ -0.0788 & 2.8395 \end{pmatrix}, & Q_4 &= \begin{pmatrix} 1.9859 & -0.2388 \\ -0.2388 & 1.4177 \end{pmatrix}, & N_1 &= \begin{pmatrix} -4.1198 & 0.4992 \\ 0.7261 & -2.7597 \end{pmatrix}, \\
N_2 &= \begin{pmatrix} 1.9399 & -0.0997 \\ -0.1962 & 1.5020 \end{pmatrix}, & N_3 &= \begin{pmatrix} 0 & 0 \\ 0 & 0 \end{pmatrix}, & N_4 &= \begin{pmatrix} -0.2957 & -0.0263 \\ 0.0959 & -0.0107 \end{pmatrix}, \\
N_5 &= \begin{pmatrix} -0.0147 & 0.0606 \\ 0.1252 & 0.2426 \end{pmatrix}, & N_6 &= \begin{pmatrix} 0.0734 & -0.1495 \\ -0.0498 & -0.0592 \end{pmatrix}, & N_7 &= (M_1 \ M_2), \\
M_1 &= \begin{pmatrix} 0.085 & 0.085 & -0.0068 & -0.0068 & 0.085 & 0.085 & -0.0068 & -0.0068 \\ 0.008 & 0.008 & 0.0892 & 0.0892 & 0.008 & 0.008 & 0.0892 & 0.0892 \end{pmatrix}, \\
M_2 &= \begin{pmatrix} 0.085 & 0.085 & -0.0068 & -0.0068 & 0.085 & 0.085 & -0.0068 & -0.0068 \\ 0.008 & 0.008 & 0.0892 & 0.0892 & 0.008 & 0.008 & 0.0892 & 0.0892 \end{pmatrix}.
\end{aligned}
\tag{4.4}$$

By Theorem 3.1, this switched interval neural network with discrete and distributed delays of neural type is globally robustly asymptotically stable under any switching rules.

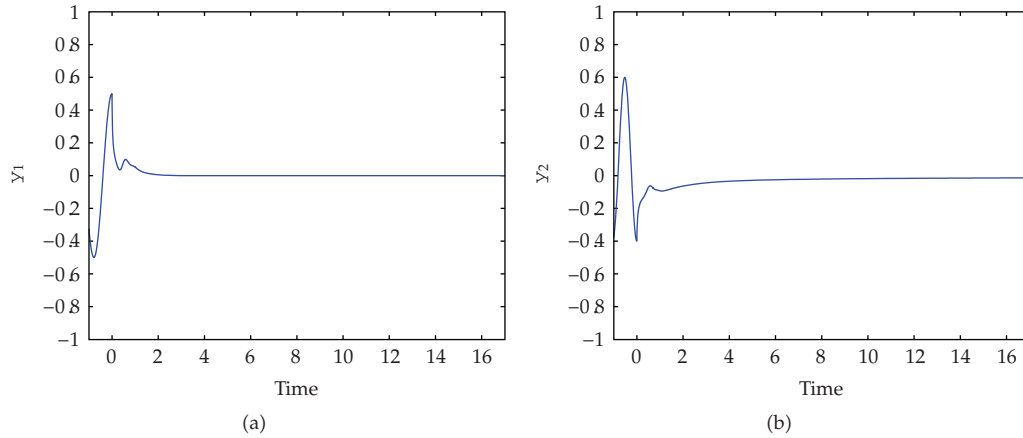


Figure 1: The state trajectories y_1 and y_2 of the network with initial value $(y_1(t), y_2(t))^T = ((\cos 2t)^2 - 0.5, (\sin 3t)^2 - 0.4)^T, t \in [-1, 0]$.

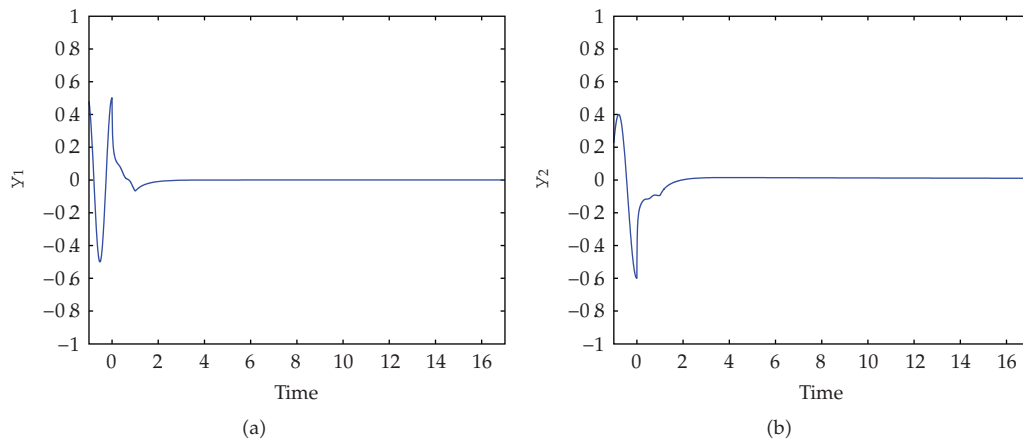


Figure 2: The state trajectories y_1 and y_2 of the network with initial value $(y_1(t), y_2(t))^T = ((\cos 3t)^2 - 0.5, (\sin 2t)^2 - 0.6)^T, t \in [-1, 0]$.

Let $A_1 = \underline{A}_1, W_{11} = \underline{W}_{11}, W_{21} = \underline{W}_{21}, W_{31} = \underline{W}_{31}, W_{41} = \underline{W}_{41}$ and $A_2 = \underline{A}_2, W_{12} = \underline{W}_{12}, W_{22} = \underline{W}_{22}, W_{32} = \underline{W}_{32},$ and $W_{42} = \underline{W}_{42}$. For numerical simulation, assume that the two subsystems are switched every four seconds. Figure 1 displays the state trajectories of this network with initial value $(y_1(t), y_2(t))^T = ((\cos 2t)^2 - 0.5, (\sin 3t)^2 - 0.4)^T, t \in [-1, 0]$. It can be seen that these trajectories asymptotically converge to the unique equilibrium $x^* = (0, 0)^T$ of the network. This is in accordance with the conclusion of Theorem 3.1.

Let $\underline{A}_1 = \underline{A}_1, \underline{W}_{11} = \underline{W}_{11}, \underline{W}_{21} = \underline{W}_{21}, \underline{W}_{31} = \underline{W}_{31}, \underline{W}_{41} = \underline{W}_{41}$ and $\underline{A}_2 = \underline{A}_2, \underline{W}_{12} = \underline{W}_{12}, \underline{W}_{22} = \underline{W}_{22}, \underline{W}_{32} = \underline{W}_{32},$ and $\underline{W}_{42} = \underline{W}_{42}$. For numerical simulation, assume that the two subsystems are switched every four seconds. Figure 2 displays the state trajectories of this network with initial value $(y_1(t), y_2(t))^T = ((\cos 3t)^2 - 0.5, (\sin 2t)^2 - 0.6)^T, t \in [-1, 0]$. It can be seen that these trajectories asymptotically converge to the unique equilibrium $x^* = (0, 0)^T$ of the network. This is in accordance with the conclusion of Theorem 3.1.

5. Conclusion

In this paper, a novel class of switched interval neural networks with discrete and distributed delays of neural type has been presented by combing the theories of the switched systems and the interval neural networks with discrete and distributed delays of neural type. Furthermore, a delay-dependent criterion expressed in the form of LMIs has been obtained to guarantee the proposed neural networks to be globally asymptotically robustly stable under interval parameter uncertainties. An illustrative example has been also given to demonstrate the effectiveness of the proposed LMI-based stability criteria.

Acknowledgments

The authors are extremely grateful to the Editor and the Reviewers for their valuable comments and suggestions, which help to enrich the content and improve the presentation of this paper. This work was supported by the Natural Science Foundation of Hebei Province of China (A2011203103) and the Hebei Province Education Foundation of China (2009157).

References

- [1] V. Singh, "A new criterion for global robust stability of interval delayed neural networks," *Journal of Computational and Applied Mathematics*, vol. 221, no. 1, pp. 219–225, 2008.
- [2] V. Singh, "On global robust stability of interval Hopfield neural networks with delay," *Chaos, Solitons & Fractals*, vol. 33, no. 4, pp. 1183–1188, 2007.
- [3] Q. Song and J. Cao, "Global robust stability of interval neural networks with multiple time-varying delays," *Mathematics and Computers in Simulation*, vol. 74, no. 1, pp. 38–46, 2007.
- [4] Y. Q. Zhang and X. Wan, "Statistical fuzzy interval neural networks for currency exchange rate time series prediction," *Applied Soft Computing Journal*, vol. 7, no. 4, pp. 1149–1156, 2007.
- [5] H. Zhang, Z. Wang, and D. Liu, "Robust stability analysis for interval Cohen-Grossberg neural networks with unknown time-varying delays," *IEEE Transactions on Neural Networks*, vol. 19, no. 11, pp. 1942–1955, 2008.
- [6] W. Su and Y. Chen, "Global robust exponential stability analysis for stochastic interval neural networks with time-varying delays," *Communications in Nonlinear Science and Numerical Simulation*, vol. 14, no. 5, pp. 2293–2300, 2009.
- [7] R. Zhang and L. Wang, "Global exponential robust stability of interval cellular neural networks with S-type distributed delays," *Mathematical and Computer Modelling*, vol. 50, no. 3-4, pp. 380–385, 2009.
- [8] H. Wu, F. Tao, L. Qin, R. Shi, and L. He, "Robust exponential stability for interval neural networks with delays and non-Lipschitz activation functions," *Nonlinear Dynamics*. In press.
- [9] S. Senan and S. Arik, "New results for global robust stability of bidirectional associative memory neural networks with multiple time delays," *Chaos, Solitons & Fractals*, vol. 41, no. 4, pp. 2106–2114, 2009.
- [10] R. Rakkiyappan and P. Balasubramaniam, "New global exponential stability results for neutral type neural networks with distributed time delays," *Neurocomputing*, vol. 71, no. 4-6, pp. 1039–1045, 2008.
- [11] R. Rakkiyappan and P. Balasubramaniam, "LMI conditions for global asymptotic stability results for neutral-type neural networks with distributed time delays," *Applied Mathematics and Computation*, vol. 204, no. 1, pp. 317–324, 2008.
- [12] L. Liu, Z. Han, and W. Li, "Global stability analysis of interval neural networks with discrete and distributed delays of neutral type," *Expert Systems with Applications*, vol. 36, no. 3, pp. 7328–7331, 2009.
- [13] J. Zhu, Q. Zhang, and C. Yang, "Delay-dependent robust stability for Hopfield neural networks of neutral-type," *Neurocomputing*, vol. 72, no. 10–12, pp. 2609–2617, 2009.
- [14] J. Qiu and J. Cao, "Delay-dependent robust stability of neutral-type neural networks with time delays," *Journal of Mathematical Control Science and Applications*, vol. 1, pp. 179–188, 2007.

- [15] J. H. Park, O. M. Kwon, and S. M. Lee, "LMI optimization approach on stability for delayed neural networks of neutral-type," *Applied Mathematics and Computation*, vol. 196, no. 1, pp. 236–244, 2008.
- [16] O. M. Kwon, J. H. Park, and S. M. Lee, "On stability criteria for uncertain delay-differential systems of neutral type with time-varying delays," *Applied Mathematics and Computation*, vol. 197, no. 2, pp. 864–873, 2008.
- [17] J. H. Park, C. H. Park, O. M. Kwon, and S. M. Lee, "A new stability criterion for bidirectional associative memory neural networks of neutral-type," *Applied Mathematics and Computation*, vol. 199, no. 2, pp. 716–722, 2008.
- [18] J. H. Park and O. M. Kwon, "Design of state estimator for neural networks of neutral-type," *Applied Mathematics and Computation*, vol. 202, no. 1, pp. 360–369, 2008.
- [19] Y. Tsividis, "Switched neural networks," US patent no. 4873661, 1989.
- [20] T. X. Brown, "Neural networks for switching," *IEEE Communications Magazine*, vol. 27, no. 11, pp. 72–81, 1989.
- [21] M. Muselli, "Gene selection through switched neural networks," in *Network Tools and Applications in Biology Workshop (NETTAB '03)*, pp. 27–28, Bologna, Italy, 2003.
- [22] H. Huang, Y. Qu, and H. X. Li, "Robust stability analysis of switched Hopfield neural networks with time-varying delay under uncertainty," *Physics Letters A*, vol. 345, no. 4–6, pp. 345–354, 2005.
- [23] K. Yuan, J. Cao, and H. X. Li, "Robust stability of switched Cohen-Grossberg neural networks with mixed time-varying delays," *IEEE Transactions on Systems, Man, and Cybernetics, Part B*, vol. 36, no. 6, pp. 1356–1363, 2006.
- [24] P. Li and J. Cao, "Global stability in switched recurrent neural networks with time-varying delay via nonlinear measure," *Nonlinear Dynamics*, vol. 49, no. 1-2, pp. 295–305, 2007.
- [25] X. Lou and B. Cui, "Delay-dependent criteria for global robust periodicity of uncertain switched recurrent neural networks with time-varying delay," *IEEE Transactions on Neural Networks*, vol. 19, no. 4, pp. 549–557, 2008.
- [26] J. Lian and K. Zhang, "Exponential stability for switched Cohen-Grossberg neural networks with average dwell time," *Nonlinear Dynamics*, vol. 63, no. 3, pp. 331–343, 2011.
- [27] C. K. Ahn, "Switched exponential state estimation of neural networks based on passivity theory," *Nonlinear Dynamics*. In press.
- [28] S. Boyd, L. El Ghaoui, E. Feron, and V. Balakrishnan, *Linear Matrix Inequalities in System and Control Theory*, vol. 15 of *SIAM Studies in Applied Mathematics*, SIAM, Philadelphia, Pa, USA, 1994.
- [29] Z. Wang, Y. Liu, and X. Liu, "On global asymptotic stability of neural networks with discrete and distributed delays," *Physics Letters A*, vol. 345, no. 4–6, pp. 299–308, 2005.
- [30] Z. Wang, Y. Liu, M. Li, and X. Liu, "Stability analysis for stochastic Cohen-Grossberg neural networks with mixed time delays," *IEEE Transactions on Neural Networks*, vol. 17, no. 3, pp. 814–820, 2006.
- [31] Z. Wang, D. W. C. Ho, and X. Liu, "State estimation for delayed neural networks," *IEEE Transactions on Neural Networks*, vol. 16, no. 1, pp. 279–284, 2005.
- [32] Z. Wang, Y. Liu, and X. Liu, "Exponential stabilization of a class of stochastic system with Markovian jump parameters and mode-dependent mixed time-delays," *IEEE Transactions on Automatic Control*, vol. 55, no. 7, pp. 1656–1662, 2010.
- [33] Z. Wang, Y. Wang, and Y. Liu, "Global synchronization for discrete-time stochastic complex networks with randomly occurred nonlinearities and mixed time delays," *IEEE Transactions on Neural Networks*, vol. 21, no. 1, pp. 11–25, 2010.
- [34] B. Shen, Z. Wang, and X. Liu, "Bounded H_∞ synchronization and state estimation for discrete time-varying stochastic complex networks over a finite-horizon," *IEEE Transactions on Neural Networks*, vol. 22, pp. 145–157, 2011.
- [35] H. Dong, Z. Wang, D. W. C. Ho, and H. Gao, "Robust H_∞ fuzzy output-feedback control with multiple probabilistic delays and multiple missing measurements," *IEEE Transactions on Fuzzy Systems*, vol. 18, no. 4, pp. 712–725, 2010.
- [36] S. Xu, J. Lam, D. W. C. Ho, and Y. Zou, "Delay-dependent exponential stability for a class of neural networks with time delays," *Journal of Computational and Applied Mathematics*, vol. 183, no. 1, pp. 16–28, 2005.
- [37] J. Cao, K. Yuan, and H. X. Li, "Global asymptotical stability of recurrent neural networks with multiple discrete delays and distributed delays," *IEEE Transactions on Neural Networks*, vol. 17, no. 6, pp. 1646–1651, 2006.
- [38] Y. Liu, Z. Wang, J. Liang, and X. Liu, "Stability and synchronization of discrete-time Markovian jumping neural networks with mixed mode-dependent time delays," *IEEE Transactions on Neural Networks*, vol. 20, no. 7, pp. 1102–1116, 2009.

- [39] P. Balasubramaniam and G. Nagamani, "Global robust passivity analysis for stochastic interval neural networks with interval time-varying delays and Markovian jumping parameters," *Journal of Optimization Theory and Applications*, vol. 149, no. 1, pp. 197–215, 2011.
- [40] Z. Wang, H. Gao, J. Cao, and X. Liu, "On delayed genetic regulatory networks with polytopic uncertainties: robust stability analysis," *IEEE Transactions on Nanobioscience*, vol. 7, no. 2, pp. 154–163, 2008.

Research Article

H_∞ Neural-Network-Based Discrete-Time Fuzzy Control of Continuous-Time Nonlinear Systems with Dither

Zhi-Ren Tsai¹ and Jiing-Dong Hwang²

¹ Department of Computer Science and Information Engineering, Asia University, No. 500 Lioufeng Road, Wufeng Distinguish, Taichung City 41354, Taiwan

² Department of Electronic Engineering, Jinwen University of Science and Technology, No. 99 Anchung Road, Xindian Distinguish, New Taipei City 23154, Taiwan

Correspondence should be addressed to Jiing-Dong Hwang, ditherman@just.edu.tw

Received 23 April 2011; Revised 26 June 2011; Accepted 6 July 2011

Academic Editor: Zidong Wang

Copyright © 2012 Z.-R. Tsai and J.-D. Hwang. This is an open access article distributed under the Creative Commons Attribution License, which permits unrestricted use, distribution, and reproduction in any medium, provided the original work is properly cited.

This study presents an effective approach to stabilizing a continuous-time (CT) nonlinear system using dithers and a discrete-time (DT) fuzzy controller. A CT nonlinear system is first discretized to a DT nonlinear system. Then, a Neural-Network (NN) system is established to approximate a DT nonlinear system. Next, a Linear Difference Inclusion state-space representation is established for the dynamics of the NN system. Subsequently, a Takagi-Sugeno DT fuzzy controller is designed to stabilize this NN system. If the DT fuzzy controller cannot stabilize the NN system, a dither, as an auxiliary of the controller, is simultaneously introduced to stabilize the closed-loop CT nonlinear system by using the Simplex optimization and the linear matrix inequality method. This dither can be injected into the original CT nonlinear system by the proposed injecting procedure, and this NN system is established to approximate this dithered system. When the discretized frequency or sampling frequency of the CT system is sufficiently high, the DT system can maintain the dynamic of the CT system. We can design the sampling frequency, so the trajectory of the DT system and the relaxed CT system can be made as close as desired.

1. Introduction

During the past decade, fuzzy control [1, 2] has attracted great attention from both the academic and industrial communities, and there have been many successful applications. Despite this success, it has become evident that many basic and important issues [3] remain to be further addressed. These stability analysis and systematic designs are among the most important issues for fuzzy control systems [4] and H_∞ control theories [1, 2, 5–10], and there has been significant research on these issues (see [4, 11, 12]). In addition, fuzzy

controller has been suggested as an alternative approach to conventional control techniques for complex control systems [1, 2]. Moreover, Neural-Network- (NN-) based modeling has become an active research field because of its unique merits in solving complex nonlinear system identification and control problems (see [12]). Neural networks (NNs) are composed of simple elements operating in parallel, inspired by biological nervous systems. As a result, we can train a neural network to represent a particular function by adjusting the weights between elements [13]. As the discrete-time (DT) controller is cheaper and more flexible than continuous-time (CT) controller, the DT control problem for CT plant is worth studying in this paper. However, an NN-model-based design method with dither has not yet been developed to adjust the parameters of a discrete-time (DT) fuzzy controller such that the original continuous-time (CT) system is uniformly ultimately bounded (UUB) stable.

Therefore, to solve this problem, this paper proposes a less conservative DT control design methodology for a CT nonlinear system with dither based on using an NN model, then these problems of the systematic control design are overcome using the simplex optimization [14] and the LMI method [3, 11]. Our design approach is to approximate a DT nonlinear system with a multilayer perceptron of which the transfer functions. Then, an LDI state-space representation [12] is established for the dynamics of the NN system. Finally, a DT fuzzy controller is designed to stabilize the CT nonlinear system. According to this approach, if the closed-loop DT system cannot be stabilized, a dither is injected into the original CT nonlinear system as an auxiliary of the controller (see Figure 1).

A dither [15] is a high-frequency signal injected into a CT nonlinear system in order to augment stability, quench undesirable limit cycles, eliminate jump phenomena, and reduce nonlinear distortion. Zames and Shneydor [16] rigorously examined the effect of a dither depending on its amplitude distribution function. Mossaheb [17] showed that when the dither frequency is high enough, the output of the smoothed system and the dithered system may be as close as desired. Desoer and Shahrz [18] studied the effect of dither in nonlinear control systems involving backlash or hysteresis. A rigorous analysis of stability in a general CT nonlinear system with a dither control was given in [19]. Based on these articles, we suggest that the trajectory of a DT system can be predicted rigorously by establishing a corresponding system the CT relaxed system, provided that the dither's frequency and the discretized frequency (or sampling frequency) are sufficiently high. This enables us to obtain a rigorous prediction of the stability of the closed-loop DT system by establishing the stability of the NN system. On the other hand, some parameters of membership functions for fuzzy controller could not be optimized by the LMI method; hence, we use the simplex optimization method [14] to search these parameters quickly. A simulation example is given to illustrate the proposed design method.

2. System Description

Consider an open-loop CT nonlinear system f_{CT} described by the following equation:

$$\dot{x}(t) = f_{CT}(x(t), u, D(\omega, A)) = f_{CT}(x, u), \quad (2.1)$$

where $D(\omega, A)$ is the dither signal and A is the maximum dither amplitude; ω is dither's lower-bound frequency [15] when $D = 0$, (2.1) is a common CT nonlinear system without dither, otherwise, it is a CT nonlinear dithered system; $x(t)$ is a CT state vector, u is a DT control input vector, and f_{CT} is a vector-valued function that satisfies the assumptions of

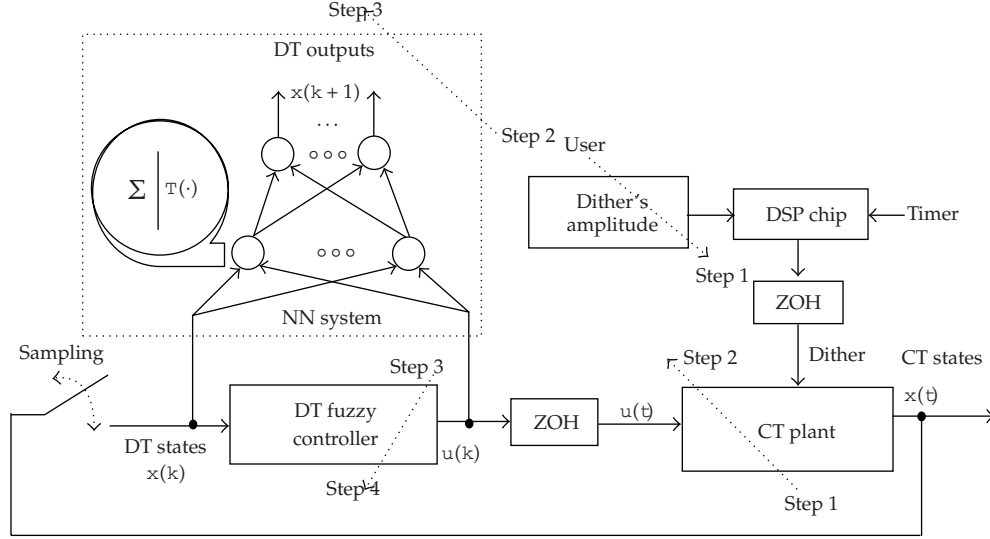


Figure 1: CT to DT fuzzy control system with dither effect and design flow chart.

boundedness given in [19]. Then f_{CT} is discretized by setting the sampling time or sampling period \bar{T} (sec), and $t = k \cdot \bar{T}$, k is a positive integer, to the following a DT nonlinear system f_{DT} :

$$x\left((k+1) \cdot \bar{T}\right) = f_{DT}\left(x\left(k \cdot \bar{T}\right), u\left(k \cdot \bar{T}\right)\right), \quad \text{or} \quad x(k+1) = f_{DT}(x(k), u(k)), \quad (2.2)$$

where k indicates the signal sequence, the DT state vector is $x(k \cdot \bar{T})$, and the DT control input vector is $u(k \cdot \bar{T})$.

In this study, an NN system is first established to approximate a CT nonlinear system (2.1). An LDI state-space representation is then established for the dynamics of the NN system. Finally, a DT fuzzy controller is designed to stabilize the CT nonlinear system.

2.1. Neural Network System

An NN system with S layers each having R^e ($r = 1^e, 2^e, \dots, R^e$; $e = 1, 2, \dots, S$) neurons is established to approximate a CT nonlinear system f_{CT} , as shown in Figure 1. Superscript text is used to distinguish these layers. Specifically, we append the number of the layer as superscript to the names of these variables. Thus, the weight matrix for the e th ($e = 1, 2, \dots, S$) layer is written as $W^{e(\bar{T})}$. Moreover, it is assumed that v_r ($r = 1^e, 2^e, \dots, R^e$) is the net input and that all the transfer functions $T_S(v_r)$ of units in the NN system are described by the following sigmoid function:

$$T_S(v_r) = \frac{1}{1 + \exp(-v_r/q)} - 1, \quad (2.3)$$

where q and α are the positive parameters associated with the sigmoid function. The transfer function vector of the e th layer is defined as

$$\Psi^e(v_r) \equiv [T_S(v_{1^e}), T_S(v_{2^e}), \dots, T_S(v_{R^e})]^T, \quad e = 1, 2, \dots, S, \quad (2.4)$$

where $T_S(v_r)$ ($r = 1^e, 2^e, \dots, R^e$) is a transfer function of the r th neuron. The final outputs of the NN system can then be inferred as follows:

$$x(k+1) = \left(W^S \left(W^{S-1} \left(W^{S-2} \left(\dots \left(W^2 \left(W^1 Z(k) \right) \right) \right) \right) \right) \right), \quad (2.5)$$

where $Z^T(k) = [x(k), u(k)]$. In next section, an LDI state-space representation is established in order to deal with the stability problem of the NN system.

2.2. Linear Difference Inclusion (LDI)

An LDI system can be described in the state-space representation as [12]:

$$y(k+1) = A(a(k))y(k), \quad A(a(k)) = \sum_{i=1}^l h_i(a(k))A_i, \quad (2.6)$$

where l is a positive integer, a is a vector signifying the dependence of h_i on its elements, A_i ($i = 1, 2, \dots, l$), and $y(k) = [y_1(k), y_2(k), \dots, y_l(k)]^T$. Moreover, it is assumed that $h_i \geq 0$, $\sum_{i=1}^l h_i = 1$. From the properties of LDI, without loss of generality, we can use $h_i(k)$ instead of $h_i(a(k))$. In the following, a procedure is taken to represent the dynamics of the NN system (2.5) by LDI state-space representation [12]:

$$g(T_S(v_r)) = \begin{cases} g_1 = \min_{v_r} \frac{dT_S(v_r)}{dv_r} = 0, \\ g_2 = \max_{v_r} \frac{dT_S(v_r)}{dv_r} = \frac{1}{2q}, \end{cases} \quad (2.7)$$

where g_1 and g_2 are the minimum and the maximum of the derivative of T_S , respectively. The min-max matrix G^e is defined as

$$G^e = \text{diag}(g), \quad e = 1, 2, \dots, S; \quad r = 1^e, 2^e, \dots, R^e. \quad (2.8)$$

Next, using the interpolation method and (2.5), we can obtain

$$\begin{aligned}
x(k+1) &= \sum_{v_1=1}^2 \sum_{v_2=1}^2 \cdots \sum_{v_{R^S}=1}^2 h_{v_1}^S(k) h_{v_2}^S(k) \cdots h_{v_{R^S}}^S(k) G^S \\
&\quad \times \left(W^S \left[\cdots \left[\sum_{v_1=1}^2 \sum_{v_2=1}^2 \cdots \sum_{v_{R^2}=1}^2 h_{v_1}^2(k) h_{v_2}^2(k) \cdots h_{v_{R^2}}^2(k) G^2 \right. \right. \right. \\
&\quad \left. \left. \left. \times \left(W^2 \left[\sum_{v_1=1}^2 \sum_{v_2=1}^2 \cdots \sum_{v_{R^1}=1}^2 h_{v_1}^1(k) h_{v_2}^1(k) \cdots h_{v_{R^1}}^1(k) G^1 (W^{-1} Z(k)) \right] \right] \right] \cdots \right] \right) \\
&= \sum_{\Omega^S} \tilde{h}_{\Omega^S}^S(k) G^S W^S \cdots \sum_{\Omega^2} \tilde{h}_{\Omega^2}^2(k) G^2 W^2 \sum_{\Omega^1} \tilde{h}_{\Omega^1}^1(k) G^1 W^{-1} Z(k) = \sum_{\Omega} \hat{h}_{\Omega}(k) E_{\Omega} Z(k),
\end{aligned} \tag{2.9}$$

where

$$\begin{aligned}
\sum_{\Omega^e} \tilde{h}_{\Omega^e}^e(k) &\equiv \sum_{v_1=1}^2 \sum_{v_2=1}^2 \cdots \sum_{v_{R^e}=1}^2 h_{v_1}^e(k) h_{v_2}^e(k) \cdots h_{v_{R^e}}^e(k), \quad \text{for } e = 1, 2, \dots, S; \\
h_{v_r}^e(k) &\in [0, 1], \quad \sum_{v_r=1}^2 h_{v_r}^e(k) = 1, \quad \text{for } r = 1^e, 2^e, \dots, R^e, \\
E_{\Omega} &\equiv G^S W^S \cdots G^2 W^2 G^1 W^{-1}, \quad \sum_{\Omega} \hat{h}_{\Omega}(k) \equiv \sum_{\Omega^S} \cdots \sum_{\Omega^2} \sum_{\Omega^1} \tilde{h}_{\Omega^S}^S(k) \cdots \tilde{h}_{\Omega^2}^2(k) \tilde{h}_{\Omega^1}^1(k).
\end{aligned} \tag{2.10}$$

Finally, using (2.6), we can rewrite the dynamics of the NN system (2.9) in the following LDI state-space representation:

$$x(k+1) = \sum_{i=1}^1 \hat{h}_i(k) E_i Z(k), \tag{2.11}$$

where $\hat{h}_i(k) \geq 0$, $\sum_{i=1}^1 \hat{h}_i(k) = 1$, 1 is a positive integer, and E_i is a constant matrix with appropriate dimension associated with E_{Ω} . The LDI state-space representations (2.11) can be further rearranged as follows:

$$x(k+1) = \sum_{i=1}^1 \hat{h}_i(k) [A_i x(k) + B_i u(k)], \tag{2.12}$$

where A_i and B_i are the partitions of E_i corresponding to the partitions of $Z(k)$. Furthermore, we obtain the LDI relaxed representations of the CT dithered system, as shown in the next section.

2.3. LDI Form of the Dithered System

The LDI form of a CT nonlinear system with dither includes the dither's maximum amplitude and can be obtained by replacing \hat{h}_i, A_i, B_i in (2.12) with the relaxed parameters $\check{h}_i, \check{A}_i(\cdot), \check{B}_i(\cdot)$, respectively. For relaxed theory and its application for dithered systems, refer to [15]. Hence, we directly obtain the LDI state-space relaxed representation of this CT dithered system as

$$x(k+1) = \sum_{i=1}^1 \check{h}_i(k) [\check{A}_i(\cdot)x(k) + \check{B}_i(\cdot)u(k)], \quad (2.13)$$

where $u(k)$ is a Takagi-Sugeno (T-S) DT fuzzy controller, as shown in the following section.

3. T-S DT Fuzzy Controller

Here, a Takagi-Sugeno (T-S) DT fuzzy controller is synthesized to stabilize the NN system (2.13). The DT fuzzy controller is in the following form.

Rule j. IF $x_1(k)$ is M_{j1} , and ...and $x_\mu(k)$ is $M_{j\mu}$, THEN $u(k) = -F_j x(k)$, where $j = 1, 2, \dots$, and μ is the number of IF-THEN rules and $M_{j\mu}$ ($\mu = 1, 2, \dots$) are the fuzzy sets. Hence, the final output of this DT fuzzy controller is inferred as follows:

$$u(k) = \frac{-\sum_{j=1}^M h_j(x) F_j x(k)}{\sum_{j=1}^M h_j(x) F_j x(k)} = -\sum_{j=1}^M \bar{h}_j(x) F_j x(k) \quad (3.1)$$

with

$$h_j(x) = \prod_{\mu=1}^M M_{j\mu}(x_\mu(k)), \quad \bar{h}_j(x) = \frac{h_j(x)}{\sum_{j=1}^M h_j(x)}, \quad (3.2)$$

in which $M_{j\mu}$ is the grade of membership of x_μ in $M_{j\mu}$. In this study, it is also assumed that $h_j(x) \geq 0$, $\sum_{j=1}^M h_j(x) > 0$, $j = 1, 2, \dots$, and $k = 1, 2, \dots, K$. Therefore, $\bar{h}_j(x) \geq 0$, $\sum_{j=1}^M \bar{h}_j(x) = 1$ for all k . Substituting (3.1) into (2.12), we have

$$x(k+1) = \sum_{i=1}^1 \sum_{j=1}^M \check{h}_i \bar{h}_j(x) [\check{A}_i(\cdot) - \check{B}_i(\cdot) F_j] x(k) = \sum_{i=1}^1 \sum_{j=1}^M \check{h}_i \bar{h}_j \check{H}_{ij}(\cdot) x(k), \quad (3.3)$$

where $\check{H}_{ij} = \check{A}_i - \check{B}_i F_j$.

Furthermore, we consider the CT system (2.1) by using the above NN system (3.3) and modeling error $e_{\text{mod}}(k)$ as follows:

$$x(k+1) = \sum_{i=1}^1 \sum_{j=1}^{\check{h}_i \bar{h}_j \check{H}_{ij}(\cdot)} \check{h}_i \bar{h}_j \check{H}_{ij}(\cdot) x(k) + e_{\text{mod}}(k), \quad \text{for } i=1,2,\dots, \check{h}; m=1,2,\dots, \bar{h}; j=1,2,\dots, \check{H}_{ij} \quad (3.4)$$

where $e_{\text{mod}}(k) \equiv f_{\text{CT}}(\cdot) - \sum_{i=1}^1 \sum_{j=1}^{\check{h}_i \bar{h}_j} \check{h}_i \bar{h}_j [\check{A}_i(\cdot) - \check{B}_i(\cdot) F_j] x(k)$.

If the closed-loop CT system's sampling frequency is sufficiently high, according to the Nyquist sampling theory, the discretized states of this dithered system can approximate its original CT states. This permits a rigorous prediction of the stability of the CT dithered system by establishing the stability of the closed-loop NN system (3.4) with the bounded condition (e_U). The modeling error $e_{\text{mod}}(k)$ satisfies the following bounded condition:

$$e_{\text{mod}}^T(k) e_{\text{mod}}(k) \leq e_U^T e_U. \quad (3.5)$$

Moreover, according to the Lyapunov approach, the following Theorem 3.1 is given to guarantee the uniformly ultimately bounded (UUB) stability of the closed-loop CT system (3.4).

Theorem 3.1. *The closed-loop CT system (3.4) is UUB stable in the large if there exists a common positive definite matrix $P > 0$, $Q > 0$, $\alpha > 0$ and $\beta \geq 0$ such that*

$$\check{H}_{ij}^T P \cdot \check{H}_{ij} - P + \alpha \check{H}_{ij}^T P^T P \check{H}_{ij} \leq -Q, \quad (3.6)$$

where $\check{H}_{ij}(\cdot) = \check{A}_i(\cdot) - \check{B}_i(\cdot) F_j$.

Proof. See the appendix. □

According to the stability conditions addressed in Theorem 3.1, the closed-loop NN system is classified into two conditions. Condition 1: if there exists a common positive definite matrix P to satisfy the stability conditions in Theorem 3.1, then the fuzzy controller can stabilize this closed-loop NN system without dither. Condition 2: if there does not exist a common positive definite matrix P to satisfy the stability conditions in Theorem 3.1, then the DT fuzzy controller and the dither (as an auxiliary of the T-S fuzzy controller) are simultaneously introduced to stabilize the closed-loop CT nonlinear system. Therefore, the rest of this paper focuses on the robust stability analysis of Condition 2.

4. T-S DT Fuzzy Controller and Dither Design Algorithm

An illustration of the flow chart in Figure 1 for DT fuzzy controller and dither design algorithm is as follows.

Step 1. If the DT fuzzy controller cannot stabilize the NN system, a dither, as an auxiliary of this controller, is simultaneously introduced to stabilize the closed-loop CT system. This study suggests users add the dither's amplitude from zero, and go to Step 2 until Step 4 has a stable solution.

Step 2. The CT nonlinear system with dither is discretized by setting the sampling time \bar{T} , and go to Step 3.

Step 3. Collect DT training input data: $x(k)$ and $u(k)$, output data: $x(k+1)$, and the NN system can be obtained by a Levenberg-Marquardt backpropagation (LM-BP) algorithm [13] and the LDI relaxed representation, then go to Step 4.

Step 4. According to the LDI relaxed representation in Step 3, a T-S DT fuzzy controller (3.1) can be designed by the linear matrix inequality (LMI) method. Finally, we can adjust the dither's amplitude in Step 1 and verify the stability condition of a system with this DT fuzzy controller in Step 4.

5. Case Study

The above T-S DT fuzzy controller and dither design algorithm discussed in the preceding section is illustrated below by the numerical example of a van der Pol control system:

$$\begin{aligned}\dot{x}_1 &= x_2, \\ \dot{x}_2 &= -x_1 + 2 \cdot (1 - x_1^2)x_2 + u,\end{aligned}\tag{5.1}$$

where the initial states $x_1(0) = -3$, $x_2(0) = 0$.

In this example, we use the dither method [19] in Case 2 to compare with our method in Case 1 as follows.

Case 1. Stability of the NN model in Figure 2 of the dithered system with a fuzzy controller, and demonstrate the control performance of dither plus fuzzy controller in the van der Pol system.

Case 2. Demonstrate the control performance of the dithering system [19] in the van der Pol system.

First, the neural-network structure 3-3-1 of Case 1 has 3 inputs, 3 sigmoid neurons of (2.3) in a hidden layer, 1 sigmoid neuron in an output layer, and their weights are 12, as shown in Figure 2.

Step 1. According to Theorem 3.1, the T-S DT fuzzy controller cannot stabilize the NN system of (5.2) without dither. Hence, we use a dither and DT fuzzy controller and rebuild the NN system of (5.2) with dither to stabilize the following closed-loop CT system with

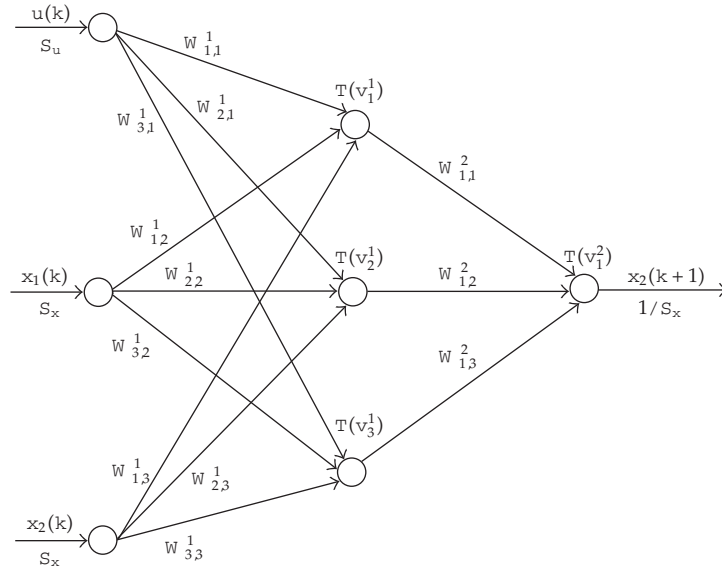


Figure 2: NN model of CT dithered system.

dither:

$$\dot{x}_1 = x_2,$$

$$\dot{x}_2 = -x_1 + 2 \cdot \left(1 - x_1^2\right)x_2 + u_D + u(t) = -x_1 + 2 \left[1 - (x_1 + D(\cdot, \cdot))^2\right] x_2 + u(t), \quad (5.2)$$

where $u_D = -2[2x_1D(\cdot, \cdot) + D^2(\cdot, \cdot)]x_2$. A periodic symmetrical square-wave dither $D(\cdot, \cdot)$ with sufficiently high frequency is added in front of $u(t)$. The lower-bound dither's maximum amplitude $= 0.5$.

Step 2. The CT nonlinear system with dither is discretized as the following equations by setting the sampling time $\bar{T} = 0.05$ sec, and go to Step 3,

$$\begin{aligned} x_1(k+1) &= x_1(k) + x_2(k)\bar{T}, \\ x_2(k+1) &= x_2(k) + \left\{-x_1(k) + 2 \left[1 - (x_1(k) + D(\cdot, \cdot))^2\right]x_2(k) + u(k)\right\}\bar{T}. \end{aligned} \quad (5.3)$$

Step 3. Collect and shuffle DT training input data: $x(k)$ and $u(k)$, output data: $x(k+1)$ to avoid most of local optimal weight values, due to the NN system is obtained by a LM-BP algorithm [13]. The training result is shown in Figure 3.

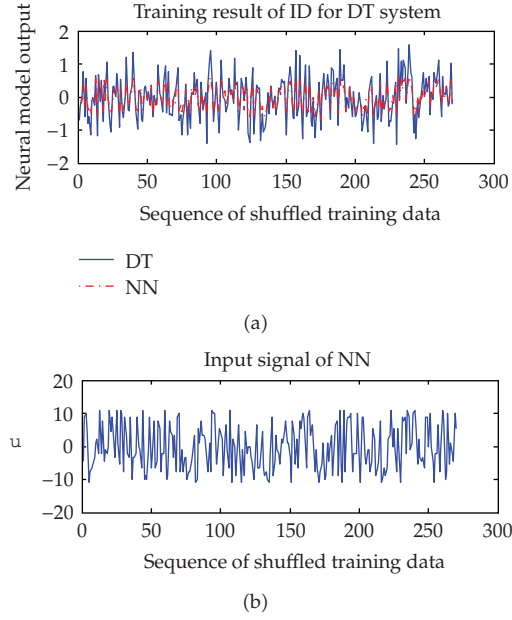


Figure 3: The training result of NN for system identification for Case 1.

The weight matrices of the hidden and the output layer are denoted by W^1 and W^2 . After training via the LM-BP algorithm, the weights can be obtained as follows:

$$\begin{aligned}
 W_{1,1}^1 &= 0.2304, & W_{2,1}^1 &= 0.6039, & W_{3,1}^1 &= 0.6846, \\
 W_{1,2}^1 &= -0.1446, & W_{2,2}^1 &= 2.4534, & W_{3,2}^1 &= -0.1107, \\
 W_{1,3}^1 &= 1.8985, & W_{2,3}^1 &= -0.1123, & W_{3,3}^1 &= 0.8417, \\
 W_{1,1}^2 &= 0.2853, & W_{1,2}^2 &= -0.0002, & W_{1,3}^2 &= 0.0267.
 \end{aligned} \tag{5.4}$$

If the symbol v_b^a denotes the net input of the b th neuron of the a th layer, then

$$v_r^1 = W_{r,1}^1 S_u u(k) + W_{r,2}^1 S_x x_1(k) + W_{r,3}^1 S_x x_2(k), \quad r = 1, 2, 3, \tag{5.5}$$

where $S_x = 1/3$ and $S_u = 1/11$ are the scaling constants to limit the range of inputs x , u in the NN model; respectively, and

$$v_1^2 = W_{1,1}^2 T_s(v_1^1) + W_{1,2}^2 T_s(v_2^1) + W_{1,3}^2 T_s(v_3^1), \quad x(k+1) = T_s(v_1^2), \tag{5.6}$$

where $T_s(v_r^1) = 2/(1 + \exp(-v_r^1/0.5)) - 1$, $r = 1, 2, 3$, $T_s(v_1^2) = 2/(1 + \exp(-v_1^2/0.5)) - 1$.

Hence, $g_1 = 0$, $g_2 = 1$, and we can obtain $\check{\mathbb{A}}_i(0.5)$, $\check{\mathbb{B}}_i(0.5)$ of the LDI relaxed representation as follows:

$$\begin{aligned}
\check{\mathbb{A}}_1 &= \begin{bmatrix} 1 & \bar{T} \\ g_2^2 W_{1,1}^2 W_{1,2}^1 & g_2^2 W_{1,1}^2 W_{1,3}^1 \end{bmatrix}, & \check{\mathbb{A}}_2 &= \begin{bmatrix} 1 & \bar{T} \\ g_2^2 W_{1,2}^2 W_{2,2}^1 & g_2^2 W_{1,2}^2 W_{2,3}^1 \end{bmatrix}, \\
\check{\mathbb{A}}_3 &= \begin{bmatrix} 1 & \bar{T} \\ g_2^2 W_{1,3}^2 W_{3,2}^1 & g_2^2 W_{1,3}^2 W_{3,3}^1 \end{bmatrix}, \\
\check{\mathbb{A}}_4 &= \begin{bmatrix} 1 & \bar{T} \\ g_2^2 (W_{1,1}^2 W_{1,2}^1 + W_{1,2}^2 W_{2,2}^1) & g_2^2 (W_{1,1}^2 W_{1,3}^1 + W_{1,2}^2 W_{2,3}^1) \end{bmatrix}, \\
\check{\mathbb{A}}_5 &= \begin{bmatrix} 1 & \bar{T} \\ g_2^2 (W_{1,1}^2 W_{1,2}^1 + W_{1,3}^2 W_{3,2}^1) & g_2^2 (W_{1,1}^2 W_{1,3}^1 + W_{1,3}^2 W_{3,3}^1) \end{bmatrix}, \\
\check{\mathbb{A}}_6 &= \begin{bmatrix} 1 & \bar{T} \\ g_2^2 (W_{1,2}^2 W_{2,2}^1 + W_{1,3}^2 W_{3,2}^1) & g_2^2 (W_{1,2}^2 W_{2,3}^1 + W_{1,3}^2 W_{3,3}^1) \end{bmatrix}, \\
\check{\mathbb{A}}_7 &= \begin{bmatrix} 1 & \bar{T} \\ g_2^2 (W_{1,1}^2 W_{1,2}^1 + W_{1,2}^2 W_{2,2}^1 + W_{1,3}^2 W_{3,2}^1) & g_2^2 (W_{1,1}^2 W_{1,3}^1 + W_{1,2}^2 W_{2,3}^1 + W_{1,3}^2 W_{3,3}^1) \end{bmatrix}, \\
\check{\mathbb{B}}_1 &= \begin{bmatrix} 0 \\ g_2^2 W_{1,1}^2 W_{1,1}^1 S_u / S_x \end{bmatrix}, & \check{\mathbb{B}}_2 &= \begin{bmatrix} 0 \\ g_2^2 W_{1,2}^2 W_{2,1}^1 S_u / S_x \end{bmatrix}, & \check{\mathbb{B}}_3 &= \begin{bmatrix} 0 \\ g_2^2 W_{1,3}^2 W_{3,1}^1 S_u / S_x \end{bmatrix}, \\
\check{\mathbb{B}}_4 &= \begin{bmatrix} 0 \\ g_2^2 (W_{1,1}^2 W_{1,1}^1 + W_{1,2}^2 W_{2,1}^1) S_u / S_x \end{bmatrix}, & \check{\mathbb{B}}_5 &= \begin{bmatrix} 0 \\ g_2^2 (W_{1,1}^2 W_{1,1}^1 + W_{1,3}^2 W_{3,1}^1) S_u / S_x \end{bmatrix}, \\
\check{\mathbb{B}}_6 &= \begin{bmatrix} 0 \\ g_2^2 (W_{1,2}^2 W_{2,1}^1 + W_{1,3}^2 W_{3,1}^1) S_u / S_x \end{bmatrix}, \\
\check{\mathbb{B}}_7 &= \begin{bmatrix} 0 \\ g_2^2 (W_{1,1}^2 W_{1,1}^1 + W_{1,2}^2 W_{2,1}^1 + W_{1,3}^2 W_{3,1}^1) S_u / S_x \end{bmatrix}.
\end{aligned} \tag{5.7}$$

Because the case of $\check{\mathbb{A}}_i = \begin{bmatrix} 0 & 0 \\ 1 & 0 \end{bmatrix}$ and $\check{\mathbb{B}}_i = \begin{bmatrix} 0 \\ 0 \end{bmatrix}$ did not have any effect on $x(k+1)$ in the LDI relaxed representation, so the relaxed LMI conditions are not considered this case.

Step 4. According to [15], the lower-bound dither's frequency is 50 Hz. In this example, we choose the sampling frequency of a T-S DT fuzzy controller (3.1) to be 20 Hz, and it can be designed by the linear matrix inequality (LMI) method in Theorem 3.1. First, we design the membership functions of Rule 1, 2 as follows:

$$\begin{aligned} \text{Rule 1 : IF } x_1(k) \text{ is } M_1(x_1(k)), \quad \text{THEN } u(k) &= -F_1x(k), \\ \text{Rule 2 : IF } x_1(k) \text{ is } M_2(x_1(k)), \quad \text{THEN } u(k) &= -F_2x(k), \end{aligned} \quad (5.8)$$

where $x(k) = [x_1(k), x_2(k)]^T$.

Next, we design

$$\bar{h}_1 = M_1 = \exp\left(-\frac{(x_1(k) - c)^2}{(2 - c)^2}\right), \quad \bar{h}_2 = M_2 = 1 - \bar{h}_1. \quad (5.9)$$

Then, we use the Simplex optimization method [14] to search $c = 2.2132$ and $c = 0.00000445$. According to (3.1), the overall T-S DT fuzzy controller is

$$u(k) = -\sum_{j=1}^2 \bar{h}_j F_j x(k). \quad (5.10)$$

Finally, we can adjust dither's amplitude in Step 1, and according to the LMI solutions:

$$P = \begin{bmatrix} 4.174 & 0.1803 \\ 0.1803 & 4.7201 \end{bmatrix}, \quad -\gamma^2 = 10^{-7}, \quad Q = \begin{bmatrix} 10^{-6} & 0 \\ 0 & 10^{-6} \end{bmatrix}, \quad (5.11)$$

we have verified the stability condition of the system with these DT fuzzy gains:

$$F_1 = [-0.0000376, 7.3814], \quad F_2 = [0.0000391, -18.8912]. \quad (5.12)$$

The DT controller of Case 1 is to check the fulfillment of (3.5). According to the recorded values shown in Figure 4, (3.5) is satisfied. Hence, the DT controller of Case 1 can stabilize the CT dithered nonlinear system (5.2), as shown in Figure 5. The DT controller of Case 1 is shown in Figure 6. However, Case 2 cannot stabilize this CT nonlinear system, as shown in Figure 7. Furthermore, the different dither's shapes did not have an effect on the stability of the system, but the system responses to different dithers' shapes of Case 1 must be clearly different.

6. Conclusion

This study presents an effective NN-based approach to stabilizing continuous-time (CT) nonlinear systems by a dither and a T-S discrete-time (DT) fuzzy controller. This NN system is established to approximate a nonlinear system with dither. The dynamics of the NN system

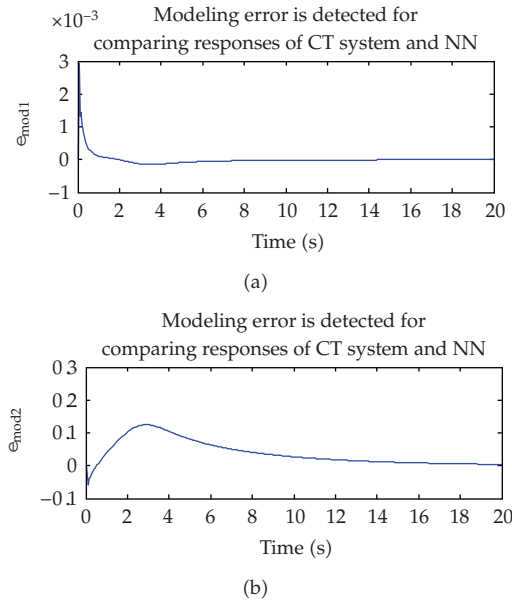


Figure 4: The result of detecting modeling error $e_{mod} = [e_{mod1}, e_{mod2}]^T$ for Case 1.

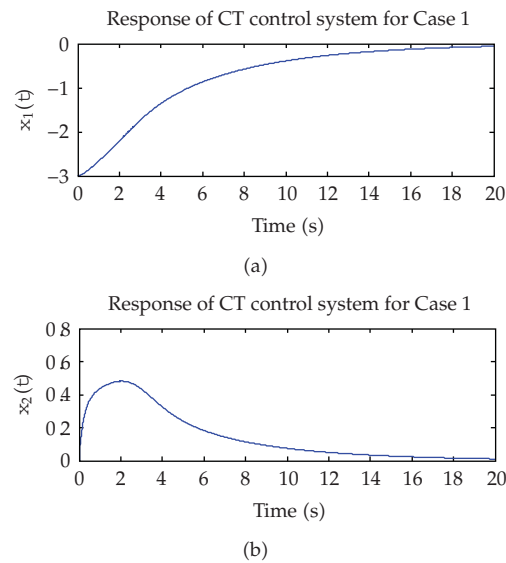


Figure 5: The detail of response of a van der Pol control system for Case 1.

are then converted into an LDI relaxed representation, and finally, a T-S DT fuzzy controller is designed to stabilize the CT nonlinear system by the LMI method. If the designed DT fuzzy controller cannot asymptotically stabilize the NN system, a dither is injected into this system. The T-S DT fuzzy controller and the dither signal are simultaneously introduced to stabilize the closed-loop CT nonlinear system. With sufficiently high dither frequency and system sampling frequency, simulation results show that the DT fuzzy controller can

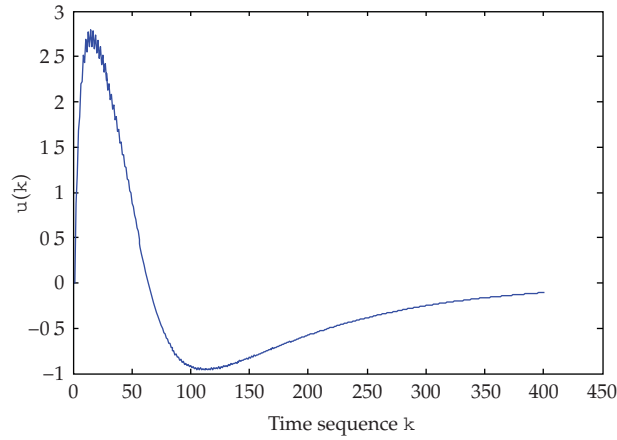


Figure 6: The digital control signal of a van der Pol CT plant for Case 1.

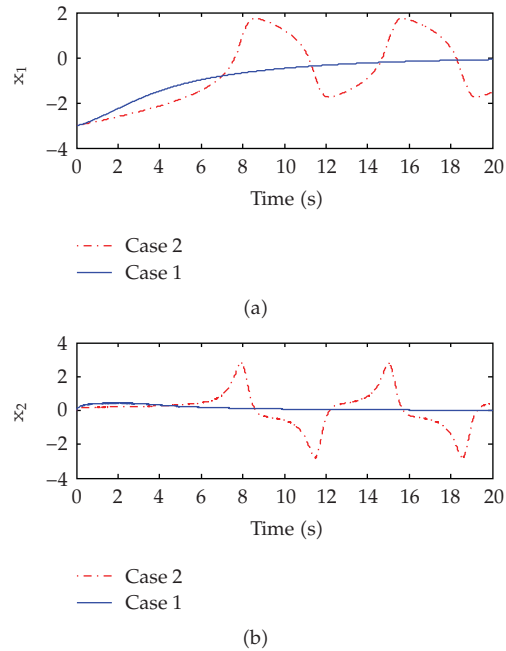


Figure 7: Comparison of results for Cases 1, 2.

stabilize the nonlinear dithered system by appropriately regulating the dither amplitude. The algorithm of LMI solver needs the special form to obtain control gains; therefore we will develop less conservative theorem by SOS algorithm for further research [20]. LM-BP has disadvantages such as getting into local minimum for the offline training stage of NN. For this reason, we will improve these disadvantages of LM-BP by studying fast convergence of genetic algorithm [14] with the multilayer perceptron (MLP) neural network [13].

Appendix

Lemma A.1 (see [11]). *For any matrices A and B with appropriate dimension, we have*

$$A^T B + B^T A \leq -2A^T A + -2B^T B. \quad (\text{A.1})$$

Let the Lyapunov function for the nonlinear system be defined as

$$V(k) = x(k)^T P x(k), \quad (\text{A.2})$$

where $P = P^T > 0$. We then evaluate the backward difference $\Delta V(k)$ of $V(k)$ to obtain

$$\begin{aligned} \Delta V(k) &= V(k+1) - V(k) = x(k+1)^T P \cdot x(k+1) - x(k)^T P \cdot x(k) \\ &= \left\{ \sum_{i=1}^1 \sum_{j=1}^1 \check{h}_i \bar{h}_j \check{H}_{ij}(\cdot) x(k) + e_{\text{mod}}(k) \right\}^T P \left\{ \sum_{i=1}^1 \sum_{j=1}^1 \check{h}_i \bar{h}_j \check{H}_{ij}(\cdot) x(k) + e_{\text{mod}}(k) \right\} \\ &\quad - x(k)^T P \cdot x(k) \\ &= \sum_{i=1}^1 \sum_{j=1}^1 \check{h}_i \bar{h}_j x(k)^T \left[\check{H}_{ij}^T(\cdot) P \check{H}_{ij}(\cdot) - P \right] x(k) + \sum_{i=1}^1 \sum_{j=1}^1 \check{h}_i \bar{h}_j x(k)^T \check{H}_{ij}^T P \cdot e_{\text{mod}}(k) \\ &\quad + \sum_{i=1}^1 \sum_{j=1}^1 \check{h}_i \bar{h}_j e_{\text{mod}}(k)^T P \cdot \check{H}_{ij} x(k) + e_{\text{mod}}(k)^T P \cdot e_{\text{mod}}(k). \end{aligned} \quad (\text{A.3})$$

According to Lemma .1, we obtain

$$\begin{aligned} &x(k)^T \check{H}_{ij}^T P \cdot e_{\text{mod}}(k) + e_{\text{mod}}(k)^T P \cdot \check{H}_{ij} x(k) \\ &\leq -2x(k)^T \check{H}_{ij}^T P^T P \check{H}_{ij} x(k) + -2e_{\text{mod}}(k)^T e_{\text{mod}}(k). \end{aligned} \quad (\text{A.4})$$

Therefore, we obtain

$$\begin{aligned} \Delta V(k) &\leq \sum_{i=1}^1 \sum_{j=1}^1 \check{h}_i \bar{h}_j x(k)^T \left(\check{H}_{ij}^T P \cdot \check{H}_{ij} - P \right) x(k) \\ &\quad + \sum_{i=1}^1 \sum_{j=1}^1 \check{h}_i \bar{h}_j \left[-2x(k)^T \check{H}_{ij}^T P^T P \cdot \check{H}_{ij} x(k) + -2e_{\text{mod}}(k)^T e_{\text{mod}}(k) \right] \\ &= \sum_{i=1}^1 \sum_{j=1}^1 \check{h}_i \bar{h}_j x(k)^T \left(\check{H}_{ij}^T P \cdot \check{H}_{ij} - P + -2\check{H}_{ij}^T P^T P \cdot \check{H}_{ij} \right) x(k) + -2e_{\text{mod}}(k)^T e_{\text{mod}}(k) \\ &\leq -x(k)^T Q \cdot x(k) + -2e_{\text{mod}}(k)^T e_{\text{mod}}(k). \end{aligned} \quad (\text{A.5})$$

In accordance with $\check{H}_{ij}^T P \cdot \check{H}_{ij} - P + \gamma^{-2} \check{H}_{ij}^T P^T P \check{H}_{ij} \leq -Q < 0$, we have

$$\Delta V(k) \leq -x(k)^T Q \cdot x(k) + \gamma^{-2} e_{\text{mod}}(k)^T e_{\text{mod}}(k) \leq -\min(Q) x(k)^T x(k) + \gamma^{-2} e_U^T e_U, \quad (\text{A.6})$$

where $\min(Q)$ denotes the minimum eigenvalue of Q . Whenever

$$\|x(k)\| > \frac{\gamma^{-1} e_U}{\sqrt{\min(Q)}}, \quad \Delta V(k) < 0. \quad (\text{A.7})$$

By a standard Lyapunov extension [21], this illustrates the trajectories of the closed-loop nonlinear systems are UUB stable. From $k = 0$ to N yields

$$\begin{aligned} V(N+1) - V(0) &< -\sum_{k=0}^N x(k)^T Q \cdot x(k) + \gamma^{-2} \sum_{k=0}^N e_{\text{mod}}(k)^T e_{\text{mod}}(k), \\ \sum_{k=0}^N x(k)^T Q \cdot x(k) &< V(0) - V(N+1) + \gamma^{-2} \sum_{k=0}^N e_{\text{mod}}(k)^T e_{\text{mod}}(k). \end{aligned} \quad (\text{A.8})$$

Hence, we have

$$\sum_{k=0}^N x(k)^T Q \cdot x(k) < x(0)^T \tilde{P} \cdot x(0) + \gamma^{-2} \sum_{k=0}^N e_{\text{mod}}(k)^T e_{\text{mod}}(k). \quad (\text{A.9})$$

Hence, the H_∞ control performance is achieved with a prescribed γ^{-2} in (3.6). Next, recasting a control problem as an LMI problem is equivalent to finding a solution to the original problem, $\check{H}_{ij}^T P \cdot \check{H}_{ij} - P < 0$. The stability conditions encountered in Theorem 3.1 are expressed in the following forms of LMIs. The conditions $\check{H}_{ij}^T P \cdot \check{H}_{ij} - P < 0$ are not jointly convex in F_j and P . Now multiplying the inequality on the left and right by P^{-1} and defining new variables $\bar{P} = P^{-1}$ and $\bar{M}_j = F_j \bar{P}$, the conditions $\check{H}_{ij}^T P \cdot \check{H}_{ij} - P < 0$ can be rewritten using

the Schur complement as follows:

$$\begin{aligned}
 & \begin{bmatrix} -\bar{P} & (\check{A}_{i\bar{P}} - \check{B}_{j\bar{M}})^T \\ \check{A}_{i\bar{P}} - \check{B}_{j\bar{M}} & -\bar{P} \end{bmatrix} < 0, \quad \text{for } i=1,2,\dots,l; j=1,2,\dots, \\
 & \begin{bmatrix} -2\bar{P} & (2\check{A}_{i\bar{P}} - \check{B}_{j\bar{M}} - \check{B}_{j\bar{M}})^T \\ 2\check{A}_{i\bar{P}} - \check{B}_{j\bar{M}} - \check{B}_{j\bar{M}} & -\bar{P} \end{bmatrix} < 0, \quad \text{for } j < = 1,2,\dots, \\
 & \begin{bmatrix} -2\bar{P} & (\check{A}_{i\bar{P}} - \check{B}_{j\bar{M}} + \check{A}_{i\bar{P}} - \check{B}_{j\bar{M}})^T \\ \check{A}_{i\bar{P}} - \check{B}_{j\bar{M}} + \check{A}_{i\bar{P}} - \check{B}_{j\bar{M}} & -\bar{P} \end{bmatrix} < 0, \quad \text{for } i < = 1,2,\dots,l, \\
 & \begin{bmatrix} -4\bar{P} & \check{M}^T \\ \check{M} & -\bar{P} \end{bmatrix} < 0, \quad \text{for } i < = 1,2,\dots,l; j < = 1,2,\dots,
 \end{aligned} \tag{A.10}$$

where $\check{M} \equiv \check{A}_{i\bar{P}} - \check{B}_{j\bar{M}} + \check{A}_{i\bar{P}} - \check{B}_{j\bar{M}} + \check{A}_{i\bar{P}} - \check{B}_{j\bar{M}} + \check{A}_{i\bar{P}} - \check{B}_{j\bar{M}}$.

The feedback gain F_j and a common P can be obtained as $P = \bar{P}^{-1}$, $F_j = \bar{M}_{j\bar{P}}^{-1}$ from the solutions \bar{P} and $\bar{M}_{j\bar{P}}$.

References

- [1] H. Dong, Z. Wang, D. W. C. Ho, and H. Gao, "Robust H_∞ fuzzy output-feedback control with multiple probabilistic delays and multiple missing measurements," *IEEE Transactions on Fuzzy Systems*, vol. 18, no. 4, pp. 712–725, 2010.
- [2] H. Dong, Z. Wang, and H. Gao, " H_∞ fuzzy control for systems with repeated scalar nonlinearities and random packet losses," *IEEE Transactions on Fuzzy Systems*, vol. 17, no. 2, pp. 440–450, 2009.
- [3] Z. Wang, Y. Liu, G. Wei, and X. Liu, "A note on control of a class of discrete-time stochastic systems with distributed delays and nonlinear disturbances," *Automatica*, vol. 46, no. 3, pp. 543–548, 2010.
- [4] H. O. Wang, K. Tanaka, and M. F. Griffin, "An approach to fuzzy control of nonlinear systems: stability and design issues," *IEEE Transactions on Fuzzy Systems*, vol. 4, no. 1, pp. 14–23, 1996.
- [5] Z. Wang, D. W. C. Ho, H. Dong, and H. Gao, "Robust \mathcal{L}_∞ finite-horizon control for a class of stochastic nonlinear time-varying systems subject to sensor and actuator saturations," *IEEE Transactions on Automatic Control*, vol. 55, no. 7, pp. 1716–1722, 2010.
- [6] Z. Wang, G. Wei, and G. Feng, "Reliable H_∞ control for discrete-time piecewise linear systems with infinite distributed delays," *Automatica*, vol. 45, no. 12, pp. 2991–2994, 2009.
- [7] B. Shen, Z. Wang, H. Shu, and G. Wei, "Robust H_∞ finite-horizon filtering with randomly occurred nonlinearities and quantization effects," *Automatica*, vol. 46, no. 11, pp. 1743–1751, 2010.
- [8] B. Shen, Z. Wang, H. Shu, and G. Wei, " H_∞ filtering for nonlinear discrete-time stochastic systems with randomly varying sensor delays," *Automatica*, vol. 45, no. 4, pp. 1032–1037, 2009.
- [9] H. Dong, Z. Wang, D. W. C. Ho, and H. Gao, "Variance-constrained \mathcal{L}_∞ filtering for a class of nonlinear time-varying systems with multiple missing measurements: the finite-horizon case," *IEEE Transactions on Signal Processing*, vol. 58, no. 5, pp. 2534–2543, 2010.
- [10] H. Dong, Z. Wang, and H. Gao, "Robust H_∞ filtering for a class of nonlinear networked systems with multiple stochastic communication delays and packet dropouts," *IEEE Transactions on Signal Processing*, vol. 58, no. 4, pp. 1957–1966, 2010.
- [11] B. S. Chen, C. S. Tseng, and H. J. Uang, "Mixed H_2/H_∞ fuzzy output feedback control design for nonlinear dynamic systems: an LMI approach," *IEEE Transactions on Fuzzy Systems*, vol. 8, no. 3, pp. 249–265, 2000.

- [12] K. Tanaka, "An approach to stability criteria of neural-network control systems," *IEEE Transactions on Neural Networks*, vol. 7, no. 3, pp. 629–642, 1996.
- [13] M. M. Gupta, L. Jin, and N. Homma, *Static and Dynamic Neural Networks from Fundamentals to Advanced Theory*, John Wiley & Sons, Hoboken, NJ, USA, 2003.
- [14] J. S. R. Jang, C. T. Sun, and E. Mizutani, *Neuro-Fuzzy and Soft Computing*, Prentice-Hall, 1997.
- [15] Z.-R. Tsai, Y.-Z. Chang, J.-D. Hwang, and J. Lee, "Robust fuzzy stabilization of dithered chaotic systems using island-based random optimization algorithm," *Information Sciences*, vol. 178, no. 4, pp. 1171–1188, 2008.
- [16] G. Zames and N. A. Shneydor, "Structural stabilization and quenching by dither in nonlinear systems," *IEEE Transactions on Automatic Control*, vol. 22, no. 3, pp. 352–361, 1977.
- [17] S. Mossaheb, "Application of a method of averaging to the study of dithers in nonlinear systems," *International Journal of Control*, vol. 38, no. 3, pp. 557–576, 1983.
- [18] C. A. Desoer and S. M. Shahruz, "Stability of dithered nonlinear systems with backlash or hysteresis," *International Journal of Control*, vol. 43, no. 4, pp. 1045–1060, 1986.
- [19] A. M. Steinberg and I. Kadushin, "Stabilization of nonlinear systems with a dither control," *Journal of Mathematical Analysis and Applications*, vol. 43, pp. 273–284, 1973.
- [20] K. Tanaka, H. Ohtake, and H. O. Wang, "Guaranteed cost control of polynomial fuzzy systems via a sum of squares approach," *IEEE Transactions on Systems, Man, and Cybernetics, Part B*, vol. 39, no. 2, pp. 561–567, 2009.
- [21] J. P. LaSalle, "Some extensions of Liapunov's second method," *IRE Transactions on Circuit Theory*, vol. 7, no. 4, pp. 520–527, 1960.

Research Article

Further Stability Criterion on Delayed Recurrent Neural Networks Based on Reciprocal Convex Technique

Guobao Zhang,¹ Tao Li,² and Shumin Fei¹

¹ Key Laboratory of Measurement and Control of CSE, School of Automation, Southeast University, Ministry of Education, Nanjing 210096, China

² School of Automation Engineering, Nanjing University of Aeronautics and Astronautics, Nanjing 210007, China

Correspondence should be addressed to Tao Li, litaotianren@yahoo.com.cn

Received 15 April 2011; Revised 3 June 2011; Accepted 6 July 2011

Academic Editor: Zidong Wang

Copyright © 2012 Guobao Zhang et al. This is an open access article distributed under the Creative Commons Attribution License, which permits unrestricted use, distribution, and reproduction in any medium, provided the original work is properly cited.

Together with Lyapunov-Krasovskii functional theory and reciprocal convex technique, a new sufficient condition is derived to guarantee the global stability for recurrent neural networks with both time-varying and continuously distributed delays, in which one improved delay-partitioning technique is employed. The LMI-based criterion heavily depends on both the upper and lower bounds on state delay and its derivative, which is different from the existent ones and has more application areas as the lower bound of delay derivative is available. Finally, some numerical examples can illustrate the reduced conservatism of the derived results by thinning the delay interval.

1. Introduction

Recently, various classes of neural networks have been increasingly studied in the past few decades, due to their practical importance and successful applications in many areas such as optimization, image processing, and associative memory design. In those applications, the key feature of the designed neural network is to be convergent. Meanwhile, since there inevitably exist communication delay which is the main source of oscillation and instability in various dynamical systems, great efforts have been made to analyze the dynamical behaviors of time-delay systems including delayed neural networks (DNNs), and many elegant results have been reported; see [1–31] and the references therein. In practical application, though it is difficult to describe the form of delay precisely, the ranges of time delay and its variation rate can be measured. Since Lyapunov functional approach imposed no restriction on delay

and its derivative and presented the simple stability results, Lyapunov-Krasovskii functional (LKF) one has been widely utilized due to that it can fully utilize the information on time-delay system. Thus recently, the delay-dependent stability or delay-derivative-dependent one for DNNs has become an important topic of primary significance, in which its main purpose was to derive the maximum allowable upper bound on time delay such that the system can be convergent [7–9, 11–16]. Meanwhile, since a neural network usually has a spatial nature due to the presence of an amount of parallel pathways of a variety of axon sizes and lengths, it is desired to model them by introducing a distributed delay over a certain duration of time such that the distant past has less influence compared to the recent behavior of the state. In other words, when studying stability for DNNs, the distributed delay should be taken into consideration simultaneously [18–26].

Presently, during tackling the effect of time delay, the delay-partitioning idea has been verified to be more effective in reducing the conservatism and widely employed [10–17]. In [11], one delay-partitioning idea has been used to tackle time-varying delay of DNNs based on the improved idea in [10] and in [12, 13], and some researchers also put forward the other novel delay-partitioning idea to tackle constant delay, which can be more evident and concise than the idea based on the one in [10]. Later, though the idea was extended to time-varying delay case [14, 15, 17], the improved idea cannot deal with the interval varying delay efficiently, especially as the lower bound of delay is greater than 0. Meanwhile, as for time-varying delay, because convex combination technique can play an important role in reducing the conservatism, it has received much attention and achieved some great improvements in studying the stability for time-delay systems including DNNs [15–18, 28–30]. Its basic idea is to approximate the integral terms of quadratic quantities into a convex combination of quadratic terms of the LMIs. However, owing to the inversely weighted nature of coefficients in Jensen inequality approach or the limitation of free-weighting matrix method, when estimating the derivative of Lyapunov-Krasovskii functional, some important terms still have been ignored based on the convex combination technique [15–18]. In [31], together with integral inequality lemma, the authors put forward the reciprocal convex technique, which can consider these previously ignorant terms. Yet, we have noticed that the reciprocal convex technique could not tackle the case that the lower and upper bound of time delay can be measured simultaneously, which still needs the convex technique. Now, together with the improved delay-partitioning idea in [17] and combining reciprocal convex technique with convex combination one, no researcher has investigated the stability for DNNs as the lower bound of delay derivative is available, which motivates the focus of this presented work.

In the paper, we make some great efforts to investigate asymptotical stability for recurrent neural networks with both time-varying and continuously distributed delay, in which both the upper and lower bounds of time delay and its derivative are treated. Through applying an improved delay-partitioning idea, one LMI-based condition is derived based on combination of reciprocal convex technique and convex one, which can present the pretty delay dependence and computational efficiency. Finally, we give three numerical examples to illustrate the reduced conservatism.

Notations

For symmetric matrices $X, Y, X > Y$ (resp., $X \geq Y$) means that $X - Y > 0$ ($X - Y \geq 0$) is a positive-definite (resp., positive-semidefinite) matrix; $\text{Tr}(A)$ denotes the trace of the matrix A ; $\begin{bmatrix} X & Y \\ Y^T & Z \end{bmatrix} = \begin{bmatrix} X & Y \\ * & Z \end{bmatrix}$ with $*$ denotes the symmetric term in a symmetric matrix.

2. Problem Formulations

Consider the DNNs with continuously distributed delay of the following form:

$$\dot{z}(t) = -Cz(t) + Ag(z(t)) + Bg(z(t-\tau(t))) + D \int_{-\infty}^t K(t-s)g(z(s))ds + J, \quad (2.1)$$

where $z(t) = [z_1(t) \cdots z_n(t)]^T \in \mathbf{R}^n$ is the neuron state vector; $C = \text{diag}\{c_1, \dots, c_n\} > 0$ and A, B, D are $n \times n$ known constant matrices; $g(z(\cdot)) = [g_1(z_1(\cdot)) \cdots g_n(z_n(\cdot))]^T \in \mathbf{R}^n$ stands for the neuron activation function, $J \in \mathbf{R}^n$ is a constant input vector, and $K(t-s) = [k_{ij}(t-s)]_{n \times n}$; here the delay kernel $k_{ij}(\cdot)$ is a real-valued nonnegative continuous function defined on $[0, +\infty)$ and satisfies $\int_0^\infty k_{ij}(\tau) d\tau = 1$ for $i, j = 1, 2, \dots, n$.

The following assumptions on system (2.1) are utilized throughout this paper.

(H1) The delay $\tau(t)$ denotes one continuous function satisfying

$$0 \leq \tau(t) \leq \tau_m, \quad \mu_0 \leq \dot{\tau}(t) \leq \mu_m, \quad (2.2)$$

in which τ_m, μ_0, μ_m are constants. Here we denote $\bar{\mu}_m = \mu_m - \mu_0$ and $\bar{\mu}_m = \mu_m - \mu_0$.

(H2) For the constants $\bar{\mu}_j^+, \bar{\mu}_j^-$, the functions $g_j(\cdot)$ in (2.1) are bounded and satisfy the following condition:

$$\bar{\mu}_j^- \leq \frac{g_j(x) - g_j(y)}{x - y} \leq \bar{\mu}_j^+, \quad \forall x, y \in \mathbf{R}, x \neq y, j = 1, 2, \dots, n. \quad (2.3)$$

In what follows, we denote $\Sigma = \text{diag}\{\bar{\mu}_1^-, \dots, \bar{\mu}_n^-\}$, $\bar{\Sigma} = \text{diag}\{\bar{\mu}_1^+, \dots, \bar{\mu}_n^+\}$ and set $\Sigma_1 = \Sigma \bar{\Sigma}$, $\Sigma_2 = (\Sigma + \bar{\Sigma})/2$, respectively.

Remark 2.1. As pointed out in [22], the constants $\bar{\mu}_i^+, \bar{\mu}_i^-$ in (H2) are allowed to be positive, negative, or zero. Thus, some previously used Lipschitz conditions are just special cases of (H2), which means that the activation functions are of more general descriptions than these previous ones.

Suppose $z^* = [z_1^* \cdots z_n^*]^T$ is the equilibrium point of the system (2.1). In order to prove the result, we will shift the equilibrium to the origin by changing the variable $x(\cdot) = z(\cdot) - z^*$. Then the system (2.1) can be transformed into

$$\dot{x}(t) = -Cx(t) + Af(x(t)) + Bf(x(t-\tau(t))) + D \int_{-\infty}^t K(t-s)f(x(s))ds, \quad (2.4)$$

where $x(t) = [x_1(t), \dots, x_n(t)]^T$, and $f(x) = [f_1(x_1), \dots, f_n(x_n)]^T$ with $f_j(x_j) = g_j(x_j + z_j^*) - g_j(z_j^*)$, $j = 1, 2, \dots, n$. Note that the function $f_j(\cdot)$ satisfies $f_j(0) = 0$, and

$$\bar{\mu}_j^- \leq \frac{f_j(x)}{x} \leq \bar{\mu}_j^+, \quad \forall x \in \mathbf{R}, x \neq 0. \quad (2.5)$$

In order to establish the stability criterion, firstly, the following lemmas are introduced.

Lemma 2.2 (see [27]). For any constant matrix $W \in \mathbf{R}^{n \times n}$, $W = W^T > 0$, scalar functional $0 \leq r(t) \leq r_M$, and a vector function $e : [-r_M, 0] \rightarrow \mathbf{R}^n$ such that the following integration is well defined, then $-r_M \int_{-r(t)}^0 e^T(t+s)W e(t+s)ds \leq [e(t) - e(t-r(t))]^T W [e(t) - e(t-r(t))]$.

Lemma 2.3 (see [31]). Let the functions $f_1(t), f_2(t), \dots, f_N(t) : \mathbf{R}^m \rightarrow \mathbf{R}$ have the positive values in an open subset \mathbf{D} of \mathbf{R}^m and satisfy

$$\frac{1}{1} f_1(t) + \frac{1}{2} f_2(t) + \dots + \frac{1}{N} f_N(t) : \mathbf{D} \rightarrow \mathbf{R}^n \quad (2.6)$$

with $\alpha_i > 0$ and $\sum_{i=1}^N \alpha_i = 1$, then the reciprocal convex technique of $f_i(t)$ over the set \mathbf{D} satisfies

$$\sum_{i=1}^N \frac{1}{\alpha_i} f_i(t) \geq \sum_{i=1}^N f_i(t) + \sum_{i \neq j} g_{ij}(t) \quad \forall g_{ij}(t) : \mathbf{R}^m \rightarrow \mathbf{R}^n, g_{ij}(t) \doteq g_{ji}(t), \begin{bmatrix} f_i(t) & g_{ij}(t) \\ g_{ji}(t) & f_j(t) \end{bmatrix} \geq 0. \quad (2.7)$$

Then the problem to be addressed in next section can be formulated as developing a condition ensuring that the DNNs (2.4) are asymptotically stable.

3. Delay-Derivative-Dependent Stability

In the section, through utilizing the reciprocal convex technique idea in [31], we present one novel delay-derivative-dependent stability criterion for the system (2.4) in terms of LMIs.

Theorem 3.1. Given a positive integer l and setting $\bar{\alpha}_m = \bar{\alpha}_m / l$, $\tilde{\Sigma}_1 = \text{diag} \{ \Sigma_1, \dots, \Sigma_1 \}_{\times l}$, $\tilde{\Sigma}_2 = \text{diag} \{ \Sigma_2, \dots, \Sigma_2 \}_{\times l}$ then the system (2.4) satisfying (2.2) and (2.5) is globally asymptotically stable if there exist $n \times n$ matrices $P > 0$, $P_1 > 0$, $H_1, Q_1 > 0$, $V > 0$, $W_j > 0 (j=1, \dots, l)$, $S_j (j=1, \dots, l)$, $E_i (i=1, 2)$, $n \times n$ diagonal matrices $K > 0, L > 0, T > 0, U_i > 0 (i=1, 2, 3)$, $V_j > 0, R_j > 0 (j=1, \dots, l)$, $n \times n$ matrices $X_{ij} > 0, Y_{ij}, Z_{ij} > 0 (i=1, 2; j=1, \dots, l)$, and $l_n \times l_n$ constant matrices $\tilde{P} > 0, \tilde{Q} > 0, \tilde{H}$ such that the LMIs in (3.1)-(3.2) hold:

$$\begin{bmatrix} P_1 & H_1 \\ * & Q_1 \end{bmatrix} > 0, \quad \begin{bmatrix} \tilde{P} & \tilde{H} \\ * & \tilde{Q} \end{bmatrix} > 0, \quad \begin{bmatrix} X_{ij} & Y_{ij} \\ * & Z_{ij} \end{bmatrix} > 0, \quad \begin{bmatrix} W_j & S_j \\ * & W_j \end{bmatrix} \geq 0, \quad (3.1)$$

$i=1, 2; j=1, \dots, l$,

$$\Upsilon_1 \Theta \Upsilon_1^T + \Upsilon_2 \Xi \Upsilon_2^T + \frac{\bar{\alpha}_m}{l} \sum_{i=1}^l I_{1i}^T \begin{bmatrix} X_{ki} & Y_{ki} \\ * & Z_{ki} \end{bmatrix} I_{1i} < 0, \quad k=1, 2, \quad (3.2)$$

where $I_{1i} = \begin{bmatrix} 0_{n \cdot (i+1)n} & -I_n & 0_{n \cdot (2i+1)n} & -I_n & 0_{n \cdot (i+4)n} \\ 0_{n \cdot (i+1)n} & I_n & 0_{n \cdot (2i+1)n} & I_n & 0_{n \cdot (i+4)n} \end{bmatrix}$, and

$$\Theta = \begin{bmatrix} \Theta_{11} & V & 0 & \Theta_{14} & 0 & 0 & \Theta_{17} & 0 & E_1^T B & E_1^T D \\ * & \Theta_{22} & 0 & 0 & -H_1 & 0 & 0 & 0 & 0 & 0 \\ * & * & -U_2 \Sigma_1 & 0 & 0 & U_2 \Sigma_2 & 0 & 0 & 0 & 0 \\ * & * & * & \Theta_{44} & 0 & 0 & \Theta_{47} & 0 & 0 & 0 \\ * & * & * & * & -Q_1 & 0 & 0 & 0 & 0 & 0 \\ * & * & * & * & * & -U_2 & 0 & 0 & 0 & 0 \\ * & * & * & * & * & * & \Theta_{77} & 0 & E_2^T B & E_2^T D \\ * & * & * & * & * & * & * & -U_3 \Sigma_1 & U_3 \Sigma_2 & 0 \\ * & * & * & * & * & * & * & * & -U_3 & 0 \\ * & * & * & * & * & * & * & * & * & -\frac{1}{n} T \end{bmatrix},$$

$$Y_1 = \begin{bmatrix} I_n & * \\ 0_{n \cdot n} & I_n & * \\ 0_{n \cdot (i+1)n} & I_n & * \\ 0_{n \cdot (2i+2)n} & I_n & * \\ 0_{n \cdot (2i+3)n} & I_n & * \\ 0_{n \cdot (3i+3)n} & I_n & * \\ 0_{n \cdot (4i+3)n} & I_n & * \\ 0_{n \cdot (4i+4)n} & I_n & * \\ 0_{n \cdot (4i+5)n} & I_n & * \\ 0_{n \cdot (4i+6)n} & I_n & * \end{bmatrix}, \quad \Xi = \begin{bmatrix} \Xi_{11} & \tilde{S} & \tilde{W}_1 - \tilde{S} & \Xi_{14} & 0 & 0 \\ * & \Xi_{22} & \tilde{W} - \tilde{S} & 0 & 0 & -\tilde{H} \\ * & * & \Xi_{33} & 0 & 0 & \Xi_{36} \\ * & * & * & \Xi_{44} & 0 & 0 \\ * & * & * & * & -\tilde{Q} & 0 \\ * & * & * & * & * & \Xi_{66} \end{bmatrix}, \quad Y_2 = \begin{bmatrix} 0_{1n \cdot n} & I_{1n} & * \\ 0_{1n \cdot 2n} & I_{1n} & * \\ 0_{1n \cdot (i+2)n} & I_{1n} & * \\ 0_{1n \cdot (2i+3)n} & I_{1n} & * \\ 0_{1n \cdot (2i+4)n} & I_{1n} & * \\ 0_{1n \cdot (3i+4)n} & I_{1n} & * \end{bmatrix} \quad (3.3)$$

with * representing the appropriately dimensional $\mathbf{0}$ matrix making Y_i ($i = 1, 2$) of $(4i+8)n$ columns, $\tilde{X}_i = \text{diag}\{X_{i1}, \dots, X_{i1}\}$, $\tilde{Y}_i = \text{diag}\{Y_{i1}, \dots, Y_{i1}\}$, $\tilde{Z}_i = \text{diag}\{Z_{i1}, \dots, Z_{i1}\}$, $i = 1, 2$, $\tilde{W} = \text{diag}\{W_1, \dots, W_1\}$, $\tilde{S} = \text{diag}\{S_1, \dots, S_1\}$, $\tilde{V} = \text{diag}\{V_1, \dots, V_1\}$, $\tilde{R} = \text{diag}\{R_1, \dots, R_1\}$, and

$$\begin{aligned} \Theta_{11} &= -E_1^T C - C^T E_1 + P_1 - V - U_1 \Sigma_1, & \Theta_{14} &= E_1^T A + H_1 + U_1 \Sigma_2, \\ \Theta_{17} &= P - \Sigma K + \tilde{\Sigma} L - E_1^T - C^T E_2, & \Theta_{22} &= -P_1 - V, \\ \Theta_{44} &= -U_1 + Q_1 + \text{Tr}(T) I_n, & \Theta_{47} &= K - L + A^T E_2, \\ \Theta_{77} &= -E_2^T - E_2 + \sum_{i=1}^1 2W_i, & \Xi_{11} &= \tilde{P} + \tilde{X}_1 - \tilde{W} - \tilde{V} \tilde{\Sigma}_1, \end{aligned}$$

$$\begin{aligned}
\Xi_{14} &= \widetilde{H} + \widetilde{V} \widetilde{\Sigma}_2 + \widetilde{Y}_1, & \Xi_{22} &= -\widetilde{P} - \widetilde{W}, & \Xi_{33} &= -2\widetilde{W} + \widetilde{S} + \widetilde{S}^T - \widetilde{R} \widetilde{\Sigma}_1, \\
\Xi_{36} &= \left(1 - \frac{\mu_m}{1}\right) \widetilde{Y}_2 - \left(1 - \frac{\mu_0}{1}\right) \widetilde{Y}_1 - \widetilde{R} \widetilde{\Sigma}_2, & \Xi_{44} &= \widetilde{Q} + \widetilde{Z}_1 - \widetilde{V}, \\
\Xi_{66} &= \left(1 - \frac{\mu_m}{1}\right) \widetilde{Z}_2 - \left(1 - \frac{\mu_0}{1}\right) \widetilde{Z}_1 - \widetilde{R}.
\end{aligned} \tag{3.4}$$

Proof. Based on (2.5) and denoting $\vartheta(t) = (\vartheta(t) - \vartheta_0)/1$, we construct the Lyapunov-Krasovskii functional candidate as

$$V(\mathbf{x}(t)) = V_1(\mathbf{x}(t)) + V_2(\mathbf{x}(t)) + V_3(\mathbf{x}(t)) + V_4(\mathbf{x}(t)), \tag{3.5}$$

where

$$\begin{aligned}
V_1(\mathbf{x}(t)) &= \mathbf{x}^T(t) P \mathbf{x}(t) + 2 \sum_{i=1}^n k_i \int_0^{x_i} [f_i(s) - \bar{f}_i s] ds + 2 \sum_{i=1}^n \underline{l}_i \int_0^{x_i} [\bar{f}_i s - f_i(s)] ds, \\
V_2(\mathbf{x}(t)) &= \int_{t_0}^t \begin{bmatrix} \mathbf{x}(s) \\ f(\mathbf{x}(s)) \end{bmatrix}^T \begin{bmatrix} P_1 & H_1 \\ * & Q_1 \end{bmatrix} \begin{bmatrix} \mathbf{x}(s) \\ f(\mathbf{x}(s)) \end{bmatrix} ds + \int_{t_0}^{t_0} \begin{bmatrix} \mathbf{x}(s) \\ h(\mathbf{x}(s)) \end{bmatrix}^T \begin{bmatrix} \widetilde{P} & \widetilde{H} \\ * & \widetilde{Q} \end{bmatrix} \begin{bmatrix} \mathbf{x}(s) \\ h(\mathbf{x}(s)) \end{bmatrix} ds \\
&\quad + \sum_{i=1}^1 \int_{t_0 - (i-1)}^{t_0 - (i-1)} \begin{bmatrix} \mathbf{x}(s) \\ f(\mathbf{x}(s)) \end{bmatrix}^T \begin{bmatrix} X_{1i} & Y_{1i} \\ * & Z_{1i} \end{bmatrix} \begin{bmatrix} \mathbf{x}(s) \\ f(\mathbf{x}(s)) \end{bmatrix} ds \\
&\quad + \sum_{i=1}^1 \int_{t_0 - i}^{t_0 - (i-1)} \begin{bmatrix} \mathbf{x}(s) \\ f(\mathbf{x}(s)) \end{bmatrix}^T \begin{bmatrix} X_{2i} & Y_{2i} \\ * & Z_{2i} \end{bmatrix} \begin{bmatrix} \mathbf{x}(s) \\ f(\mathbf{x}(s)) \end{bmatrix} ds, \\
V_3(\mathbf{x}(t)) &= \sum_{i=1}^n \sum_{j=1}^n t_{ij} \int_0^\infty k_{ij}(\cdot) \int_{t_0}^t f_j^2(x_j(s)) ds d\cdot, \\
V_4(\mathbf{x}(t)) &= \int_{-0}^0 \int_{t_0}^t \mathbf{x}^T(s) V \dot{\mathbf{x}}(s) ds d\cdot + \sum_{i=1}^1 \int_{-0-i}^{-(i-1)} \int_{t_0}^t \dot{\mathbf{x}}^T(s) W_i \dot{\mathbf{x}}(s) ds d\cdot
\end{aligned} \tag{3.6}$$

with $K = \text{diag}\{k_1, \dots, k_n\} > 0$, $L = \text{diag}\{\underline{l}_1, \dots, \underline{l}_n\} > 0$, $T = \text{diag}\{t_1, \dots, t_n\} > 0$ waiting to be determined, and

$$\mathbf{h}^T(s) = \begin{bmatrix} \mathbf{x}^T(s) \cdots \mathbf{x}^T(s - (1-1)) \end{bmatrix}, \quad \mathbf{h}^T(\mathbf{x}(s)) = \begin{bmatrix} f^T(\mathbf{x}(s)) \cdots f^T(\mathbf{x}(s - (1-1))) \end{bmatrix}. \tag{3.7}$$

Through directly calculating and using any $n \times n$ constant matrices $E_i (i = 1, 2)$, the time derivative of functional (3.5) along the trajectories of system (2.4) yields

$$\begin{aligned} \dot{V}_1(x(t)) = & 2x^T(t)P\dot{x}(t) + 2\left[f^T(x(t))(K - L) + x^T(t)(\bar{\Sigma}L - \Sigma K)\right]\dot{x}(t) \\ & + 2\left[x^T(t)E_1^T + \dot{x}^T(t)E_2^T\right] \left[-\dot{x}(t) - Cx(t) + Af(x(t)) + Bf(x(t-\tau)) \right. \\ & \left. + D \int_{-\infty}^t K(t-s)f(x(s))ds \right], \end{aligned} \quad (3.8)$$

$$\begin{aligned} \dot{V}_2(x(t)) = & \left[x^T(t)P_1x(t) + 2x^T(t)H_1f(x(t)) + f^T(x(t))Q_1f(x(t)) \right] \\ & - \left[x^T(t-\tau)P_1x(t-\tau) + 2x^T(t-\tau)H_1f(x(t-\tau)) + f^T(x(t-\tau))Q_1f(x(t-\tau)) \right] \\ & + \left[{}^T(t-\tau)\tilde{P}(t-\tau) + 2{}^T(t-\tau)\tilde{H}h(t-\tau) + h^T(t-\tau)\tilde{Q}h(t-\tau) \right] \\ & - \left[{}^T(t-\tau_0)\tilde{P}(t-\tau_0) + 2{}^T(t-\tau_0)\tilde{H}h(t-\tau_0) + h^T(t-\tau_0) \right. \\ & \left. \times \tilde{Q}h(t-\tau_0) \right] \\ & + \left[{}^T(t-\tau)\tilde{X}_1(t-\tau) + {}^T(t-\tau_0-\tau)\left(1 - \frac{\tau}{1}\right)(\tilde{X}_2 - \tilde{X}_1)(t-\tau_0-\tau) \right. \\ & \left. - {}^T(t-\tau_0-\tau)\tilde{X}_2(t-\tau_0-\tau) \right] \\ & + \left[2{}^T(t-\tau)\tilde{Y}_1h(t-\tau) + 2{}^T(t-\tau_0-\tau)\left(1 - \frac{\tau}{1}\right)(\tilde{Y}_2 - \tilde{Y}_1) \right. \\ & \left. \times h(t-\tau_0-\tau) - 2{}^T(t-\tau_0-\tau)\tilde{Y}_2h(t-\tau_0-\tau) \right] \\ & + \left[h^T(t-\tau)\tilde{Z}_1h(t-\tau) + h^T(t-\tau_0-\tau)\left(1 - \frac{\tau}{1}\right)(\tilde{Z}_2 - \tilde{Z}_1) \right. \\ & \left. \times h(t-\tau_0-\tau) - h^T(t-\tau_0-\tau)\tilde{Z}_2h(t-\tau_0-\tau) \right], \end{aligned} \quad (3.9)$$

$$\begin{aligned} \dot{V}_3(x(t)) = & \sum_{i=1}^n \sum_{j=1}^n \tau_i \int_0^\infty k_{ij}(\tau) f_j^2(x_j(t)) d\tau - \sum_{i=1}^n \sum_{j=1}^n \int_0^\infty k_{ij}(\tau) f_j^2(x_j(t-\tau)) d\tau \\ & \leq \sum_{i=1}^n \tau_i f^T(x(t)) f(x(t)) - \sum_{i=1}^n \sum_{j=1}^n \left(\int_0^\infty k_{ij}(\tau) f_j(x_j(t-\tau)) d\tau \right)^2 \end{aligned}$$

$$\begin{aligned} &\leq \text{Tr}(\mathbb{T}) f^T(\mathbf{x}(t)) f(\mathbf{x}(t)) - \left(\int_{-\infty}^t \mathbb{K}(t-s) f(\mathbf{x}(s)) ds \right)^T \left(\frac{1}{n} \mathbb{T} \right) \\ &\quad \times \left(\int_{-\infty}^t \mathbb{K}(t-s) f(\mathbf{x}(s)) ds \right), \end{aligned} \quad (3.10)$$

$$\begin{aligned} \dot{V}_4(\mathbf{x}(t)) &= \dot{\mathbf{x}}^T(t) \left[{}_0^2 V + \sum_{i=1}^1 ({}^2 W_i) \right] \dot{\mathbf{x}}(t) - \int_{t_0}^t {}_0 \dot{\mathbf{x}}^T(s) V \dot{\mathbf{x}}(s) ds \\ &\quad - \sum_{i=1}^1 \int_{t_0-i}^{t_0-(i-1)} \dot{\mathbf{x}}^T(s) W_i \dot{\mathbf{x}}(s) ds. \end{aligned} \quad (3.11)$$

Moreover, together with Lemmas 2.2 and 2.3 and (3.1), we can estimate $-\sum_{i=1}^1 \int_{t_0-i}^{t_0-(i-1)} \dot{\mathbf{x}}^T(s) W_i \dot{\mathbf{x}}(s) ds$ as follows:

$$\begin{aligned} &-\sum_{i=1}^1 \int_{t_0-i}^{t_0-(i-1)} \dot{\mathbf{x}}^T(s) W_i \dot{\mathbf{x}}(s) ds \\ &\leq -\sum_{i=1}^1 \left\{ \frac{-m}{m-(t)} [\mathbf{x}(t_0-(i-1)-(t)) - \mathbf{x}(t_0-i)]^T \right. \\ &\quad \times W_i [\mathbf{x}(t_0-(i-1)-(t)) - \mathbf{x}(t_0-i)] - \frac{-m}{(t)-0} \\ &\quad \times [\mathbf{x}(t_0-(i-1)) - \mathbf{x}(t_0-(i-1)-(t))]^T \\ &\quad \left. \times W_i [\mathbf{x}(t_0-(i-1)) - \mathbf{x}(t_0-(i-1)-(t))] \right\} \\ &\leq -\sum_{i=1}^1 \begin{bmatrix} \mathbf{x}(t_0-(i-1)) \\ \mathbf{x}(t_0-(i-1)-(t)) \\ \mathbf{x}(t_0-i) \end{bmatrix}^T \begin{bmatrix} W_i & S_i - W_i & -S_i \\ * & 2W_i - S_i - S_i^T & S_i^T - W_i \\ * & * & W_i \end{bmatrix} \\ &\quad \times \begin{bmatrix} \mathbf{x}(t_0-(i-1)) \\ \mathbf{x}(t_0-(i-1)-(t)) \\ \mathbf{x}(t_0-i) \end{bmatrix} \\ &= - \begin{bmatrix} (t_0) \\ (t_0-(t)) \\ (t_0-) \end{bmatrix}^T \begin{bmatrix} \widetilde{W} & \widetilde{S} - \widetilde{W} & -\widetilde{S} \\ * & 2\widetilde{W} - \widetilde{S} - \widetilde{S}^T & \widetilde{S}^T - \widetilde{W} \\ * & * & \widetilde{W} \end{bmatrix} \begin{bmatrix} (t_0) \\ (t_0-(t)) \\ (t_0-) \end{bmatrix}. \end{aligned} \quad (3.12)$$

From (2.5), the following inequality holds for any diagonal matrices $U_i > 0$ ($i=1,2,3$), $V_j > 0$, $R_j > 0$ ($j = 1, \dots, l$) with the compatible dimensions and setting $\tilde{V} = \text{diag}\{V_1, \dots, V_l\}$, $\tilde{R} = \text{diag}\{R_1, \dots, R_l\}$,

$$\begin{aligned}
0 \leq & \left[-x^T(t)U_1 \Sigma_1 x(t) + 2x^T(t)U_1 \Sigma_2 f(x(t)) - f^T(x(t))U_1 f(x(t)) \right] \\
& + \left[-x^T(t-m)U_2 \Sigma_1 x(t-m) + 2x^T(t-m)U_2 \Sigma_2 f(x(t-m)) - f^T(x(t-m))U_2 f(x(t-m)) \right] \\
& + \left[-x^T(t-\vartheta)U_3 \Sigma_1 x(t-\vartheta) + 2x^T(t-\vartheta)U_3 \Sigma_2 f(x(t-\vartheta)) - f^T(x(t-\vartheta)) \right. \\
& \quad \left. \times U_3 f(x(t-\vartheta)) \right] \\
& + \left[-h^T(t) \tilde{V} \tilde{\Sigma}_1 h(t) + 2h^T(t) \tilde{V} \tilde{\Sigma}_2 h(t) \right] - h^T(t) \tilde{V} h(t) \\
& + \left[-h^T(t-\vartheta) \tilde{R} \tilde{\Sigma}_1 h(t-\vartheta) + 2h^T(t-\vartheta) \tilde{R} \tilde{\Sigma}_2 h(t-\vartheta) \right. \\
& \quad \left. - h^T(t-\vartheta) \tilde{R} h(t-\vartheta) \right].
\end{aligned} \tag{3.13}$$

Now, adding the terms on the right-hand side of (3.8)–(3.12) and employing inequality (3.13), we can deduce

$$\begin{aligned}
\dot{V}(x(t)) \leq & h^T(t) \left\{ \Upsilon_1 \Theta \Upsilon_1^T + \Upsilon_2 \Xi \Upsilon_2^T + \frac{\mu_0 - \mu_1}{1} \sum_{i=1}^l I_{3i}^T \begin{bmatrix} X_{1i} & Y_{1i} \\ * & Z_{1i} \end{bmatrix} I_{3i} + \frac{\mu_m - \mu_1}{1} \right. \\
& \left. \times \sum_{i=1}^l I_{3i}^T \begin{bmatrix} X_{2i} & Y_{2i} \\ * & Z_{2i} \end{bmatrix} I_{3i} \right\} h(t) \doteq h^T(t) \Lambda(t) h(t),
\end{aligned} \tag{3.14}$$

in which Θ, Ξ, Υ_i ($i=1,2$) are presented in (3.2), and

$$\begin{aligned}
\Lambda(t) = & \begin{bmatrix} x^T(t) & h^T(t) & x^T(t-m) & h^T(t-\vartheta) & f^T(x(t)) \\ & h^T(t) & f^T(x(t-m)) & h^T(t-\vartheta) & \dot{x}^T(t) \\ & & & & x^T(t-\vartheta) & f^T(x(t-\vartheta)) \end{bmatrix} \left(\int_{-\infty}^t K(t-s) f(x(s)) ds \right)^T.
\end{aligned} \tag{3.15}$$

Then by employing convex combination technique, the LMIs in (3.2) can guarantee $\Lambda(t) < 0$, which indicates that there must exist a positive scalar $\alpha > 0$ such that $\dot{V}(x(t)) \leq -\alpha \|x(t)\|^2 < 0$ for $x(t) \neq 0$. Then it follows from Lyapunov-Krasovskii stability theory that the system (2.4) is asymptotically stable, and the proof is completed. \square

Remark 3.2. Presently, the convex combination technique has been widely employed to tackle time-varying delay owing to the truth that it could reduce the conservatism more effectively than the previous ones, see [15–18, 28–30]. In [31], the authors put forward the reciprocal convex approach, which can reduce the conservatism more effectively than convex combination ones. Yet, it has come to our attention that no researchers have utilized both of them simultaneously to tackle the stability for DNNs.

Remark 3.3. One can easily check that the theorem in this work achieves some great improvements over the one in [17], which can be illustrated in the following. Firstly, some ignored terms in [17] have been fully considered in this paper when estimating the derivative of Lyapunov-Krasovskii functional in (3.11), such as the ignored ones.

Secondly, owing to the introduction of reciprocal convex approach, Theorem 3.1 can be much less complicated than the ones in [17], which will result in some computation simplicity in some degree. Thirdly, though reciprocal convex approach plays an important role in tackling the range of time delay, it cannot efficiently deal with the effect of lower and upper bound on delay derivative, which can be checked in (3.14). Thus we employ the convex combination technique to overcome this shortcoming.

Remark 3.4. When τ is not differentiable or μ_0 (resp., μ_m) is unknown, through setting $\begin{bmatrix} X_{ij} & Y_{ij} \\ * & Z_{ij} \end{bmatrix} = 0$ ($i=1,2$) or $\begin{bmatrix} X_{2j} & Y_{2j} \\ * & Z_{2j} \end{bmatrix} = 0$ (resp., $\begin{bmatrix} X_{1j} & Y_{1j} \\ * & Z_{1j} \end{bmatrix} = 0$) in (3.5), our theorem still can be true.

Remark 3.5. Owing to the introduction of delay-partitioning idea in this work, the difficulty and complexity in checking the theorem will become more and more evident when the integer l increases and the dimension of the LMIs in (3.2) will become much higher. Yet based on the results in [12–16], the maximum allowable upper bound of μ_m would become unapparent enlarging as $l \geq 5$. Thus if we want to employ the idea to real cases, we do not necessarily partition the interval $[0, \mu_m]$ into more than $l \geq 5$ subintervals.

4. Numerical Examples

In the section, three numerical examples will be presented to illustrate that our results are superior over the ones by convex combination technique.

Example 4.1. We revisit the system considered in [9, 11, 17] with the following parameters:

$$\begin{aligned} C &= \begin{bmatrix} 2 & 0 \\ 0 & 2 \end{bmatrix}, & A &= \begin{bmatrix} 1 & 1 \\ -1 & -1 \end{bmatrix}, & B &= \begin{bmatrix} 0.88 & 1 \\ 1 & 1 \end{bmatrix}, \\ D = \Sigma &= \begin{bmatrix} 0 & 0 \\ 0 & 0 \end{bmatrix}, & \bar{\Sigma} &= \begin{bmatrix} 0.4 & 0 \\ 0 & 0.8 \end{bmatrix}, \end{aligned} \quad (4.1)$$

in which $\mu_0 = 0$ is set. If we do not consider the existence of μ_0 , then by utilizing Theorem 3.1 and Remark 3.2, the corresponding maximum allowable upper bounds (MAUBs) μ_{\max} for different μ_m derived by Theorem 3.1 in [17] and in the paper can be summarized in Table 1,

Table 1: Calculated MAUBs μ_{\max} for various τ , unavailable μ_0 in Example 4.1.

Methods\ μ_m		0.6	0.8	0.9	1.2
Li et al. [17]	$\tau = 1$	3.4878	2.8458	1.9150	1.1167
	$\tau = 2$	3.7458	3.1150	2.1153	1.3189
Theorem 3.1	$\tau = 1$	3.5664	2.9316	2.0552	1.2107
	$\tau = 2$	3.8543	3.2311	2.2115	1.4445

Table 2: Calculated MAUBs μ_{\max} for various τ and $\mu_0 = 0.5$ in Example 4.1.

Methods\ μ_m		0.6	0.8	0.9	1.2
Zhang et al. [9]		3.5209	2.8654	1.9508	—
Li et al. [17]	$\tau = 1$	3.5872	2.8815	1.9657	1.2055
Theorem 3.1	$\tau = 1$	3.6435	2.9443	2.0112	1.2899

which demonstrates that Theorem 3.1 in this paper of $\tau = 1$ is less conservative than the theorem in [17]. Yet, if we set $\mu_0 = 0.5$, it is still easy to verify that our results can yield much less conservative results than the one in [17], which can be shown in Table 2.

Based on Tables 1 and 2, it indicates that the conservatism of stability criterion can be greatly deduced if we take μ_0 into consideration. Moreover, though the delay-partitioning idea has been used in [17], the corresponding MAUBs μ_{\max} derived by [17] and Theorem 3.1 are summarized in Table 3, which shows that the idea in this work can be more efficient than the one in [17] even for $\tau = 1, 2$.

Example 4.2. Consider the delayed neural networks (2.1) with

$$C = \text{diag}\{1.2769, 0.6231, 0.9230, 0.4480\}, \quad \Sigma = 0_{3 \times 3}, \quad \bar{\Sigma} = \text{diag}\{0.1137, 0.1279, 0.7994, 0.2368\},$$

$$A = \begin{bmatrix} -0.0373 & 0.4852 & -0.3351 & 0.2336 \\ -1.6033 & 0.5988 & -0.3224 & 1.2352 \\ 0.3394 & -0.0860 & -0.3824 & -0.5785 \\ -0.1311 & 0.3253 & -0.9534 & -0.5015 \end{bmatrix}, \quad B = \begin{bmatrix} 0.8674 & -1.2405 & -0.5325 & 0.0220 \\ 0.0474 & -0.9164 & 0.0360 & 0.9816 \\ 1.8495 & 2.6117 & -0.3788 & 0.8428 \\ -2.0413 & 0.5179 & 1.1734 & -0.2775 \end{bmatrix}, \tag{4.2}$$

which has been addressed extensively, see [2, 15, 17] and the references therein. Together with the delay-partitioning idea and for different μ_m , the works [15, 17] have calculated the MAUBs μ_{\max} such that the origin of the system is globally asymptotically stable for (τ) satisfying $3 = \tau_0 \leq (\tau) \leq \tau_m \leq \mu_{\max}$. By resorting to Theorem 3.1 and Remark 3.2, the corresponding results can be given in Table 4, which indicates that our delay-partitioning idea can be more effective than the relevant ones in [15, 17] for $\tau = 1, 2$ and $\mu_0 = 0$.

Table 3: Calculated MAUBs $\mu_{m \max}$ for various $\mu_0 = 0.5$ in Example 4.1

Methods \ μ_m		0.8	0.9	Unknown μ_m
Li et al. [17]	1= 1	2.8815	1.9657	1.2055
	1= 2	3.1488	2.1968	1.4078
Theorem 3.1	1= 1	2.9668	2.0113	1.3115
	1= 2	3.2350	2.2778	1.4890

Table 4: Calculated MAUBs $\mu_{m \max}$ for various μ_0, μ_m in Example 4.2.

Methods \ μ_m		0.1	0.5	0.9	Unknown μ_m
Hu et al. [15]	1= 1	3.33	3.16	3.10	3.09
	1= 2	3.65	3.32	3.26	3.24
Li et al. [17]	1= 1	3.35	3.21	3.20	3.19
	1= 2	3.77	3.41	3.38	3.37
Theorem 3.1	1= 1	3.40	3.32	3.31	3.24
	1= 2	3.86	3.49	3.42	3.40

Table 5: Calculated MAUBs $\mu_{m \max}$ for various $[\mu_0, \mu_m]$, and μ_0 in Example 4.3.

Methods \ $[\mu_0, \mu_m]$		[0.1, 0.4]	[0.4, 0.8]	[0.8, 0.9]	[0.9, 1.1]
Li et al. [17]	1= 1	0.8712	0.8257	0.9327	0.9805
	1= 2	1.1872	1.1815	1.2657	1.3028
Theorem 3.1	1= 1	0.9221	0.9115	0.9995	1.1134
	1= 2	1.2315	1.2189	1.3012	1.3898

Example 4.3. Consider the delayed neural networks (2.4) with

$$\begin{aligned}
 C &= \begin{bmatrix} 4.2 & 0 \\ 0 & 3.8 \end{bmatrix}, & A &= \begin{bmatrix} 1 & -1.66 \\ 0 & -1 \end{bmatrix}, & B &= \begin{bmatrix} 1 & 0 \\ -2.475 & 1 \end{bmatrix}, & D &= \begin{bmatrix} 0.5 & 0.2 \\ 0.3 & 0.4 \end{bmatrix}, \\
 K(t-s) &= \begin{bmatrix} 2e^{-2(t-s)} & 3e^{-3(t-s)} \\ 4e^{-4(t-s)} & 2e^{-2(t-s)} \end{bmatrix},
 \end{aligned} \tag{4.3}$$

and $f(x_i) = \tanh(x_i), i = 1, 2$. For $\mu_0 = 0.5$, choosing various $[\mu_0, \mu_m]$ in Table 5 and applying Theorem 3.1 in our work and the one in [17], we can find the MAUBs on μ_m for which the system remains asymptotically stable.

Based on Table 5, it can indicate that the delay-partitioning idea in our work can be less conservative than the ones in [17].

5. Conclusion

This paper has investigated the asymptotical stability for DNNs with continuously distributed delay. Through employing one improved delay-partitioning idea and combining

reciprocal convex technique with convex combination one, one stability criterion with significantly reduced conservatism has been established in terms of LMIs. The proposed stability condition benefits from the partition of delay intervals and reciprocal convex technique. Three numerical examples have been given to demonstrate the effectiveness of the presented criteria and the improvements over some existent ones. Finally, it should be worth noting that the delay-partitioning idea presented in this work is widely applicable in many cases.

Acknowledgment

This work is supported by the National Natural Science Foundation of China no. 60875035, no. 60904020, no. 61004064, no. 61004032, and the Special Foundation of China Postdoctoral Science Foundation Projects no. 201003546.

References

- [1] B. Shen, Z. Wang, H. Shu, and G. Wei, " H_∞ filtering for nonlinear discrete-time stochastic systems with randomly varying sensor delays," *Automatica*, vol. 45, no. 4, pp. 1032–1037, 2009.
- [2] B. Shen, Z. Wang, Y. S. Hung, and G. Chesi, "Distributed H_∞ filtering for polynomial nonlinear stochastic systems in sensor networks," *IEEE Transactions on Industrial Electronics*, vol. 58, no. 5, pp. 1971–1979, 2011.
- [3] H. Dong, Z. Wang, D. W. C. Ho, and H. Gao, "Robust H_∞ fuzzy output-feedback control with multiple probabilistic delays and multiple missing measurements," *IEEE Transactions on Fuzzy Systems*, vol. 18, no. 4, pp. 712–725, 2010.
- [4] B. Shen, Z. Wang, and Y. S. Hung, "Distributed H_∞ -consensus filtering in sensor networks with multiple missing measurements: the finite-horizon case," *Automatica*, vol. 46, no. 10, pp. 1682–1688, 2010.
- [5] H. Dong, Z. Wang, and H. Gao, "Robust H_∞ filtering for a class of nonlinear networked systems with multiple stochastic communication delays and packet dropouts," *IEEE Transactions on Signal Processing*, vol. 58, no. 4, pp. 1957–1966, 2010.
- [6] G. Wei, Z. Wang, and B. Shen, "Error-constrained filtering for a class of nonlinear time-varying delay systems with non-Gaussian noises," *IEEE Transactions on Automatic Control*, vol. 55, no. 12, pp. 2876–2882, 2010.
- [7] Z. Wang, H. Zhang, and W. Yu, "Robust stability criteria for interval Cohen-Grossberg neural networks with time varying delay," *Neurocomputing*, vol. 72, no. 4–6, pp. 1105–1110, 2009.
- [8] P. Balasubramaniam and S. Lakshmanan, "Delay-range dependent stability criteria for neural networks with Markovian jumping parameters," *Nonlinear Analysis: Hybrid Systems*, vol. 3, no. 4, pp. 749–756, 2009.
- [9] Y. Zhang, D. Yue, and E. Tian, "New stability criteria of neural networks with interval time-varying delay: a piecewise delay method," *Applied Mathematics and Computation*, vol. 208, no. 1, pp. 249–259, 2009.
- [10] K. Gu, "Refined discretized Lyapunov functional method for systems with multiple delays," *International Journal of Robust and Nonlinear Control*, vol. 13, no. 11, pp. 1017–1033, 2003.
- [11] W. H. Chen and W. X. Zheng, "Improved delay-dependent asymptotic stability criteria for delayed neural networks," *IEEE Transactions on Neural Networks*, vol. 19, no. 12, pp. 2154–2161, 2008.
- [12] S. Mou, H. Gao, J. Lam, and W. Qiang, "A new criterion of delay-dependent asymptotic stability for Hopfield neural networks with time delay," *IEEE Transactions on Neural Networks*, vol. 19, no. 3, pp. 532–535, 2008.
- [13] R. Yang, H. Gao, and P. Shi, "Novel robust stability criteria for stochastic Hopfield neural networks with time delays," *IEEE Transactions on Systems, Man, and Cybernetics, Part B*, vol. 39, no. 2, pp. 467–474, 2009.
- [14] X. M. Zhang and Q. L. Han, "New Lyapunov-Krasovskii functionals for global asymptotic stability of delayed neural networks," *IEEE Transactions on Neural Networks*, vol. 20, no. 3, pp. 533–539, 2009.

- [15] L. Hu, H. Gao, and W. X. Zheng, "Novel stability of cellular neural networks with interval time-varying delay," *Neural Networks*, vol. 21, no. 10, pp. 1458–1463, 2008.
- [16] L. Hu, H. Gao, and P. Shi, "New stability criteria for Cohen-Grossberg neural networks with time delays," *IET Control Theory & Applications*, vol. 3, no. 9, pp. 1275–1282, 2009.
- [17] T. Li, A. Song, S. Fei, and T. Wang, "Delay-derivative-dependent stability for delayed neural networks with unbound distributed delay," *IEEE Transactions on Neural Networks*, vol. 21, no. 8, pp. 1365–1371, 2010.
- [18] T. Li, S.-M. Fei, Y.-Q. Guo, and Q. Zhu, "Stability analysis on Cohen-Grossberg neural networks with both time-varying and continuously distributed delays," *Nonlinear Analysis. Real World Applications*, vol. 10, no. 4, pp. 2600–2612, 2009.
- [19] J. H. Park, "On global stability criterion of neural networks with continuously distributed delays," *Chaos, Solitons & Fractals*, vol. 37, no. 2, pp. 444–449, 2008.
- [20] P. Balasubramaniam and R. Rakkiyappan, "Global asymptotic stability of stochastic recurrent neural networks with multiple discrete delays and unbounded distributed delays," *Applied Mathematics and Computation*, vol. 204, no. 2, pp. 680–686, 2008.
- [21] Q. Song and J. Cao, "Stability analysis of Cohen-Grossberg neural network with both time-varying and continuously distributed delays," *Journal of Computational and Applied Mathematics*, vol. 197, no. 1, pp. 188–203, 2006.
- [22] Z. Wang, Y. Liu, and X. Liu, "On global asymptotic stability of neural networks with discrete and distributed delays," *Physics Letters A*, vol. 345, no. 4-6, pp. 299–308, 2005.
- [23] Z. Wang, H. Shu, Y. Liu, D. W. C. Ho, and X. Liu, "Robust stability analysis of generalized neural networks with discrete and distributed time delays," *Chaos, Solitons & Fractals*, vol. 30, no. 4, pp. 886–896, 2006.
- [24] R. Rakkiyappan and P. Balasubramaniam, "Dynamic analysis of Markovian jumping impulsive stochastic Cohen-Grossberg neural networks with discrete interval and distributed time-varying delays," *Nonlinear Analysis: Hybrid Systems*, vol. 3, no. 4, pp. 408–417, 2009.
- [25] T. Li and S. M. Fei, "Stability analysis of Cohen-Grossberg neural networks with time-varying and distributed delays," *Neurocomputing*, vol. 71, no. 4-6, pp. 1069–1081, 2008.
- [26] R. Samidurai, S. M. Anthoni, and K. Balachandran, "Global exponential stability of neutral-type impulsive neural networks with discrete and distributed delays," *Nonlinear Analysis: Hybrid Systems*, vol. 4, no. 1, pp. 103–112, 2010.
- [27] Q.-L. Han, "On designing time-varying delay feedback controllers for master-slave synchronization of Lur'e systems," *IEEE Transactions on Circuits and Systems I*, vol. 54, no. 7, pp. 1573–1583, 2007.
- [28] D. Yue, E. Tian, Y. Zhang, and C. Peng, "Delay-distribution-dependent stability and stabilization of T-S fuzzy systems with probabilistic interval delay," *IEEE Transactions on Systems, Man, and Cybernetics, Part B*, vol. 39, no. 2, pp. 503–516, 2009.
- [29] H. Shao, "New delay-dependent stability criteria for systems with interval delay," *Automatica*, vol. 45, no. 3, pp. 744–749, 2009.
- [30] P. Park and J. W. Ko, "Stability and robust stability for systems with a time-varying delay," *Automatica*, vol. 43, no. 10, pp. 1855–1858, 2007.
- [31] P. Park, J. W. Ko, and C. Jeong, "Reciprocally convex approach to stability of systems with time-varying delays," *Automatica*, vol. 47, no. 1, pp. 235–238, 2011.

Research Article

Abstract Description of Internet Traffic of Generalized Cauchy Type

Ming Li¹ and Wei Zhao²

¹ School of Information Science and Technology, East China Normal University, 500 Dong-Chuan Road, Shanghai 200241, China

² Department of Computer and Information Science, University of Macau, Avenue Padre Tomas Pereira, Taipa, Macau, China

Correspondence should be addressed to Ming Li, ming_lihk@yahoo.com

Received 10 March 2011; Accepted 6 July 2011

Academic Editor: Zidong Wang

Copyright © 2012 M. Li and W. Zhao. This is an open access article distributed under the Creative Commons Attribution License, which permits unrestricted use, distribution, and reproduction in any medium, provided the original work is properly cited.

Self-similar process with long-range dependence (LRD), that is, fractional Gaussian noise (fGn) with LRD is a widely used model of Internet traffic. It is indexed by its Hurst parameter H_{fGn} that linearly relates to its fractal dimension D_{fGn} . Note that, on the one hand, the fractal dimension D of traffic measures local self-similarity. On the other hand, LRD is a global property of traffic, which is characterized by its Hurst parameter H . However, by using fGn, both the self-similarity and the LRD of traffic are measured by H_{fGn} . Therefore, there is a limitation for fGn to accurately model traffic. Recently, the generalized Cauchy (GC) process was introduced to model traffic with the flexibility to separately measure the fractal dimension D_{GC} and the Hurst parameter H_{GC} of traffic. However, there is a fundamental problem whether or not there exists the generality that the GC model is more conformable with real traffic than single parameter models, such as fGn, *irrelevant of traffic traces used in experimental verification*. The solution to that problem remains unknown but is desired for model evaluation in traffic theory or for model selection against specific issues, such as queuing analysis relating to the autocorrelation function (ACF) of arrival traffic. The key contribution of this paper is our solution to that fundamental problem (see Theorem 3.17) with the following features in analysis. (i) Set-valued analysis of the traffic of the fGn type. (ii) Set-valued analysis of the traffic of the GC type. (iii) Revealing the generality previously mentioned by comparing metrics of the traffic of the fGn type to that of the GC type.

1. Introduction

This paper explores the Internet traffic (traffic for short) modeling which plays a role in telecommunications [1]. Let $x[t(i)]$ be an arrival traffic function, implying the number of bytes in the i th packet arriving at $t(i)$ ($i = 0, 1, 2, \dots$), where $t(i)$ is the timestamp of the i th packet [2]. To avoid confusion, we use $x(t)$ and $x(i)$ to represent a traffic time series in

the continuous case and the discrete one, respectively, where $x(i)$ implies the size of the i th packet. Note that traffic statistics for $x(i)$ corresponds with the statistics of the traffic time series represented by either byte count or packet size [3].

The pioneer in stochastic modeling of traffic refers to the Danish scientist A. K. Erlang, see Bojkovic et al. [4]. As early as the 1920s, he contributed to his experimental work on the statistics of the traffic in telephony networks and introduced the traffic models of the Poisson type [5, 6]. Erlang's work was so successful in characterizing the old telephony traffic such that it was applied as a law in traffic engineering, see for example, Yue et al. [7], Papoulis [8], Gibson [9], Cooper [10], Pitts and Schormans [11], and McDysan [12]. Note that the autocorrelation function (ACF) of the traffic of the Poisson type, which is Markovian, is exponentially decayed [13]. In fact, the ACF of a Markov process decays exponentially [14]. The Poisson-type models fit in with the traffic in old telephony networks, which are circuit-switched, see for example, [9], Le Gall [15], Lin et al. [16], Manfield and Downs [17], Reiser [18], and Lu [19]. Those types of models, however, fail to effectively characterize the traffic in the Internet, which is packet switched. As a matter of fact, the ACF, the probability density function (PDF), and the power spectrum density (PSD) function of traffic, follow power law, see for example, Resnick [20], Csabai [21], Leland et al. [22], Beran et al. [23], López-Ardao et al. [24], and Cleveland and Sun [25]. Therefore, system responses to the Internet have to take into account the arrival traffic with long-range dependence (LRD), see for example, Tsybakov and Georganas [26], Norros [27], Fishman and Adan [28], Li and Zhao [29], Dahl and Willemain [30], and Kingman [31].

Theoretically, on one hand, Taqqu's Theorem relates a heavy-tailed PDF in power law to a hyperbolically decayed ACF, that is, power law-type ACF [3, 32]. On the other hand, the Fourier transform connects a hyperbolically decayed ACF with $1/f^\alpha$ ($\alpha > 0$) noise (power law-type PSD), see for example, Li [33].

Note that, before the Internet's worldwide prevalence, in the seventies of the last century, Tobagi et al. [34] reported a noticeable behavior of traffic, which is called "burstiness" [12]. It implies that there would be no packets transmitted for a while, then flurry of transmission, no transmission for another long period of time, and so on if one observes traffic over a long period of time. This also means that traffic has intermittency. In 1986, Jain and Routhier [35] further described the intermittency or burstiness of traffic using the term "packet trains." They inferred that traffic is neither a Poisson process nor a compound Poisson one [35]. The results in [34, 35] are quite qualitative but they may be considered as early work with respect to fractal-type traffic. The concept of packet train is interesting [36] but we utilize the concept of fractal time series for traffic modeling in this paper.

The early literature quantitatively describing the statistical properties of traffic from a view of fractals refers to Csabai [21], Leland et al. [22], Beran et al. [23], Paxson and Floyd [37], and Crovella and Bestavros [38]. Those scientists revealed some of the main properties of traffic, such as LRD and asymptotic self-similarity. The traffic model described in [22, 23, 37, 39–43], just citing a few, is the fGn that was introduced by Mandelbrot and Van Ness in mathematics [44].

The model of fGn is characterized by a single parameter H , called the Hurst parameter. Its limitation in accurately modeling traffic was noticed by Paxson and Floyd [37], and Tsybakov and Georganas [39]. Paxson and Floyd noted that "it might be difficult to characterize the correlations over the entire traffic traces with a single Hurst parameter [37, Section 7.4]." They suggested that "further work is required to fully understand the correlational structure of wide-area traffic [37]." Tsybakov and Georganas remarked that "the class of exactly self-similar processes, that is, fGn or fractional Brownian motion (fBm),

is too narrow for modeling actual network traffic [39, Section II].” The authors of [37, 39] qualitatively stated the limitation of fGn in traffic modeling without mentioning how to release the limitation. In this regard, Beran [45, page 101-102] suggested to develop a sufficiently flexible class of parametric correlation models. The key of the Beran’s idea implies that the ACF of an LRD series may be fitted by a correlation model with several parameters instead of one, but he did not mention what concrete parametric correlation models are.

Li and Lim recently reported a two-parameter traffic model called the GC process with the demonstrations based on sets of real-traffic traces in [46, 47]. Li [48] discussed its simulation. Nevertheless, whether or not it has the generality to be more agreement with traffic than single parameter models, such as fGn, remains an unsolved problem. Therefore, it may be useful, especially for traffic engineers, to exhibit that generality. Motivated by this, we, in this paper, aim at presenting a solution to it based on the abstract analysis, more precisely, the set-valued analysis in Hilbert spaces, to thoroughly reveal that generality, irrelevant of traces used in experimental verification. To the best of our knowledge, the set-valued analysis of traffic models is rarely seen.

The rest of paper is organized as follows. Related work is explained in Section 2. The set-valued analysis is presented in Section 3. An application case is demonstrated in Section 4. Discussions are provided in Section 5, followed by our conclusions.

2. Related Work

We first respectively brief the ACFs of the fGn and the GC process. Then, fractal dimension and the Hurst parameter are discussed.

2.1. fGn

The continuous fGn is the derivative of the smoothed fractional Brownian motion (fBm) in the sense of the generalized functions over the Schwartz space of test functions, refer to Kanwal [49] for generalized functions.

Denote by $r_{\text{fGn}}(\tau)$ the ACF of the fGn as the increment process of the fBm of the Weyl type. Then, for time lag $\tau \in \mathbb{R}$, which is the set of real numbers,

$$r_{\text{fGn}}(\tau) = \frac{\tau^{2-2H}}{2} \left[\left(\frac{|\tau|}{2} + 1 \right)^{2H} + \left| \frac{|\tau|}{2} - 1 \right|^{2H} - 2 \left| \frac{|\tau|}{2} \right|^{2H} \right], \quad (2.1)$$

where $H \in (0,1)$ is the Hurst parameter, $\epsilon > 0$ is used by smoothing the fBm so that the smoothed fBm is differentiable, and $\tau^2 = (H - \epsilon)^{-1} \Gamma(1 - 2H + \epsilon) \cos(H - \epsilon)$ [44]. The PSD of fGn is given by [50]

$$S_{\text{fGn}}(\omega) = \tau^2 \sin(H - \epsilon) \Gamma(2H + 1) |\omega|^{1-2H}, \quad (2.2)$$

where ω is angular frequency.

fGn includes three classes of time series. When $H \in (0.5,1)$, $r_{\text{fGn}}(\tau)$ is positive and finite for all τ . It is nonintegrable and the corresponding series is LRD. For $H \in (0,0.5)$, the integral of $r_{\text{fGn}}(\tau)$ is zero, corresponding series with short-range dependence (SRD). Besides

$r_{fGn}(\tau)$ for $0 < H < 0.5$ changes its sign and becomes negative for some τ proportional to $|\tau|$. It reduces to the white noise when $H = 0.5$.

The ACF of fGn in the discrete case is given by

$$r_{fGn}(k) = 0.5^2 \left[(|k|+1)^{2H} - 2|k|^{2H} + (|k|-1)^{2H} \right], \quad (2.3)$$

where $k \in \mathbb{I}$, where \mathbb{I} is the set of integers. To avoid confusion, we often consider ACFs for $k \geq 0$ in the normalized case in what follows as an ACF is an even function. Thus, for $k \geq 0$, one has

$$r_{fGn}(k) = 0.5 \left[(k+1)^{2H} - 2k^{2H} + (k-1)^{2H} \right]. \quad (2.4)$$

Considering the right side of (2.4) as the finite 2-order difference of $0.5(k)^{2H}$ and approximating it with the 2-order differential of $0.5(k)^{2H}$ yields the following equation. Its right side is quite accurate to the left for $k > 10$ [51]:

$$0.5 \left[(k+1)^{2H} - 2k^{2H} + (k-1)^{2H} \right] \approx H(2H-1)(k)^{2H-2}. \quad (2.5)$$

2.2. GC Process

A random function $x(t)$ is called the GC process if it is stationary Gaussian with the ACF given by

$$r_{GC}(\tau) = E[X(t+\tau)X(t)] = (1 + |\tau|^\alpha)^{-\beta}, \quad (2.6)$$

where $0 < \alpha \leq 2$ and $\beta > 0$. When $\alpha = 2$, one gets the usual Cauchy process the ACF of which is expressed by

$$r_C(\tau) = \left(1 + |\tau|^2\right)^{-1}, \quad (2.7)$$

which is used in geostatistics, see Chilès and Delfiner [52].

The PSD of the GC process is given by (see [47])

$$S_{GC}(\omega) = \sum_{k=0}^{\infty} \frac{(-1)^k \Gamma((\alpha/\omega) + k)}{\Gamma(\alpha/\omega) \Gamma(1+k)} \mathbb{I}_1(\omega) * \text{Sa}(\omega) + \sum_{k=0}^{\infty} \frac{(-1)^k \Gamma((\alpha/\omega) + k)}{\Gamma(\alpha/\omega) \Gamma(1+k)} \left[\mathbb{I}_2(\omega) - \mathbb{I}_2(\omega) * \text{Sa}(\omega) \right], \quad (2.8)$$

where $\text{Sa}(x) = \sin(x)/x$ and

$$\begin{aligned} \mathbb{I}_1(x) &= -2 \sin\left(\frac{k}{2}\right) \Gamma(k+1) |x|^{-k-1}, \\ \mathbb{I}_2(x) &= 2 \sin\left[\frac{(1+k)}{2}\right] \Gamma[1-(1+k)] |x|^{(1+k)-1}. \end{aligned} \quad (2.9)$$

The PSD of the GC process for $x \rightarrow 0$ is given by (see [53])

$$S_{GC}(x) \sim \frac{1}{\Gamma(1+k) \cos(\pi/2)} |x|^{-1}, \quad x \rightarrow 0. \quad (2.10)$$

On the other hand, $S_{GC}(x)$ for $x \rightarrow \infty$ is given by

$$S_{GC}(x) \sim \frac{\Gamma(1+k) \sin(\pi/2)}{\Gamma(1+k)} |x|^{-(1+k)}, \quad x \rightarrow \infty. \quad (2.11)$$

The above exhibits the power law of $S_{GC}(x)$. The GC process is LRD if $0 < k < 1$ and is SRD if $1 < k$.

As noted in [53], “the GC process is non-Markovian since $r_{GC}(t_1, t_2)$ does not satisfy the triangular relation given by

$$r_{GC}(t_1, t_3) = \frac{r_{GC}(t_1, t_2)r_{GC}(t_2, t_3)}{r_{GC}(t_2, t_2)}, \quad t_1 < t_2 < t_3, \quad (2.12)$$

which is a necessary condition for a Gaussian process to be Markovian, see Todorovic [54].” In fact, up to a multiplicative constant, the Ornstein-Uhlenbeck process is the only stationary Gaussian Markov process, see Lim and Muniandy [55] and Wolpert and Taqqu [56].

2.3. Fractal Dimension and the Hurst Parameter

On the one hand, fractal dimension, denoted by D , of traffic $x(t)$ is a measure to characterize its local self-similarity or irregularity. On the other hand, the Hurst parameter H is used to measure its statistical dependence, see Mandelbrot [57]. Thus, we respectively use D and H to describe the local property and the global property of $x(t)$, see Li and Lim [46, 47] and Li and Zhao [58]. In fact, if the ACF $r_{xx}(x)$ is sufficiently smooth on $(0, \infty)$ and if

$$r_{xx}(0) - r_{xx}(x) \sim c_1 |x|^{-D} \quad \text{for } |x| \rightarrow 0, \quad (2.13)$$

where c_1 is a constant and D is the fractal index of $x(t)$, D of $x(t)$ is expressed by

$$D = 2 - \frac{1}{H}, \quad (2.14)$$

see, for example, Kent and Wood [59], Hall and Roy [60], Chan et al. [61], and Adler [62]. Applying the binomial series to $r_{fGn}(\cdot)$ yields

$$r_{fGn}(0) - r_{fGn}(\cdot) \sim c|\cdot|^{2H} \quad \text{for } |\cdot| \rightarrow 0. \quad (2.15)$$

Therefore, one has

$$D_{fGn} = 2 - H_{fGn}. \quad (2.16)$$

Consequently, the fGn , as the incremental process of the fBm of the Weyl type, is stationary. Its D happens to linearly relate to its H , see [57, page 27] and Gneiting and Schlather [63]. Hence, a single parameter model fails to separately capture the local irregularity and the LRD of traffic.

Recall that a self-similar process $x(t)$ with the self-similarity index α requires for $\alpha > 0$,

$$x(at) \stackrel{=}_d a^{-\alpha} x(t), \quad (2.17)$$

where $\stackrel{=}_d$ denotes equality in joint finite distribution. It is known that a stationary Gaussian random function $x(t)$ that is not exactly self-similar may satisfy a weaker self-similar property known as local self-similarity. Taking into account the definition of the local self-similarity provided in [59–62], we say that a Gaussian stationary process is locally self-similar of order α if its ACF satisfies for $\tau \rightarrow 0$,

$$r_{xx}(\tau) = 1 - |\tau|^\alpha \{1 + o(|\tau|^\alpha)\}, \quad \alpha > 0. \quad (2.18)$$

The fractal dimension D of a locally self-similar process of order α is given by (2.14). Therefore, we have the asymptotic expressions given by

$$\begin{aligned} r_{GC}(\tau) &\sim |\tau|^{-\alpha}, \quad \tau \rightarrow 0, \\ r_{GC}(\tau) &\sim |\tau|^{-\alpha}, \quad \tau \rightarrow \infty. \end{aligned} \quad (2.19)$$

Note that traffic $x(t)$ is LRD if its ACF $r_{xx}(\tau)$ satisfies

$$r_{xx}(\tau) \sim |\tau|^{-b}, \quad \tau \rightarrow \infty, \quad (2.20)$$

where $0 < b < 1$. Denote by D_{GC} and H_{GC} the fractal dimension and the Hurst parameter of traffic of the GC type, respectively. Then, according to (2.19), one has

$$\begin{aligned} D_{GC} &= 2 - \frac{\alpha}{2}, \\ H_{GC} &= 1 - \frac{\alpha}{2}. \end{aligned} \quad (2.21)$$

Replacing α and β , respectively, by D_{GC} and H_{GC} according to (2.21), we have

$$r_{GC}(\lambda) = \left(1 + |\lambda|^{4-2D_{GC}}\right)^{-(1-H_{GC})/(2-D_{GC})}, \quad (2.22)$$

where D_{GC} is independent of H_{GC} . Thus,

$$D_{GC} \neq D_{fGn}. \quad (2.23)$$

3. Set-Valued Analysis

A physically measured traffic trace has single history with finite length. Without losing generality, the maximum possible length of a traffic series is assumed as $N \in \mathbb{I}_+ (= 1, 2, \dots)$. Let \mathbb{I}_N^2 be a space containing all ACFs, including ACFs of real traffic. Let r be an ACF of a real-traffic series. Define the norm of r as an inner product given by

$$\|r\| = \sqrt{\langle r, r \rangle} = \sqrt{\sum_{k=0}^{N-1} |r|^2}. \quad (3.1)$$

Then, the inner space given by

$$\mathbb{I}_N^2 = \left\{ r; \sqrt{\sum_{k=0}^{N-1} |r|^2} < \infty \right\} \quad (3.2)$$

is a Hilbert space when all limits are included [64, 65].

Remark 3.1. \mathbb{I}_N^2 is a finite-dimensional normed space.

Now, we consider the following consequences of a linear normed space with finite dimensions.

Lemma 3.2. *In a linear finite-dimensional space, all norms are equivalent [66].*

Lemma 3.3. *Every finite-dimensional subspace of a linear normed space is closed [67].*

Lemma 3.4. *Let \mathcal{H} be a Hilbert space and \mathcal{M} be a closed subspace of \mathcal{H} . Let $x \in \mathcal{H}$, $x \notin \mathcal{M}$. Then there exists a unique element $\hat{x} \in \mathcal{M}$ satisfying $\|x - \hat{x}\| = \inf_{y \in \mathcal{M}} \|x - y\|$ [66, 67], Aubin [68].*

From the above, we obtain the following theorem. Its proof is straightforward according to Lemmas 3.2–3.4.

Theorem 3.5. *Let $r \in \mathbb{I}_N^2$ be an ACF of a real-traffic series. Let \mathcal{S} be a closed subspace of \mathbb{I}_N^2 . Then, there exists a unique $R \in \mathcal{S}$ such that $\|r - R\| = \inf_{s \in \mathcal{S}} \|r - s\|$ [64, 65].*

Let $e = R - r$ be the error. Its norm is defined by

$$\|e\| = \sqrt{\langle e, e \rangle} = \frac{1}{N} \sum_{k=0}^{N-1} |e|^2. \quad (3.3)$$

Let the functional of e be $F(e) = \|e\|$. Then, $F(e)$ is convex. Thus, the optimal approximation of r in \mathcal{S} can be expressed by

$$R = \arg \min F(e), \quad r \in \mathbb{L}_N^2, \quad R \in \mathcal{S}. \quad (3.4)$$

Suppose R has m parameters such that

$$R(k) = R(k; a_1, a_2, \dots, a_m). \quad (3.5)$$

Then, the error by taking the approximation (3.5) as a traffic model is a function of a_j ($j = 1, 2, \dots, m$). To clarify this point, we utilize the cost function of m dimensions expressed by

$$J(a_1, a_2, \dots, a_m) = \frac{1}{N} \sum_k [R(k) - r(k)]^2. \quad (3.6)$$

The partial derivative of J with respect to m parameters, which will be zero at the J minimum, yields [69]

$$\frac{J}{a_j} = \frac{2}{N} \sum_k (R - r) \frac{R}{a_j}, \quad j = 1, 2, \dots, m. \quad (3.7)$$

Let $(a_{10}, a_{20}, \dots, a_{m0})$ be the solution of $J / a_j = 0$. Then, $R(k; a_{10}, a_{20}, \dots, a_{m0})$ is the optimal approximation of r in \mathcal{S} .

The above discussions draw attention to the fact that an optimal approximation of r in \mathcal{S} may have m parameters. Obviously, an approximation of r is related to a subspace of \mathbb{L}_N^2 as can be seen from Theorem 3.5. For this reason, we, below, consider the extensions of the fGn's ACF towards constructing the ACF of the GC process.

Definition 3.6. Let \mathcal{H} be a Hilbert space equipped with a distance d . When K is a subset of \mathcal{H} , the distance from r to K is denoted by $d(r, K) = \inf_{s \in K} d(r, s)$ [70, 71].

Definition 3.7 (see [70]). Let $\{K_n\} (n \in \mathbb{L}_+)$ be a sequence of subspaces of a Hilbert space \mathcal{H} . Then, the subset

$$\limsup_{n \rightarrow \infty} K_n = \left\{ r \in \mathcal{H} : \liminf_{n \rightarrow \infty} d(r, K_n) = 0 \right\} \quad (3.8)$$

is the upper limit of the sequence K_n . Besides, the subset

$$\liminf_{n \rightarrow \infty} K_n = \left\{ r \in \mathcal{H} : \lim_{n \rightarrow \infty} d(r, K_n) = 0 \right\} \quad (3.9)$$

is the lower limit of K_n . A subset K is said to be the limit or the set limit of K_n if

$$K = \liminf_{n \rightarrow \infty} K_n = \limsup_{n \rightarrow \infty} K_n = \lim_{n \rightarrow \infty} K_n. \quad (3.10)$$

Considering the above terms, one has the lemma below.

Lemma 3.8. *Any monotone sequence of subsets K_n has a limit [70].*

According to Lemma 3.8, therefore, the following holds.

Corollary 3.9 (see [70, 71]). *Let $\{K_n\}$ ($n \in \mathbb{L}_+$) be a family of increasing closed subspaces of a Hilbert space $\mathcal{H} : K_0 \subset K_1 \subset K_2 \subset \dots$. Then,*

$$\begin{aligned} d(r; K_0) &\geq d(r; K_1) \geq d(r; K_2) \geq \dots, \\ \lim_{n \rightarrow \infty} d(r; K_n) &= 0. \end{aligned} \quad (3.11)$$

We now turn to constructing the ACF of the GC process.

Corollary 3.10. $(c/2^H (2^H - 1))[(+1)^{2^H} - 2^{2^H} + (-1)^{2^H}] \approx c(+1)^{2^H - 2}$.

Proof. According to (2.5), this corollary results. \square

Let

$$\mathcal{G} = \left\{ r; r = r_{fGn}, \|r\| = \sqrt{\sum_{k=0}^{N-1} |r|^2} < \infty \right\}, \quad c > 0. \quad (3.12)$$

Then, \mathcal{G} is the set containing the ACF of fGn . Therefore, we have the following remark.

Remark 3.11. $\mathcal{G} \subset \mathbb{L}_N^2$. Besides, it is closed according to Lemma 3.3.

We now construct the second space. Let \mathcal{GA} be the set containing ACFs of traffic in the form $c(|+1|)^{2^H - 2}$ for $c > 0$. Then,

$$\mathcal{GA} = \left\{ r; r = c(|+1|)^{2^H - 2}, \|r\| = \sqrt{\sum_{k=0}^{N-1} |r|^2} < \infty \right\}. \quad (3.13)$$

According to Corollary 3.10, element in \mathcal{GA} is an approximation of the ACF of fGn . Hence, we have $d(r; \mathcal{GA}) \approx d(r; \mathcal{G})$. Based on \mathcal{GA} , we further construct a space as follows.

Proposition 3.12. *The following \mathcal{GA}_1 is an extension of \mathcal{GA} , where $c > 0$;*

$$\mathcal{GA}_1 = \left\{ r; r = c(|^{a_2} + 1|)^{2^H - 2}, a_2 \in (0, 1), \|r\| = \sqrt{\sum_{k=0}^{N-1} |r|^2} < \infty \right\}. \quad (3.14)$$

Proof. $(| |^{a_2+1})^{2H-2}$ equals to $(| |^{+1})^{2H-2}$ for $a_2 = 1$, meaning $\mathcal{G}_{a_1} \supset \mathcal{G}_{a_2}$. Thus, this proposition results. \square

Remark 3.13. $(| |^{a_2+1})^{2H-2}$ is nonintegrable for $a_2(2-2H) \in (0,1)$ because $(| |^{a_2+1})^{2H-2} \sim | |^{a_2(2H-2)}$ ($\rightarrow \infty$). Clearly, $\mathcal{G}_{a_1} \subset \mathbb{I}_N^2$. In addition, it is closed according to Lemma 3.3.

The space \mathcal{G}_{a_1} can be further extended into the following.

Proposition 3.14. *The following \mathcal{G}_{a_2} is an extension of \mathcal{G}_{a_1} ;*

$$\mathcal{G}_{a_2} = \left\{ r; r = r_{GC}, \|r\| = \sqrt{\sum_{k=0}^{N-1} |r|^2} < \infty \right\}, \quad (3.15)$$

where $r_{GC} = (| |^{a_2+1})^{-a_1}$, $a_1 > 0$, $a_2 \in (0,1)$, $a_1 a_2 \in (0,1)$.

Proof. $(| |^{a_2+1})^{2H-2}$ is a special case of $(| |^{a_2+1})^{-a_1}$ for $a_1 = 2-2H$, implying $\mathcal{G}_{a_2} \supset \mathcal{G}_{a_1}$. Thus, Proposition 3.14 holds. \square

According to Proposition 3.14, therefore, we have the remarks below.

Remark 3.15. $(| |^{a_2+1})^{-a_1}$ is nonintegrable for $a_1 a_2 \in (0,1)$ because $(| |^{a_2+1})^{-a_1} \sim | |^{a_1 a_2}$ ($\rightarrow \infty$). Clearly, $\mathcal{G}_{a_2} \subset \mathbb{I}_N^2$. It is closed according to Lemma 3.3.

Remark 3.16. Proposition 3.14 presents a class of parametric ACF structures.

From the above, we have the theorem below.

Theorem 3.17. *Let $r \in \mathbb{I}_N^2$ be an ACF of real traffic. Then,*

$$d(r; \mathcal{G}_{a_2}) \leq d(r; \mathcal{G}_{a_1}) \leq d(r; \mathcal{G}_{\mathcal{A}}). \quad (3.16)$$

Proof. Because $\mathcal{G}_{a_2} \supset \mathcal{G}_{a_1} \supset \mathcal{G}_{\mathcal{A}}$, Theorem 3.17 holds according to Corollary 3.9. \square

Theorem 3.17 exhibits the generality of the GC process in accurate modeling of traffic. In what follows, we let $a_2 =$ and $a_1 = /$ so as to be consistent with (2.6) in computations.

In the end of this section, we note that the purpose for using the abstract expression of m -parameter model (3.5) as well as (3.6) and (3.7) is simply to mention the concept of multiparameter model of ACF. For traffic, the GC model equipped with two parameters can be well explained because one parameter is the fractal index for local property and the other the LRD index for global one.

4. Application of Theorem 3.17 to Traffic Modeling

As an application of Theorem 3.17, we show the ACF modeling of $x(i)$ of real-traffic trace named by AMP-1131669938-1.psize, which was collected by the US National Laboratory for Applied Network Research (NLNR) in November 2005 [73]. We first model it in \mathcal{G}_{a_2} . Then, we compare it with that in \mathcal{G} (i.e., fGn model). Because $d(r; \mathcal{G}_{\mathcal{A}}) \approx d(r; \mathcal{G})$, we use $d(r; \mathcal{G})$ in this section.

Denote the measured ACF of $x(i)$ by $r(k)$. Denote by $Rgc(k)$ and $Rfgn(k)$ the modeled ACFs in \mathcal{G}_{a_2} and \mathcal{G} , respectively. Let $M^2(Rgc) = E[(Rgc - r)^2]$ be the mean square error (MSE) by using $Rgc(k)$ and $M^2(Rfgn) = E[(Rfgn - r)^2]$ be the MSE by using $Rfgn(k)$. For the sake of demonstration, we use (4.1) for the MSE in \mathcal{G}_{a_2} and (4.2) for that in \mathcal{G} ;

$$J1(\alpha, \beta) = \frac{1}{N} \sum_k [Rgc(k) - r(k)]^2, \quad (4.1)$$

$$J2(H) = \frac{1}{N} \sum_k [Rfgn(k) - r(k)]^2. \quad (4.2)$$

Figure 1(a) shows the first 2048 points of AMP-1131669938-1.size. Figure 1(b) is the right part, that is, the part for $k \geq 0$, of the measured ACF $r(k)$ with the block size $L = 2048$ and average count = 30. By least squares fitting, we obtain the estimates $(\alpha, \beta) = (0.020, 0.028)$. Thus, we have

$$Rgc(k) = \left(k^{0.020} + 1 \right)^{-0.028/0.020}, \quad (4.3)$$

with $M^2(Rgc) = 5.157 \times 10^{-5}$. Figure 1(c) shows $Rgc(k)$ and Figure 1(d) indicates that $Rgc(k)$ fits well with $r(k)$. Figure 2 illustrates the estimates of α and β . According to (2.21), H_{GC} and D_{GC} of that series equal to 0.986 and 1.990, respectively.

With least squares fitting in \mathcal{G} , however, we have

$$Rfgn(k) = 0.5 \left[(k+1)^{2H} - 2k^{2H} + (k-1)^{2H} \right]_{H=0.930}, \quad (4.4)$$

with $M^2(Rfgn) = 1.347 \times 10^{-3}$. Figure 3(a) plots the $Rfgn(k)$ and Figure 3(b) shows the data fitting in \mathcal{G} . Figures 1(d) and 3(b) exhibit an application case of (3.16) in Theorem 3.17. Judging from them, it is obvious that the GC process is more effective with that trace for both short-term and long-term lags.

Purely from a view of curve fitting, the fitting accuracy of 10^{-3} in \mathcal{G} may not be too large. The unsatisfactory point of the modeling in \mathcal{G} is in two aspects. One is that $Rfgn(k)$ may overestimate autocorrelations of traffic for small lags (around the knee of the ACF curve). The other is that it may underestimate autocorrelations for large lags as evidenced by Figure 3(b), refer to Li and Lim [46] for more cases regarding modeling real-traffic traces in \mathcal{G}_{a_2} .

5. Discussion

A conventional method to assess whether a model is appropriate is goodness-of-fit test in statistics ([3, 69], Press et al. [74]). However, it still needs sets of traffic data involved in the test. In fact, experimental processing of specific sets of real traffic, no matter how many traces are involved in experimental verification or goodness-of-fit test, may not deterministically infer the generality of the GC process expressed by Theorem 3.17, theoretically speaking.

Recall that an ACF of arrival traffic has a considerable impact on queuing systems, see, for example, Hajek and He [75], Livny et al. [72], Li and Hwang [76, 77], Wittevrongel and Bruneel [78], and Geist and Westall [79]. Therefore, using the ACF of the arrival traffic

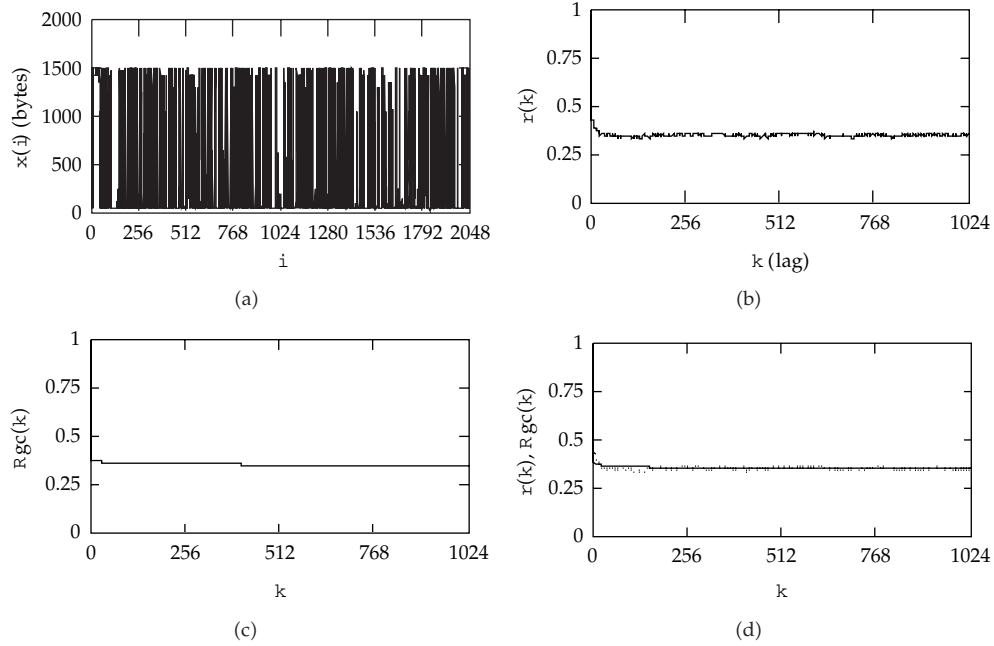


Figure 1: Modeling procedure using the GC process. (a) Traffic series: AMP-1131669938-1.psize. (b) Measured ACF $r(k)$. (c) Modeled ACF $R_{gc}(k)$. (d) Fitting the data: dot line, $r(k)$; solid line, $R_{gc}(k)$.

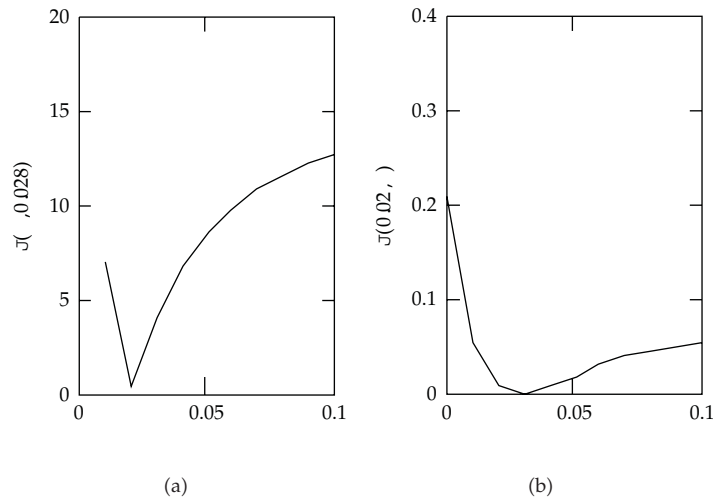


Figure 2: Estimations of $J(0.028)$ and $J(0.02, \cdot)$ for $R_{gc}(k)$ of AMP-1131669938-1.psize.

of the GC type may bring in considerable advances in practice, such as system analysis or evaluation, which we will work on in the future.

The GC model has one significance to separately characterize the local self-similarity and the LRD. In the case study in the previous section, we have $H_{GC} = 0.986$ and $D_{GC} = 1.990$ for AMP-1131669938-1.psize. Both H_{GC} and D_{GC} are of large value for this trace since $H_{GC} \in (0.5, 1)$ for LRD and $D_{GC} \in (1, 2)$. Note that a large value of H corresponds to strong

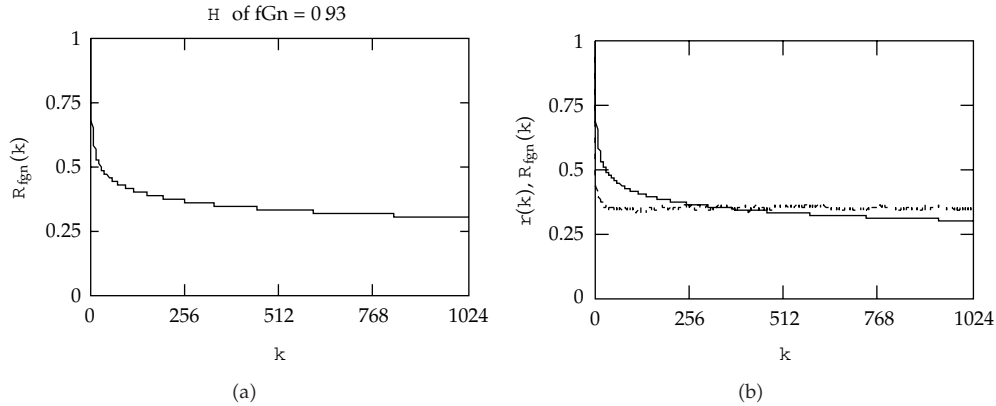


Figure 3: Modeling ACF of AMP-1131669938-1.psize in \mathcal{G} . (a) Modeled ACF in \mathcal{G} . (b) Fitting the data: dot line, $r(k)$; solid line, $R_{fGn}(k)$.

LRD while a large value of D implies highly local irregularity. The phenomenon of traffic like this was demonstrated with more real-traffic traces in [46]. This phenomenon may not be satisfactorily observed using single parameter models, that is, fGn due to the restrictive relationship $D_{fGn} = 2 - H_{fGn}$.

The GC model has another significance to explain the complicated phenomenon of traffic, which was observed by Paxosn and Floyd [37] and Feldmann et al. [80], and which was stated like this. Traffic has robust long-term persistence at large time scales but high irregularity at small time scales. This phenomenon may be described by $\text{Var}[D(n)] > \text{Var}[H(n)]$, where $D(n)$ and $H(n)$ are the fractal dimension and the Hurst parameter of traffic in the n th interval on an interval-by-interval basis for $n = 1, 2, \dots$, respectively. This complicated phenomenon of traffic can be well characterized by the GC model because H_{GC} is independent of D_{GC} , refer to [46] for the demonstrations of this phenomenon with real traffic. Again, we note that it may not be described by single parameter models, such as fGn. In fact, $\text{Var}[H_{fGn}(n)] = \text{Var}[D_{fGn}(n)]$ because D_{fGn} and H_{fGn} are restricted by $D_{fGn} = 2 - H_{fGn}$.

The third significance of the traffic model of the GC type can be briefed as follows. It is well known that the amount of traffic accumulated in the interval $[0, t]$ is upper bounded by

$$\int_0^t x(u)du \leq \alpha + \beta t, \tag{5.1}$$

where α and β are constants and $t > 0$, see Cruz [81]. It is obviously that a tightened bound of $\int_0^t x(u)du$ is particularly desired in practice, such as delay computations. By applying the GC model to the traffic bound, we have the tightened bound expressed by

$$\int_0^t x(u)du \leq r^{2D-5} [u(t) - u(t-)] + a^{-H} u(t-), \tag{5.2}$$

where $r > 0$ is a small-scale factor, $a > 0$ is a large-scale factor, and $\tau > 0$, $u(t)$ is the unit step function, see Li and Zhao [58] for details. For instance, if we let $D = 1.8$, $H = 0.9$, $r = 1.5$, and $a = 10$, then we have a tightened bound given by

$$\int_0^t x(u) du \leq 0.567 [u(t) - u(t-\tau)] + 0.126 u(t-\tau)t. \quad (5.3)$$

The conventional traffic bound, that is, the right side of (5.1), is a special case of (5.2) for $r = a = 1$. We should emphasize that the fractal dimension D and the Hurst parameter H in (5.2) have to be considered in the sense of the GC model of traffic [58].

Our future work is in two ways. One is to explore more specific significances of the GC model of traffic in practical issues, for example, queuing. The other is to study whether the GC model of random processes may provide new explanation for the random phenomena in nonlinear time-varying systems or complex systems discussed by Dong et al. [82–84], and Shen et al. [85–87], Chen et al. [88], and Sheng et al. [89, 90].

6. Conclusions

fGn, which is a self-similar process with LRD for $H \in (0.5, 1)$ and a widely used model in traffic engineering, was proposed as a traffic model by Leland et al. [22], Beran et al. [23], and Paxson and Floyd [37], based on their data processing of sets of real-traffic traces. The GC process, which is a locally self-similar process with LRD for $H \in (0, 1)$, was recently reported by Li and Lim [46], also based on their processing the same sets of traffic traces as those in [22, 37]. However, experimental processing of real traffic relying on selected sample records of traffic may be limited, in methodology, to be used to abstractly evaluate which is more conformable with real traffic without relating to the selected sample records of traffic. The theoretical significance of this paper is to provide us with the abstract assessment in terms of the generality described by (3.16) in Theorem 3.17 that the GC model is more conformable with real traffic than single parameter models, for example, fGn, regardless of any sample records of traffic, which may yet be a theoretical supplement with respect to the traffic model of the GC type. In addition, we have given our construction procedure of the ACF of the GC process in Hilbert spaces with the technique of extensions based on fGn.

Acknowledgments

This paper was supported in part by the National Natural Science Foundation of China under the project Grant numbers 60873264 and 61070214, the 973 plan under the project number 2011CB302801/2011CB302802, and by the University of Macau. Thanks go to NLNR for allowing the authors to use its real-traffic data in the research.

References

- [1] H. Akimaru and K. Kawashima, *Teletraffic: Theory and Applications*, Springer, New York, NY, USA, 1993.
- [2] M. Li, W. Jia, and W. Zhao, "Correlation form of timestamp increment sequences of self-similar traffic on Ethernet," *Electronics Letters*, vol. 36, no. 19, pp. 1668–1669, 2000.

- [3] P. Abry, P. Borgnat, F. Ricciato, A. Scherrer, and D. Veitch, "Revisiting an old friend: on the observability of the relation between long range dependence and heavy tail," *Telecommunication Systems*, vol. 43, no. 3-4, pp. 147–165, 2010.
- [4] Z. Bojkovic, M. Bakmaz, and B. Bakmaz, "Originator of teletraffic theory," *Proceedings of the IEEE*, vol. 98, no. 1, pp. 123–127, 2010.
- [5] A. K. Erlang, "Telefon-ventetider. et stykke sandsynlighedsregning," *Matematisk Tidsskrift B*, vol. 31, pp. 25–42, 1920.
- [6] E. Brockmeyer, H. L. Halstrøm, and A. Jensen, "The life of A. K. Erlang," *Transactions of the Danish Academy of Technical Sciences*, no. 2, pp. 23–100, 1948.
- [7] W. Yue, H. Takagi, and Y. Takahashi, *Advances in Queueing Theory and Network Applications*, Springer, New York, NY, USA, 2009.
- [8] A. Papoulis, *Probability, Random Variables and Stochastic Processes*, McGraw-Hill Series in Electrical Engineering. Communications and Information Theory, McGraw-Hill, New York, NY, USA, 4th edition, 2002.
- [9] J. D. Gibson, *The Communications Handbook*, IEEE Press, New York, NY, USA, 1997.
- [10] R. B. Cooper, *Introduction to Queueing Theory*, Elsevier, New York, NY, USA, 2nd edition, 1981.
- [11] J. M. Pitts and J. A. Schormans, *Introduction to ATM Design and Performance: With Applications Analysis Software*, John Wiley & Sons, New York, NY, USA, 1996.
- [12] D. McDysan, *QoS & Traffic Management in IP & ATM Networks*, McGraw-Hill, New York, NY, USA, 2000.
- [13] J. S. Bendat and A. G. Piersol, *Random Data Analysis and Measurement Procedures*, John Wiley & Sons, New York, NY, USA, 3rd edition, 2000.
- [14] J. L. Doob, *Stochastic Processes*, John Wiley & Sons, New York, NY, USA, 1953.
- [15] F. Le Gall, "One moment model for telephone traffic," *Applied Mathematical Modelling*, vol. 6, no. 6, pp. 415–423, 1982.
- [16] P. M. Lin, B. J. Leon, and C. R. Stewart, "Analysis of circuit-switched networks employing originating-office control with spill-forward," *IEEE Transactions on Communications*, vol. 26, no. 6, pp. 754–765, 1978.
- [17] D. R. Manfield and T. Downs, "On the one-moment analysis of telephone traffic networks," *IEEE Transactions on Communications*, vol. 27, no. 8, pp. 1169–1174, 1979.
- [18] M. Reiser, "Performance evaluation of data communication systems," *Proceedings of the IEEE*, vol. 70, no. 2, pp. 171–196, 1982.
- [19] D.-X. Lu, *Random Processes and Their Applications*, Press of Tsinghua University, Beijing, China, 2006.
- [20] S. I. Resnick, "Heavy tail modeling and teletraffic data," *The Annals of Statistics*, vol. 25, no. 5, pp. 1805–1869, 1997, with discussion and a rejoinder by the author.
- [21] I. Csabai, "1/f noise in computer network traffic," *Journal of Physics A*, vol. 27, no. 12, pp. L417–L421, 1994.
- [22] W. E. Leland, M. S. Taqqu, W. Willinger, and D. V. Wilson, "On the self-similar nature of Ethernet traffic (extended version)," *IEEE/ACM Transactions on Networking*, vol. 2, no. 1, pp. 1–15, 1994.
- [23] J. Beran, R. Sherman, M. S. Taqqu, and W. Willinger, "Long-range dependence in variable-bit-rate video traffic," *IEEE Transactions on Communications*, vol. 43, no. 234, pp. 1566–1579, 1995.
- [24] J. C. López-Ardao, C. López-García, A. Suárez-González, M. Fernández-Veiga, and R. Rodríguez-Rubio, "On the use of self-similar processes in network simulation," *ACM Transactions on Modeling and Computer Simulation*, vol. 10, no. 2, pp. 125–151, 2000.
- [25] W. S. Cleveland and D. X. Sun, "Internet traffic data," *Journal of the American Statistical Association*, vol. 95, no. 451, pp. 979–985, 2000.
- [26] B. Tsybakov and N. D. Georganas, "On self-similar traffic in atm queues: definitions, overflow probability bound, and cell delay distribution," *IEEE/ACM Transactions on Networking*, vol. 5, no. 3, pp. 397–409, 1997.
- [27] I. Norros, "A storage model with self-similar input," *Queueing Systems. Theory and Applications*, vol. 16, no. 3-4, pp. 387–396, 1994.
- [28] G. S. Fishman and I. J. B. F. Adan, "How heavy-tailed distributions affect simulation-generated time averages," *ACM Transactions on Modeling and Computer Simulation*, vol. 16, no. 2, pp. 152–173, 2006.
- [29] C. Li and W. Zhao, "Stochastic performance analysis of non-feedforward networks," *Telecommunication Systems*, vol. 43, no. 3-4, pp. 237–252, 2010.
- [30] T. A. Dahl and T. R. Willemain, "The effect of long-memory arrivals on queue performance," *Operations Research Letters*, vol. 29, no. 3, pp. 123–127, 2001.

- [31] J. F. C. Kingman, "The first Erlang century and the next," *Queueing Systems*, vol. 63, no. 1-4, pp. 3–12, 2009.
- [32] P. Loiseau, P. Gonçalves, G. Dewaele, P. Borgnat, P. Abry, and P. V. B. Primet, "Investigating self-similarity and heavy-tailed distributions on a large-scale experimental facility," *IEEE/ACM Transactions on Networking*, vol. 18, no. 4, Article ID 5422706, pp. 1261–1274, 2010.
- [33] M. Li, "Fractal time series—a tutorial review," *Mathematical Problems in Engineering*, vol. 2010, Article ID 157264, 26 pages, 2010.
- [34] F. A. Tobagi, R. W. Peebles, and E. G. Manning, "Modeling and measurement techniques in packet communication networks," *Proceedings of the IEEE*, vol. 66, no. 11, pp. 1423–1447, 1978.
- [35] R. Jain and S. A. Routhier, "Packet trains—measurements and a new model for computer network traffic," *IEEE Journal on Selected Areas in Communications*, vol. 4, no. 6, pp. 986–995, 1986.
- [36] F. Kamoun, "Performance analysis of a discrete-time queueing system with a correlated train arrival process," *Performance Evaluation*, vol. 63, no. 4-5, pp. 315–340, 2006.
- [37] V. Paxson and S. Floyd, "Wide area traffic: the failure of Poisson modeling," *IEEE/ACM Transactions on Networking*, vol. 3, no. 3, pp. 226–244, 1995.
- [38] M. E. Crovella and A. Bestavros, "Self-similarity in world wide web traffic: evidence and possible causes," *IEEE/ACM Transactions on Networking*, vol. 5, no. 6, pp. 835–846, 1997.
- [39] B. Tsybakov and N. D. Georganas, "Self-similar processes in communications networks," *IEEE Transactions on Information Theory*, vol. 44, no. 5, pp. 1713–1725, 1998.
- [40] A. Adas, "Traffic models in broadband networks," *IEEE Communications Magazine*, vol. 35, no. 7, pp. 82–89, 1997.
- [41] H. Michiel and K. Laevens, "Teletraffic engineering in a broad-band era," *Proceedings of the IEEE*, vol. 85, no. 12, pp. 2007–2032, 1997.
- [42] A. Erramilli, M. Roughan, D. Veitch, and W. Willinger, "Self-similar traffic and network dynamics," *Proceedings of the IEEE*, vol. 90, no. 5, pp. 800–819, 2002.
- [43] W. Willinger, M. S. Taqqu, W. E. Leland, and D. V. Wilson, "Self-similarity in high-speed packet traffic: analysis and modeling of Ethernet traffic measurements," *Statistical Science*, vol. 10, no. 1, pp. 67–85, 1995.
- [44] B. B. Mandelbrot and J. W. Van Ness, "Fractional Brownian motions, fractional noises and applications," *SIAM Review*, vol. 10, pp. 422–437, 1968.
- [45] J. Beran, *Statistics for Long-Memory Processes*, vol. 61 of *Monographs on Statistics and Applied Probability*, Chapman & Hall, New York, NY, USA, 1994.
- [46] M. Li and S. C. Lim, "Modeling network traffic using generalized Cauchy process," *Physica A*, vol. 387, no. 11, pp. 2584–2594, 2008.
- [47] M. Li and S. C. Lim, "Power spectrum of generalized Cauchy process," *Telecommunication Systems*, vol. 43, no. 3-4, pp. 219–222, 2010.
- [48] M. Li, "Generation of teletraffic of generalized Cauchy type," *Physica Scripta*, vol. 81, no. 2, Article ID 025007, 2010.
- [49] R. P. Kanwal, *Generalized Functions: Theory and Application*, Birkhäuser, Boston, Mass, USA, 3rd edition, 2004.
- [50] M. Li and S. C. Lim, "A rigorous derivation of power spectrum of fractional Gaussian noise," *Fluctuation and Noise Letters*, vol. 6, no. 4, pp. C33–C36, 2006.
- [51] B. B. Mandelbrot, *Gaussian Self-Affinity and Fractals*, Springer, New York, NY, USA, 2002.
- [52] J.-P. Chiles and P. Delfiner, *Geostatistics: Modeling Spatial Uncertainty*, Wiley Series in Probability and Statistics: Applied Probability and Statistics, John Wiley & Sons, New York, NY, USA, 1999.
- [53] S. C. Lim and M. Li, "A generalized Cauchy process and its application to relaxation phenomena," *Journal of Physics A*, vol. 39, no. 12, pp. 2935–2951, 2006.
- [54] P. Todorovic, *An Introduction to Stochastic Processes and Their Applications*, Springer Series in Statistics: Probability and Its Applications, Springer, New York, NY, USA, 1992.
- [55] S. C. Lim and S. V. Muniandy, "Generalized Ornstein-Uhlenbeck processes and associated self-similar processes," *Journal of Physics A*, vol. 36, no. 14, pp. 3961–3982, 2003.
- [56] R. L. Wolpert and M. S. Taqqu, "Fractional Ornstein-Uhlenbeck Lévy processes and the telecom process: upstairs and downstairs," *Signal Processing*, vol. 85, no. 8, pp. 1523–1545, 2005.
- [57] B. B. Mandelbrot, *The Fractal Geometry of Nature*, W.H. Freeman, New York, NY, USA, 1982.
- [58] M. Li and W. Zhao, "Representation of a stochastic traffic bound," *IEEE Transactions on Parallel and Distributed Systems*, vol. 21, no. 9, pp. 1368–1372, 2010.
- [59] J. T. Kent and A. T. A. Wood, "Estimating the fractal dimension of a locally self-similar Gaussian process by using increments," *Journal of the Royal Statistical Society B*, vol. 59, no. 3, pp. 679–699, 1997.

- [60] P. Hall and R. Roy, "On the relationship between fractal dimension and fractal index for stationary stochastic processes," *The Annals of Applied Probability*, vol. 4, no. 1, pp. 241–253, 1994.
- [61] G. Chan, P. Hall, and D. S. Poskitt, "Periodogram-based estimators of fractal properties," *The Annals of Statistics*, vol. 23, no. 5, pp. 1684–1711, 1995.
- [62] R. J. Adler, *The Geometry of Random Fields*, John Wiley & Sons, New York, NY, USA, 1981, Wiley Series in Probability and Mathematical Statistics.
- [63] T. Gneiting and M. Schlather, "Stochastic models that separate fractal dimension and the Hurst effect," *SIAM Review*, vol. 46, no. 2, pp. 269–282, 2004.
- [64] M. Li, "Modeling autocorrelation functions of long-range dependent teletraffic series based on optimal approximation in Hilbert space-A further study," *Applied Mathematical Modelling*, vol. 31, no. 3, pp. 625–631, 2007.
- [65] M. Li, W. Zhao, W. Jia, D. Long, and C. H. Chi, "Modeling autocorrelation functions of self-similar teletraffic in communication networks based on optimal approximation in Hilbert space," *Applied Mathematical Modelling*, vol. 27, no. 3, pp. 155–168, 2003.
- [66] D. H. Griffel, *Applied Functional Analysis*, Ellis Horwood, Chichester, UK, 1981, Ellis Horwood Series in Mathematics and its Application.
- [67] N. Young, *An Introduction to Hilbert Space*, Cambridge Mathematical Textbooks, Cambridge University Press, Cambridge, UK, 1988.
- [68] J.-P. Aubin, *Applied Functional Analysis*, Pure and Applied Mathematics, Wiley-Interscience, New York, NY, USA, 2nd edition, 2000.
- [69] J. A. Rice, *Mathematical Statistics and Data Analysis*, Wadsworth, 2nd edition, 1995.
- [70] J.-P. Aubin and H. Frankowska, *Set-Valued Analysis*, vol. 2 of *Systems & Control: Foundations & Applications*, Birkhäuser, Boston, Mass, USA, 1990.
- [71] G. V. Smirnov, *Introduction to the Theory of Differential Inclusions*, vol. 41 of *Graduate Studies in Mathematics*, American Mathematical Society, Providence, RI, USA, 2002.
- [72] M. Livny, B. Melamed, and A. K. Tsiolis, "The impact of autocorrelation on queuing systems," *Management Science*, vol. 39, no. 3, pp. 322–339, 1993.
- [73] <http://pma.nlanr.net/Traces/Traces/daily>.
- [74] W. H. Press, S. A. Teukolsky, W. T. Vetterling, and B. P. Flannery, *Numerical Recipes in C: The art of scientific computing*, Cambridge University Press, Cambridge, UK, 2nd edition, 1992.
- [75] B. Hajek and L. He, "On variations of queue response for inputs with the same mean and autocorrelation function," *IEEE/ACM Transactions on Networking*, vol. 6, no. 5, pp. 588–598, 1998.
- [76] S. Q. Li and C. L. Hwang, "Queue response to input correlation functions: discrete spectral analysis," *IEEE/ACM Transactions on Networking*, vol. 1, no. 5, pp. 522–533, 1993.
- [77] S. Q. Li and C. L. Hwang, "Queue response to input correlation functions: continuous spectral analysis," *IEEE/ACM Transactions on Networking*, vol. 1, no. 6, pp. 678–692, 1993.
- [78] S. Wittevrongel and H. Bruneel, "Correlation effects in ATM queues due to data format conversions," *Performance Evaluation*, vol. 32, no. 1, pp. 35–56, 1998.
- [79] R. M. Geist and J. M. Westall, "Correlational and distributional effects in network traffic models," *Performance Evaluation*, vol. 44, no. 1-4, pp. 121–138, 2001.
- [80] A. Feldmann, A. C. Gilbert, W. Willinger, and T. G. Kurtz, "The changing nature of network traffic: scaling phenomena," *Computer Communication Review*, vol. 28, no. 2, pp. 5–29, 1998.
- [81] R. L. Cruz, "A calculus for network delay. I. Network elements in isolation," *IEEE Transactions on Information Theory*, vol. 37, no. 1, pp. 114–131, 1991.
- [82] H. Dong, Z. Wang, D. W. C. Ho, and H. Gao, "Robust H_∞ fuzzy output-feedback control with multiple probabilistic delays and multiple missing measurements," *IEEE Transactions on Fuzzy Systems*, vol. 18, no. 4, pp. 712–725, 2010.
- [83] H. Dong, Z. Wang, and H. Gao, "Observer-based H_∞ control for systems with repeated scalar nonlinearities and multiple packet losses," *International Journal of Robust and Nonlinear Control*, vol. 20, no. 12, pp. 1363–1378, 2010.
- [84] H. Dong, Z. Wang, D. W. C. Ho, and H. Gao, "Variance-constrained H_∞ filtering for a class of nonlinear time-varying systems with multiple missing measurements: the finite-horizon case," *IEEE Transactions on Signal Processing*, vol. 58, no. 5, pp. 2534–2543, 2010.
- [85] B. Shen, Z. Wang, Y. S. Hung, and G. Chesi, "Distributed H_∞ filtering for polynomial nonlinear stochastic systems in sensor networks," *IEEE Transactions on Industrial Electronics*, vol. 58, no. 5, pp. 1971–1979, 2011.

- [86] B. Shen, Z. Wang, and X. Liu, "Bounded H_∞ synchronization and state estimation for discrete time-varying stochastic complex networks over a finite horizon," *IEEE Transactions on Neural Networks*, vol. 22, no. 1, pp. 145–157, 2011.
- [87] B. Shen, Z. Wang, and Y. S. Hung, "Distributed H_∞ -consensus filtering in sensor networks with multiple missing measurements: the finite-horizon case," *Automatica*, vol. 46, no. 10, pp. 1682–1688, 2010.
- [88] Y. Q. Chen, R. Sun, and A. Zhou, "An improved Hurst parameter estimator based on fractional Fourier transform," *Telecommunication Systems*, vol. 43, no. 3-4, pp. 197–206, 2010.
- [89] H. Sheng, H. Sun, Y. Q. Chen, and T. Qiu, "Synthesis of multifractional Gaussian noises based on variable-order fractional operators," *Signal Processing*, vol. 91, no. 7, pp. 1645–1650, 2011.
- [90] H. Sheng, Y. Q. Chen, and T. Qiu, "On the robustness of Hurst estimators," *IET Signal Processing*, vol. 5, no. 2, pp. 209–225, 2011.

Research Article

Energy-Aware Topology Evolution Model with Link and Node Deletion in Wireless Sensor Networks

Xiaojuan Luo, Huiqun Yu, and Xiang Wang

School of Information Science and Engineering, East China University of Science and Technology, Shanghai 200237, China

Correspondence should be addressed to Xiaojuan Luo, luoxj@ecust.edu.cn

Received 20 April 2011; Revised 10 June 2011; Accepted 6 July 2011

Academic Editor: Zidong Wang

Copyright © 2012 Xiaojuan Luo et al. This is an open access article distributed under the Creative Commons Attribution License, which permits unrestricted use, distribution, and reproduction in any medium, provided the original work is properly cited.

Based on the complex network theory, a new topological evolving model is proposed. In the evolution of the topology of sensor networks, the energy-aware mechanism is taken into account, and the phenomenon of change of the link and node in the network is discussed. Theoretical analysis and numerical simulation are conducted to explore the topology characteristics and network performance with different node energy distribution. We find that node energy distribution has the weak effect on the degree distribution $P(k)$ that evolves into the scale-free state, nodes with more energy carry more connections, and degree correlation is nontrivial disassortative. Moreover, the results show that, when nodes energy is more heterogeneous, the network is better clustered and enjoys higher performance in terms of the network efficiency and the average path length for transmitting data.

1. Introduction

Recently, complex networks have attracted considerable attention to investigate various real-world dynamic networks, such as scientific collaboration, the Internet, worldwide web, social networks, biological networks, transportation networks, e-mail networks, software engineering, and ad hoc networks; see [1–9] and the references therein. In the original theoretical description of these findings, the Watts-Strogatz (WS) model [10] provided a simple way to generate networks with the “small-world” properties. Barabási and Albert [11] proposed a “scale-free” network with a power-law degree distribution. Further studies show that real networked systems may undergo the more complex evolution process governed by multiple mechanisms on which the occurrence of network structures depends [12–15]. Therefore, to get a better understanding of the real-world system, it is necessary to describe such evolution processes of complex network in more detailed and realistic manner.

The motivation for considering dynamic networks comes, in part, from the recent interest in designing wireless sensor networks as a prime example. Sensor networks have recently received increasing interests due to their extensive application in areas such as information collection, environmental monitoring, industrial automation, health tracking, and military surveillance [16, 17]. Consequently, many critical techniques in sensor network have gained much research efforts [18–22]. The motivations of this work is to continue such efforts aimed at discovering new mechanism to construct optimal network structures and that might be useful in designing engineered sensor networks.

Well-known examples of such dynamical network models are proposed including preferential attachment and its variants [11, 23, 24]. Very recently, Zhu et al. [25] have proposed two scale-free networks-based models for wireless sensor networks, named energy-aware evolution model (EAEM) and energy-balanced evolution model (EBEM) which can organize the networks in an energy-efficient way. Chen et al. [26] have proposed a topology control of wireless sensor networks under an average degree constraint. Actually, the above evolving models have considered energy efficiency of WSNs using by energy-aware mechanism. These mechanisms, however, model the dynamics WSN as a monotonously growing network, where the effect of node deletion is not considered to be significant. Sensor networks experience significant rates of links and nodes deletion for several kinds of cases as follows and beyond. Nodes join and depart from sensor networks in a random and rapid manner for artificial mobility. The links and nodes are probably removed for many factors such as environment deteriorated, hostile attack because the sensor nodes are usually deployed over some inaccessible and dangerous geographical area. Usually the energy of sensor node is limited and nonrecharged and would be exhausted after working for a period of time. Hence, developing a network dynamic model for the real-world sensor networks with a significant deletion component is necessary.

Several recently proposed models have addressed the link and node deletion process for dynamical sensor network. Kong and Roychowdhury [27] proposed an ad hoc network with node addition and removal, focusing on the compensatory process for node removal to preserve true scale-free state. Sarshar and Roychowdhury [28] investigated stable ad hoc network where nodes deletion is dominated by preferential survival mechanism. A local-world heterogeneous model of wireless sensor networks with node and link diversity was proposed in [29]. Unfortunately, those works have not considered the node energy problem in the network. Energy efficiency is a critical factor for prolonging the life of the network system. If the topology is constructed based on the node energy, then the traffic load is properly adjusted, that is, nodes with more energy carry more connections and the node with less energy will carry few connections. The energy consumption is balanced in the whole network, and the network lifetime will be effectively extended.

Motivated by the above analysis, in this paper, we aim to investigate the topological evolving model for wireless sensor network, which is combined energy-aware mechanism with both addition and removal of link and node based on complex network theory. To the best of the authors' knowledge, the proposed mechanism has not yet been addressed for WSNs. The main contributions of this paper are summarized as follows. (1) a new evolution model is proposed to describe dynamical sensor network. (2) a combination of two important mechanisms of energy preferential attachment for link and node addition and energy antipreferential attachment for link and deletion contributes to investigating the complexity of WSNs. (3) Degree distribution $P(k)$ is solved by utilizing mean-field analysis and shows how the network evolves into the scale-free state. Numerical simulations

of several critical topology characteristics are used to demonstrate the effectiveness of the proposed model in this paper.

The rest of this paper is organized as follows. In Section 2, we present our new energy-aware topology evolving model for wireless sensor networks. In Section 3, we give the numerical analysis and simulations experiments discussion about the network characteristics under the effect of different node energy distribution. Its effectiveness is analytically investigated by its topology properties, such as degree distribution, node degree, and the average degree of neighboring node, the average clustering coefficient, the average path length, and the network efficiency. The results are validated through numerical calculations and simulations. Finally in Section 4, we conclude the investigation and point out the further research direction.

2. The Proposed Model for WSNs

In this section, we present the following model to capture the particular features of such WSNs evolving networks. In the initial state, the network has a small number n_0 of connected nodes and small number e_0 of edges. Then, the iterative algorithm during the evolving process is outlined as follows.

(1) Preferential Attachment

At each time step, a new node is added to the system. And m ($0 < m \leq n_0$) new links from the new node are connected to m existing nodes. We assume that the preferential probability $\Pi(k_i)$ of a new node will be connected to node i depending on the connectivity k_i and energy (E_i) of that node. In this paper, we use the definition of the function $f(E_i)$ to present the relationship between the energy of a node and its ability to be linked just as in [25]. Then

$$\Pi(k_i) = \frac{f(E_i)k_i}{\sum_j f(E_j)k_j}. \quad (2.1)$$

In real wireless sensor network, the node which has more connectivities will carry more traffic load and consume its energy more quickly. For the balance the energy consumption, we assume the more energy a node has, the strong ability it will have of being connected to the new coming nodes. Therefore, $f(E_i)$ must be an increasing function here, and the form may be as E_i , E_i^2 and so on. Here α is the coefficient. In this paper, we just set $f(E_i) = E_i^\alpha$, where $\alpha = 1$. And the form of $\Pi(k_i)$ is expressed as

$$\Pi(k_i) = \frac{E_i k_i}{\sum_j E_j k_j}. \quad (2.2)$$

(2) Links Deletion

At each time step, with probability p ($0 \leq p < 1$), $m * p$ old links are removed. So the parameter p denotes the deletion rate, which is defined as the rate of links removed divided by the rate of links addition. We first select a node i as an end of a deleted link with the antipreferential

probability as (2.2). The less energy the node has, the more probability it will have for being deleted:

$$\Pi^*(k_i) = \frac{(k_i E_i)^{-1}}{\sum_i (k_i E_i)^{-1}}. \quad (2.3)$$

Then node j is then chosen from the linked neighborhood of node i (denoted by O_i) with probability $K_i^{-1} \Pi^*(k_j)$, where $K_i = \sum_{j \in O_i} \Pi^*(k_j)$. Then the link connecting nodes i and j is removed; this process is repeated $m * p$ times. Once an isolated node appears, it should be removed from the network to maintain the connectivity of networks. The antipreferential removal mechanism is more reasonable for deleting links that are parallel with the preferential connection. It is consistent with the real wireless sensor networks environment. The wireless links that have not been active may be removed from the network when the energy of the connecting nodes falls down to a certain level. The particular antipreferential removal phenomenon is also reasonable for many real networks. For example, users' e-mail networks can be constructed by considering user address books as nodes and addresses in the address books as links. Some old addresses that have become inactive below the threshold may be deleted in the evolving e-mail network [8]. Furthermore, in the evolving words network, there will be link and node removals over time because some old expressions and sentences are no longer used and some words may become obsolete [12].

3. Network Analysis

Topological characterization is of great importance for network structure in reality. To have a better understanding of the complex dynamics in the considered model and of the influence of (E) , in this section we give theoretical analysis and numerical simulation of these statistical properties parameters—the degree distribution $P(k)$, node degree (k_E) , the average nearest-neighbor connectivity $(k_{nn}(k))$, the average clustering coefficient (C) , the average path length (L) , and the network efficiency (E) .

3.1. Degree Distribution

The degree distribution $P(k)$, which indicates the probability that a randomly selected node has k connections, is very important statistical character of large-scale complex network. In fact, $P(k)$ has been suggested to be used as the first criterion to classify real-world networks. Now we adopt the mean field theory [30] to give a qualitative analysis of $P(k)$ for our energy-aware evolving model with link and node deletions.

By the mean-field theory, let $k_i(t)$ be the degree of the i th node at time t , then in the limit of large t , the increasing rate of $k_i(t)$ satisfies the following dynamical equation:

$$\frac{k_i}{t} = m \Pi(k_i) - m p \left[\Pi^*(k_i) + \sum_{j \in \text{linked}(i)} \Pi^*(k_j) K_i^{-1} \Pi^*(k_i) \right]. \quad (3.1)$$

It is easy to know that the first term in (3.1) accounts for the increasing number of links of the i th node by the preferential attachment due to the newly added node. The second

term in (3.1) explains the losing of links by antipreferential attachment during the evolving process.

From the mean-field sense, we have

$$\sum_j E_j k_j = N(t) * \bar{E} * \langle k(t) \rangle, \quad (3.2)$$

where \bar{E} is the expected value of the node energy in the whole network; $N(t)$ is the number of the nodes at time step t ; $\langle k(t) \rangle$ is the average degree of the network at time t . For large t , $N(t) = n_0 + t \approx t$, $\langle k(t) \rangle = (2m(1-p)t + e_0) / (m_0 + t) \approx 2m(1-p)$ with e_0 being the number of edges that were initially linked to n_0 nodes. Moreover we can have $\sum_{j \in O(i)} K_i^{-1} \Pi^*(k_i) \approx 1$. Then, at time step t , $\Pi^*(k_i) \approx 1/N(t) \approx 1/t$, which indicates that link deletion with the antipreferential probability is equivalent to deleting links with equal probability by mean-field sense. This phenomenon is also observed in [12].

Supposing that sensor networks which undergo a large number of time steps t have sufficiently large scale, we obtain

$$\frac{k_i}{t} \approx m \frac{E_i k_i}{2m(1-p)\bar{E}t} - \frac{2mp}{t}. \quad (3.3)$$

It is obvious that, at every time step t , $0 \leq p < 1$. Since $p = 1$, the network cannot grow. We then consider two cases in the above proposed evolving network model: $p = 0$ and $0 < p < 1$, which are further discussed below.

Case A ($p = 0$). In this case, there are only link and node additions without link and node deletions in the evolving process as in [25]. It is usually fit for topology discovery state of WSNs in which the all nodes have enough power in the ideal environment. So $k_i(t)$ satisfies

$$\frac{k_i}{t} = m \frac{E_i k_i}{N \bar{E} \langle k(t) \rangle} = \frac{E_i k_i}{2(n_0 + t)\bar{E}} \approx \frac{E_i k_i}{2t\bar{E}}. \quad (3.4)$$

With the initial condition $k_i(t_0) = m$, then we can get

$$k_i(t) = m \frac{E_i}{2\bar{E}} \left(\frac{t}{t_0} \right)^{1/2}. \quad (3.5)$$

The probability that a node has a connectivity which satisfy $k_i(t) < k$ is

$$P(k_i(t) < k) = P\left(t_0 > \frac{1}{2} \left(\frac{m E_i}{2\bar{E}} \right)^2 \frac{t}{k^2} \right). \quad (3.6)$$

Assuming that we add the node to the network at equal time intervals in evolving process for WSNs, the probability density at the time t_0 is $P(t_0) = 1/(n_0 + t)$. Therefore, we get

$$P(k_i(t) < k) = 1 - \frac{1}{2} \left(\frac{m E_i}{2\bar{E}} \right)^2 \frac{t}{k^2} \frac{1}{n_0 + t}. \quad (3.7)$$

The probability density function of the degree of a node with energy E is

$$P(k_E) = \frac{P(k_i(t) < k)}{k} = \frac{2}{n_0 + t} \left(\frac{m E}{2\bar{E}} \right)^2 \frac{t}{k^3}. \quad (3.8)$$

The overall probability density function is

$$\begin{aligned} P(k) &= \int_{E_{\min}}^{E_{\max}} (E) P(k_E) dE = \int_{E_{\min}}^{E_{\max}} (E) \frac{1}{2(n_0 + t)} \left(\frac{m E}{\bar{E}} \right)^2 \frac{t}{k^3} dE \\ &= \int_{E_{\min}}^{E_{\max}} \frac{1}{2} (E) \left(\frac{m E}{\bar{E}} \right)^2 \frac{1}{k^3} dE, \quad t \rightarrow \infty, \end{aligned} \quad (3.9)$$

where (E) is the probability density distribution of node energy E in the whole network; E_{\min} and E_{\max} are the bounds of node energy values. Obviously, $p(k) \propto k^{-3}$, where $= \int_{E_{\min}}^{E_{\max}} (1/2) (E) (m E / \bar{E})^2 dE$. The degree distribution follows the same power law as the Barabási-Albert scale-free model [11].

Case B ($0 < p < 1$). In this case, links and nodes in the evolving network model are not monotonously growing. Instead, links and nodes can be added in some occasion and removed in other case. We rewrite (3.3) as follows:

$$\frac{k_i}{t} = m \frac{E_i k_i}{2m(1-p)\bar{E}t} - \frac{2m p}{t}. \quad (3.10)$$

With the initial condition that node i at its introduction has $k_i(t_i) = m$, one can get

$$k_i(t) = B \left(\frac{t}{t_i} \right)^{-B+m} \quad \text{for large } t, \quad (3.11)$$

where the dynamic exponent is

$$= (m, p) = \frac{m E_i}{[2m(1-p) + 1] \bar{E}} \quad (3.12)$$

and the coefficient is

$$B = B(m, p) = m - \frac{m - 2m p [2m(1-p) + 1] \bar{E}}{m E_i}. \quad (3.13)$$

We can get from (3.11) that

$$P(k_i(t) < k) = P\left(t_i > \left(\frac{B}{B-m+k} \right)^{1/} t\right) \quad \text{for } k > m. \quad (3.14)$$

With the same about the probability density at the time t , $P(t) = 1/(n_0 + t)$. Hence,

$$P(k_i(t) < k) = 1 - \left(\frac{B}{B - m + k} \right)^{1/\tau} \frac{t}{n_0 + t}. \quad (3.15)$$

The probability density function of the degree of a node with energy E is

$$P(k_E) = \frac{P(k_i(t) < k)}{k} = \frac{t}{n_0 + t} \frac{1}{B^{1/\tau}} (k + B - m)^{-(1+1/\tau)}. \quad (3.16)$$

To obtain the overall probability density function

$$P(k) = \int_{E_{\min}}^{E_{\max}} P(E) P(k_E) dE = \int_{E_{\min}}^{E_{\max}} P(E) \frac{t}{n_0 + t} \frac{1}{B^{1/\tau}} (k + B - m)^{-(1+1/\tau)} dE, \quad (3.17)$$

where $P(E)$, E_{\min} , and E_{\max} have the same definition as in (3.9). We compute numerical results and compare them with simulation as follows.

In this paper, we consider three kinds of node energy distribution $P(E)$ in the whole network within the interval $[0, 1]$: (1) the same node energy with value 0.5 with $\sigma = 0$; (2) uniform distribution ($U[0, 1]$) with $\sigma = 1/12$; (3) exponential distribution ($\exp(-E)$) with $\sigma = 1$, where σ is the standard deviation used to indicate the node energy heterogeneity. The nodes energy in the network becomes more and more heterogeneous as σ increases. So, the node energy with exponential distribution is the most heterogeneous among the three cases, while the node energy is homogeneous with $\sigma = 0$ for the first case.

In Figure 1, we make the simulations for $m = 4$ and $m = 1$, where $p = 0$. We can find that the degree distributions $P(k)$ are power law as B-A model. Moreover, it is easy to understand that the network makes higher connectivity as m increases. We also can see that the network degree distribution curves obtained by the mathematic method and by simulation match very well.

In Figures 2, 3(a) and 3(b), we, respectively, give the simulations for $p = 0.5$, $p = 0.75$, and $p = 0.25$, where $m = 4$, $\tau = 2000$. We observe that the results of $P(k)$ display a horse-head-like curve, with its middle section showing the expected scale-free state whatever the value of p is. We can see that the network degree distribution curves obtained by the mean-field method and by simulation match very well for degree larger than m . The figures also show that the mean-field solution cannot provide probabilities for degrees smaller than m . The overall horse-head-like distribution curve has also been observed in [12] by Markov process. Thus, from Figures 1, 2, and 3, there is little distinction among the plots for three kinds of nodes energy distribution. So we think the different nodes energy distribution in the network has the weakest affect on the degree distribution.

3.2. Connectivity Correlation

To clearly understand the influence of $P(E)$ on the network connectivity and uncover the internal complexity of the topological structure, it is worth investigating the connectivity correlation through k_E (the average degree of node with energy E) and $k_{nn}(k)$ (the average

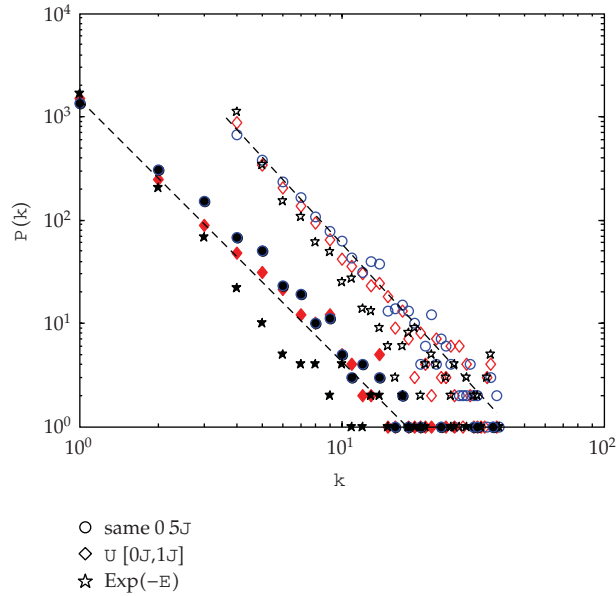


Figure 1: The degree distribution $P(k)$ obtained by simulations as hollow symbol for $m = 4$; face color marked symbol for $m = 1$, with three kinds of (E) , by the mean-field method as dashed line, where $p = 0$, $t = 2000$.

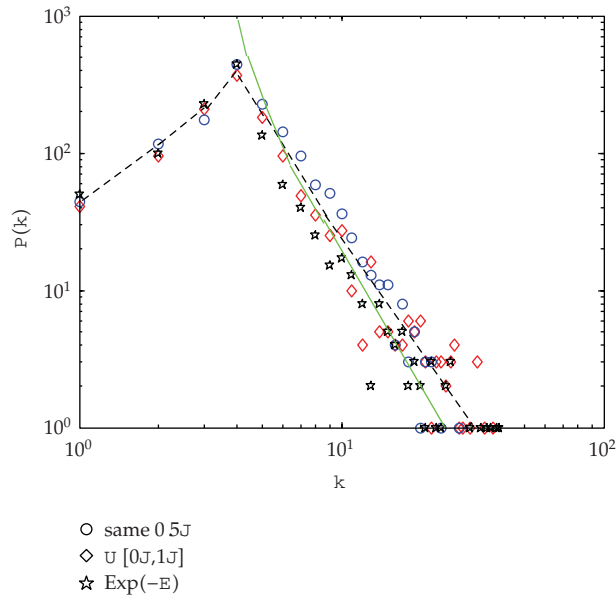


Figure 2: The degree distribution $P(k)$ obtained by simulations with three kinds of (E) : same (0.5J), U [0,1], exp(-E) and by fitting line as dashed line, by the mean-field method as solid green line, where $m = 4$, $p = 0.5$, $t = 2000$.

degree of neighboring nodes of a given node with degree k). We find from Figure 4 that the node which has more energy has a larger degree. The node degree is linearly increased with node energy when (E) is uniform distribution. But for the exponential distribution, there

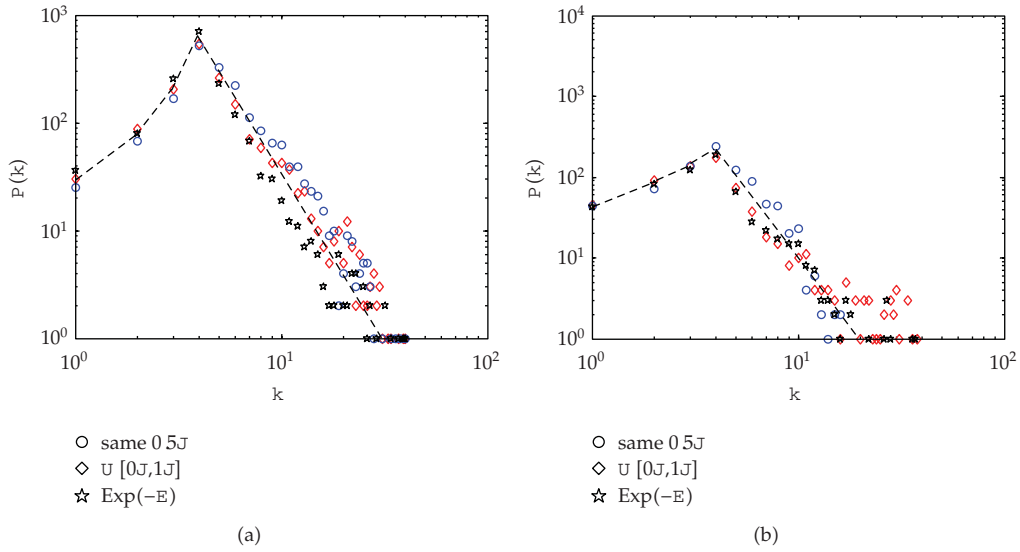


Figure 3: The degree distribution $P(k)$ obtained by simulations for three kinds of node energy distribution (E) and by fitting line as dashed line; (a) $p = 0.25$, (b) $p = 0.75$; where $m = 4$, $\tau = 2000$.

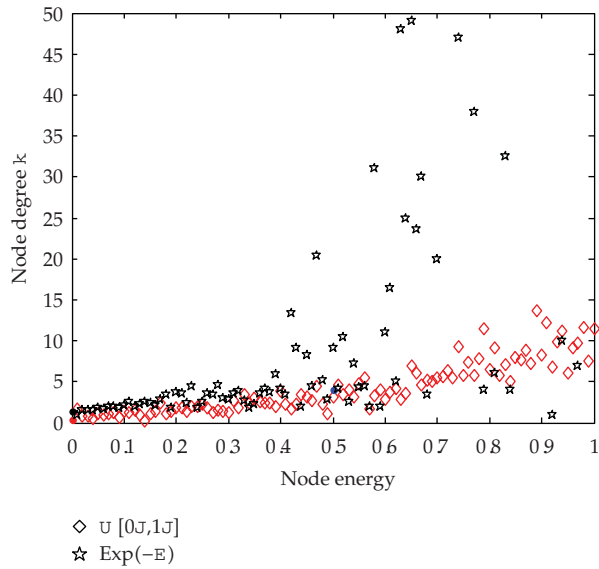


Figure 4: The relation between node degree and node energy obtained by simulations for two kinds of node energy distribution (E): $U [0,1]$, $\exp(-E)$, where $m = 4$, $p = 0.5$.

is an inward bend at the middle of the data curve that most high energy nodes carry much more links and a few of them keep relatively less links. It is because we can only perform a finite number of computation steps, and then possibly some nodes with high energy newly come into the network. There are a few hubs, that have much more links than the others nodes, emerging in the evolving process for the energy exponential distribution case. Thus the connectivity becomes more inhomogeneous when nodes energy is more heterogeneous.

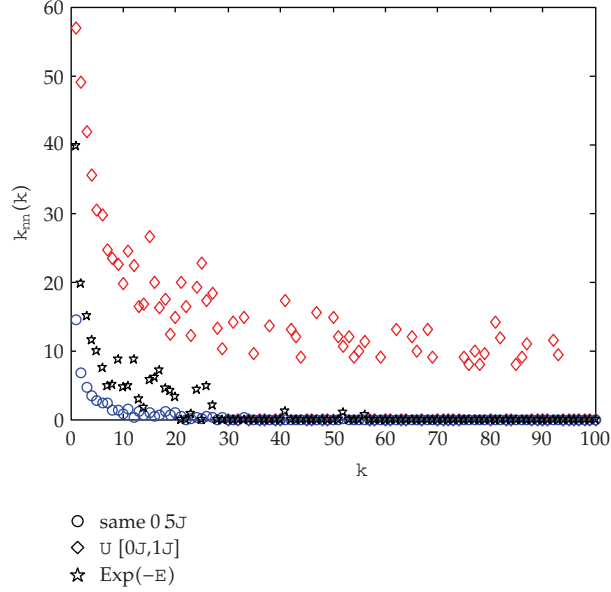


Figure 5: The average degree of neighboring node $k_{nn}(k)$ obtained by simulations for three kinds of node energy distribution (E) , where $m = 4, p = 0.5$.

Connectivity correlation is also quantified by reporting the numerical value of the slope of $k_{nn}(k)$ as a function of k . We compute $k_{nn}(k)$ which is defined as in [31]:

$$k_{nn}(k) = \frac{1}{N_k} \sum_{i \in \Omega_k} \left(\frac{1}{k} \sum_{j \in O_i} k_j \right), \quad (3.18)$$

where Ω_k is the set of nodes with degree k of the amount N_k in the evolving WSNs. O_i is the set of linked neighbors of node i . In Figure 5, it is found that $k_{nn}(k)$ is independent of k for nodes with large degree, that is, nodes with large k show no obvious biases in their connections. But there is a short disassortative region when k is relatively small, that is, nodes with low degree are more likely linked with the highly connected ones. Such phenomenon can be explained by the effect of network growth with energy preferential attachment and elements removals with antipreferential mechanism.

3.3. Clustering Coefficient

We investigate the effect of node energy distribution on network's cluster coefficient, which quantifies the extent to which nodes adjacent to a given node are linked [15, 31]. Let E_i denote the number of edges among the neighbor nodes of a selected node i with degree k_i in the network; C_i is local clustering coefficient of node i . Then the clustering coefficient of the whole network is the average of all individual C_i . It is defined as follows:

$$C = \frac{1}{N} \sum_i C_i = \frac{1}{N} \sum_i \frac{E_i}{k_i(k_i - 1)/2}. \quad (3.19)$$

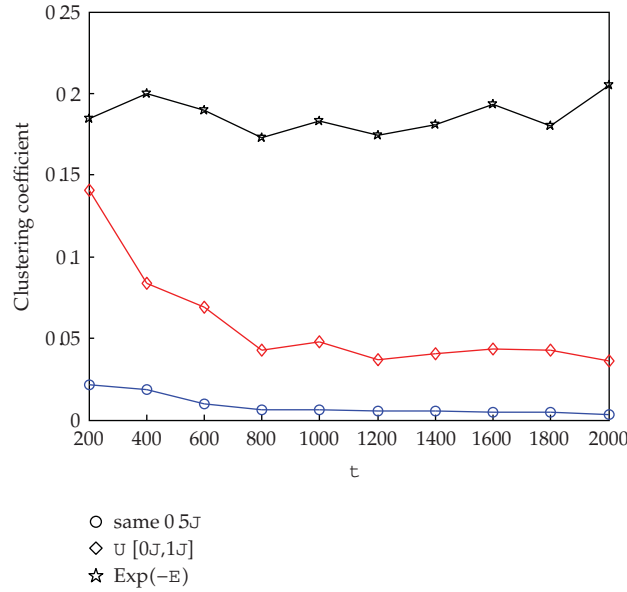


Figure 6: The clustering coefficient obtained by simulations for three kinds of node energy distribution (E), where $m = 4$, $p = 0.5$.

In Figure 6, we give the clustering coefficient (C) changing by network size with three kinds of node energy distribution. C keeps very small value of 0.005 when node energy is same in the network. But when (E) is exponential distribution, C keeps large value with the average value 0.185. The result indicates that nodes energy heterogeneity makes the network more clustering.

3.4. Average Shortest Path Length and Network Efficiency

In WSN, the sensor nodes forward the data by multihops. The average path length L is defined to be the average length of the shortest paths between any two nodes in the network that is written as in (3.20). Usually we use it to measure the average hops among the nodes for data processing. Simultaneously we use the network efficiency E to measure how efficiently the information is exchanged over the network. Let d_{ij} denote the length of the shortest path between node i and node j . The efficiency between node i and j is assumed to be inversely proportional to the shortest distance: $e_{ij} = 1/d_{ij}$. With this definition, when there is no path between i and j , $d_{ij} = \infty$. The global efficiency of the network is defined as the average of the efficiencies over all couples of nodes. Its calculation can be defined as (3.21):

$$L = \frac{1}{N(N-1)} \sum_{i \neq j} d_{ij}, \quad (3.20)$$

$$E = \frac{1}{N(N-1)} \sum_{i \neq j} \frac{1}{d_{ij}}. \quad (3.21)$$

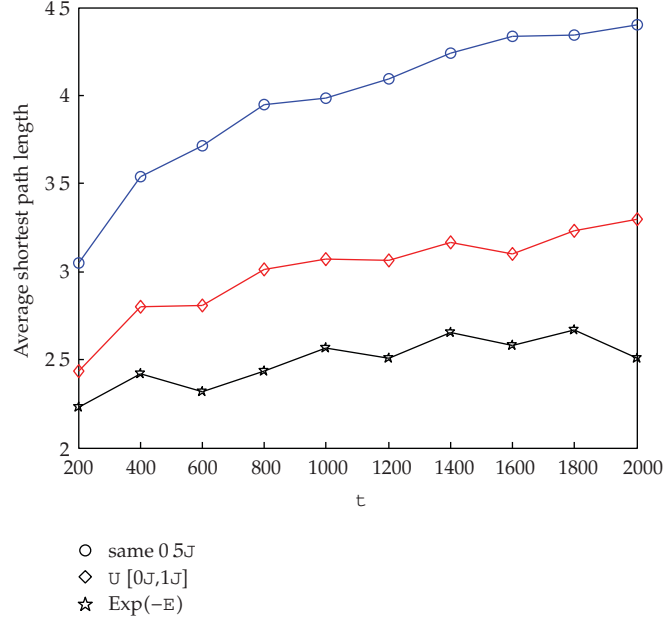


Figure 7: The average shortest path length obtained by simulations for three kinds of node energy distribution (E), where $m = 4$, $p = 0.5$.

Since L and E characterize the ability of two nodes to communicate with each other, the smaller L and the larger E mean fewer hops and less energy consumption for data processing. In Figures 7 and 8, we plot the average shortest path length (L) and network efficiency (C) with evolving time step t which denoted network size, for three kinds of node energy distribution. We observe that L increases, and E decreases with the network size increasing. We also find, by the same evolving time step t that the network obtains the smallest L and the largest E when (E) is exponential distribution among the three kinds of (E). Conversely, L is the largest and E is the smallest when node energy is same in the network for the same network size. The results verify that nodes in energy inhomogeneous networks are more efficient to communicate with others.

4. Conclusion

In this paper, we have addressed a novel topology evolution model for wireless sensor networks. A notion of energy-aware mechanism combined with additions and removals of link and node has been first defined to characterize the evolution model of WSNs. Subsequently, by using mean-field approach, numerical calculation shows the network evolving into the scale-free state with a horse-head-like initial section. Finally, experimental simulations have been employed to demonstrate the effectiveness of the results derived in this paper. Node energy distribution has a weak effect on the degree distribution $P(k)$ but it has much effect on the network internal topological characterizations. The node which has more energy will have more degrees for balancing energy consumption, and the model exhibits the nontrivial disassortative degree correlation as a natural property of network evolution. In addition, the connectivity is tighter and the network is higher clustering for

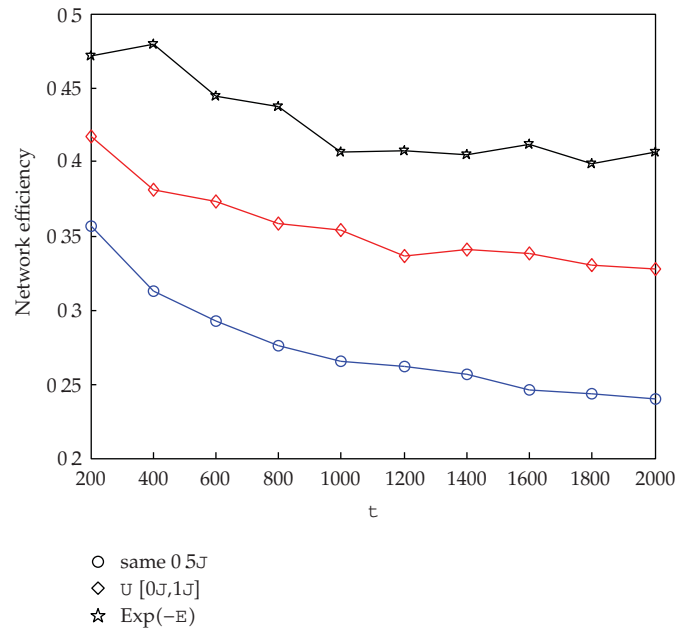


Figure 8: The network efficiency obtained by simulations for three kinds of node energy distribution (E) where $m = 4$, $p = 0.5$.

the sensor network system in which node energy is more heterogeneous. Then, from the perspective of the average path length and the network efficiency, we find that, when node energy distribution is more heterogeneous, the network enjoys better performance in energy efficiency for transmitting data. The analysis of the robustness against the random failures and intentional attacks for the proposed model is beyond the scope of the current work and is left for future investigations.

This model articulates the topology dynamics of the real WSNs and provides some useful guidelines for constructing WSNs.

Acknowledgments

This work was partially supported by the NSF of China under Grants no. 60773094 and no. 50803016 and Shanghai Shuguang Program under Grant no. 07SG32.

References

- [1] M. E. J. Newman, "The structure of scientific collaboration networks," *Proceedings of the National Academy of Sciences of the United States of America*, vol. 98, no. 2, pp. 404–409, 2001.
- [2] M. Faloutsos, P. Faloutsos, and C. Faloutsos, "On power-law relationships of the internet topology," *Computer Communication Review*, vol. 29, no. 4, pp. 251–261, 1999.
- [3] R. Albert, H. Jeong, and A. L. Barabási, "Diameter of the world-wide web," *Nature*, vol. 401, no. 6749, pp. 130–131, 1999.
- [4] B. A. Huberman, P. L. T. Pirolli, J. E. Pitkow, and R. M. Lukose, "Strong regularities in world wide web surfing," *Science*, vol. 280, no. 5360, pp. 95–97, 1998.
- [5] G. González-Parra, L. Acedo, R.-J. V. Micó, and A. J. Arenas, "Modeling the social obesity epidemic with stochastic networks," *Physica A*, vol. 389, no. 17, pp. 3692–3701, 2010.

- [6] V. Colizza, A. Flammini, A. Maritan, and A. Vespignani, "Characterization and modeling of protein-protein interaction networks," *Physica A*, vol. 352, no. 1, pp. 1–27, 2005.
- [7] J. R. Banavar, A. Maritan, and A. Rinaldo, "Size and form in efficient transportation networks," *Nature*, vol. 399, no. 6732, pp. 130–132, 1999.
- [8] J. Wang and P. De Wilde, "Properties of evolving e-mail networks," *Physical Review E*, vol. 70, no. 6, Article ID 066121, 8 pages, 2004.
- [9] L. Wen, R. G. Dromey, and D. Kirk, "Software engineering and scale-free networks," *IEEE Transactions on Systems, Man, and Cybernetics B*, vol. 39, no. 3, pp. 648–657, 2009.
- [10] D. J. Watts and S. H. Strogatz, "Collective dynamics of 'small-world' networks," *Nature*, vol. 393, no. 6684, pp. 440–442, 1998.
- [11] A.-L. Barabási and R. Albert, "Emergence of scaling in random networks," *American Association for the Advancement of Science*, vol. 286, no. 5439, pp. 509–512, 1999.
- [12] D. Shi, L. Liu, S. X. Zhu, and H. Zhou, "Degree distributions of evolving networks," *Europhysics Letters*, vol. 76, no. 4, pp. 731–737, 2006.
- [13] B. Shen, Z. Wang, and X. Liu, "Bounded H_∞ synchronization and state estimation for discrete time-varying stochastic complex networks over a finite horizon," *IEEE Transactions on Neural Networks*, vol. 22, no. 1, pp. 145–157, 2011.
- [14] Q. Chen and D. Shi, "The modeling of scale-free networks," *Physica A*, vol. 335, no. 1-2, pp. 240–248, 2004.
- [15] Y. Gu and J. Sun, "A local-world node deleting evolving network model," *Physics Letters A*, vol. 372, no. 25, pp. 4564–4568, 2008.
- [16] I. F. Akyildiz, W. Su, Y. Sankarasubramaniam, and E. Cayirci, "A survey on sensor networks," *IEEE Communications Magazine*, vol. 40, no. 8, pp. 102–114, 2002.
- [17] G. Anastasi, M. Conti, M. Di Francesco, and A. Passarella, "Energy conservation in wireless sensor networks: a survey," *Ad Hoc Networks*, vol. 7, no. 3, pp. 537–568, 2009.
- [18] B. Shen, Z. Wang, Y. S. Hung, and G. Chesi, "Distributed H_∞ filtering for polynomial nonlinear stochastic systems in sensor networks," *IEEE Transactions on Industrial Electronics*, vol. 58, no. 5, pp. 1971–1979, 2011.
- [19] J. Yick, B. Mukherjee, and D. Ghosal, "Wireless sensor network survey," *Computer Networks*, vol. 52, no. 12, pp. 2292–2330, 2008.
- [20] H. Dong, Z. Wang, D. W. C. Ho, and H. Gao, "Variance-constrained H_∞ filtering for a class of nonlinear time-varying systems with multiple missing measurements: the finite-horizon case," *IEEE Transactions on Signal Processing*, vol. 58, no. 5, pp. 2534–2543, 2010.
- [21] B. Shen, Z. Wang, and Y. S. Hung, "Distributed H_∞ -consensus filtering in sensor networks with multiple missing measurements: the finite-horizon case," *Automatica*, vol. 46, no. 10, pp. 1682–1688, 2010.
- [22] H. Dong, Z. Wang, and H. Gao, "Robust H_∞ filtering for a class of nonlinear networked systems with multiple stochastic communication delays and packet dropouts," *IEEE Transactions on Signal Processing*, vol. 58, no. 4, pp. 1957–1966, 2010.
- [23] A. Vázquez, "Growing network with local rules: preferential attachment, clustering hierarchy, and degree correlations," *Physical Review E*, vol. 67, no. 5, Article ID 056104, 15 pages, 2003.
- [24] X. Li and G. Chen, "A local-world evolving network model," *Physica A*, vol. 328, no. 1-2, pp. 274–286, 2003.
- [25] H. Zhu, H. Luo, H. Peng, L. Li, and Q. Luo, "Complex networks-based energy-efficient evolution model for wireless sensor networks," *Chaos, Solitons and Fractals*, vol. 41, no. 4, pp. 1828–1835, 2009.
- [26] L. J. Chen, Y. C. Mao, D. X. Chen, and L. Xie, "Topology control of wireless sensor networks under an average degree constraint," *Chinese Journal of Computers*, vol. 30, no. 9, pp. 1544–1550, 2007.
- [27] J. S. Kong and V. P. Roychowdhury, "Preferential survival in models of complex ad hoc networks," *Physica A*, vol. 387, no. 13, pp. 3335–3347, 2008.
- [28] N. Sarshar and V. Roychowdhury, "Scale-free and stable structures in complex ad hoc networks," *Physical Review E*, vol. 69, no. 2, Article ID 026101, 6 pages, 2004.
- [29] S. Li, L. Li, and Y. Yang, "A local-world heterogeneous model of wireless sensor networks with node and link diversity," *Physica A*, vol. 390, no. 6, pp. 1182–1191, 2011.
- [30] A. L. Barabási, R. Albert, and H. Jeong, "Mean-field theory for scale-free random networks," *Physica A*, vol. 272, no. 1, pp. 173–187, 1999.
- [31] S. Boccaletti, V. Latora, Y. Moreno, M. Chavez, and D.-U. Hwang, "Complex networks: structure and dynamics," *Physics Reports*, vol. 424, no. 4-5, pp. 175–308, 2006.

Research Article

A Novel Algorithm of Stochastic Chance-Constrained Linear Programming and Its Application

Xiaodong Ding and Chengliang Wang

School of Management, University of Shanghai for Science and Technology, Shanghai 200093, China

Correspondence should be addressed to Chengliang Wang, usstwcl@163.com

Received 20 April 2011; Accepted 6 July 2011

Academic Editor: Zidong Wang

Copyright © 2012 X. Ding and C. Wang. This is an open access article distributed under the Creative Commons Attribution License, which permits unrestricted use, distribution, and reproduction in any medium, provided the original work is properly cited.

The computation problem is discussed for the stochastic chance-constrained linear programming, and a novel direct algorithm, that is, simplex algorithm based on stochastic simulation, is proposed. The considered programming problem in this paper is linear programming with chance constraints and random coefficients, and therefore the stochastic simulation is an important implement of the proposed algorithm. By theoretical analysis, the theory basis of the proposed algorithm is obtained and, by numerical examples, the feasibility and validness of this algorithm are illustrated. The detailed algorithm procedure is given, which is easily converted into the executable codes of software tools. Then, we compare it with some algorithms to verify its superiority. Finally, a practical example is presented to show its practicability.

1. Introduction

In the late 1950s, stochastic linear programming (SLP) appeared with the further application of linear programming. SLP is a special kind of linear programming problem in which a part or all of coefficients are random variables with joint probability distribution. Generally speaking, there are two sorts of SLP models, one of which can be described as “wait-and-see” model based on the hypothesis that the decision maker can wait until the random variables come true and another one is called “here-and-now” model in which the decision maker must make decision before the random variables come true.

Stochastic chance-constrained programming (SCP), firstly proposed by Charnes and Cooper [1], offers a powerful means of modeling stochastic decision and control systems (see, e.g., [2, 3]). SCP is mainly concerned with the problem that the decision maker must give his solution before the random variables come true. In this problem, the made decision

may not satisfy the constraints in some degree, but the probability of decision satisfying the constraints cannot be less than some given confidence level α . Stochastic chance-constrained linear programming (SCLP) is an important part of SCP.

As we know the traditional method to solve SCLP is converting it into an equivalent deterministic linear programming and then obtaining the optimal solution by some deterministic algorithms [4]. However, this method is only effective for some special cases. Generally, SCLP cannot be converted into some deterministic linear programming and convex programming, see the work of Kall and Wallace in [5]. However, for those which can be converted to deterministic problem, it is usually a difficult work to convert and one can always obtain a complicated nonlinear programming which is traditional hard problem. Therefore, it is necessary and urgent to find the direct and effective algorithm to solve SCLP. Luckily, with the rapid development of computer, genetic algorithms based on stochastic simulation were designed for SCP, see, for example, [6–8]. These intelligent algorithms are more direct and effective than the method of converting SCP to deterministic programming. However, the disadvantages of these genetic algorithms are obvious. That is, they are always designed aiming to solve every specified problem, depending on experiment and lacking the common theory basis. Therefore, it is a necessary and urgent task to find a better algorithm, which gives rise to the motivation for the present study in this paper.

Summarizing the above discussion, we aim to develop a novel direct and universal algorithm to solve the computation problem of the stochastic chance-constrained linear programming. The main contribution of this paper can be given as follows: (i) several simple approaches are illustrated to be ineffective or limited to SCLP by numerical example; (ii) a novel and direct algorithm, that is, simplex algorithm based on stochastic simulation, is proposed; (iii) the theory basis of the proposed algorithm is proved; (iv) the detailed procedures of the simplex algorithm are given. By numerical examples, our algorithm is compared with the traditional methods and genetic algorithm based on stochastic simulation and verified to be feasible, valid, and better than the traditional ones and intelligent technique. Finally, a real-world example is given to illustrate the practicability of the developed algorithm.

2. Research Model and Computation Problem of SCLP

In this paper, unless otherwise specified, $(\Omega, \mathcal{F}, \mathcal{P})$ denotes a complete probability space, where Ω is a nonempty sample space, \mathcal{F} is the power set of Ω , and \mathcal{P} is a probability measure on \mathcal{F} , and a random variable is defined as a function from the probability space $(\Omega, \mathcal{F}, \mathcal{P})$ to the set of \mathcal{F} .

2.1. Stochastic Linear Programming (SLP) Model

Firstly, introduce the following SLP model

$$\begin{aligned} \min \quad & C^T X \\ \text{s.t.} \quad & A X \leq b \\ & X \geq 0, \end{aligned} \tag{2.1}$$

where X is an n dimensional vector to be determined, and $A = (a_{ij}(\omega))_{m \times n}$, $b = (b_i(\omega))_{m \times 1}$, $C = (c_j(\omega))_{n \times 1}$, with $a_{ij}(\omega)$, $b_i(\omega)$, $c_j(\omega)$ ($i = 1, \dots, m$, $j = 1, \dots, n$) being random variables and $\omega \in \Omega$.

2.2. Stochastic Chance-Constrained Linear Programming (SCLP) Model

SCLP usually includes two sorts of models which can be formulated as follows:

$$\begin{aligned} \min \quad & C^T X \\ \text{s.t.} \quad & P(A X \leq b) \geq \alpha \\ & X \geq 0, \end{aligned} \quad (2.2)$$

$$\begin{aligned} \min \quad & C^T X \\ \text{s.t.} \quad & P(A_i X \leq b_i) \geq \alpha_i, \quad i=1,2,\dots,m \\ & X \geq 0, \end{aligned} \quad (2.3)$$

where A_i is the i th row of A , b_i is the i th element of b , and α_i is the i th confidence level of the constraints.

2.3. Computation Problem of SCLP

In this subsection, by solving a numerical example of SLP, the computation problem of SCLP is analyzed and several possible approaches are tried to obtain the optimal solution to the example.

Example 2.1. Let (a, b) be the random variables with uniform distribution in rectangle $\{1 \leq a \leq 4, 1/3 \leq b \leq 1\}$ and consider the following SLP problem:

$$\begin{aligned} \min \quad & x_1 + x_2 \\ \text{s.t.} \quad & ax_1 + x_2 \geq 7 \\ & bx_1 + x_2 \geq 4 \\ & x_1 \geq 0, \quad x_2 \geq 0. \end{aligned} \quad (2.4)$$

Solution 1. In (2.4), the expectations of the random variables a and b are easily derived. Therefore, a very simple idea is to replace the stochastic parameters a and b by their

expectations, respectively, and solve the corresponding deterministic linear programming problem described as follows:

$$\begin{aligned}
 \min \quad & x_1 + x_2 \\
 \text{s.t.} \quad & \frac{5}{2}x_1 + x_2 \geq 7 \\
 & \frac{2}{3}x_1 + x_2 \geq 4 \\
 & x_1 \geq 0, \quad x_2 \geq 0.
 \end{aligned} \tag{2.5}$$

From (2.5), by deterministic linear programming algorithms, it is easy to derive the unique optimal solution $x_1^* = 18/11$, $x_2^* = 32/11$.

Now, in order to analyze the feasibility of this approach, we assume $*$ = (18/11, 32/11), and, from the example, we can easily know the feasible region $D = \{(x_1, x_2) \mid ax_1 + x_2 \geq 7, bx_1 + x_2 \geq 4\}$. Then

$$\begin{aligned}
 P(* \in D) &= P\left(\frac{18}{11}a + \frac{32}{11} \geq 7, \frac{18}{11}b + \frac{32}{11} \geq 4\right) \\
 &= P\left(a \geq \frac{5}{2}, b \geq \frac{2}{3}\right) = 0.25.
 \end{aligned} \tag{2.6}$$

That is, the probability of the solution $*$ taking value in the feasible region D is only 0.25, which verifies that the method of directly replacing random parameters by their expectations is invaluable.

Solution 2. It is well known that the samples of random variables are also easily obtained; therefore, another simple technique is to produce some random samples of these random parameters and solve all the deterministic linear programming problems corresponding to the samples, and then we choose the best solution as the optimal solution. Now, produce 10 samples of a and b in (2.4):

$$\begin{aligned}
 a: & (1.99, 2.02, 2.47, 3.23, 2.56, 3.78, 1.68, 3.95, 2.33, 3.65), \\
 b: & (0.63, 0.62, 0.41, 0.58, 0.85, 0.59, 0.47, 0.80, 0.57, 0.62).
 \end{aligned} \tag{2.7}$$

From Table 1, it is easy to see that the largest probability $P(* \in D)$ is no more than 0.5. Consequently, this approach is almost useless for any practical problems.

To further testify the above conclusion about the technique in Solution 2, we consider the following stochastic chance-constrained programming, which relaxes the constraints in (2.4):

$$\begin{aligned}
 \min \quad & x_1 + x_2 \\
 \text{s.t.} \quad & P\{ax_1 + x_2 \geq 7, bx_1 + x_2 \geq 4\} \geq 0.95 \times 0.95 \\
 & x_i \geq 0, \quad i=1,2.
 \end{aligned} \tag{2.8}$$

Table 1: The solutions and their probabilities $* \in D$.

Number	Solution (x_1, x_2)	$x_1 + x_2$	$P(* \in D)$
1	(2.20, 2.62)	4.82	0.37
2	(2.13, 2.68)	4.81	0.38
3	(1.46, 3.40)	4.86	0.45
4	(1.13, 3.34)	4.48	0.16
5	(1.75, 2.50)	4.26	0.11
6	(0.95, 3.44)	4.39	0.05
7	(3.18, 1.66)	4.84	0.37
8	(0.95, 3.23)	4.19	0.00
9	(1.70, 3.03)	4.74	0.36
10	(0.99, 3.39)	4.81	0.38

Generate 10000 samples of (a, b) , replace (a, b) by the samples, and calculate all the deterministic programming problems. We can find that there is almost no solution satisfying the constraints of (2.8) among 10000 solutions.

Solution 3. In the following, we analyze a traditional but indirect approach, which is to convert SLP into an equivalent deterministic programming problem and obtain the optimal solution by some deterministic programming algorithms.

From the constraints in (2.8), we have

$$\begin{aligned}
 P\{ax_1 + x_2 \geq 7, bx_1 + x_2 \geq 4\} &= P\left\{a \geq \frac{7-x_2}{x_1}, b \geq \frac{4-x_2}{x_1}\right\} \\
 &= P\{a \geq a^*, b \geq b^*\} \\
 &= [(4-a^*)(1-b^*)] \div \left(3 \times \frac{2}{3}\right),
 \end{aligned} \tag{2.9}$$

where $a^* = (7-x_2)/x_1$, $b^* = (4-x_2)/x_1$.

Therefore, the constraints in (2.8) are equivalent to

$$\begin{aligned}
 \left[\left(4 - \frac{7-x_2}{x_1}\right) \times \left(1 - \frac{4-x_2}{x_1}\right)\right] \div \left(3 \times \frac{2}{3}\right) &\geq 0.9025, \\
 \left(4 - \frac{7-x_2}{x_1}\right) \div 3 &\geq 0.9025, \\
 \left(1 - \frac{4-x_2}{x_1}\right) \div \frac{2}{3} &\geq 0.9025,
 \end{aligned} \tag{2.10}$$

and then the SCLP model (2.8) is equivalent to the following deterministic nonlinear programming:

$$\begin{aligned}
 \min \quad & x_1 + x_2 \\
 \text{s.t.} \quad & 1.805x_1^2 - (4x_1 + x_2 - 7)(x_1 + x_2 - 4) \leq 0 \\
 & 0.9025x_1 - \frac{4x_1 - (7 - x_2)}{3} \leq 0 \\
 & 0.9025x_1 - \frac{x_1 - (4 - x_2)}{2/3} \leq 0 \\
 & x_1 \geq 0, \quad x_2 \geq 0.
 \end{aligned} \tag{2.11}$$

Setting the initial value $x_0 = (0,0)$, then the optimal solution x^* and the optimal value f^* of this nonlinear programming model are

$$x^* = (3.36, 2.84)^T, \quad f^* = 6.19, \tag{2.12}$$

and we can have the probability $P(x^* \in D) = 0.9025$.

From the above calculation and analysis of the three methods, we can conclude that the former two are not feasible regardless of their simpleness and the third one is valid. However, the third measure is indirect and the obtained equivalent deterministic programming is usually a nonlinear programming whose calculation is difficult and sometimes impossible. Therefore, it is necessary to find some novel direct computation method. Recently, a direct and effective algorithm, that is, genetic algorithms, has been put forward and rapidly developed to solve the stochastic chance-constrained linear programming, see, for example, the work of Liu in [9], of Ding et al. in [10], and of Ding and Sun in [11]. However, they are always designed aiming to solve every specified problem, depending on experiment and lacking the common theory basis.

In next section, we propose a direct and universal algorithm of SCLP, simplex algorithm based on stochastic simulation, and build its theory basis. Then we design the detailed procedures of the algorithm, which are easily changed into the executable codes of software.

3. Simplex Algorithm Based on Stochastic Simulation

In SCLP model, on one hand, the meaning of "min" is not clear because of C being random vector; on the other hand, it is difficult to judge the convexity of SCLP which is required by optimization theory. Therefore, the computation problem of the SCLP is very difficult. In this section, we propose a satisfying algorithm, that is, simplex algorithm based on stochastic simulation, to overcome this difficulty. Firstly, several problems in SCLP are handled by stochastic simulation. Then, we build the theory basis of this algorithm by theoretical analysis. Finally, the detailed procedures of this algorithm are designed.

According to the theory of stochastic chance-constrained linear programming, we can transform (2.2) into the following programming model:

$$\begin{aligned}
 & \min \quad f \\
 & \text{s.t.} \quad P\left(C^T X \leq f\right) \geq \alpha \\
 & \quad \quad P(A X \leq b) \geq \beta \\
 & \quad \quad X \geq 0,
 \end{aligned} \tag{3.1}$$

where f is the target function and α, β are the confidence levels of the target function and constraint, respectively.

Similarly, model (2.3) can be transformed into

$$\begin{aligned}
 & \min \quad f \\
 & \text{s.t.} \quad P\left(C^T X \leq f\right) \geq \alpha \\
 & \quad \quad P\left(A_{ij} X \leq b_i\right) \geq \beta_i, \quad i=1,2,\dots,m \\
 & \quad \quad X \geq 0.
 \end{aligned} \tag{3.2}$$

3.1. Stochastic Simulation

3.1.1. Judging the Chance Constraint

Consider the chance constraints in (3.1):

$$P\{A X \leq b\} \geq \beta, \tag{3.3}$$

where the random matrix A and the random vector b have a known joint probability distribution $\Phi(A, b)$. Then we check whether the chance constraint holds or not if we have a solution X by applying the stochastic simulation method (the Monte Carlo simulation). The algorithm is as follows.

Algorithm 3.1. Chance constraint judging algorithm.

Step 1. Set $N' = 0$.

Step 2. Sample a random vector $\{(a_{ij}^k, b_i^k), i = 1, 2, \dots, m, j = 1, 2, \dots, n\}$ according to the joint probability distribution of $\Phi(A, b)$.

Step 3. Calculate $A X$; if $A X \leq b$, then $N' ++$.

Step 4. Repeat Step 2 to Step 3 N times.

Step 5. If $N'/N \geq \beta$, return FEASIBLE, or else return INFEASIBLE.

3.1.2. Handling the Target Function

Consider the target function with the random parameter vector C :

$$P\left(C^T X \leq f\right) \geq \alpha. \quad (3.4)$$

For any given vector X , the minimum objective function f can always be found by stochastic simulation, and the algorithm is as follows.

Algorithm 3.2. Minimum target function searching algorithm.

Step 1. Sample a random vector $\{C_k, k = 1, 2, \dots, N\}$ according to the probability distribution of $\Phi(C)$.

Step 2. Compute $\{C_k^T X, k = 1, 2, \dots, N\}$ and arrange the results according to the ascending order.

Step 3. Set N' as the integer part of αN .

Step 4. Return the N' th largest element in the set $\{C_k^T X, k = 1, 2, \dots, N\}$ as the estimation of f .

3.1.3. Checking the Estimation Number

In order to check the estimate of probability, we test and return the random variable t_j , such that

$$P\left\{\omega \in \Omega \mid t_j - \hat{c}_j > 0\right\} \geq \alpha, \quad (3.5)$$

where t_j is a random variable, \hat{c}_j is a deterministic number, and α is a prescribed confidence level.

Algorithm 3.3. Estimation number checking algorithm.

Step 1. Set $N' = 0$.

Step 2. Sample random vectors $\{t_j^{(k)}, k = 1, 2, \dots, N\}$ according to the probability distribution of $\Phi(t_j)$.

Step 3. If $t_j - \hat{c}_j > 0$, then $N' = N' + 1$.

Step 4. Repeat Step 2 to Step 3 N times.

Step 5. If $N'/N \geq \alpha$, return FEASIBLE and execute Step 6.

Step 6. Letting K' be the integer part of αN , array $\{t_j - \hat{c}_j, k = 1, 2, \dots, N\}$ according to ascending order, return the $(N - K' + 1)$ 'th element.

Step 7. Otherwise return INFEASIBLE.

3.2. Theoretical Analysis

In this subsection, we aim to build the theory basis of simplex algorithm based on stochastic simulation by theoretical analysis. To begin with, we recall the basic principle of deterministic linear programming. According to the convexity of deterministic linear programming, the programming has optimal solution if the feasible solutions are finite, and the optimal solution must be in the range of the feasible solutions (see the work of Zhang and Xu in [12]). Based on this theory, the simplex method is designed. Specifically, the basic principles of simplex method can be formulated as follows. First of all, find a feasible solution stochastically and check whether it is optimal; if it is not optimal, then we find another feasible solution which can improve the target function and check this solution again; repeat the above process until we find the optimal solution and the corresponding target value, or we can confirm that the programming does not have the optimal solution. According to these principles, we further consider the stochastic chance-constrained linear programming (3.1).

In (3.1), replace $AX \leq b$ by $AX + Y = b$ with $Y \geq 0$ according to the slack variable method and assume $H = (A, E_Y)$, where E_Y is an $m \times m$ unit matrix. Then the constraint is equivalent to

$$P(HZ = b) \geq \alpha, \quad (3.6)$$

where $Z = (X^T \ Y^T)^T$. Still mark $(C^T \ 0_Y^T)^T$ as C^T , where 0_Y is a $m \times 1$ zero vector, and then we have $C^T X = C^T Z$.

Based on the above assumption, the main principle of simplex algorithm based on stochastic simulation can be described as follows. Firstly, find a base matrix from H by random sample or Big M method (Big M method is the most direct method and the base matrix is deterministic unit matrix). Secondly, search a feasible basic solution satisfying the chance constraint according to stochastic simulation, calculate the corresponding b (denoted by \hat{b}), then check whether it is the optimal solution by the sample value of C (denoted by \hat{C}), which is calculated by stochastic simulation method; if it is not optimal, according to the improvement principle, we can find the sample value of H (denoted by \hat{H}). Thirdly, solve the deterministic programming defined by \hat{H} , \hat{b} and \hat{C} by simplex algorithm, and we can obtain a solution \bar{X} which can improve the value of target function. Fourthly, check whether the solution satisfies the constraint. If it does not, change \hat{H} , \hat{b} , and \hat{C} and check once more until we derive an improved solution satisfying the constraint. Repeat the above steps until we find the optimal solution or are sure that there is no optimal solution (infinite optimal solutions).

Assume \bar{Z} , B , \hat{b} , U ($H = (B, U)$) are the initial feasible solution, the feasible base, a sample value of b (\hat{b} is determined by checking whether $B^{-1}\hat{b}$ satisfies the constraint through stochastic simulation), and the nonbase matrix, respectively, and then we have

$$\begin{aligned} \bar{Z} &= \begin{pmatrix} B^{-1}\hat{b} \\ 0 \end{pmatrix} = \begin{pmatrix} \bar{b} \\ 0 \end{pmatrix}, \\ C^T \bar{Z} &= \begin{pmatrix} C_B^T & C_U^T \end{pmatrix} \begin{pmatrix} \bar{b} \\ 0 \end{pmatrix} = C_B^T \bar{b}, \end{aligned} \quad (3.7)$$

with C_B and C_U being corresponding to the base variable and the nonbase variable of C , respectively.

Computing the value of target function by stochastic simulation and chance constraint

$$P\left(C^T \begin{pmatrix} \bar{b} \\ 0 \end{pmatrix} \leq \bar{f}\right) \geq \alpha, \quad (3.8)$$

it is easy to obtain the sample value \hat{C} of C and the target value $\bar{f} = \hat{C}^T \bar{b}$.

Set $Z = (Z_B^T \ Z_U^T)^T$ as being any feasible solution and consider the following stochastic chance constrained programming:

$$\begin{aligned} \min \quad & f = \hat{C}^T Z \\ \text{s.t.} \quad & P\left(H Z = \bar{b}\right) \geq \alpha \\ & Z = \begin{pmatrix} X^T & Y^T \end{pmatrix}^T \geq 0. \end{aligned} \quad (3.9)$$

From (3.9) and the above discussion, we have

$$\begin{aligned} P\left(Z_B = B^{-1}\bar{b} - B^{-1}U Z_U\right) &\geq \alpha, \\ f = \hat{C}^T Z &= \hat{C}_B^T Z_B + \hat{C}_U^T Z_U. \end{aligned} \quad (3.10)$$

therefore,

$$P\left(f = \hat{C}_B^T \bar{b} - \left(\hat{C}_B^T B^{-1}U - \hat{C}_U^T\right) Z_U\right) \geq \alpha. \quad (3.11)$$

Let $H = (h_1, h_2, \dots, h_n)$ and J_U be the lower label set of nonbase variables and

$$t_j - \hat{c}_j = \hat{C}_B^T B^{-1} h_j - \hat{c}_j, \quad j \in J_U, \quad (3.12)$$

where $t_j - \hat{c}_j$ is defined as the estimation number. Then we can derive

$$P\left(f = \bar{f} - \sum_{j \in J_U} (t_j - \hat{c}_j) z_j\right) \geq \alpha. \quad (3.13)$$

Then, the programming (3.9) is converted into

$$\begin{aligned}
 \min \quad & f = \widehat{C}^T Z \\
 \text{s.t.} \quad & P \left(f = \bar{f} - \sum_{j \in J_U} (t_j - \widehat{c}_j) z_j \right) \geq \\
 & P \left(Z_B = B^{-1} \widehat{b} - B^{-1} U Z_U \right) \geq \\
 & Z = \begin{pmatrix} X^T & Y^T \end{pmatrix}^T \geq 0,
 \end{aligned} \tag{3.14}$$

where $\bar{f} = \widehat{C}^T B^{-1} \widehat{b}$ with \widehat{b} and \widehat{C} being obtained by stochastic simulation in (3.1).

If the feasible base solutions in programming (3.14) are nondegenerative, from the above discussion, we can have the following theorem.

Theorem 3.4. *If $P(t_j - \widehat{c}_j \leq 0, \forall j \in J_U) \geq \alpha$, then \bar{Z} is the optimal solution of SCLP (3.14) and is denoted as Z^* .*

Proof. Since $P(t_j - \widehat{c}_j \leq 0) \geq \alpha$ holds for all $j \in J_U$, there is no new feasible solution satisfying the constraint and reducing target function value. Therefore \bar{Z} must be the optimal solution. \square

Given a probability space (Ω, \mathcal{F}, P) , assume

$$\begin{aligned}
 \Omega_1 &= \{ \omega \in \Omega \mid t_j - \widehat{c}_j \leq 0, \forall j \in J_U \}, \\
 \Omega_2 &= \{ \omega \in \Omega \mid t_j - \widehat{c}_j > 0, \forall j \in J_U \}.
 \end{aligned} \tag{3.15}$$

Then it is easy to know that $\Omega = \Omega_1 \cup \Omega_2$, $\Omega_1 \cap \Omega_2 = \emptyset$, and $P(\Omega_1) + P(\Omega_2) = 1$. According to Theorem 3.4, if $P(\Omega_1) \geq \alpha$ does not hold, there may be other new feasible solutions satisfying the constraint and reducing the target function value. Since $P(\Omega_1) < \alpha$ is equivalent to $P(\Omega_2) \geq 1 - \alpha$, we can compute estimation number $P(\Omega_2) \geq 1 - \alpha$ by stochastic simulation and return some sample values of t_j and also obtain some sample values of h_j which is denoted as \widehat{H} . Then we can derive a feasible solution by solving the following deterministic linear programming by simplex method (see the work of Zhang and Xu in [12]).

$$\begin{aligned}
 \min \quad & \widehat{C}^T Z \\
 \text{s.t.} \quad & \widehat{H} Z = \widehat{b} \\
 & Z \geq 0.
 \end{aligned} \tag{3.16}$$

Now, we can begin solve the SCLP problem (3.1) by simplex algorithm based on stochastic simulation, and the steps are as follows.

Firstly, check the initial feasible solution \bar{Z} . If all of the estimation numbers $t_j - \widehat{c}_j \leq 0$ hold, then \bar{Z} is the optimal solution; if $t_j - \widehat{c}_j > 0$ and $B^{-1} h_k \leq 0$, there is no optimal solution;

otherwise, if $t_j - \hat{c}_j > 0$ and some of elements of $B^{-1}h_k$ are positive, there must be a new feasible solution \hat{Z} to reduce the target function value.

Secondly, check whether \hat{Z} satisfies the constraint of (3.1) by stochastic simulation. If it does, continue to check whether it is the optimal one; if it does not, change a new \hat{H} and the corresponding new \hat{b} and repeat the above checking.

Finally, repeat the above two steps. The number of basic feasible solutions is finite; therefore, it is sure that we can find an optimal solution or the programming problem has no optimal solution.

In order to find a new basic feasible solution \hat{Z} , let the vector h_k (k is the biggest estimation number of $t_k - \hat{c}_k$) enter the base vector and change the nonbase vector into a base vector. Set

$$z_k = \min \left\{ \frac{\bar{b}_i}{h_{ik}} \mid \bar{h}_{ik} > 0 \right\} \triangleq \frac{\bar{b}_i}{h_{ik}}, \quad i = 1, 2, \dots, m \quad (3.17)$$

and let $z_{B_r} = 0$. Then we obtain a new basic feasible solution

$$\hat{Z} = (\hat{z}_{B_1}, \dots, \hat{z}_{B_{r-1}}, 0, \hat{z}_{B_{r+1}}, \dots, \hat{z}_{B_m}, 0, \dots, z_k, \dots, 0)^T, \quad (3.18)$$

where $\hat{z}_{B_i} = \bar{b}_i - \bar{h}_{ik}z_k \geq 0$, ($i = 1, \dots, r-1, r+1, \dots, m$) and $\hat{z}_{B_r} = z_k > 0$. This is to say $\hat{Z}_B \geq 0$. Then, check whether \hat{Z} satisfies the constraints by stochastic simulation. If it does, we figure out a new feasible solution.

3.3. Computation Procedure

In this subsection, we design the detailed steps for the simplex algorithm based on stochastic simulation according to the above algorithm analysis. These procedures can easily be converted into the executable codes of some software tools.

Algorithm 3.5. Simplex algorithm based on stochastic simulation.

Step 1. Find an initial feasible base B .

Step 2. Find a basic feasible solution satisfying the chance constraints and the corresponding sample value of b (denoted by \hat{b}).

Step 3. Computing $z_B = B^{-1}\hat{b} \triangleq \bar{b}$ and the target function value $\bar{f} = \hat{C}_B^T \bar{b}$ by stochastic simulation, return the sample value \hat{C} .

Step 4. Check $P(t_j - \hat{c}_j > 0) > 1 - \alpha$ by stochastic simulation, and return sample value t_j which satisfies the constraint. Produce a group of \hat{H} by stochastic simulation.

Step 5. Select an \hat{H} , and calculate the estimation number by $t_j - \hat{c}_j = \hat{C}_B^T B^{-1}h_j - \hat{c}_j$. Determine the lower label k by $t_k - \hat{c}_k = \max\{t_j - \hat{c}_j \mid j = 1, 2, \dots, n\}$, and then let z_k enter the base vector.

Step 6. If $\bar{t}_k - \hat{c}_k \leq 0$, end the procedure. Then, the basic feasible solution is the optimal one and the target function can be calculated as $\bar{f} = \hat{C}_B^T \bar{b}$, or else, go to Step 7.

Step 7. Calculate $\bar{h}_k = B^{-1} \hat{h}_k$; if $\bar{h}_k \leq 0$, end the steps. We can get the programming is infinite, or else, go to Step 8.

Step 8. Calculate the ratio

$$z_k = \min \left\{ \frac{\bar{b}_i}{\bar{h}_{ik}} \mid \bar{h}_{ik} > 0 \right\} \triangleq \frac{\bar{b}_i}{\bar{h}_{ik}} \quad (3.19)$$

to find the lower label r , and set $\hat{z}_{B_r} = 0$.

Step 9. Replace \hat{h}_{B_r} by h_k , and we have a new base. Then, compute the new basic feasible solution \hat{Z} .

Step 10. Check whether \hat{Z} satisfies the chance constraints by stochastic simulation. If it does, go to Step 2; otherwise, go to Step 5. If, for all of \hat{H} obtained in Step 4, \hat{Z} does not satisfy the chance constraint, go to Step 2 to find a new \hat{b} .

4. A Numerical Example

In this section, a simulation example is presented to illustrate the feasibility and effectiveness of the simplex algorithm based on stochastic simulation developed in this paper.

Example 4.1. Consider the stochastic chance-constrained linear programming (2.8) again.

According to Big M method, (2.8) is equivalent to

$$\begin{aligned} \min \quad & (x_1 + x_2 + M x_3 + N x_4) \\ \text{s.t.} \quad & P \left\{ \begin{array}{l} ax_1 + x_2 + x_3 - x_5 = 7 \\ bx_1 + x_2 + x_4 - x_6 = 4 \end{array} \right\} \geq 0.95 \times 0.95 \\ & x_i \geq 0, \quad i = 1, 2, \dots, 6, \end{aligned} \quad (4.1)$$

where x_4 and x_5 are slack variables.

According to Algorithm 3.5, the above SCLP (4.1) can be solved by using MATLAB toolbox and the optimal solution and optimal target function value can be obtained as follows:

$$x^* = (3.2010, 2.9245)^T, \quad f^* = 6.1255. \quad (4.2)$$

Moreover, we can find that, for the above optimal solution,

$$P \{ ax_1 + x_2 \geq 7, bx_1 + x_2 \geq 4 \} = 0.9035 \geq 0.95 \times 0.95. \quad (4.3)$$

Table 2: The solutions and their probabilities $* \in D$.

Number	Solution (x_1, x_2)	f^*	$P(* \in D)$
1	(3.2802, 2.8907)	6.1709	0.9091
2	(3.2708, 2.8899)	6.1607	0.9061
3	(3.4615, 2.8299)	6.2914	0.9252

Remark 4.2. In SCLP, the coefficients, x and f , are all random variables; therefore, the optimal solution may be different for different computation. In Table 2, we obtain three couples of optimal solutions by executing Algorithm 3.5 three times.

From the above results, we can know that every optimal solution satisfies the constraints, and there is a different confidence level corresponding to the optimal solution.

Remark 4.3. From Solution 2 of Example 2.1, it is very difficult to obtain an effective result even if 10000 random samples are utilized. But we can obtain a satisfactory optimal solution using less than 20 samples in our experiment by simplex algorithm based on stochastic simulation. So it is clear that Algorithm 3.5, that is, simplex algorithm based on stochastic simulation, is effective and much better than the method in Solution 2 to Example 2.1.

Remark 4.4. Apparently, simplex algorithm based on stochastic simulation is a direct method and can be applied to any SCLP problem. Thereby, Algorithm 3.5 is also better than the traditional approach in Solution 3 to Example 2.1, which is indirect measure and only effective for some special cases.

Example 4.5. In this example, we consider a typical optimal decision problem in oil refinery production (Kall and Wallace [5]). An oil refinery factory refines two kinds of crude oil (denoted by raw_1 and raw_2) and provides gas (denoted by $prod_1$) for the gas company and burning oil (denoted by $prod_2$) for power company. A plan is needed one week before production. Assume that the yield $(raw_1, prod_1)$ of gas by raw_1 and yield $(raw_2, prod_2)$ of burning oil by raw_2 are random and yields of other products are deterministic. Therefore, set

$$\begin{aligned} (raw_1, prod_1) &= 2 + \xi_1, & (raw_1, prod_2) &= 3, \\ (raw_2, prod_1) &= 6, & (raw_2, prod_2) &= 3 + \xi_2, \end{aligned} \quad (4.4)$$

where ξ_1 is uniform distribution $\mathcal{U}(-0.8, 0.8)$ and ξ_2 is exponential distribution $\mathcal{E}\mathcal{X}\mathcal{P}(0.4)$. And let the requirement h_1 of gas and h_2 of burning oil be also random variables

$$h_1 = 180 + \eta_1, \quad h_2 = 162 + \eta_2, \quad (4.5)$$

where η_1 is normal distribution $\mathcal{N}(0, \sqrt{12})$ and η_2 is normal distribution $\mathcal{N}(0, 3)$.

The amount of expending raw_1 and raw_2 are denoted as x_1 and x_2 , respectively, and the unit prices of raw_1 and raw_2 are $c_1 = 2$ and $c_2 = 3$, respectively. Therefore, the total cost is $2x_1 + 3x_2$. Again assume the production capability (the largest amount of raw consumed) per week is 100, that is, the constraint

$$x_1 + x_2 \leq 100. \quad (4.6)$$

This problem has been dealt with by using a two-stage complement model in [5], and now we solve it by our simplex algorithm based on stochastic simulation developed in this paper.

As we know that the decision (x_1, x_2) is made a week before production and cannot be changed during the next week. Moreover, in these decisions, confidence levels are necessary; these are

$$\begin{aligned} P((2 + \delta_1)x_1 + 6x_2 \geq 180 + \delta_1) &\geq \alpha_1, \\ P(3x_1 + (3.4 - \delta_2)x_2 \geq 162 + \delta_2) &\geq \alpha_2. \end{aligned} \quad (4.7)$$

According to the decision principles: satisfying customer and minimizing loss, we can have the following SCLP problem:

$$\begin{aligned} \min \quad & f = 2x_1 + 3x_2 \\ \text{s.t.} \quad & P((2 + \delta_1)x_1 + 6x_2 \geq 180 + \delta_1) \geq \alpha_1 \\ & P(3x_1 + (3.4 - \delta_2)x_2 \geq 162 + \delta_2) \geq \alpha_2 \\ & x_1 + x_2 \leq 100 \\ & x_1, x_2 \geq 0. \end{aligned} \quad (4.8)$$

If the confidence levels α_1 and α_2 are 0.8 and 0.7, respectively, by our simplex algorithm based on stochastic simulation, we can obtain an optimal solution

$$\begin{aligned} X^* &= (33.0944, 21.7716)^T, \quad f^* = 131.5035, \\ P((2 + \delta_1)x_1 + 6x_2 \geq 180 + \delta_1) &\geq 0.8149, \\ P(3x_1 + (3.4 - \delta_2)x_2 \geq 162 + \delta_2) &\geq 0.715. \end{aligned} \quad (4.9)$$

Remark 4.6. In this SCLP problem, the random variables δ_1 , δ_2 , δ_1 , and δ_2 obey uniform, exponential and normal distributions, respectively; therefore the joint distribution of them is so complicated that it is nearly impossible to find Φ^{-1} . Therefore the programming problem is difficult to be solved by using the approach in Solution 3 to Example 2.1.

Remark 4.7. Genetic algorithm based on stochastic simulation has been put forward by Iwamura and Liu [6] for SCL problems, which is also a direct and effective method. Supposing the scale popsize = 30, the cross probability $P_c = 0.5$, the mutation probability $P_m = 0.05$, and the parameter in the rank-based evaluation function $\beta = 0.05$, after running 500 generations, we obtain an optimal solution

$$\begin{aligned} X^* &= (31.95, 22.65)^T, \quad f^* = 131.85, \\ P((2 + \delta_1)x_1 + 6x_2 \geq 180 + \delta_1) &\geq 0.8859, \\ P(3x_1 + (3.4 - \delta_2)x_2 \geq 162 + \delta_2) &\geq 0.6849. \end{aligned} \quad (4.10)$$

Comparing (4.9) and (4.10), we can see both of them satisfying all of the constraints. However, (4.9) can obtain a less minimum value; this is a better result than (4.10). We should notice that their confidence levels are different. So simplex algorithm based on stochastic simulation is a practicable method.

5. Conclusion

This paper has studied the computation problem of stochastic chance-constrained linear programming and proposed a novel algorithm, simplex algorithm based on stochastic simulation. By a numerical example, several simple approaches have been tried to solve the SCLP problem, and the disadvantages of these methods have been analyzed. By theoretical analysis, the theory basis of the simplex algorithm based on stochastic simulation has been built and a theorem has been proved. Then the detailed procedures of the proposed algorithm have been designed, which are easily executed by some software tools. Finally, by two examples, the introduced algorithm has been verified to be better than the approaches used in Example 2.1 and be more effective than genetic algorithm based on stochastic simulation.

Based on the algorithm proposed in this paper, some possible further research topics include (i) the direct and universal algorithm for uncertain programming, such as fuzzy programming and nonlinear stochastic programming, see, for example, [10, 13, 14]; (ii) the control and state estimate problems, see, for example, [3, 15–19] and the references therein.

References

- [1] A. Charnes and W. W. Cooper, "Chance-constrained programming," *Management Science*, vol. 6, no. 1, pp. 73–79, 1959.
- [2] B. Liu, *Theory and Practice of Uncertain Programming*, Springer, Heidelberg, Germany, 2002.
- [3] T. B. M. J. Ouarda and J. W. Labadie, "Chance-constrained optimal control for multireservoir system optimization and risk analysis," *Stochastic Environmental Research and Risk Assessment*, vol. 15, no. 3, pp. 185–204, 2001.
- [4] J.-M. Bismut, "An introductory approach to duality in optimal stochastic control," *SIAM Review*, vol. 20, no. 1, pp. 62–78, 1978.
- [5] P. Kall and S. W. Wallace, *Stochastic Programming*, Wiley-Interscience Series in Systems and Optimization, John Wiley & Sons, Chichester, UK, 1994.
- [6] K. Iwamura and B. Liu, "A genetic algorithm for chance constrained programming," *Journal of Information & Optimization Sciences*, vol. 17, no. 2, pp. 409–422, 1996.
- [7] J. Ren, R. Zhao, and B. Liu, "The combination model of stochastic optimal dependence investment," *The Theory and Practice of Systemic Engineering*, vol. 9, no. 1, pp. 14–18, 2000.
- [8] S. He, S. S. Chaudhry, Z. Lei, and W. Baohua, "Stochastic vendor selection problem: chance-constrained model and genetic algorithms," *Annals of Operations Research*, vol. 168, pp. 169–179, 2009.
- [9] B. Liu, "Dependent-chance programming: a class of stochastic optimization," *Computers & Mathematics with Applications*, vol. 34, no. 12, pp. 89–104, 1997.
- [10] X. Ding, R. Wu, and S. Shao, "Fixed chance-constrained programming model with fuzzy and stochastic parameter," *Control and Decision*, vol. 17, no. 5, pp. 587–590, 2002.
- [11] X. Ding and X. Sun, "A hybrid chance-constrained integer programming model and its application," *Systems Engineering—Theory Methodology Application*, vol. 14, no. 2, pp. 141–144, 2005.
- [12] J. Zhang and S. Xu, *Linear Programming*, Science, Beijing, China, 1990.
- [13] B. Liu, R. Zhao, and G. Wang, *Uncertain Programming with Applications*, Springer, Beijing, China, 2003.
- [14] H. Dong, Z. Wang, D. W. C. Ho, and H. Gao, "Robust H_∞ fuzzy output-feedback control with multiple probabilistic delays and multiple missing measurements," *IEEE Transactions on Fuzzy Systems*, vol. 18, no. 4, pp. 712–725, 2010.
- [15] B. Shen, Z. Wang, and X. Liu, "Bounded H_∞ Synchronization and state estimation for discrete time-varying stochastic complex networks over a finite horizon," *IEEE Transactions on Neural Networks*, vol. 22, no. 1, pp. 145–157, 2011.

- [16] H. Dong, Z. Wang, and H. Gao, "Observer-based H_∞ control for systems with repeated scalar nonlinearities and multiple packet losses," *International Journal of Robust and Nonlinear Control*, vol. 20, no. 12, pp. 1363–1378, 2010.
- [17] B. Shen, Z. Wang, and Y. S. Hung, "Distributed H_∞ -consensus filtering in sensor networks with multiple missing measurements: The finite-horizon case," *Automatica*, vol. 46, no. 10, pp. 1682–1688, 2010.
- [18] H. Dong, Z. Wang, D. W. C. Ho, and H. Gao, "Variance-constrained \mathcal{L}_∞ filtering for a class of nonlinear time-varying systems with multiple missing measurements: the finite-horizon case," *IEEE Transactions on Signal Processing*, vol. 58, no. 5, pp. 2534–2543, 2010.
- [19] B. Shen, Z. Wang, Y. S. Hung, and G. Chesi, "Distributed H_∞ filtering for polynomial nonlinear stochastic systems in sensor networks," *IEEE Transactions on Industrial Electronics*, vol. 58, no. 5, pp. 1971–1979, 2011.

Research Article

Adaptive-Impulsive Control of the Projective Synchronization in Drive-Response Complex Dynamical Networks with Time-Varying Coupling

Song Zheng^{1,2}

¹ School of Mathematics and Statistics, Zhejiang University of Finance and Economics, Hangzhou, Zhejiang 310018, China

² Faculty of Science, Jiangsu University, Zhenjiang, Jiangsu 212013, China

Correspondence should be addressed to Song Zheng, songzheng07318@yahoo.com.cn

Received 25 February 2011; Accepted 6 July 2011

Academic Editor: Zidong Wang

Copyright © 2012 Song Zheng. This is an open access article distributed under the Creative Commons Attribution License, which permits unrestricted use, distribution, and reproduction in any medium, provided the original work is properly cited.

This paper investigates the projective synchronization (PS) of drive-response time-varying coupling complex dynamical networks with time delay via an adaptive-impulsive controlling method, in which the weights of links are time varying. Based on the stability analysis of impulsive control system, sufficient conditions for the PS are derived, and a hybrid controller, that is, an adaptive feedback controller with impulsive control effects, is designed. Numerical simulations are performed to verify the correctness and effectiveness of theoretical result.

1. Introduction

Complex network models widely exist in the real world including the spread of infectious diseases, the World Wide Web, food webs, various wireless communication networks, metabolic networks, biological neural works, and scientific citation webs. Since the discovery of small-world effect [1] and scale-free feature [2] of complex networks, many scientists and engineers from various disciplines, such as mathematics, physics, biology, engineering, have paid increasing attention to the studies of complex networks.

Synchronization, one of the typical collective behaviours of complex dynamical networks, has received rapidly increasing attention from different fields in recent years [3–24]. And different control schemes including adaptive control [10–12], pinning control [13–16], and impulsive control [17–22] have been used to study the above problem. Recently, some authors presented hybrid control strategy to investigate the synchronization of complex networks [23–26]. Compared to the conventional control method, hybrid control method is more effective to the networks with evolutionary features [23]. In many practical situations, some complex networks may change suddenly and sharply and thus the modes switch

simultaneously. This kind of networks can be found in many evolutionary processes, such as optimal control model in economics, bursting rhythm model in pathology, mobile communication networks, and social networks.

The typical configuration of chaotic synchronization consists of drive and response systems and has been widely investigated. The PS, a new chaos synchronization phenomenon, was first studied in two coupled partially linear systems by Mainieri and Rehacek in [27]. Later, the PS between two complex networks has obtained much more attention [28–32]. In [28], Guo et al. studied the PS in drive-response networks via impulsive control. In [29, 30], authors discussed the PS of a drive-response dynamical network model without the time delay. Sun et al. studied the PS in drive-response dynamical networks of partially linear systems with time-varying coupling delay in [31]. Xu et al. [32] investigated the PS of a class of the drive-response dynamical networks with coupling delays. However, the time-varying coupling was not considered in the above studies. To simulate more realistic networks, time-varying coupling [33–35] should be taken into account. Motivated by the above discussions, this paper will focus on the adaptive-impulsive PS problem of drive-response time-varying coupling dynamical networks with time delay. Based on the stability theory of the impulsive differential equation, some criteria for the PS are derived. Furthermore, analytical results show that the drive-response networks can realize the PS.

The rest of this paper is organized as follows. In Section 2, we present the model of drive-response time-varying coupling dynamical networks with time delay and a hybrid controller is designed. In Section 3, synchronization criteria for PS are derived. Numerical simulations are shown in Section 4. The conclusion is finally drawn in Section 5.

2. Model Description and Preliminaries

Consider the following drive-response time-varying coupling dynamical network model with time delay:

$$\begin{aligned} \dot{u}_d(t) &= M(z) \cdot u_d(t), \\ \dot{z}(t) &= f(u_d(t), z(t)), \\ \dot{u}_{ri}(t) &= M(z) \cdot u_{ri}(t) + c \sum_{j=1}^N c_{ij}(t) \Gamma(t) u_{rj}(t-\tau), \quad i = 1, 2, \dots, N, \end{aligned} \quad (2.1)$$

where the drive system and the response network systems are linked through the variable $z(t) \in \mathbb{R}^1$, $u_d(t) = (u_d^1(t), u_d^2(t), \dots, u_d^n(t))^T \in \mathbb{R}^n$, $u_{ri}(t) = (u_{ri}^1(t), u_{ri}^2(t), \dots, u_{ri}^n(t))^T \in \mathbb{R}^n$ and the d and r stand for the drive system and response system, respectively. The constant $c > 0$ is the coupling strength to be adjusted, $\tau \geq 0$ is the time-delay. $M(z) \in \mathbb{R}^{n \times n}$ is a matrix which depends on the variable $z(t)$. $\Gamma(t) \in \mathbb{R}^{n \times n}$ is the time-varying inner-coupling link matrix at time t $C(t) = (c_{ij}(t))_{N \times N}$ is the outer-coupling configuration matrix, in which $c_{ij}(t) \neq 0$ if there is a link from node i to node j ($i \neq j$), and $c_{ij}(t) = 0$ ($i \neq j$) otherwise, the diagonal elements of matrix $C(t)$ are given by

$$c_{ii}(t) = - \sum_{j=1, j \neq i}^N c_{ij}(t), \quad i = 1, 2, \dots, N. \quad (2.2)$$

If there exists a constant $\rho \neq 0$ such that $\lim_{t \rightarrow \infty} \|e_i(t)\| = \|u_{ri}(t) - \rho u_d(t)\| = 0$ for $i = 1, 2, \dots, N$, then the PS of network (2.1) is achieved. ρ is a desired scaling factor.

The aim of this paper is to discuss the adaptive-impulsive PS in the drive-response time-varying coupling complex dynamical network with time delay. We choose the linear impulsive controller B_{i_k} which is a $n \times n$ constant matrix, and design an adaptive feedback controller U_i . Therefore, the network (2.1) can be rewritten as the following impulsive differential equations:

$$\begin{aligned} \dot{u}_d(t) &= M(z) \cdot u_d(t), \\ \dot{z}(t) &= f(u_d(t), z(t)), \\ \dot{u}_{ri}(t) &= M(z) \cdot u_{ri}(t) + c \sum_{j=1}^N c_{ij}(t) \Gamma(t) u_{rj}(t^-) + U_i, \quad t \neq t_k, \\ \Delta u_{ri} &= u_{ri}(t_k^+) - u_{ri}(t_k^-) = B_{i_k} [u_{ri} - u_d], \quad t = t_k, \end{aligned} \tag{2.3}$$

where $u_{ri}(t_k^+) = \lim_{t \rightarrow t_k^+} u_{ri}(t)$, $u_{ri}(t_k^-) = \lim_{t \rightarrow t_k^-} u_{ri}(t)$. Moreover, any solution of (2.3) is left continuous at each t_k , that is, $u_{ri}(t_k) = u_{ri}(t_k^-)$.

Letting the PS error $e_i(t) = u_{ri}(t) - u_d(t)$, the adaptive controllers U_i and updating laws are designed as follows:

$$\begin{aligned} U_i &= -d_i e_i(t), \\ \dot{d}_i &= k_i e_i^T(t) e_i(t) = k_i \|e_i(t)\|^2, \quad k_i > 0. \end{aligned} \tag{2.4}$$

The system (2.3) is said to be synchronized if $\lim_{t \rightarrow \infty} \|e_i(t)\| = 0$.

Under the adaptive-impulsive control, the error dynamical network is characterized by

$$\begin{aligned} \dot{e}_i(t) &= M(z) \cdot e_i(t) + c \sum_{j=1}^N c_{ij}(t) \Gamma(t) e_j(t^-) + U_i, \quad t \neq t_k, \\ \dot{z}(t) &= f(u_d(t), z(t)), \\ \Delta e_i &= B_{i_k} e_i, \quad t = t_k, \quad k = 1, 2, \dots \end{aligned} \tag{2.5}$$

Before proceeding, we give some necessary assumptions and lemmas to derive the main results of the paper.

Lemma 2.1. *The matrix inequality $2x^T y \leq x^T Q x + y^T Q^{-1} y$ holds, for any vectors $x, y \in \mathbb{R}^n$ and a positive-definite matrix $Q \in \mathbb{R}^{n \times n}$.*

Assumption 2.2. *Suppose there exists a positive constant δ , such that $\|e_i(t^-)\|^2 \leq \|e_i(t)\|^2$ holds.*

3. PS Analysis

In this section, we will make drive-response time-varying coupling complex dynamical networks achieve the PS by using the adaptive-impulsive controlling method.

Theorem 3.1. For given synchronization scaling factor α , the PS in drive-response dynamical networks will occur if the following conditions hold:

(i) If there exist two constants a_k , satisfying $0 \leq a_k < 1$ and $\dot{t}_k \leq -\alpha < 0$ such that

$$\ln(a_k) - a_k(t_k - t_{k-1}) \leq 0, \quad k = 1, 2, \dots, \quad (3.1)$$

then the trivial solution of error system (2.5) is global asymptotically stable, which implies drive-response networks achieve the projective synchronization under the adaptive-impulsive control.

(ii) If $\dot{t}_k \geq 0$ and there exists a constant $a \geq 1$ such that

$$\ln(a_k) + \int_{t_k}^{t_{k+1}} (s) ds \leq 0, \quad k = 1, 2, \dots, \quad (3.2)$$

then $a = 1$ implies that the trivial solution of error system (2.5) is stable and $a > 1$ implies that the trivial solution of error system (2.5) is global asymptotically stable where

$$\begin{aligned} \alpha &= \max_{1 \leq k \leq N} \left\{ \left(\frac{1}{\min(P)} \right) \sup \left[\max \left(P M(z) + M^T(z) P - 2d^* P \right) \right] + N, \right. \\ &\quad \left. + \sum_{j=1}^N (c_{ij}(t))^2 \|P \Gamma(t)\|^2 \right\}, \\ \max_k \left(\|I + B_k\|^2 \right) &= \alpha_k < 1, \quad \alpha_k \geq \left(\frac{\|P\|}{\min(P)} \right), \end{aligned} \quad (3.3)$$

P is a positive-definite matrix. d^* is the minimum value of the initial feedback strength d_{i0} ($d_{i0} \leq d_i$), $i = 1, 2, \dots, N$.

Proof. Consider the following Lyapunov functional:

$$V(t) = \frac{1}{2} \sum_{i=1}^N e_i^T(t) P e_i(t). \quad (3.4)$$

For $t \neq t_k$, the derivative of $V(t)$ along the trajectories of (2.5) is

$$\begin{aligned} \dot{V}(t) &= \frac{1}{2} \sum_{i=1}^N \dot{e}_i^T(t) P e_i(t) + \frac{1}{2} \sum_{i=1}^N e_i^T(t) P \dot{e}_i(t) \\ &= \frac{1}{2} \sum_{i=1}^N \left[M(z) e_i(t) + c \sum_{j=1}^N c_{ij}(t) \Gamma(t) e_j(t - \tau) - d_i e_i(t) \right]^T P e_i(t) \\ &\quad + \frac{1}{2} \sum_{i=1}^N e_i^T(t) P \left[M(z) e_i(t) + c \sum_{j=1}^N c_{ij}(t) \Gamma(t) e_j(t - \tau) - d_i e_i(t) \right] \end{aligned}$$

$$\begin{aligned}
&= \frac{1}{2} \sum_{i=1}^N e_i^T(t) \left[P M(z) + M^T(z) P - 2d_i P \right] e_i(t) + \frac{1}{2} \sum_{i=1}^N \sum_{j=1}^N e_j^T(t^-) c c_{ij}(t) \Gamma^T(t) P e_i(t) \\
&\quad + \frac{1}{2} \sum_{i=1}^N \sum_{j=1}^N e_i^T(t) c c_{ij}(t) P \Gamma(t) e_j(t^-) \\
&\leq \frac{1}{2} \sum_{i=1}^N \left\{ \sup \left[\max \left(P M(z) + M^T(z) P - 2d_i P \right) \right] \right\} e_i^T(t) e_i(t) \\
&\quad + \frac{1}{2} \sum_{i=1}^N \sum_{j=1}^N e_i^T(t) (c c_{ij}(t))^2 P \Gamma(t) \Gamma^T(t) P^T e_i(t) \\
&\quad + \frac{1}{2} \sum_{i=1}^N \sum_{j=1}^N e_j^T(t^-) e_j(t^-) \\
&\leq \frac{1}{2} \sum_{i=1}^N \left\{ \sup \left[\max \left(P M(z) + M^T(z) P - 2d_i P \right) \right] \right\} e_i^T(t) e_i(t) \\
&\quad + \frac{1}{2} \sum_{i=1}^N \sum_{j=1}^N e_i^T(t) (c c_{ij}(t))^2 P \Gamma(t) \Gamma^T(t) P^T e_i(t) + \frac{N}{2} \sum_{i=1}^N e_i^T(t^-) e_i(t^-).
\end{aligned} \tag{3.5}$$

From Assumption 2.2, we get

$$\frac{N}{2} \sum_{i=1}^N e_i^T(t^-) e_i(t^-) \leq \frac{N}{2} \sum_{i=1}^N e_i^T(t) e_i(t). \tag{3.6}$$

Thus we have

$$\begin{aligned}
\dot{V}(t) &\leq \frac{1}{2} \sum_{i=1}^N \left\{ \sup \left[\max \left(P M(z) + M^T(z) P - 2d^* P \right) \right] + N \right. \\
&\quad \left. + \sum_{j=1}^N (c c_{ij}(t))^2 \|P \Gamma(t)\|^2 \right\} e_i^T(t) e_i(t) \\
&\leq \max_{1 \leq i \leq N} \left\{ \frac{1}{\min(P)} \sup \left[\max \left(P M(z) + M^T(z) P - 2d^* P \right) \right] + N \right. \\
&\quad \left. + \sum_{j=1}^N (c c_{ij}(t))^2 \|P \Gamma(t)\|^2 \right\} \sum_{i=1}^N \frac{1}{2} e_i^T(t) P e_i(t) \\
&= (t) \sum_{i=1}^N \frac{1}{2} e_i^T(t) P e_i(t) \\
&= (t) V(t).
\end{aligned} \tag{3.7}$$

This implies that

$$V(t) \leq (V_{k-1}^+) \exp \int_{t_{k-1}}^t (s) ds, \quad k = 1, 2, \dots, t \in (t_{k-1}, t_k]. \quad (3.8)$$

When $t = t_k$, we have

$$\begin{aligned} V(t_k^+) &= \frac{1}{2} \sum_{i=1}^N e_i^T(t) (\mathbb{I}_2 + B_{i_k})^T P (\mathbb{I}_2 + B_{i_k}) e_i(t) \\ &\leq \frac{\|P\|}{\min(P)} V(t_k) \\ &\leq \kappa V(t_k), \quad k = 1, 2, \dots \end{aligned} \quad (3.9)$$

When $k = 1$ in inequality (3.8), then for any $t \in (t_0, t_1]$,

$$V(t) \leq V(t_0^+) \exp \int_{t_0}^t (s) ds. \quad (3.10)$$

This leads to

$$V(t_1) \leq V(t_0^+) \exp \int_{t_0}^{t_1} (s) ds. \quad (3.11)$$

Also from (3.9) we have

$$V(t_1^+) \leq \kappa V(t_1) \leq \kappa V(t_0^+) \exp \int_{t_0}^{t_1} (s) ds. \quad (3.12)$$

In the same way for $t \in (t_1, t_2]$, we have

$$\begin{aligned} V(t) &\leq V(t_1^+) \exp \int_{t_1}^t (s) ds \\ &\leq \kappa V(t_0^+) \exp \int_{t_0}^{t_1} (s) ds \exp \int_{t_1}^t (s) ds, \\ &= \kappa V(t_0^+) \exp \int_{t_0}^t (s) ds. \end{aligned} \quad (3.13)$$

In general for any $t \in (t_k, t_{k+1}]$, one finds that

$$V(t) \leq \kappa_1 \kappa_2 \cdots \kappa_k V(t_0^+) \exp \int_{t_0}^t (s) ds. \quad (3.14)$$

(i) If there exist two constants a , satisfying $0 \leq a < \dots$, $(t) \leq - < 0$ and (3.1), we have

$$k \leq e^{a(t_k - t_{k-1})}, \quad k = 1, 2, \dots \quad (3.15)$$

From (3.14), one finds that

$$\begin{aligned} V(t) &\leq V(t_0^+) e^{-a(t-t_0)} \\ &= V(t_0^+) e^{-a(t-t_0) - (-a)(t-t_0)} \\ &\leq V(t_0^+) e^{-a(t_k - t_0) - (-a)(t-t_0)} \\ &\leq V(t_0^+) e^{a(t_1 - t_0)} e^{a(t_2 - t_1)} \dots e^{a(t_k - t_{k-1})} e^{-a(t_k - t_0) - (-a)(t-t_0)} \\ &= V(t_0^+) e^{-(-a)(t-t_0)}, \quad t \in (t_k, t_{k+1}]. \end{aligned} \quad (3.16)$$

Then the trivial solution of error system (2.5) is global asymptotically stable, which implies drive-response time-varying coupling dynamical networks (2.3) achieve the PS under the adaptive-impulsive control.

(ii) If $(t) \geq 0$ and there exists a constant $a \geq 1$ satisfying (3.2), we have

$$k \leq \frac{1}{a} \exp \int_{t_{k+1}}^{t_k} (s) ds. \quad (3.17)$$

From (3.14), we have

$$\begin{aligned} V(t) &\leq V(t_0^+) \exp \int_{t_0}^t (s) ds \\ &\leq V(t_0^+) \exp \int_{t_0}^{t_{k+1}} (s) ds \\ &\leq V(t_0^+) \frac{1}{a} \exp \int_{t_2}^{t_1} (s) ds \frac{1}{a} \exp \int_{t_3}^{t_2} (s) ds \dots \frac{1}{a} \exp \int_{t_{k+1}}^{t_k} (s) ds \exp \int_{t_0}^{t_{k+1}} (s) ds \\ &= V(t_0^+) \frac{1}{a^k} \exp \int_{t_0}^{t_k} (s) ds, \quad t \in (t_k, t_{k+1}]. \end{aligned} \quad (3.18)$$

This implies that error system (2.5) is global asymptotically stable about zero. Therefore, the PS of the drive-response dynamical networks (2.3) is achieved. The proof is completed. \square

Remark 3.2. The conditions given by Theorem 3.1 do not require the network configuration to be symmetric and irreducible, which can be applied to more real-world dynamical networks. Moreover, Theorem 3.1 does not impose any bound on the time-delay constant τ . Thus, our synchronization results are a time-delay-independent stability criteria.

4. Numerical Simulation

In this section, to verify and demonstrate the effectiveness of the proposed methods, we consider the unified chaotic system as the drive system. It is well known that the unified chaotic system is described by

$$\begin{aligned}\dot{x}_1 &= (25 + 10)(x_2 - x_1), \\ \dot{x}_2 &= (28 - 35 - z)x_1 - x_1x_2 + (29 - 1)x_2, \\ \dot{z} &= x_1x_2 - \frac{8 + z}{3}z,\end{aligned}\tag{4.1}$$

where $M(z) = \begin{pmatrix} -(25+10) & 25+10 \\ 28-35-z & 29-1 \end{pmatrix}$, $f(x, z) = x_1x_2 - (8 + z/3)z$, $x = (x_1, x_2)^T$, $z \in [0, 1]$. System (4.1) especially is always chaotic in the whole interval $z \in [0, 1]$.

The drive-response time-varying coupling dynamical networks with time delay are described as follows:

$$\begin{aligned}\dot{x} &= (25 + 10)(y - x), \\ \dot{y} &= (28 - 35 - z)x + (29 - 1)y, \\ \dot{z} &= xy - \frac{8 + z}{3}z,\end{aligned}\tag{4.2}$$

$$\begin{aligned}\dot{x}_i &= (25 + 10)(y_i - x_i) + c \sum_{j=1}^5 c_{ij}(t)x_j(t - \tau) + u_{i1}, \\ \dot{y}_i &= (28 - 35 - z)x_i + (29 - 1)y_i + c \sum_{j=1}^5 c_{ij}(t)x_j(t - \tau) + u_{i2}.\end{aligned}$$

Choose the time-varying coupling configuration matrix:

$$C(t) = \begin{pmatrix} -2 \sin t & -1 & 0 & 2 \sin t & 1 \\ \sin t & -\sin t - \cos t & 0 & 0 & \cos t \\ 0 & \cos t & 0 & -\cos t & 0 \\ 0 & \sin t \cos t & 1 & -\sin t \cos t & -1 \\ -1 & 2 \sin t & 0 & -1 & 2 - 2 \sin t \end{pmatrix}.\tag{4.3}$$

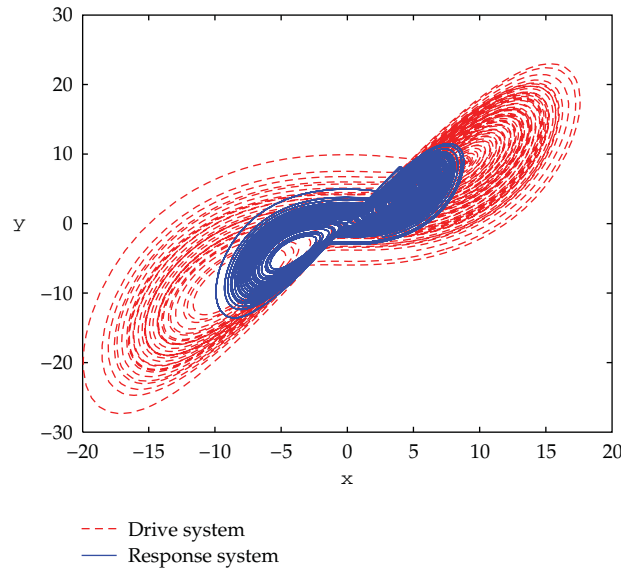


Figure 1: The trajectories of PS in the x - y plane.

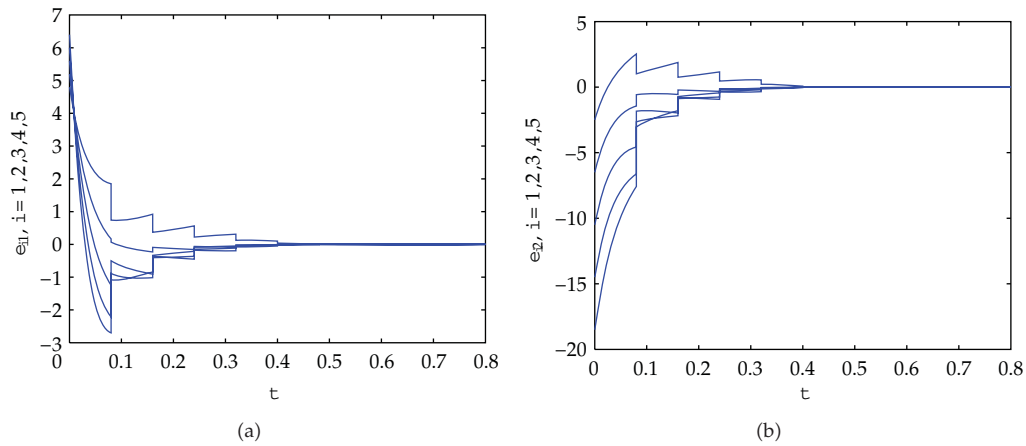


Figure 2: PS errors under the adaptive-impulsive control: (a) $e_{1i}(t) = x_{1i} - 0.5x_1$, (b) $e_{2i}(t) = x_{2i} - 0.5x_2$.

For simplicity, in the numerical simulations, we assume $P = \Gamma(t) = I_2, c = 0.1, k_i = 1, \tau = 1, \delta = 0.03$, the time-delay $\tau = 0.07$, and the impulsive interval $t_{k+1} - t_k = 0.08$. The initial values of the drive systems and the response systems are chosen as $-2, 1, 2, 3.8, -2, 4.2, -6, 4.6, -10, 5, -14, 5.4, -18, B_{ik} = \text{diag}\{-0.79, -0.79\}, \alpha_k = 0.0441 > 0, d_{i0} = 5$. After calculations, we get $\lambda_1(t) = \max_{1 \leq i \leq N} \{ (1 / \min(P)) \sup [\max(PM(z) + M^T(z)P - 2d^*P)] + N + \sum_{j=1}^N (cc_{ij}(t))^2 \|P\Gamma(t)\|^2 \} = 31.667 > 0$. Let $a = 1.02$. Then $\ln(a^{-k}) + \int_{t_k}^{t_{k+1}} (s) ds = -0.5681 < 0$, according to Theorem 3.1, and the trivial solution of error system (2.5) is global asymptotically stable. Therefore, the adaptive-impulsive PS of the drive-response dynamical networks (2.3) is achieved. Figure 1 displays the trajectories of PS in the x - y plane when $\alpha = 0.5$. The synchronization errors $e_{1i}(t) = x_{1i} - 0.5x_1$ and $e_{2i}(t) = x_{2i} - 0.5x_2$ ($i = 1, 2, \dots, 5$) are shown, respectively, in Figure 2. Figure 3 show the evolution of the feedback strength $d_{i,k}$.

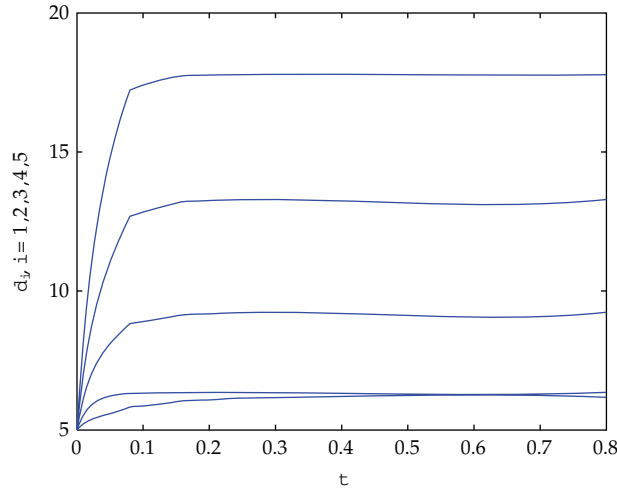


Figure 3: The evolution of the feedback strength d_i , $i = 1, 2, \dots, 5$.

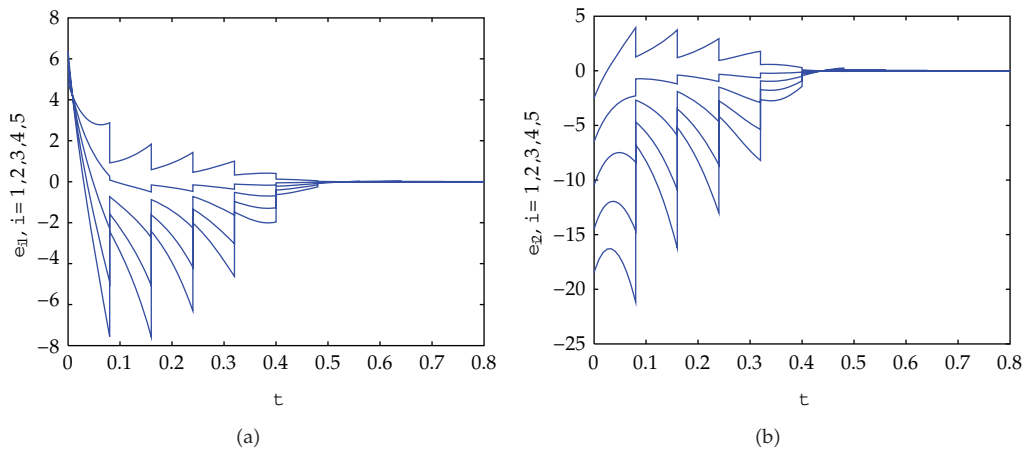


Figure 4: PS errors under the impulsive control.

The numerical results show that the adaptive-impulsive controlling scheme for the drive-response complex network is effective in Theorem 3.1.

Remark 4.1. We only consider the impulsive control; the other conditions are chosen as above, and simulation results are shown in Figure 4. From Figures 2 and 4, it is easy to find that the control effect is not as well as the adaptive-impulsive control method.

Remark 4.2. In [31, 32], the authors investigated the PS of the drive-response dynamical networks model, but the time-varying coupling was not taken into account. Here, the PS of the drive-response time-varying coupling dynamical networks with time delay is studied by employing the adaptive-impulsive control. Furthermore, the proposed adaptive-impulsive control scheme is more effective than the adaptive control scheme in [31] and the impulsive control scheme in [32].

5. Conclusion

In this paper, the adaptive-impulsive PS of the drive-response time-varying coupling dynamical networks with time delay has been investigated. Based on the stability analysis of impulsive functional differential equations, some sufficient conditions for realizing the PS are established under the adaptive-impulsive control. And the results are a time delay independent stability criteria. Finally, numerical simulations have also been given to show effectiveness of the proposed method by an example of the unified chaotic systems. In the near future, we will extend the proposed method to discrete complex dynamical networks and discuss the delay-dependent case.

Acknowledgments

The author would like to thank the associate editor and the anonymous reviewers for their constructive comments and suggestions to improve the quality of the paper and Professor Qinsheng Bi for his help. This work was supported by the National Natural Science Foundation of China (nos. 10872080, 20976075, 10972091).

References

- [1] D. J. Watts and S. H. Strogatz, "Collective dynamics of 'small-world' networks," *Nature*, vol. 393, no. 6684, pp. 440–442, 1998.
- [2] A. -L. Barabási and R. Albert, "Emergence of scaling in random networks," *Science*, vol. 286, no. 5439, pp. 509–512, 1999.
- [3] C. W. Wu, *Synchronization in Complex Networks of Nonlinear Dynamical Systems*, World Scientific, Singapore, 2007.
- [4] B. Shen, Z. Wang, and Y. S. Hung, "Distributed H_∞ -consensus filtering in sensor networks with multiple missing measurements: the finite-horizon case," *Automatica*, vol. 46, no. 10, pp. 1682–1688, 2010.
- [5] H. Dong, Z. Wang, D. W. C. Ho, and H. Gao, "Robust H_∞ fuzzy output-feedback control with multiple probabilistic delays and multiple missing measurements," *IEEE Transactions on Fuzzy Systems*, vol. 18, no. 4, Article ID 5444946, pp. 712–725, 2010.
- [6] H. Dong, Z. Wang, and H. Gao, "Observer-based H_∞ control for systems with repeated scalar nonlinearities and multiple packet losses," *International Journal of Robust and Nonlinear Control*, vol. 20, no. 12, pp. 1363–1378, 2010.
- [7] H. Dong, Z. Wang, D. W. C. Ho, and H. Gao, "Variance-constrained H_∞ filtering for a class of nonlinear time-varying systems with multiple missing measurements: the finite-horizon case," *IEEE Transactions on Signal Processing*, vol. 58, no. 5, pp. 2534–2543, 2010.
- [8] B. Shen, Z. Wang, Y. S. Hung, and G. Chesi, "Distributed H_∞ filtering for polynomial nonlinear stochastic systems in sensor networks," *IEEE Transactions on Industrial Electronics*, vol. 58, no. 5, pp. 1971–1979, 2011.
- [9] B. Shen, Z. Wang, and X. Liu, "Bounded H_∞ synchronization and state estimation for discrete time-varying stochastic complex networks over a finite horizon," *IEEE Transactions on Neural Networks*, vol. 22, no. 1, pp. 145–157, 2011.
- [10] P. De Lellis, M. di Bernardo, and F. Garofalo, "Synchronization of complex networks through local adaptive coupling," *Chaos*, vol. 18, no. 3, Article ID 037110, 8 pages, 2008.
- [11] S. Wen, S. Chen, and W. Guo, "Adaptive global synchronization of a general complex dynamical network with non-delayed and delayed coupling," *Physics Letters A*, vol. 372, no. 42, pp. 6340–6346, 2008.
- [12] S. Zheng, Q. Bi, and G. Cai, "Adaptive projective synchronization in complex networks with time-varying coupling delay," *Physics Letters A*, vol. 373, no. 17, pp. 1553–1559, 2009.
- [13] X. F. Wang and G. Chen, "Pinning control of scale-free dynamical networks," *Physica A*, vol. 310, no. 3–4, pp. 521–531, 2002.

- [14] X. Li, X. Wang, and G. Chen, "Pinning a complex dynamical network to its equilibrium," *IEEE Transactions on Circuits and Systems*, vol. 51, no. 10, pp. 2074–2087, 2004.
- [15] T. Chen, X. Liu, and W. Lu, "Pinning complex networks by a single controller," *IEEE Transactions on Circuits and Systems*, vol. 54, no. 6, pp. 1317–1326, 2007.
- [16] W. Guo, F. Austin, S. Chen, and W. Sun, "Pinning synchronization of the complex networks with non-delayed and delayed coupling," *Physics Letters A*, vol. 373, no. 17, pp. 1565–1572, 2009.
- [17] J. Zhou, L. Xiang, and Z. Liu, "Synchronization in complex delayed dynamical networks with impulsive effects," *Physica A*, vol. 384, no. 2, pp. 684–692, 2007.
- [18] G. Zhang, Z. Liu, and Z. Ma, "Synchronization of complex dynamical networks via impulsive control," *Chaos*, vol. 17, no. 4, Article ID 043126, 9 pages, 2007.
- [19] P. Li, J. Cao, and Z. Wang, "Robust impulsive synchronization of coupled delayed neural networks with uncertainties," *Physica A*, vol. 373, pp. 261–272, 2007.
- [20] Q. Song, J. Cao, and F. Liu, "Synchronization of complex dynamical networks with nonidentical nodes," *Physics Letters A*, vol. 374, no. 4, pp. 544–551, 2010.
- [21] H. Jiang and Q. Bi, "Impulsive synchronization of networked nonlinear dynamical systems," *Physics Letters A*, vol. 374, no. 27, pp. 2723–2729, 2010.
- [22] Y. Tang, S. Y. S. Leung, W. K. Wong, and J. A. Fang, "Impulsive pinning synchronization of stochastic discrete-time networks," *Neurocomputing*, vol. 73, no. 10–12, pp. 2132–2139, 2010.
- [23] M. Yang, Y. W. Wang, H. O. Wang, K. Tanaka, and Z. H. Guan, "Delay independent synchronization of complex network via hybrid control," in *Proceedings of the American Control Conference (ACC '08)*, pp. 2266–2271, Seattle, Wash, USA, June 2008.
- [24] K. Li and C. H. Lai, "Adaptive-impulsive synchronization of uncertain complex dynamical networks," *Physics Letters A*, vol. 372, no. 10, pp. 1601–1606, 2008.
- [25] H. B. Jiang, "Hybrid adaptive and impulsive synchronisation of uncertain complex dynamical networks by the generalised Barbalat's lemma," *IET Control Theory & Applications*, vol. 3, no. 10, pp. 1330–1340, 2009.
- [26] Z.-H. Guan, D. J. Hill, and J. Yao, "A hybrid impulsive and switching control strategy for synchronization of nonlinear systems and application to Chua's chaotic circuit," *International Journal of Bifurcation and Chaos*, vol. 16, no. 1, pp. 229–238, 2006.
- [27] R. Mainieri and J. Rehacek, "Projective synchronization in three-dimensional chaotic systems," *Physical Review Letters*, vol. 82, no. 15, pp. 3042–3045, 1999.
- [28] L. X. Guo, Z. Y. Xu, and M. F. Hu, "Projective synchronization in drive-response networks via impulsive control," *Chinese Physics Letters*, vol. 25, no. 8, pp. 2816–2819, 2008.
- [29] M. Hu, Y. Yang, Z. Xu, R. Zhang, and L. Guo, "Projective synchronization in drive-response dynamical networks," *Physica A*, vol. 381, no. 1–2, pp. 457–466, 2007.
- [30] Y. Zhao and Y. Yang, "The impulsive control synchronization of the drive-response complex system," *Physics Letters A*, vol. 372, no. 48, pp. 7165–7171, 2008.
- [31] M. Sun, C. Zeng, and L. Tian, "Projective synchronization in drive-response dynamical networks of partially linear systems with time-varying coupling delay," *Physics Letters A*, vol. 372, no. 46, pp. 6904–6908, 2008.
- [32] X. Xu, Y. Gao, Y. Zhao, and Y. Yang, "The impulsive control of the projective synchronization in the drive-response dynamical networks with coupling delay," *Advances in Neural Networks*, vol. 6063, no. 1, pp. 520–527, 2010.
- [33] J. Lü and G. Chen, "A time-varying complex dynamical network model and its controlled synchronization criteria," *IEEE Transactions on Automatic Control*, vol. 50, no. 6, pp. 841–846, 2005.
- [34] M. Chen, "Synchronization in time-varying networks: a matrix measure approach," *Physical Review E*, vol. 76, no. 1, Article ID 016104, 10 pages, 2007.
- [35] P. Li and Z. Yi, "Synchronization analysis of delayed complex networks with time-varying couplings," *Physica A*, vol. 387, no. 14, pp. 3729–3737, 2008.

Research Article

Two Quarantine Models on the Attack of Malicious Objects in Computer Network

Bimal Kumar Mishra¹ and Aditya Kumar Singh²

¹ Department of Applied Mathematics, Birla Institute of Technology, Mesra, Ranchi 835215, India

² Department of Applied Mathematics, Nilai Educational Trust's Group of Institutions, Thakurgaon, Ranchi 835205, India

Correspondence should be addressed to Bimal Kumar Mishra, drbimalmishra@gmail.com

Received 5 April 2011; Accepted 3 June 2011

Academic Editor: Zidong Wang

Copyright © 2012 B. K. Mishra and A. K. Singh. This is an open access article distributed under the Creative Commons Attribution License, which permits unrestricted use, distribution, and reproduction in any medium, provided the original work is properly cited.

SEIQR (Susceptible, Exposed, Infectious, Quarantined, and Recovered) models for the transmission of malicious objects with simple mass action incidence and standard incidence rate in computer network are formulated. Threshold, equilibrium, and their stability are discussed for the simple mass action incidence and standard incidence rate. Global stability and asymptotic stability of endemic equilibrium for simple mass action incidence have been shown. With the help of Poincare Bendixson Property, asymptotic stability of endemic equilibrium for standard incidence rate has been shown. Numerical methods have been used to solve and simulate the system of differential equations. The effect of quarantine on recovered nodes is analyzed. We have also analyzed the behavior of the susceptible, exposed, infected, quarantine, and recovered nodes in the computer network.

1. Introduction

It is a well-known fact that cyber world brought massive changes in the society. But nowadays cyber world is being threatened by the attack of malicious objects. Electronic mails and use of secondary devices are the major sources for the transmission of malicious objects in the computer network these days [1]. In accordance with their propagating behavior and characteristic, malicious objects spread in different way to each other. To curb the spread and impact of these malicious objects, it is important to study about their feature propagating methods, means, and limitation. Isolation may also be a very important and easy way to curb the transmission of these malicious objects. The word quarantine has evolved, meaning a forced isolation or stoppage of interactions with others. In biological world, quarantine has been adopted to reduce the transmission of human diseases, such as Leprosy, Plague, and Smallpox. Same concept has been adopted in the cyber world; the most infected nodes are isolated from the computer network till they get recovered. Anderson

and May [2, 3] discussed the spreading nature of biological viruses, parasite, and so forth. leading to infectious diseases in human population through several epidemic models. The action of malicious objects throughout a network can be studied by using epidemiological models for disease propagation [4–9]. Richard and Mark [10] proposed an improved SEI (Susceptible-Exposed-Infected) model to simulate virus propagation. However, they do not show the length of latency and take into account the impact of antivirus software. Mishra and Saini [11, 12] presented a SEIRS model with latent and temporary immune periods to overcome limitation, which can reveal common worm propagation. Feng and Thieme [13–15] considered very general endemic models that include SEIQR model, with arbitrarily distributed periods of infection including quarantine and with a general form for the incidence term that includes the three forms. Wa and Feng [16] showed that an epidemic approximation near threshold number ($R_q = 1$) can have a homoclinic bifurcation, so that some perturbation of the original model might also have a homoclinic bifurcation. Several authors studied the global stability of several epidemiological models [17–24]. Wang et al. studied the robustness of filtering on nonlinearities in packet losses, sensors, and so forth, [25–30].

In the SEIQR models for infection that confers immunity, susceptible nodes go to latent period, that is, nodes become infected but not infectious called exposed nodes, thereafter some nodes go to infectious class. Some infected nodes remain in the infected class while they are infectious and then move to the recovered class after the run of antimalicious software. Other most infected nodes are transferred into the quarantine class while they are infectious and then move to the recovered class after their recovery. The models here have a variable total population size, because they have recruitment into the susceptible class by inclusion of some new nodes and they have both crashing of nodes due to reason other than the attack of malicious codes and crashing of nodes due to the attack of malicious codes. We have developed two models and have taken simple mass action incidence and standard incidence rate, because standard incidence rate is more realistic than the simple mass action incidence [31].

2. Model 1: Mathematical Formulation for the SEIQR Model with Simple Mass Action Incidence

Let $S(t)$ be the number of susceptible at time t , $E(t)$ be the number of exposed, $I(t)$ be the number of infected nodes, $Q(t)$ be the number of quarantined nodes, $R(t)$ be the recovered nodes after the run of antimalicious software, and $N(t)$ be the total population size in time t . The schematic diagram for the flow of malicious objects is depicted in Figure 1.

As per our assumption, we have the following system of equations:

$$\begin{aligned}
 \frac{dS}{dt} &= A - SI - dS, \\
 \frac{dE}{dt} &= SI - (\delta + d)E, \\
 \frac{dI}{dt} &= E - (d + \delta_1 + \delta_2 - \delta)I, \\
 \frac{dQ}{dt} &= I - (d + \delta_2)Q, \\
 \frac{dR}{dt} &= Q + I - dR,
 \end{aligned} \tag{2.1}$$

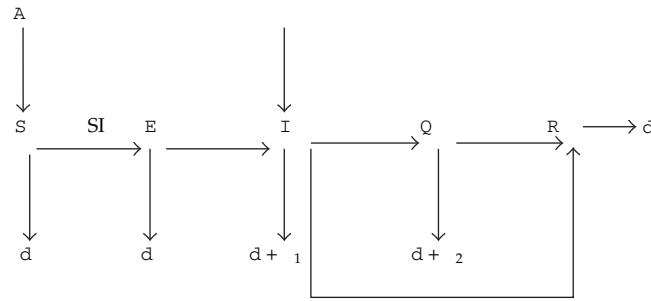


Figure 1: Schematic diagram for the flow of malicious objects in computer network.

where A is the recruitment rate of susceptible nodes, d is the per capita natural mortality rate, d_1 the death rate in infective compartment due to malicious objects, and d_2 the death rate in quarantine class due to malicious objects. The per capita contact rate β is average number of effective contacts with other nodes per unit time, σ is the rate constant which leaves the exposed compartment for infective class, γ is the rate constant which leaves the infective class for quarantine class, δ is the rate by which the nodes go from quarantine class into recovered class, and ν is the rate of vertical transmission into the infective class.

Lemma 2.1. Consider the following two systems:

$$\frac{dx}{dt} = f(t, x), \quad \frac{dy}{dt} = g(y), \tag{2.2}$$

where x, y belong to \mathbb{R}^n , f and g are continuous function which satisfy a local Lipschitz condition in any compact set X which belongs to \mathbb{R}^n , and $f(t, x) \rightarrow g(x)$ as t tends to infinity so that the second system is the limit system. Let (t, t_0, x_0) and (t, t_0, y_0) be the solutions of these systems, respectively. Suppose that $e \in X$ is a locally asymptotically stable equilibrium of the limit system and its attractive region is

$$W(e) = \{y \in X / (t, t_0, x_0) \rightarrow e, t \rightarrow +\infty\}. \tag{2.3}$$

Let W be the omega limit set of (t, t_0, x_0) . If $W \cap W(e) = \emptyset$, then $\lim_{t \rightarrow \infty} (t, t_0, x_0) = 0$.

Lipschitz's condition

If for some function $F(y)$, the following condition is satisfied:

$$|F(y_2) - F(y_1)| \leq K |y_2 - y_1|. \tag{2.4}$$

where y_1 and y_2 are any points in the domain and K is a constant, this condition is called the Lipschitz's condition.

Now, the total population size $N(t)$ satisfies the equation

$$\frac{dN}{dt} = A - dN - \beta I - \gamma Q. \quad (2.5)$$

When $t \rightarrow \infty$, then from the above equation $N \rightarrow A/d$.

Let us define the solution region by $D = \{(S, E, I, Q, R) / S \geq 0; E \geq 0; I \geq 0, Q \geq 0; R \geq 0; S + E + I + Q + R \leq A/d\}$.

The system (2.1) always has the malicious oject-free equilibrium $P_0 = (A/d, 0, 0, 0, 0)$.

Here the quarantine reproduction number is

$$R_q = \frac{(A/d)}{(\beta + d)(\beta + \gamma + \delta - \epsilon)}. \quad (2.6)$$

If $R_q > 1$, then D also contains a unique positive, endemic equilibrium $P^* = (S^*, E^*, I^*, Q^*, R^*)$.

Now from (2.1), on simplification, we have

$$\begin{aligned} S^* &= \frac{A/d}{R_q}, & I^* &= (R_q - 1) \frac{d}{\beta}, \\ E^* &= \frac{A(R_q - 1)}{(\beta + d)R_q}, & R^* &= \frac{1}{d} \left\{ \frac{(\beta + d)(R_q - 1)d}{(\beta + \gamma + \delta - \epsilon)} + \frac{d(R_q - 1)}{(\beta + \gamma + \delta - \epsilon)} \right\}, & Q^* &= \frac{(\beta + \gamma + \delta - \epsilon)(R_q - 1)d}{(\beta + \gamma + \delta - \epsilon)}. \end{aligned} \quad (2.7)$$

We have $N^* = S^* + E^* + I^* + Q^* + R^*$, Hence,

$$N^* = \frac{A/d}{R_q} + \frac{A(R_q - 1)}{(\beta + d)R_q} + \frac{d}{\beta}(R_q - 1) + \frac{1}{d} \left\{ \frac{(\beta + d)(R_q - 1)d}{(\beta + \gamma + \delta - \epsilon)} + \frac{d(R_q - 1)}{(\beta + \gamma + \delta - \epsilon)} \right\}. \quad (2.8)$$

Theorem 2.2. Consider the system (2.1). If $R_q < 1$, then solution set $D = \{(S, E, I, Q, R) / S \geq 0; E \geq 0; I \geq 0, Q \geq 0; R \geq 0; S + E + I + Q + R \leq A/d\}$ is locally asymptotically stable for disease-free equilibrium P_0 . If $R_q > 1$, then the region $D - \{(S, E, I, Q, R) / I = 0\}$, is an asymptotically stable region for the endemic equilibrium P^* .

Proof. For local stability, Jacobian of system (2.1) at equilibrium P_0 is

$$J_{P_0} = \begin{bmatrix} -d & 0 & -\beta(A/d) & 0 & 0 \\ 0 & -(\beta + d) & \beta(A/d) & 0 & 0 \\ 0 & 0 & -(\beta + \gamma + \delta - \epsilon) & 0 & 0 \\ 0 & 0 & 0 & -(\beta + \gamma + \delta - \epsilon) & 0 \\ 0 & 0 & 0 & 0 & -d \end{bmatrix}. \quad (2.9)$$

The eigenvalues of J_{P_0} are $-d; -(\beta + d); -(\beta + \gamma + \delta - \epsilon); -(\beta + \gamma + \delta - \epsilon); -d$. Since all the roots are real and negative, system is locally asymptotically stable.

In order to prove the global stability when $R_q \leq 1$, consider the Liapunov function $V = I$. Liapunov derivative $dV/dt = E - I(d + \dots)$:

$$\begin{aligned} \frac{dV}{dt} &= (R_q - 1) \frac{d}{dt} (d + \dots), \\ \frac{dV}{dt} &= \{ R_q - 1 \} \frac{d}{dt} (d + \dots) I \leq 0, \quad (\text{since } R_q - 1 \leq 0). \end{aligned} \tag{2.10}$$

As we know the Liapunov Lasalle theorem [17] implies that solutions in D approach the largest positively invariant subset of the set where $dV/dt = 0$, which is the set where $I = 0$.

In this set,

$$\begin{aligned} \frac{dQ}{dt} &= -(d + \dots) Q, \\ \frac{dS}{dt} &= A - dS. \end{aligned} \tag{2.11}$$

We have

$$Q = \frac{1}{e^{(d + \dots)t}}, \tag{2.12}$$

when

$$t \rightarrow \infty, \tag{2.13}$$

then

$$\begin{aligned} Q &\rightarrow 0, \\ S &\rightarrow \frac{A}{d}. \end{aligned} \tag{2.14}$$

We have from (2.1),

$$\frac{dR}{dt} = Q + I - dR; \tag{2.15}$$

this implies

$$R = e^{-t}. \tag{2.16}$$

Thus,

$$R \rightarrow 0 \quad (2.17)$$

when

$$t \rightarrow \infty. \quad (2.18)$$

Thus, all solutions in the set $I = 0$ go to the disease, free equilibrium P_0 . By Lemma 2.1, the system is globally asymptotically stable, when $R_0 < 1$.

From the fourth equation in system (2.1), we can solve to obtain

$$Q(t) = \frac{\left\{ Q_0 + \int_{t_0}^t I(\tau) e^{-(d+\alpha_2)(t-\tau)} d\tau \right\}}{e^{-(d+\alpha_2)(t-t_0)}}. \quad (2.19)$$

Now, $\lim_{t \rightarrow \infty} Q(t) = \lim_{t \rightarrow \infty} (I(t) / (d + \alpha_2))$. This implies $Q^* = I^* / (d + \alpha_2)$;

The similarly, solving for R by using, fifth equation in (2.1), we obtain

$$\lim_{t \rightarrow \infty} R(t) = \lim_{t \rightarrow \infty} \frac{Q(t) + I(t)}{d}, \implies R^* = \frac{I^* + Q^*}{d}. \quad (2.20)$$

An application of Lemma 2.1 shows that the endemic equilibrium P^* of model (2.1) is globally asymptotically stable in the region $D = \{(S, E, I, Q, R) / I = 0\}$. \square

3. Model 2: The SEIQR Model with the Standard Incidence Rate

The flow chart for the SEIQR model will be the same as depicted in Figure 1, but instead of simple mass action incidence βSI , we take standard incidence rate $\beta SI/N$, where $N = S + E + I + Q + R$.

The system of differential equations for this model is

$$\begin{aligned} \frac{dS}{dt} &= A - \frac{\beta SI}{N} - dS, \\ \frac{dE}{dt} &= \frac{\beta SI}{N} - (d + \alpha_1)E, \\ \frac{dI}{dt} &= E - (d + \alpha_1 + \alpha_2 + \alpha_3)I, \\ \frac{dQ}{dt} &= I - (d + \alpha_2 + \alpha_3)Q, \\ \frac{dR}{dt} &= Q + I - dR, \end{aligned} \quad (3.1)$$

where the parameters are the same as in the previous model,

$$\frac{dN}{dt} = A - dN - \beta I - \beta Q. \quad (3.2)$$

When $t \rightarrow \infty$ then $N \rightarrow A/d$. When there are malicious objects free equilibrium $P_0 = (A/d, 0, 0, 0, 0)$. For this model basic reproduction number is

$$R_q = \frac{\beta}{(d + \delta)(d + \beta_1 + \beta_2 - \delta)}. \quad (3.3)$$

If $R_q > 1$, then D also contains a unique positive, endemic equilibrium $P^* = (S^*, E^*, I^*, Q^*, R^*)$ where

$$\begin{aligned} S^* &= \left[\frac{1}{\left\{ -(d + \delta)(d + \beta_2 + \delta) + R_q(d + \delta)(d + \beta_2 + \delta) + d(d + \beta_2 + \delta) \right.} \right. \\ &\quad + R_q(d + \delta)(\beta_2 + \delta) + R_q d(d + \delta) + R_q(d + \delta) \\ &\quad \left. + R_q(d + \delta)(d + \beta_2 + \delta) \right\]} \\ &\quad \times \left[A d(d + \beta_2 + \delta) + R_q d(d + \delta)(d + \beta_2 + \delta) \right. \\ &\quad \left. + R_q A(d + \delta)d + R_q A(d + \delta) + R_q A(d + \delta)(d + \beta_2 + \delta) \right], \\ E^* &= \frac{1}{(d + \delta)}(A - dS^*), \\ I^* &= \frac{R_q(A - dS^*)}{(d + \beta_2 + \delta)}, \quad Q^* = \frac{R_q(A - dS^*)}{(d + \beta_2 + \delta)}, \\ R^* &= \frac{R_q(A - dS^*)}{d(d + \beta_2 + \delta)} + \frac{R_q(A - dS^*)}{d}. \end{aligned} \quad (3.4)$$

Theorem 3.1. Consider the system (3.1). If $R_q < 1$, then solution set $D = \{(S, E, I, Q, R) / S \geq 0; E \geq 0; I \geq 0; Q \geq 0; R \geq 0; S + E + I + Q + R \leq A/D\}$ is locally asymptotic stable for disease-free equilibrium P_0 . If $R_q > 1$, then the region $D - \{(S, E, I, Q, R) / I = 0\}$ is an asymptotically stable region for the endemic equilibrium P^* .

Proof. For the local stability, Jacobian of the system (3.1) at equilibrium P_0 is

$$J_{P_0} = \begin{bmatrix} -d & 0 & -\frac{(A/D)}{N} & 0 & 0 \\ 0 & -(d + \delta) & \left(\frac{A/D}{N}\right) & 0 & 0 \\ 0 & & -(d + \beta_1 + \beta_2 - \delta) & 0 & 0 \\ 0 & 0 & & -(d + \beta_2 + \delta) & 0 \\ 0 & 0 & & & -d \end{bmatrix}. \quad (3.5)$$

Table 1: Parametric values used in simulating the models.

Parameters	Simple mass action	Standard incidence rate
N	10,000	10,000
S(0)	9900	9900
E(0)	100	100
I(0)	0	0
Q(0)	0	0
R(0)	0	0
	0.1	0.01
	0.09	0.09
	0.01	0.09
	0.07	0.07
	0.09	0.03
A	0.01	0.01
d	0.01	0.01
μ_1	0.1	0.03
μ_2	0.1	0.04
	0.01	0.03

The eigenvalues of J_{P_0} are $-\bar{d}$; $-(\bar{d} + \mu_1)$; $-(\bar{d} + \mu_1 + \mu_2 - \mu_3)$; $(\bar{d} + \mu_2 + \mu_3)$; $-\bar{d}$. Since all the roots are real and negative, system is locally asymptotically stable.

With a view to prove the global stability when $R_q \leq 1$, we use the Liapunov function by putting $V = I$, we get the same equation as we have found in the model 1; therefore, the proof will be analogous with the proofs in the previous section.

In order to prove the global stability when $R_q > 1$ and $\mu_1 = \mu_2 = 0$, first we get $dN/dt = A - N\bar{d}$, this implies $N \rightarrow A/\bar{d}$ when t tends to infinity.

The limit system for (3.1) is

$$\begin{aligned} \frac{dS}{dt} &= A - \frac{dSI}{A} - dS, \\ \frac{dE}{dt} &= \frac{dSI}{A} - (\mu_1 + d)E, \\ \frac{dI}{dt} &= E - (\bar{d} + \mu_1 + \mu_2 - \mu_3)I, \\ \frac{dQ}{dt} &= I - (\bar{d} + \mu_2 + \mu_3)Q, \\ \frac{dR}{dt} &= Q + I - dR, \end{aligned} \tag{3.6}$$

where $N = A/\bar{d}$. The first three equations are independent of Q and R . In the three dimensional $S E I$ first octant region with $S + E + I \leq A/\bar{d}$, the equilibrium $(0, 0, 0)$ is saddle, that is, attractive along $I = 0$ and has a repulsive direction into the region. The other equilibrium (S^*, I^*) in the region is locally asymptotically stable.

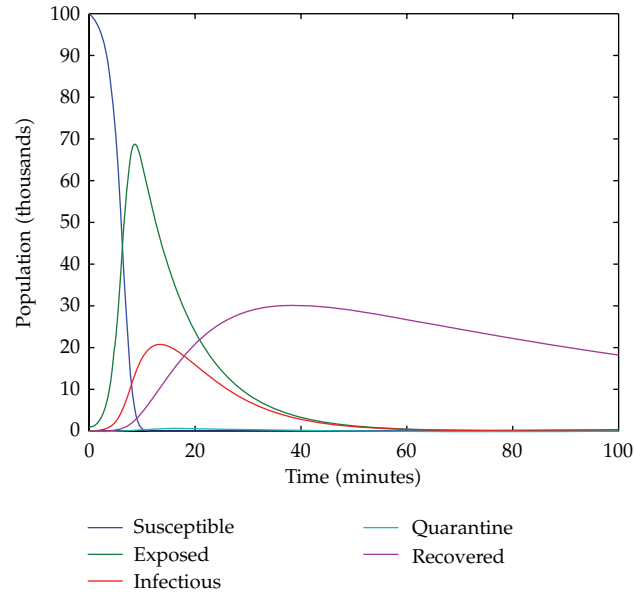


Figure 2: Time series of susceptible population $S(t)$, $E(t)$, $I(t)$, $Q(t)$, and $R(t)$ of the system (2.1).

Using Dulac’s criteria with multiplier $1/I$, we have

$$\begin{aligned}
 &-\frac{1}{S} \left[\frac{A}{I} - \frac{d}{A} \frac{S}{I} - \frac{dS}{I} \right] + \frac{1}{E} \left[\frac{d}{A} \frac{S}{I} - \frac{E}{I} (d + \dots) \right] + \frac{1}{I} \left[\frac{E}{I} - (d + \dots) \right] \\
 &= -\frac{d}{A} - \frac{d}{I} - (d + \dots) \frac{1}{I} - \frac{E}{I^2} < 0,
 \end{aligned}
 \tag{3.7}$$

so that there are no periodic solutions in the region. Thus, by the Poincare-Bendixson theory, all solutions starting in the first octant region with $I > 0$ and $S + E + I \leq A/d$ approach (S^*, E^*, I^*) as t tends infinity.

In this case, the differential equation for Q has the limiting equation

$$\frac{dQ}{dt} = I - (d + \dots)Q,
 \tag{3.8}$$

so that Q tends to Q^* by Lemma 2.1.

Similarly, the differential equation for R has the limiting equation

$$\frac{dR}{dt} = Q^* + I^* - dR,
 \tag{3.9}$$

so that R tends to R^* by Lemma 2.1. Thus P^* is a globally asymptotically stable equilibrium for the limit system (3.6). Hence, by Lemma 2.1, all solutions starting in the region $D - \{(S, E, I, Q, R) / I = 0\}$ of the system (3.1) approach the endemic equilibrium P^* as t tends to infinity.

□

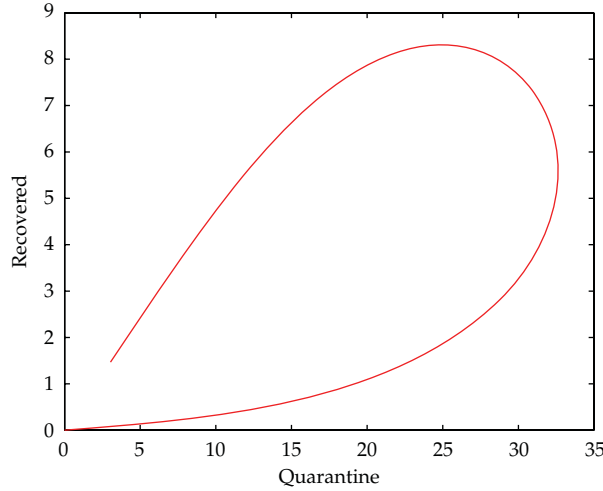


Figure 3: Effect of quarantine Q on recovered nodes R .

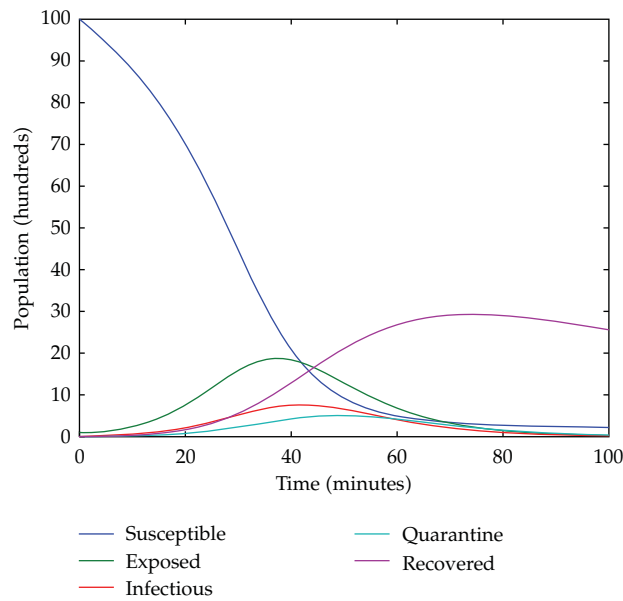


Figure 4: Time series of susceptible population $S(t)$, $E(t)$, $I(t)$, $Q(t)$, and $R(t)$ of the system (3.1).

4. Conclusion

Inspired by the biological compartmental epidemic model, we made an attempt to develop two SEIQR models, one using simple mass action incidence and the other using standard incidence rate. Vertical transmission has been included into infectious compartment. Runge Kutta Fehlberg fourth-fifth order method is used to solve and simulate the system (2.1) and (3.1) by using parametrical values mentioned in Table 1. The model has a constant recruitment of the nodes and exponential natural and infection-related death (crashing) of the nodes. Global stability of the unique endemic equilibrium for the epidemic model has been established. We observe that the behavior of the Susceptible, Exposed, Infected, and

Quarantined nodes with respect to time is asymptotically stable, which is depicted in Figures 2 and 4. The effect of Q on R is depicted in Figure 3. When the nodes are highly infected by different kinds of malicious objects, quarantine is one of the remedy. We run antimicrobial software of latest signature against quarantined nodes, and these nodes are kept under observation. The more we quarantine the most infected nodes, the more the recovery is; the lesser we quarantine, the lesser the recovery is. Also at a very specific short interval of time, the recovery of the nodes is constant when the quarantine node decreases. These can be observed in Figure 3. Simulation result agrees with the real life situation. The basic reproduction number R_q is obtained and has been identified as a threshold parameter. If $R_q \leq 1$, the disease-free equilibrium D is globally stable in the feasible region and the disease always dies out. If $R_q > 1$, a unique endemic equilibrium P^* exists and is globally stable in the interior of the feasible region, and once the disease appears, it eventually persists at the unique endemic equilibrium level. Lyapunov function is used to prove the global stability of D when $R_q \leq 1$. In our model, the number of contacts is influenced by the size of the quarantine class Q . The quarantine process is an alternative method for reducing the average infectious period by isolating some infectives, so that they do not transmit the malicious objects in the computer network. We have observed that both the effective infectious period $1/(d + \mu + \nu)$ and R_q decrease as the quarantine rate ν increases.

The analysis of quarantine reproduction number R_q by Feng and Thieme [14, 15] and Hethcote et al. [31] agrees with our model. Feng and Thieme [14, 15] in their SIQR model observed that the quarantine reproduction number was independent of the mean residence time in the quarantine class Q . Hethcote et al. [31] also had their same observation regarding the independence of the mean residence time in the Q class for all of their endemic models. We also have the same observation for our SEIQRS model. The mean residence time in the class Q for our model SEIQRS is $1/\nu$. The expression for the threshold does not involve the parameter ν . This comes from our assumption that the nodes in the quarantine class Q do not infect other nodes and nodes are not infectious when they move out of the quarantine class. The quarantine reproduction number R_{qr} depends on parameter ν . For example, if $\nu = n, n \in \mathbb{Z}^+$, then transfer out of infectious class I to quarantine class Q is n times as frequent as transfer to the removed class R . A positive rate constant ν to transfer out of infectious class I by quarantine does decrease the quarantine reproduction number R_{qr} so that it is less than its value without quarantine. Hence the use of quarantine to control a disease not only decreases the endemic infective class size when R_q remains above 1, but also makes it easier to obtain $R_q \leq 1$ leading to disease extinction.

The future work will involve in taking time delay constraints in various compartments which may lead to more interesting result.

Acknowledgment

The authors are thankful to the editor and anonymous referees for their comments which substantially improved the quality of the paper.

References

- [1] M. E. J. Newman, S. Forrest, and J. Balthrop, "Email networks and the spread of computer viruses," *Physical Review E*, vol. 66, no. 3, Article ID 035101, 4 pages, 2002.
- [2] R. M. Anderson and R. M. May, *Infection Disease of Humans, Dynamics and Control*, Oxford University Press, Oxford, UK, 1992.

- [3] R. M. Anderson and R. M. May, "Population biology of infectious diseases," *Nature*, vol. 180, pp. 361–367, 1999.
- [4] S. Forrest, S. Hofmeyr, A. Somayaji, and T. Longstaff, "Self-nonsel self discrimination in a computer," in *Proceedings of the IEEE Symposium on Research in Security and Privacy*, pp. 202–212, May 1994.
- [5] E. Gelenbe, "Keeping viruses under control," in *Proceedings of the 20th International Symposium on Computer and Information Sciences (ISCIS '05)*, vol. 3733 of *Lecture Notes in Computer Science*, pp. 304–311, Springer, October 2005.
- [6] E. Gelenbe, "Dealing with software viruses: a biological paradigm," *Information Security Technical Report*, vol. 12, no. 4, pp. 242–250, 2007.
- [7] E. Gelenbe, V. Kaptan, and Y. Wang, "Biological metaphors for agent behavior," in *Computer Science*, pp. 667–675, Springer-Verlag, 2004.
- [8] J. R. C. Piqueira and F. B. Cesar, "Dynamical models for computer viruses propagation," *Mathematical Problems in Engineering*, vol. 2008, Article ID 940526, 11 pages, 2008.
- [9] J. R. C. Piqueira, B. F. Navarro, and L. H. A. Monteiro, "Epidemiological models applied to virus in computer networks," *Journal of Computer Science*, vol. 1, no. 1, pp. 31–34, 2005.
- [10] W. T. Richard and J. C. Mark, "Modeling virus propagation in peer-to-peer networks," in *Proceedings of the 5th International Conference on Information, Communications and Signal Processing*, pp. 981–985, December 2005.
- [11] B. K. Mishra and D. K. Saini, "SEIRS epidemic model with delay for transmission of malicious objects in computer network," *Applied Mathematics and Computation*, vol. 188, no. 2, pp. 1476–1482, 2007.
- [12] B. K. Mishra and D. K. Saini, "Mathematical models on computer viruses," *Applied Mathematics and Computation*, vol. 187, no. 2, pp. 929–936, 2007.
- [13] Z. Feng and H. R. Thieme, "Recurrent outbreaks of childhood diseases revisited: the impact of isolation," *Mathematical Biosciences*, vol. 128, no. 1-2, pp. 93–130, 1995.
- [14] Z. Feng and H. R. Thieme, "Endemic models with arbitrarily distributed periods of infection I: general theory," *SIAM Journal on Applied Mathematics*, vol. 61, no. 3, pp. 803–833, 2000.
- [15] Z. Feng and H. R. Thieme, "Endemic models with arbitrarily distributed periods of infection II: fast disease dynamics and permanent recovery," *SIAM Journal on Applied Mathematics*, vol. 61, no. 3, pp. 983–1012, 2000.
- [16] L. I. Wu and Z. Feng, "Homoclinic bifurcation in an SIQR model for childhood diseases," *Journal of Differential Equations*, vol. 168, no. 1, pp. 150–167, 2000.
- [17] K. L. Cooke and P. van den Driessche, "Analysis of an SEIRS epidemic model with two delays," *Journal of Mathematical Biology*, vol. 35, no. 2, pp. 240–260, 1996.
- [18] M. Y. Li, J. R. Graef, L. C. Wang, and J. Karsai, "Global dynamics of a SEIR model with varying total population size," *Mathematical Biosciences*, vol. 160, no. 2, pp. 191–213, 1999.
- [19] D. Greenhalgh, "Hopf bifurcation in epidemic models with a latent period and nonpermanent immunity," *Mathematical and Computer Modelling*, vol. 25, no. 2, pp. 85–107, 1997.
- [20] J. K. Hale, *Ordinary Differential Equations*, Krieger, Basel, Switzerland, 2nd edition, 1980.
- [21] H. W. Hethcote, H. W. Stech, and P. van dan Driessche, "Periodicity and stability in epidemic models: a survey," in *Differential Equations and Applications in Ecology, Epidemics and Population Problems*, K. L. Cook, Ed., pp. 65–85, Academic Press, New York, NY, USA, 1981.
- [22] M. Y. Li and J. S. Muldowney, "Global stability for the SEIR model in epidemiology," *Mathematical Biosciences*, vol. 125, no. 2, pp. 155–164, 1995.
- [23] M. Y. Li and L. Wang, "Global stability in some SEIR epidemic models," in *Mathematical Approaches for Emerging and Reemerging Infectious Diseases: Models, Methods, and Theory*, C. Chavez, S. Blower, P. van den Driessche, D. Kirschner, and A. Yakhdu, Eds., vol. 126, pp. 295–311, Springer, New York, NY, USA, 2002.
- [24] Y. Michel, H. Smith, and L. Wang, "Global dynamics of an seir epidemic model with vertical transmission," *SIAM Journal on Applied Mathematics*, vol. 62, no. 1, pp. 58–69, 2001.
- [25] H. Dong, Z. Wang, and H. Gao, "Observer-based H_∞ control for systems with repeated scalar nonlinearities and multiple packet losses," *International Journal of Robust and Nonlinear Control*, vol. 20, no. 12, pp. 1363–1378, 2010.
- [26] Z. Wang, D. W. C. Ho, H. Dong, and H. Gao, "Robust H_∞ finite-horizon control for a class of stochastic nonlinear time-varying systems subject to sensor and actuator saturations," *IEEE Transactions on Automatic Control*, vol. 55, no. 7, Article ID 5441037, pp. 1716–1722, 2010.
- [27] B. Shen, Z. Wang, and Y. S. Hung, "Distributed H_∞ -consensus filtering in sensor networks with multiple missing measurements: the finite-horizon case," *Automatica*, vol. 46, no. 10, pp. 1682–1688, 2010.

- [28] B. Shen, Z. Wang, H. Shu, and G. Wei, "Robust H_∞ finite-horizon filtering with randomly occurred nonlinearities and quantization effects," *Automatica*, vol. 46, no. 11, pp. 1743–1751, 2010.
- [29] B. Shen, Z. Wang, and X. Liu, "Bounded H -infinity synchronization and state estimation for discrete time-varying stochastic complex networks over a finite-horizon," *IEEE Transactions on Neural Networks*, vol. 22, no. 1, pp. 145–157, 2011.
- [30] H. Dong, Z. Wang, D. W. C. Ho, and H. Gao, "Variance-constrained H_∞ filtering for a class of nonlinear time-varying systems with multiple missing measurements: the finite-horizon case," *IEEE Transactions on Signal Processing*, vol. 58, no. 5, Article ID 5410142, pp. 2534–2543, 2010.
- [31] H. Hethcote, M. Zhen, and L. Shengbing, "Effects of quarantine in six endemic models for infectious diseases," *Mathematical Biosciences*, vol. 180, pp. 141–160, 2002.